uOttawa

L'Université canadienne
Canada's university

FACULTÉ DES ÉTUDES SUPÉRIEURES ET POSTOCTORALES

uOttawa

L'Université canadienne
Canada's university

FACULTY OF GRADUATE AND POSDOCTORAL STUDIES

Jennifer L. Chaytor
AUTEUR DE LA THÈSE / AUTHOR OF THESIS

Ph.D (Chemistry)
GRADE / DEGREE

Department of Chemistry
FACULTÉ, ÉCOLE, DÉPARTEMENT / FACULTY, SCHOOL, DEPARTMENT

Examining the Role of Carbohydrate Hydration and Structure in Preventing Ice-Recrystallization

TITRE DE LA THÈSE / TITLE OF THESIS

Robert Ben
DIRECTEUR (DIRECTRICE) DE LA THÈSE / THESIS SUPERVISOR

CO-DIRECTEUR (CO-DIRECTRICE) DE LA THÈSE / THESIS CO-SUPERVISOR

Amit Basu (Brown University)

André Beauchemin

William Willmore

Christoper Boddy

Gary W. Slater
Le Doyen de la Faculté des études supérieures et postdoctorales / Dean of the Faculty of Graduate and Postdoctoral Studies

Examining the Role of Carbohydrate Hydration and Structure in Preventing Ice-Recrystallization

Jennifer L. Chaytor

Thesis submitted to the Faculty of Graduate & Postdoctoral Studies

University of Ottawa

In partial fulfillment of the requirements for the Ph.D. degree in the Ottawa-Carleton Chemistry Institute

Your file Votre référence
ISBN: 978-0-494-65564-1
Our file Notre référence
ISBN: 978-0-494-65564-1

Abstract

Antifreeze glycoproteins (AFGPs) are a subclass of biological antifreezes that are found in many species of Antarctic and Atlantic teleost fish. These compounds restrict the growth of ice and therefore protect these organisms from cryo-injury and death. Our laboratory is exploring the rational design of chemically and biologically stable AFGPs that have biological activity and therefore have potential medical and industrial applications. To this end, we have prepared a series of *C*-linked AFGP analogues that possess thermal hysteresis (TH) and ice-recrystallization inhibition (IRI) activity.

This thesis examines the effect of stereochemical and structural modifications of carbohydrates on IRI activity. Recently, our laboratory evaluated several commercially available *O*-linked mono- and disaccharides with varying stereochemical configurations for antifreeze activity. It was discovered that these sugars do not display thermal hysteresis activity, but do display IRI activity. Furthermore, their IRI activity is related to their solvation or hydration, which affects their ability to fit into the three-dimensional hydrogen-bonded network of ice. The ability of a sugar to be solvated depends on the stereochemical relationship of the hydroxyl groups on C2 and C4.

The IRI activity of these mono- and disaccharides was then correlated to their ability to protect human embryonic kidney cells at sub-zero temperatures. It has been proposed that the majority of damage to cells and tissues is caused by the recrystallization of ice during freeze-thaw protocols. Carbohydrates have been used as cryoprotective agents in the past, however, a systematic study that compares the IRI activity of these compounds to their cryoprotective ability has not been reported. Our observations support the theory that ice-recrystallization is a major cause of damage to cells during the freeze-thaw cycle, and that we can design novel cryoprotectants based upon the results of our IRI activity assessment.

I have recently prepared several new classes of substituted *C*-linked carbohydrates, which have been designed to disrupt the hydration of carbohydrates through hydrophobic interactions. It is believed that hydrophobic groups will affect the fit of these compounds into the three-dimensional hydrogen-bonded network of water, and

therefore change their ability to inhibit the recrystallization of ice. In the first series, the IRI activity of compounds with an alpha *C*-allyl group mirrored the trend of their *O*-linked parent monosaccharides. Through the synthesis of these and other compounds, it was found that for galactose, the anomeric stereochemistry does play a role in RI activity.

Methyl-α/β-galactopyranoside has been observed to have a poor compatibility with the three-dimensional hydrogen-bonded structure of ice. Compounds with a methoxy group at C2, C3, C4, and C6 respectively were prepared using standard protecting group chemistry. These compounds form the basis of a second series of *C*-linked carbohydrates that all showed a decrease in IRI activity compared to a non-methylated control. These results suggest that the methyl group disturbs the hydration of the carbohydrate and affects its ability to interact with ice. Interestingly, when longer groups (ethyl, propyl, butyl, and hexyl) were added to C2 to form a third series of compounds, we saw a steady increase in IRI activity. These compounds may be forming liquid-crystals or gelators, which is affecting their hydration and increasing their interaction with the ice-water interface. Thioglycoside derivatives of galactose were also found to have moderate IRI activity.

In another drastic structural variation, we examined the addition of a geminal-difluoromethylene group at the anomeric position in a fourth series of *C*-linked compounds. The results of the IRI assay of fluorinated sugars suggest that the fluorine atoms do not result in increased IRI activity. A fluorinated sugar showed lower levels of IRI activity when compared to an appropriate non-fluorinated control.

In order to develop an understanding of the role that biological antifreezes play at the ice-water interface, we undertook a series of Coherent Anti-Stokes Raman Scattering (CARS) experiments to observe the OH-stretching regions of solutions of water and biological antifreezes at sub-zero and room temperatures. The results of these experiments will be described in this dissertation.

Acknowledgements

I would first like to thank my supervisor, Dr. Robert Ben, for his invaluable guidance and assistance during the course of my doctoral studies. He was always available for helpful discussions and suggestions for my research as well as my career path, and he made it possible for me to attend several interesting scientific conferences during my Ph.D. Dr. Ben was also very helpful in proof-reading the various drafts of this thesis. I would also like to thank all of the past and present members of the Ben group for their assistance and friendship, including: Dr. Vincent Bouvet, Dr. Suhuai Lui, Pawel Czechura, Liz von Moos, Roger Tam, John Trant, Ruoying Gong, Sandra Ferreira, Wendy Campbell, Taline Boghossian, Jacqueline Tokarew, Taz Cheema, and Chantelle Capicciotti. Special thanks also to Dr. Mathieu Leclere and Dr. Michael Souweha, members of the Fallis group, who always had valuable suggestions.

Thank you to the members of my Research Proposal Committee (Dr. Bill Ogilvie and Dr. Christopher Boddy) and the members of my Thesis Committee (Dr. Amit Basu, Dr. Andre Beauchemin, Dr. Christopher Boddy, and Dr. Bill Willmore) for valuable discussions and suggestions to improve these documents.

I was privileged to supervise two wonderful undergraduate students, Rachelle Denis and Jackie Tokarew. I would like to thank both of them for helping to prepare starting materials for my projects. They also assisted my with my biology experiments, along with Liz von Moos, Luke Wu, and Louise Guolla. Thanks also to Dr. Tom Woo and Christopher Rowley for calculating hydration numbers for several of the carbohydrates discussed in this thesis. Thank you to Dr. Glenn Facey for NMR assistance and for setting up a ^{1}H-^{19}F HOESY experiment for my research.

I would like to thank the National Research Council for allowing us access to their CARS microscope. A special thank you to Adrian Pegoraro, Doug Moffatt and Andy Ridsdale for assisting me with these CARS experiments, as well as to Dr. John Pezacki and Dr. Albert Stolow for collaborating with us on this project.

I would like to acknowledge the National Sciences and Engineering Research Council and the University of Ottawa for their generous scholarships that assisted me financially during the course of this research.

Finally, thank you to my friends and family, especially my parents, for their love, support, and constant encouragement during the course of my studies.

Table of Contents

List of Figures

List of Tables

List of Abbreviations

2-D	two-dimensional
3-D	three-dimensional
10-CSA	10-camphor sulfonic acid
Ac	acetyl
Ac_2O	acetic anhydride
AcOH	acetic acid
AFGP(s)	antifreeze glycoprotein(s)
AFGP8	antifreeze glycoprotein fraction 8
AFP(s)	antifreeze protein(s)
AFP I	antifreeze protein type I
Ala	alanine
Allyl-MgBr	allyl magnesium bromide
ATR-FTIR	attenuated total reflection – fourier transform infrared
$BF_3{\bullet}OEt_2$	boron trifluoride diethyl etherate
Bn	benzyl
BnBr	benzyl bromide
Boc	*tert*-butyloxycarbonyl
br	broad
Bu	butyl
BuLi	butyl lithium
Bz	benzoyl
BzCl	benzoyl chloride
CARS	coherent anti-Stokes Raman scattering
CD	circular dichroism
CDI	carbonyl diimidazole

CF_2	*geminal*-difluoromethylene
CH_3CN	acetonitrile
CH_3NO_2	nitromethane
cm^{-1}	wavenumber
CPA	cryoprotective agent
$CuSO_4$	copper sulfate
d	doublet
dd	doublet of doublets
ddd	doublet of doublets of doublets
DCM	dichloromethane, CH_2Cl_2
DIPA	diisopropyl amine
DIPEA	diisopropylethyl amine
DFT	density functional theory
DIS	dynamic ice shaping
DMAP	dimethylaminopyridine
DMF	dimethyl formamide
DMSO	dimethyl sulfoxide
dt	doublet of triplets
EDTA	ethylene diamine tetraacetic acid
ESI	electrospray ionization
Et	ethyl
Et_2O	diethyl ether
EtOAc	ethyl acetate
EtOH	ethanol
Et_3SiH	triethyl silane
EXAFS	extended X-ray absorption fine structure
FBS	fetal bovine serum

Fmoc	9-fluorenylmethyloxycarbonyl
FTIR	fourier transform infrared
fs	femtosecond
Gal	galactose
GalNAc	*N*-acetyl-galactosamine
Glc	glucose
GlcNAc	*N*-acetyl glucosamine
Gly	glycine
HBTU	2-(1H-benzotriazole-1-yl)-1,1,3,3-tetramethylaminium hexafluorophosphate
Hex	hexyl
HN	hydration number
HOBT	*N*-hydroxyl benzotriazole
HOESY	heteronuclear overhauser enhancement spectroscopy
HPLC	high performance liquid chromatography
Ic	crystalline ice
Ih	hexagonal ice
iPrOH	isopropanol
IRI	ice-recrystallization inhibition
IR resin	Amberlite ion exchange resin
K_2CO_3	potassium carbonate
kDa	kiloDaltons
k_{as}	anti-Stokes wave vector
k_i	inhibition constant
k_p	pump wave vector
k_s	Stokes wave vector
Lac	lactose
LDA	lithium diisopropyl amide

LiOH	lithium hydroxide
m	multiplet
M	molar
M^+	parent molecular ion
Man	mannose
MD	molecular dynamics
Me	methyl
$MeC(OEt)_3$	triethyl orthoformate
MEM	minimal essential medium
MeI	iodomethane (methyl iodide)
MeOAc	methyl acetate
MeOH	methanol
MGS	mean grain size
$MgSO_4$	magnesium sulfate
MHz	mega Hertz
mM	millimolar
MMPP	magnesium monoperoxyphthalate
mOsmol	milliOsmolars
MS	mass spectrometry
MS	molecular sieves
MTT	methylthiazolydiphenyl-tetrazolium bromide
NAc	*N*-acetyl
NaH	sodium hydride
$NaHCO_3$	sodium bicarbonate
NaOAc	sodium acetate
NaOH	sodium hydroxide
NaOMe	sodium methoxide

NBS	*N*-bromosuccinamide
NH_4Cl	*tert*-butyl ammonium chloride
NH_4I	*tert*-butyl ammonium iodide
NTR	neurotrophin receptor
OGG	ornithine-glycine-glycine
OMe	*O*-methoxy
Orn	ornithine
P	protecting group
PBS	phosphate-buffered saline
Pd/C	palladium on carbon
$PhCH(OMe_2)$	benzaldehyde dimethyl acetal
PMC	partial molar compressibility
PMV	partial molar volume
ppm	parts per million
Pr	propyl
pTsOH	para-toluene sulfonic acid
q	quartet
QLL	quasi-liquid layer
Quant.	quantitative yield
s	singlet
SEM	standard error of the mean
Ser	serine
SM	starting material
SPPS	solid phase peptide synthesis
t	triplet
T	temperature
Tal	talose

TBAF	*tert*-butylammonium fluoride
TBDMSCl	*tert*-butyldimethyl silyl chloride
TBS	*tert*-butyldimethyl silyl
TBSOTf	*tert*-butyldimethyl silyl trifluoromethane sulfonate
tBuOAc	*tert*-butyl acetate
tdd	triplet of doublets of doublets
TFA	trifluoroacetic acid
TH	thermal hysteresis
THF	tetrahydrofuran
Thr	threonine
TMS	trimethylsilyl
TMSCl	trimethylsilyl chloride
TNBS	2,4,6-trinitrobenzene sulfonic acid
tt	triplet of triplets
ω_{as}	anti-Stokes frequency
ω_p	pump frequency
ω_s	Stokes frequency

Chapter 1 : Introduction

1.1: Carbohydrates in Biological Systems:

Carbohydrates play a significant role in several biological processes, both on their own and upon incorporation in glycoproteins and glycolipids.[1, 2] For example, proteoglycans are necessary for the maintenance of tissue structure and integrity and the formation of cellular and extracellular matrices,[3] and the carbohydrate portion of glycoproteins has been implicated in polypeptide folding and in maintaining protein stability, solubility, and conformation.[1, 4-7] Adoption of the correct protein tertiary and quaternary structure and protein aggregation often requires oligosaccharides.[8]

Furthermore, binding of carbohydrates to their receptors is essential for mediating biological functions. For example, chains of carbohydrate have been shown to affect the biological activity and secretion of erythropoietin, a protein involved in the differentiation of erythrocytes.[9] Carbohydrates have also been implicated in mammal sperm-egg interactions,[10] and specifically in human reproduction, where carbohydrates affect binding of the acrosome-reaction inhibiting glycoprotein to spermatozoa and ultimately regulate sperm exocytosis.[11] In addition, the survival and function of neurons requires binding of neurotrophic factors to the neurotrophin receptor (NTR), which is mediated by *O*-glycosylation of the NTR.[12]

Oligosaccharides and glycoproteins are essential for cell signalling, recognition, activation, trafficking, and enzymatic activity.[13-15] For example, Maly et al. have shown that fucosylated oligosaccharides play an important role in the trafficking of leukocytes.[16] Sialic acid residues, found in many biological materials, affect the overall concentration and transportation of calcium ions into and out of the heart.[17] Furthermore, carbohydrates are perfectly designed to encode biological information, because differences in their stereochemical configuration, anomeric configuration, attachment sites, location of substituents, and formation of isomers (such as pyranose and furanose forms) allow for many different structures that can hold distinct

information.[18] Clearly, carbohydrates are involved in nearly all biological processes and are essential in controlling our cellular processes.

In addition to mediating biological functions within the body, carbohydrates have been utilized in the preservation of cells, tissues, and organisms. Crowe et al. have shown that the disaccharide trehalose (Table 1.1) is responsible for membrane stabilization in anhydrobiotic organisms such as fungal spores, yeast, brine shrimp cysts, and nematodes that undergo dehydration in dry environments.[19] Since that observation, several groups have reported that trehalose can be used for the protection of cells against freezing[20, 21] and dehydration.[22] Other sugars that have been used for the cryopreservation of cells include sucrose,[21, 23] glucose,[21, 24] fructose,[21, 24] galactose,[21] xylose,[21] lactose,[21] maltose,[21] and the non-metabolizable glucose derivative 3-*O*-methyl-glucose (Table 1.1).[25] These sugars have been used on their own and in combination with other known cryoprotectants such as dimethyl sulfoxide (DMSO).[21, 26] The ability of a carbohydrate to act as a cryoprotectant has been linked to their hydration, or the way that they interact with water molecules, and this will be discussed below.

Table 1.1: Examples of carbohydrates previously used in cryopreservation protocols

Carbohydrate	Structure	Carbohydrate	Structure
Trehalose	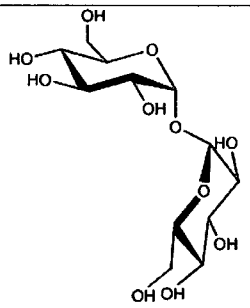	Sucrose	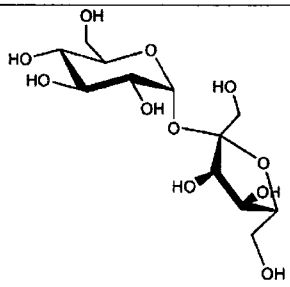
Glucose	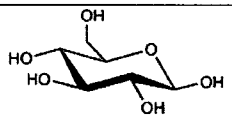	Fructose	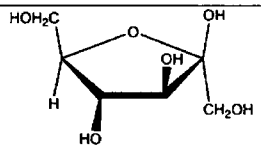
Galactose	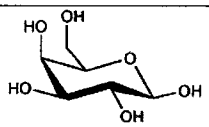	Xylose	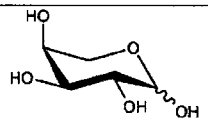
Lactose	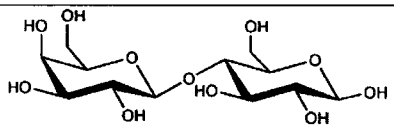	Maltose	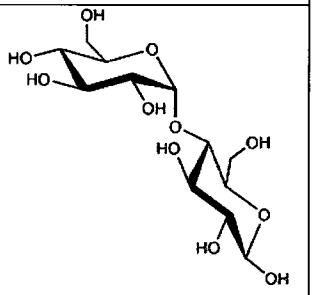
3-*O*-Methyl-Glucose	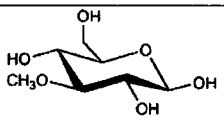		

1.2: Hydration of Carbohydrates:

The hydration or solvation of carbohydrates is important in mediating all biological functions, just as protein-water interactions have been shown to affect the

biological properties of proteins.[27] The solution conformation of an oligosaccharide (the way that it folds about its glycosidic bonds and forms hydrogen bonds within aqueous solutions) can determine its function.[28] Several of the properties of carbohydrates are affected by their hydration, including melting temperature, glass transition temperature, solubility, and osmotic pressure.[29] Molecular dynamics simulations have shown that water plays a critical role in determining the conformation of disaccharides, and that the primary role of the water is to competitively hydrogen bond to the carbohydrate and therefore weaken the internal hydrogen bond network of the carbohydrates.[30] Furthermore, the hydration of carbohydrates and other solutes can affect the dynamics of hydration and the water structure around other biological materials that are in the vicinity of the solute.[31]

Water is also important in maintaining protein stability.[32] For example, researchers have suggested that protein stabilization by carbohydrate stabilizers such as sucrose is due to the preferential exclusion of the carbohydrate from the protein surface, which serves to increase the chemical potential of the protein.[33] In other words, the concentration of solute is lower in the water immediately surrounding the protein than in the bulk water, resulting in a concentration and chemical potential gradient, leaving the protein preferentially hydrated.

Several researchers have examined the hydration of carbohydrates in an effort to understand its role in biological functions. It has been observed that the hydration of sugars depends on their structure. One theory is that hydration depends on the number of equatorial hydroxyl groups, which are reported to be better hydrated than axial hydroxyl groups.[34-36] Others have proposed the formation of hydrogen bond networks. Lopez de la Paz et al. have shown that carbohydrate hydroxyl groups act as hydrogen bond arrays as opposed to forming independent hydrogen bonds, and that the hydrogen bonding network within carbohydrates is significantly influenced by the nearby functional groups.[37] Galema et al. have reported that the hydration differs based on the distance of the next nearest neighbouring hydroxyl group, which is mainly dependent on the relative stereochemistry of the hydroxyl groups at C-2 and C-4.[38] In other words, the compatibility of the carbohydrate with the three-dimensional hydrogen bonded network

of water is dependent on the oxygen distances within the carbohydrate. Dashnau et al. have a similar hypothesis, where the orientation of the carbohydrate hydroxyl groups affects the water structure in the first surrounding hydration shell.[39] The hydroxyl group at position four (OH-4) was shown to be particularly important because it is able to be involved in several different hydrogen bond networks within the carbohydrate. The formation of an intramolecular hydrogen bond between OH-2 and OH-4 in talose has been observed and is suggested to account for the observation that talose is more hydrophobic and less hydrated than galactose or glucose.[40, 41]

As mentioned above, trehalose has been implicated in the survival of anhydrobiotic organisms (those that live in extremely dry or desiccated environments) and the preservation of cells. To explain these observations, three mechanisms have been proposed to account for the stabilization of desiccated proteins by trehalose.[42] The first is a *water replacement hypothesis*, where direct hydrogen bonding between the carbohydrate and the protein results in stabilization of dry proteins.[43, 44] In a second theory, there is no direct binding of the carbohydrate to the protein. Instead, the carbohydrate traps water molecules at the protein-carbohydrate interface by vitrification or glass formation, forming the *preferential hydration hypothesis*.[45] Finally, researchers have proposed the *high viscosity hypothesis*, in which an increase in the viscosity of the sugar solution restricts motion of the protein domains.[46] Others have suggested that a combination of these mechanisms is in effect. For example, Crowe et al. have proposed that carbohydrates protect organisms from dehydration both by vitrification (glass formation), and by hydrogen bonding to the protein as a substitute for bound water.[44] It is clear that trehalose interacts with water in some way and that its hydration can account for its ability to stabilize proteins and preserve cells.

Interestingly, trehalose has been reported to be a considerably better cryoprotectant than other disaccharides of very similar structure, such as sucrose and maltose.[47] Of particular interest in recent years has been the origin of this so-called "trehalose anomaly". Several researchers have undertaken experiments to explain the improved cryoprotection ability of trehalose over that of other disaccharides. Green and Angell have shown that trehalose has a significantly higher glass transition temperature

than maltose, sucrose, and glycerol, and that the order of glass transition temperatures mirrors their ability to preserve membrane structure and integrity.[47] Density, acoustic, and ultrasound measurements have shown that trehalose displays different hydration properties than other disaccharides that have been examined (maltose and sucrose) and shows a greater interaction with water.[48-50] Ultrasound measurements have further suggested that in concentrated solutions, intramolecular hydrogen bonds between the two pyranose rings of trehalose cause it to fold in on itself and therefore have very few trehalose-water interactions at high concentrations.[51] However, when the solution is less concentrated, the trehalose opens up and is more accessible for interactions with the water.[51] The hydration of trehalose is also decreased as the temperature is increased, because the trehalose rings form more intramolecular hydrogen bonds at higher temperatures.[51]

Of all the disaccharides that have been examined, trehalose is the only one that contains a 1,1 glycosidic linkage. Molecular dynamics (MD) simulations of several glucose disaccharides have shown that the position of the disaccharide linkage affects the flexibility and intramolecular hydrogen bonding, and this may account for the enhanced activity of trehalose.[52] Other MD experiments have contributed to our understanding of carbohydrate hydration. Lee et al. have shown using molecular dynamics that carbohydrates can disrupt the tetrahedral arrangement of water molecules surrounding themselves and can also reduce the rotational and translational motion.[32] Furthermore, trehalose and sucrose (disaccharides) cause greater restrictions in the movement of water molecules than glucose (a monosaccharide).[32] In addition, disaccharides are able to influence the dynamics of water into the second hydration shell, while monosaccharides display a smaller influence, and this has been correlated to the number of hydrogen bonds formed between the carbohydrate and water.[31] Therefore, the size of the carbohydrate clearly plays a role in hydration.

Hydration has also been suggested to play a role in freezing and ice recrystallization and growth. Kawai et al. have examined the hydration ability of several disaccharides in terms of the amount of unfrozen water using NMR experiments. They have observed that the amount of unfrozen water molecules in a sugar solution is

correlated to the number of equatorial hydroxyl groups on the sugar, which in turn have been correlated with the hydration of carbohydrates.[53] A similar study by Furuki has shown that there is a greater amount of unfrozen water in aqueous solutions of carbohydrates that have a poorer compatibility with the hydrogen bond network of water.[54] Others have suggested that the effective cryoprotection imparted by trehalose may be due to its ability to bind water molecules more tightly than other disaccharides, which hinders molecular motion of itself and the surrounding solution components.[55] Furthermore, it has been hypothesized by Branca and co-workers that by disrupting the tetrahedral hydrogen bond network of water, trehalose can prevent water molecules from adopting orientations that are compatible with the formation of ice and therefore act as a cryoprotectant.[48, 56] Magazu et al. have further suggested that the disruption of the tetrahedral network of water by trehalose reduces the amount of hydrogen bonds that are arranged in a manner that would normally promote the formation of ice.[57]

1.3: Biological Antifreezes:

In addition to the hydration of carbohydrates playing a role in ice growth and cryopreservation, water-carbohydrate and water-protein interactions are important in the actions of antifreeze proteins and glycoproteins. Researchers have reported that antifreeze proteins require interactions with water and the ice-water interface in order to display antifreeze activity.[54, 58] For example, McDonald et al. have observed through molecular dynamics simulations that the winter flounder antifreeze polypeptide gains stabilization by forming hydrogen bonds with water.[59] Further studies have shown that the polypeptide binds strongly to the ice surface, and that several hydrogen bonds are formed to both solid and liquid water.[60]

The winter flounder antifreeze polypeptide studied by McDonald et al. belongs to a class of molecules known as biological antifreezes. These compounds are found in several different species, such as insects, fish, and plants that inhabit arctic environments, and they have evolved to protect these organisms from freezing and ice damage. Biological antifreezes were first described by DeVries and Wohlschlag in 1969

when they discovered them in the blood serum of fish that live in areas with -1.87 ºC sea water.[61] These proteins were able to lower the freezing point of the blood of the fish below that of the freezing point of sea water, enabling their survival in subzero temperatures.[62] There are two main types of biological antifreezes, which are the antifreeze proteins and the antifreeze glycoproteins. The structure and the activity of these compounds, as well as the nature of their interactions with water and ice and their exciting medical and commercial applications, will be described below.

1.3.1: Structure of Biological Antifreezes:

1.3.1.1: Antifreeze Proteins:

There are several different types of antifreeze proteins (AFP) found in fish, which differ significantly in their structures (Table 1.2). Fish AFPs are classified into Types I, II, III, and IV. AFP Type I is mainly found in the winter flounders and sculpins and is rich in alanine residues. It has a molecular weight of 3.3-4.5 kDa and forms an α-helix. The α-helix is stabilized by several charged amino acids, which form charge dipole interactions, salt bridges, hydrogen bonds, and hydrophobic interactions with the helix.[63] Type I AFPs can be repetitive, with the primary structure consisting of 11 repeating amino acids TX_2AsxX_7 where X is mainly alanine and Asx is aspartic acid or asparagine, or contain a non-repetitive amino acid sequence.

Table 1.2: Comparison of biological antifreezes (modified from Harding et al,[64] Davies and Sykes,[65] and Venketesh and Dayanand[64-66])

Characteristic	AFGP	AFP I	AFP II	AFP III	AFP IV
Mass (kDa)	2.6 – 33	3.3 – 4.5	11 – 24	6.5	12.3
Primary Structure	(AAT)-repeat	Alanine-rich	Cysteine rich, disulfide-stabilized	General	Glutamine/ Glutamate rich
Secondary Structure	Extended 3-fold helix	α-helix	Mixed coil	β-sandwich	α-helix
Tertiary Structure	Extended	Single α-helix	Globular, C-type lectin fold	Globular	Helical Bundle
Heterogeneity	Polymer of 1-8 units	Repetitive/ non-repetitive	Ca dependent/ independent	Isoforms, dimers	NA
Natural Source	Antarctic notothenoids, northern cods	Right-eyed flounders	Sea raven, smelt, herring	Ocean pout, wolfish, eel pout	Longhorn sculpin
Structure	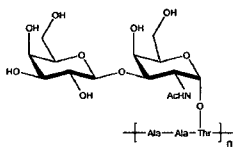				

Type II AFP is larger in size, ranging in weight from 11-24 kDa, and is stabilized by disulfide bridges due to its high cysteine content.[67] Its secondary structure forms a mixed coil, and in turn forms a globular C-type lectin fold. This AFP shows some structural similarity to the C-type lectin carbohydrate recognition domain.[67] The AFP from the sea raven has been shown to contain a relatively large amount of reverse turns, which may be involved in hydrogen bonding to water.[68] AFPs Type II are further

divided into two subtypes, based on their calcium dependence.[69, 70] It has been proposed that in the calcium dependent AFPs, the calcium cation is directly involved in the binding of the protein to ice, and plays a role in protein stabilization. This class of AFP is found in species such as the Rainbow smelt and the Atlantic herring.

The third class of AFPs, Type III, are found in the eel pouts. These proteins range in weight from 6-7 kDa and their 87-amino acid sequence is non-repetitive and not rich in any particular amino acid.[71] They form a β-sandwich and their tertiary structure is globular. More recently, a fourth class of fish AFPs was discovered by Deng et al. in the longhorn sculpin.[72] Type IV AFPs are enriched in glutamine and glutamate residues and contain repeats of a 22 amino acid sequence, which comprises their 12.3 kDa molecular weight.[72] They mainly form α-helices and may fold into a four-helix bundle, and are often found as dimers in solutions. Other non-fish AFPs are found in insects,[73-75] plants,[76-78] bacteria,[79] and fungi.[80]

1.3.1.2: Antifreeze Glycoproteins

Antifreeze glycoproteins (AFGPs), unlike their non-glycosylated counterparts, have a high degree of structural similarity. These proteins are comprised of a repeating threonine-alanine-alanine tripeptide, in which the threonine is glycosylated with a β-D-galactosyl-(1,3)-α-D-*N*-acetyl-galactosamine disaccharide (Table 1.2). This structure was originally proposed by DeVries et al. in 1970 when it was observed that Antarctic fish contain approximately 4-8 mg of AFGP per mL of blood serum.[81] AFGPs are divided into eight classes that differ mainly in their molecular weight, as the structure is generally conserved throughout the classes. AFPGs 1-4 range in molecular weight from 33-20 kDa, and AFGPs 5-8 weigh less than 20 kDa, with AFGP8 being the lightest at 2.6 kDa.[64] Although the tripeptide sequence is largely conserved, the glycosylated threonine can be replaced by arginine,[82, 83] and proline can replace one or both alanine residues.[84, 85]

The conformation of AFGPs has been extensively studied, although it remains somewhat undefined, unlike the fish AFPs which have a well-understood solution conformation. Early circular dichroism (CD) experiments suggested that AFGPs 3, 5, and 8 adopt a random coil conformation, since there was no evidence of α-helices or β-structures.[81] In 2006, Bouvet et al. examined the structure of AFGP8 at various concentrations using CD and observed that the conformation appeared to be concentration and temperature-dependent (Table 1.3).[86] Like earlier experiments, the predominant secondary structure was found to be random coil, although significant portions of α–helix and β–sheet were observed in solution.[86]

Table 1.3: Percentages of secondary structures in an AFGP8 solution at various concentrations, as determined by circular dichroism.[86] (--- indicates a negligible contribution)

Temperature	Concentration (mM)	Random Coil	α-helix	β-sheet	Other
21 ºC	0.01 – 0.05	41%	13%	20%	β-turn, polyproline type II helix
	0.1 – 5.0	41%	30%	8%	---
	10	85%	---	---	---
	20 – 100	40-48%	---	35%	6-17% Polyproline
-0.5 ºC	0.5 – 1.0	41%	13%	20%	13% β-turn, 13% polyproline
	5	40%	30%	---	---
	10	42%	---	34%	---
	20 – 100	20-55%	---	37-45%	---

Other studies have examined the dynamics and conformation of modified AFGPs (di-methylated at the *N*-terminus) in the presence of ice.[87] The solution conformation of the modified AFGP did not change dramatically upon freezing, and the structure of the

freeze-dried protein was similar to the fully hydrated protein.[87] Several conformers with varying secondary structure were observed, which suggested that the protein was highly flexible with the timescale of motion being in the nanosecond range.[87] Furthermore, water and ice played a large role in modulating the motion between conformers, suggesting that the conformation in the presence of ice is important for antifreeze activity.[87] Further studies using proline-containing AFGP showed that the protein is made up of four segments that are linked by flexible pivot points of alanine residues 5, 8, and 11.[88] Hydrogen bonds were observed between the *N*-acetyl group of the disaccharide and the protein backbone, which imparted stability to the AFGP.[88] The protein adopted a poly-proline II structure, although several other conformations were observed during the course of the experiment.[88] The lowest free energy conformations were found to be structurally very different, resulting in several energy minima that were approximately equal in energy.[88] The authors suggested that interconversion between the multiple energy minima acts as a thermal reservoir that restricts the growth of ice in locations where the AFGP has accumulated on the ice surface.[88]

1.3.2: Antifreeze-Specific Activity:

1.3.2.1: Thermal Hysteresis and Dynamic Ice Shaping:

There are two main properties of biological antifreezes, and the first is called thermal hysteresis. These proteins are able to depress the freezing point of a solution and therefore prevent the solution from freezing (Figure 1.1).[81, 89] However, the melting point of the solution remains the same, leaving a gap between the melting and freezing points known as the thermal hysteretic gap (Figure 1.2).[89] This depression occurs in a non-colligative manner (Figure 1.1, 1.2).[90] It has been suggested that biological antifreezes have activity that is 200-500 times greater than substances such as sodium chloride that lower freezing points by colligative properties (Figure 1.1, Table 1.4).[81, 91]

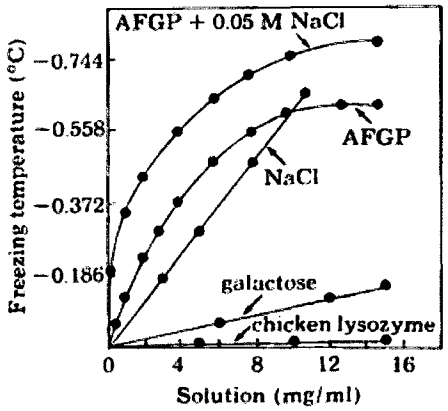

Figure 1.1: Freezing temperatures of several solutions as a function of solute concentration.[81, 91] The curved lines indicate non-colligative freezing point depression which becomes saturated at high concentrations, whereas the straight lines show the freezing temperatures of solutions that act in a colligative manner. Note that on a molar basis, a 4 mg/mL solution of NaCl is approximately 50 times more concentrated than a 4 mg/mL solution of AFGP due to the large difference in molecular weights.

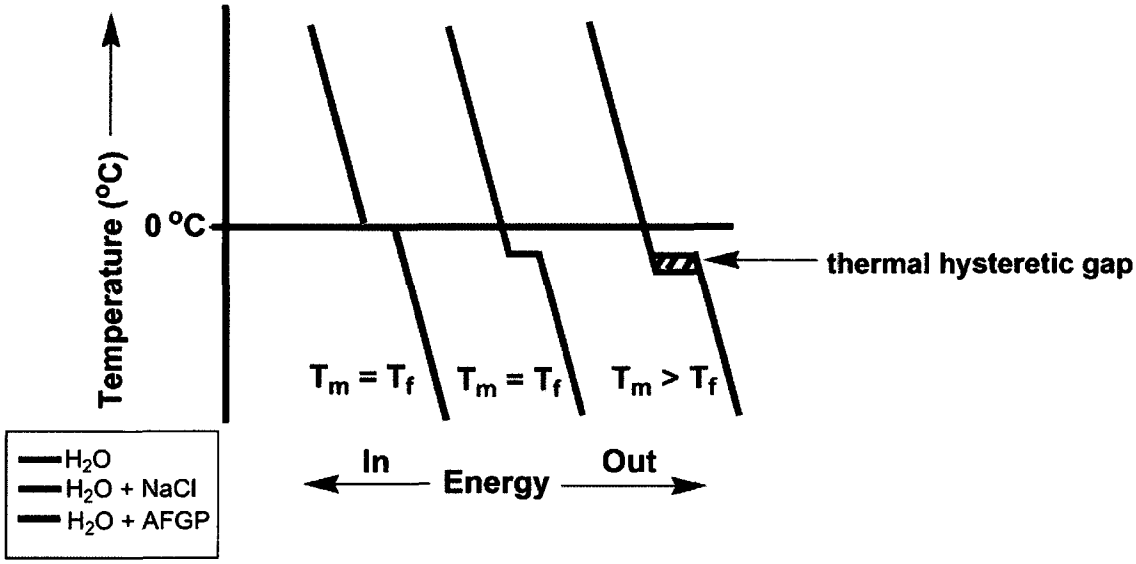

Figure 1.2: Schematic representation of thermal hysteresis: freezing/melting curves for water (black), NaCl solution (blue), and AFGP8 solution (red). In the salt solution the melting point and freezing points are depressed by the same amount due to colligative properties. The AFGP solution causes a further depression of the freezing point below the colligatively-lowered melting point, leaving a thermal hysteretic gap between them.

Table 1.4: Maximal thermal hysteresis activity (dependent on concentration) of AFPs from various sources[66]

Source of AFP	Thermal Hysteresis Activity
Bacteria/fungal AFPs	Negligible (IRI activity only)
Plant AFPs	0.2-0.4 ºC
Fish AFPs	0.6-1.5 ºC
Insect AFPs	6.0 ºC and greater

Associated with thermal hysteresis is a phenomenon called dynamic ice shaping, which is a direct result of the binding of the protein to ice. Antifreeze proteins are able to change the growth habit and rate of growth of ice.[89] Due to the binding of the protein to only certain faces of the growing ice crystal, the crystal begins to change its shape and form hexagonal bipyramids and ultimately forms needle-shaped ice crystals as the temperature drops below the thermal hysteretic gap (Figure 1.3).[92]

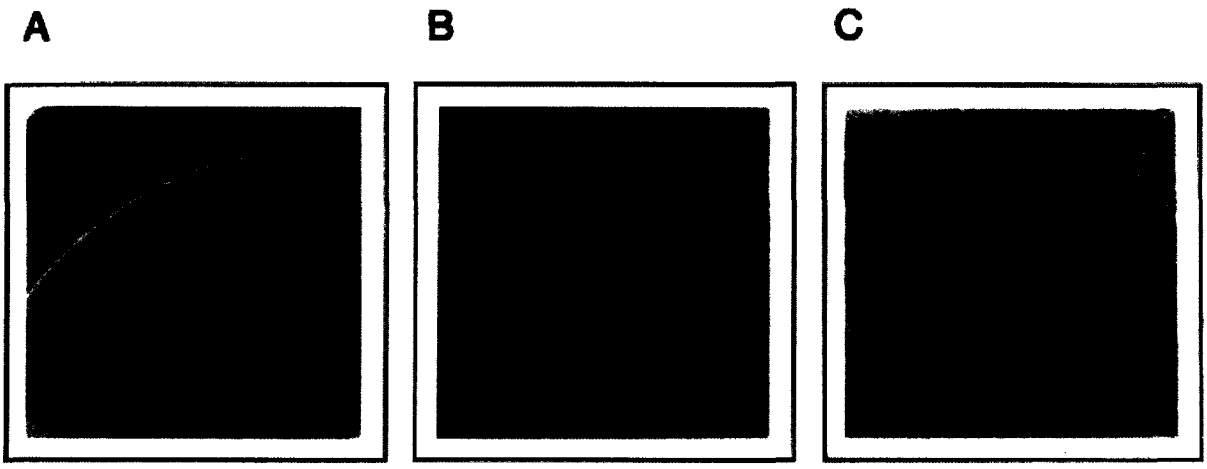

Figure 1.3: Dynamic ice shaping results in hexagonal (A), hexagonal bipyramidal (B), and needle-shaped (C) ice crystals.[65]

Through several studies of ice crystal habit in the presence of biological antifreezes, researchers have observed that biological antifreezes cause ice to grow in long needles with axes that are parallel to the c-axis.[91, 92] From this observation, a general model for the binding of AFPs and AFGPs to ice has emerged. Biological antifreezes appear to preferentially bind to the prism faces of a growing ice crystal through hydrogen bonds and dipolar interactions.[63, 93] These bound proteins therefore restrict the addition of further water molecules to the prism face, and those additional water molecules can only add to the basal plane (Figure 1.4).[65] This causes growth to occur parallel to the c-axis, and restricts growth perpendicular to the c-axis, accounting for the formation of needle-shaped ice crystals.[82, 94] The mechanism of ice-binding will be described in detail later in this chapter.

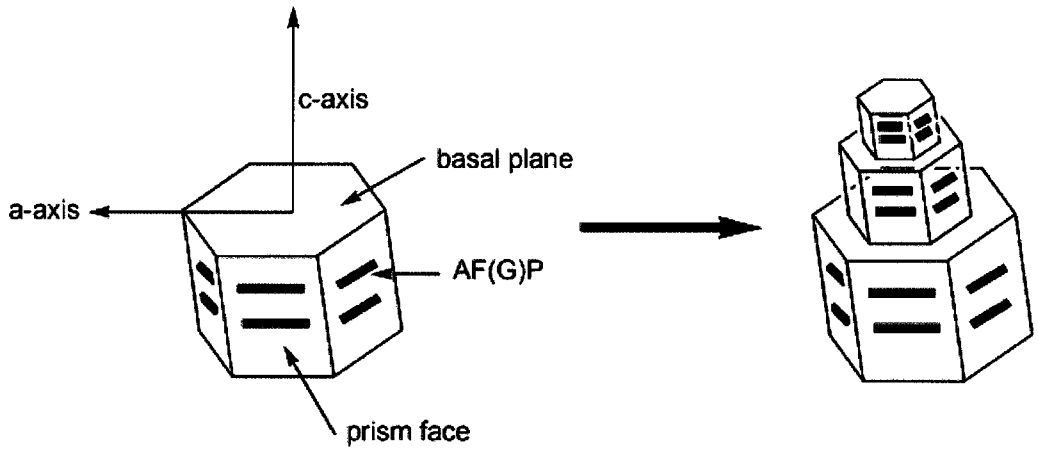

Figure 1.4: Schematic representation of the interaction of biological antifreezes with ice (adapted from Davies and Hew[65] and Hew and Yang[95]). Biological antifreezes selectively bind to the prism faces of an ice crystal and prevent further growth along the a-axis.

1.3.2.2: Inhibition of Ice-Recrystallization:

The second property of biological antifreezes is their ability to inhibit the recrystallization of ice. Ice recrystallization is a process whereby large ice crystals get larger at the expense of smaller ones.[96] Biological antifreezes are able to inhibit this

process and therefore restrict the growth of large ice crystals.[93] Figure 1.5 shows the difference in ice crystal size between a 10 mg/mL AFGP8 solution (Image **A**) and a phosphate-buffered saline solution (Image **B**). In the AFGP8 solution, the formation of larger ice crystals by recrystallization has been minimized, resulting in much smaller crystals. It has been suggested that ice-recrystallization inhibition (IRI) activity is especially important in organisms that are able to survive intracellular freezing, although it is not essential in organisms which are freeze-tolerant but are unable to survive intracellular freezing.[97] In most cases, thermal hysteresis and ice-recrystallization inhibition activity are thought to go hand-in-hand, but some researchers have observed thermal hysteresis in the absence of IRI activity, and others have observed ice-recrystallization inhibition when thermal hysteresis was not present.[97, 98]

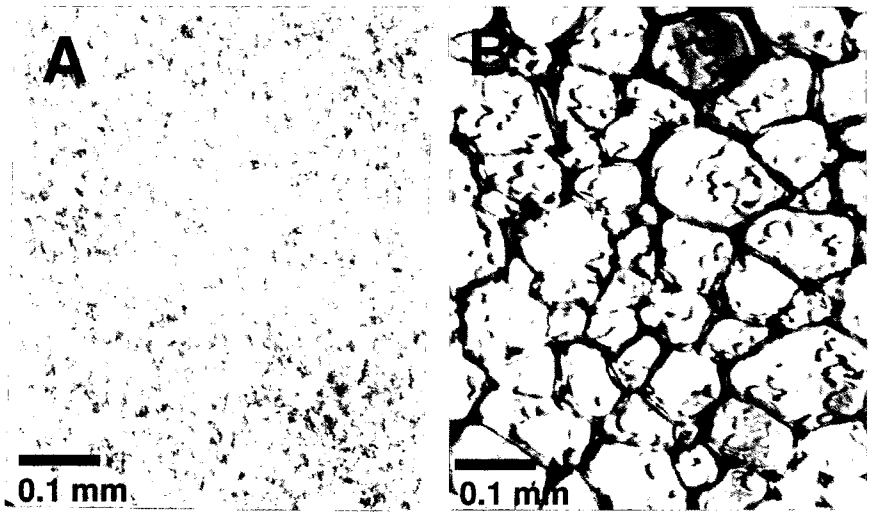

Figure 1.5: Size of ice crystals of a 10 mg/mL AFGP8 solution (Image **A**) compared to a phosphate-buffered saline (PBS) as a negative control (Image **B**) (Ben lab, unpublished results). The magnification is the same in both images. AFGP8 has inhibited the recrystallization of ice, resulting in much smaller ice crystals in Image **A**.

1.3.3: Proposed Mechanisms of Action of Biological Antifreezes:

It is generally accepted that the antifreezes directly bind to the surface of a growing ice crystal in an absorption-inhibition process.[82, 99, 100] A few researchers have proposed a reversible kinetic model for antifreeze binding;[101-103] however, much more evidence exists for irreversible binding. Once the antifreeze has bound, additional water molecules are added only to the ice surfaces between adjacent antifreeze molecules. As water molecules are added to these areas, the ice begins to grow with a high degree of curvature. There are two theories as to how this curvature affects ice growth.[104] In the first theory, more energy is required to add additional water molecules to these curved surfaces that have a large surface area (Figure 1.6).[82] This ultimately leads to a non-equilibrium freezing point depression, although the melting point remains the same. In other words, surface water molecules and biological antifreezes act as an energy barrier towards ice growth.

In a second theory, the build up of pressure from the increasing convexity of the interface can account for the inhibition of ice growth.[104] Within the thermal hysteretic gap, ice crystals do not increase in size, so the biological antifreezes must cause a vapour pressure equilibrium between the ice vapour pressure and the vapour pressure of the surrounding water.[104] In this model, the "vapour pressure" of the solid or liquid phase reflects the tendency of a molecule to leave that phase.[104] Therefore, in order to reach a vapour pressure equilibrium, the ice vapour pressure is raised to match that of the surrounding supercooled water.[104] This process, whereby the vapour pressure at the ice crystal surface is affected by curvature at the surface, is called the Kelvin Effect.[104] There is a maximum amount that the ice crystal surface can expand, and when this point is reached the ice crystal is said to have reached the critical convexity. At the hysteresis freezing point, one area of the ice surface will reach this critical convexity, where the vapour pressure will be suddenly lowered and spontaneous ice nucleation will occur at that location.[104]

Three different adsorption-inhibition mechanisms that incorporate curvature of the ice surface have been proposed to account for the properties of biological

antifreezes, of which the first two are the mattress model and the step-pinning molecule (Figure 1.6). In the mattress model, the bound antifreezes prevent ice from growing perpendicular to the surface of the ice.[105] The step-pinning model, in a more three-dimensional view, suggests that the antifreezes block the growth of a step.[101, 106] These models both assume irreversible absorption. In accordance with this model, Pertaya et al. have shown using AFPs bound to green fluorescent protein that attachment of AFPs to ice is quasi-permanent (lasting at least seven days).[107] The third mechanism is a two step model, in which the antifreezes originally bind reversibly and then switch to irreversible binding. This two-step model has been proposed by Hall and Lips to account for the fact that some of the proteins remain in solution in the presence of ice.[1, 108-111] This observation is not consistent with entirely irreversible binding of biological antifreezes to ice. However, although activity does increase with increasing antifreeze concentration, AFGPs display a plateau in activity at high concentrations.[101]

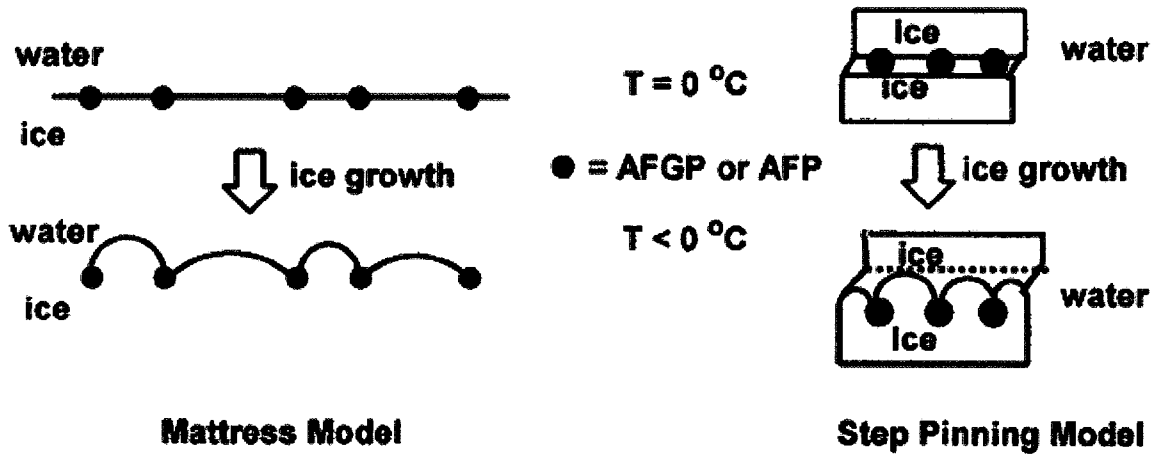

Figure 1.6: Adsorption-inhibition mechanisms: the mattress model and the step pinning model.[112] Both models show that ice grows with a high degree of curvature between each bound antifreeze molecule.

The nature of the binding of antifreezes to ice and the interactions involved has been heavily studied. Some researchers have proposed that the antifreezes adopt a structure that is complimentary to the structure of ice, which helps to dock the proteins.

For example, DeVries and Price observed that several of the hydroxyl groups of the disaccharide of AFGP are spaced 4.5 Å apart, which matches the distances between the oxygen atoms that are parallel to the a-axes of the ice lattice.[93] Baruch et al. have also observed that carbohydrates that contain at least two hydroxyl groups that are spaced 4.2 to 4.5 Å apart, such as galactose, have a good steric match to the three-dimensional hydrogen-bonded structure of water.[113] This would account for the affinity of certain antifreezes for the prism faces of growing ice crystals. Furthermore, in AFPs the distance between the aspartate and threonine residues is also 4.5 Å.[93] In addition, some AFPs from insects have been shown to adopt a β-helical structure stabilized by disulfide and hydrogen bonds.[114] The conserved ice binding surface of these insect AFPs contains a series of threonine-cysteine-threonine residues, which form a flat β-sheet.[114] The spacing of the hydroxyl groups of the threonine residues on the ice-binding face is a very good match to the ice lattice.[114] Similar results have been obtained when studying the crystal structure of a globular AFP,[111] although it should be noted that the crystal structure may not be representative of the solution structure in the presence of water or ice. In the spruce budworm AFP, the hydroxyls on the ice-binding face match the ice lattice on both the prism and basal planes, which suggests that this protein is able to bind to both planes, possibly accounting for its much greater ("hyperactive") activity than the fish AFPs.[75]

The ability of biological antifreezes to bind to ice must be dependent upon their structure. However, there is great debate over the role of the various functional groups on ice binding. For many years, is has been believed that polar groups such the side chains of threonine and aspartate are involved in the structuring of water and in ice-binding.[81, 115] The ice lattice-complimentarity described above seemed to be in support of this theory. Although AFP III does not have a regular repeating structure like AFGPs and AFP I, several polar amino acids in the *C*-terminal β-sheet were determined to be essential for protein-ice interactions and antifreeze activity by the synthesis of mutants.[116] Dipolar interactions and hydrogen bonding seemed to be very important in ice binding of all antifreezes.[63, 117] In addition to polar residues on the ice-binding face, Yang et al. have suggested that hydrophobic residues on the non-ice binding face are

also important in antifreeze activity, because they prevent the addition of more water molecules to the ice surface.[118]

When examining the effect of hydrophobic residues on antifreeze activity, Wen and Laursen observed that placing bulky glutamine or leucine residues on one side of the helix resulted in a complete loss of activity.[119] They suggested that this is due to steric hindrance which prevents effective packing of AFPs on the ice surface, and therefore propose that AFPs must interact with each other by side-by-side hydrophobic interactions.[119] Sonnichsen et al. have studied the solution structure of AFP III and observed that the ice binding site is planar and fairly non-polar.[65] Although the spacing of the polar groups matches that of the prism face of the ice lattice, many of the residues in the ice-binding site have low solvent accessibility, and the conformation of the protein limits the number of ice-protein hydrogen bonds that can be formed.[65] They therefore suggest that hydrophobic groups may be involved in protein-ice adsorption.[65] Similar observations led Yang et al. to propose that AFP III binds to ice based on atomic surface complimentarity arising from van der Waals interactions.[120] Mutations that extend or shorten the side chain of an ice-binding amino acid residue have been shown to result in dramatic decreases in ice-binding.[58] These mutations decrease van der Waals interactions and interrupt the required ice-protein surface-surface complimentarity.[58] Finally, molecular dynamics simulations showed that during ice binding, although strong ice-peptide hydrogen bonds were formed, the threonine side chains were oriented away from the ice-protein interface.[60] This suggests that the protein was a good steric fit to the ice-water interface and that it is this matching, and not the polar threonine groups, that controls binding.

Additional support for hydrophobic effects in determining antifreeze activity came with several studies of AFP mutants. Replacing threonine residues with serine, which retains the hydroxyl group of threonine, resulted in moderate to complete loss of activity.[121-123] However, replacement by valine residues, which retains the γ-methyl group of threonine but eliminates the hydroxyl group, had a much less drastic effect on antifreeze activity.[110, 122] These results show that hydrogen bonds involving the threonine hydroxyls are not solely responsible for protein-ice binding, and suggest that

entropic effects and van der Waals interactions are important.[121] Researchers suggested that the methyl groups of the threonine residues provide a driving force for the initial binding and are involved in overall stability of the protein, while the polar residues control binding specificity, aid in irreversible binding, prevent the proteins from moving along the ice surface, and impart stability.[123, 124] Serine mutants were unable to bind at all because they lack hydrophobic methyl groups that control the initial binding. The valine mutants were able to bind but they display altered ice crystal growth because they do not have hydroxyl groups that are positioned for hydrogen bonding to ice.[123] Ice growth was not at all inhibited by serine mutants, which suggests that the methyl group of threonine is also involved in excluding water from the protein-ice adsorption site.[104, 122]

One of the factors affecting antifreeze activity is the solubility of the AFP or AFGP. Variants of antifreeze proteins that are more soluble than the wild-type protein have been shown to have lower amounts of antifreeze activity.[122] Factors affecting the solubility of the proteins include their size and hydrophobicity, and this accounts for the fact that larger proteins, and those that are more hydrophobic, are more active.[104] Aggregates of AFGP8 at high concentrations (consisting of mainly dimers) have been shown to have significantly greater thermal hysteresis activity than less concentrated solutions that do not form aggregates.[86] Furthermore, the decreased activity of AFGPs upon complexation of the disaccharide with borate was attributed to the necessity of cis-hydroxyl groups for antifreeze activity.[62, 125] However, this loss of activity with increasing borate concentration may in fact be due to the increased solubility of the complexed proteins.[104]

All of these results show that hydrophobic moieties on the biological antifreezes are equally as important as their hydrophilic counterparts in tuning their antifreeze activity.

1.3.4: Hydration of Biological Antifreezes:

As mentioned at the end of the previous section, hydration has been implicated in the mechanism of action of biological antifreezes. Jorov et al. performed Monte Carlo minimization modelling experiments of AFP from the winter flounder.[126] Their calculations suggest that the gain in free energy upon binding of AFPs to ice is a result of the stabilization gained by de-solvation of the hydrophobic residues on the AFP, which occurs upon ice binding.[126] Comparison of the structure of water in the ice-binding site of active proteins and inactive mutants has revealed that hydration is important in imparting antifreeze activity.[127] For the active AFPs, the hydration of the polar groups in the ice binding site was observed to be "ice-like", and more similar to the hydration of apolar groups.[127] In contrast, the polar groups of the inactive AFPs displayed typical polar hydration.[127] The authors suggest that the "ice-like" hydrated water gives the ice-binding face of the active AFP a specificity and affinity for ordered, "ice-like" water and therefore for ice crystals.[127]

NMR spectroscopy, molecular dynamics simulations, and density functional theory studies of a small glycopeptide mimic (α-GalNAc-Ser, Figure 1.7) suggest that intramolecular hydrogen bonds between the sugar and peptide residues are not strong enough to maintain the conformation or stabilize the molecule.[128] Instead, the conformation is believed to be stabilized by water pockets or water bridges between the peptide and the sugar.[128] Furthermore, the DFT calculations suggest that in addition to the bridging water molecules, the water molecules in the first hydration shell surrounding the glycopeptide are important in maintaining the conformation.[128]

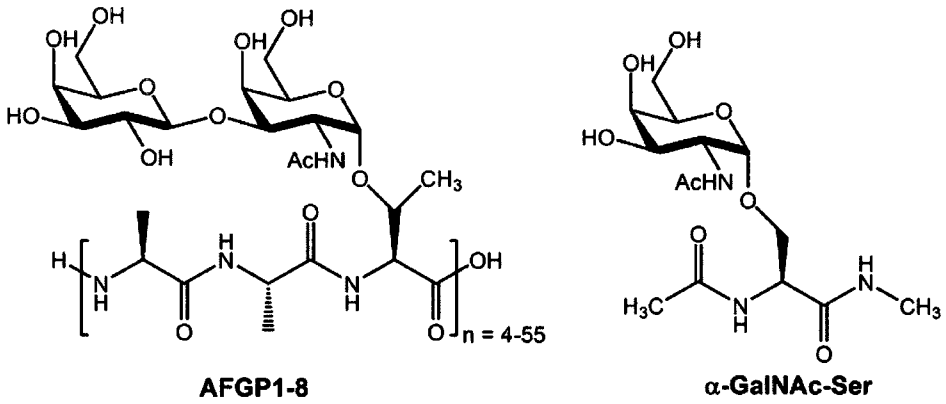

Figure 1.7: Structure of native AFGP1-8 and the small glycopeptide mimic used by Corzana et al.[128] in NMR studies

These observations suggest that the hydration of the biological antifreezes modulates their activity and that antifreeze-water interactions are very important. This is a logical conclusion since the properties of biological antifreezes (thermal hysteresis and ice-recrystallization inhibition) require an interaction with water molecules. In order to further explore this hypothesis, a greater understanding of the hydration of the structural components of biological antifreezes is necessary. The requirement for each structural feature of biological antifreezes has been assessed through structure-activity relationship studies.

1.3.5: Structure-Activity Relationship Studies of AFGPs:

Unlike the antifreeze proteins, as mentioned above AFGPs display a large degree of sequence homology across several species of fish, differing only in their length (Figure 1.7).[112] This makes them attractive compounds for structure-activity relationship studies, which must be done if the potential applications of AFGPs are to be realized. AFGPs are difficult to obtain, isolate and purify,[64] and relatively few syntheses of AFGPs or their analogues have been attempted (Figure 1.8).[98, 129-134] As a result, very little AFGP is available for detailed experiments. Therefore, determining the

essential components for antifreeze activity is especially important, as custom-designed analogues could be prepared and used in potential applications.

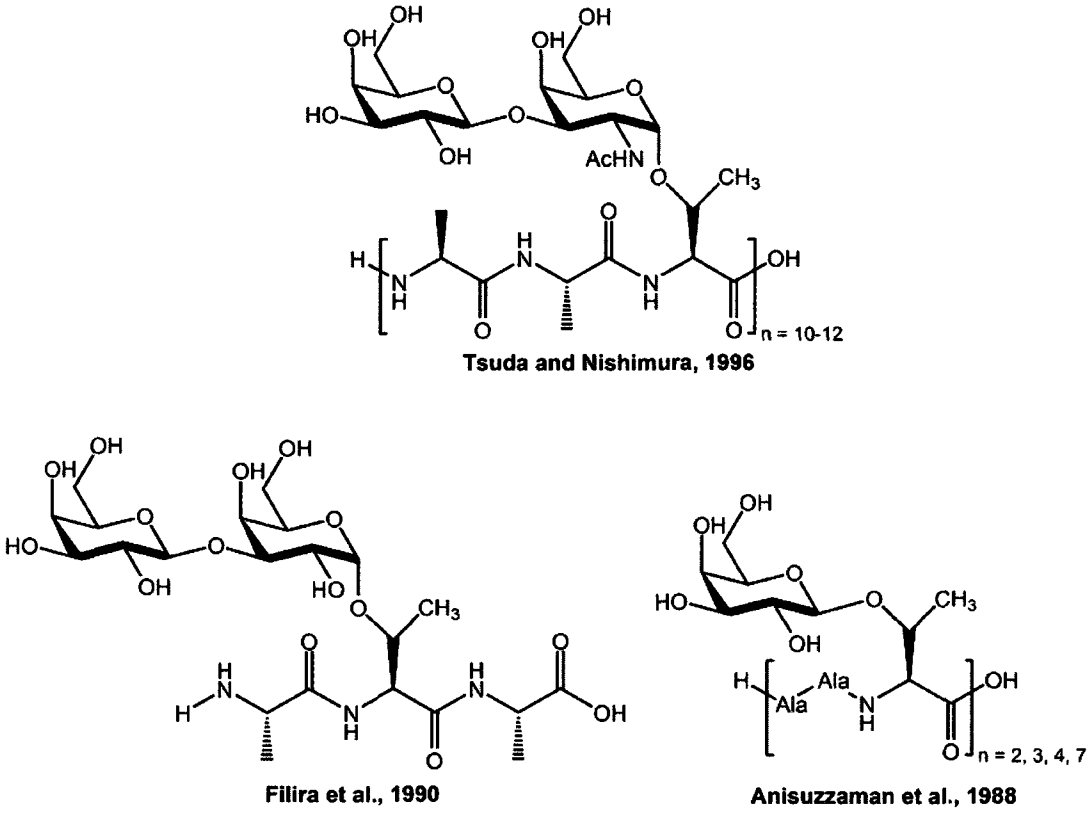

Figure 1.8: Native AFGP and *O*-linked AFGP analogues that have been synthesized by Anisuzzaman et al.,[129] Filira et al.,[130] and Tsuda and Nishimura.[131]

Early degradation studies by Komatsu et al. revealed the importance of the carbohydrate moiety.[135] Periodate oxidation of the terminal galactose residues and NaOH-catalyzed β-elimination of the disaccharide both resulted in a complete loss of antifreeze activity.[135, 136] Furthermore, acetylation of only 35% of the carbohydrate hydroxyl groups caused a loss of all TH activity, but activity was restored upon de-acetylation.[135, 136] In a separate study, borate-complexation of the carbohydrate cis-

hydroxyl groups eliminated TH activity, suggesting that these hydroxyl groups are important for antifreeze activity.[125] Although these studies demonstrated the necessity for the carbohydrate moiety, the question of the nature of the carbohydrate, including the number and stereochemistry of the hydroxyls, remained. In addition, it was not known whether the C-2-acetamide group, the α-anomeric stereochemistry, or both sugars of the disaccharide were required. Furthermore, the requirement for alanine and threonine residues in the peptide backbone was not probed and the question of whether other amino acids could be used remained. In response to these questions, one of the most extensive studies AFGP analogues was performed by Tachibana et al. in 2004.[137] Through the synthesis of several analogues, they discovered the key features required for thermal hysteresis activity (Figure 1.9).[137]

Thermal hysteresis activity increased as the length and concentration of the analogues was increased, although weak DIS was observed with a tripeptide monomer and a dimer was large enough to display TH activity.[137] Four to five tripeptide repeating units appeared to be an optimal length for activity, as increasing the length to six and seven units did not result in an increase in TH.[137] The carbohydrate moiety was determined to be essential for TH activity; however, the terminal galactose residue was not required for DIS activity.[137] Both GalNAc- and LacNAc-containing analogues showed TH activity, although the activity was weaker than in the native protein.[137] This suggests that the configuration of the hydroxyl groups in Gal-GalNAc is important for effective ice-binding and thermal hysteresis activity. Furthermore, synthesis of a Gal-Gal-containing analogue confirmed that the C-2 acetamide group on the reducing end sugar is required for TH activity.[137] In addition, the α-configuration of the disaccharide-threonine linkage is necessary, as a β-analogue displayed no activity.[137] Activity was abolished when a glycosylated Ala-Ser-Ala analogue was tested, indicating that the γ-methyl groups on the threonine residues are essential for activity.[137] Conformational experiments suggested that the AFGP needs to be able to adopt a specific-ordered helix in order to display effective activity.[137]

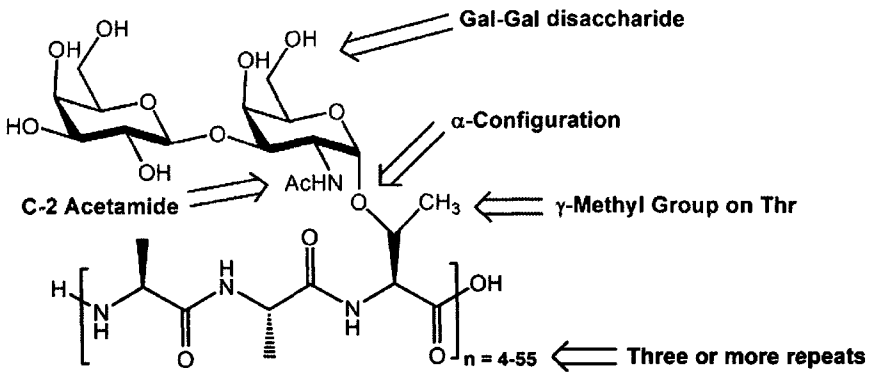

Figure 1.9: Structural features of AFGPs that are required for TH activity are the Gal-Gal disaccharide, the C-2 acetamide, the γ-methyl groups on threonine, an α-configuration of the sugar joined to the peptide, and three or more tripeptide repeats.

1.3.6: Synthesis of C-Linked AFGP Analogues:

It is noteworthy that although this study was extremely comprehensive, it did not take into account the factors required for ice-recrystallization inhibition activity. Recently, Budke et al. have prepared a synthetic AFGP which contains a single *N*-acetyl-D-galactosamine monosaccharide in place of the native disaccharide, and this compound displayed efficient IRI activity.[138] This suggests that the disaccharide is not required for ice-recrystallization inhibition.[138] The Ben lab is currently examining the structural features required for IRI activity through the synthesis of *C*-linked AFGP analogues, and have shown that thermal hysteresis and recrystallization inhibition activity can be decoupled.[98, 139] This is exciting because the needle-like ice crystals formed during thermal hysteresis due to dynamic ice shaping are extremely damaging to cells.[140] If biological antifreezes are going to be used for the preservation of cells and tissues at low temperatures, the damaging effects of these sharp ice crystals must be minimized. However, ice-recrystallization inhibition activity is very desirable in a potential cryoprotectant, because ice-recrystallization and large ice crystals are known to be causes of cell death during freeze-thaw protocols.[141]

Our laboratory has been interested in the synthesis of *C*-linked glycoprotein analogues, since the *O*-linkage of the native system can be unstable under strongly

acidic, basic, or biological enzymatic conditions.[142, 143] These *C*-linked compounds could be potentially used for the cryopreservation of cells. Two *C*-linked analogues were developed that display potent IRI activity but do not display TH activity and have little to no dynamic ice shaping activity. The first is a *C*-serine derivative (Figure 1.10),[98] and the second is an analogue consisting of an galactosyl-ornithine building block ("OGG-Gal") (Figure 1.11).[132-134]

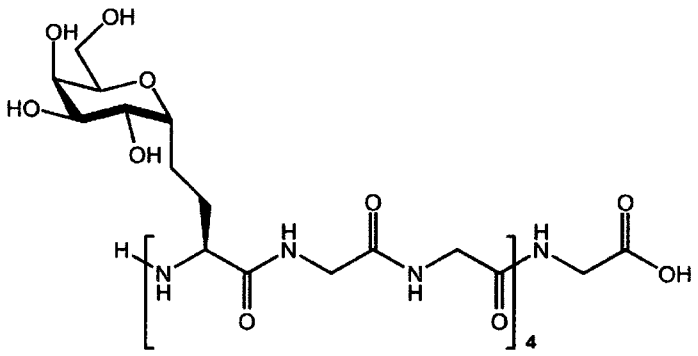

Figure 1.10: *C*-serine derivative prepared by Liu et al.[98]

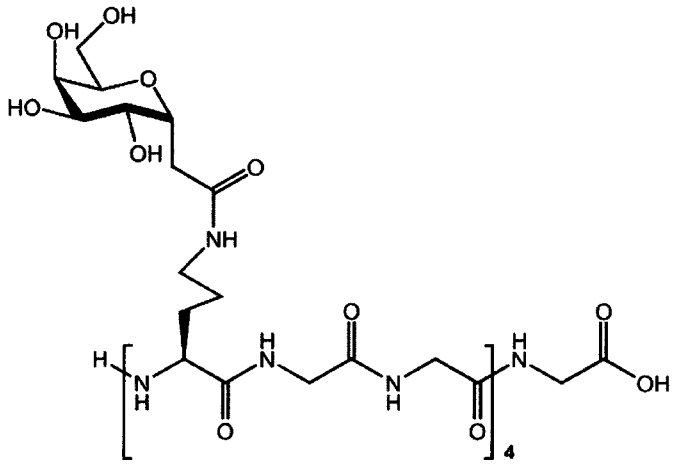

Figure 1.11: Galactose-ornithine derivative "OGG-Gal" prepared by Eniade and co-workers.[132-134]

OGG-Gal was thought to be an excellent substrate for structure-activity relationship studies of the ice-recrystallization inhibition activity of AFGPs. Based upon the observations that the hydration of biological antifreezes is important for their activity, and that the hydration of carbohydrates is strongly dependent on the orientation of their hydroxyl groups, the carbohydrate portion of OGG-Gal was chosen as the initial site for modification.

Four analogues were prepared, which have a galactose (Gal), glucose (Glc), mannose (Man), and talose (Tal) pyranose ring, respectively (Figure 1.12).[139] The authors observed that the IRI activity of these analogues decreased in the order OGG-Gal > OGG-Glc > OGG-Man > OGG-Tal (Figure 1.13). This trend mirrored the trend observed by Galema and Hoiland.[38] They observed that talose had a high molar compressibility value, meaning that it fits well into the three-dimensional (3-D) hydrogen bonded structure of water, and galactose has a low molar compressibility and therefore fits very poorly into water.[38] It was suggested that this ability of galactose to disrupt the 3-D hydrogen bonded network of water is related to the ability of OGG-Gal to restrict the growth of ice crystals.[139] In other words, these AFGP analogues may function by disturbing the order of supercooled water molecules and thus affecting their ability to be incorporated into the ice lattice. These results will be discussed in greater detail in the next chapter of this thesis. This custom-tailored antifreeze activity (potent IRI but no TH activity) of the AFGP analogues makes them attractive compounds to be used in the food and medical industries.

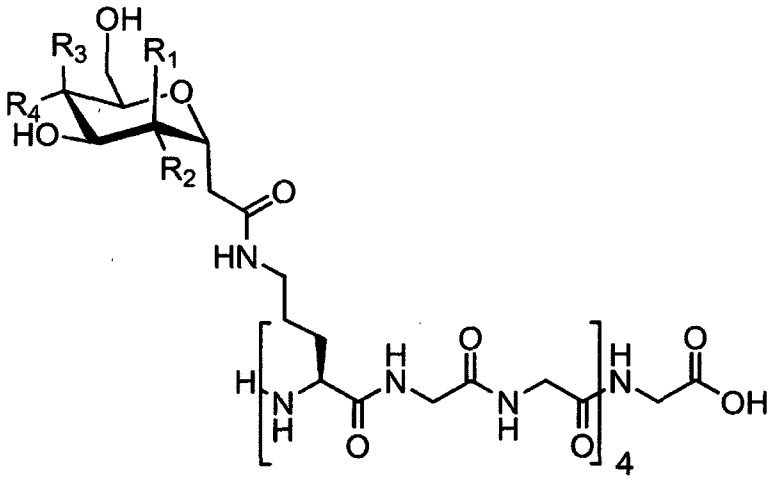

1: OGG Gal: R_1=H;R_2=OH;R_3=OH;R_4=H
2: OGG Glc: R_1=H;R_2=OH;R_3=H;R_4=OH
3: OGG Man: R_1=OH;R_2=H;R_3=H;R_4=OH
4: OGG Tal: R_1=OH;R_2=H;R_3=OH;R_4=H

Figure 1.12: Structure of C-linked AFGP analogues prepared by Czechura et al.[139]

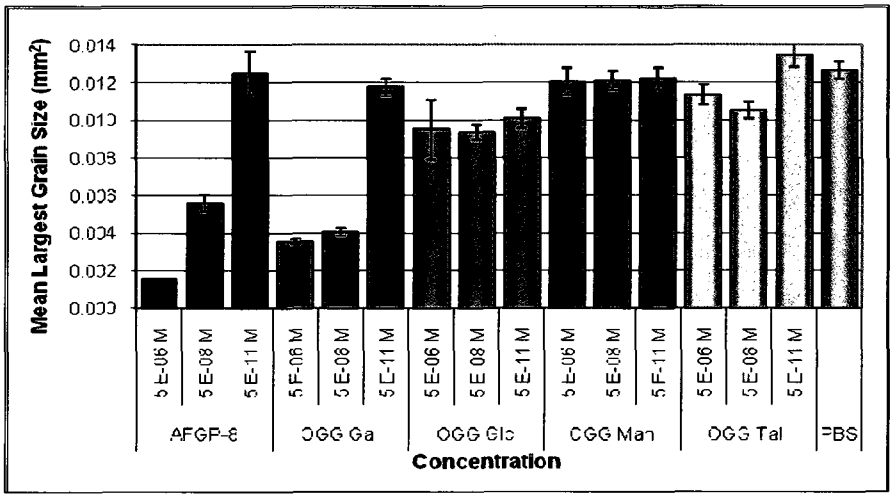

Figure 1.13: IRI activity of C-linked AFGP analogues compared to AFGP8 (positive control) and PBS (negative control).[139] Small bars indicate a small mean grain size of ice crystals (good IRI activity) and large bars indicate poor IRI activity.

1.3.7: Applications of Biological Antifreezes:

The intriguing properties of the biological antifreezes render them potentially useful in several applications. They can be used in the food industry to improve the flavour and quality of frozen food, due to their ability to restrict the growth of ice crystals and possibly maintain a smooth texture.[144] One of the benefits of AFPs is that they are already found in food that is used for human consumption (such as Antarctic fish), and no adverse side effects have been observed in people that have consumed these fish.[145] AFPs have also been explored in the storage of frozen meat. Payne et al. have shown that ice crystal size is reduced in frozen bovine samples containing 0.1 mg/mL AFP compared to frozen controls, while no improvement was seen in meat that was chilled but not frozen.[146] In another study of lamb meat, the authors observed that ice crystal size was reduced after frozen storage for 2-16 weeks when the samples were injected with AFGP either 1 or 24 hours before slaughter.[147]

Alternatively, AFPs and AFGPs can be used in the medical industry, both to protect and damage cells, depending on which properties are exploited. Several studies have examined the protective effects of AFPs on cells, membranes, and tissues at low temperatures. One of the first experiments reported that AFGPs can protect pig oocyte membranes at hypothermic temperatures by inhibiting ion leakage across the membrane.[148] In a further study, similar results were seen with bovine oocytes which were protected by the addition of AFPs.[149] The development of the AFP-treated oocytes post-thaw was similar to unfrozen oocytes, unlike the frozen controls.[149] Winter flounder AFPs are able to block ion channels and suppress potassium and calcium currents of porcine granulose cells.[150] It is important to note that in most cases the cryoprotection is dependent on the concentration and type of biological antifreeze used.[151] These experiments are not limited to cells and tissues, and Rubinsky et al. have observed that a combination of glycerol and antifreeze proteins have a cryoprotective effect on whole rat livers during freezing and subsequent storage.[152]

As mentioned above, biological antifreezes can also have a damaging effect on cells and tissues. This property has been exploited in cryosurgery, where the ability of

AFPs and AFGPs to form needle-like ice crystals due to dynamic ice shaping can be used in the destruction of undesirable cells such as cancerous tumours. In a cryosurgery model, Type I AFP was explored as a chemical adjuvant to cryosurgery, where it was able to greatly increase cell damage due to increased formation of intracellular ice.[140] A further study showed that the addition of AFP during surgery increased the destruction of undesirable tissues that often survive freezing.[153] Increased destruction of tumours may reduce complications, such as the re-emergence of cancer, that occur when these undesirable tissues survive.[153] It is interesting to note that the increased cell death resulting from the actions of AFPs is increased when two freeze-thaw cycles are employed during cryosurgery, possibly because the AFPs are better able to access the cells during the second cycle.[140, 154]

Recrystallization inhibitors have potential as cryoprotectant agents, since it has been suggested that the intracellular and extracellular formation and recrystallization of ice are the main causes of damage to cells and tissues during the freezing and thawing processes. A discussion of the role of ice formation and recrystallization in cryopreservation protocols is described below.

1.4: Cryopreservation:

Five stages of cryopreservation have been described, which are extension and cooling, addition of cryoprotectant, freezing, storage, and thawing.[155] There are three main methods of cryopreservation, described as vitrification, slow-cooling cryopreservation, and rapid-cooling cryopreservation. Vitrification is a process whereby a glass forms when a high concentration of cryoprotectants are added to the solution. The solution is cooled to very low temperatures, where the solutions become supercooled and very viscous to the point where they solidify without the formation of ice.[156, 157] In some cases, there is direct contact between the solution to be frozen that contains the cells, and the liquid nitrogen in partially sealed containers, resulting in an "open" system.[158] As their names suggest, the two other methods of cryopreservation differ mainly in their cooling rates.

Interestingly, cells and tissues can be stored at temperatures below -80 ºC for several years, because very few reactions can take place at these low temperatures.[159] It is actually the intermediate temperature zone (approximately -15 to -60 ºC) that provides the major challenge to cells.[159] The cells must pass through this temperature both during the freezing and the thawing cycles, and therefore damage can occur during each of these cycles.[159]

When freezing is initiated, the cells and the surrounding solution become supercooled, but do not freeze at temperatures down to approximately -5 ºC.[159] As the temperature is lowered further, extracellular ice begins to form, but the cells remain unfrozen.[159] Many of the problems observed during cryopreservation are a result of the formation of this extracellular ice.[159] As the extracellular ice forms, the extracellular solution becomes more concentrated, giving the water inside the cells a higher chemical potential than the extracellular water.[159] In response to this imbalance, water begins to flow out of the cells by ex-osmosis and freezes in the extracellular solution, and this may result in osmotic shrinkage of the cell.[159] In addition, extracellular ice causes mechanical damage and deforms the cells, and is thought to induce intracellular ice nucleation and formation.[160] The events that follow extracellular ice formation depend on the rate of cooling (Figure 1.14).[159]

During slow cooling, water is able to move out of the cells at a satisfactory rate to allow the intracellular solution to become adequately concentrated and viscous enough to prevent supercooling.[159] This allows time to re-establish the chemical potential balance inside and outside the cell.[159] As a result, the cell becomes dehydrated before it reaches its nucleation temperature, so it does not freeze intracellularly.[159, 160] However, during rapid cooling, water cannot leave the cells quickly enough to establish equilibrium, so the cell becomes supercooled and eventually reaches equilibrium by freezing intracellularly.[159] It is believed that the intracellular freezing is due to nucleation by the passage of extracellular ice crystals into the cell through the plasma membrane.[161, 162]

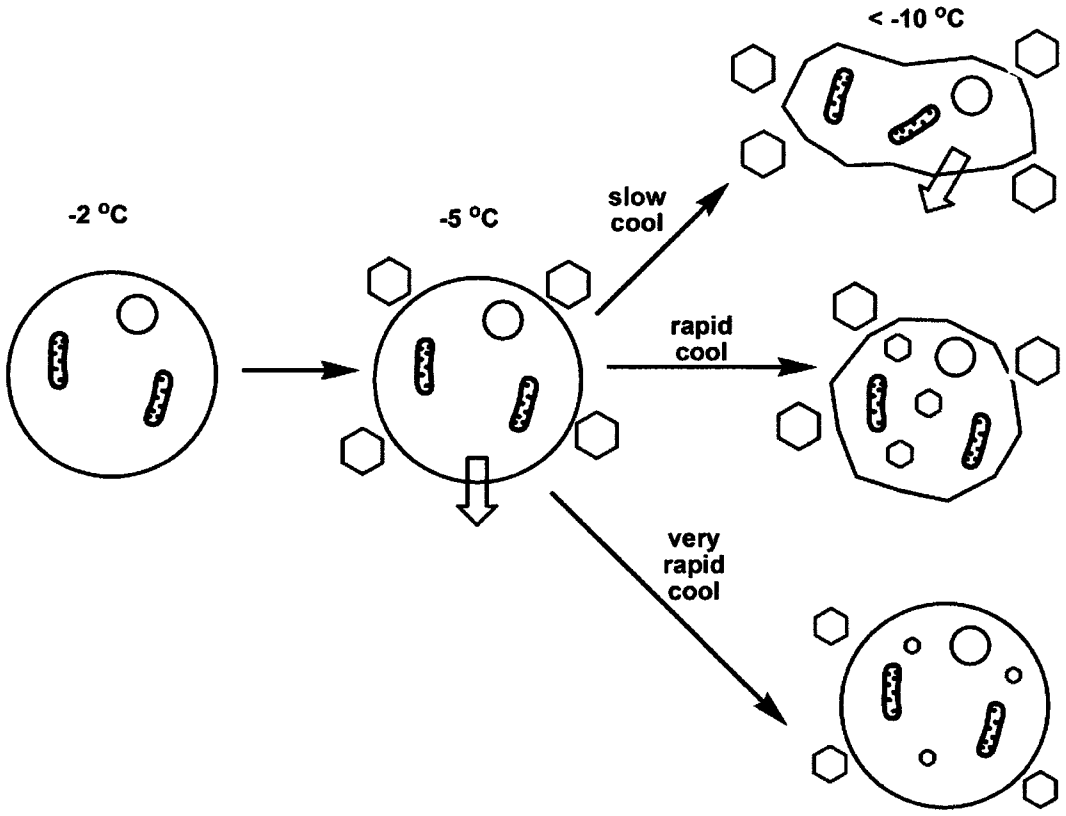

Figure 1.14: Schematic description of the physical events that occur in cells during freezing (adapted from Mazur, 1977).[159] The blue hexagons represent ice crystals and the blue arrows represent movement of water. During a slow cool, intracellular ice does not form due to the efflux of water out of the cells. Ice does form inside the cells during rapid cooling, and their size depends on whether the cooling is rapid or very rapid.

During very rapid cooling, the intracellular ice crystals are often quite small (Figure 1.14).[159] During thawing, however, these small, thermodynamically unstable ice crystals undergo recrystallization and aggregation to form larger crystals.[159, 163] Slow warming can be more damaging to frozen cells because there is time for recrystallization to occur during the thawing process.[159] Intracellular freezing often causes considerable cell damage and death.[159] The damage may be due to the size of the ice crystals, or the total amount of intracellular ice. [163] Damage due to recrystallization is not observed when rapid thawing is employed.[163] From these results, it is clear that the rate of thawing is also important when designing a cryopreservation

procedure. Best results are obtained when the rate of thawing matches the rate of cooling, that is, cells that underwent slow-cooling cryopreservation should also undergo slow-thawing and vice versa.[160]

There are two main mechanisms of cell injury in frozen tissue, one of which is immediate and the other is delayed.[141] The immediate cause of injury is direct cell injury during freeze-thaw protocols. The function and structure of cellular components such as proteins and lipids is stressed as soon as the temperature of the tissue is lowered.[141] Cell metabolism is slowed and begins to fail, which can lead to cell death if the tissues remain in a hypothermic state for too long, even if freezing does not occur.[141] However, freezing temperatures have even more damaging consequences. Ice crystals form in the extracellular medium, causing water to flow out of the cells and resulting in cell shrinkage.[159] Intracellular ice formation may also occur, which is almost always lethal to cells.[141] Ice crystals may enter the cells from the extracellular space either through micropores in the cell membrane,[159] or through membranes that have been compromised by cell shrinkage.[164] During thawing cycles, recrystallization results in the formation of large ice crystals due to the fusion of small ice crystals.[141] These large ice crystals resulting from recrystallization are extremely damaging to cell membranes.[141] They also create "shearing forces" that disrupt the tissues.[165] Furthermore, they can cause water to enter the cells which causes the cell volume to increase and may result in cell rupture.[159]

The second mechanism of cell injury occurs once the cells have been thawed, and is known as vascular stasis.[141] Circulation slows upon cooling and stops when the cells freeze. Once the tissue is thawed, circulation begins again, causing vasodilatation and increased vascular permeability.[141] Blood supply is lost, resulting in necrosis (pathological cell death) of the cells.[141] In addition to physical cell rupture and necrosis, apoptosis (gene-regulated cell death) also occurs during freezing.[166] All three of these mechanisms are ultimately involved in the destruction of cells at low temperatures.

1.4.1: Cryoprotective agents:

Cryoprotective agents (CPAs) are often used to minimize cell damage during cryopreservation. There are two forms of cryoprotectants that are used: those that are cell-penetrating (such as glycerol and dimethyl sulfoxide), and those that are non-penetrating (such as sugars). The first report of using a penetrating cryoprotective agent was published in 1949, where researchers observed that glycerol solutions were able to increase the percentage of human sperm cells that could be revived following vitrification.[167] Lovelock further examined several compounds for cryoprotective properties and observed that glycerol is the most effective.[168] Dimethyl sulfoxide (DMSO) was observed to be more cell-permeating than glycerol by Lovelock and Bishop, and in some cases it was found to be a more effective CPA than glycerol.[169]

The criteria for an efficient cryoprotectant are a low molecular weight, a high solubility in aqueous solutions, and the ability to permeate the cell.[168, 169] The weight concentration of cryoprotectant required for efficient cryoprotection was found to be proportional to its molecular weight.[168] It is believed that glycerol and other penetrating CPAs operate by a colligative mechanism.[168] When added to a salt solution, neutral solutes will decrease the concentration of salt that is in equilibrium with ice at subzero temperatures, and prevent damage that results from exposure to high concentrations of electrolytes.[168] It is possible to add a sufficient amount of neutral solute to maintain the salt concentration below the level where it becomes damaging.[168] Ultimately, the damage due to dehydration and high electrolyte concentration will be minimized by the use of CPAs. In addition, CPAs decrease the amount of ice that is formed during freezing, which results in less cellular damage during the freeze-thaw cycle.[170] Others have suggested that a non-colligative mechanism may be operating in the stabilization of phospholipid bilayers by DMSO, in which there is an ionic interaction between the oxygen atom of DMSO and the positively charged groups on the phospholipid bilayers.[170]

The generally accepted mechanism for cryoprotection by DMSO is two-fold. First, it is believed to replace water in the cell membrane and therefore prevent fractionation

of the cell membrane as the temperature changes.[171, 172] Secondly, researchers have suggested that DMSO molecules may form ion channels in the cell membrane and therefore allow the transport of water into and out of the cell, which minimizes damage due to osmotic stress.[171, 172]

Unfortunately, there are several problems involved with the use of DMSO as a CPA. The most significant is that DMSO is known to be toxic to cells, particularly at the high concentrations required for cryopreservation.[127, 173] This toxicity means that several steps have to be added to the cryopreservation cycle, in which the cells are washed to remove the DMSO before they are used post-thaw. Furthermore, residual DMSO causes several side effects in patients that are treated with cryopreserved stem cells, including nausea, vomiting, cardiac symptoms, and anaphylaxis.[174] There is evidence that solutions of 5% DMSO are actually more effective than the higher concentrations that are typically used (10-20%);[174] however, it would be desirable to further decrease the amount of DMSO used in cryopreservation protocols. For these reasons, several researchers have turned to the use of non-penetrating CPAs to replace the toxic penetrating DMSO.

The most commonly used non-penetrating cryoprotective agents are carbohydrates. Sucrose and trehalose are used most often; however, other sugars have been used as well. Solutions of 100 mM sucrose are able to improve motility and viability of dog spermatozoa following freezing and thawing.[23] Trehalose has been shown to be as effective as DMSO in preserving hematopoietic progenitor and stem cells, without the high toxicity associated with DMSO.[175] Sugimachi et al. have explored the use of non-metabolizable glucose derivative 3-*O*-methyl glucose in the preservation of rat hepatocytes, based on findings that freeze-tolerant wood frogs respond to cold temperatures by producing large amounts of glucose.[25] Since glucose is rapidly metabolized by many organisms, the non-metabolizable derivative was suggested as an alternative.[25] 3-Methoxy-glucose is taken into cells via GLUT receptors and was shown to be an effective cryoprotectant.[25]

Unlike glucose and 3-*O*-methyl glucose, most sugars require permeabilization of the plasma membrane so that the sugar can provide full protection by reaching both sides of the membrane.[20] Beattie et al. took advantage of the fact that trehalose can enter the cell through membranes that become slightly permeable as they pass through thermotropic lipid-phase transitions during cooling in order to achieve trehalose-mediated cryoprotection of human pancreatic islet cells.[176] Sugars have also been used in combination with DMSO and more effective cryopreservation of human hepatocytes was observed with the combination of trehalose with 10% DMSO.[26] One of the reasons for decreased damage to cells that are frozen in the presence of sugars may be that certain sugars are able to restrict the rate of growth of ice.[177, 178] The inhibition of ice growth seems to be correlated to the sugar's ability to bind water molecules. Interestingly, the addition of 1.7 or 9.9 mg/mL of AFP Type I to 50 w/w % glycerol solutions did not affect the ice crystal growth rate compared to the glycerol solution alone,[31] although this may be due to the extremely high glycerol concentration masking any effect from the antifreeze.

It should be noted that although biological antifreezes can inhibit the recrystallization of ice and therefore prevent damage to cells resulting from this process, they are not ideal cryoprotectants due to their thermal hysteresis activity. Thermal hysteresis is not damaging in itself, however the dynamic ice shaping that occurs within the thermal hysteretic gap results in needle-shaped ice crystals that can rupture cell membranes.[65, 141] The mechanical damage resulting from these sharp ice crystals generally causes cell death, rather than cell preservation.[141] As mentioned above, thermal hysteresis and dynamic ice shaping activity have been exploited in cryosurgery, where cells belonging to cancerous tumours are destroyed at low temperatures following being punctured by needle-like ice crystals.[140, 153] In order to use analogues of biological antifreezes for cryopreservation, their thermal hysteresis activity and the associated dynamic ice shaping must be eliminated. Furthermore, Liu et al. have observed that AFGP8 is cytotoxic to human embryonic kidney cells, possibly due to an apoptotic mechanism.[179] This precludes their use as cryoprotectants until the nature of this cytotoxicity is addressed and understood.

There remains considerable room for improvement in the field of cryopreservation, especially in the area of development of new small, non-toxic cryoprotectant agents. Since damage due to ice growth and recrystallization of ice is one of the major causes of cell death during freeze-thaw cycles, a greater understanding of the mechanism of ice-recrystallization and the factors affecting recrystallization inhibitors will ultimately aid in this goal. This understanding will come as new inhibitors of ice-recrystallization are synthesized and tested for IRI activity, and the link between ice-recrystallization inhibition and cryopreservation is explored. A greater understanding of the mechanism of ice-recrystallization inhibition will come from further studies of hydration of carbohydrates and its role in IRI activity, and in studies of the nature of the ice-water interface. These are the goals of the current research project, and they will be described in greater detail in the following chapter.

1.5: References:

1. Varki, A., Biological Roles of Oligosaccharides: All of the Theories are Correct. *Glycobiology* **1993,** 3, 97-130.

2. Steen, P. V. d.; Rudd, P. M.; Dwek, R. A.; Opdenakker, G., Concepts and Principles of *O*-Linked Glycosylation. *Critical Reviews in Biochemistry and Molecular Biology* **1998,** 33, 151-208.

3. Hardingham, T. E.; Fosang, A. J., Proteoglycans: Many Forms and Many Functions. *FASEB J.* **1992,** 6, 861-870.

4. Williamson, G.; Belshaw, N. J.; Noel, T. R.; Ring, S. G.; Williamson, M. P., O-Glycosylation and Stability: Unfolding of Glucoanylase Induced by Heat and Guanidine Hydrochloride. *Eur. J. Biochem.* **1992,** 207, 661-670.

5. Rose, M. C.; Voter, W. A.; Sage, H.; Brown, C. F.; Kaufman, B., Effects of Deglycosylation on the Architecture of Ovine Submaxillary Mucin Glycoprotein. *J. Biol. Chem.* **1984,** 259, 3167-3172.

6. Narhi, L. O.; Arakawa, T.; Aoki, K. H.; Elmore, R.; Rohde, M. F.; Boone, T.; Strickland, T. W., The Effect of Carbohydrate on the Structure and Stability of Erythropoietin. *J. Biol. Chem.* **1991,** 266, 23022-23026.

7. Riederer, M. A.; Hinnen, A., Removal of N-Glycosylation Sites of the Yeast Acid Phosphatase Severely Affects Protein Folding. *J. Bacteriol.* **1991,** 173, 3539-3546.

8. Langeveld, J. P. M.; Noelken, M. E.; Karl Hard, P. T.; Vliegenthart, J. F. G.; Rouse, J.; Hudson, B. G., Bovine Glomerular Basement Membrane: Location and Structure of the Asparagine-Linked Oligosaccharide Units and their Potential Role in the Assembly of the 7 S Collagen IV Tetramer. *J. Biol. Chem.* **1991,** 266, 2622-2631.

9. Delorme, E.; Lorenzini, T.; Giffin, J.; Martin, F.; Jacobsen, F.; Boone, T.; Elliott, S., Role of Glycosylation on the Secretion and Biological Activity of Erythropoietin. *Biochemistry* **1992,** 31, 9871-9876.

10. Youakim, A.; Hathaway, H. J.; Miller, D. J.; Gong, X.; Shur, B. D., Overexpressing Sperm Surface β1,4-Galactosyltransferase in Transgenic Mice Affects Multiple Aspects of Sperm-Egg Interactions. *J. Cell Biol.* **1994,** 126, 1573-1583.

11. Drisdel, R. C.; Mack, S. R.; Anderson, R. A.; Zaneveld, L. J. D., Purification and Partial Characterization of Acrosome Reaction Inhibiting Glycoprotein from Human Seminal Plasma. *Biol. Reprod.* **1995,** 53, 201-208.

12. Chapman, B. S.; Eckart, M. R.; Kaufman, S. E.; Lapointe, G. R., *O*-Linked Oligosaccharide on the 75-kDa Neurorophin Receptor. *J. Neurochem.* **1996,** 66, 1707-1716.

13. Su, B.; Waneck, G. L.; Flavell, R. A.; Bothwell, A. L. M., The Glycosyl Phosphatidylinositol Anchor Is Critical for Ly-6A/E-mediated T Cell Activation. *J. Cell Biol.* **1991,** 112, 377-384.

14. Gong, X.; Dubois, D. H.; Miller, D. J.; Shur, B. D., Activation of a G Protein Complex by Aggregation of β-1,4-Galactosyltransferase on the Surface of Sperm. *Science* **1995,** 269, 1718-1721.

15. Naim, H. Y.; Lentze, M. J., Impact of O-Glycosylation on the Function of Human Intestinal Lactase-Phlorizin Hydrolase: Characterization of Glycoforms Varying in Enzyme Activity and Localization of *O*-Glycoside Addition. *J. Biol. Chem.* **1992,** 267, 25494-25504.

16. Maly, P.; Thall, A. D.; Petryniak, B.; Rodgers, C. E.; Smith, P. L.; Marks, R. M.; Kelly, R. J.; Gersten, K. M.; Cheng, G.; Saunders, T. L.; Camper, S. A.; Camphausen, R. T.; Sullivan, F. X.; Isogai, Y.; Hindsgaul, O.; Andrian, U. H. v.; Lowe, J. B., The α(1,3)Fucosyltransferase Fuc0TVII Controls Leukocyte Trafficking through an Essential Role in L-, E-, and P-selectin Ligand Biosynthesis. *Cell* **1996,** 86, 643-653.

17. Langer, G. A.; Frank, J. S.; Nudd, L. M.; Seraydarian, K., Sialic Acid: Effect of Removal on Calcium Exchangeability of Cultured Heart Cells. *Science* **1976,** 193, (4257), 1013-1015.

18. Gabius, H.-J.; Siebert, H.-C.; Andre, S.; Jimenez-Barbero, J.; Rudiger, H., Chemical Biology of the Sugar Code. *ChemBioChem* **2004,** 5, 740-764.

19. Crowe, J. H.; Crowe, L. M.; Chapman, D., Preservation of Membranes in Anhydrobiotic Organisms: The Role of Trehalose. *Science* **1984,** 223, 701-703.

20. Eroglu, A.; Russo, M. J.; Bieganski, R.; Fowler, A.; Cheley, S.; Bayley, H.; Toner, M., Intracellular Trehalose Improves the Survival of Cryopreserved Mammalian Cells. *Nat. Biotechnol.* **2000,** 18, 163-167.

21. Yildiz, C.; Kaya, A.; Aksoy, M.; Tekeli, T., Influence of Sugar Supplementation of the Extender on Motility, Viability, and Acrosomal Integrity of Dog Spermatozoa During Freezing. *Theriogenology* **2000,** 54, 579-585.

22. Guo, N.; Puhlev, I.; Brown, D. R.; Mansbridge, J.; Levine, F., Trehalose Expression Confers Desiccation Tolerance on Human Cells. *Nat. Biotechnol.* **2000,** 18, 168-171.

23. Hossain, A. M.; Osuamkpe, C. O., Sole Use of Sucrose in Human Sperm Cryopreservation. *Arch. Andrology* **2007,** 53, 99-103.

24. Terry, C.; Dhawan, A.; Mitry, R. R.; Lehec, S. C.; Hughes, R. D., Preincubation of Rat and Human Hepatocytes With Cytoprotectants Prior to Cryopreservation Can Improve Viability and Function Upon Thawing. *Liver Transplant.* **2005,** 11, 1533-1540.

25. Sugimachi, K.; Roach, K. L.; Rhoads, D. V.; Tompkins, R. G.; Toner, M., Nonmetabolizable Glucose Compounds Impart Cryotolerance to Primary Rat Hepatocytes. *Tissue Eng.* **2006,** 12, 579-588.

26. Katenz, E.; Vondran, F. W. R.; Schwartlander, R.; Pless, G.; Gong, X.; Cheng, X.; Neuhaus, P.; Sauer, I. M., Cryopreservation of Primary Human Hepatocytes: The Benefit of Trehalose as an Additional Cryoprotective Agent. *Liver Transplant.* **2007,** 13, 38-45.

27. Svergun, D. I.; Richard, S.; Koch, M. H. J.; Sayers, Z.; Kuprin, S.; Zacca, G., Protein Hydration in Solution: Experimental Observation by X-Ray and Neutron Scattering. *Proc. Nat. Acad. Sci. USA* **1998,** 95, 2267-2272.

28. Gharsallaoui, A.; Roge, B.; Mathlouthi, M., Water-Disaccharides Interactions in Saturated Solution and the Crystallisation Conditions. *Food Chem.* **2008,** 106, 1329-1339.

29. Gaida, L. B.; Dussap, C. G.; Gros, J. B., Variable Hydration of Small Carbohydrates for Predicting Equilibrium Properties in Diluted and Concentrated Solutions. *Food Chem.* **2006,** 96, 387-401.

30. Kirschner, K. N.; Woods, R. J., Solvent Interactions Determine Carbohydrate Conformation. *Proc. Nat. Acad. Sci. USA* **2001,** 98, 10541-10545.

31. Heyden, M.; Brundermann, E.; Heugen, U.; Niehues, G.; Leitner, D. M.; Havenith, M., Long-Range Influence of Carbohydrates on the Solvation Dynamics of Water - Answers from Terahertz Absorption Measurements and Molecular Modeling Simulations. *J. Am. Chem. Soc.* **2008,** 130, 5773-5779.

32. Lee, S. L.; Debenedetti, P. G.; Errington, J. R., A Computational Study of Hydration, Solution Structure, and Dynamics in Dilute Carbohydrate Solutions. *J. Chem. Phys.* **2005,** 122, 204511-204520.

33. Timasheff, S. N., The Control of Protein Stability and Association by Weak Interactions with Water: How Do Solvents Affect These Processes? *Annu. Rev. Biophys. Biomol. Struct.* **1993,** 22, 67-97.

34. Hoiland, H.; Holvik, H., Partial Molar Volumes and Compressibilities of Carbohydrates in Water. *J. Solution Chem.* **1978,** 7, 587-596.

35. Uedaira, H.; Uedaira, H., Sugar-Water Interaction from Diffusion Measurements. *J. Solution Chem.* **1985,** 14, 27-34.

36. Uedaira, H.; Ikura, M.; Uedaira, H., Natural-Abundance Oxygen-17 Magnetic Relaxation in Aqueous Solutions of Carbohydrates. *Bull. Chem. Soc. Jpn.* **1989,** 62, 1-4.

37. Lopez de la Paz, M.; Ellis, G.; Perez, M.; Perkins, J.; Jimenez-Barbero, J.; Vicent, C., Carbohydrate Hydrogen-Bonding Cooperativity - Intramolecular Hydrogen Bonds and Their Cooperative Effect on Intermolecular Processes - Binding to a Hydrogen-Bond Acceptor Molecule *Eur. J. Org. Chem.* **2002,** 2002, 840-855.

38. Galema, S. A.; Hoiland, H., Stereochemical Aspects of Hydration of Carbohydrates in Aqueous Solutions. 3. Density and Ultrasound Measurements. *J. Phys. Chem.* **1991,** 95, 5321-5326.

39. Dashnau, J. L.; Sharp, K. A.; Vanderkooi, J. M., Carbohydrate Intramolecular Hydrogen Bonding Cooperativity and Its Effect on Water Structure. *J. Phys. Chem. B* **2005,** 109, 24152-24159.

40. Galema, S. A.; Howard, E.; Engberts, J. B. F. N.; Grigera, J. R., The Effect of Stereochemistry upon Carbohydrate Hydration. A Molecular Dynamics Simulation of β-D-Galactopyranose and (α,β)-D-Talopyranose. *Carbohydrate Res.* **1994,** 265, 215-225.

41. Cheetham, N. W. H.; Lam, K., Molecular Dynamics Simulations of Glycosides in Aqueous Solution. *Carbohydrate Res.* **1996,** 282, 13-23.

42. Cordone, L.; Cottone, G.; Giuffrida, S., Role of Residual Water Hydrogen Bonding in Sugar/Water/Biomolecule Systems: A Possible Explanation for Trehalose Peculiarity. *J. Phys. Condens. Matter* **2007,** 19, 205110: 1-14.

43. Carpenter, J. F.; Crowe, J. H., An Infrared Spectroscopic Study of the Interactions of Carbohydrates with Dried Proteins. *Biochemistry* **1989,** 28, 3916-3922.

44. Crowe, J. H.; Carpenter, J. F.; Crowe, L. M., The Role of Vitrification in Anhydrobiosis. *Annual Review of Physiology* **1998,** 60, 73-103.

45. Belton, P. S.; Gil, A. M., IR and Raman Spectroscopic Studies of the Interaction of Trehalose with Hen Egg White Lysozyme. *Biopolymers* **1994,** 34, 957-961.

46. Uribe, J. G. S. a. S., Trehalose-Enzyme Interactions Result in Structure Stabilization and Activity Inhibition. The Role of Viscosity. *Mol. Cell. Biochem.* **2004,** 256/257, 319-327.

47. Green, J. L.; Angell, C. A., Phase Relations and Vitrification in Saccharide-Water Solutions and the Trehalose Anomaly. *J. Phys. Chem.* **1989,** 93, 2880-2882.

48. Branca, C.; Magazu, S.; G.Maisano; Migliardo, F.; P.Migliardo; Romeo, G., α, α-Trehalose/Water Solutions. 5. Hydration and Viscosity in Dilute and Semidilute Disaccharide Solutions. *J. Phys. Chem. B* **2001,** 105, 10140-10145.

49. Gharsallaoui, A.; Roge, B.; Genotelle, J.; Mathlouthi, M., Relationships Between Hydration Number, Water Activity and Density of Aqueous Sugar Solutions. *Food Chem.* **2008,** 106, 1443-1453.

50. Matsuoka, T.; Okada, T.; Murai, K.; Koda, S.; Nomura, H., Dynamics and Hydration of Trehalose and Maltose in Concentrated Solutions. *J. Mol. Liq.* **2002,** 98-99, 317-327.

51. Magazu, S.; Migliardo, P.; Musolino, A. M.; Sciortino, M. T., α,α-Trehalose-Water Solutions. 1. Hydration Phenomena and Anomalies in the Acoustic Properties. *J. Phys. Chem. B* **1997,** 101, 2348-2351.

52. Pereira, C. S.; Kony, D.; Baron, R.; Muller, M.; Gunsteren, W. F. v.; Hunenberger, P. H., Conformational and Dynamical Properties of Disaccharides in Water: a Molecular Dynamics Study. *Biophys. J.* **2006,** 90, 4337-4344.

53. Kawai, H.; Sakurai, M.; Inoue, Y.; Chujo, R.; Kobayashi, S., Hydration of Oligosaccharides: Anomalous Hydration Ability of Trehalose. *Cryobiology* **1992,** 29, 599-606.

54. Furuki, T., Effect of Stereochemistry on the Anti-Freeze Characteristics of Carbohydrates. A Thermal Study of Aqueous Monosaccharides at Subzero Temperatures. *Carbohydrate Res.* **2000,** 323, 185-191.

55. Ekdawi-Sever, N. C.; Conrad, P. B.; de Pable, J. J., Molecular Simulation of Sucrose Solutions near the Glass Transition Temperature. *J. Phys. Chem. A* **2001,** 105, 734-742.

56. Branca, C.; Magazu, S.; Maisano, G.; Migliardo, P., alpha,alpha-Trehalose - Water Solutions. 3. Vibrational Dynamics Studies by Inelastic Light Scattering. *J. Phys. Chem. B* **1999,** 103, 1347-1353.

57. Magazu, S.; Villari, V.; Migliardo, P.; Maisano, G.; Telling, M. T. F., Diffusive Dynamics of Water in the Presence of Homologous Disaccharides: A Comparative Study by Quasi Elastic Neutron Scattering. IV. *J. Phys. Chem. B* **2001,** 105, 1851-1855.

58. Baardsnes, J.; Davies, P. L., Contribution of Hydrophobic Residues to Ice Binding by Fish Type III Antifreeze Protein. *Biochim. Biophys. Acta* **2002,** 1601, 49-54.

59. McDonald, S. M.; Brady, J. W.; Clancy, P., Molecular Dynamics Simulations of a Winter Flounder "Antifreeze" Polypeptide in Aqueous Solution. *Biopolymers* **1993,** 33, 1481-1503.

60. McDonald, S. M.; White, A.; Clancy, P.; Brady, J. W., Binding of an Antifreeze Polypeptide to an Ice/Water Interface via Computer Simulation. *AIChE J.* **1995,** 41, 959-973.

61. DeVries, A. L.; Wohlschlag, D. E., Freezing Resistance in Some Antarctic Fishes. *Science* **1969,** 163, 1073-1075.

62. DeVries, A. L., Glycoproteins as Biological Antifreeze Agents in Antarctic Fishes. *Science* **1971,** 172, 1152-1155.

63. Chakrabartty, A.; Hew, C. L., The Effect of Enhanced Alpha-Helicity on the Activity of a Winter Flounder Antifreeze Polypeptide. *Eur. J. Biochem.* **1991,** 202, 1057-1063.

64. Harding, M. M.; Anderberg, P. I.; Haymet, A. D. J., 'Antifreeze' Glycoproteins from Polar Fish. *Eur. J. Biochem.* **2003,** 270, 1381-1392.

65. Sonnichsen, F. D.; DeLuca, C. I.; Davies, P. L.; Sykes, B. D., Refined Ssolution Structure of Type III Antifreeze Protein: Hydrophobic Groups May Be Involved in the Energetics of the Protein-Ice Interactions. *Structure* **1996,** 4, 1325-1337.

66. Venketesh, S.; Dayananda, C., Properties, Potentials, and Prospects of Antifreeze Proteins. *Crit. Rev. Biotechnol.* **2008,** 19, 57-82.

67. Ng, N. F. L.; Hew, C. L., Structure of an Antifreeze Polypeptide from the Sea Raven: Disulfide bonds and similarity to lectin binding proteins. *J. Biol. Chem.* **1992,** 267, 16069-16075.

68. Street, I. P.; Armstrong, C. R.; Withers, S. G., Hydrogen Bonding and Specificity. Fluorodeoxy Sugars as Probes of Hydrogen Bonding in the Glycogen Phosphorylase-Glucose Complex. *Biochemistry* **1986,** 25, 6021-6027.

69. Yamashita, Y.; Miura, R.; Takemoto, Y.; Tsuda, S.; Kawahara, H.; Obata, H., Type II Antifreeze Protein from a Mid-latitude Freshwater Fish, Japanese Smelt (*Hypomesus nipponensis*). *Biosci., Biotechnol., Biochem.* **2003,** 67, (3), 461-466.

70. Loewen, M. C.; Gronwald, W.; Sonnichsen, F. D.; Sykes, B. D.; Davies, P. L., The Ice-Binding Site of Sea Raven Antifreeze Protein Is Distinct from the Carbohydrate-Binding Site of the Homologous C-Type-Lectin. *Biochemistry* **1998,** 37, 17745-17753.

71. Li, X.-M.; Trinh, K.-Y.; Hew, C. L.; Buettner, B.; Baenziger, J.; Davies, P. L., Structure of an Antifreeze Polypeptide and Its Precursor from the Ocean Pout, *Macrozoarces americanus*. *J. Biol. Chem.* **1985,** 260, (24), 12904-12909.

72. Deng, G.; Andrews, D. W.; Laursen, R. A., Amino Acid Sequence of a New Type of Antifreeze Protein, from the Longhorn Sculpin *Myoxocephalus octodecimspinosis*. *FEBS Lett.* **1997,** 402, 17-20.

73. Tyshenko, M. G.; Doucet, D.; Davies, P. L.; Walker, V. K., The Antifreeze Potential of the Spruce Budworm Thermal Hysteresis Proteins. *Nat. Biotechnol.* **1997,** 15, 887-890.

74. Graham, L. A.; Liou, Y.-C.; Walker, V. K.; Davies, P. L., Hyperactive Antifreeze Protein from Beetles. *Nature* **1997,** 388, 727-728.

75. Graether, S. P.; Kuiper, M. J.; Gagne, S. M.; Walker, V. K.; Jia, Z.; Sykes, B. D.; Davies, P. L., β-Helix Structure and Ice-Binding Properties of a Hyperactive Antifreeze Protein from an Insect. *Nature* **2000,** 406, 325-328.

76. Griffith, M.; Antikainen, M.; Hon, W.-C.; Pihakaski-Maunsbach, K.; Yu, X.-M.; Chun, J. U.; Yang, D. S. C., Antifreeze proteins in winter rye. *Physiol. Plantarum* **1997,** 100, 327-332.

77. Griffith, M.; Yaish, M. W. F., Antifreeze Proteins in Overwintering Plants: A Tale of Two Activities. *Trends Plant Sci.* **2004,** 9, 399-405.

78. Smallwood, M.; Worrall, D.; Byass, L.; Elias, L.; Ashford, D.; Doucet, C. J.; Holt, C.; Telford, J.; Lillford, P.; Bowles, D. J., Isolation and Characterization of a Novel Antifreeze Protein from Carrot (*Daucus carota*). *Biochem. J.* **1999,** 340, 385-391.

79. Gilbert, J. A.; Hill, P. J.; Dodd, C. E. R.; Laybourn-Parry, J., Demonstration of Antifreeze Protein Activity in Antarctic Lake Bacteria. *Microbiology* **2004,** 150, 171-180.

80. Hoshino, T.; Kiriaki, M.; Ohgiya, S.; Fukiwara, M.; Kondo, H.; Nishimiya, Y.; Yumoto, I.; Tsuda, S., Antifreeze Proteins from Snow Mold Fungi. *Can. J. Bot.* **2003,** 81, 1175-1181.

81. DeVries, A. L.; Komatsu, S. K.; Feeney, R. E., Chemical and Physical Properties of Freezing Point-depressing Glycoproteins from Antarctic Fishes. *J. Biol. Chem.* **1970,** 245, 2901-2908.

82. Lemieux, R. U., How Water Provides the Impetus for Molecular Recognition in Aqueous Solution. *Acc. Chem. Res.* **1996,** 29, 373-380.

83. Burcham, T. S.; Osuga, D. T.; Rao, B. N. N.; Bush, C. A.; Feeney, R. E., Purification and Primary Sequences of the Major Arginine-containing Antifreeze Glycopeptides from the Fish *Eleginus gracilis*. *J. Biol. Chem.* **1986,** 261, 6384-6389.

84. Morris, H. R.; Thompson, M. R.; Osuga, D. T.; Ahmed, A. I.; Chan, S. M.; Vandenheede, J. R.; Feeney, R. E., Antifreeze Glycoproteins from the Blood of an Antarctic Fish: The Structure of the Proline-Containing Glycopeptides. *J. Biol. Chem.* **1978,** 253, 5155-5162.

85. Lin, Y.; Duman, J. G.; DeVries, A. L., Studies on the Structure and Activity of Low Molecular Weight Glycoproteins from an Antarctic Fish. *Biochem. Biophys. Res. Commun.* **1972,** 46, 87-92.

86. Bouvet, V. R.; Lorello, G. R.; Ben, R. N., Aggregation of Antifreeze Glycoprotein Fraction 8 and Its Effect on Antifreeze Activity. *Biomacromolecules* **2006,** 7, 565-571.

87. Tsvetkova, N. M.; Phillips, B. L.; Krishnan, V. V.; Feeney, R. E.; Fink, W. H.; Crowe, J. H.; Risbud, S. H.; Tablin, F.; Yeh, Y., Dynamics of Antifreeze Glycoproteins in the Presence of Ice. *Biophys. J.* **2002,** 82, 464-473.

88. Nguyen, D. H.; Colvin, M. E.; Yeh, Y.; Feeney, R. E.; Fink, W. H., The Dynamics, Structure, and Conformational Free Energy of Proline-Containing Antifreeze Glycoprotein. *Biophys. J.* **2002,** 82, 2892-2905.

89. Scholander, P. F.; Maggert, J. E., Supercooling and Ice Propagation in Blood from Arctic Fishes. *Cryobiology* **1971,** 8, 371-374.

90. Duman, J. G.; DeVries, A. L., Freezing Resistance in Winter Flounder *Pseudopleuronectes americanus*. *Nature* **1974,** 247, 237-238.

91. Yeh, Y.; Feeney, R. E., Antifreeze Proteins: Structures and Mechanisms of Function. *Chem. Rev.* **1996,** 96, 601-617.

92. Wilson, P. W.; Gould, M.; DeVries, A. L., Hexagonal Shaped Ice Spicules in Frozen Antifreeze Protein Solutions. *Cryobiology* **2002,** 44, 240-250.

93. DeVries, A. L.; Price, T. J., Role of Glycopeptides and Peptides in Inhibition of Crystallization of Water in Polar Fishes [and Discussion]. *Philosophical Transactions of The Royal Society B* **1984,** 304, 575-588.

94. Knight, C. A.; DeVries, A. L.; Oolman, L. D., Fish Antifreeze Protein and the Freezing and Recrystallization of Ice. *Nature* **1984,** 308, 295-296.

95. Hew, C. L.; Yang, D. S. C., Protein Interaction with Ice. *Eur. J. Biochem.* **1992,** 203, 33-42.

96. Tomczak, M. M.; Marshall, C. B.; Gilbert, J. A.; Davies, P. L., A Facile Method for Determining Ice Recrystallization Inhibition by Antifreeze Proteins. *Biochem. Biophys. Res. Commun.* **2003,** 311, 1041-1046.

97. Ramlov, H.; Wharton, D. A.; Wilson, P. W., Recrystallization in a Freezing Tolerant Antarctic Nematode, *Panagrolaimus davide*, and an Alpine Weta, *Hemideina maori* (Orthoptera; Stenopelmatidae). *Cryobiology* **1996,** 33, 607-613.

98. Liu, S.; Ben, R. N., C-Linked Galactosyl Serine AFGP Analogues as Potent Recrystallization Inhibitors. *Org. Lett.* **2005,** 7, 2385-2388.

99. Brown, R. A.; Yeh, Y.; Burcham, T. S.; Feeney, R. E., Direct Evidence for Antifreeze Glycoprotein Adsorption Onto an Ice Surface. *Biopolymers* **1985,** 24, 1265-1270.

100. Brigaud, T.; Lefebvre, O.; Plantier-Royon, R.; Portella, C., Mixed Organofluorine - Organosilicon Chemistry. 6. Synthesis of gem-Difluoro-*C*-glycosides and *C*-

Disaccharides from Acylsilanes and Trifluoromethyltrimethylsilane. An Exploratory Study. *Tetrahedron Lett.* **1996,** 37, 6115-6116.

101. Burcham, T. S.; Osuga, D. T.; Yeh, Y.; Feeney, R. E., A Kinetic Description of Antifreeze Glycoprotein Activity. *J. Biol. Chem.* **1986,** 261, 6390-6397.

102. Li, Q.; Luo, L., The Kinetic Theory of Thermal Hysteresis of a Macromolecule Solution. *Chem. Phys. Lett.* **1993,** 216, (3,4,5,6), 453-457.

103. Li, Q.; Luo, L., Further Discussion on the Thermal Hysteresis of the Ice Growth Inhibitor. *Chem. Phys. Lett.* **1994,** 223, 181-184.

104. Kristiansen, E.; Zachariassen, K. E., The Mechanism By Which Fish Antifreeze Proteins Cause Thermal Hysteresis. *Cryobiology* **2005,** 51, 262-280.

105. Knight, C. A.; Cheng, C. C.; DeVries, A. L., Adsorption of α-Helical Antifreeze Peptides on Specific Ice Crystal Surface Planes. *Biophys. J.* **1991,** 59, 409-418.

106. Knight, C. A.; DeVries, A. L., Melting Inhibition and Superheating of Ice by an Antifreeze Glycopeptide. *Science* **1989,** 245, 505-507.

107. Pertaya, N.; Marshall, C. B.; DiPrinzio, C. L.; Wilen, L.; Thomson, E. S.; Wettlaufer, J. S.; Davies, P. L.; Braslavsky, I., Fluorescence Microscopy Evidence for Quasi-Permanent Attachment of Antifreeze Proteins to Ice Surfaces. *Biophys. J.* **2007,** 92, 3663-3673.

108. Huffman, W. F.; Hall, R. F.; Grant, J. A.; Holden, K. G., Nuclear Analogues of beta-Lactam Antibiotic. 4. Total Synthesis of Bisnorisopenicillins from Antibacterially Active Monocyclic beta-Lactam Precursors. *J. Med. Chem.* **1978,** 21, 413-415.

109. Houston, M. E., Jr.; Chao, H.; Hodges, R. S.; Sykes, B. D.; Kay, C. M.; Sonnichsen, F. D.; Loewen, M. C.; Davies, P. L., Binding of an Oligopeptide to a Specific Plane of Ice. *J. Biol. Chem.* **1998,** 273, 11714-11718.

110. Bar, M.; Celik, Y.; Fass, D.; Braslavsky, I., Interactions of β-Helical Antifreeze Protein Mutants with Ice. *Cryst. Growth Des.* **2008,** 8, 2954-2963.

111. Witczak, Z. J.; Sun, J.; Mielguj, R., Synthesis of L-Fucopyranosyl-4-Thiodisaccharides from Levoglucosenone and their Inhibitory Activity on alpha-L-Fucosidase. *Bioorg. Med. Chem. Lett.* **1995,** 5, 2169-2174.

112. Bouvet, V.; Ben, R. N., Antifreeze Glycoproteins. *Cell Biochem. Biophys.* **2003,** 39, 133-144.

113. Baruch, E.; Belostotskii, A. M.; Mastai, Y., Relationship Between the Antifreeze Activities and the Chemical Structure of Polyols. *J. Mol. Struct.* **2008,** 874, 170-177.

114. Liou, Y.-C.; Tocllj, A.; Davies, P. L.; Jia, Z., Mimicry of Ice Structure by Surface Hydroxyls and Water of a β-Helix Antifreeze Protein. *Nature* **2000,** 406, 322-324.

115. Wen, D.; Laursen, R. A., Structure-Function Relationships in an Antifreeze Polypeptide: The Role of Neutral, Polar Amino Acids. *J. Biol. Chem.* **1992,** 267, 14102-14108.

116. Chao, H.; Sonnichsen, F. D.; DeLuca, C. I.; Sykes, B. D.; Davies, P. L., Structure-Function Relationship in the Globular Type II Antifreeze Protein: Identification of a Cluster of Surface Residues Required for Binding to Ice. *Protein Sci.* **1994,** 3, 1760-1769.

117. Wen, D.; Laursen, R. A., A Model for Binding of an Antifreeze Polypeptide to Ice. *Biophys. J.* **1992,** 63, 1659-1662.

118. Yang, D. S. C.; Sax, M.; Chakrabartty, A.; Hew, C. L., Crystal Structure of an Antifreeze Polypeptide and its Mechanistic Implications. *Nature* **1988,** 333, 232-237.

119. Wen, D.; Laursen, R. A., Structure-Funciton Relationships in an Antifreeze Polypeptide. *J. Biol. Chem.* **1993,** 268, 16401-16405.

120. Yang, D. S. C.; Hon, W.-C.; Bubanko, S.; Xue, Y.; Seetharaman, J.; Hew, C. L.; Sicheri, F., Identification of the Ice-Binding Surface on a Type III Antifreeze Protein with a "Flatness Function" Algorithm. *Biophys. J.* **1998** 74, 2142-2151.

121. Chao, H.; Housten, M. E. J.; Hodges, R. S.; Kay, C. M.; Sykes, B. D.; Loewen, M. C.; Davies, P. L.; Sonnichsen, F. D., A Diminished Role for Hydrogen Bonds in Antifreeze Protein Binding to Ice. *Biochemistry* **1997,** 36, 14652-14660.

122. Karim, O. A.; Haymet, A. D. J., The Ice/Water Interface. *Chem. Phys. Lett.* **1987,** 138, 531-534.

123. Zhang, W.; Laursen, R. A., Structure-Function Relationships in a Type I Antifreeze Polypeptide: The Role of Threonine Methyl and Hydroxyl Groups in Antifreeze Activity. *J. Biol. Chem.* **1998,** 273, 34806-34812.

124. Graether, S. P.; DeLuca, C. I.; Baardsnes, J.; Hill, G. A.; Davies, P. L.; Jia, Z., Quantitative and Qualitative Analysis of Type III Antifreeze Protein Structure. *J. Biol. Chem.* **1999,** 274, 11842-11847.

125. Ahmed, A. I.; Yeh, Y.; Osuga, D. T.; Feeney, R. E., Antifreeze Glycoproteins from Antarctic Fish: Inactivation by Borate. *J. Biol. Chem.* **1976,** 251, 3033-3036.

126. Jorov, A.; Zhorov, B. S.; Yang, D. S. C., Theoretical Study of Interaction of Winter Flounder Antifreeze Protein with Ice. *Protein Sci.* **2004,** 13, 1524-1537.

127. Yang, C.; Sharp, K. A., Hydrophobic Tendency of Polar Group Hydration as a Major Force in Type I Antifreeze Protein Recognition. *PROTEINS: Struct., Funct., Bioinf.* **2005,** 59, 266-274.

128. Corzana, F.; Busto, J. H.; Jimenez-Oses, G.; Garcia de Luis, M.; Asensio, J. L.; Jimenez-Barbero, J.; Peregrina, J. M.; Avenoza, A., Serine versus Threonine Glycosylation: The Methyl Group Causes a Drastic Alteration on the Carbohydrate Orientation and on the Surrounding Water Shell. *J. Am. Chem. Soc.* **2007,** 129, 9458-9467.

129. Anisuzzaman, A. K. M.; Anderson, L.; Navia, J. L., Synthesis of a Close Analog of the Repeating Unit of the Antifreeze Glycoproteins of Polar Fish. *Carbohydrate Res.* **1988,** 174, 265-278.

130. Filira, F.; Biondi, L.; Scolaro, B.; Foffani, M. T.; Mammi, S.; Peggion, E.; Rocchi, R., Solid Phase Synthesis and Conformation of Sequential Glycosylated Polytripeptide Sequences Related to Antifreeze Glycoproteins. *Int. J. Biol. Macromol.* **1990,** 12, 41-49.

131. Uedaira, H.; Okouchi, S.; Tsuda, S.; Uedaira, H., Hydration of Glucose and Galactose Derivatives. *Bull. Chem. Soc. Jpn.* **2001,** 74, 1857-1861.

132. Ben, R. N.; Eniade, A. A.; Hauer, L., Synthesis of a *C*-linked Antifreeze Glycoprotein (AFGP) Mimic: Probes for Investigating the Mechanism of Action. *Org. Lett.* **1999,** 1, 1759-1762.

133. Eniade, A. A.; Ben, R. N., Fully Convergent Solid Phase Synthesis of Antifreeze Glycoprotein Analogues. *Biomacromolecules* **2001,** 2, 557-561.

134. Eniade, A. A.; Purushotham, M.; Ben, R. N.; Wang, J. B.; Horwath, K., A Serendipitous Discovery of Antifreeze Protein-Specific Activity in *C*-Linked Antifreeze Glycoprotein Analogs. *Cell Biochem. Biophys.* **2003,** 38, 115-124.

135. Komatsu, S. K.; DeVries, A. L.; Feeney, R. E., Studies of the Structure of Freezing Point-depressing Glycoproteins from an Antarctic Fish. *J. Biol. Chem.* **1970,** 245, 2909-2913.

136. Ahmed, A. I.; Osuga, D. T.; Feeney, R. E., Antifreeze Glycoprotein from an Antarctic Fish: Effects of Chemical Modifications of Carbohydrate Residues on Antifreeze and Antilectin Activities. *J. Biol. Chem.* **1973,** 248, 8524-8527.

137. Tachibana, Y.; Fletcher, G. L.; Fujitani, N.; Tsuda, S.; Monde, K.; Nishimura, S.-I., Antifreeze Glycoproteins: Elucidation of the Structural Motifs That Are Essential for Antifreeze Activity. *Angew. Chem. Int. Ed.* **2004,** 43, 856-862.

138. Budke, C.; Heggemann, C.; Koch, M.; Sewald, N.; Koop, T., Ice Recrystallization Kinetics in the Presence of Synthetic Antifreeze Glycoprotein Analogues Using the Framework of LSW Theory. *J. Phys. Chem. B* **2009,** 113, 2865-2873.

139. Czechura, P.; Tam, R. Y.; Dimitrijevic, E.; Murphy, A. V.; Ben, R. N., The Importance of Hydration for Inhibiting Ice Recrystallization with *C*-Linked Antifreeze Glycoproteins. *J. Am. Chem. Soc.* **2008,** 130, 2928-2929.

140. Koushafar, H.; Pham, L.; Lee, C. Y.; Rubinsky, B., Chemical Adjuvant Cryosurgery With Antifreeze Proteins. *J. Surg. Oncol.* **1997,** 66, 114-121.

141. Gage, A. A.; Baust, J., Mechanisms of Tissue Injury in Cryosurgery. *Cryobiology* **1998,** 37, 171-186.

142. Feather, M. S.; Harris, J. F., The Acid-Catalyzed Hydrolysis of Glycopyranosides. *Journal of Organic Chemistry* **1965,** 30, 153-157.

143. Harbon, S.; Herman, G.; Clauser, H., Quantitiatve Evaluation of O-Glycosidic Linkages between Sugars and Aminoacids in Ovine Submaxillary Gland Mucoprotein. *European Journal of Biochemistry* **1968,** 4, 265-272.

144. Griffith, M.; Ewart, K. V., Antifreeze Proteins and their Potential Use in Frozen Foods. *Biotechnol. Adv.* **1995,** 13, 375-402.

145. Crevel, R. W. R.; Fedyk, J. K.; Spurgeon, M. J., Antifreeze Proteins: Characteristics, Occurrence and Human Wxposure. *Food. Chem. Toxicol.* **2002,** 40, 899-903.

146. Payne, S. R.; Sandford, D.; Harris, A.; Young, O. A., The Effects of Antifreeze Proteins on Chilled and Frozen Meat. *Meat Sci.* **1994,** 37, 429-438.

147. Payne, S. R.; Young, O. A., Effects of Pre-slaughter Administration of Antifreeze Proteins on Frozen Meat Quality. *Meat Sci.* **1995,** 41, 147-155.

148. Rubinsky, B.; Arav, A.; Mattioli, M.; DeVries, A. L., The Effect of Antifreeze Glycopeptides on Membrane Potential Changes at Hypothermic Temperatures. *Biochem. Biophys. Res. Commun.* **1990,** 173, 1369-1374.

149. Rubinsky, B.; Arav, A.; Fletcher, G. L., Hypothermic Protection - A Fundamental Property of "Antifeeze" Proteins. *Biochem. Biophys. Res. Commun.* **1991,** 180, 566-571.

150. Rubinsky, B.; Mattioli, M.; Arav, A.; Barboni, B.; Fletcher, G. L., Inhibition of Ca^{2+} and K^{+} currents by "antifreeze" proteins. *Am. J. Physiol. Regul. Intr. Comp. Physiol.* **1992,** 262, R542-R545.

151. Park, T.-J.; Weiwer, M.; Yuan, X.; Baytas, S. N.; Munoz, E. M.; Murugesan, S.; Linhardt, R. J., Glycosylation in Room Temperature Ionic Liquid using Unprotected and Unactivated Donors. *Carbohydrate Res.* **2007,** 342, 614-620.

152. Rubinsky, B.; Arav, A.; Hong, J.-S.; Lee, C. Y., Freezing of Mammalian Livers with Glycerol and Antifreeze Proteins. *Biochem. Biophys. Res. Commun.* **1994,** 200, 732-741.

153. Pham, L.; Dahiya, R.; Rubinsky, B., An *in Vivo* Study of Antifreeze Protein Adjuvant Cryosurgery. *Cryobiology* **1999,** 38, 169-175.

154. Muldrew, K.; Rewcastle, J.; Donnelly, B. J.; Saliken, J. C.; Liang, S.; Goldie, S.; Olson, M.; Baissalov, R.; Sandison, G., Flounder Antifreeze Peptides Increase the Efficacy of Cryosurgery. *Cryobiology* **2001,** 42, 182-189.

155. Hammerstedt, R. H.; Graham, J. K.; Nolan, J. P., Cryopreservation of Mammalian Sperm: What We Ask Them to Survive. *J. Androl.* **1990,** 11, 73-88.

156. Rall, W. F.; Fahy, G. M., Ice-Free Cryopreservation of Mouse Embryos at -196 ºC by Vitrification. *Nature* **1985,** 313, 573-575.

157. Uechi, H.; Tsutsumi, O.; Morita, Y.; Takai, Y.; Taketain, Y., Comparison of the Effects of Controlled-Rate Cryopreservation and Vitrification on 2-cell Mouse Embryos and their Subsequent Development. *Hum. Reprod.* **1999,** 14, 2827-2832.

158. Liebermann, J.; Tucker, M., Comparison of Vitrification and Conventional Cryopreservation of Day 5 and Day 6 Blastocysts During Clinical Application. *Fertil. Steril.* **2006,** 86, 20-26.

159. Mazur, P., Principles of Cryobiology. In *Life in the Frozen State*, 1 ed.; Fuller, B.; Lane, N.; Benson, E. E., Eds. CRC Press: 2004; pp 3-66.

160. Karlsson, J. O. M.; Toner, M., Long-Term Storage of Tissues by Cryopreservation: Critical Issues. *Biomaterials* **1996,** 17, 243-256.

161. Brown, M. S.; Reuter, F. W., Freezing of Nonwoody Plant Tissues: III. Videotape Micrography and the Correlation Between Individual Cellular Freezing Events and Temperature Changes in the Surrounding Tissue. *Cryobiology* **1974,** 11, 185-191.

162. Melcarek, P. K.; Brown, G. N., Chlorophyll Fluorexcence Monitoring of Freezing Point Exotherms in Leaves. *Cryobiology* **1979,** 16, 69-73.

163. Farrant, J.; Walter, C. A.; Lee, H.; McGann, L. E., Use of Two-Step Cooling Procedures to Examine Factors Influencing Cell Survival Following Freezing and Thawing. *Cryobiology* **1977,** 14, 273-286.

164. Muldrew, K.; McGann, L. E., The Osmotic Rupture Hypothesis of Intracellular Freezing Injury. *Biophys. J.* **1994,** 66, 532-541.

165. Baust, J. G.; Gage, A. A., The Molecular Basis of Cryosurgery. *BJU Int.* **2005,** 95, 1187-1191.

166. Baust, J. M., Molecular Mechanisms of Cellular Demise Associated with Cryopreservation Failure. *Cell Preserv. Technol.* **2002,** 1, 17-31.

167. Polge, A.; Smith, A. U.; Parkes, A. S., Revival of Spermatozoa after Vitrification and Dehydration at Low Temperatures. *Nature* **1949,** 164, 666-667.

168. Lovelock, J. E., The Protective Action of Neutral Solutes against Haemolysis by Freezing and Thawing. *Biochem. J.* **1954,** 56, 265-270.

169. Lovelock, J. E.; Bishop, M. W. H., Prevention of Freezing Damage to Living Cells by Dimethyl Sulphoxide. *Nature* **1959,** 183, 1394-1395.

170. Anchordoguy, T. J.; Cecchini, C. A.; Crowe, J. H.; Crowe, L. M., Insights into the Cryoprotective Mechanism of Dimethyl Sulfoxide for Phospholipid Bilayers. *Cryobiology* **1991,** 28, 467-473.

171. Gurtovenko, A. A.; Anwar, J., Modulating the Structure and Properties of Cell Membranes: The Molecular Mechanism of Action of Dimethyl Sulfoxide. *J. Phys. Chem. B* **2007,** 111, 10453-10460.

172. Notman, R.; Noro, M.; O'Malley, B.; Anwar, J., Molecular Basis for Dimethylsulfoxide (DMSO) Action on Lipid Membranes. *J. Am. Chem. Soc.* **2006,** 128, 13982-13983.

173. Fahy, G. M., The Relevance of Cryoprotectant "Toxicity" to Cryobiology. *Cryobiology* **1986,** 21, 1-13.

174. Liseth, K.; Abrahamsen, J. F.; Bjorsvik, S.; Grottebo, K.; Bruserud, O., The Viability of Cryopreserved PBPC Depends on the DMSO Concentration and the Concentration of Nucleated Cells in the Graft. *Cryotherapy* **2005,** 7, 328-333.

175. Scheinkonig, C.; Kappicht, S.; Kolb, H.-J.; Schleuning, M., In Vitro Studies: Adoption of Long-Term Cultures to Evaluate the Cryoprotective Potential of Trehalose for Freezing Hematopoietic Stem Cells. *Bone Marrrow Transpl.* **2004,** 34, 531-536.

176. Beattie, G. M.; Crowe, J. H.; Lopez, A. D.; Cirulli, V.; Ricordi, C.; Hayek, A., Trehalose: A Cryoprotectant That Enhances Recovery and Preserves Function of Human Pancreatic Islets After Long-Term Storage. *Diabetes* **1997,** 46, 519-523.

177. Sei, T.; Gonda, T.; Arima, Y., Growth Rate and Morphology of Ice Crystals Growing in a Solution of Trehalose and Water. *J. Cryst. Growth* **2002,** 240, 218-229.

178. Tam, R. Y.; Ferreira, S. S.; Czechura, P.; Chaytor, J. L.; Ben, R. N., Hydration Index - A Better Parameter for Explaining Small Molecule Hydration in Inhibition of Ice Recrystallization. *J. Am. Chem. Soc.* **2008,** 130, 17494-17501.

179. Liu, S.; Wang, W.; von Moos, E.; Jackman, J.; Mealing, G.; Monette, R.; Ben, R. N., In Vitro Studies of Antifreeze Glycoprotein (AFGP) and a *C*-Linked AFGP Analogue. *Biomacromolecules* **2007,** 8, 1456-1462.

Chapter 2 : Goals and Objectives

2.1: Introduction to C-Glycosides

In biological systems, carbohydrates are almost always bound to proteins through an *O*-linkage or an *N*-linkage. For example, the most common glycoprotein linkage is an *O*-linkage to the hydroxyl group on the side chain of serine or threonine,[1] as is observed in native AFGP. Alternatively, carbohydrates can be bound to the side chain of asparagine residues via an *N*-linkage.[1] Unfortunately, although *O*-linkages are commonly found in nature, they are also inherently unstable, making chemical synthesis of *O*-linked glycoproteins difficult. They are hydrolyzed under strongly acidic[2] or strongly basic conditions,[3] and can also be easily degraded enzymatically through the action of glycosidases.[4]

Recently, some interest has been shown in using *C*-glycosides as mimetics to *O*-linked glycosides.[1] In these compounds, a methylene group replaces either the inter-saccharide oxygen between two pyranose rings, or the oxygen linkage to the peptide in glycoproteins. *C*-Glycosides have been found in nature in the structures of palytoxin (Figure 2.1),[5] maitotoxin (Figure 2.2),[6] aquayamycin (Figure 2.3),[7] and human RNase2 (Figure 2.3).[8-10]

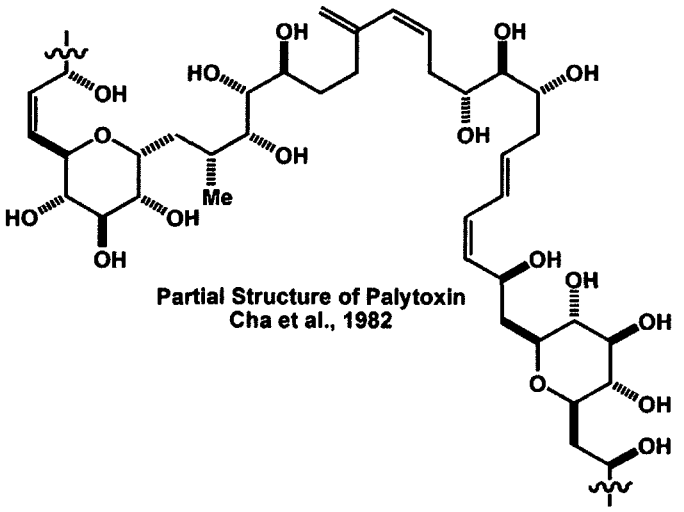

Figure 2.1: Palytoxin contains several *C*-linked monosaccharides, of which two are shown in this partial structure (adapted from Cha et al.).[5]

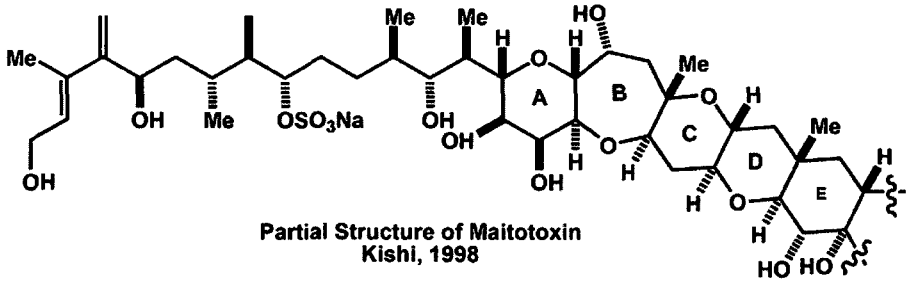

Figure 2.2: Maitotoxin contains a *C*-linked monosaccharide as its A-ring (adapted from Kishi).[6]

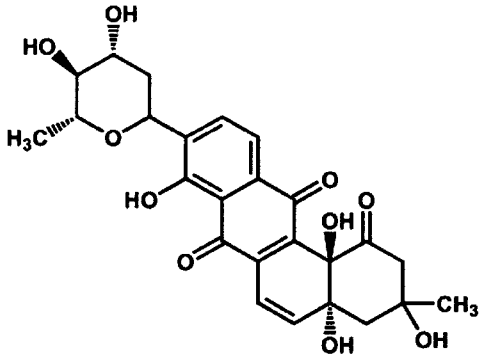

Structure of Aquaymycin
Sezaki et al., 1970

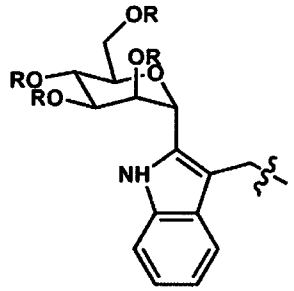

Partial Structure of Human RNase2
Hofsteenge et al., 1994

Figure 2.3: Aquaymycin has a naphthoquinone *C*-linked to a dihydropyran,[7] and Human RNase2 contains an α-mannose *C*-linked to a tryptophan residue.[8]

Although this motif has been found in nature, researchers were reluctant to incorporate it into *O*-glycoside analogues due to two main concerns. The first was that the *C*-glycosides, being more flexible, would be able to adopt several different conformations and would not be as conformationally constrained as the *O*-glycosides. Secondly, there was concern that the anomeric oxygen was required for mediating binding to carbohydrate receptors, and therefore that the *C*-glycosides would not bind with the same affinities as *O*-glycosides.

Several studies have been conducted to address these concerns. First, researchers have studied the solution conformations of *C*-glycoside analogues of mono- and disaccharides, and they observed that the predominant and preferred conformations are virtually identical to that of their parent *O*-glycosides.[11-13] Furthermore, Ravishankar et al. observed that *C*-lactose binds to peanut lectin in a conformation that is extremely similar to that of lectin-bound *O*-lactose.[14] In addition, Wei et al. have shown that *C*-glycosides adopt the same staggered exo-anomeric conformation as *O*-glycosides.[15] They also observed that *C*-linked analogues of H-type II trisaccharides have identical binding affinities as the native *O*-linked system. To further address the second issue, Wang et al. examined the binding affinities of oligosaccharides to monoclonal immunoglobulins.[16] Synthetic *C*-linked oligosaccharides

were observed to bind to the immunoglobulins with affinities nearly identical to their parent oligosaccharides.[16] These experiments confirm that *C*-linked analogues behave very similarly to their parent *O*-linked compounds *in vitro*, and suggest that they can be effectively used as *O*-mimetics with increased stability in biological systems without a loss in binding affinity or conformation.

2.2: C-Linked AFGP Analogues

C-Glycosides can be used as stable mimetics of *O*-glycosides, because the methylene group is quite stable to acidic and basic conditions, and is not hydrolyzed by glycosidases which act only on the *O*-linkage. The Ben lab has used this approach to synthesize several *C*-linked AFGP analogues, two of which are the *C*-serine derivative[17] and OGG-Gal (Figure 2.4).[18-20] These analogues exhibited potent IRI activity (Figure 2.5) but did not show any TH activity. Our lab is currently synthesizing new AFGP analogues based upon these lead compounds in hopes of determining which structural features are necessary for potent IRI activity.

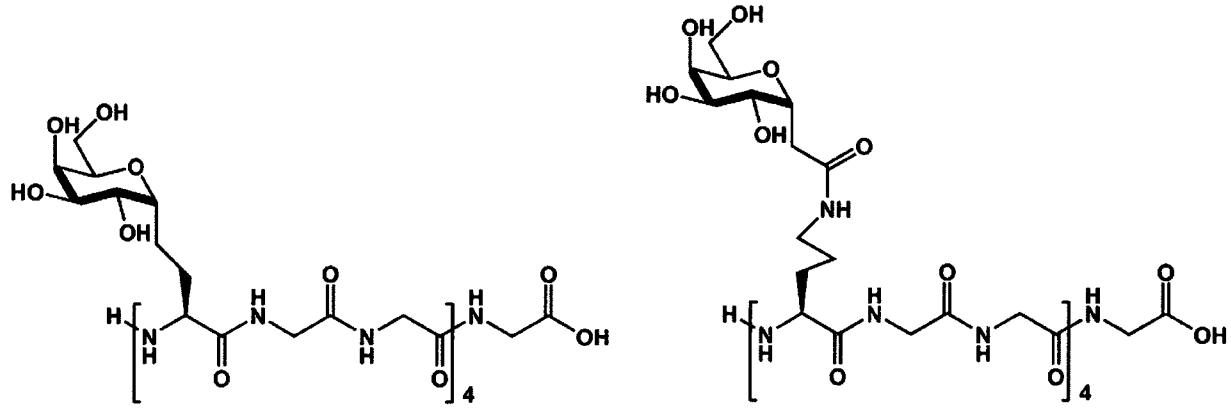

Figure 2.4: Structures of AFGP analogues *C*-Serine (prepared by Liu et al.),[17] and OGG-Gal (prepared by Eniade et al.)[18-20]

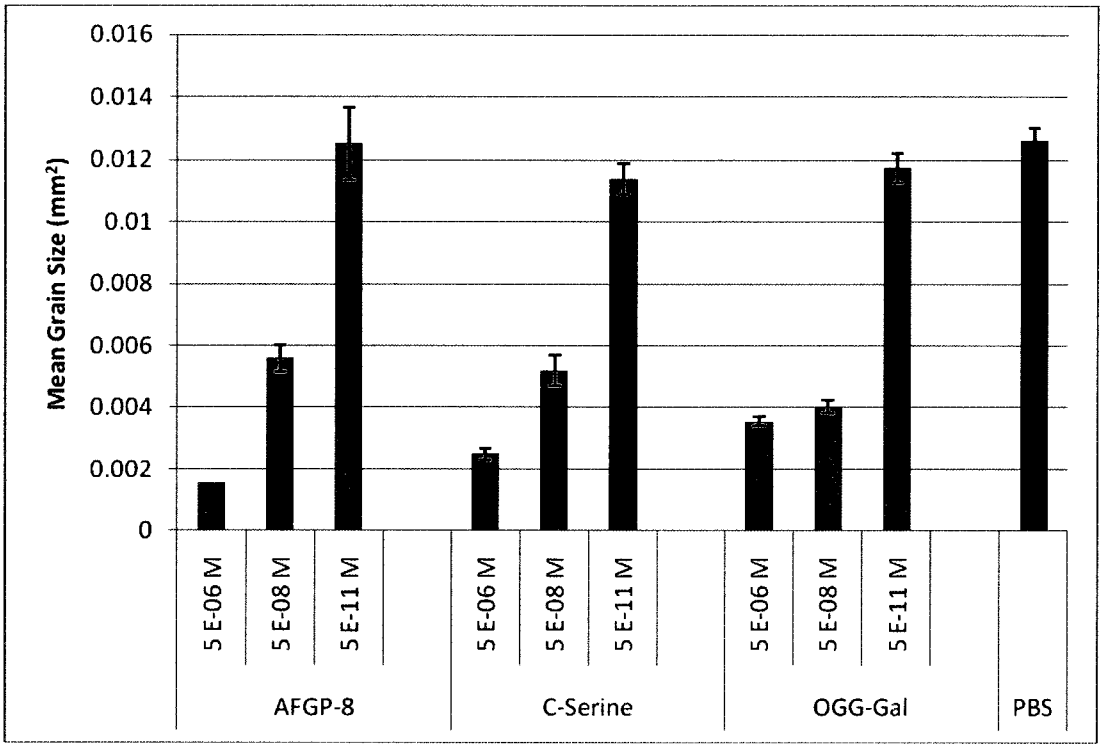

Figure 2.5: Ice-recrystallization inhibition activity of *C*-Serine[17] and OGG-Gal[18] compared to AFGP8 (positive control) and phosphate buffered saline solution (PBS) (negative control). *C*-Serine and OGG-Gal solutions produced ice crystals that were nearly as small as those in an AFGP8 solution at 5×10^{-6} M.

As introduced in the previous chapter, a series of analogues (**1-4**) were prepared by varying the carbohydrate moiety of OGG-Gal (Figure 2.6) in order to assess the structural and functional importance of the carbohydrate moiety on IRI activity. An interesting trend was observed, in which the IRI activity was observed to decrease in the order OGG-Gal (**1**) > OGG-Glc (**2**) > OGG-Man (**3**) > OGG-Tal (**4**) (Figure 2.7).[21] These four monosaccharides (galactose, glucose, mannose, and talose) differ only in the stereochemistry of the hydroxyl groups at C-2 and C-4. Galema and Hoiland observed a similar trend when they determined that the isentropic partial molar compressibilities (PMCs) of several monosaccharides were dependent on the configuration of the hydroxyl groups (Figure 2.8).[22] These PMC values are an estimate of the "fit" of a carbohydrate into the three-dimensional hydrogen bonded network of

water. From these results, it was demonstrated that talose had the best fit within the hydrogen bonded network of bulk water, followed by mannose and glucose, and galactose has the worst fit. Based on these recent results from our laboratory, it appears that the IRI activity of AFGP analogues is correlated to the partial molar compressibilities of the monosaccharide portion and therefore on the "fit" of the carbohydrate into the bulk water. Czechura et al. suggested that the poor fit of galactose into water results in a large disturbance of the ordered structure of supercooled water. This disorder slows the growth of ice by slowing the addition of water molecules to the ice lattice, resulting in inhibition of recrystallization.[21] These results are not surprising, as Furuki has suggested that nature chose to incorporate galactose into AFGPs because of its unique ability to prevent the freezing of water.[23]

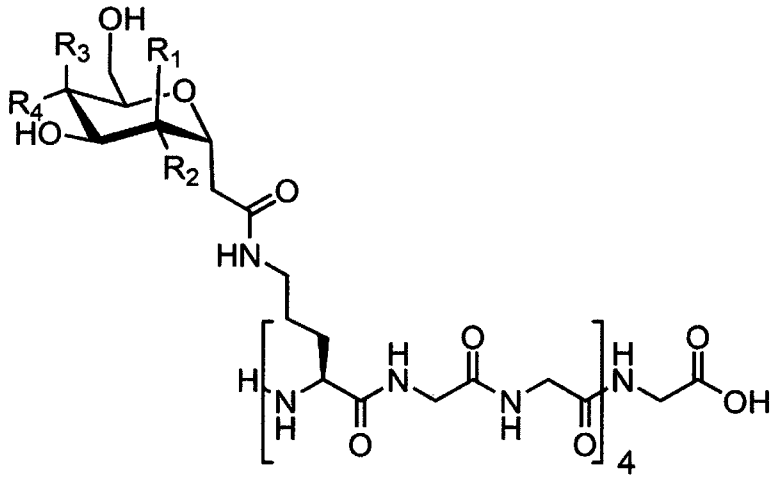

1: OGG Gal: R_1=H;R_2=OH;R_3=OH;R_4=H
2: OGG Glc: R_1=H;R_2=OH;R_3=H;R_4=OH
3: OGG Man: R_1=OH;R_2=H;R_3=H;R_4=OH
4: OGG Tal: R_1=OH;R_2=H;R_3=OH;R_4=H

Figure 2.6: AFGP analogues (**1-4**) containing a varied carbohydrate moiety.

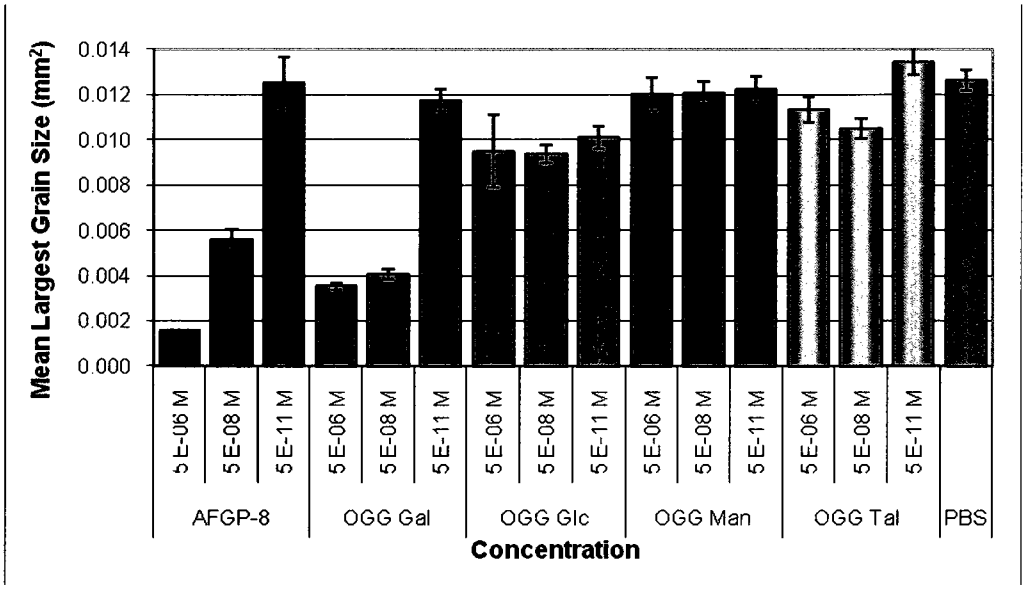

Figure 2.7: IRI activity of AFGP analogues (**1-4**) containing different *C*-linked monosaccharide moieties

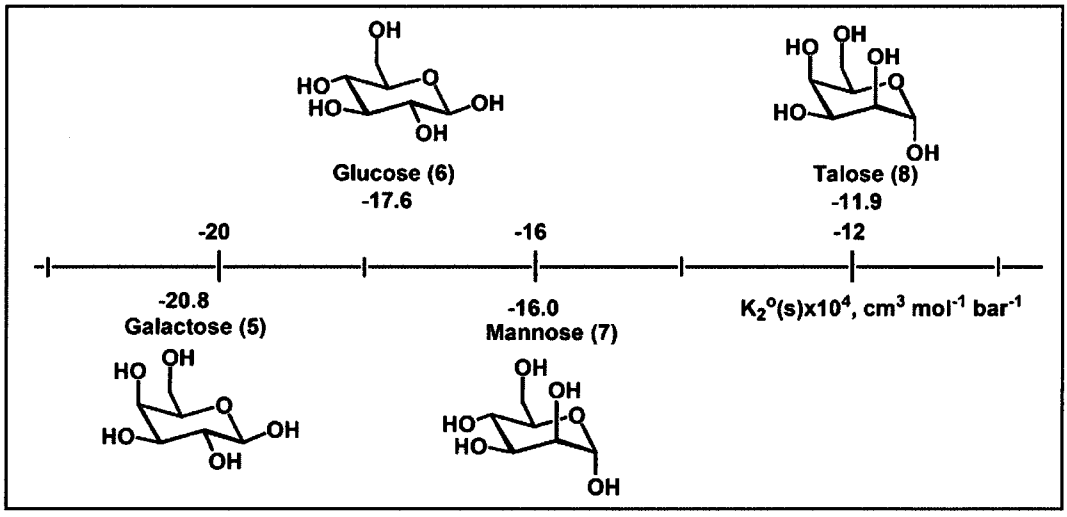

Figure 2.8: Partial molar compressibilities of galactose (**5**), glucose (**6**), mannose (**7**), and talose (**8**)[22]

2.3: Objectives of this thesis:

Based on these previous observations, the six objectives of this thesis are as follows:

Objective 1:

Examine several mono- and disaccharides for ice-recrystallization inhibition (IRI) activity and determine whether there is a correlation to the hydration of the carbohydrates

The results from Czechura et al. suggest that the hydration of carbohydrates, as described by Galema and Hoiland, plays a role in the ice-recrystallization inhibition activity of AFGP analogues. A few researchers have observed the morphology and growth rate of ice crystals in carbohydrate solutions. Sei et al. observed that trehalose is more effective than sucrose in inhibiting the growth of ice crystals, possibly due to the greater ability of trehalose to bind water molecules.[24] Others have suggested that the ability of fructose, glucose, maltose, and sucrose to affect the rate of recrystallization of ice crystals is related to their respective diffusion coefficients.[25] However, to the best of our knowledge, a systematic study to determine whether carbohydrates can act as ice-recrystallization inhibitors has not been previously conducted. Furthermore, the correlation between IRI activity and hydration of simple carbohydrates has not been explored.

Several monosaccharides (galactose (**5**), glucose (**6**), mannose (**7**), and talose (**8**), (Figure 2.8) and disaccharides (melibiose (**9**), lactose (**10**), trehalose (**11**), maltose (**12**), and sucrose (**13**), (Figure 2.9) will be evaluated for IRI activity at appropriate concentrations. Furthermore, the ability of these compounds to inhibit ice-recrystallization will be compared to that of dimethyl sulfoxide (DMSO), a known cryoprotectant. If IRI activity is observed in simple carbohydrates, this will support their use as cryoprotective agents and may allow us to further understand the role they play in cryoprotection.

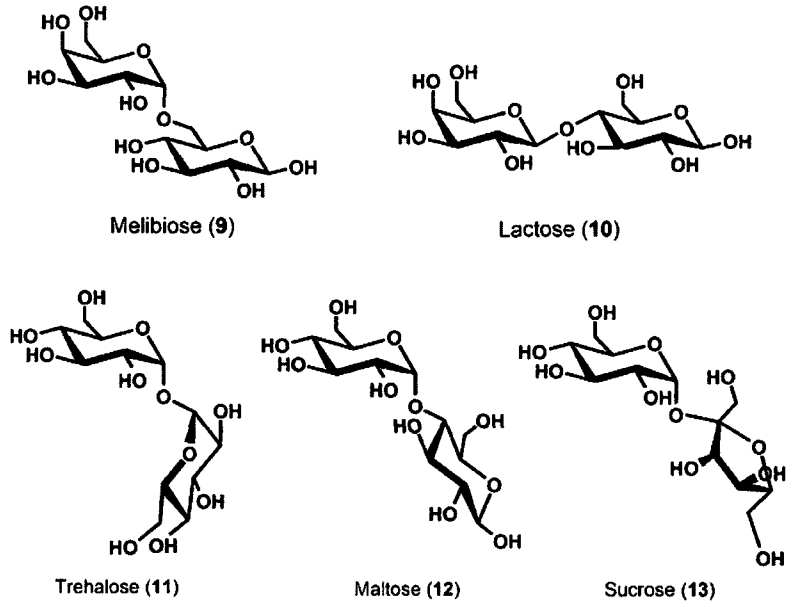

Figure 2.9: Structures of melibiose (**9**), lactose (**10**), trehalose (**11**), maltose (**12**), and sucrose (**13**)

These IRI results will be compared to their partial molar compressibilities and hydration numbers to see if a correlation exists between carbohydrate IRI activity and the hydration of the carbohydrate. The hydration describes the number of water molecules that are surrounding a carbohydrate and also describes how the hydrated carbohydrate fits into the three dimensional structure of ice. If a correlation is observed with IRI activity, this will suggest that the interaction of the carbohydrate with bulk water is involved in the mechanism of ice-recrystallization inhibition. Furthermore, an observed correlation may allow us to "predict" the IRI activity of carbohydrates based upon the amount of hydration that they exhibit, aiding in our design of novel ice-recrystallization inhibitors.

Objective 2:

Test a series of carbohydrates for IRI activity, in vitro cytotoxicity, and in vitro cryopreservation ability at various concentrations and attempt to correlate these properties

It is the recrystallization of ice during the thawing cycle of cryopreservation protocols that causes the most damage,[26-28] as described in Section 1.4. For this reason, ice-recrystallization inhibitors could be very useful in decreasing the damage to frozen samples if they were incorporated into cryopreservation media. Although several researchers have observed the beneficial protective effect of carbohydrates during freeze-thaw cycles,[29-33] a systematic study that compares the IRI activity of carbohydrates to their cryoprotective ability has not been carried out. Furthermore, the potential cytotoxicity of these samples at high concentrations should also be considered, as this could preclude them from being used as cryoprotectants. If a link is established between IRI and cryopreservation, novel ice-recrystallization inhibitors could be custom-designed for use in cryopreservation protocols. This could decrease or eliminate the amount of toxic DMSO that is required during the freeze-thaw cycle.

Towards this end, several mono- (**5-8**) and disaccharides (**9-11** and **13**) will be tested for IRI activity at various concentrations. Their IRI activity will be compared to the results of MTT cytotoxicity assays and any observed correlation will be discussed. Subsequent to this, the IRI activity of these compounds will be compared to results of viability assays post freeze-thaw using flow cytometry and the results will be presented. Furthermore, these carbohydrates will be compared to DMSO solutions and will also be evaluated in combination with DMSO (a known cryoprotectant).

Once the IRI activity of simple mono- and disaccharides is established, the following three objectives are to examine how modifications of these sugars affect their ability to inhibit the recrystallization of ice.

Objective 3:

Synthesize C-linked carbohydrates and compare them to their natural O-linked counterparts to determine whether the substituent at C-1 influences IRI activity

As previously mentioned, our laboratory has observed that the IRI activity of *C*-linked AFGP analogues is correlated to the hydration properties reported for the

corresponding *O*-linked monosaccharide. Based upon these results, it seems reasonable to predict that *C*-linked monosaccharides will display IRI activity that is comparable that of their parent *O*-linked monosaccharides. In order to test this hypothesis and determine the effect of the nature of the anomeric linkage, a series of *C*-linked carbohydrates (**14-19**, Figure 2.10) will be prepared and tested for IRI activity.

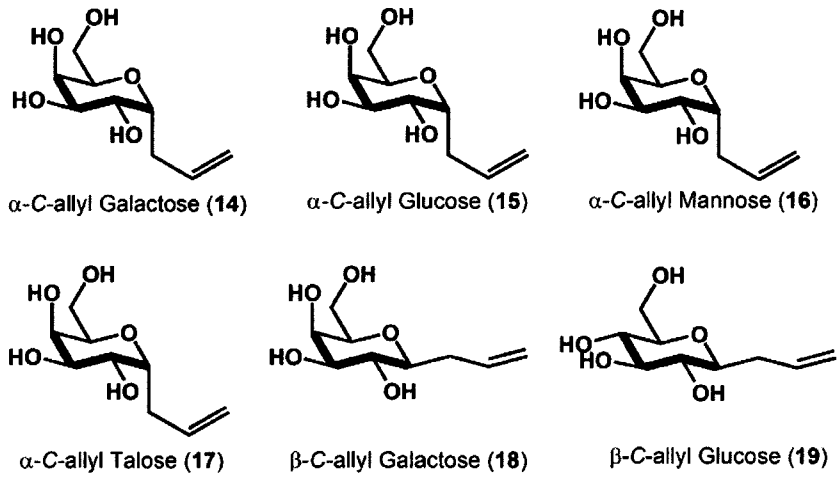

Figure 2.10: α-*C*-allyl monosaccharides (**14-17**) and β-*C*-allyl galactose (**18**) and glucose (**19**) will be evaluated for IRI activity. The results will be compared to those for their *O*-linked parent monosaccharides galactose (**5**) and glucose (**6**).

It has been proposed that the stereochemistry of the hydroxyl group at C-1 is not as important in determining the hydration of carbohydrates as the stereochemistry at C-2 and C-4.[22, 34] This hypothesis will be further examined with the synthesis of a series of *C*-linked analogues (**20-23**) with varying stereochemistry at C-1 (Figure 2.11). These compounds will be evaluated for IRI activity and compared to the compounds described in Figure 2.10.

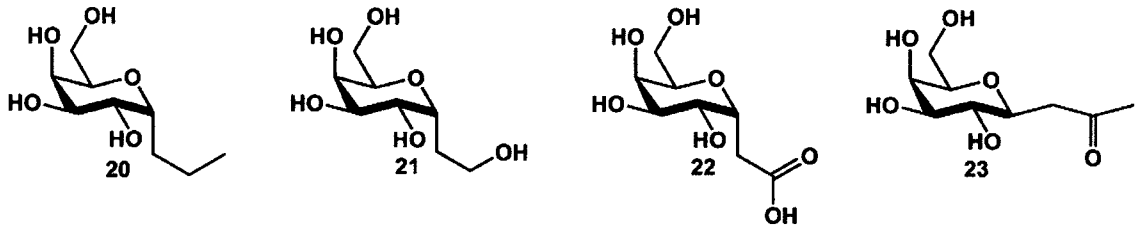

Figure 2.11: *C*-linked compounds (**20**, **21**, **22**, and **23**) will be evaluated for IRI activity

Objective 4:

Evaluate the effect of the acetamide group in glucose and galactose

The acetamide group in native AFGP has been reported to be essential for thermal hysteresis activity;[35] however, whether it is a requirement for ice-recrystallization inhibition activity has not been fully explored. A series of galactose and glucose derivatives with amino and amide functionalities at C-2 (**24-27**, Figure 2.12) will be tested for IRI activity to attempt to see if this functional group increases antifreeze activity.

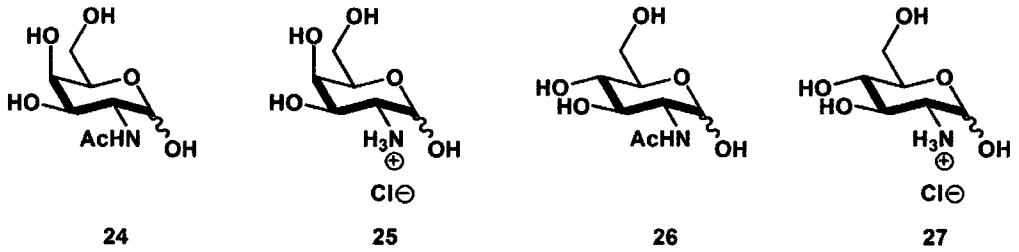

Figure 2.12: *N*-acetyl-galactosamine (**24**), galactosamine hydrochloride (**25**), *N*-acetyl-glucosamine (**26**), and glucosamine hydrochloride (**27**) will be purchased and tested for IRI activity. These compounds will be compared to D-galactose (**5**) and D-glucose (**6**).

Objective 5:

Prepare several galactose derivatives containing dramatic structural modifications and determine the effect of these modifications on hydration and IRI activity.

As mentioned previously, several researchers have studied the interactions of biological antifreezes with ice and the ice-water interface. McDonald et al. have suggested that AFPs may act by perturbing the structure of liquid water and therefore decreasing the likelihood of additional water molecules adding to the ice surface.[36] They have also observed that there is a steric match between the ice-binding face of AFP and the ice surface, and that the threonine residues are oriented away from the ice-binding face.[37] Baardsnes and Davies have observed the importance of hydrophobic groups in affecting the steric match of the ice-binding site to ice.[38] Furthermore, several groups have observed that the γ-methyl groups of threonine, and not the hydroxyl groups, are required for ice-binding and effective IRI activity.[39-41]

Hydration has also been implicated in antifreeze activity, and hydrophobic groups have been shown to influence hydration. Jorov et al. demonstrated that the hydrophobic groups on AFP are de-solvated upon binding to ice, and that this de-solvation lowers the energy of AFP-ice binding.[42] Yang and Sharp have observed that the hydration structure of the ice-binding site of AFP is altered upon binding, and active antifreezes display very apolar-like hydration compared to bulk water.[43] All of these experiments have confirmed that hydrophobic groups are very important for antifreeze activity, and that the hydration of these hydrophobic groups is implicated in effective recognition and ice-binding. Therefore, carbohydrates and AFGP analogues with increased hydrophobicity will affect the hydrogen bonded network of water at the ice-water interface, and this should have an effect on IRI activity.

Once a correlation between the IRI activity of monosaccharides and their hydration properties is established, this will be further explored through the synthesis of monosaccharides derivatives. Structural modifications that are likely to disrupt the hydration network will be prepared and evaluated for IRI activity.

5a) Systematically replace each hydroxyl group with a methoxy group to evaluate the role of hydrogen bonding to each hydroxyl group

Researchers have suggested that the stereochemistry of the hydroxyl groups at C-2 and C-4 are most important in determining how effectively a carbohydrate is hydrated.[22, 34] The internal hydrogen bonding network within a carbohydrate is dependent upon the stereochemistry of these hydroxyl groups.[22, 34] For example, the formation of an intramolecular hydrogen bond between OH-2 and OH-4 in talose has been observed and this disrupts the internal hydrogen bond network of this monosaccharide.[44, 45] This has been suggested to account for the observation that talose is more hydrophobic and less hydrated than galactose or glucose.[44, 45] By adding structural modifications that disrupt the hydrogen bonding ability of the hydroxyl groups and therefore the hydrogen bond network, we can determine whether this has an effect on IRI activity in conjunction with the change in the hydration of the carbohydrate.

In order to realize this goal, I will prepare a series of *C*-allyl galactose analogues with a methoxy group replacing each hydroxyl group in turn (**28-31**, Figure 2.13). The methoxy group is capable of being a hydrogen bond acceptor, but is unable to act as a hydrogen bond donor. By testing each of these analogues for IRI activity, we will examine whether hydrogen bonding plays a significant role in determining IRI activity at each position on galactose. These results will be compared to those for α- and β-methylgalactopyranoside (**32** and **33**, Figure 2.14) as well as to α-*C*-allyl galactose (**14**, Figure 2.10).

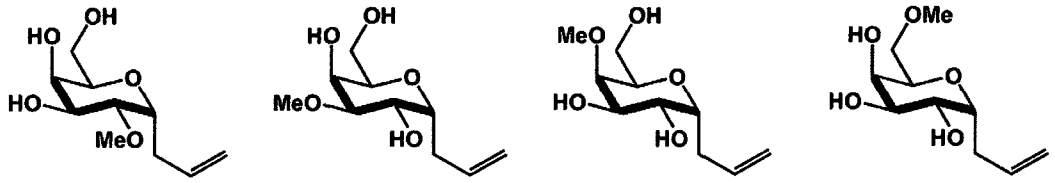

Figure 2.13: Methylated *C*-allyl galactose derivatives to be synthesized and tested for IRI activity.

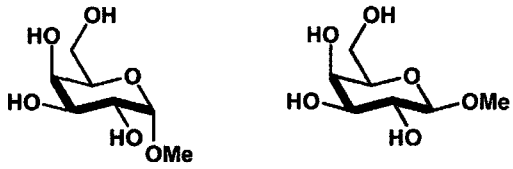

32 33

Figure 2.14: Structures of α-methylgalactopyranoside (**32**) and β-methylgalactopyranoside (**33**) which will be compared to methylated *C*-allyl galactose derivatives (**28-31**)

O-Linked compounds with similar structural modifications (Figure 2.15) will be prepared in order to confirm whether the *C*-linkage in compounds (**18**) and (**28**) is responsible for changes in IRI activity. In addition, efforts to determine the hydration properties of these compounds using molecular dynamics simulations will be presented.

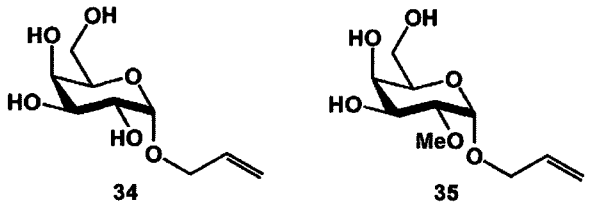

34 35

Figure 2.15: *O*-linked compounds (**34**) and (**35**) will be synthesized and evaluated for IRI activity.

*5b) Synthesize fluorinated analogues as hydrophobic mimetics of the anomeric oxygen in OGG-Gal (**1**) and compare to non-fluorinated controls*

In 2006, Quirion and Castelot-Deliencourt-Godefroy reported that fluorinated AFGP analogues (Figure 2.16) are able to preserve human embryonic kidney cells, blood platelets, rat heart myoblasts, and human skin fibroblasts at physiological and sub-zero temperatures.[46] However, these compounds were not evaluated for antifreeze

activity, and this reported preservation effect may be due to an inhibition of ice recrystallization by these compounds.

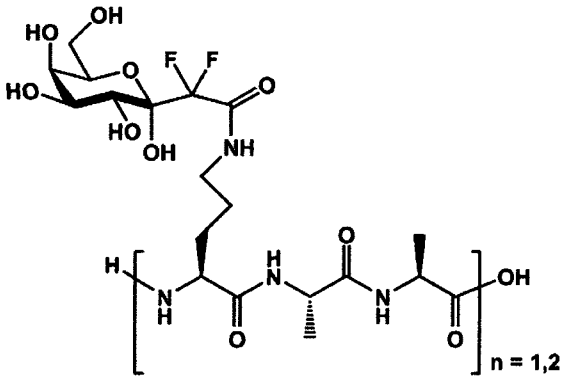

Figure 2.16: Fluorinated AFGP analogues prepared by Quirion and Castelot-Deliencourt-Godefroy[46]

The *geminal*-difluoromethylene group in these compounds is generally regarded as a good steric mimic to an anomeric oxygen atom.[47, 48] However, it can be considered to be much more hydrophobic than oxygen since it has been proposed that covalently bound fluorine is not able to form hydrogen bonds.[49, 50] A similar analogue (Figure 2.17) will be prepared and tested for IRI activity. The retrosynthesis of this analogue is outlined in Figure 2.17.

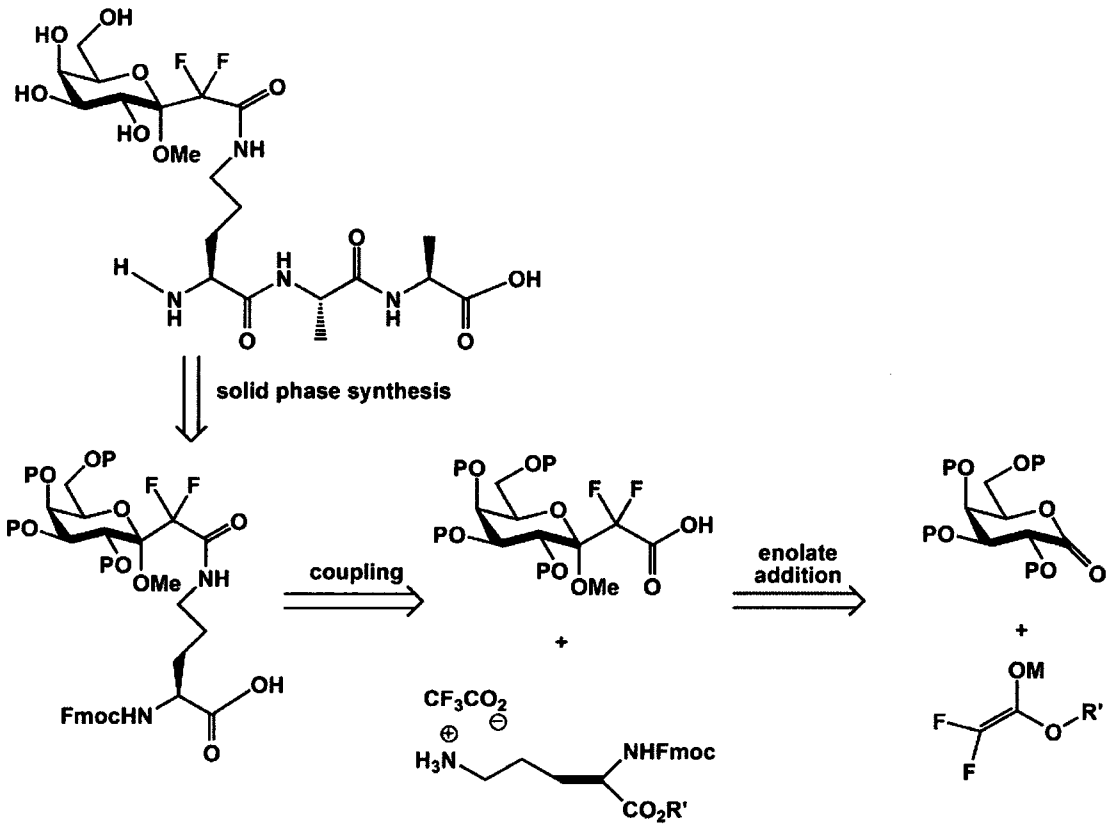

Figure 2.17: Retrosynthesis of fluorinated AFGP analogue to be prepared

In addition, the role of the CF_2 will be examined by synthesizing non-fluorinated controls. The role of the anomeric hydroxyl group will be evaluated by testing methylated derivatives which will be unable to act as hydrogen bond donors (Figure 2.18). If analogues such as those prepared by Quirion et al. (Figure 2.16) display IRI activity, the additional hydroxyl group at C-1 may be responsible, rather than the *geminal*-difluoromethylene group. The anomeric hydroxyl group will be able to form strong hydrogen bonds with water, perhaps increasing the hydration of the carbohydrate and increasing the IRI activity. By preparing analogues with a methoxy group replacing this anomeric hydroxyl group, we will be able to determine whether the hydrogen-bond donating ability of the anomeric hydroxyl group is responsible for imparting any observed IRI activity. Based upon our previous results, it is proposed that the IRI activity of monosaccharides will show the same trend as glycopeptides containing those

monosaccharides, allowing us to screen for IRI activity of the carbohydrate component as an indicator of the ability of the associated glycopeptide to inhibit the recrystallization of ice.

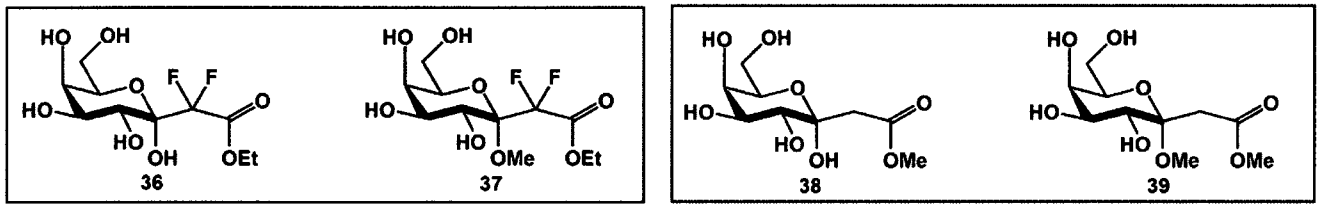

Figure 2.18: Fluorinated (**36**, **37**) and non-fluorinated (**38**, **39**) monosaccharides that will be prepared and tested for IRI activity. These four compounds will allow us to determine the effect of the fluorine atoms and the hydrogen bond donating ability of the anomeric hydroxyl group on the IRI activity of monosaccharides.

5c) Examine the potential for gel formation and its effect on IRI activity by synthesizing carbohydrates containing alkyl chains

Carbohydrate-based low molecular weight gelators have recently been reported in the literature (Figure 2.19).[51] These compounds have been observed to form gels in aqueous DMSO, ethanol, and pure water solutions. These gels depend on intermolecular forces such as π-π stacking, hydrogen bonding, hydrophobic interactions, and van der Waals forces.[51]

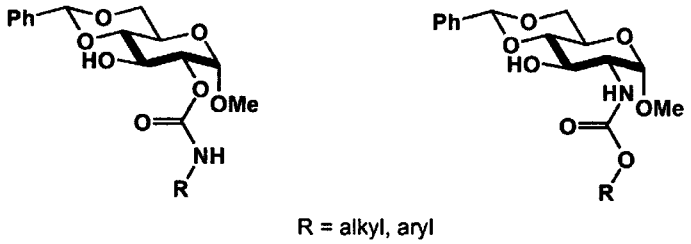

Figure 2.19: Carbohydrate-based gelators synthesized by Wang et al.[51]

Recent data in our laboratory has caused us to propose that gel or liquid crystal formation may result in increased IRI activity. Several C-1 amides with alkyl chains of increasing lengths were found to display IRI activity (Trant, Biggs, and Ben, unpublished results). In order to further explore the effect of alkyl chains on IRI activity, a series of compounds with alkyl chains at C-1 (**26** and **27**, Figure 2.20), and alkyl chains of increasing length at C-2 (**28-31**, Figure 2.20) will be prepared and evaluated for IRI activity.

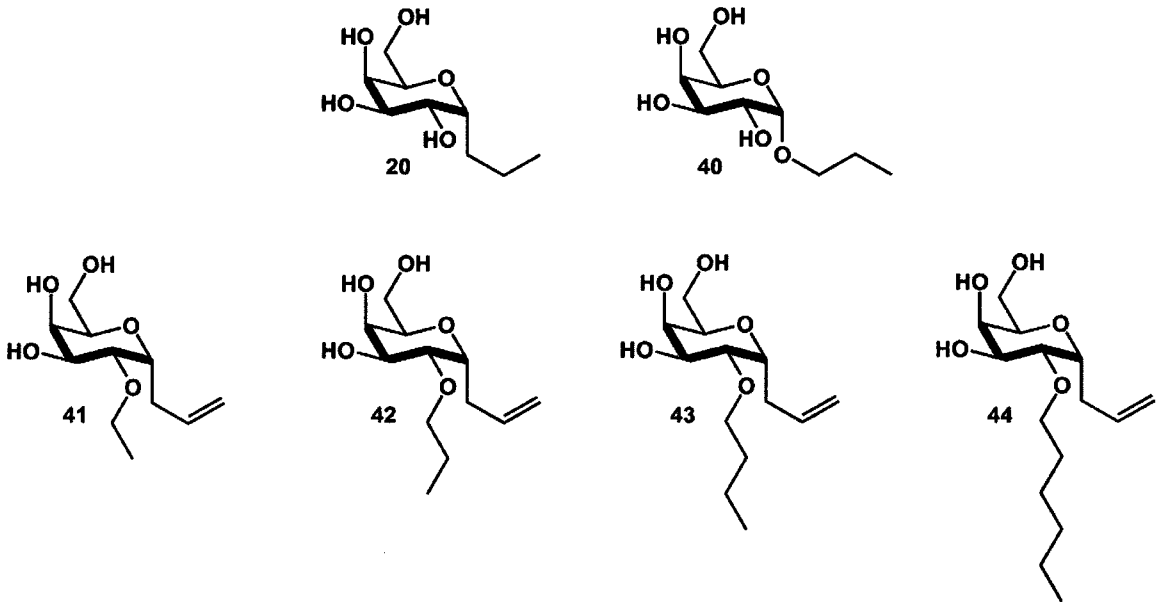

Figure 2.20: Alkylated compounds (**20** and **40-44**) will to be synthesized to explore the effect of alkyl chains on IRI activity

Thioglycosides have also been reported to act as gelators. Consistent with our hypothesis that compounds with gel-forming potential may act as potent inhibitors of ice recrystallization, a series of thioglycoside derivatives of galactose (Figure 2.21) will also be prepared and evaluated for IRI activity.

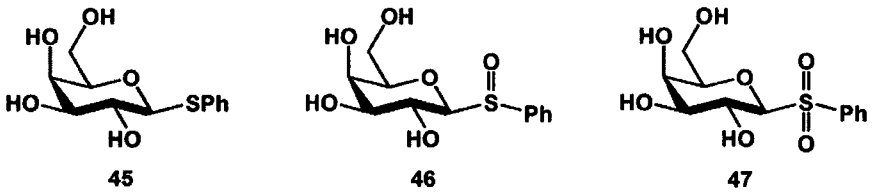

Figure 2.21: Thioglycosides (**45-47**) will be synthesized and evaluated for IRI activity

Objective 6:

Explore the nature of the ice-water interface using CARS

As previously mentioned, recrystallization of ice is one of the major causes of damage during freeze-thaw protocols. Understanding the mechanisms of ice recrystallization and the ice-water interface may aid us in designing novel cryoprotectants. Although hydration has been implicated in the activity of biological antifreezes, the nature of the ice-water interface is not well understood. Furthermore, during freezing protocols, the samples remain in a supercooled state for an extended period of time before freezing occurs. The differences between water, supercooled water, and ice have not been fully explored.

A spectroscopic tool that has received much interest in recent years is Coherent Anti-Stokes Raman Scattering (CARS) microscopy. This is a non-linear optical form of Raman spectroscopy.[52] CARS uses two lasers that generate a strong anti-Stokes signal.[52] A strong vibrational signal is generated, which can allow for real-time monitoring of dynamic processes. Benefits of this technique includes the fact that it is non-invasive and does not cause heating or photobleaching, and it does not require

dyes or stains.[53] Also, much stronger signals are observed as compared to regular Raman spectroscopy.[53] When combined with a cryostage, CARS can be used to examine the differences in vibrational frequencies between water, supercooled water, and ice. The addition of biological antifreezes to this system can allow one to examine the nature of the ice-water interface in the presence of these compounds. The goals of this final project include the following:

6a) Use CARS to study the differences between water, supercooled water, and ice.

The structure of water, supercooled water, and ice has been extensively studied using Raman spectroscopy. However, to the best of our knowledge, CARS spectroscopy has not been used for this purpose. Understanding the differences in the CARS spectra of water, supercooled water, and ice will be necessary before we move to examine these solutions in cell-based systems.

6b) Study the effect of biological antifreezes on the ice-water interface during freezing.

The advantage of using CARS combined with a cryostage is that water, supercooled water, and ice can be easily monitored in the presence of living cells without the need for probes or dyes. Therefore, we may increase our understanding of the effect that supercooled water and ice have on biological membranes. The effect of biological antifreezes on the ice-water interface will be evaluated using this experimental setup.

Summary of the goals and objectives of this thesis:

The successful fulfillment of these studies will improve our current understanding of the factors affecting ice-recrystallization inhibition activity of carbohydrates and will allow us to determine the effect of hydration on antifreeze activity. In addition, through cellular based assays we will evaluate whether carbohydrates could potentially be used

for the preservation of cells and tissues at sub-zero temperatures. Furthermore, a greater understanding of the ice-water interface will aid in the design of new recrystallization-inhibitors. In summary, this dissertation will address the following goals:

1) Evaluate carbohydrates for antifreeze activity and determine whether IRI activity is linked to the hydration of the carbohydrates.
2) Observe through *in vitro* cell-based assays whether IRI activity can be correlated to cytotoxicity and/or cryopreservation ability of carbohydrates.
3) Determine whether *C*-linked monosaccharides display IRI activity and whether the anomeric stereochemistry affects IRI activity levels.
4) Test carbohydrates containing amine and acetamide moieties for IRI activity
5) Synthesize several monosaccharides containing drastic structural modifications (methoxy groups, alkyl groups, and *geminal*-difluoromethylene groups) and assess their IRI activity.
6) Examine the nature of the ice-water interface using CARS.

The results of these experiments will be presented in the following three chapters of this dissertation.

2.4: References:

1. Marcaurelle, L. A.; Bertozzi, C. R., New Directions in the Synthesis of Glycopeptide Mimetics. *Chem. Eur. J.* **1999,** 5, 1384-1390

2. Feather, M. S.; Harris, J. F., The Acid-Catalyzed Hydrolysis of Glycopyranosides. *J. Org. Chem.* **1965,** 30, 153-157.

3. Harbon, S.; Herman, G.; Clauser, H., Quantitiatve Evaluation of *O*-Glycosidic Linkages between Sugars and Aminoacids in Ovine Submaxillary Gland Mucoprotein. *Eur. J. Biochem.* **1968,** 4, 265-272.

4. Capon, B., Mechanism in Carbohydrate Chemistry. *Chem. Rev.* **1969,** 69, 407-498.

5. Cha, J. K.; Christ, W. J.; Finan, J. M.; Fujioka, H.; Kishi, Y.; Klein, L. L.; Ko, S. S.; Leder, J.; McWhorter, W. W. J.; Pfaff, K.-P.; Yonaga, M.; Uemura, D.; Hirata, Y., Stereochemistry of Palytoxin. 4. Complete Structure. *J. Am. Chem. Soc.* **1982,** 104, 7369-7371.

6. Kishi, Y., Complete Structure of Maitotoxin. *Pure Appl. Chem.* **1998,** 70, 339-344.

7. Sezaki, M.; Kondo, S.; Maeda, K.; Umezawa, H., The Structure of Aquayamycin. *Tetrahedron* **1970,** 26, 5171-5180.

8. Hofsteenge, J.; Muller, D. R.; Beer, T. d.; Loffler, A.; Richter, W. J.; Vliegenthart, J. F. G., New Type of Linkage between a Carbohydrate and a Protein: *C*-Glycosylation of a Specific Tryptophan Residue in Human RNase U_S. *Biochemistry* **1994,** 33, 13524-13530.

9. Vliegenthart, J. F. G.; Casset, F., Novel Forms of Protein Glycosylation. *Curr. Opin. Struct. Biol.* **1998,** 8, 565-571.

10. de Beer, T.; Vliegenthart, J. F. G.; Loffler, A.; Hofsteenge, J., The Hexopyranosyl Residue That Is C-Glycosidically Linked to the Side Chain of Tryptophan-7 in Human RNase Us Is α-Mannopyranose. *Biochemistry* **1995,** 34, 11785-11789.

11. Wu, T.-C.; Goekjian, P. G.; Kishi, Y., Preferred Conformation of *C*-Glycosides. 1. Conformational Similarity of Glycosides and Corresponding *C*-Glycosides. *J. Org. Chem.* **1987,** 52, 4819-4823.

12. Babirad, S. A.; Wang, Y.; Goekjian, P. G.; Kishi, Y., Preferred Conformation of *C*-Glycosides. 3. Preferred Conformation of Carbon Analogues of 1,4-Disaccharides. *J. Org. Chem.* **1987,** 52, 4825-4827.

13. Goekjian, P. G.; Wu, T.-C.; Kishi, Y., Preferred Conformation of *C*-Glycosides. 6. Conformational Similarity of Glycosides and Corresponding *C*-Glycosides. *J. Org. Chem.* **1991,** 56, 6412-6422.

14. Ravishankar, R.; Surolia, A.; Vijayan, M.; Lim, S.; Kishi, Y., Preferred Conformation of *C*-Lactose at the Free and Peanut Lectin Bound States. *J. Am. Chem. Soc.* **1998,** 120, 11297-11303.

15. Wei, A.; Boy, K. M.; Kishi, Y., Biological Evaluation of Rationally Modified Analogs of the H-Type II Blood Group of Trisaccharide. A Correlation between Solution Conformation and Binding Affinity. *J. Am. Chem. Soc.* **1995,** 117, 9432-9436.

16. Wang, J.; Kovac, P.; Sinay, P.; Glaudemans, C. P. J., Synthetic *C*-Oligosaccharides Mimic their Natural, Analogous Immunodeterminants in Binding to Three Monoclonal Immunoglobulins. *Carbohydrate Res.* **1998,** 308, 191-193.

17. Liu, S.; Ben, R. N., *C*-Linked Galactosyl Serine AFGP Analogues as Potent Recrystallization Inhibitors. *Org. Lett.* **2005,** 7, 2385-2388.

18. Eniade, A. A.; Purushotham, M.; Ben, R. N.; Wang, J. B.; Horwath, K., A Serendipitous Discovery of Antifreeze Protein-Specific Activity in *C*-Linked Antifreeze Glycoprotein Analogs. *Cell Biochem. Biophys.* **2003,** 38, 115-124.

19. Ben, R. N.; Eniade, A. A.; Hauer, L., Synthesis of a *C*-linked Antifreeze Glycoprotein (AFGP) Mimic: Probes for Investigating the Mechanism of Action. *Org. Lett.* **1999,** 1, 1759-1762.

20. Eniade, A. A.; Ben, R. N., Fully Convergent Solid Phase Synthesis of Antifreeze Glycoprotein Analogues. *Biomacromolecules* **2001,** 2, 557-561.

21. Czechura, P.; Tam, R. Y.; Dimitrijevic, E.; Murphy, A. V.; Ben, R. N., The Importance of Hydration for Inhibiting Ice Recrystallization with *C*-Linked Antifreeze Glycoproteins. *J. Am. Chem. Soc.* **2008,** 130, 2928-2929.

22. Galema, S. A.; Hoiland, H., Stereochemical Aspects of Hydration of Carbohydrates in Aqueous Solutions. 3. Density and Ultrasound Measurements. *J. Phys. Chem.* **1991,** 95, 5321-5326.

23. Furuki, T., Effect of Stereochemistry on the Anti-Freeze Characteristics of Carbohydrates. A Thermal Study of Aqueous Monosaccharides at Subzero Temperatures. *Carbohydrate Res.* **2000,** 323, 185-191.

24. Sei, T.; Gonda, T.; Arima, Y., Growth Rate and Morphology of Ice Crystals Growing in a Solution of Trehalose and Water. *J. Cryst. Growth* **2002,** 240, 218-229.

25. Hagiwara, T.; Hartel, R. W.; Matsukawa, S., Relationship between Recrystallization Rate of Ice Crystals in Sugar Solutions and Water Mobility in Freeze-Concentrated Matrix. *Food Biophys.* **2006,** 1, 74-82.

26. Gage, A. A.; Baust, J., Mechanisms of Tissue Injury in Cryosurgery. *Cryobiology* **1998,** 37, 171-186.

27. Mazur, P., Principles of Cryobiology. In *Life in the Frozen State*, 1 ed.; Fuller, B.; Lane, N.; Benson, E. E., Eds. CRC Press: 2004; pp 3-66.

28. Farrant, J.; Walter, C. A.; Lee, H.; McGann, L. E., Use of Two-Step Cooling Procedures to Examine Factors Influencing Cell Survival Following Freezing and Thawing. *Cryobiology* **1977,** 14, 273-286.

29. Hossain, A. M.; Osuamkpe, C. O., Sole Use of Sucrose in Human Sperm Cryopreservation. *Arch. Andrology* **2007,** 53, 99-103.

30. Scheinkonig, C.; Kappicht, S.; Kolb, H.-J.; Schleuning, M., In Vitro Studies: Adoption of Long-Term Cultures to Evaluate the Cryoprotective Potential of Trehalose for Freezing Hematopoietic Stem Cells. *Bone Marrow Transplant.* **2004,** 34, 531-536.

31. Sugimachi, K.; Roach, K. L.; Rhoads, D. V.; Tompkins, R. G.; Toner, M., Nonmetabolizable Glucose Compounds Impart Cryotolerance to Primary Rat Hepatocytes. *Tissue Eng.* **2006,** 12, 579-588.

32. Beattie, G. M.; Crowe, J. H.; Lopez, A. D.; Cirulli, V.; Ricordi, C.; Hayek, A., Trehalose: A Cryoprotectant That Enhances Recovery and Preserves Function of Human Pancreatic Islets After Long-Term Storage. *Diabetes* **1997,** 46, 519-523.

33. Katenz, E.; Vondran, F. W. R.; Schwartlander, R.; Pless, G.; Gong, X.; Cheng, X.; Neuhaus, P.; Sauer, I. M., Cryopreservation of Primary Human Hepatocytes: The Benefit of Trehalose as an Additional Cryoprotective Agent. *Liver Transplant.* **2007,** 13, 38-45.

34. Dashnau, J. L.; Sharp, K. A.; Vanderkooi, J. M., Carbohydrate Intramolecular Hydrogen Bonding Cooperativity and Its Effect on Water Structure. *J. Phys. Chem. B* **2005,** 109, 24152-24159.

35. Tachibana, Y.; Fletcher, G. L.; Fujitani, N.; Tsuda, S.; Monde, K.; Nishimura, S.-I., Antifreeze Glycoproteins: Elucidation of the Structural Motifs That Are Essential for Antifreeze Activity. *Angew. Chem. Int. Ed.* **2004,** 43, 856-862.

36. McDonald, S. M.; Brady, J. W.; Clancy, P., Molecular Dynamics Simulatoins of a Winter Flounder "Antifreeze" Polypeptide in Aqueous Solution. *Biopolymers* **1993,** 33, 1481-1503.

37. McDonald, S. M.; White, A.; Clancy, P.; Brady, J. W., Binding of an Antifreeze Polypeptide to an Ice/Water Interface via Computer Simulation. *AIChE J.* **1995,** 41, 959-973.

38. Baardsnes, J.; Davies, P. L., Contribution of Hydrophobic Residues to Ice Binding By Fish Type III Antifreeze Protein. *Biochim. Biophys. Acta* **2002,** 1601, 49-54.

39. Chao, H.; Housten, M. E. J.; Hodges, R. S.; Kay, C. M.; Sykes, B. D.; Loewen, M. C.; Davies, P. L.; Sonnichsen, F. D., A Diminished Role for Hydrogen Bonds in Antifreeze Protein Binding to Ice. *Biochemistry* **1997,** 36, 14652-14660.

40. Karim, O. A.; Haymet, A. D. J., The Ice/Water Interface. *Chem. Phys. Lett.* **1987,** 138, 531-534.

41. Zhang, W.; Laursen, R. A., Structure-Function Relationships in a Type I Antifreeze Polypeptide: The Role of Threonine Methyl and Hydroxyl Groups in Antifreeze Activity. *J. Biol. Chem.* **1998,** 273, 34806-34812.

42. Jorov, A.; Zhorov, B. S.; Yang, D. S. C., Theoretical Study of Interaction of Winter Flounder Antifreeze Protein with Ice. *Protein Sci.* **2004,** 13, 1524-1537.

43. Yang, C.; Sharp, K. A., Hydrophobic Tendency of Polar Group Hydration as a Major Force in Type I Antifreeze Protein Recognition. *PROTEINS: Struct., Funct., Bioinf.* **2005,** 59, 266-274.

44. Galema, S. A.; Howard, E.; Engberts, J. B. F. N.; Grigera, J. R., The Effect of Stereochemistry upon Carbohydrate Hydration. A Molecular Dynamics Simulation of β-D-Galactopyranose and (α,β)-D-Talopyranose. *Carbohydrate Res.* **1994,** 265, 215-225.

45. Cheetham, N. W. H.; Lam, K., Molecular Dynamics Simulations of Glycosides in Aqueous Solution. *Carbohydrate Research* **1996,** 282, 13-23.

46. Quirion, J.-C.; Castelot-Deliencourt-Godefroy, G. Gem Difluorinated C-Glycopeptides, their Preparation and their Use for the Preservation of Biological Materials and/or in Cryosurgery. WO 2006/059227 A1, June 8 2006, 2006.

47. Cuenca, A. B.; D'Hooge, F.; Gouge, V.; Castelot-Deliencourt, G.; Oulyadi, H.; Leclerc, E.; Jubault, P.; Pannecoucke, X.; Quirion, J.-C., Addition of Ethyl Bromodifluoroacetate to Lactones: Reactivity and Stereoselectivity. *Synlett* **2005,** 2005, 2627-2630.

48. Plantier-Royon, R.; Portella, C., *C*-Difluoromethylene-Containing, *C*-Trifluoromethyl and *C*-Perfluoroalkyl Carbohydrates. Synthesis by Carbohydrate Transformation or Building Block Methods. *Carbohydrate Res.* **2000,** 327, 119-146.

49. Brigaud, T.; Lefebvre, O.; Plantier-Royon, R.; Portella, C., Mixed Organofluorine - Organosilicon Chemistry. 6. Synthesis of Gem-Difluoro-*C*-Glycosides and *C*-Disaccharides from Acylsilanes and Trifluoromethyltrimethylsilane. An Exploratory Study. *Tetrahedron Lett.* **1996,** 37, 6115-6116.

50. Dunitz, J. D.; Taylor, R., Organic Fluorine Hardly Ever Accepts Hydrogen Bonds. *Chem. Eur. J.* **1997,** 1, 89-98.

51. Wang, G.; Cheuk, S.; Yang, H.; Goyal, N.; Reddy, P. V. N.; Hopkinson, B., Synthesis and Characterization of Monosaccharide-Derived Carbamates as Low-Molecular-Weight Gelators. *J. Am. Chem. Soc.* **2009,** DOI: 10.1021/la804337g.

52. Evans, C. L.; Potma, E. O.; Puoris'haag, M.; Cote, D.; Lin, C. P.; Xie, X. S., Chemical imaging of tissue in vivo with video-rate coherent anti-Stokes Raman scattering microscopy. *Proc. Nat. Acad. Sci. USA* **2005,** 102, 16807-16812.

53. Muller, M.; Zumbusch, A., Coherent anti-Stokes Raman Scattering Microscopy. *ChemPhysChem* **2007,** 8, 2156-2170.

Chapter 3 : Antifreeze Activity of Simple Mono- and Disaccharides

3.1 Evaluation of the IRI Activity of Mono- and Disaccharides and the Link to Carbohydrate Hydration

3.1.1: Hydration of Carbohydrates

Carbohydrates are involved in nearly all biological processes. Their biological activity has been shown to be linked to their hydration, or their interaction with water molecules. Water is important in maintaining protein stability[1] and carbohydrate conformation;[2, 3] and it mediates the solubility, osmotic pressure, and melting temperature of carbohydrates,[4] among other functions. Several researchers have examined the hydration of carbohydrates in an effort to further understand its role in biological functions.

The hydration of sugars depends on their structure. One theory is that hydration depends on the number of equatorial hydroxyl groups, which are reported to be better hydrated than axial hydroxyl groups.[5-7] Lopez de la Paz et al. have proposed that hydrogen bond networks of water molecules form when carbohydrates are hydrated.[8] Galema et al. have reported that the hydration differs based on the distance of the next nearest neighbouring hydroxyl group, which is dependent on the relative stereochemistry of the hydroxyl groups at C-2 and C-4.[9] In other words, the compatibility of the carbohydrate with the oxygen distances in water is dependent on the oxygen distances within the carbohydrate.[9] Dashnau et al., in a similar hypothesis, suggest that the orientation of the carbohydrate hydroxyl groups affects the water structure in the first surrounding hydration shell.[10] The hydroxyl group at position four (OH-4) was shown to be particularly important because it is able to be involved in several different hydrogen bond networks within the carbohydrate.[10] The formation of an intramolecular hydrogen bond between OH-2 and OH-4 in talose has been observed. This intramolecular hydrogen bond is suggested to account for the observation that talose is said to be more hydrophobic and less hydrated than galactose or glucose.[11, 12]

Hydration has been also implicated in ice growth and recrystallization. Kawai et al. have observed using NMR that the amount of unfrozen water molecules in a sugar solution is correlated to the number of equatorial hydroxyl groups on the sugar, which in turn have been correlated with the hydration of carbohydrates.[13] Furuki has used differential scanning calorimetry to show that there is a greater amount of unfrozen water in aqueous solutions of carbohydrates that have a poorer compatibility with the hydrogen bond network of water.[14] To explain the ability of the disaccharide trehalose to act as an efficient cryoprotectant, Branca and co-workers have hypothesized that by disrupting the tetrahedral hydrogen bond network of water, trehalose can prevent water molecules from adopting orientations that are compatible with the formation of ice.[15, 16] Magazu et al. have further suggested that the disruption of the tetrahedral network of water by trehalose reduces the number of hydrogen bonds that are oriented in a manner that would normally promote the formation of ice.[17]

The activity of biological antifreezes depends on their ability to interact with water and ice. Antifreeze-water and antifreeze-ice hydrogen bonds have been implicated both in maintaining stability of the AFP and in binding to ice,[18, 19] which is necessary for thermal hysteresis and ice-recrystallization inhibition (IRI) activity. Recently, our laboratory has shown that the IRI activity of *C*-linked AFGP analogues is dependent on the hydration of the carbohydrate portion of the analogue (see Figures 2.6, 2.7, 2.8).[20] These observations led us to question whether simple carbohydrates display IRI activity in the absence of a peptide component. The trends observed for the *C*-linked glycopeptide series (**1-4**) suggest that this may be the case. However, to the best of our knowledge, a systematic study of the IRI activity of carbohydrates has not been conducted. Furthermore, we sought to determine whether the potential IRI activity of carbohydrates is linked to their hydration.

Molecular dynamics experiments have contributed to our understanding of carbohydrate hydration. Lee et al. have shown that carbohydrates can disrupt the tetrahedral arrangement of water molecules surrounding themselves and can also reduce the rotational and translational motion.[1] Furthermore, trehalose (**11**) and sucrose (**13**) (disaccharides) cause greater restrictions in the movement of water molecules than

glucose (**6**) (a monosaccharide).[1] In addition, disaccharides are able to influence the dynamics of water into the second hydration shell, while monosaccharides display a smaller influence, and this has been correlated to the number of hydrogen bonds formed between the carbohydrate and water.[21] In agreement with these results, Galema and Hoiland have predicted through density ultrasound measurements that disaccharides have partial molar compressibilities and hydration numbers that are nearly double that of monosaccharides.[9] The isentropic partial molar compressibility (PMC) of a solute is a measure of how much the hydrogen-bonded structure of water is disturbed by that solute. The more negative the PMC value, the more the hydration layer is disturbed compared to pure water. Based upon these results for mono- and disaccharides, we can conclude that in addition to the structure, the size of the carbohydrate clearly plays a role in hydration. For these reasons, we chose a series of mono- and disaccharides for our study, and their partial molar compressibilities, hydration numbers, and chemical structures are reported in Table 3.1.

Table 3.1: Isentropic molar compressibility ($10^4K_2^o(s)$, $cm^3\ mol^{-1}\ bar^{-1}$) and hydration numbers of various monosaccharides and disaccharides.[22] Errors of molar compressibility values and hydration numbers are shown in parentheses.[5, 9]

Carbohydrate	Molar Compressibility ($K_2^o(s)x10^4$, $cm^3\ mol^{-1}\ bar^{-1}$)	Hydration Number[9]	Carbohydrate	Molar Compressibility ($K_2^o(s)x10^4$, $cm^3\ mol^{-1}\ bar^{-1}$)	Hydration Number[9]
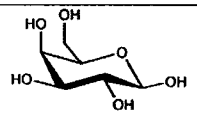 D-Galactose (**5**)	-20.8 (0.5)[5] -20.4 (0.4)[9]	8.7 (0.2)	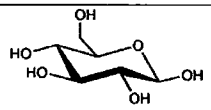 D-Glucose (**6**)	-17.6 (0.3)[9]	8.4 (0.2)
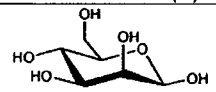 D-Mannose (**7**)	-16.0 (0.5)[5]	8.1 (0.2)	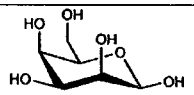 D-Talose (**8**)	-11.9 (0.3)[9]	7.7 (0.2)
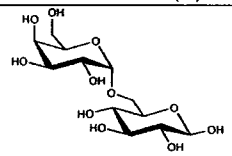 D-Melibiose (**9**)	-31.2 (1.0)[9]	15.5 (0.3)	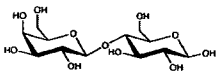 D-Lactose (**10**)	-31.1 (0.2)[9] -30.4 (1.0)[5]	15.3 (0.3)
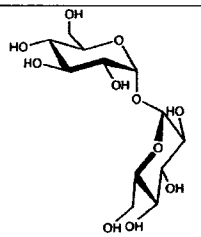 D-Trehalose (**11**)	-30.2 (0.3)[9]	15.3 (0.3)	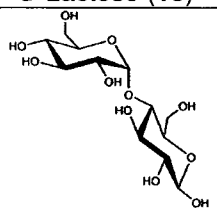 D-Maltose (**12**)	-23.7 (1.0)[5]	14.5 (0.3)
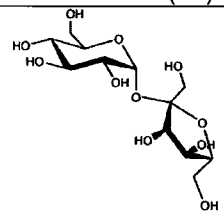 D-Sucrose (**13**)	-17.8 (0.5)[5]	13.9 (0.3)			

3.1.2: Antifreeze Activity of Native Mono- and Disaccharides

We initially tested three monosaccharides and three disaccharides for thermal hysteresis activity (Table 3.2).[22] The ice crystal morphology was disk-like for each carbohydrate tested, indicating that there was no dynamic ice shaping activity.

Furthermore, thermal hysteresis activity was not observed. Colligative properties of the carbohydrates accounted for the slight freezing point depressions that were observed. The lack of dynamic ice shaping (the ice crystal morphology for the carbohydrate solutions was the same as that of pure distilled water) indicated that there is no direct interaction of the carbohydrates with the ice lattice. This is in contrast to results from Baruch et al., who proposed that the structure of the carbohydrate determines its ability to interact with the ice lattice.[23] They suggest that pyranose rings with 1,3-trans-configured hydroxyl groups are able to depress freezing points because the 4.2-4.5 Å distance between these hydroxyl groups is a direct match to the ice lattice.[23] However, no clear trends in freezing point depression based on carbohydrate structure were observed in our study. Furthermore, the lack of dynamic ice shaping in our study suggests that there is no interaction at all between the carbohydrates and the ice.

Table 3.2: Ice crystal morphology and melting points of 10 mg/mL solutions of carbohydrates in double-distilled water, determined using nanoliter osmometry.[22, 24]

Carbohydrate	Melting Point (ºC)	Crystal Morphology	Carbohydrate	Melting Point (ºC)	Crystal Morphology
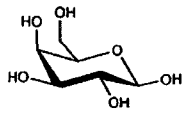 D-Galactose (**5**)	-0.069	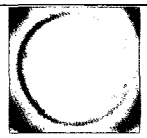	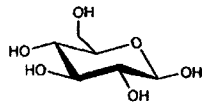 D-Glucose (**6**)	-0.055	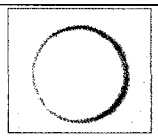
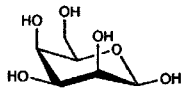 D-Talose (**8**)	-0.22	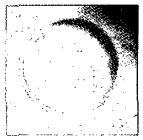	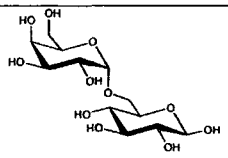 D-Melibiose (**9**)	-0.17	
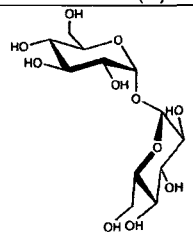 D-Trehalose (**11**)	-0.015	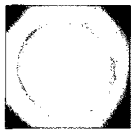	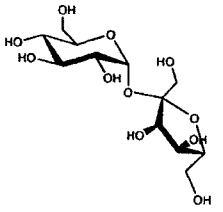 D-Sucrose (**13**)	-0.12	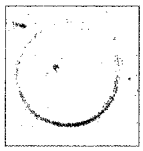

With these results in hand, we examined the IRI activity of several mono- and disaccharides as a second measure of antifreeze activity. All IRI experiments were conducted according to the procedure reported by Jackman et al.[25] In order to determine an appropriate carbohydrate concentration for these experiments, a concentration scan of D-galactose (**5**) was performed. A 0.22 M solution of galactose (**5**) was found to be a potent inhibitor of recrystallization (Figure 3.1).[22] However, the solution was very viscous which adversely affected the performance of the assay and made quantification of ice crystal mean grain size difficult. For this reason, a lower concentration was desired for future studies. There was no statistically significant difference between 0.044 M and 0.022 M solutions of galactose as determined using a Student's T-test,[26] so concentrations of 0.022 M were employed for all carbohydrates.

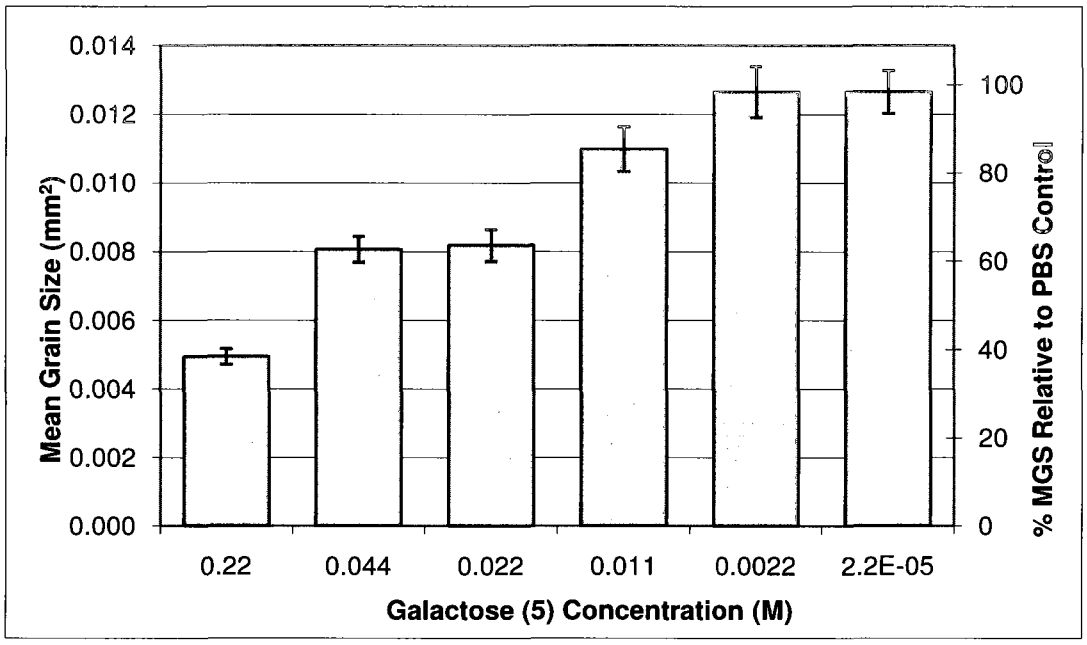

Figure 3.1: IRI activity of various concentrations of D-galactose (**5**) in PBS[22]

When this data was plotted in a log plot, a logarithmic relationship was observed between galactose concentration and IRI activity (Figure 3.2). There appears to be a limiting effect at concentrations below 0.0022 M, whereby the ice crystals in dilute galactose solutions were approaching the size of ice crystals in the PBS negative control. These results suggest that at higher concentrations, the recrystallization inhibition activity of galactose is non-colligative, as has been suggested by Uchida et al. when examining ice crystal size in the presence of trehalose solutions.[27]

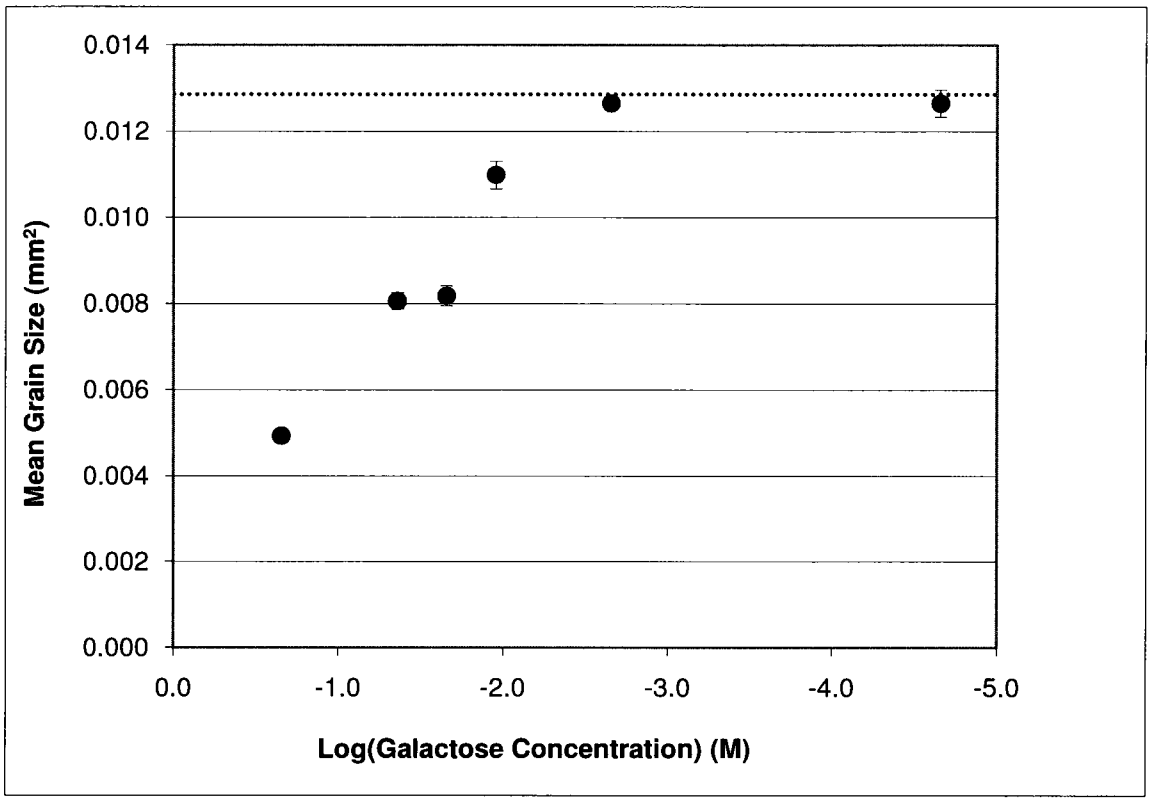

Figure 3.2: IRI activity of various galactose concentrations in PBS solution. The dashed line represents the IRI activity of the PBS negative control. The x-axis represents the $\log_{10}$(concentration) of galactose.[22]

Once we had determined that 0.022 M was an appropriate concentration for our IRI assay, we tested four monosaccharides and five disaccharides (Table 3.1) for ice-recrystallization inhibition (IRI) activity and the results are displayed in Figure 3.3. It is clear that some carbohydrates do display reasonable IRI activity, with galactose and melibiose solutions forming ice crystals that were approximately 40% smaller than in the PBS control. However, the structure of the carbohydrate clearly plays a role in determining whether a saccharide will have IRI activity.

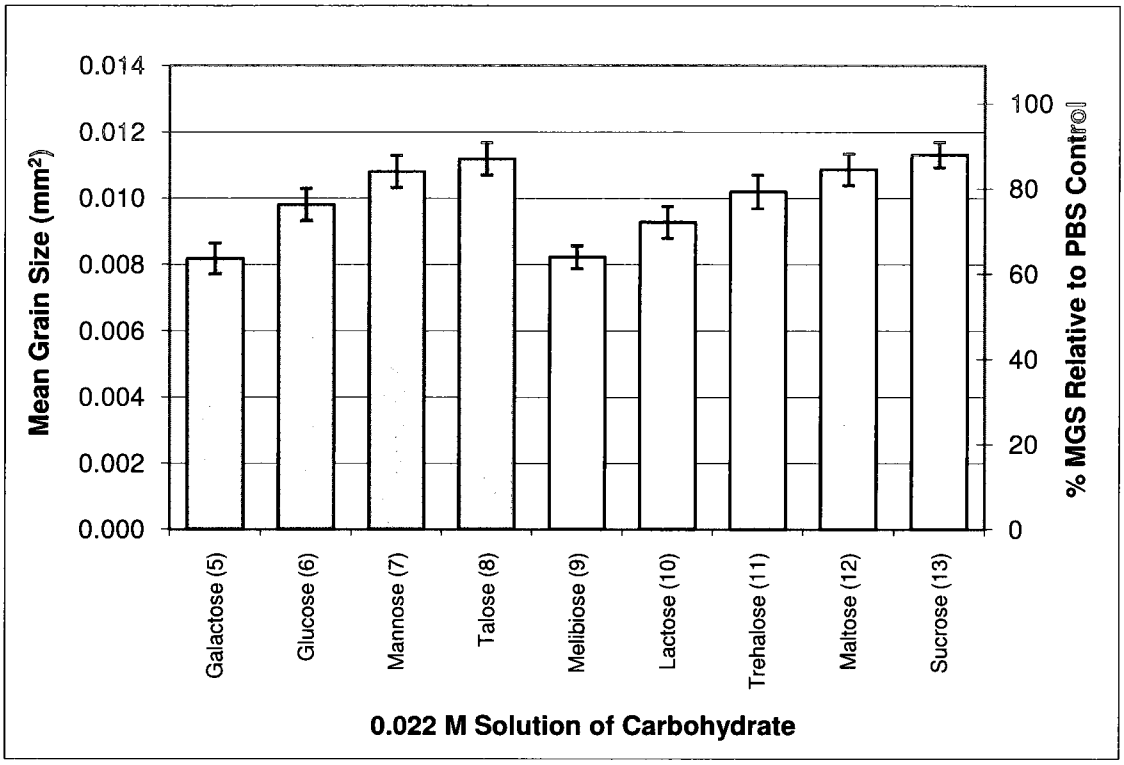

Figure 3.3: IRI activity of 0.022 M solutions of mono- and disaccharides in PBS. Monosaccharides are represented in blue and disaccharides are shown in yellow.[22]

3.1.3: Hydration of Native Mono- and Disaccharides and its Link to IRI Activity

It has been suggested that the stereochemistry of the hydroxyl groups of a carbohydrate is important in determining that carbohydrate's hydration properties.[9] The compatibility of the hydroxyl groups on the carbohydrate with the hydrogen bonded network of water is dependent on the hydroxyl stereochemistry and the distance between the hydroxyl groups.[9] We have observed that the IRI activity of a series of *C*-linked AFGP analogues can be linked to the hydration of the carbohydrate component.[20] In this study, we observed that analogues with low isentropic molar compressibilities (such as galactose) that have a poor fit into the three-dimensional hydrogen bonded network of water were good recrystallization-inhibitors.[20] While these earlier observations were based on hydration as a function of isentropic molar compressibilities (Figure 2.8),[20] there may be measures of solute hydration that are more reflective of the hydration state in solution.

Density ultrasound measurements have emerged as one of the best techniques for studying solute hydration because it is able to delineate between very subtle differences in solution structure.[28] This experimental method is able to distinguish between water molecules that are tightly bound to a solute from those that are only loosely associated with the solute. Density ultrasound has been used to determine molar compressibility coefficients, but recent studies have shown that hydration numbers (HNs) calculated from these coefficients more accurately represent the contributions to hydration of a carbohydrate.[29] Hydration numbers predict the total number of water molecules that are hydrogen bonded to the carbohydrate. They can also be thought of as a dynamic measurement which calculates the number of water molecules that are tightly bound to the carbohydrate, and thus move with the carbohydrate in solution.

We proposed that the hydration of the carbohydrates, which is dependent on carbohydrate structure, is responsible for imparting antifreeze activity. In order to explore this hypothesis, we examined the IRI activity as a function of carbohydrate hydration. Since hydration numbers have been reported to be a more accurate representation of carbohydrate hydration than partial molar compressibilities, we plotted the IRI activity as a function of hydration number (Figure 3.4).

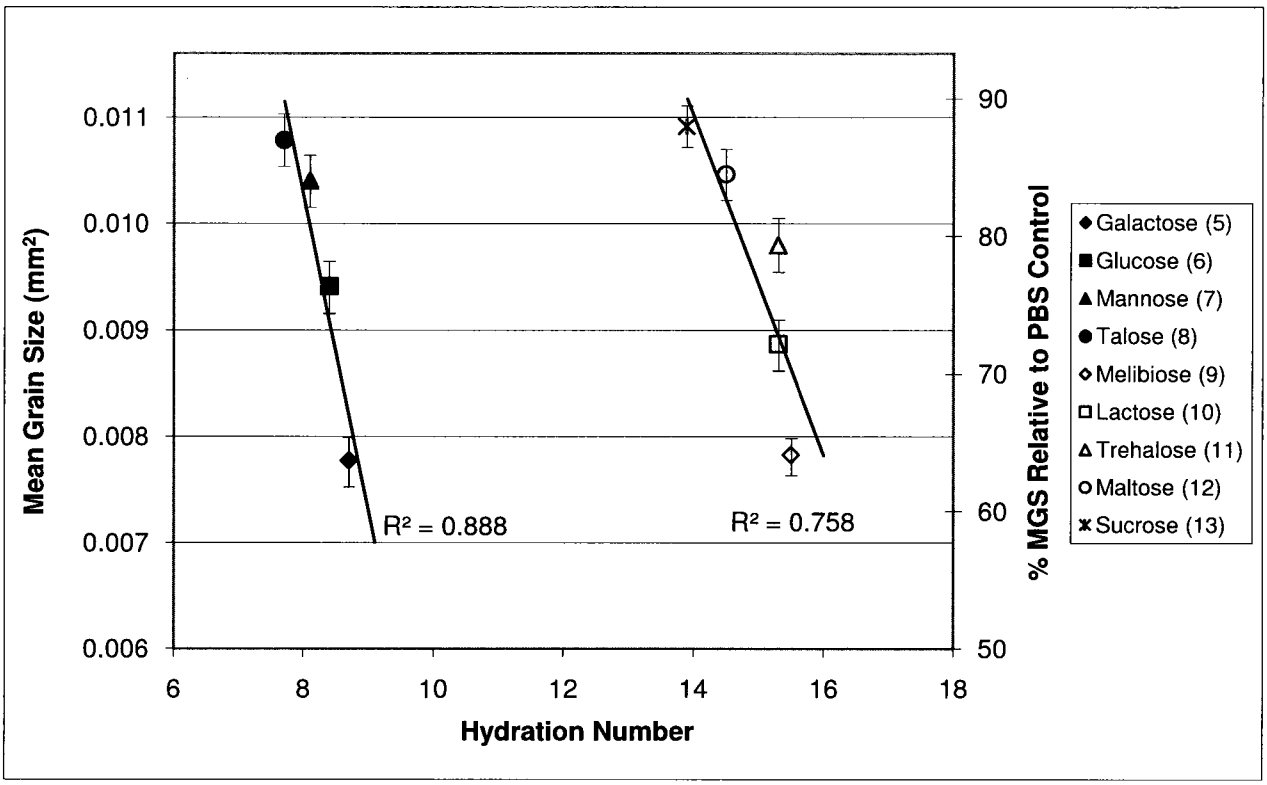

Figure 3.4: IRI activity of 0.022 M solutions of various mono- and disaccharides in PBS, plotted against their respective hydration numbers. Monosaccharides are represented in blue and disaccharides are shown in yellow.[22]

From this graph, it is clear that the monosaccharides and disaccharides show two distinct linear relationships between hydration number and IRI activity. However, the increase in hydration for disaccharides compared to monosaccharides did not result in the expected increase in IRI activity. As mentioned above, disaccharides have been shown to be better hydrated than monosaccharides, and they disturb the three-dimensional structure of water more than monosaccharides. This is evident by the fact that disaccharides have hydration numbers and partial molar compressibilities that are nearly double that of monosaccharides (Table 3.1). In our experiments, the IRI activity of galactose (**5**) and melibiose (**9**) were approximately identical, despite the fact that melibiose (**9**) has a hydration number (HN) of 15.5 which is nearly twice that of galactose (**5**) (HN = 8.7). More surprisingly, the larger hydration number of sucrose (**13**) (HN = 13.9) compared to galactose (**5**) actually resulted in a decrease in IRI activity.

At this point, we had to consider the factors that affect hydration and IRI activity. Firstly, the stereochemistry of the hydroxyl groups on the carbohydrate seems to play a role. This factor is represented in the hydration number, which describes the number of water molecules that are tightly bound to the solute, because the hydration number is dependent on carbohydrate hydroxyl stereochemistry. Secondly, it seems reasonable that the size or volume of the carbohydrate would affect the "fit" into bulk water and would therefore affect hydration and the carbohydrate's ability to inhibit ice recrystallization. There is a difference in steric volume in going from monosaccharides to disaccharides. In order to account for this factor, we corrected the hydration numbers for a volume component. To do so, the hydration numbers obtained from the literature were divided by the partial molar volumes (PMV) for each carbohydrate. This gives a description of the number of tightly bound water molecules per molar volume of carbohydrate, and we refer to this value as a *hydration index*. When the IRI activity was plotted against the hydration index of carbohydrates, a single correlation was observed for all mono- and disaccharides (Figure 3.5).

This result is significant because it suggests that although the absolute number of water molecules surrounding a carbohydrate is important for predicting IRI activity, the number of water molecules per unit volume also plays a significant role. Therefore, a higher concentration (number of water molecules per unit volume) of water molecules around a solute must cause a greater disturbance of the surrounding bulk water, which leads to increased IRI activity.

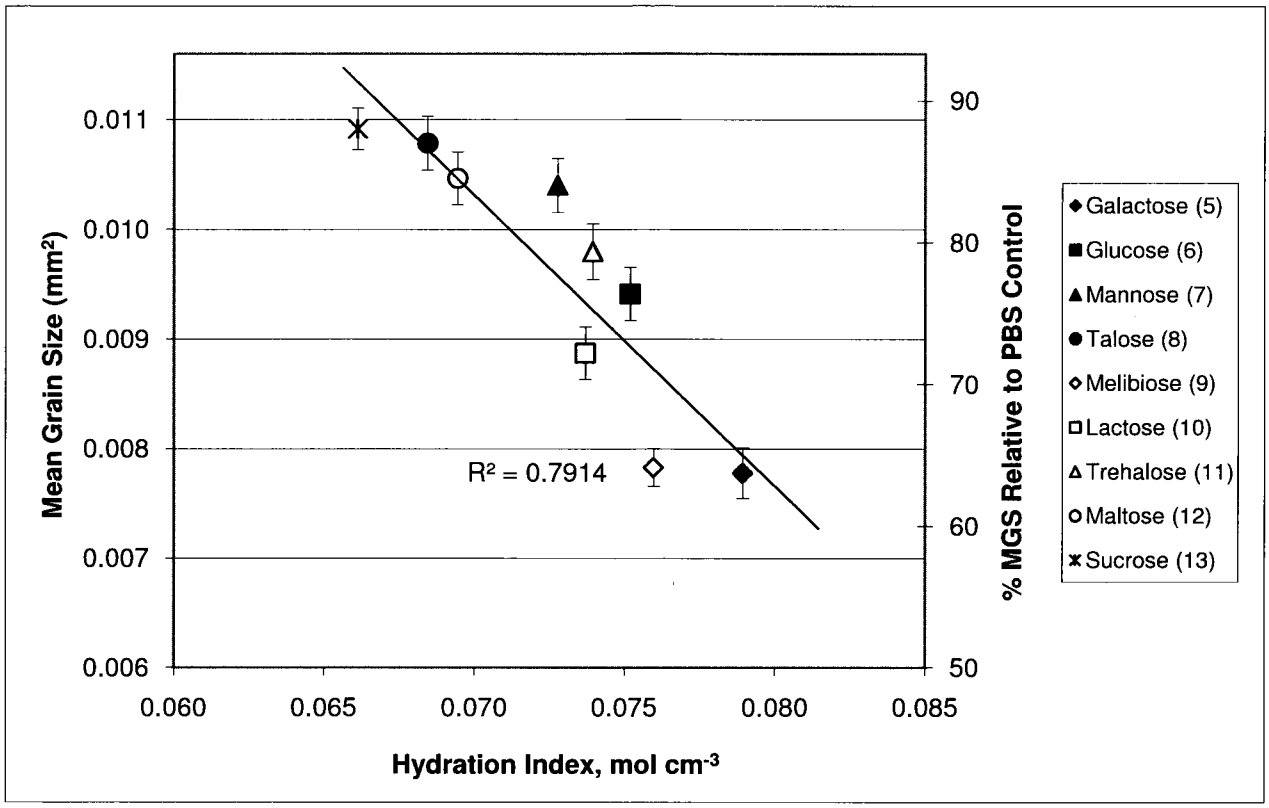

Figure 3.5: IRI activities of monosaccharides (blue points) and disaccharides (yellow points) plotted against their respective hydration index. Hydration index = hydration number ÷ partial molar volume (mol^1 cm^{-3})[22]

3.1.4: Comparison to DMSO:

Since recrystallization of ice is known to be the main cause of damage to cells during the thawing cycle of cryopreservation protocols, the IRI activity of galactose (**5**) was compared to that of a known cryoprotectant, dimethyl sulfoxide (DMSO). DMSO is often added to cryopreservation protocols to increase cell viability post thaw at concentrations between 1 and 20%. Recent studies have suggested that little additional cryoprotection is achieved at concentrations above 5%.[30] To the best of our knowledge, the ability of DMSO to inhibit recrystallization of ice has not been explored. We performed a concentration scan of DMSO, and the results are displayed in Figure 3.10.

DMSO concentrations of 0.1 to 4% were assessed in our study. At concentrations of 6% and higher, large portions of the wafer remained unfrozen during

the assay and therefore results were inconsistent. For this reason, only concentrations below 6% were reliably assessed and are presented in Figure 3.6. A 0.1% solution of DMSO was unable to function as a recrystallization inhibitor and produced ice crystals that were statistically identical to the PBS control. However, a 4% DMSO solution showed IRI activity that was greater than 0.022 M galactose (**5**). A 0.022M solution of galactose (**5**) was approximately as good at inhibiting recrystallization of ice as a 3% solution of DMSO. These results suggest that galactose may be used as a suitable cryoprotectant. Studies are ongoing to observe the cryoprotective effect of galactose (**5**) and to determine if there is a correlation between IRI activity and cryopreservation ability. The results of these studies will be discussed in the next section of this dissertation.

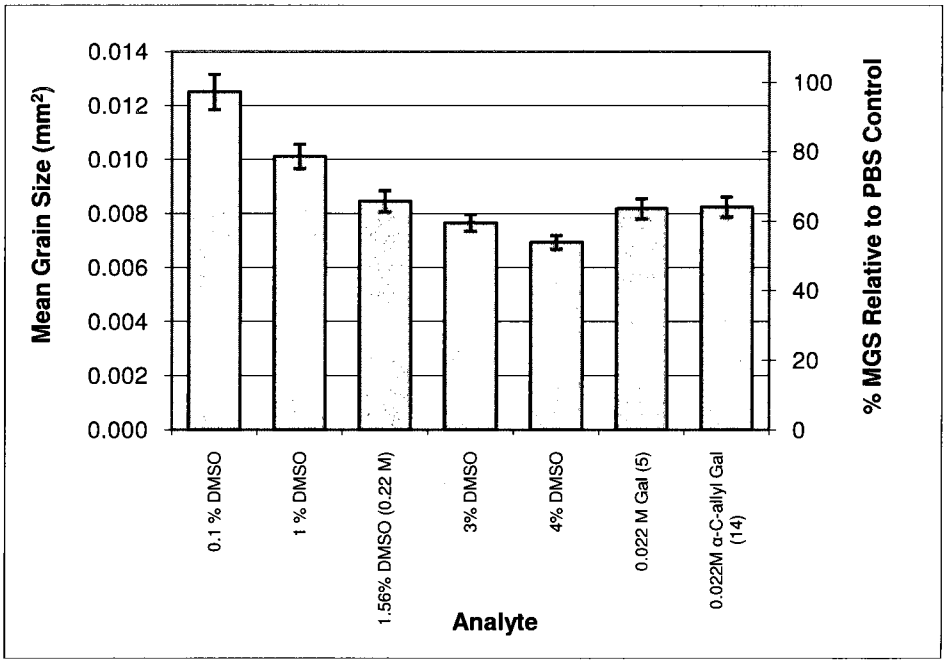

Figure 3.6: IRI activity of various concentrations of DMSO and 0.022 M solutions of galactose (**5**) and α-*C*-allyl-galactose (**14**) in PBS.[22]

3.1.5: Proposed Mechanism of Ice-Recrystallization Inhibition

Recrystallization has been well studied in metallurgy in reference to inorganic composites,[31-33] however the mechanism of ice-recrystallization has yet to be fully understood. Several researchers have observed the existence of a semi-ordered layer of ice (called the quasi-liquid layer, QLL) between the highly ordered ice lattice and the bulk water.[34, 35] When proposing a mechanism for ice-recrystallization the QLL should be taken into account, although this has only rarely been the case in the past. Our results suggest that a direct interaction between carbohydrates and the ice lattice is not occurring, since we observed no dynamic ice shaping or thermal hysteretic activity. Carbohydrates are not thought to be incorporated into growing ice crystals, and it is proposed that they will become concentrated in the interface between two adjacent ice crystals and their QLLs as they are excluded from the ice lattice during ice growth and recrystallization. Figure 3.7 shows a representation of a carbohydrate being solvated in bulk water between two adjacent ice crystals and their QLLs.

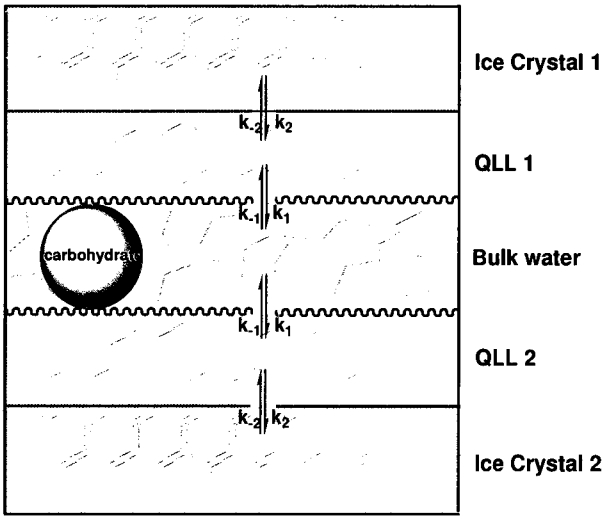

Figure 3.7: Schematic representation of the proposed mechanism for ice recrystallization inhibition. Carbohydrates reside at the QLL-bulk water interface between two adjacent ice crystals. Water molecules surrounding a carbohydrate with a high hydration index are more disordered than those surrounding a low hydration index carbohydrate or in the absence of a solute. The red shaded area represents a hydrated solute. QLL = quasi-liquid layer[22]

The exact location of the carbohydrate in relation to the QLL is difficult to ascertain, given the difficulties in studying the QLL, although two possibilities exist. In the first, the carbohydrate is located at the bulk water – QLL interface, whereas in the second, the carbohydrate is incorporated directly into the QLL. No precedent has been shown for the second possibility, whereas Uchida et al. have also suggested that carbohydrates such as trehalose function at the QLL – bulk water interface.[27] We propose that ice recrystallization inhibition is dependent on the interaction of the carbohydrate with the QLL, which in turn is dependent on the carbohydrate's hydration and stereochemistry.

Based on the results of this study, it seems that carbohydrates with a large hydration index positioned at the QLL – bulk water interface disturb the order of bulk water surrounding the hydration shell more than those with a smaller hydration index. This greater disorder of the bulk water increases the energy associated with transferring a water molecule from the bulk water to the QLL. Therefore, carbohydrates with larger hydration indices (such as galactose (**5**) and melibiose (**9**)) function as better ice-recrystallization inhibitors. Furthermore, disaccharides with larger hydration numbers than monosaccharides do not necessarily act as improved recrystallization inhibitors. In order to inhibit recrystallization effectively, a carbohydrate must have a large number of water molecules in its hydration shell and more importantly, they must be concentrated around the solute, which increases the entropy of the surrounding bulk water and slows the transfer of water molecules from bulk water to the QLL.

3.2: Correlating IRI activity with Cytotoxicity and Cryopreservation Ability

It has been proposed that the recrystallization of ice during the thawing cycle of cryopreservation protocols causes the most damage to the sample.[36-39] For this reason, recrystallization inhibitors could be very useful in decreasing the damage to frozen samples if they were incorporated into cryopreservation media. Biological antifreezes have been explored as potential cryoprotectants due to their potent ice-recrystallization inhibition activity.

Our laboratory has observed that the ice-recrystallization inhibition activity of AFGP analogues is correlated to the hydration of the carbohydrate moiety.[20] Furthermore, we recently showed that simple mono- and disaccharides display IRI activity, and that this activity is also correlated to the hydration of the carbohydrate as described in Section 3.1.[22] Although several researchers have observed the beneficial protective effect of carbohydrates during freeze-thaw cycles,[40-44] to the best of our knowledge, a systematic study that compares the IRI activity of carbohydrates to their cryoprotective ability has not been carried out. That is the goal of the present study. Furthermore, the potential cytotoxicity of these samples at high concentrations will also be considered, as this could preclude them from being used as cryoprotectants.

In order to examine the effect of carbohydrate concentration on both IRI activity and on human liver cells at various temperatures, mono- and disaccharides were evaluated at two extreme concentrations. Figure 3.8 shows the IRI activity of several mono- and disaccharides at 22 and 220 mM. The monosaccharides show a distinct trend where the IRI activity is proportional to the hydration of the carbohydrate (galactose (**5**) > glucose (**6**) > mannose (**8**) ≈ talose (**9**)) for both concentrations. There was no statistically significant difference between the mean grain sizes for mannose and talose at either concentration, as determined using a Student's T-test Two Sample with Unequal Variance.[26] At 220 mM concentration, each of the monosaccharides formed ice crystals that were approximately 30% smaller than at 22 mM concentration.

A different trend was seen for the disaccharides. At 22 mM concentration, again the IRI activity was proportional to the hydration of the carbohydrate, in the order melibiose (**9**) > lactose (**10**) > trehalose (**11**) > sucrose (**13**). However, at 220 mM all of the disaccharides displayed very efficient IRI activity, with ice crystals being approximately 80-85% smaller than in the PBS negative control. More interestingly, the structure of the disaccharide did not seem to have a large effect on IRI activity at this high concentration. In fact, there was no statistically significant difference[26] between the mean crystal sizes for melibiose (**9**) and trehalose (**11**) at 220 mM, and lactose (**10**) and sucrose (**13**) had only slightly increased activity (less than 8%) at the same concentration. In contrast, there was a 25% difference in activity between melibiose (**9**)

and sucrose (**13**) at 22 mM. It appears that disaccharides are potent inhibitors of ice-recrystallization at 220 mM, regardless of their structure.

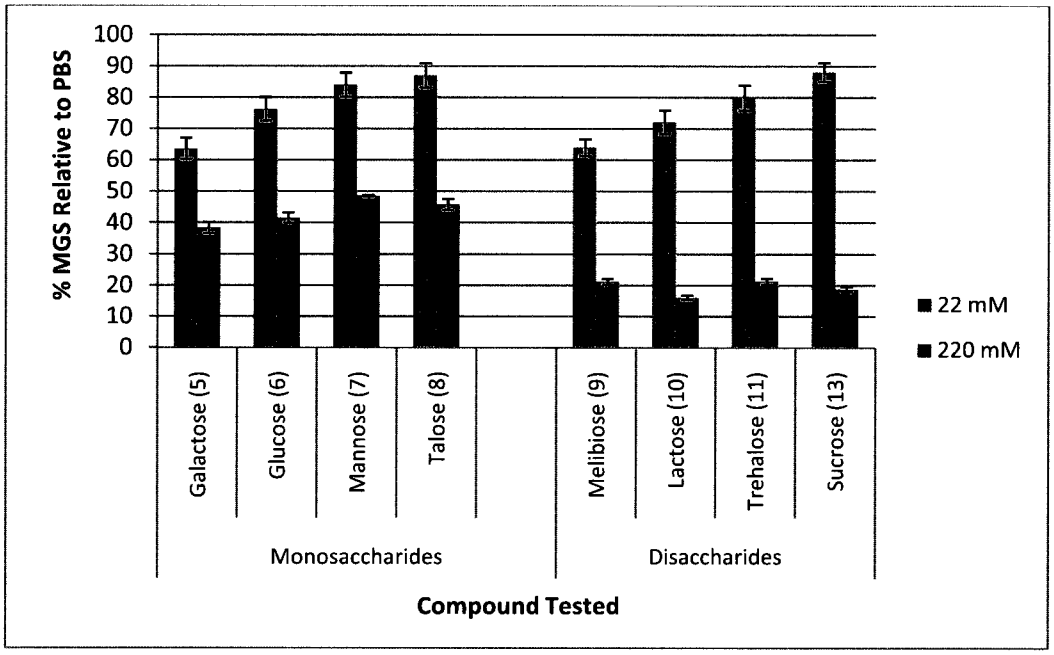

Figure 3.8: RI assay of mono- and disaccharides at two extreme concentrations of 22 mM (blue bars) and 220 mM (pink bars).

3.2.1: Preservation of Cells at Physiological Temperature

In order to determine whether there was a correlation between IRI activity and preservation of cells at physiological and sub zero temperatures, we compared the IRI activity of several carbohydrates to the results of cytotoxicity and cryopreservation assays. Cell viability assays have been previously performed in our laboratory (Wu, von Moos, Guolla, Allan, and Ben, unpublished results). Cell viability at physiological temperature (37 ºC) was assessed using an MTT viability assay, and cryopreservation ability was assessed by flow cytometry of treated cells following freeze-thaw protocols. The results of the MTT assay at physiological temperature are displayed in Figure 3.9.

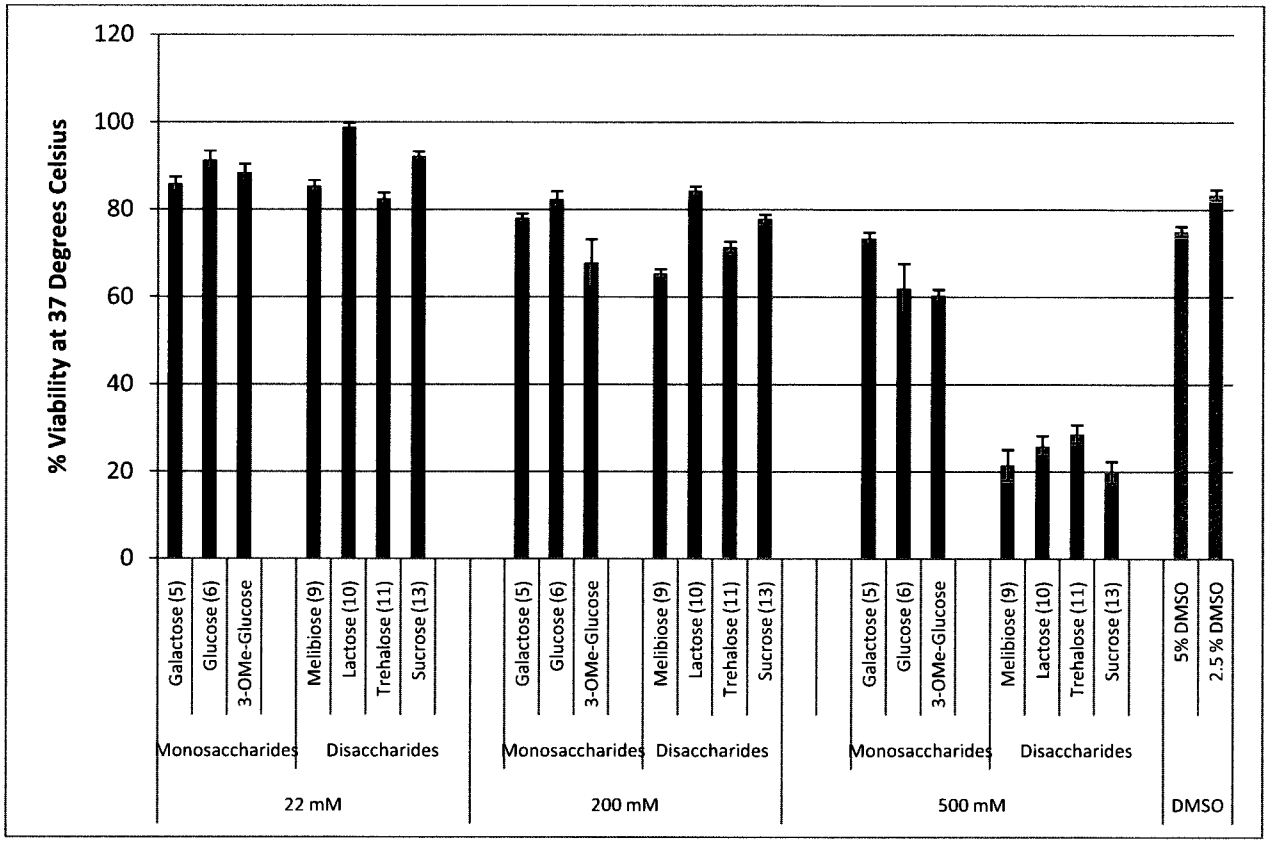

Figure 3.9: MTT assay of monosaccharides (blue bars) and disaccharides (pink bars) at 22, 200, and 500 mM. The MTT assay results for the known cryoprotectant DMSO (green) at 2.5% and 5% are shown for comparison. The y-axis represents the percentage of viable cells following treatment with the sugar for 18 hours. Data collected by Louise Guolla and Liz von Moos, unpublished results.

There are no clear trends based on carbohydrate structure in Figure 3.9. The mono- and disaccharides show similar trends at 22 and 200 mM, with glucose (**6**) being the best monosaccharide and lactose (**10**) being the best disaccharide. However, the results were different at 500 mM, where galactose (**5**) was the best monosaccharide and trehalose (**11**) was the best disaccharide. More importantly, there was a drastic decrease in cell viability for the disaccharides at 500 mM compared to the other concentrations, but only a slight decrease for the monosaccharides at 500 mM. Furthermore, cell viability following treatment with 22 and 200 mM carbohydrates was approximately equal to that following treatment with 2.5% and 5% solutions of DMSO, which is often used as a cryoprotectant.

With this cell viability data in hand, we plotted cell viability at 37 ºC versus % MGS (as a measure of IRI activity) to see if there was a correlation between these activities (Figure 3.10). Unfortunately, the viscosity of the 500 mM solutions prevented them from being assayed for IRI activity, however, concentrations of 22 mM and 200 mM were reliably assessed and are displayed in Figure 3.10. There does not appear to be a strong correlation between these parameters. This is not overly surprising, as no ice formation is occurring at physiological temperature and therefore IRI activity would not be expected to have an effect on cell preservation at 37 ºC. However, a few other observations can be made from this graph. The carbohydrates at 220 mM are clustered on the left side of the graph, and the 22 mM solutions of carbohydrates are clustered on the right. Therefore, although the 220 mM concentration resulted in potent IRI activity, they also caused more cell death in the MTT assay. The cell viability at 200 mM ranged from 84% for lactose (**10**) to only 65% for melibiose (**9**).

The exact mechanisms for the cytotoxicity of high concentrations of carbohydrates are unknown, although it has been observed that not all carbohydrates support the growth of cells at the same rate.[45] There are three mechanisms by which carbohydrates can enter viable cells, which are bidirectional transbilayer diffusion, protein-mediated bidirectional facilitated diffusion, and protein mediated active transport.[46] Monosaccharides such as glucose are able to enter the cell through GLUT receptors in the membranes.[46] However, disaccharides can only enter the cells via endocytosis.

High concentrations of carbohydrates in the medium outside the cells will certainly result in a concentration gradient, causing water to flow out of the cell by ex-osmosis. This will result in cell shrinkage, leading to osmotic and oxidative stress.[47] It has been observed that cell shrinkage is associated with apoptotic cell death, and this resulted in the suggestion that cell shrinkage may trigger signals that lead to apoptosis.[47] Therefore, it is possible that in the presence of high concentrations of carbohydrates, particularly those that are unable to penetrate the cells rapidly, cell shrinkage will occur in response to the concentration gradient that forms. This cell shrinkage may trigger apoptosis in the presence of these solutions. This theory is

supported by our observations that high concentrations of disaccharides resulted in many early apoptotic and late apoptotic cells.

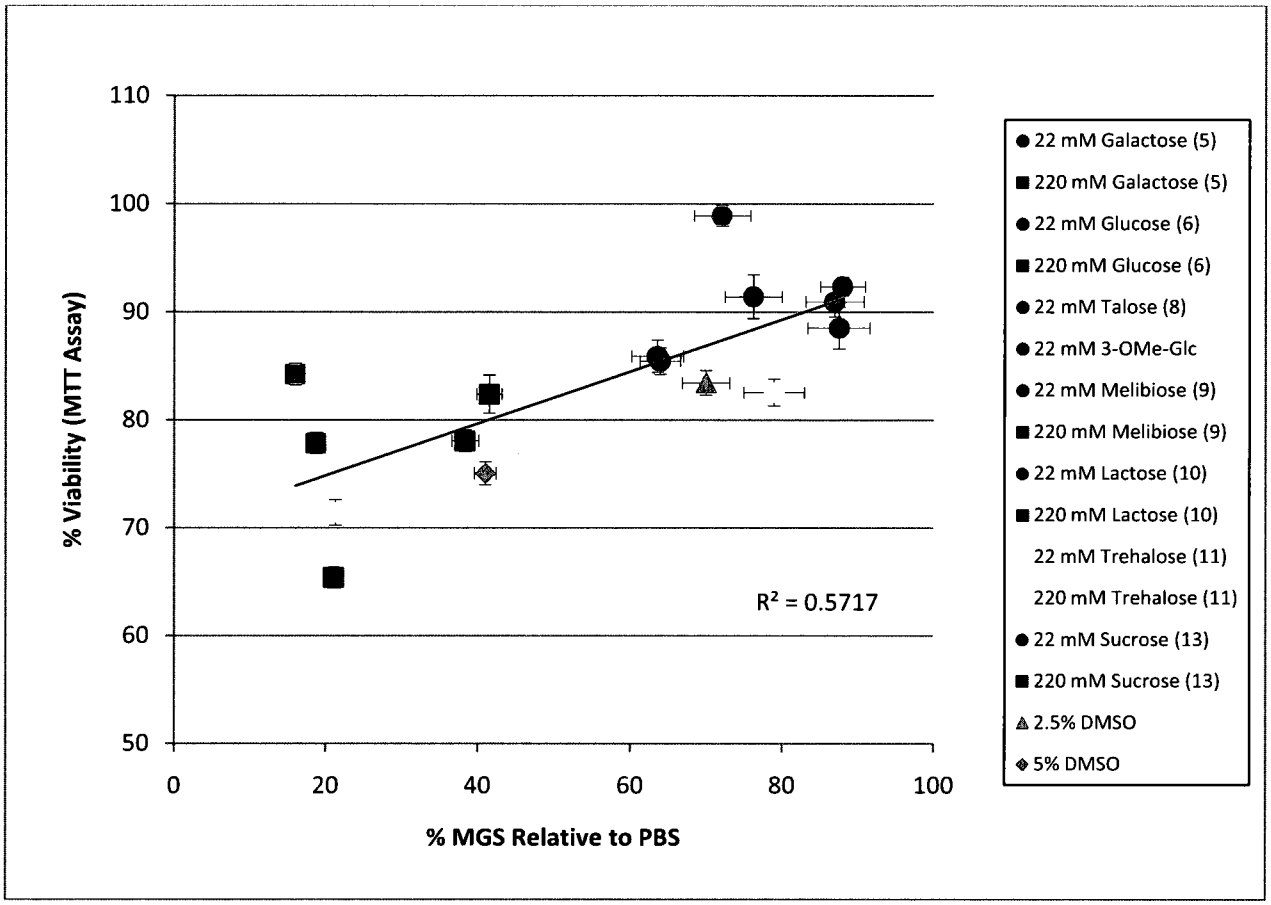

Figure 3.10: Cell viability at 37 ºC vs. RI activity for monosaccharides and disaccharides at 22 mM (circles) and 220 mM (squares) and 5% DMSO (triangle) and 2.5% DMSO (diamond) solutions.

3.2.2: Preservation of Cells at Sub-Zero Temperatures

Based on the fact that recrystallization of ice is known to cause damage during freeze-thaw protocols, we would expect there to be a positive correlation between cell viability at subzero temperatures and IRI activity. In order to evaluate this, the percentage of viable cells post freeze-thaw was determined using a flow cytometry technique. The cells are treated with the sample and then frozen to -80 ºC for one week. After this time, the cells are thawed and passed through a flow cytometer which is able

to distinguish between viable cells and necrotic cells by looking for appropriate markers. The percentage of viable cells following storage at -80 ºC is displayed in Figure 3.11.

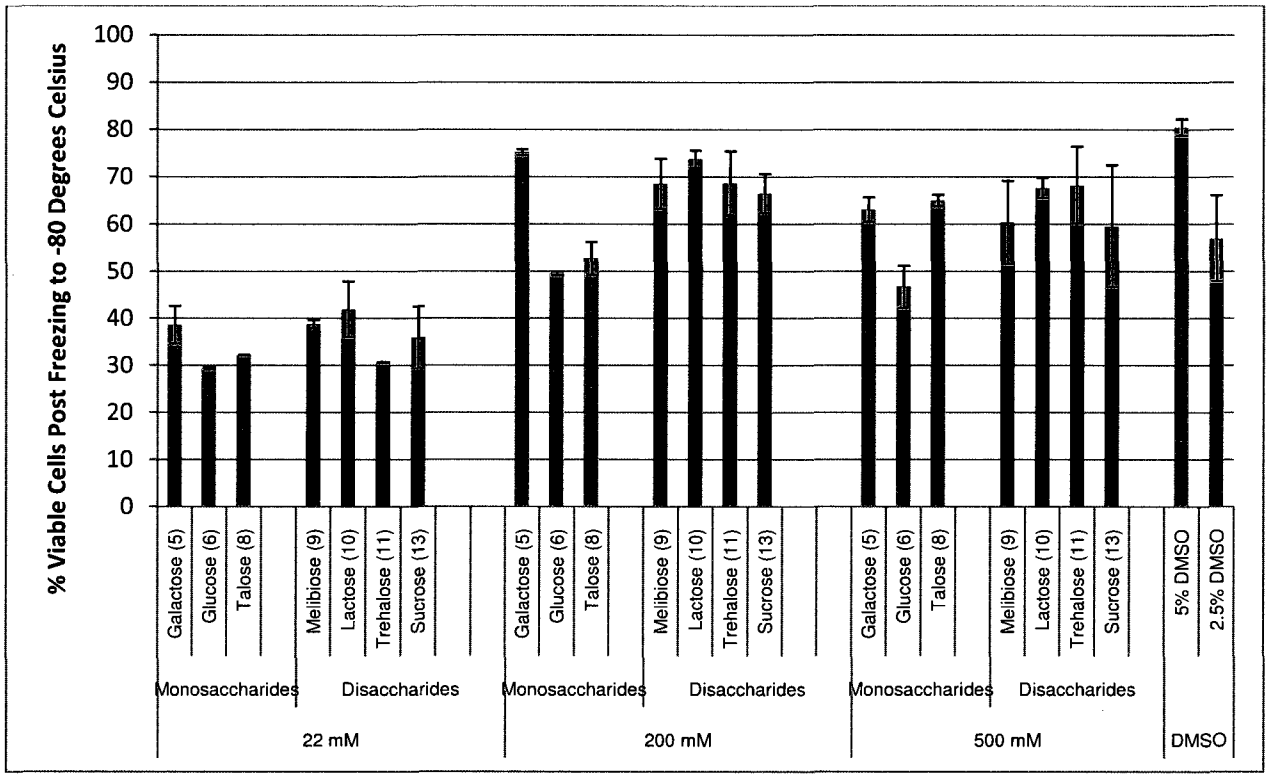

Figure 3.11: Flow cytometry results for monosaccharides (blue bars) and disaccharides (pink bars) at 22, 200, and 500 mM concentrations. Flow cytometry results for DMSO solutions (green) at 5% and 2.5% are included for comparison. The y-axis represents the number of viable cells remaining viable following freezing to -80 ºC. (Wu, von Moos, Allan, and Ben, unpublished results).

Again, no clear trends are seen based on sugar structure in Figure 3.11. At 22 and 200 mM, galactose (**5**) was the best monosaccharide and lactose (**10**) was the best disaccharide. Interestingly, galactose (**5**) was a considerably more effective cryoprotectant than the other monosaccharides at 22 and 200 mM. In general, concentrations of 200 mM and 500 mM were much more effective than concentrations of 22 mM, although very little additional protection was conferred at 500 mM compared to 200 mM in most cases. Several of the carbohydrates showed comparable activity at

200 mM to a 5% solution of DMSO, which is commonly used in cryoprotection protocols.

With these results in hand, we sought to determine whether a correlation exists between IRI activity and cryopreservation ability of mono- and disaccharides. The results are displayed in Figure 3.12. Two important initial observations can be made when comparing this graph to Figure 3.10. Firstly, the fit of the line of regression is 0.88, indicating that there is a very good correlation between cell viability following freeze-thaw and IRI activity. Secondly, the sign of the slope has changed from a positive slope in Figure 3.10 to a negative slope in Figure 3.12. This suggests that although potent IRI inhibitors result in more cell death at 37 ºC, they result in increased cell viability post freeze-thaw.

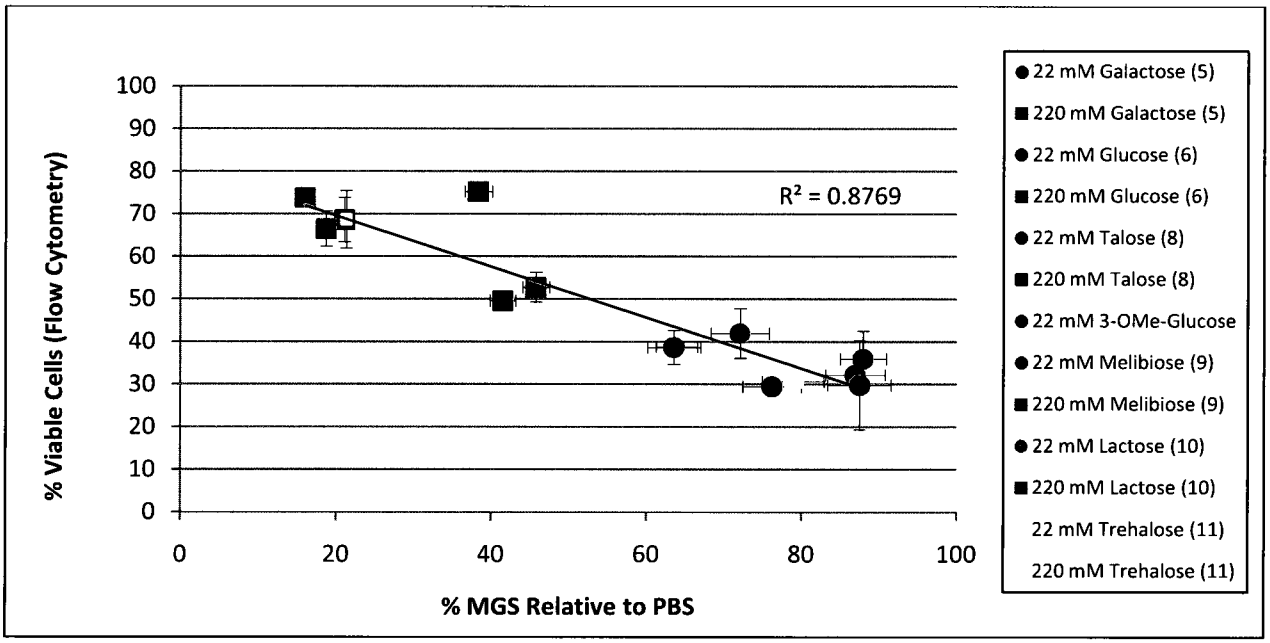

Figure 3.12: Cell viability following freeze-thaw vs. IRI activity for monosaccharides and disaccharides at 22 mM (circles) and 220 mM (squares).

There is one outlier in Figure 3.12, which is the data point representing a 220 mM galactose solution, which resulted in much higher cell viability post freeze-thaw than

other compounds with similar IRI activity. This led us to examine the change in viability in going from physiological temperature to -80 ºC and these results are displayed in Table 3.3. In general, there was a much smaller change between the viabilities at 200 mM than at 22 mM. Furthermore, at 200 mM, galactose (**5**) and trehalose (**11**) both had decreases in viabilities of less than 3% and melibiose (**9**) actually saw an increase in viability going from 37 ºC to -80 ºC. However, of these compounds, galactose (**5**) appears to be the best cryoprotectant because it gave the highest percentage of viable cells in addition to having only a slight decrease in viability upon freeze-thaw.

Table 3.3: Cell viability at 37 ºC and -80 ºC and the difference between these values.

Concentration	Carbohydrate	% Cell Viability at 37 ºC	% Cell Viability at -80 ºC	Difference
22 mM	Galactose (**5**)	85.9	38.6	47.3
	Glucose (**6**)	91.4	29.5	62.0
	Melibiose (**9**)	85.5	38.8	46.7
	Lactose (**10**)	98.9	41.9	57.0
	Trehalose (**11**)	82.5	30.6	51.9
	Sucrose (**13**)	92.4	35.9	56.4
200 mM	Galactose (**5**)	78.1	75.2	2.9
	Glucose (**6**)	82.4	49.6	32.8
	Melibiose (**9**)	65.4	68.6	-3.2
	Lactose (**10**)	84.3	73.8	10.5
	Trehalose (**11**)	71.4	68.7	2.8
	Sucrose (**13**)	77.9	66.5	11.4

3.2.3: Comparison to a Known Cryoprotectant

At this point, we sought to compare the effect of carbohydrates to that of a known cryoprotectant, DMSO. We have already observed that a 22 mM galactose (**5**) solution is as effective a recrystallization inhibitor as a 3% DMSO solution (Figure 3.6).[22] However, further investigation was necessary to determine the correlation between IRI activity of DMSO solutions and cell viability. In order to do so, 2.5% and 5% solutions of DMSO were evaluated for IRI activity. The results are displayed in Figure 3.13. A 5%

DMSO solution was found to have statistically identical IRI activity to a 220 mM solution of galactose.

We were interested in seeing the effect of combinations of DMSO and carbohydrates on IRI activity, since combinations are often used for the preservation of cells and tissues at low temperatures. When we tested a combination of 5% DMSO with 220 mM galactose (**5**), there was no statistically significant difference between the mean grain size in this solution and in a 5% DMSO solution alone (Figure 3.13). Therefore, there was no increase in activity resulting from the addition of the carbohydrate. Surprisingly, a combination of 5% DMSO with 22 mM galactose (**5**) gave ice crystals that were statistically identical in size to those from in a solution of 5% DMSO with 220 mM galactose (Figure 3.13). Again, the sugar seemed to have little effect on the IRI activity when in combination with DMSO.

In order to investigate this further, we chose to test combinations of DMSO with various concentrations of sucrose (**13**). Sucrose (**13**) was chosen because it showed the largest increase in IRI activity upon going from a 22 mM sucrose solution to a 220 mM solution. The 220 mM sucrose (**13**) solution was a much more potent inhibitor of IRI activity than a 5% DMSO solution, so we were interested in seeing the effect of this combination on ice-recrystallization. As seen in Figure 3.13, there was only a slight difference in IRI activity between a combination of 5% DMSO with 22 mM sucrose (**13**), and a 5% DMSO with 220 mM sucrose (**13**) combination. Even more interestingly, there was no statistically significant difference[26] between the combination of 5% DMSO with 220 mM sucrose (**13**) and the 5% DMSO solution, despite the fact that 220 mM sucrose (**13**) on its own was a much more potent ice-recrystallization inhibitor. There seems to be a potentiating effect with DMSO, where the 5% DMSO has same amount of ice recrystallization, regardless of the carbohydrate concentration added to the 5% DMSO.

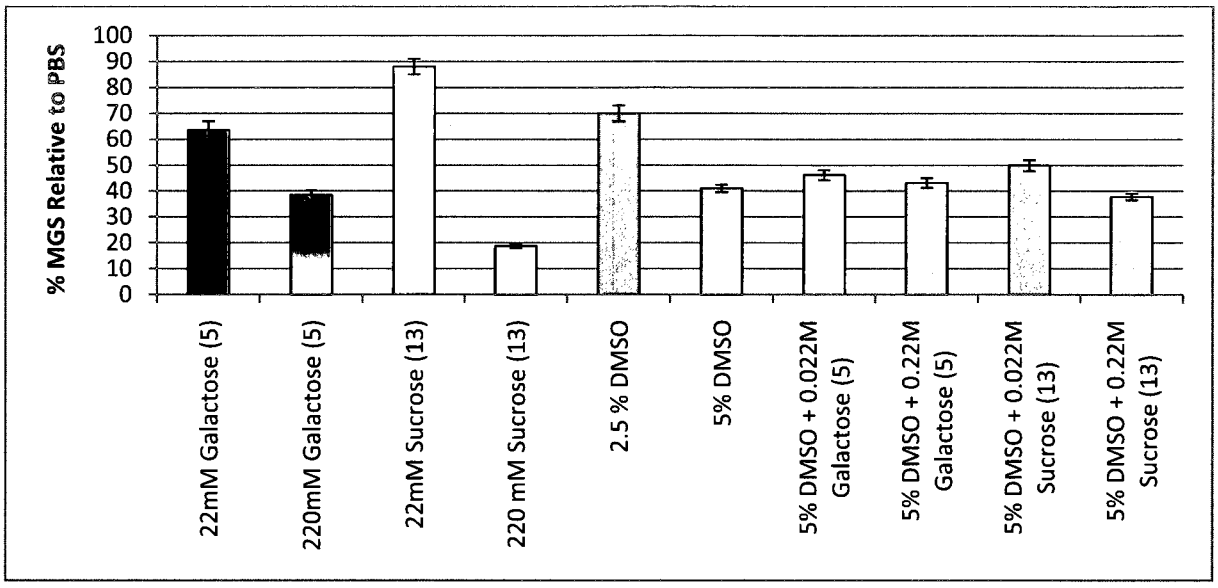

Figure 3.13: IRI activity of various concentrations of galactose (**5**), sucrose (**13**), DMSO, and combinations of DMSO with sugars.

We added the 2.5% and 5% DMSO solutions to our graph showing cell viability at 37 ºC in order to see how the sugars compare to DMSO (Figure 3.14). The DMSO points are shown in gray and they were observed to be towards the bottom of the graph. Therefore, in most cases, the sugars resulted in greater cell viability than the DMSO solutions at physiological temperatures. This is not surprising because DMSO has been observed to be cytotoxic to human cells at physiological temperatures,[19, 48] although this is generally not a significant problem at low DMSO concentrations.

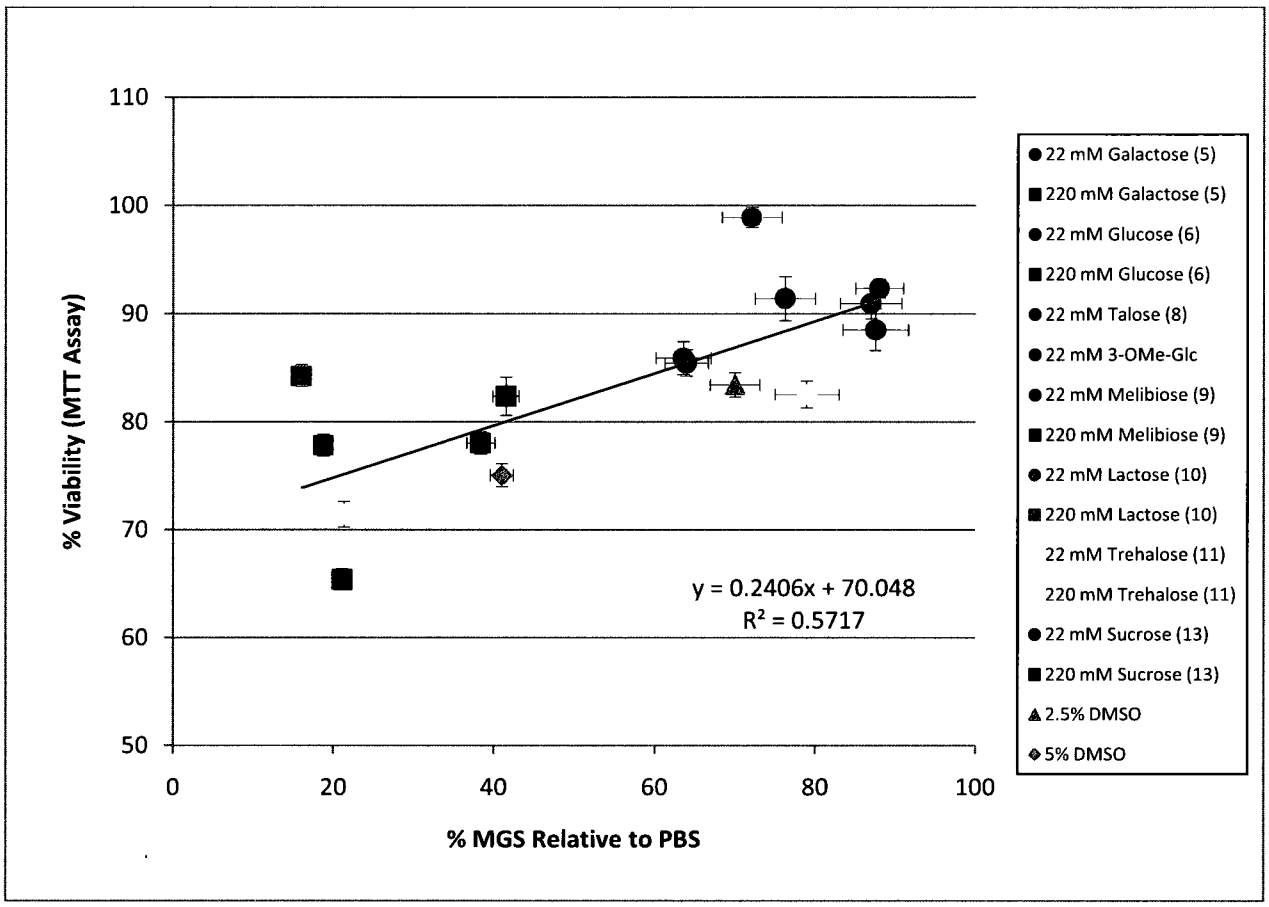

Figure 3.14: Percent cell viability at 37 ºC vs. IRI activity for monosaccharides and disaccharides at 22 mM (circles) and 220 mM (squares) as compared to 2.5% DMSO (gray triangle) and 5% DMSO (gray diamond).

When the 2.5% and 5% DMSO points (gray points) were included in our graph of percent cell viability following freeze-thaw versus IRI activity, we noticed that they were located above the majority of the other data points (Figure 3.15). Furthermore, when we added in the data points representing the combinations of 5% DMSO with galactose (light purple points) and 5% DMSO with sucrose (light green points), all of the DMSO-containing points were clustered together at the top of the graph. Interestingly, one sugar data point falls into the "DMSO-area" of the graph, which is the data point belonging to 220 mM galactose. Therefore, 220 mM galactose appears to be an equally effective cryoprotectant as 5% DMSO.

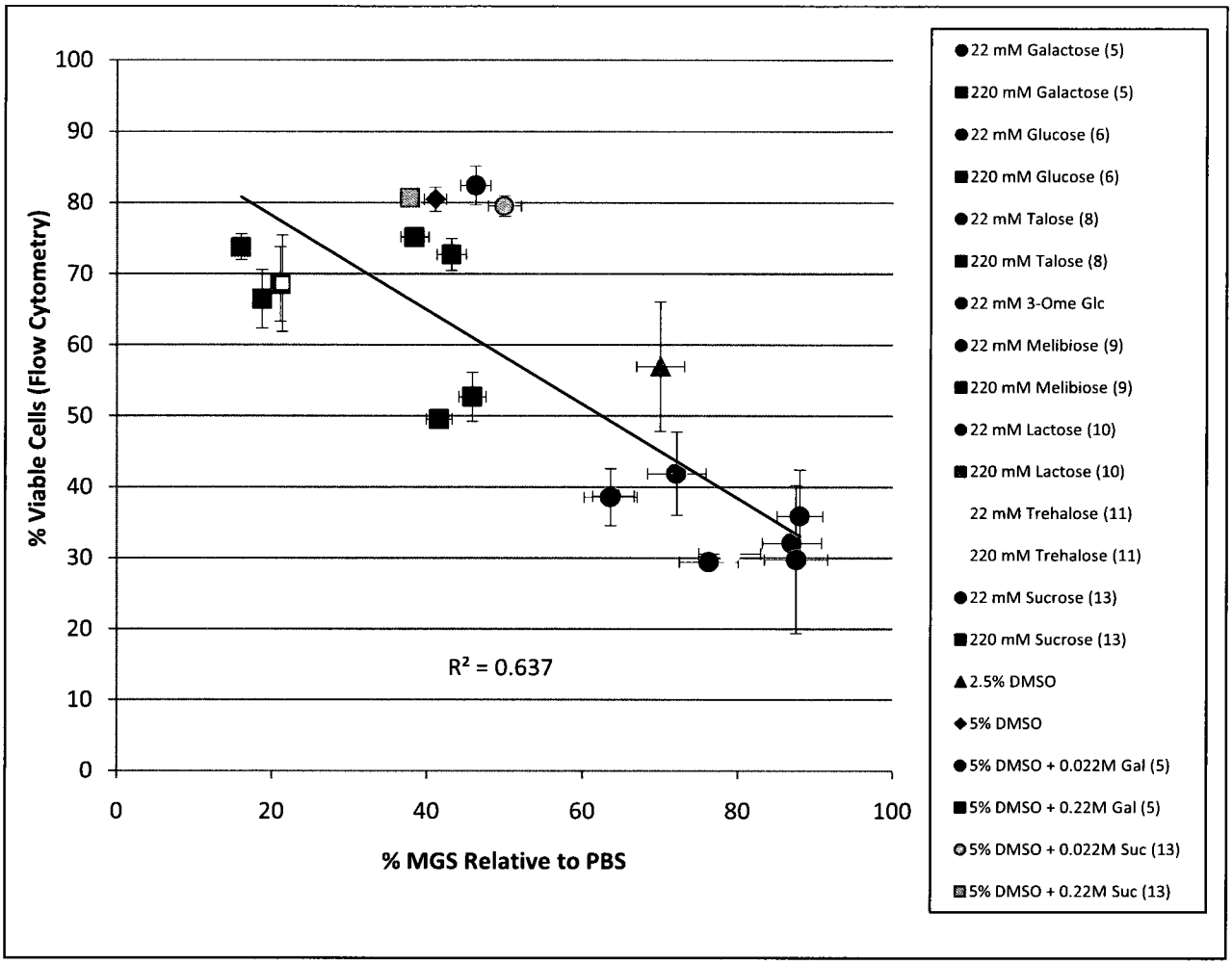

Figure 3.15: Cell viability following freeze-thaw vs. IRI activity for monosaccharides and disaccharides at 22 mM (circles) and 220 mM (squares) compared to 2.5% DMSO (gray triangle), 5% DMSO (gray diamond), and combinations of DMSO with galactose and sucrose.

As mentioned above, a 220 mM solution of galactose (**5**) was found to be as effective a cryoprotectant as a 5% DMSO solution. This is extremely exciting as DMSO is known to have harmful toxic effects on human cells, so it must be removed immediately following freeze-thaw protocols. Interestingly, DMSO seems to have a balancing effect on IRI activity when used in combination with carbohydrates. This is evidenced by the fact that a solution of 5% DMSO with 22 mM sucrose (**13**) was as effective as a combination of 5% DMSO with 22 mM galactose (**5**), although 22 mM galactose (**5**) showed much greater IRI activity than 22 mM sucrose (**13**) in the absence of DMSO.

The results presented here show that high concentrations of carbohydrates result in improved IRI activity but also cause an increase in cell death at physiological temperatures. However, although a decrease in cell viability was observed at physiological temperature, a drastic increase in cell viability was observed following freeze-thaw. Furthermore, IRI activity was found to be well correlated to cryopreservation ability. This suggests that 200 mM concentrations of carbohydrates, particularly galactose (**5**) as well as combinations of carbohydrates with DMSO, should be explored for the preservation of cells during freeze-thaw protocols. Based upon these results, it seems that the rational design of novel carbohydrate-based cryoprotectants based on their IRI activity is an attainable goal.

3.3: Evaluation of the Effect of a C-Linkage on IRI Activity

Our laboratory has previously prepared several *C*-linked AFGP analogues (Figures 2.4 and 2.6). Although the conformation of *C*-linked carbohydrates has been reported to be similar to that of *O*-linked saccharides,[49, 50] hydration numbers for *C*-linked carbohydrates have not been determined through experiment or computer simulations. The relationship between antifreeze activity and hydration of *C*-linked carbohydrates has not been explored, possibly due to this lack of hydration numbers for *C*-linked carbohydrates. However, precedent from our laboratory has suggested that the hydration of the *C*-linked carbohydrate moiety in AFGP analogues determines their IRI activity (Figures 2.7 and 2.8). In addition, researchers have proposed that hydration of carbohydrates is largely dependent on the substituents and stereochemistry at C-2 and C-4,[9, 10] and that the contribution from the substituent at C-1 plays a lesser role. This suggests that the nature of the substituent at C-1 will not greatly affect the IRI activity of carbohydrates. If this hypothesis is correct, *C*-linked analogues of galactose should display similar levels of IRI activity to the native *O*-linked galactose (**5**). To examine this hypothesis, several *C*-allyl derivatives of monosaccharides were prepared in order to be evaluated for IRI activity.

In order to determine the effect of anomeric stereochemistry, α- and β-derivatives of *C*-allyl monosaccharides were prepared (Figure 3.16). α-*C*-allyl galactose,

glucose, mannose, and talose were previously prepared in our laboratory. β–allyl derivatives of galactose and glucose were prepared for use in this study to examine the effect of a β-linkage.

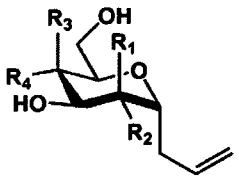

14: Gal: R_1=H;R_2=OH;R_3=OH;R_4=H
15: Glc: R_1=H;R_2=OH;R_3=H;R_4=OH
16: Man: R_1=OH;R_2=H;R_3=H;R_4=OH
17: Tal: R_1=OH;R_2=H;R_3=OH;R_4=H

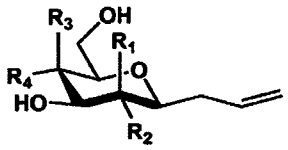

18: Gal: R_1=H;R_2=OH;R_3=OH;R_4=H
19: Glc: R_1=H;R_2=OH;R_3=H;R_4=OH

Figure 3.16: *C*-allylated derivatives of galactose (**14**, **18**), glucose (**15**, **19**), mannose (**16**), and talose (**17**).

β-*C*-allyl galactose **18** was prepared according to the following procedure (Figure 3.17). Galactose pentaacetate was allylated by treatment with allyl-trimethylsilane and boron trifluoride diethyl etherate. Performing the reaction in anhydrous nitromethane gives predominantly the β-anomer in approximately 2:1 β:α ratio. The anomers could not be separated with acetate protecting groups. Therefore, the acetates were removed and replaced with TBS groups by treatment with *tert*-butyl dimethylsilyl triflate and 2,6-lutidine in dichloromethane. The anomers were then separated by flash chromatography. Removal of the silyl groups using tetrabutylammonium fluoride gave a polar product that was very difficult to isolate from the reaction components. Therefore, a two-step de-silylation-acetylation protocol was performed to give (**52**) as a pure β-anomer. De-acetylation under basic conditions followed by acidic workup gave the desired product (**18**).

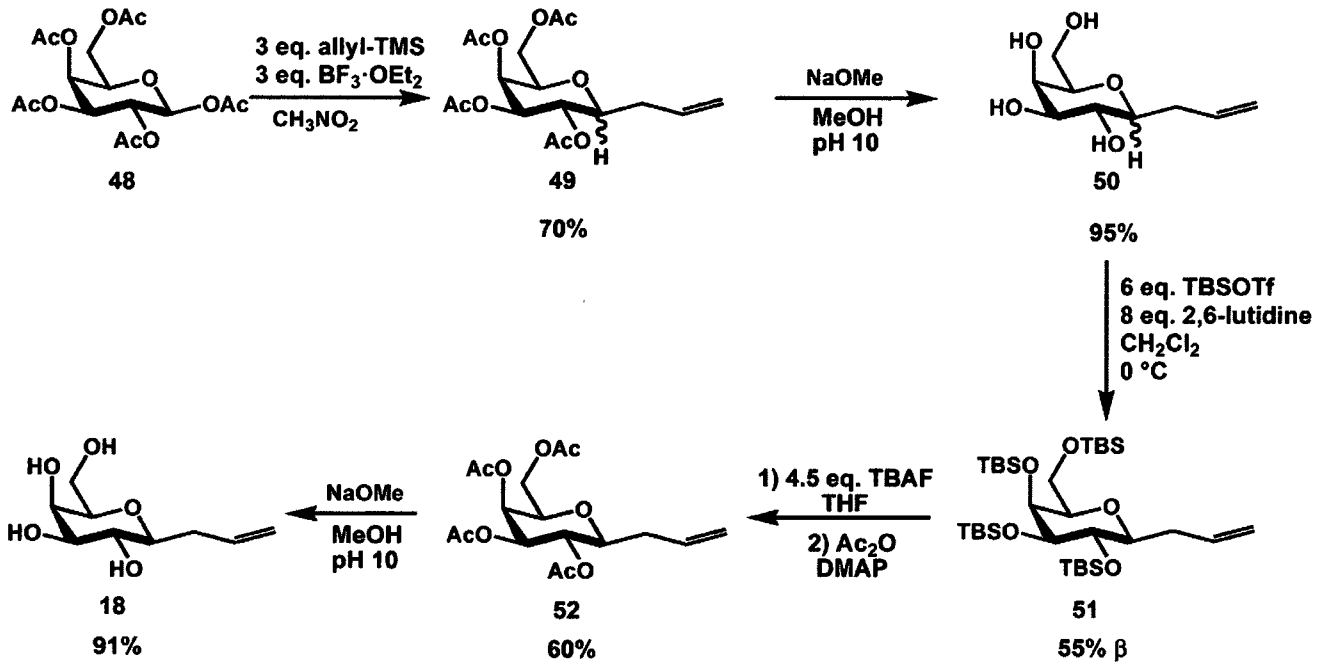

Figure 3.17: Preparation of β-*C*-allyl galactose (**18**) from galactose pentaacetate (**48**).

Although a similar scheme was attempted using glucose pentaacetate, allylation with allyl-trimethylsilane was unsuccessful for glucose under all conditions attempted. Instead, glucosyl bromide (**54**) was prepared by treating glucose pentaacetate (**53**) with a solution of HBr in acetic acid (Figure 3.18). Treatment of the bromide (**54**) with allyl-magnesium bromide under Grignard conditions gave the allylated product (**55**). When the residue from this reaction was treated with acetic anhydride and sodium acetate in order to simplify purification, compound (**55**) was obtained in low yield due to complications with the experimental setup. Despite this low yield, (**55**) was de-acetylated to give the desired product (**19**) which was ready for IRI testing.

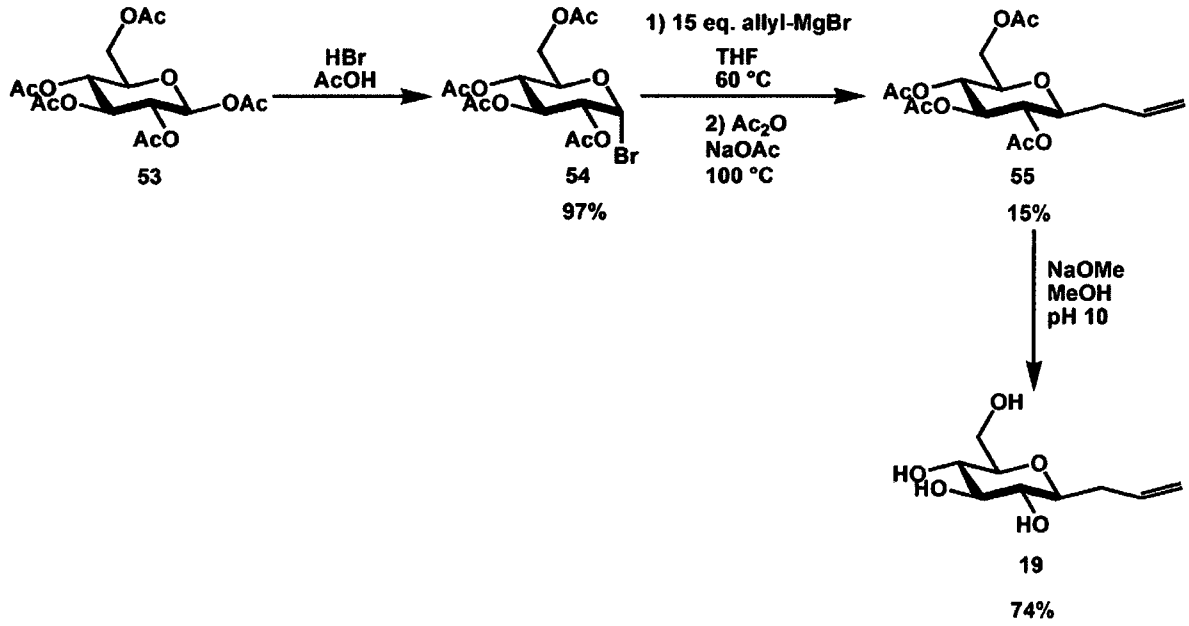

Figure 3.18: Preparation of β-*C*-allyl glucose (**19**) from glucose pentaacetate (**53**).

The IRI activity of *C*-allylated derivatives were plotted and compared to their parent monosaccharides in Figure 3.19. Unfortunately, the lack of hydration numbers for *C*-linked monosaccharides prevented us from plotting IRI activity against a measure of hydration for these compounds. α-*C*-allyl galactose (**14**) was found to be the most active of the *C*-linked derivatives, with a mean grain size that was statistically identical to D-galactose (**5**). The IRI trend of the α-*C*-allyl derivatives decreased in the order α-*C*-allyl galactose (**14**) > α-*C*-allyl glucose (**15**) > α-*C*-allyl mannose (**16**) > α-*C*-allyl talose (**17**), which was the same as for their respective parent *O*-linked monosaccharides. These results are consistent with the hypothesis that the substituent at C-1 has little effect on the hydration of the carbohydrate and therefore on their IRI activity. However, β-*C*-allyl-galactose (**18**) displayed a marked decrease in IRI activity compared to α-*C*-allyl-galactose (**14**) and D-galactose (**5**), which suggests that the anomeric stereochemistry may affect carbohydrate hydration. In contrast, β-*C*-allyl-glucose (**19**) showed the same amount of IRI activity as α-*C*-allyl-glucose (**15**), with no statistically significant difference in mean grain size. Based on these results, further studies were required to determine the exact effect of anomeric configuration on IRI activity.

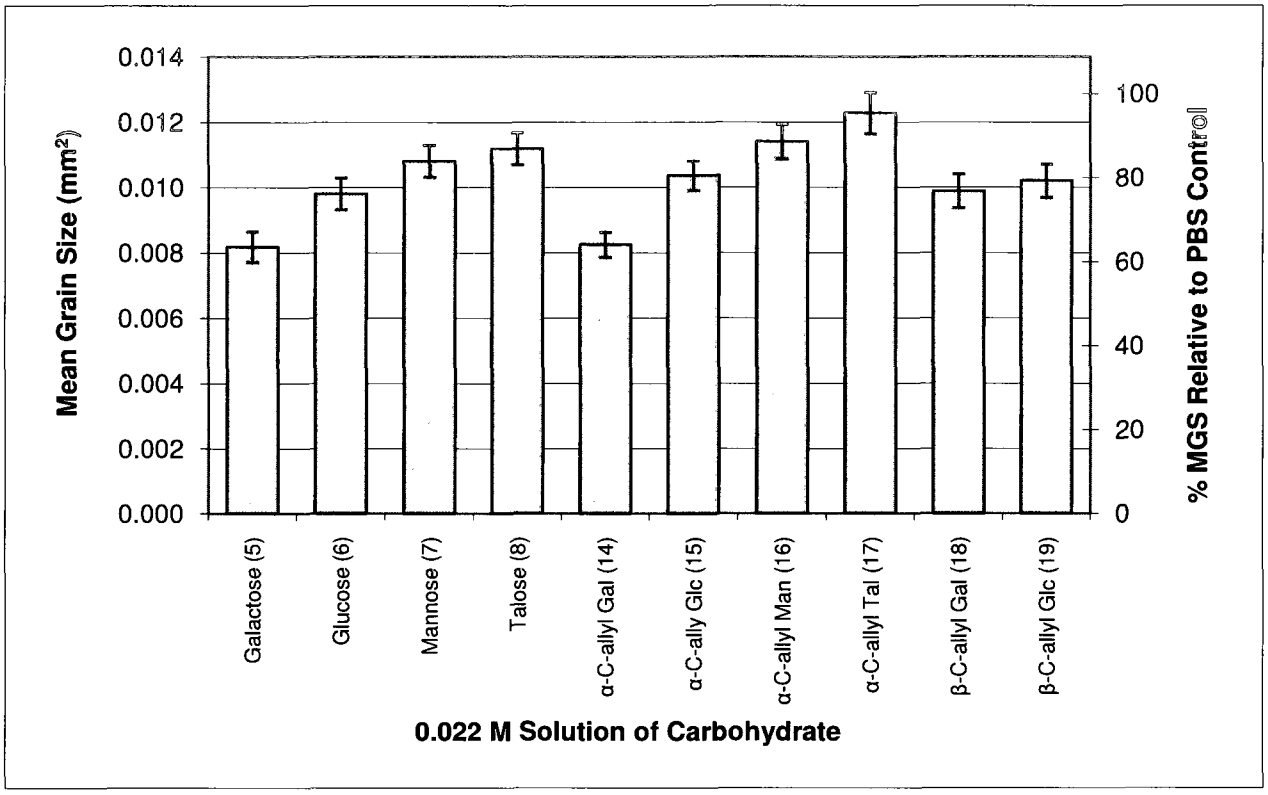

Figure 3.19: IRI activity of native *O*-linked monosaccharides (**5 - 8**) and their *C*-linked derivatives (**14 – 19**) as 0.022 M solutions in PBS.[22]

The anomeric configuration of the carbohydrate has previously been shown to play a role in hydration. Cheetham and Lam have observed that the β-anomers of methyl-D-galactopyranoside and methyl-D-glucopyranoside are more compatible with the structure of water than their α-anomers, causing them to be less hydrated.[12] Suggett has suggested that in the case of α-D-glucose (**6**), the anomeric proton is the only one in an axial conformation, and is therefore more susceptible to intermolecular proton-proton interactions.[51] The other protons are believed to be shielded by the movement of other hydrated hydroxyl groups on the pyranose ring.[51] These results by Cheetham and Lam and Suggett suggest that α-linked compounds are more effectively hydrated than β-linked compounds. Our observation that compounds with an α-configuration display greater IRI activity than those with a β-configuration support our hypothesis that well hydrated compounds are more effective inhibitors of ice-recrystallization.

Additional *C*-linked carbohydrates were tested for IRI activity in order to further examine the effect of the linkage at the anomeric position, based on our results for α-*C*-allyl-galactose (**14**) (Figure 3.19). The *C*-linkage is a useful modification to observe the necessity of having a hydrogen bond donor or acceptor at C-1. The C-1 hydroxyl group in native carbohydrates is able to act as both a hydrogen bond donor and acceptor, while a carbon atom is not. Therefore, if hydrogen bonding at C-1 is involved in ice-binding, we would expect to see a decrease in IRI activity when replacing this hydroxyl group with a *C*-linkage.

The compounds to be evaluated in this study are displayed in Figure 3.20. Compounds (**21**) and (**22**) have been previously prepared in our laboratory (Tam, Ferreira, and Ben, unpublished results). These compounds were included in this study to examine the effect of the oxidation state and the hybridization of the atom that is β to the anomeric carbon. In addition, compound (**20**) was prepared from (**14**) in order to further examine the effect of hybridization (Figure 3.21. Compound (**23**) was prepared in one step from D-galactose (**5**) (Figure 3.22). The synthesis and IRI activity of (**14**) and (**18**) has been described previously, and these compounds were included for comparison. (Figures 3.17-3.19).

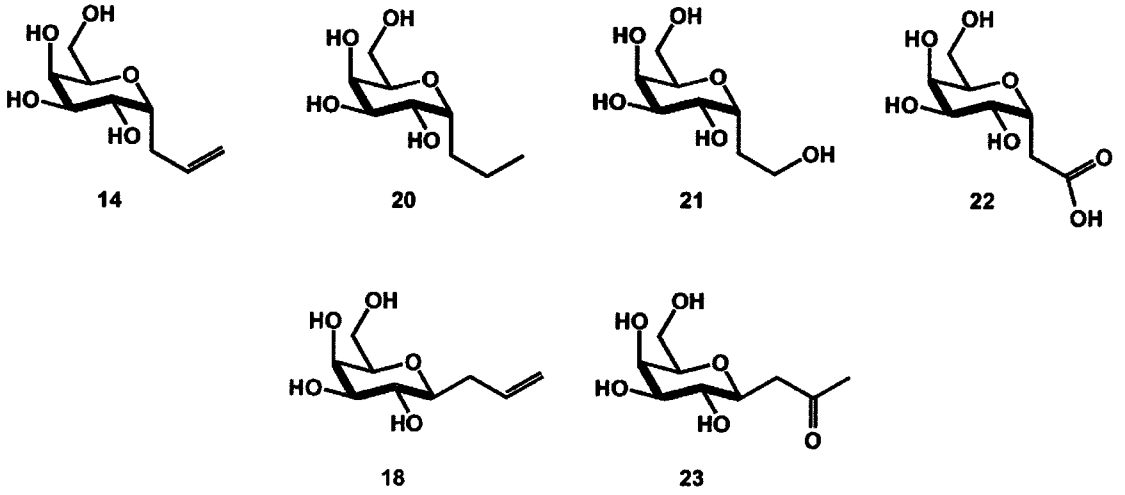

Figure 3.20: *C*-linked monosaccharides (**14**), (**18**), (**20**), (**21**), (**22**), and (**23**) to be used in this study.

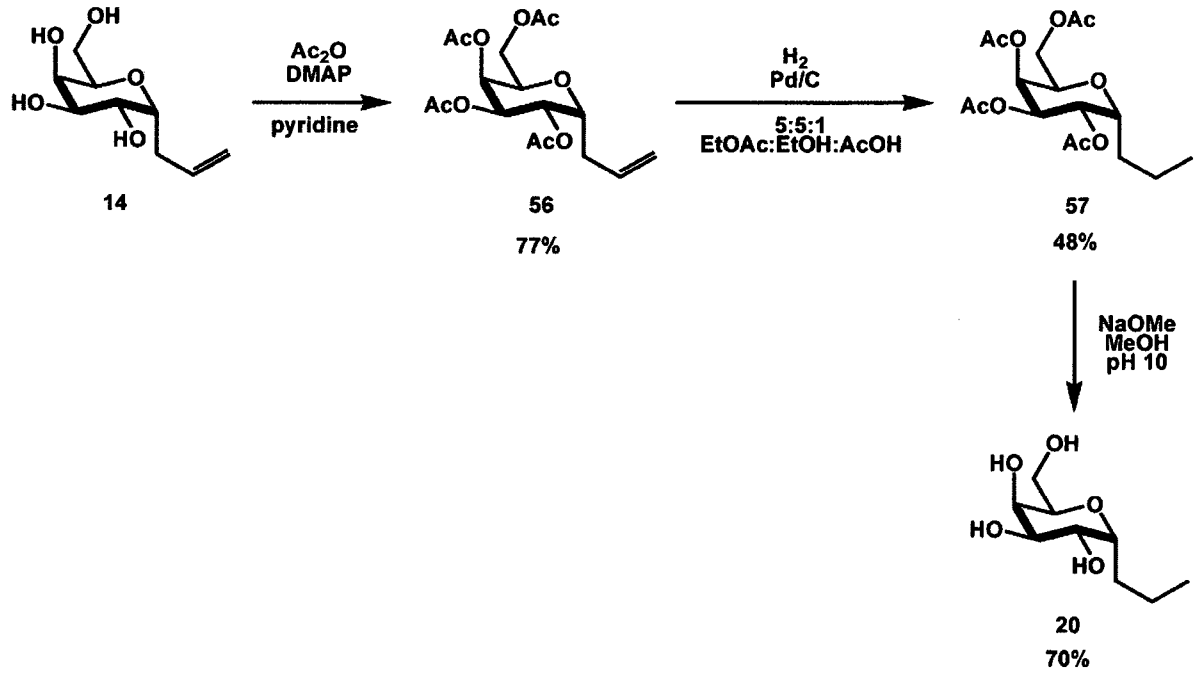

Figure 3.21: Preparation of α-*C*-propyl galactose (**20**) from α-*C*-allyl galactose (**14**).

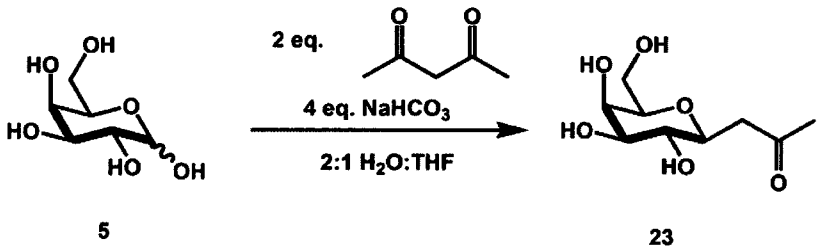

Figure 3.22: Preparation of compound (**23**) from D-galactose (**5**).

The IRI activity of these *C*-linked compounds is displayed in Figure 3.23. It can be seen from this graph that there was a decrease in activity going from α-*C*-allyl galactose (**14**) to the other α-*C*-linked galactose derivatives (**20 – 22**). Interestingly, however, compounds (**20 – 22**) all formed ice crystals with statistically identical mean grain sizes. This suggests that the *C*-allyl group imparts the best IRI activity, possibly due to the conformation that this compound adopts in solution. The β-linked compounds both showed a decrease in activity compared to α-*C*-allyl galactose (**14**). Despite this decrease, both compounds (**18**) and (**23**) displayed statistically identical[26] IRI activity within experimental error. It appears that in compounds such as the β-linked derivatives

which have only moderate IRI activity (20-30% more active than the PBS negative control), structural changes have very little additional effect on ice recrystallization. This is similar to the results observed for *C*-allyl-glucose derivatives (**15**) and (**19**) (Figure 3.19).

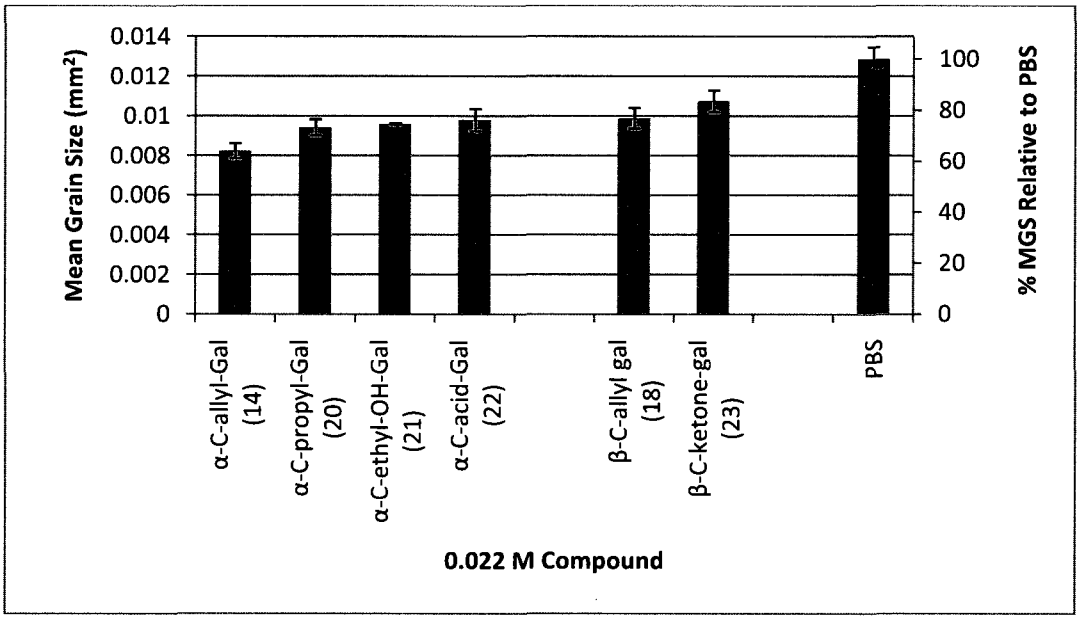

Figure 3.23: IRI activity of α-*C*-linked galactose derivatives (**14**), (**20**), (**21**), and (**22**), and β-*C*-linked galactose derivatives (**18**) and (**23**).

In nearly every case examined, a decrease in IRI activity was observed for the *C*-linked galactose derivatives compared to galactose (**5**). In each of these cases, a carbon chain of two or three carbons was added to the anomeric position. Interestingly, the nature of the oxidation state did not affect the IRI ability of these compounds, because galactose derivatives containing an all-carbon propyl chain (**20**), a hydroxyl group (**21**), a carboxylic acid (**22**), and a methyl ketone (**23**) all showed similar amounts of IRI activity.

The only exception to this is *C*-allyl galactose (**14**), which showed identical IRI activity to native galactose itself. It is possible that the double bond causes this compound to adopt a conformation which allows it to be effectively hydrated, resulting in

efficient IRI activity. This will need to be explored further through the synthesis of additional derivatives of galactose, such as compounds that have fewer and more sp^3 hybridized carbon atoms before the double bond (i.e. a vinyl group and a homo-allylic group).

In order to confirm that the hydration of carbohydrates is correlated to IRI activity, we must determine the previously unstudied hydration properties of monosaccharide derivatives, such as *C*-allyl galactose. Furthermore, if this goal is realized, we would be able to design carbohydrates that have efficient IRI activity and that may be used as novel cryoprotectants. Initial efforts to calculate the hydration properties of unnatural carbohydrates using molecular dynamics simulations are currently underway in collaboration with the Woo lab and this will be described in the next chapter of this thesis.

3.4: Evaluation of the Effect of the Acetamide Group on IRI Activity of Glucose and Galactose

Native AFGP contains a C-2 acetamide in its disaccharide moiety, and this has been shown by several researchers to be essential for thermal hysteresis activity. However, its necessity for ice-recrystallization inhibition activity has not been fully explored. Previous work in our laboratory has shown that incorporation of a C-2 acetamide into a *C*-Serine AFGP analogue (**59**) actually causes a decrease in IRI activity relative to *C*-Serine (**58**) which has a C-2 hydroxyl group (Figures 3.24 and 3.25).[52] However, it was observed by circular dichroism that the structure of (**58**) was largely random coil, whereas (**59**) was almost entirely α-helical.[52] Therefore, this change in conformation may account for the significant decrease in IRI activity.

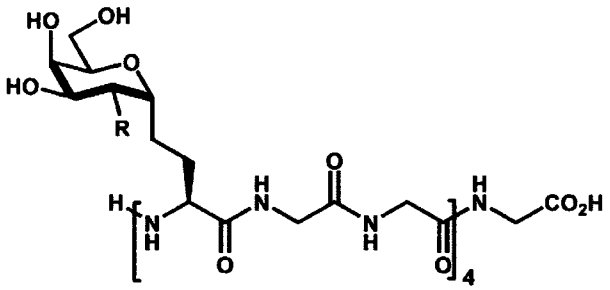

58: R=OH
59: R=NHAc

Figure 3.24: *C*-Serine AFGP analogues (**58**) and (**59**) prepared by Suhuai Liu[52, 53]

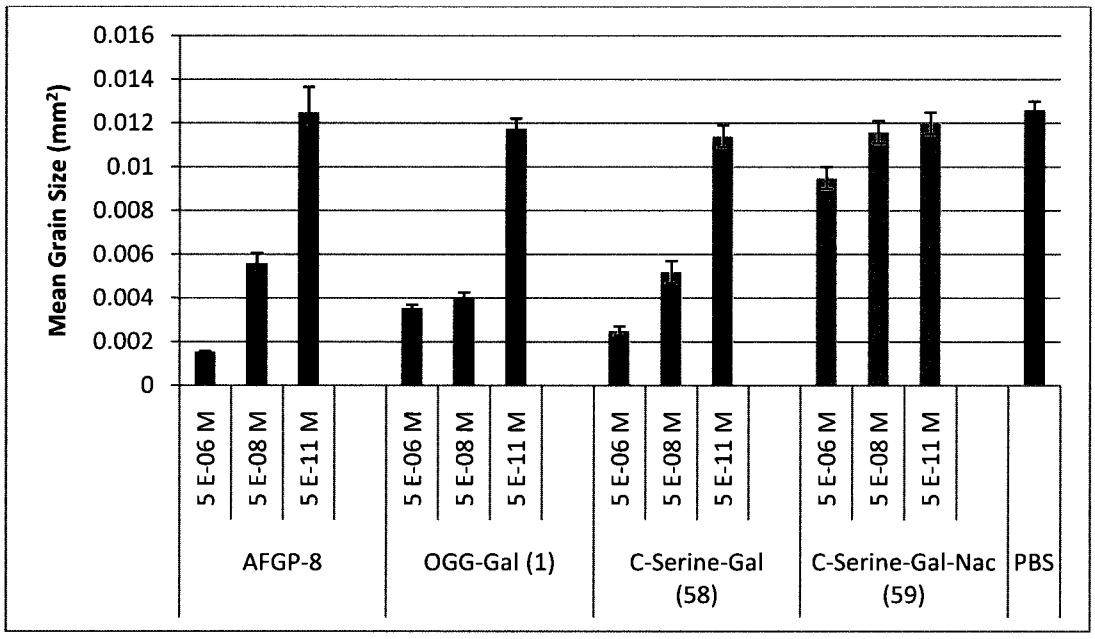

Figure 3.25: IRI activity of *C*-serine AFGP analogues (**58**) and (**59**) compared to OGG-Gal (**1**) and native AFGP8.[52, 53]

To the best of our knowledge, the effect of a C-2 acetamide group on the IRI activity of monosaccharides has not been previously investigated. For this reason, we obtained samples of *N*-acetyl-galactosamine (**24**), galactosamine hydrochloride (**25**), *N*-acetyl-glucosamine (**26**), and glucosamine hydrochloride (**27**) (Figure 3.26) and submitted them to our IRI assay.

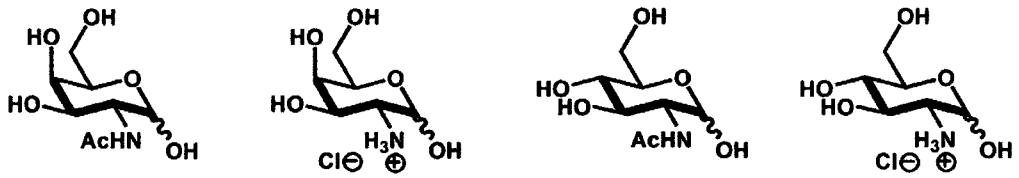

24 25 26 27

Figure 3.26: Structures of *N*-acetyl-D-galactosamine (**24**), D-galactosamine hydrochloride (**25**), *N*-acetyl-D-glucosamine (**26**), and D-glucosamine hydrochloride (**27**)

The results of these experiments are displayed in Figure 3.27. The C-2 amine and acetamide compounds are compared to their parent monosaccharides galactose (**5**) and glucose (**6**). For the galactose series, there was a significant decrease in activity (from 64% to 89% relative to PBS) when the C-2 hydroxyl group of galactose (**5**) was replaced with a C-2 acetamide in compound (**24**). Some of the IRI activity was restored for galactosamine hydrochloride (**25**), which has a C-2 amine and formed ice crystals that were 75% the size of those in the PBS negative control. In this case, we saw a significant decrease in activity when the C-2 substituent was changed from an amine (**25**) to an acetamide (**24**). In PBS solution, compound (**25**) will have a protonated amine at C-2, although the nature of the counter ion is not fully known. The chloride ion of the galactosamine hydrochloride salt may exchange for one of the other anions in the PBS solution. Further experiments are required to examine the effect of this counter ion. Regardless of the nature of the anion, it is likely that both the anion and the protonated amine group in (**25**) will have their own hydration shells, as has been observed for other charged species.[54-56] This will affect the hydrogen bonding in solution and the overall hydration bonding network of the carbohydrate, and this may account for the moderate activity seen for compound (**25**) compared to the good activity observed for galactose (**5**).

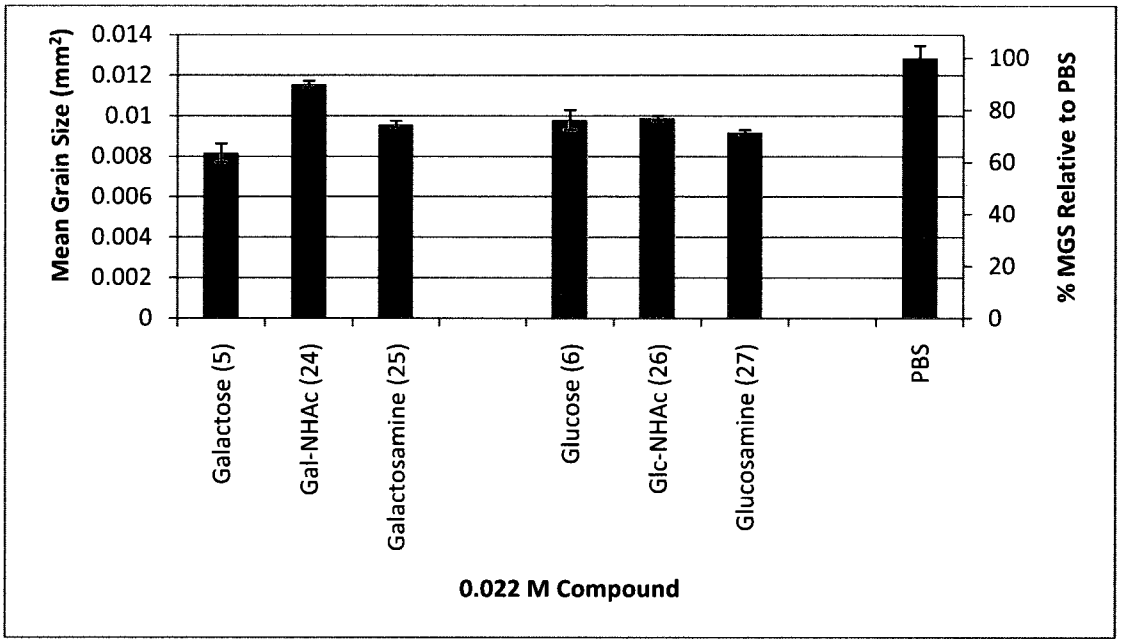

Figure 3.27: IRI activity of galactose (**5**), *N*-acetyl-galactosamine (**24**), galactosamine hydrochloride (**25**), glucose (**6**), *N*-acetyl-glucosamine (**26**), and glucosamine hydrochloride (**27**)

The results for the glucose series were quite different. Glucose (**6**) and its amine and acetamide derivatives (**26**) and (**27**) all formed ice crystals with similar mean grain sizes. Therefore, for the glucose series, small structural and electronic changes did not affect IRI activity, similar to our results for β-*C*-allyl glucose (**19**) (Figure 3.19). Our observations for the acetamide and amine derivatives are supported by experiments by Corzana et al.[57] and Uedaira et al.,[58] which will be discussed below.

Corzana and co-workers have observed the orientations of two truncated glycopeptides, D-GalNAC-Ser and D-GalNAc-Thr (Figure 3.28).[57] They observed that although both compounds contain water pockets or bridges between the carbohydrate and peptide moieties, the locations of the water pockets differ between the two structures.[57] This suggests that D-GalNAc-Ser has a different ability to structure water around itself, resulting in a less efficient hydrogen-bonding network than for the threonine analogue.[57] The authors propose that this accounts for the greater antifreeze activity for threonine-containing AFGPs.[57] These results indicate that a small structural

modification (in this case the presence or absence of the γ-methyl group on the amino acid) has the ability to completely disrupt the hydrogen-bonded network of water. It is possible that this is also true for our monosaccharides. The protonated amine in galactosamine (**25**), which is likely to be highly hydrated, may have a different ability to structure water than the acetamide of (**24**), allowing the hydrogen-bonded network caused by hydroxyl groups in galactose to remain undisturbed and effectively hydrated. This would account for our observations that (**25**) showed greater IRI activity than (**24**).

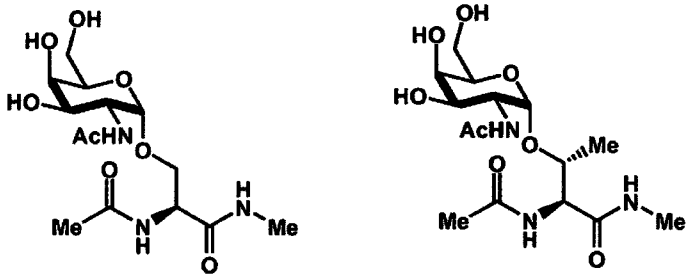

Figure 3.28: Compounds prepared by Corzana et al. to examine the carbohydrate orientation and its effect on surrounding water molecules.[57]

In a separate study, Uedaira et al. examined the hydration properties of several mono- and disaccharides using NMR experiments, and they postulated that their hydration is proportional to the number of equatorial hydroxyl groups in the carbohydrate.[6, 7] Based upon these results, they studied the hydration of substituted galactose and glucose derivatives including *N*-acetyl-D-galactosamine (**24**) and galactosamine (**25**).[58] The effect of substitutions was found to be two-fold. Firstly, the hydration of the carbohydrate is influenced by the interaction between water and the substituted group itself.[58] Secondly, the hydration layer around the carbohydrate is disturbed by the mismatch between bulk water and the conformation of the substituted carbohydrate.[58]

Specifically, one of the substitutions that were studied was that of a C-2 amine group. It was observed that the rotational correlation time, a measure of carbohydrate

hydration, decreased for glucosamine relative to glucose. These observations suggest that the amino group of glucosamine (**27**) breaks the three-dimensional water network by disrupting many water molecules. As a result, the thermal motion of water molecules that are in close proximity to the carbohydrate increases, so the amount of time that these molecules remain closely associated with the solute is decreased.[58] This accounts for the decrease in the rotational correlation time relative to glucose.[58] The acetamide group of *N*-acetyl-D-glucosamine (**26**) was also found to disrupt the structure of water molecules, but to a lesser amount than the amino group of glucosamine (**27**).[58] This suggests that glucosamine (**27**) is more effectively hydrated than *N*-acetyl-D-glucosamine (**26**). Based upon these results, we would expect that glucosamine (**27**) would show greater IRI activity than *N*-acetyl-D-glucosamine (**26**) and this is what was observed (Figure 3.27), although the increase in IRI activity for glucosamine was small.

When galactose derivatives were observed by Uedaira et al., slightly different results were seen.[58] It was observed that galactose has a weaker stabilizing effect on the water structure than glucose, suggesting that galactose would result in a greater disruption of the three-dimensional water network.[58] More importantly, the hydration of galactose derivatives was strongly dependent on the hydration of the substituted groups, such that the hydration of the substituents showed a larger overall effect on the hydration of galactose derivatives than for glucose derivatives.[58] Our IRI activity results support these findings. We observed that there was a much larger difference in IRI activity among the three compounds in the galactose series than in the glucose series, which supports the theory that the hydration of the substituted groups has a larger effect for galactose than for glucose.[58] Furthermore, as in the glucose series, we observed that galactosamine (**25**) was a better inhibitor of ice recrystallization than *N*-acetyl-D-galactosamine (**24**). Since Uedaira et al. report that the amine group disrupts water molecules more than an acetamide group,[58] this is what we would expect to see if hydration is correlated to IRI activity. In addition, our observation that *N*-acetyl-D-galactosamine (**24**) has lower IRI activity than galactose (**5**) is consistent with the results observed by Liu when examining C-serine AFGP analogues (**58**) and (**59**) with and without an acetamide group at C-2 (Figure 3.25).[52]

In the future, galactose derivatives with different charged groups should be prepared in order to further examine the effects of these modifications on hydration and IRI activity further. In addition, the effect of the chloride counter-ion of glucosamine hydrochloride and galactosamine hydrochloride must be explored.

3.5: Summary:

In summary, mono- and disaccharides were observed to display moderate IRI activity in the absence of a peptide component. Furthermore, the IRI was related to the hydration of the carbohydrates. Hydration index (hydration number divided by partial molar volume) was observed to be the best predictor of IRI activity. A model for the interaction of carbohydrates with water and ice and the resulting effect on ice recrystallization is proposed. In this model, compounds that are well hydrated cause a large disruption of the water molecules in the bulk surrounding the carbohydrate's hydration shell. More energy is required to transfer these poorly-ordered water molecules to the QLL of a growing ice crystal, so the recrystallization of ice is inhibited.

The ability of carbohydrates to prevent cell death at physiological and sub-zero temperatures was observed. Higher concentrations of mono- and disaccharides resulted in more cell death at physiological temperatures than lower concentrations. However, higher concentrations of carbohydrates were found to be more effective at maintaining cell viability following freeze-thaw protocols. An exciting correlation was observed between IRI activity and cryoprotection ability, suggesting that we can use a compound's IRI activity to design efficient cryoprotectants for cells and tissues.

The nature of the atom at C-1 has an interesting effect on IRI activity. *C*-allyl galactose (**14**) was observed to display identical IRI activity to native galactose (**5**), but all other modifications resulted in a decrease in activity. The anomeric stereochemistry has an effect on IRI activity in almost all cases, where compounds with an α–configuration show increased activity over those with a β–configuration.

The effect of an amine and an acetamide group at C-2 of galactose and glucose was observed. Galactosamine (**25**) and glucosamine (**27**) showed greater IRI activity

than *N*-acetyl-D-galactosamine (**24**) and *N*-acetyl-D-glucosamine (**26**), respectively. It has been proposed that amine groups disrupt the three dimensional structure of water more than acetamide groups and therefore that galactosamine (**25**) is more effectively hydrated than *N*-acetyl-D-galactosamine (**24**). Our observations that galactosamine (**25**) has greater IRI activity than *N*-acetyl-D-galactosamine (**24**) provides support for our hypothesis that hydration of the carbohydrate is correlated to the ability of the carbohydrate to inhibit ice-recrystallization.

This chapter has shown that mono- and disaccharides display IRI activity and this appears to be correlated to their hydration. Galactose (**5**) was observed to be the best monosaccharide in displaying effective IRI activity. In the following chapter, the effect of more dramatic structural modifications that disrupt the hydration of galactose will be explored.

3.6: References:

1. Lee, S. L.; Debenedetti, P. G.; Errington, J. R., A Computational Study of Hydration, Solution Structure, and Dynamics in Dilute Carbohydrate Solutions. *J. Chem. Phys.* **2005,** 122, 204511-204520.

2. Gharsallaoui, A.; Roge, B.; Mathlouthi, M., Water-Disaccharides Interactions in Saturated Solution and the Crystallisation Conditions. *Food Chem.* **2008,** 106, 1329-1339.

3. Kirschner, K. N.; Woods, R. J., Solvent Interactions Determine Carbohydrate Conformation. *Proc. Nat. Acad. Sci. USA* **2001,** 98, 10541-10545.

4. Gaida, L. B.; Dussap, C. G.; Gros, J. B., Variable Hydration of Small Carbohydrates for Predicting Equilibrium Properties in Diluted and Concentrated Solutions. *Food Chem.* **2006,** 96, 387-401.

5. Hoiland, H.; Holvik, H., Partial Molar Volumes and Compressibilities of Carbohydrates in Water. *J. Solution Chem.* **1978,** 7, 587-596.

6. Uedaira, H.; Uedaira, H., Sugar-Water Interaction from Diffusion Measurements. *J. Solution Chem.* **1985,** 14, 27-34.

7. Uedaira, H.; Ikura, M.; Uedaira, H., Natural-Abundance Oxygen-17 Magnetic Relaxation in Aqueous Solutions of Carbohydrates. *Bull. Chem. Soc. Jpn.* **1989,** 62, 1-4.

8. Lopez de la Paz, M.; Ellis, G.; Perez, M.; Perkins, J.; Jimenez-Barbero, J.; Vicent, C., Carbohydrate Hydrogen-Bonding Cooperativity - Intramolecular Hydrogen Bonds and Their Cooperative Effect on Intermolecular Processes - Binding to a Hydrogen-Bond Acceptor Molecule *Eur. J. Org. Chem.* **2002,** 2002, 840-855.

9. Galema, S. A.; Hoiland, H., Stereochemical Aspects of Hydration of Carbohydrates in Aqueous Solutions. 3. Density and Ultrasound Measurements. *J. Phys. Chem.* **1991,** 95, 5321-5326.

10. Dashnau, J. L.; Sharp, K. A.; Vanderkooi, J. M., Carbohydrate Intramolecular Hydrogen Bonding Cooperativity and Its Effect on Water Structure. *J. Phys. Chem. B* **2005,** 109, 24152-24159.

11. Galema, S. A.; Howard, E.; Engberts, J. B. F. N.; Grigera, J. R., The Effect of Stereochemistry upon Carbohydrate Hydration. A Molecular Dynamics Simulation of β-D-Galactopyranose and (α,β)-D-Talopyranose. *Carbohydrate Res.* **1994,** 265, 215-225.

12. Cheetham, N. W. H.; Lam, K., Molecular Dynamics Simulations of Glycosides in Aqueous Solution. *Carbohydrate Res.* **1996,** 282, 13-23.

13. Kawai, H.; Sakurai, M.; Inoue, Y.; Chujo, R.; Kobayashi, S., Hydration of Oligosaccharides: Anomalous Hydration Ability of Trehalose. *Cryobiology* **1992,** 29, 599-606.

14. Furuki, T., Effect of Stereochemistry on the Anti-Freeze Characteristics of Carbohydrates. A Thermal Study of Aqueous Monosaccharides at Subzero Temperatures. *Carbohydrate Res.* **2000,** 323, 185-191.

15. Branca, C.; Magazu, S.; G.Maisano; Migliardo, F.; P.Migliardo; Romeo, G., α, α-Trehalose/Water Solutions. 5. Hydration and Viscosity in Dilute and Semidilute Disaccharide Solutions. *J. Phys. Chem. B* **2001,** 105, 10140-10145.

16. Branca, C.; Magazu, S.; Maisano, G.; Migliardo, P., alpha,alpha-Trehalose - Water Solutions. 3. Vibrational Dynamics Studies by Inelastic Light Scattering. *J. Phys. Chem. B* **1999,** 103, 1347-1353.

17. Magazu, S.; Villari, V.; Migliardo, P.; Maisano, G.; Telling, M. T. F., Diffusive Dynamics of Water in the Presence of Homologous Disaccharides: A Comparative Study by Quasi Elastic Neutron Scattering. IV. *J. Phys. Chem. B* **2001,** 105, 1851-1855.

18. Jorov, A.; Zhorov, B. S.; Yang, D. S. C., Theoretical Study of Interaction of Winter Flounder Antifreeze Protein with Ice. *Protein Sci.* **2004,** 13, 1524-1537.

19. Yang, C.; Sharp, K. A., Hydrophobic Tendency of Polar Group Hydration as a Major Force in Type I Antifreeze Protein Recognition. *PROTEINS: Struct., Funct., Bioinf.* **2005,** 59, 266-274.

20. Czechura, P.; Tam, R. Y.; Dimitrijevic, E.; Murphy, A. V.; Ben, R. N., The Importance of Hydration for Inhibiting Ice Recrystallization with C-Linked Antifreeze Glycoproteins. *J. Am. Chem. Soc.* **2008,** 130, 2928-2929.

21. Heyden, M.; Brundermann, E.; Heugen, U.; Niehues, G.; Leitner, D. M.; Havenith, M., Long-Range Influence of Carbohydrates on the Solvation Dynamics of Water - Answers from Terahertz Absorption Measurements and Molecular Modeling Simulations. *J. Am. Chem. Soc.* **2008,** 130, 5773-5779.

22. Tam, R. Y.; Ferreira, S. S.; Czechura, P.; Chaytor, J. L.; Ben, R. N., Hydration Index - A Better Parameter for Explaining Small Molecule Hydration in Inhibition of Ice Recrystallization. *J. Am. Chem. Soc.* **2008,** 130, 17494-17501.

23. Baruch, E.; Belostotskii, A. M.; Mastai, Y., Relationship Between the Antifreeze Activities and the Chemical Structure of Polyols. *J. Mol. Struct.* **2008,** 874, 170-177.

24. Chakrabartty, A.; Hew, C. L., The Effect of Enhanced alpha-Helicity on the Activity of a Winter Flounder Antifreeze Polypeptide. *Eur. J. Biochem.* **1991,** 202, 1057-1063.

25. Jackman, J.; Noestheden, M.; Moffat, D.; Pezacki, J. P.; Findlay, S.; Ben, R. N., Assessing Antifreeze Activity of AFGP 8 using Domain Recognition Software. *Biochem. Biophys. Res. Commun.* **2007,** 354, 340-344.

26. Ruxton, G. D., The Unequal Variance t-Test is an Underused Alternative to Student's t-Test and the Mann-Whitney U Test. *Behav. Ecol.* **2006,** 17, 688-690.

27. Uchida, T.; Nagayama, M.; Shibayama, T.; Gohara, K., Morphological Investigations of Disaccharide Molecules for Growth Inhibition of Ice Crystals. *J. Cryst. Growth* **2007,** 299, 125-135.

28. Gharsallaoui, A.; Roge, B.; Genotelle, J.; Mathlouthi, M., Relationships Between Hydration Number, Water Activity and Density of Aqueous Sugar Solutions. *Food Chem.* **2008,** 106, 1443-1453.

29. Glinski, J.; Burakowski, A., Is the Hydration Number of a Non-Electrolyte Additive with Length and Constituents of the Solute Molecule? *Eur. Phys. J. Spec. Topics* **2008,** 154, 275-279.

30. Liseth, K.; Abrahamsen, J. F.; Bjorsvik, S.; Grottebo, K.; Bruserud, O., The Viability of Cryopreserved PBPC Depends on the DMSO Concentration and the Concentration of Nucleated Cells in the Graft. *Cryotherapy* **2005,** 7, 328-333.

31. Pronk, P.; Ferreira, C. A. I.; Witkamp, G. J., A Dynamic Model of Ostwald Ripening in Ice Suspensions. *J. Cryst. Growth* **2005,** 275, e1355-e1361.

32. Huige, N. J. J.; Thijssen, H. A. C., Production of Large Crystals by Continuous Ripening in a Stirrer Tank. *J. Cryst. Growth* **1972,** 13/14, 483-487.

33. Inada, T.; Modak, P. R., Growth Control of Ice Crystals by Poly(Vinyl Alcohol) and Antifreeze Protein in Ice Slurries. *Chem. Eng. Sci.* **2006,** 61, 3149-3158.

34. Karim, O. A.; Haymet, A. D. J., The Ice/Water Interface. *Chem. Phys. Lett.* **1987,** 138, 531-534.

35. Sadtchenko, V.; Ewing, G. E., Interfacial Melting of Thin Ice Films: An Infrared Study. *J. Chem. Phys.* **2002,** 116, 4686-4697.

36. Gage, A. A.; Baust, J., Mechanisms of Tissue Injury in Cryosurgery. *Cryobiology* **1998,** 37, 171-186.

37. Mazur, P., Principles of Cryobiology. In *Life in the Frozen State*, 1 ed.; Fuller, B.; Lane, N.; Benson, E. E., Eds. CRC Press: 2004; pp 3-66.

38. Farrant, J.; Walter, C. A.; Lee, H.; McGann, L. E., Use of Two-Step Cooling Procedures to Examine Factors Influencing Cell Survival Following Freezing and Thawing. *Cryobiology* **1977,** 14, 273-286.

39. Baust, J. G.; Gage, A. A., The Molecular Basis of Cryosurgery. *BJU International* **2005,** 95, 1187-1191.

40. Hossain, A. M.; Osuamkpe, C. O., Sole Use of Sucrose in Human Sperm Cryopreservation. *Archives of Andrology* **2007,** 53, 99-103.

41. Scheinkonig, C.; Kappicht, S.; Kolb, H.-J.; Schleuning, M., In Vitro Studies: Adoption of Long-Term Cultures to Evaluate the Cryoprotective Potential of Trehalose for Freezing Hematopoietic Stem Cells. *Bone Marrow Transplant.* **2004,** 34, 531-536.

42. Sugimachi, K.; Roach, K. L.; Rhoads, D. V.; Tompkins, R. G.; Toner, M., Nonmetabolizable Glucose Compounds Impart Cryotolerance to Primary Rat Hepatocytes. *Tissue Engineering* **2006,** 12, 579-588.

43. Beattie, G. M.; Crowe, J. H.; Lopez, A. D.; Cirulli, V.; Ricordi, C.; Hayek, A., Trehalose: A Cryoprotectant That Enhances Recovery and Preserves Function of Human Pancreatic Islets After Long-Term Storage. *Diabetes* **1997,** 46, 519-523.

44. Katenz, E.; Vondran, F. W. R.; Schwartlander, R.; Pless, G.; Gong, X.; Cheng, X.; Neuhaus, P.; Sauer, I. M., Cryopreservation of Primary Human Hepatocytes: The Benefit of Trehalose as an Additional Cryoprotective Agent. *Liver Transplant.* **2007,** 13, 38-45.

45. Morgan, M. J.; Faik, P., Carbohydrate Metabolism in Cultured Animal Cells. *Bioscience Reports* **1981,** 1, 669-686.

46. Carruthers, A., Facilitated Diffusion of Glucose. *Physiological Rev.* **1990,** 70, 1135-1176.

47. Schliess, F.; Haussinger, D., The Cellular Hydration State: A Critical Determinant for Cell Death and Survival. *Biol. Chem.* **2002,** 383, 577-583.

48. Fahy, G. M., The Relevance of Cryoprotectant "Toxicity" to Cryobiology. *Cryobiology* **1986,** 21, 1-13.

49. Liu, S.; Wang, W.; von Moos, E.; Jackman, J.; Mealing, G.; Monette, R.; Ben, R. N., In Vitro Studies of Antifreeze Glycoprotein (AFGP) and a C-Linked AFGP Analogue. *Biomacromolecules* **2007,** 8, 1456-1462.

50. Ravishankar, R.; Surolia, A.; Vijayan, M.; Lim, S.; Kishi, Y., Preferred Conformation of *C*-Lactose at the Free and Peanut Lectin Bound States. *J. Am. Chem. Soc.* **1998,** 120, 11297-11303.

51. Suggett, A., Molecular Motion and Interactions in Aqueous Carbohydrate Solutions. III. A Combined Nuclear Magnetic and Dielectric-Relaxation Strategy. *J. Solution Chem.* **1976,** 5, 33-46.

52. Liu, S. Novel C-linked Antifreeze Glycoprotein (AFGP) Analogues as Potent Recrystallization Inhibitors: Preparation, Assessment, and In Vitro Studies. University of Ottawa, Ottawa, 2006.

53. Liu, S.; Ben, R. N., *C*-Linked Galactosyl Serine AFGP Analogues as Potent Recrystallization Inhibitors. *Org. Lett.* **2005,** 7, 2385-2388.

54. Koneshan, S.; Rasaiah, J. C.; Lynden-Bell, R. M.; Lee, S. H., Solvent Structure, Dynamics, and Ion Mobility in Aqueous Solutions at 25 ºC. *J. Phys. Chem. B* **1998,** 102, 4193-4204.

55. Tuckerman, M.; Laasonen, K.; Sprik, M.; Parrinello, M., Ab Initio Molecular Dynamics Simulation of the Solvation and Transport of H_3O^+ and OH^- Ions in Water. *J. Phys. Chem.* **1995,** 99, 5749-5752.

56. Grossfield, A., Dependence of Ion Hydration on the Sign of the Ion's Charge. *J. Chem. Phys.* **2005,** 122, 024506-1 to 024506-10.

57. Corzana, F.; Busto, J. H.; Jimenez-Oses, G.; Garcia de Luis, M.; Asensio, J. L.; Jimenez-Barbero, J.; Peregrina, J. M.; Avenoza, A., Serine versus Threonine Glycosylation: The Methyl Group Causes a Drastic Alteration on the Carbohydrate Orientation and on the Surrounding Water Shell. *J. Am. Chem. Soc.* **2007,** 129, 9458-9467.

58. Uedaira, H.; Okouchi, S.; Tsuda, S.; Uedaira, H., Hydration of Glucose and Galactose Derivatives. *Bull. Chem. Soc. Jpn.* **2001,** 74, 1857-1861.

Chapter 4 : Dramatic Structural Modifications to Galactose and Their Effect on IRI Activity

Hydrophobic groups have been implicated in the action of biological antifreezes. Although it was initially believed that only polar residues were involved in ice binding, this theory was disproven by several experiments. For example, Sonnichsen et al. have observed that the ice binding site of AFP III is planar and fairly non-polar.[1] Although the spacing of the polar groups matches that of the prism face of the ice lattice, many of the residues in the ice-binding site are not accessible to the solvent, and the number of ice-antifreeze hydrogen bonds is restricted by the conformation of the protein.[1] They therefore suggest that hydrophobic groups may be involved in protein-ice adsorption.[1] Yang et al. have proposed that AFP III binds to ice based on atomic surface complimentarity arising from van der Waals interactions.[2] Mutations that extend or shorten the side chain of an ice-binding amino acid residue decrease van der Waals interactions and interrupt the required ice-protein surface-surface complimentarity, thereby decreasing antifreeze activity.[3] Finally, molecular dynamics simulations showed that during ice binding, the threonine side chains were oriented away from the ice-protein interface.[4] This suggests that the protein was a good steric fit to the ice-water interface and that it is this matching that controls binding.[4]

Additional studies using AFP mutants have confirmed the necessity of hydrophobic groups for antifreeze ice-binding and activity. Replacing threonine residues with serine, which retains the hydroxyl group of threonine, resulted in moderate to complete loss of activity;[5-7] although replacement by valine residues, which retains the γ-methyl group of threonine but eliminates the hydroxyl group, had a much less drastic effect on antifreeze activity.[6, 8] These experiments have led researchers to conclude that hydrogen bonds involving the threonine hydroxyls are not solely responsible for protein-ice binding, and suggest that entropic effects and van der Waals interactions are important.[5] The current theory is that the methyl groups of the threonine provide a driving force for the initial binding and are involved in overall stability of the protein, while the polar residues control binding specificity, impart stability, aid in irreversible

binding, and prevent the proteins from moving along the ice surface.[7, 9] All of these results show that hydrophobic moieties on the biological antifreezes are equally as important as their hydrophilic moieties in imparting their antifreeze activity.

Recent work in our laboratory has suggested that the hydration of carbohydrates is important in antifreeze activity.[10] The way that a carbohydrate fits into the three-dimensional hydrogen bonded network of ice, and consequently the degree of disorder of bulk water that it imparts, seems to affect the ability of water molecules to transfer from the QLL and bulk water to growing ice crystals. Adding hydrophobic moieties to carbohydrates will certainly affect their fit into the hydrogen bonded network of water, and will therefore likely affect their ability to act as ice-recrystallization inhibitors. This will be explored in the current chapter of this thesis.

4.1: Synthesis and Evaluation of Carbohydrates Containing Methoxy Groups

Substituting a hydroxyl group with a methoxy group is an ideal modification to examine the effect of hydrophobic groups on antifreeze activity. The methoxy group is relatively small and is comparable in size to a free hydroxyl group,[11] so it should not result in a drastic change of the solution conformation of the carbohydrate. Furthermore, the methoxy group adds steric hindrance and is unable to act as a hydrogen bond donor, but is still able to act as a hydrogen bond acceptor.[11] Incorporating methyl groups into simple galactose derivatives will allow us to determine the effect of hydrogen bond donating ability on IRI activity. In addition, systematically moving the methoxy group around each position of the carbohydrate will allow us to examine the effect of each hydroxyl group on antifreeze activity. Many researchers have proposed that the hydroxyl groups at C-2 and C-4 are especially important in determining the hydration of carbohydrates.[12, 13] We will explore this hypothesis through the synthesis and IRI assessment of methylated α-C-allyl derivatives (**28-31**) (Figure 4.1) and α/β-methylgalactopyranosides (**32**) and (**33**) (Figures 2.14 and 4.3).

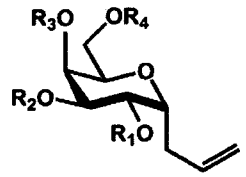

28: R_1 = Me, R_2=R_3=R_4=H
29: R_2 = Me, R_1=R_3=R_4=H
30: R_3 = Me, R_1=R_2=R_4=H
31: R_4 = Me, R_1=R_2=R_3=H

Figure 4.1: Methylated compounds (**28-31**) to be prepared for evaluation of IRI activity

Galema and Hoiland have calculated partial molar compressibilities and hydration numbers for methylated derivatives of several monosaccharides, including galactose and glucose.[12] These are summarized in Table 4.1. They have observed that hydration numbers of α- and β-methylgalactopyranoside (**32**) and (**33**) have larger hydration numbers than galactose (**5**), which suggests that they are more effectively hydrated. However, the partial molar compressibilities for both anomers of methyl-galactopyranoside (**32** and **33**) are both smaller than for galactose (**5**), suggesting that the methylated derivatives have a better fit into the hydrogen bonded network of water. Based on these results, it is difficult to say what the effect of this substitution will be on ice-recrystallization inhibition activity.

Table 4.1: Partial molar compressibilities and hydration numbers of a series of monosaccharides.[12] Errors are shown in parentheses.

Carbohydrate	Partial Molar Compressibility ($K_2°(s)x10^4$, $cm^3\ mol^{-1}\ bar^{-1}$)	Hydration Number
Galactose (**5**)	-20.8 (0.5)	8.7
α-Methyl-Galactopyranoside (**32**)	-17.0 (0.2)	9.4
β-Methyl-Galactopyranoside (**33**)	-17.0 (0.1)	9.4
Glucose (**6**)	-17.6 (0.3)	8.4
α-Methyl-Glucopyranoside (**60**)	-13.0 (0.1)	9.2
β-Methyl-Glucopyranoside (**61**)	-5.9 (0.4)	8.8
3-Methoxy-Glucose (**62**)	-5.6 (0.2)	8.1

More interesting results are seen with the methylated glucose derivatives (Figure 4.2).[12] For this monosaccharide, the anomeric stereochemistry was found to play a large role in determining hydration. α-Methylglucopyranoside (**60**) has a larger hydration number than β-methylglucopyranoside (**61**) and glucose (**6**) (Figure 4.2),[12] suggesting that in this case the anomeric stereochemistry affects the hydration of the carbohydrate. This supports our observations reported in Chapter 3 that compounds with an α-configuration display greater IRI activity than compounds with a β-configuration. Again, the partial molar compressibilities were lower for the methylated derivatives than for glucose (**6**) itself, suggesting that they have a good fit into water.[12] Even more interestingly, not only does the anomeric stereochemistry have an effect, but the position of the methyl group on the ring also plays a role. This can be seen by examining 3-methoxy-glucose (**62**, Figure 4.2), which has a smaller hydration number and smaller partial molar compressibility than the other methylated derivatives and glucose itself,[12] suggesting that it causes very little disturbance to the hydrogen bonded network of water.

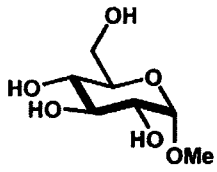

α-methylglucopyranoside
60

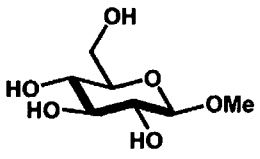

β-methylglucopyranoside
61

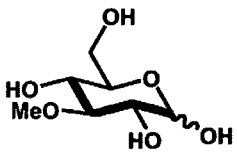

3-methoxy-glucose
62

Figure 4.2: Structures of α- and β-methylglucopyranoside (**60** and **61**) and 3-methoxy-glucose (**62**)

4.1.1: IRI Activity of α/β-Methylgalactopyranosides

In order to examine the effect of the anomeric methoxy group on IRI activity, α- and β- methylgalactopyranoside (**32**) and (**33**) were prepared using Fischer glycosylation conditions (Figure 4.3).[14, 15] (**33**) was obtained as a pure β-anomer by recrystallization, in which the minor β-anomer selectively crystallized out of solution. Unfortunately, several cycles of purification gave (**32**) as a 3:1 α:β mixture. This mixture was tested for IRI activity and compared to a sample of commercially-available (**32**) in order to further examine the effect of anomeric stereochemistry on these compounds. Figure 3.15 shows that both (**32**) and (**33**) result in a decrease in IRI activity compared to galactose (**5**). Furthermore, α-methylgalactopyranoside (**32**) produced smaller ice crystals than β-methylgalactopyranoside (**33**), mirroring our results for α- and β-*C*-allyl galactose (**14**) and (**18**). β-methylgalactopyranoside (**33**) showed no IRI activity at all, with ice crystals being the same size as in the PBS negative control as determined using a Student's T-test Two Sample with Unequal Variance.[16, 17] Interestingly, despite the majority of the mixture being in the α-configuration, the 3:1 α:β methylgalactopyranoside mixture showed identical IRI activity to pure β-methylgalactopyranoside (**33**).

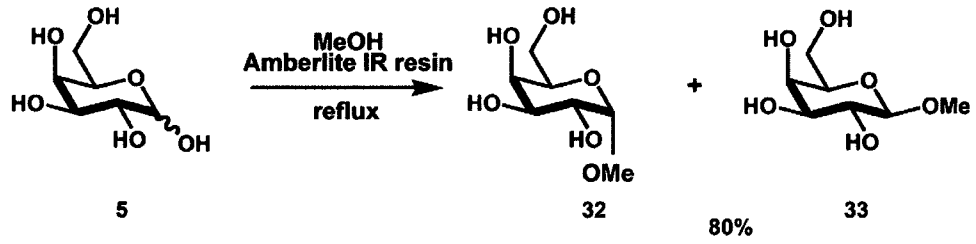

5 32 33

Figure 4.3: Preparation of α-methylgalactopyranoside (**32**) and β-methylgalactopyranoside (**33**)

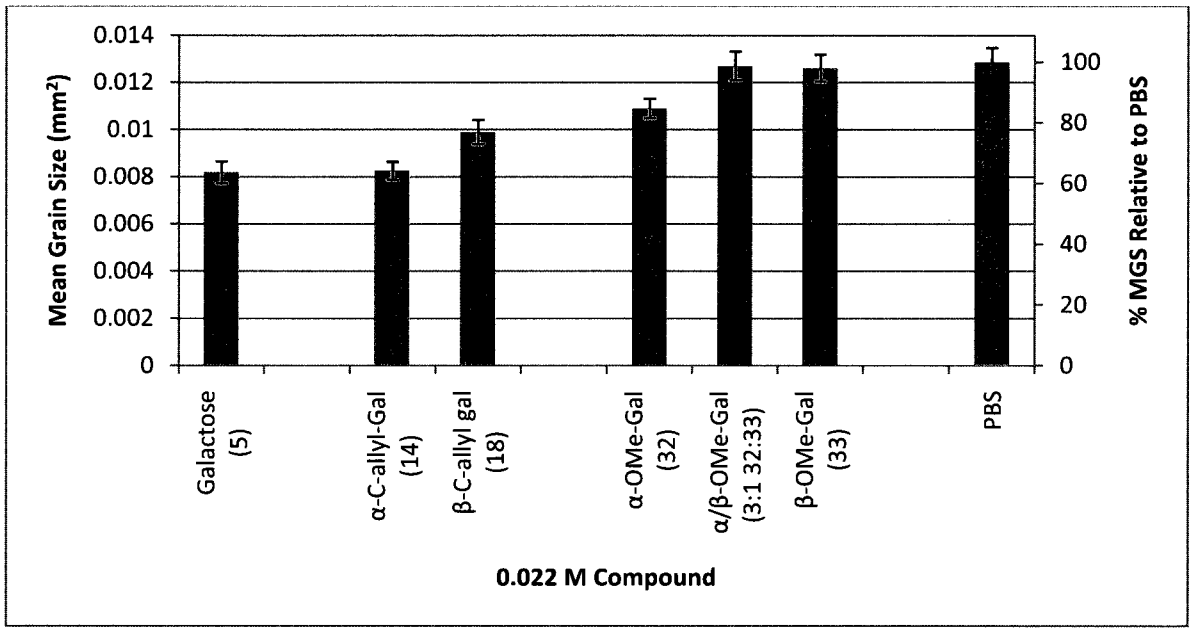

Figure 4.4: IRI activity of galactose (**5**), *C*-allyl-galactose derivatives (**14**) and (**18**), and α- and β-methylgalactopyranoside (**32**) and (**33**)

These results were quite interesting, especially since Galema and Hoiland have reported that both α- and β-methylgalactopyranoside (**32**) and (**33**) have higher hydration numbers than galactose (**5**). Based on these results, our original hypothesis was that these compounds would have greater IRI activity than galactose (**5**). However, with our IRI results in hand, we chose to calculate the hydration indices from Galema and Hoiland's values of hydration numbers and partial molar volumes for these compounds.[12] The results are portrayed in Figure 4.5. The hydration index of both compounds (**32**) and (**33**) predict that they would have poor IRI activity relative to galactose (**5**). It can be seen from this graph that these new values fit extremely well

into our correlation between IRI activity and hydration index, with an increase in the fit of the line of regression from $R^2 = 0.79$ (Figure 3.5) to $R^2 = 0.82$ in Figure 4.5. Hydration index is therefore shown to be an excellent predictor of IRI activity, unlike hydration numbers.

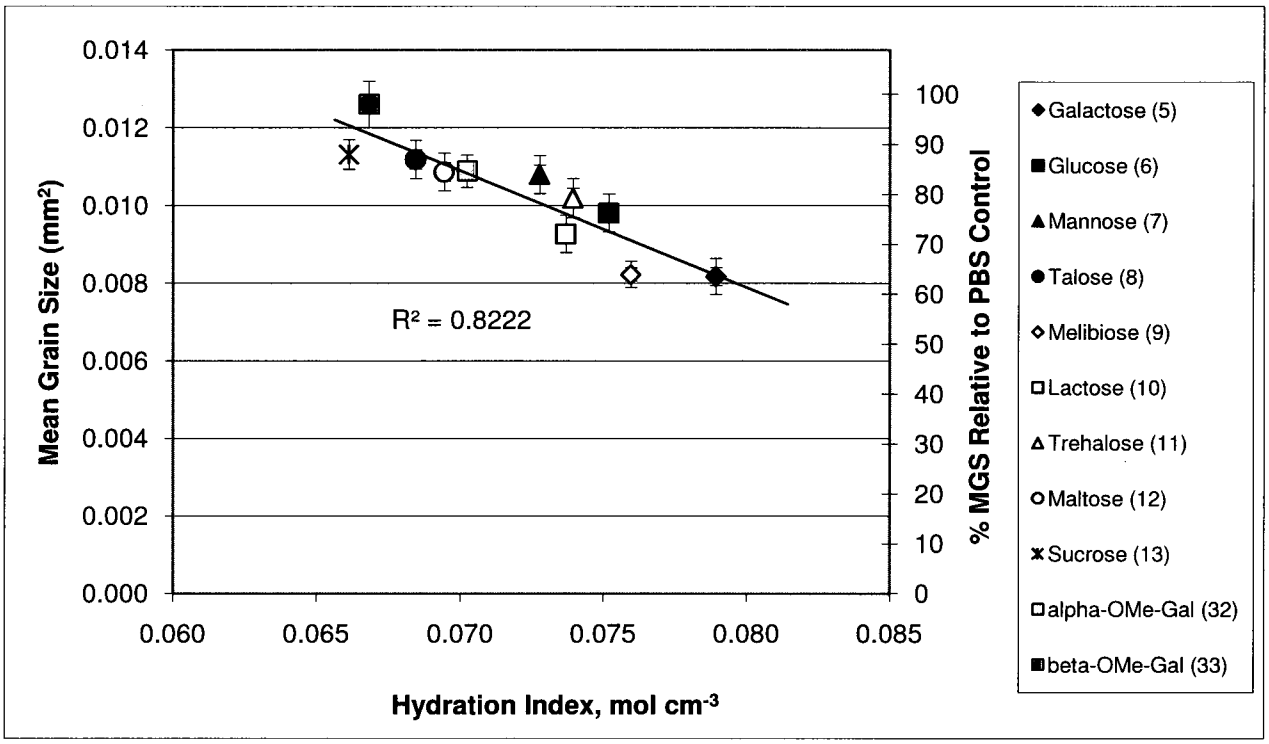

Figure 4.5: IRI activities of monosaccharides (**5 – 8**) (blue points), disaccharides (**9 – 13**) (yellow points), α-methylgalactopyranoside (**32**) (green), and β-methylgalactopyranoside (**33**) (red) plotted against their respective hydration index. Hydration index = hydration number ÷ partial molar volume (mol^1 cm^{-3})

4.1.2: Preparation and IRI activity of C*-Linked Methylated Galactose Derivatives*

With these results in hand, we turned our attention to the synthesis of methylated compounds (**28 - 31**) (Figure 4.6). These compounds will allow us to examine the role of hydrogen bond donors at each position on galactose. For this study, a large amount of α-*C*-allyl-galactose (**14**) was required. During the course of preparing β-*C*-allyl-galactose (Figure 3.17), it was discovered that the allylation with allyl-trimethylsilane in distilled acetonitrile gives a large excess of α-*C*-allyl-galactose (approximately 9:1 α:β

by ^{1}H NMR) (Figure 4.7). Furthermore, once the anomeric mixture is de-acetylated, the α-anomer selectively recrystallizes out of solution in good yield. This was found to be an efficient synthesis of the key intermediate for these studies.

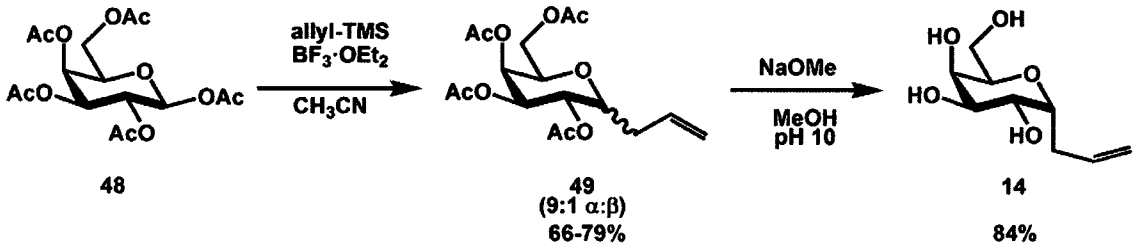

Figure 4.6: Short, efficient synthesis of α-*C*-allyl-galactose (**14**)

With (**14**) in hand, C-2 methylated galactose derivative (**28**) was prepared by a series of protecting group manipulations (Figure 4.7). First, the hydroxyl groups at C-3 and C-4 were protected as an isopropylidine acetal. Subsequent treatment with *tert*-butyldimethylsilyl chloride selectively protected the primary hydroxyl group at C-6, leaving the hydroxyl group at C-2 free to be methylated using methyl iodide and a strong base. Removal of the other protecting groups occurred in a single step to give the desired product (**28**).

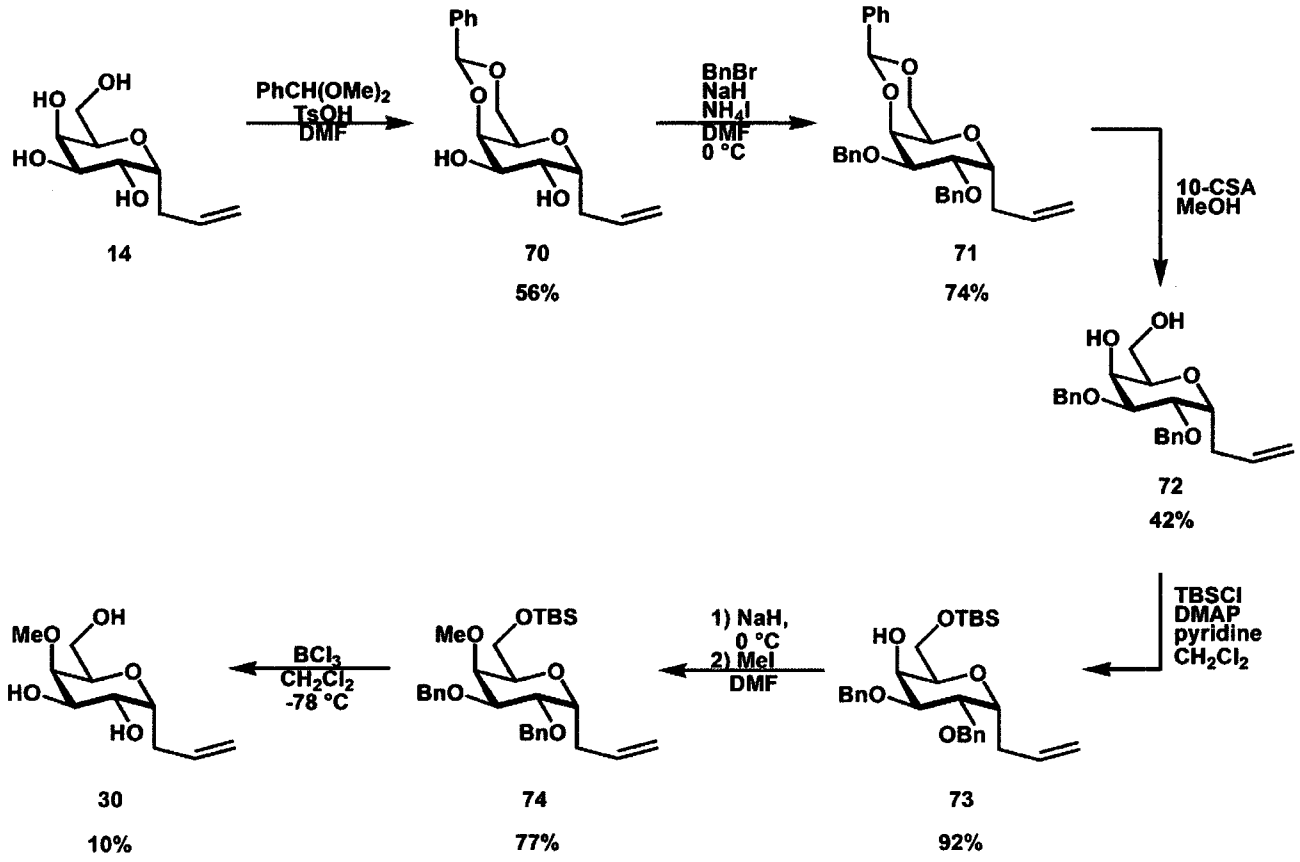

Figure 4.7: Preparation of C-2 methylated *C*-allyl-galactose (**28**) from compound (**14**)

Preparation of C-3 methylated galactose derivative (**29**) began from intermediate (**63**) (Figure 4.8). Benzoylation of C-2 and C-6 followed by removal of the isopropylidine group gave compound (**67**). This compound underwent a selective acetylation of C-4 by treatment with triethyl orthoformate followed by acid-catalyzed ring opening to give compound (**68**). Methylation of the free hydroxyl group at C-3 gave the desired compound (**69**). However, the poor yield in this reaction is likely due to acetate migration under the basic conditions of the methylation reaction, which is known to occur in partially acylated compounds.[18-20] De-acetylation of compound (**69**) gave the desired methylated compound (**29**) in good yield.

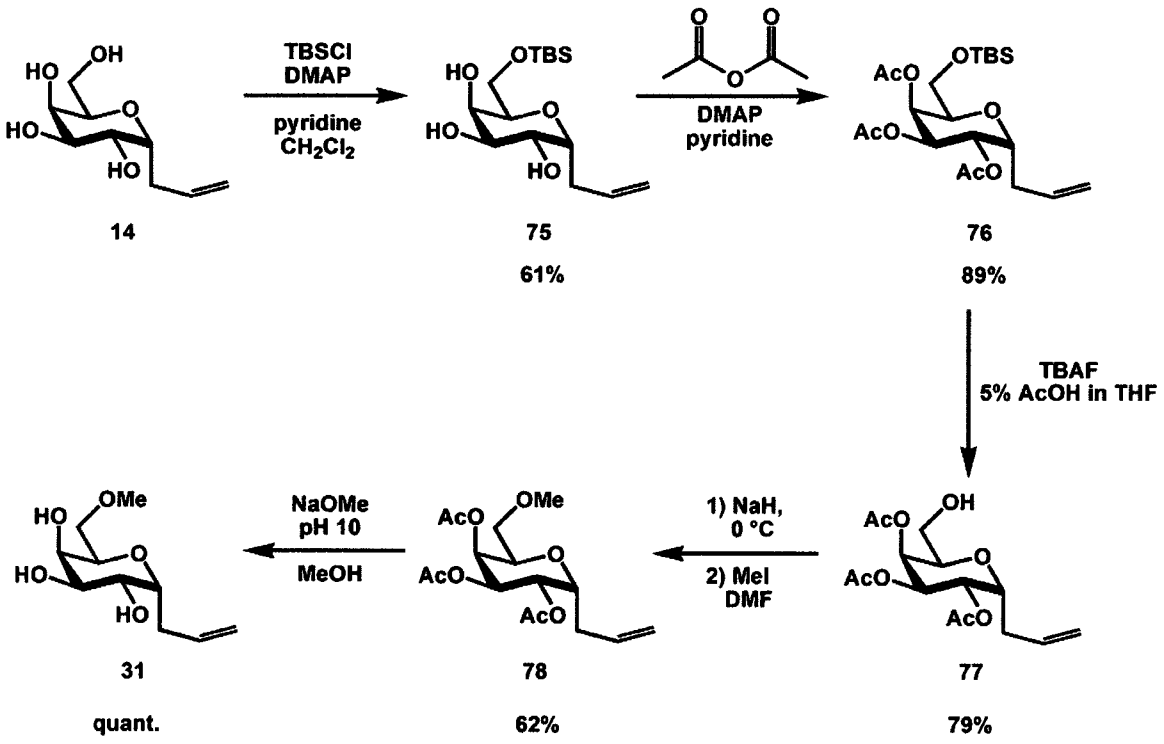

Figure 4.8: Preparation of C-3 methylated *C*-allyl-galactose (**29**) begins from intermediate (**63**).

To prepare the C-4 methylated galactose derivative (**30**), C-4 and C-6 of compound (**14**) were protected as a benzylidene acetal (Figure 4.9). Benzylation of positions C-2 and C-3 was conducted in order to avoid problems with acetate migration later in the synthesis. Acidic removal of the benzylidene acetal and selective protection of the primary hydroxyl group at C-6 with a TBS group gave compound (**73**). Methylation of the free hydroxyl group occurred in good yield. At this point, the benzyls could not be removed under standard hydrogenation conditions because of the potential for side reactions with the *C*-allyl group. Treating compound (**74**) with boron trichloride as a 1.0 M solution in dichloromethane gave a mixture of products, one of which was the desired product (**30**). The mixture of partially de-protected products accounts for the low yield of this reaction.

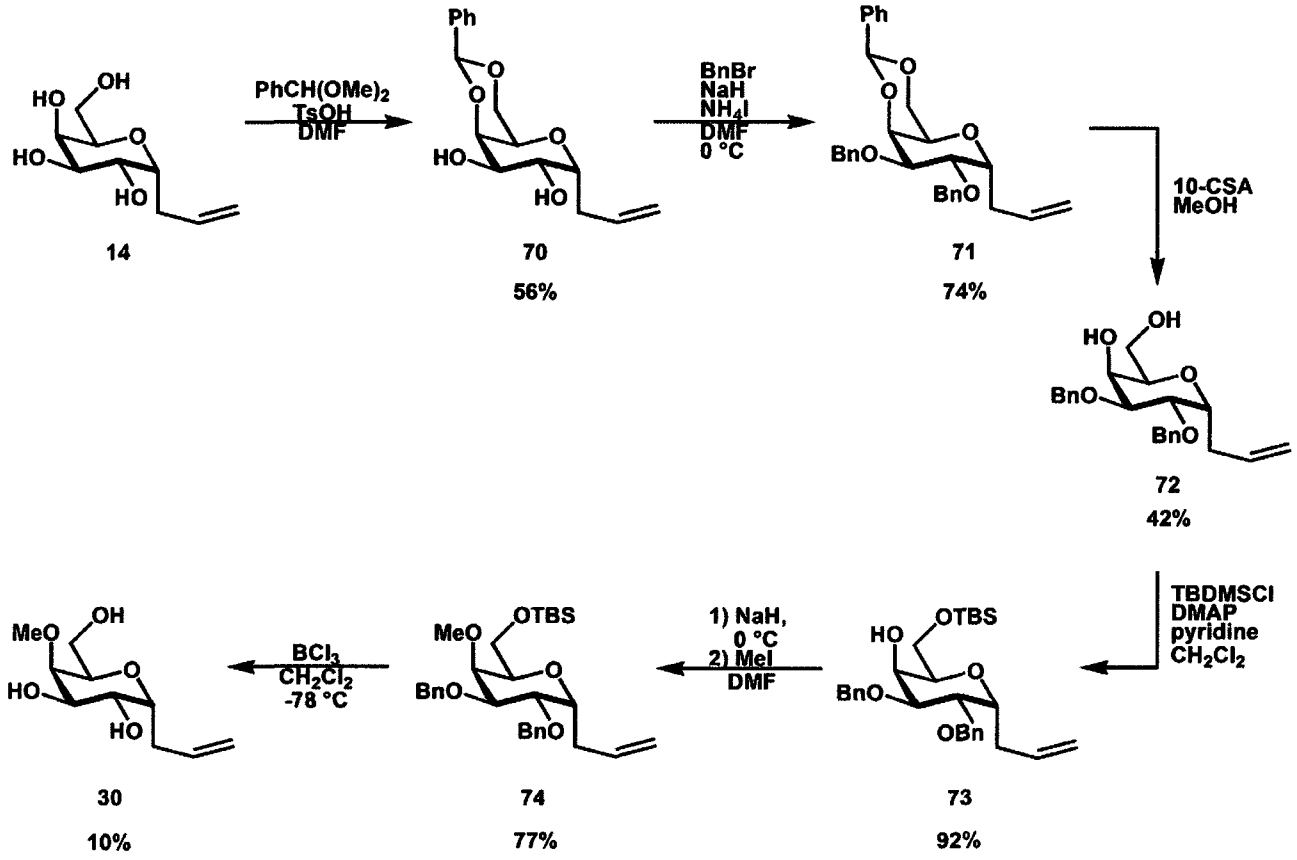

Figure 4.9: Preparation of C-4 methylated *C*-allyl-galactose derivative (**30**)

Selective protection of the primary hydroxyl group at C-6 of (**14**) began the synthesis of C-6 methylated galactose derivative (**31**) (Figure 4.10). Acetate protection of the remaining hydroxyl groups and removal of the TBS group gave compound (**77**) which was ready for methylation at the free hydroxyl group. Again, acetate migration resulted in a mixture of products that accounts for the low yield of desired compound (**78**). Flash chromatography gave pure (**78**) which was de-acetylated to give the desired compound (**31**) in quantitative yield.

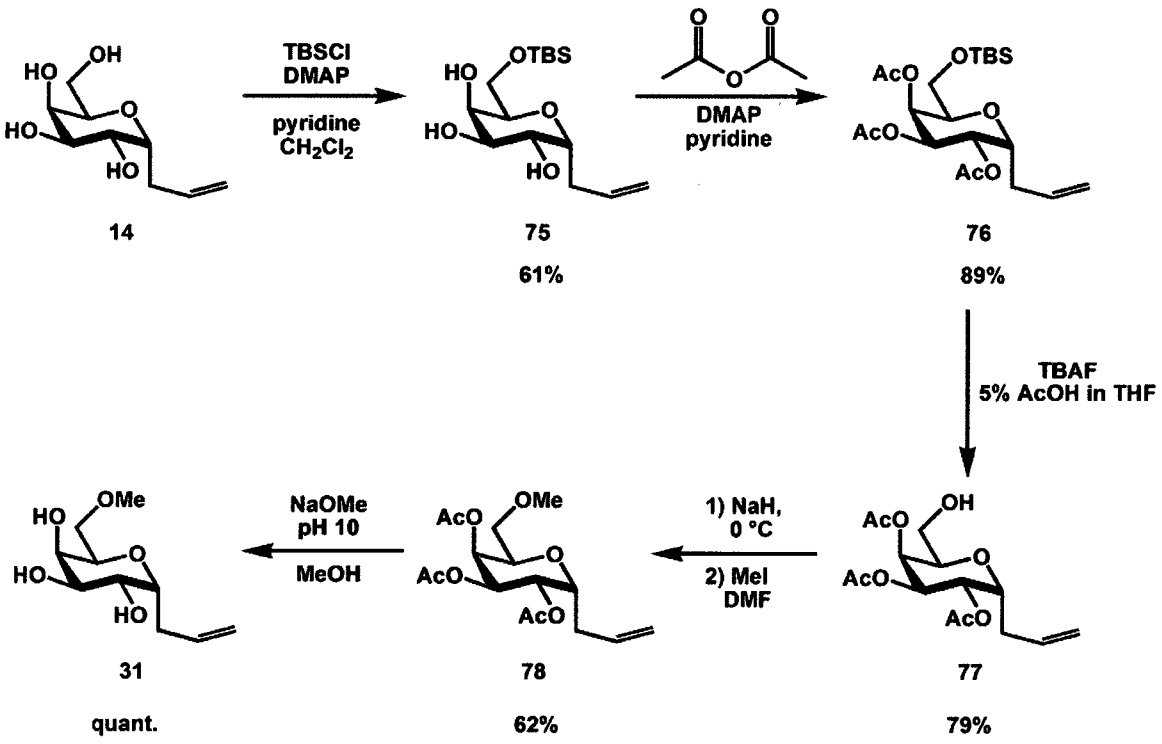

Figure 4.10: Preparation of C-6 methylated *C*-allyl galactose derivative (**31**)

These compounds (**28 - 31**) were all evaluated for ice-recrystallization inhibition activity as a measure of antifreeze activity. The results are presented in Figure 4.11 and are compared to galactose (**5**) and α-*C*-allyl-galactose (**14**). α-methylgalactopyranoside (**32**) and methylated *C*-allyl derivatives (**30**) and (**31**) all showed statistically identical activity. In all cases, there was a statistically significant decrease in activity compared to α-*C*-allyl galactose (**14**), which suggests that the methyl groups were responsible for this loss of IRI activity. Furthermore, the position of the methyl group did not seem to have an effect on IRI activity, since (**28 - 31**) showed mean grain sizes with no statistically significant differences[16] between them. These results suggest that the presence of hydrogen bond donors is extremely important for IRI activity and possibly the hydration of the carbohydrates.

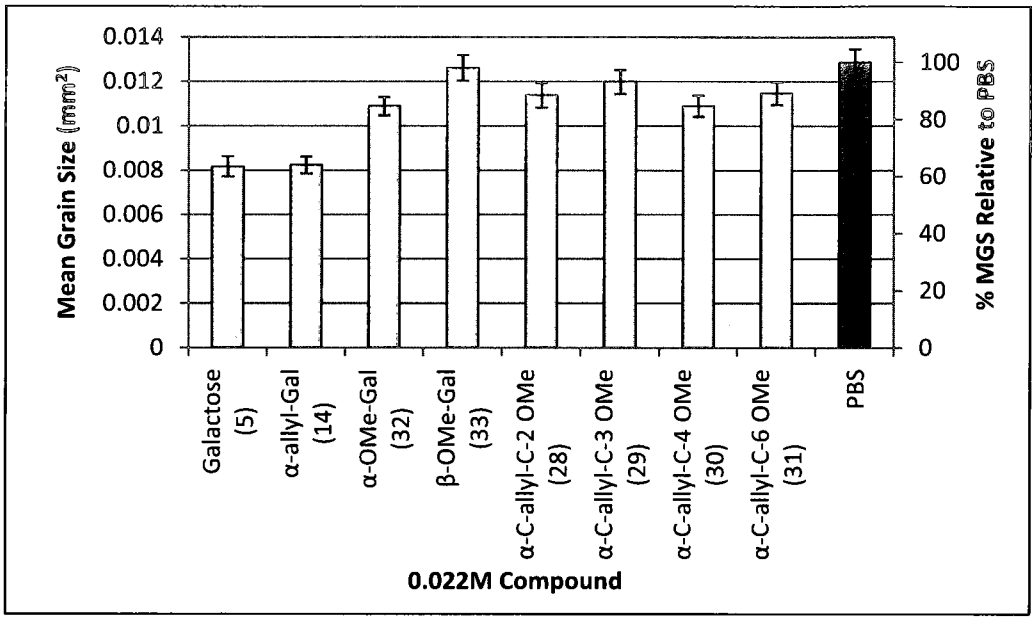

Figure 4.11: IRI activity of galactose (**5**), methylgalactopyranosides (**32**) and (**33**), and methylated derivatives (**28 – 31**)

4.1.3: Preparation and IRI Activity of an O-Linked Methylated Galactose Derivative

In order to examine whether the *C*-allyl group was having an effect during this study, compounds with an anomeric *O*-allyl group (Figure 4.12) were prepared and compared to the results for compounds (**14**) and (**28**). We have previously observed that *C*-allyl galactose (**14**) displays identical IRI activity to galactose (**5**), and we wished to probe whether the same was true for an *O*-allyl group. Figure 4.13 shows that compound (**34**) was prepared in one step from D-galactose (**5**) by refluxing with allyl alcohol in the presence of a Lewis acid. With this material in hand, (**35**) was prepared in the same manner as (**28**) (Figure 4.13).

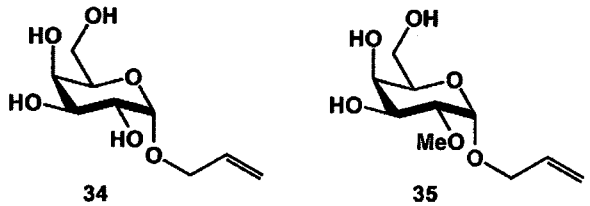

Figure 4.12: *O*-Allylated compounds (**34**) and (**35**) to be prepared for IRI testing.

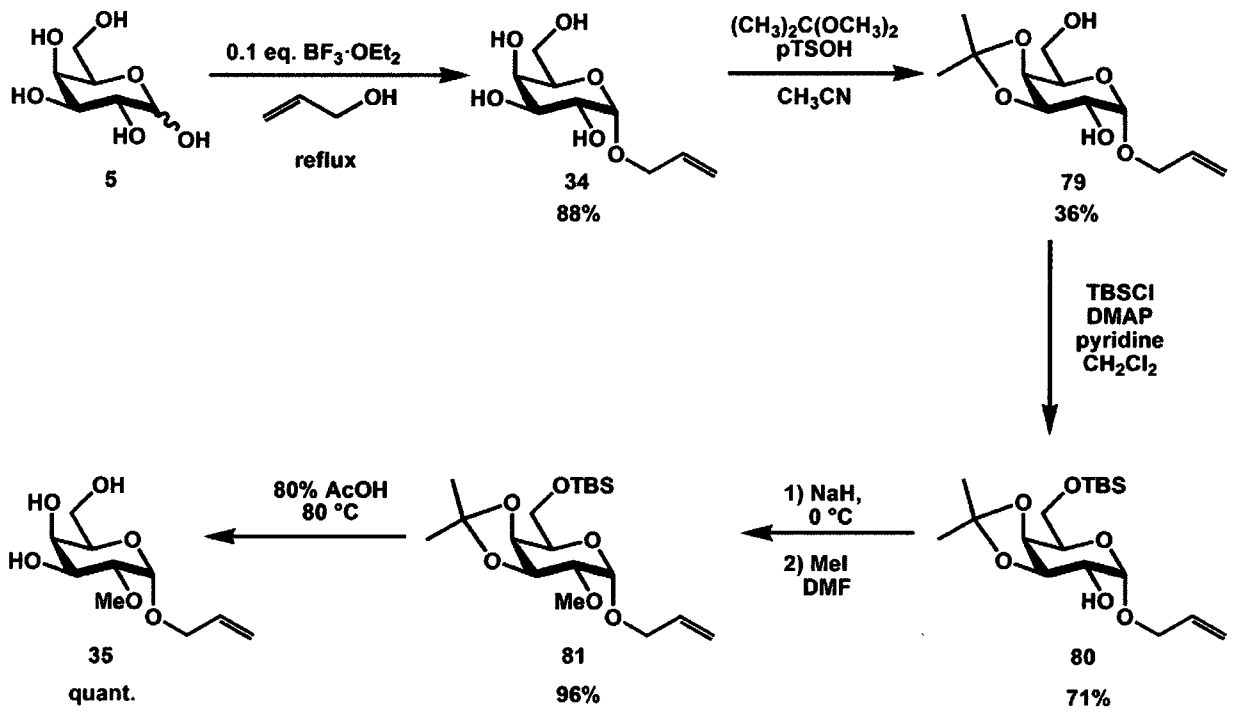

Figure 4.13: Preparation of *O*-allylated compounds (**34**) and (**35**) from D-galactose (**5**).

These compounds were tested for IRI activity and the results are displayed in Figure 4.14. α-*O*-Allyl galactose (**34**) showed statistically identical[16] activity to both galactose (**5**) and α-*C*-allyl galactose (**14**). This supports our earlier observation that the nature of the atom at C-1 has little effect on IRI activity for compounds with an α-configuration. Furthermore, methylated *O*-allyl derivative (**35**) had a mean grain size of ice crystals that was statistically identical to methylated *C*-allyl derivative (**28**). Based upon these results, we suspected that putting a methoxy group at the remaining positions of *O*-allyl galactose (**34**) would have similar results to that seen for *C*-allyl derivative (**14**). Again, the decrease in activity upon methylating one position of *O*-allyl galactose suggests that hydrogen bond donating ability is extremely important for conferring antifreeze activity.

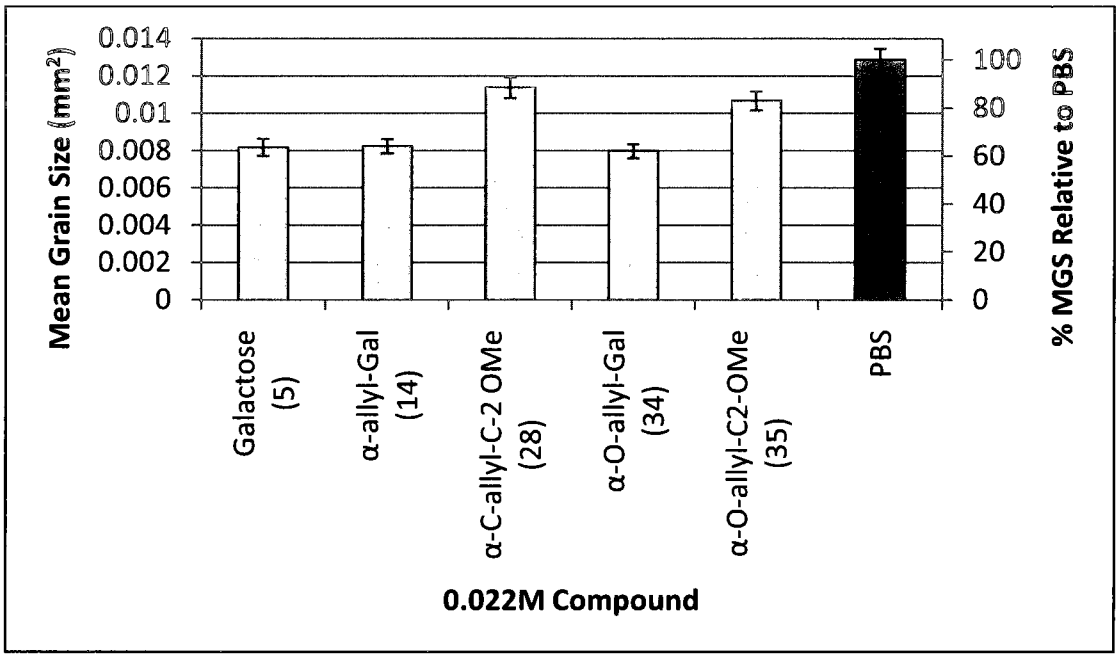

Figure 4.14: IRI activity of *O*-allylated compounds (**34**) and (**35**) compared to galactose (**5**), α-*C*-allyl galactose (**14**), and *C*-allylated C-2 methylated derivative (**28**)

4.1.4: Proposed Mechanism of Ice-Recrystallization Inhibition by Carbohydrates with Hydrophobic Groups

The experiments undertaken in this section of the thesis have provided much insight into the effect of hydrophobic groups (specifically methoxy groups) on hydration and antifreeze activity. Caffarena and Grigera have reported that water molecules tend to form a more ordered structure around hydrophobic surfaces.[21] In other words, hydrophobic molecules can increase the number of ordered water molecules by stabilizing the hydrogen bonded water network surrounding the solute.[21] Furthermore, Cheetham and Lam have observed that molecules that have a good fit into the three-dimensional structure of water and cause minimal disruption of water molecules behave in a more "hydrophobic-like" manner than molecules that have a poor fit.[22] For example, they report that the intramolecular hydrogen bonds that form in talose solutions cause talose to behave in a hydrophobic manner,[22] and talose is known to have a good fit into the 3-D structure of water.[12] When studying 1,5-anhydro-D-fructose solutions using molecular dynamics simulations, Behler et al. observed a large and tight accumulation

of water molecules close to the hydrogen atoms of the hydroxyl groups, while the water molecules were more diffuse around the lone pair sites of the oxygen atoms.[23]

Dashnau et al. have examined the role of hydrogen bonding on the cryoprotective and recrystallization inhibition properties of glycerol.[24] They propose that upon dissolution of glycerol, some of the bulk water molecules must leave the bulk phase and become incorporated into the first hydration shell of glycerol.[24] Glycerol is able to disrupt the hydrogen bonding of water molecules, becoming effectively hydrated.[24] At high glycerol concentrations, the water molecules in the hydration shell become more ice-like.[24] This ice-like hydration is typical of apolar groups, and has been observed for antifreeze proteins and is believed to aid in the recognition and binding of biological antifreezes to ice.[2] As the glycerol concentration is increased, the number of water molecules in the first hydration shell also increases at the expense of bulk water.[24] At higher concentrations, the water molecules in the first hydration shell become clustered around the hydroxyl groups of glycerol, causing the alkyl backbone to be surrounded by other glycerol molecules in a phenomenon called "alkyl backbone clustering" where hydrophobic clusters form.[24] At lower concentrations, the alkyl backbone of glycerol forms weak interactions with solvating water molecules.[24]

All of these results suggest that hydrophobic groups will cause a smaller disruption in the structure of bulk water than hydrophilic groups, resulting in their surrounding water molecules becoming quite ordered in the first hydration shell. This fits into our proposed model of how carbohydrates affect ice recrystallization depicted in Figure 3.7. As mentioned above, carbohydrates that have a large hydration index are believed to cause a greater disturbance of the order of bulk water surrounding the hydration shell. This results in greater disorder of the bulk water, and therefore more energy is required to transfer water molecules from the bulk water to the QLL of a growing ice crystal. If the carbohydrate contains hydrophobic groups, the water molecules become more ordered in the hydration shell of the carbohydrate in order to minimize unfavourable non-polar – polar interactions. Due to this increased order of the hydration shell, the bulk water is less disrupted and less energy is required to transfer

water molecules from the bulk water to the growing ice crystal. This is depicted in Figure 4.15.

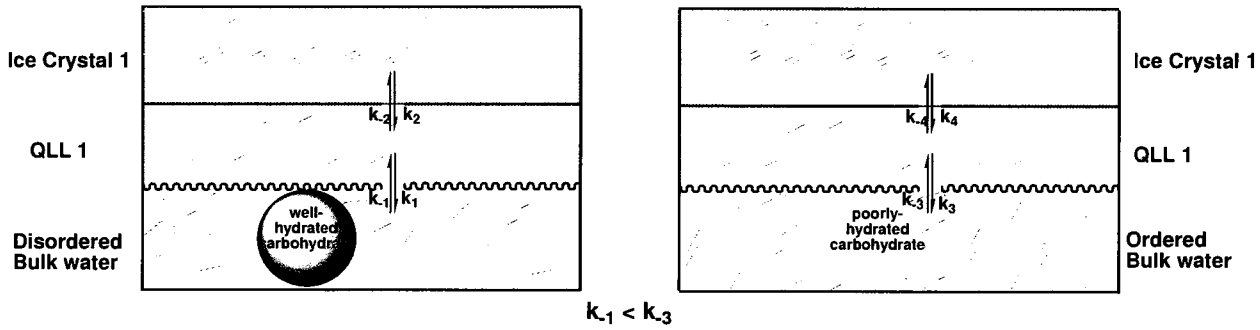

Figure 4.15: Schematic representation of the proposed mechanism for ice recrystallization inhibition with well-hydrated and poorly-hydrated carbohydrates. Carbohydrates reside at the QLL-bulk water interface between two adjacent ice crystals. Water molecules surrounding a carbohydrate that is well hydrated are more disordered than those surrounding a poorly ordered carbohydrate or in the absence of a solute. The red sphere represents a well-hydrated solute and the yellow sphere represents a poorly-hydrated solute. QLL = quasi-liquid layer[17]

Lemieux has studied the role of water in recognition of biological materials such as enzymes.[25] He has observed that the interaction of water molecules with a solute causes the hydrated water molecules to be higher in energy than those in bulk water.[25] However, there is an increase in entropy when hydrated water molecules are released back into bulk water.[25] These observations can be incorporated into our model of carbohydrate – ice and carbohydrate – water interactions. We hypothesize that carbohydrates that have a large hydration index and therefore disturb the 3-D network of water molecules greatly will result in a hydration shell containing poorly ordered water molecules. Only a small gain in entropy will be achieved upon releasing the hydrated water molecules into the bulk phase, giving an overall higher energy requirement to release these water molecules into bulk and releasing bulk water into the QLL. In contrast, carbohydrates that have a more hydrophobic hydration shell with well-ordered water molecules will attain a large gain in entropy upon releasing these hydrated water molecules into the bulk water. Furthermore, compounds that are poorly hydrated fit well into the 3D structure of water, causing minimal disruption and resulting in bulk water

that is more ordered. Less energy will be required to transfer these ordered bulk water molecules into the QLL, resulting in a faster rate of transition from the bulk water to the QLL and from the QLL to the ice. Figure 4.15 describes this process. Therefore, these poorly hydrated compounds would undergo more rapid ice-recrystallization. Compounds with hydrophobic groups are believed to be poorly hydrated and result in ordered bulk water molecules. Ultimately, we would therefore expect carbohydrates containing hydrophobic groups to be poorer inhibitors of ice-recrystallization, and this is what we observed during the current study.

This model is supported by recent observations from Nutt and Smith during their MD simulations on the hydration layer surrounding an insect AFP.[26] They observed that the ice binding face of AFP is able to increase the amount of three-dimensional ordering of the surrounding water molecules.[26] In contrast, the non-ice binding face disturbs the surrounding water molecules.[26] The authors propose that by ordering the water molecules near the ice binding face, the AFP is able to decrease the entropic loss that occurs upon binding.[26] This lowers the energy barrier and allows binding to occur.[26] Furthermore, by disrupting the water molecules surrounding the non-ice binding face, the AFP avoids being incorporated into the growing ice lattice and prevents ice growth.[26] Therefore, compounds containing structural modifications that increase the amount of ordered water molecules would be expected to be poorer inhibitors of ice recrystallization than those compounds that disturb the surrounding water molecules.

This proposed model supports our results that methylated galactose derivatives showed lower IRI activity than galactose (**5**) itself. Interestingly, the location of the methoxy groups did not have a large impact on the amount of IRI activity, as methylated derivatives (**28 – 31**) all showed comparable inhibition of ice-recrystallization. Two explanations are possible. The first is that the stereochemistry at C-2 and C-4 is not as important for hydration as initially thought. In order to confirm this, methylated derivatives of other monosaccharides with varying stereochemistry at C-2 and C-4 (i.e. glucose, mannose, and talose) would need to be prepared. A second explanation is that the methyl group is "large" enough to cause the entire molecule to adopt a more

hydrophobic hydration shell or to disrupt the entire hydration network, regardless of its position.

Despite these results, some questions remain to be answered. Through the synthesis of methylated derivatives of other monosaccharides such as glucose, mannose, and talose, we can further examine the effect of these groups on hydration. This will allow a greater understanding of the effect of the stereochemistry of the hydroxyl groups at C-2 and C-4. Furthermore, preparing deoxy-carbohydrates would allow further examination of the effect of hydrophobicity on hydration and IRI activity and would either support or refute the hydrophobic hydration model proposed above.

Our observations that methyl galactopyranosides (**32**) and (**33**) fit well into our correlation graph of IRI activity and hydration index (Figure 3.5) are extremely exciting. This suggests that the hydration index is an excellent predictor of IRI activity and that we can use this to design carbohydrates and glycoproteins that have very efficient IRI activity. These results highlight the importance of being able to calculate hydration properties of unnatural carbohydrates, such as methylated galactose derivatives (**28 – 31**). If the hydration index of these carbohydrates could be easily determined through experimental or computational methods, this would aid in the design of novel recrystallization inhibitors based upon natural carbohydrates. We have undertaken efforts towards this goal and these will be described in the next section.

4.1.5: MD Simulations to Determine the Hydration Properties of Natural and Unnatural Carbohydrates

Based on these results, we looked into the possibility of calculating hydration properties for unnatural galactose derivatives using computer simulations. To do so, we approached Dr. Tom Woo, a computational chemist in our department, for assistance. As a starting point, mono- and disaccharides with known partial molar compressibilities and hydration numbers were subjected to the Glycam force field in order to test the accuracy of the simulation. The results of these simulations are shown in Table 4.2 (Rowley and Woo, unpublished results). Two methods of evaluating hydrogen bonds

were used. The first method, "hydrogen bonded waters", counts only water molecules that are in a hydrogen bonding interaction with the carbohydrate. In the second method, "coordination sphere", any water molecule within 2.8 A of a carbohydrate atom is considered to be coordinated, although this includes any molecule that's "in the neighbourhood" and not just those in a hydrogen bonding interaction with a carbohydrate hydroxyl.

Table 4.2: Hydration numbers calculated from computer simulations compared to literature hydration numbers and the experimentally determined mean grain size

Entry	Carbohydrate	"Hydrogen bonded waters" HN	"Coordination sphere" HN	Literature hydration number[12]	IRI Mean Grain Size (mm^2)
1	Galactose (**5**)	10.9	18.1	8.7	0.008572
2	Glucose (**6**)	12.4	18.3	8.4	0.009807
3	Mannose (**7**)	10.0	---	8.1	0.010807
4	Talose (**8**)	10.4	17.3	7.7	0.01119
5	Melibiose (**9**)	19.0	28.9	15.5	0.008184
6	Trehalose (**11**)	19.3	28.2	15.3	0.01043
7	Maltose (**12**)	19.0	28.4	14.5	0.01074
8	Sucrose (**13**)	17.6	26.6	13.9	0.01058
9	α-methyl-galactopyranoside (**32**)	10.0	19.1	9.2	0.01089
10	α-*O*-allyl-galactose (**34**)	10.3	20.5	--	0.007981
11	C-2-methoxy-α-*O*-allyl-galactose (**35**)	2.2	21.4	--	0.01067

These calculated hydration numbers are compared against the experimentally determined IRI mean grain sizes in Figures 4.16 and 4.17. As is seen in these figures, these data points cannot be fit into a single correlation. The disaccharides (shown in yellow) differed from the native monosaccharides (shown in blue) and the *O*-linked monosaccharide derivatives (shown in pink). This is not surprising based on our previous observations that a hydration index is required to give a single correlation for

mono- and disaccharides. Using the hydration numbers calculated using the hydrogen bonded definition, the correlations for both native and unnatural mono- and disaccharides were quite poor (Figure 4.16). This suggests that the computer simulations used in this experiment were not able to accurately predict the hydration number for these carbohydrates. Better correlations were seen for the native mono- and disaccharides using hydration numbers calculated using the coordination sphere method (Figure 4.17). However, the correlation for unnatural carbohydrates was extremely poor. This suggests that we will need to modify the parameters used for the simulation when carbohydrate derivatives are used. The deviations in structure from the native monosaccharide must require more advanced parameters in order to accurately model the hydration of these substituents.

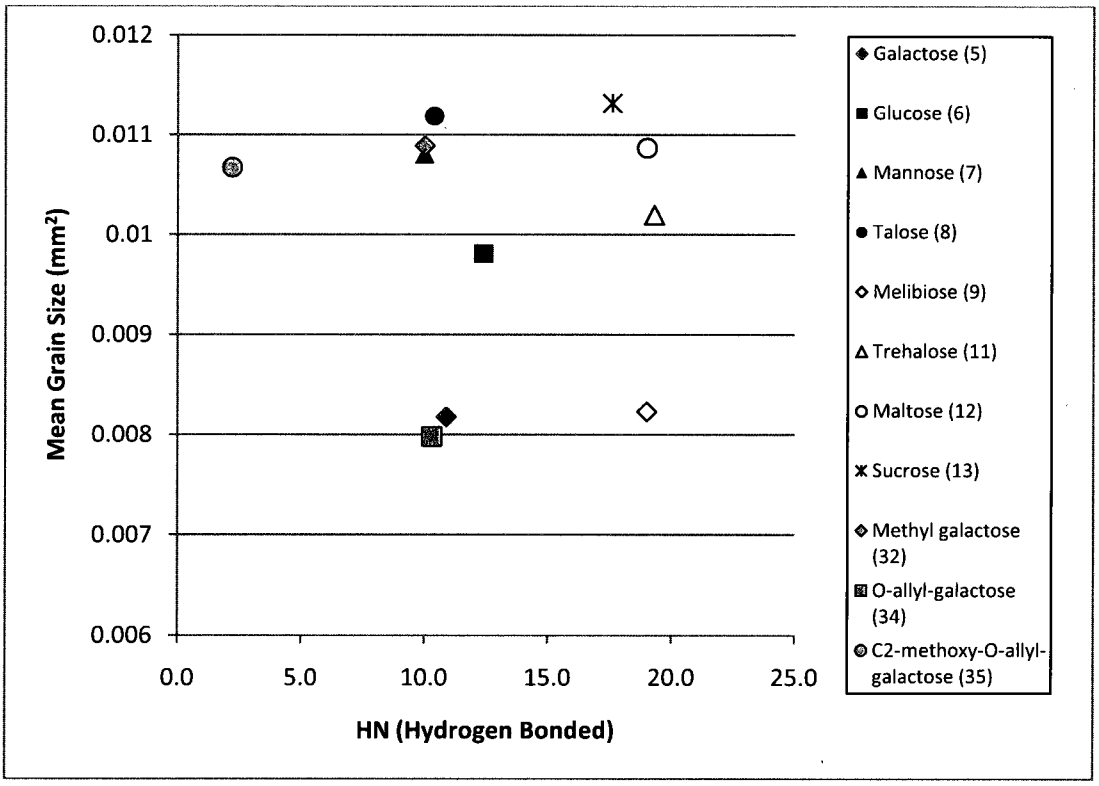

Figure 4.16: IRI activities of native monosaccharides (blue), *O*-linked monosaccharide derivatives (pink), and disaccharides (yellow) plotted against their respective hydration numbers calculated using the "hydrogen bonded" definition.

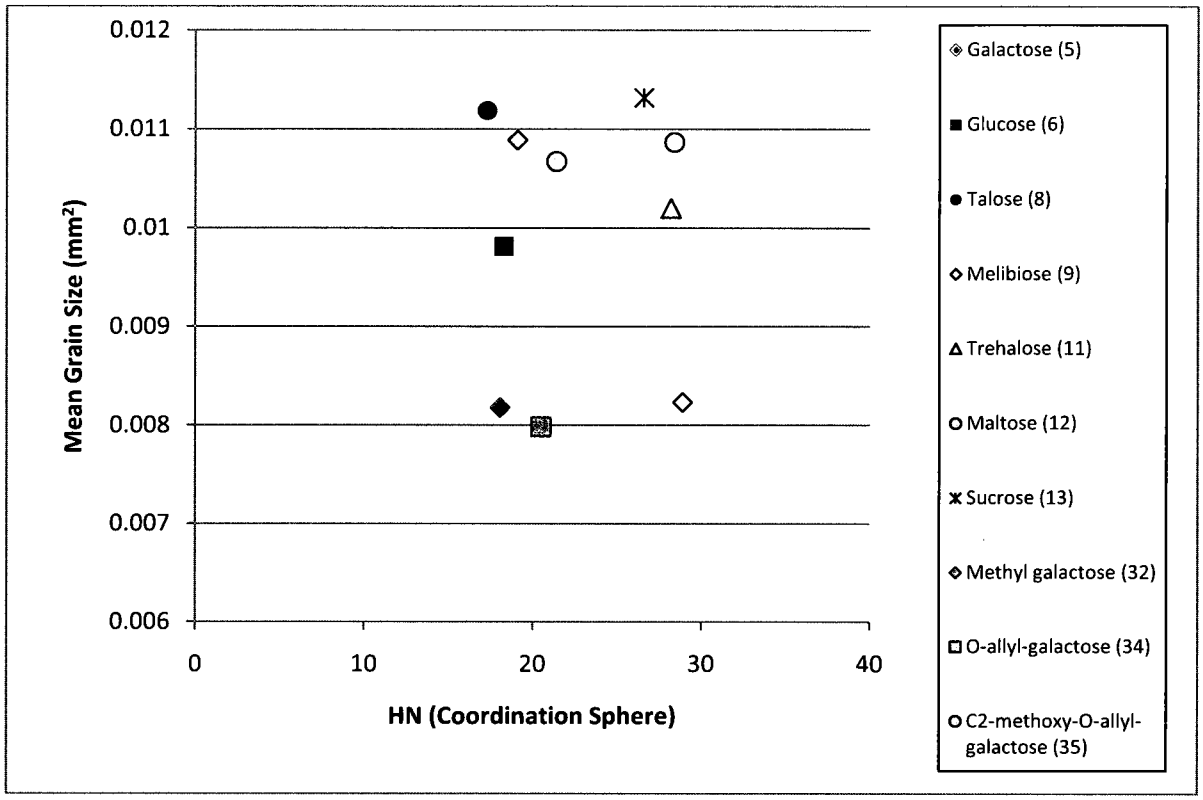

Figure 4.17: IRI activities of native monosaccharides (blue), *O*-linked monosaccharide derivatives (pink), and disaccharides (yellow) plotted against their respective hydration numbers calculated using the "coordination sphere" definition

In Table 4.2 our experimentally calculated hydration numbers are compared to those reported in the literature by Galema and Hoiland.[12] It is clear from this table that the density ultrasound measurements used by Galema and Hoiland give different hydration numbers than our computer simulations. Although the absolute values of the hydration numbers do not match those obtained by Galema and Hoiland, the trends are similar in that galactose was found to be more hydrated than talose and melibiose was more effectively hydrated than sucrose. However, in both cases glucose was observed to be more hydrated than galactose, which is opposite to the results obtained by Galema and Hoiland. In addition, mannose was also out of place in that it was calculated to be less hydrated than talose. Based upon these results, it seems that determining hydration numbers using molecular dynamics simulations is an attainable goal, although additional effort is required in order to find a computational model that is

able to accurately predict hydration numbers. We are currently working to adjust our simulation parameters to attempt to calculate more accurate hydration number values.

When we noticed that IRI activity seemed to be correlated to hydration, we initially used partial molar compressibilities as the measure of hydration of carbohydrates.[10] However, based upon a report in the recent literature that hydration numbers are often a more accurate representation of carbohydrate hydration,[27] we used hydration numbers in our hydration index calculations (Figure 3.3).[17] Since our hydration numbers obtained through modelling did not all fit the trends observed by Galema and Hoiland,[12] we chose to evaluate whether hydration indices based on partial molar compressibilities were also correlated to IRI activity, as the calculations of partial molar compressibilities may be a more attainable goal.

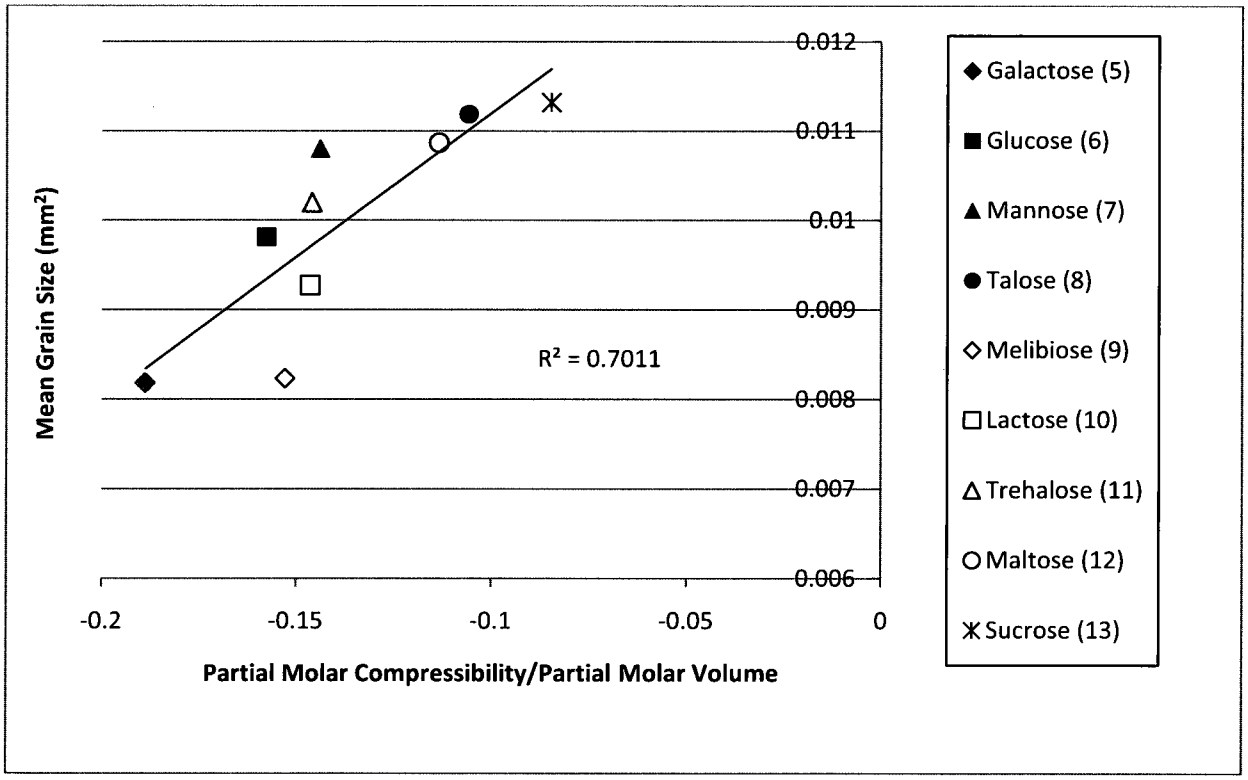

Figure 4.18: IRI activity of various monosaccharides (blue) and disaccharides (yellow) plotted against an alternate hydration index (partial molar compressibility/partial molar volume).

When we plotted the IRI activity of several mono- and disaccharides against an alternate hydration index (partial molar compressibility ÷ partial molar volume) that uses PMC as a measure of hydration, we observed that a correlation does exist (Figure 4.18). The fit of the line of regression was slightly decreased compared to the previously described hydration index (hydration number ÷ partial molar volume), 0.79 for Figure 3.3 and 0.70 for Figure 4.35. However, these results did suggest that partial molar compressibilities, when incorporated into a hydration index based upon PMCs, are correlated to IRI activity. Therefore, we sought to determine the partial molar compressibilities of a series of carbohydrates using molecular dynamics simulations. The results are displayed in Table 4.3.

Table 4.3: Partial molar volumes and partial molar compressibilities calculated by Christopher Rowley (Rowley and Woo, unpublished results) and compared to Galema's literature values.[12]

	Molar Volume (Rowley)	PMV (Galema)	Solution Compressibilty	PMC (Rowley)	PMC (Galema)
Water			4.51		
Galactose (**5**)	116.7	112.5	4.56	0.027	-11.9
Mannose (**7**)	124.4	111.0	4.36	-0.090	-16.0
Talose (**8**)	104.1	111.3	4.23	-0.17	-20.8
Sucrose (**13**)	228.9	211.6	4.30	-0.15	-17.8

Again, the absolute values of partial molar compressibilities calculated by Rowley are very different from the literature values obtained by Galema and Hoiland. However, the trend is retained in which galactose (**5**) > mannose (**7**) > talose (**8**) ≈ sucrose (**13**). It is possible that our partial molar volume calculations are inaccurate, and that this is responsible for the poor partial molar compressibility values. Despite these differences in absolute values compared to the literature, the calculation of partial molar compressibilities may be a more immediately attainable goal for determining the hydration properties of carbohydrates. This will need to be explored in the future.

In order to confirm that the hydration of carbohydrates is correlated to IRI activity, we must determine the previously unstudied hydration properties of monosaccharide derivatives, such as *C*-allyl galactose and *O*-allyl galactose. Furthermore, if this goal is realized, we would be able to design carbohydrates that have efficient IRI activity and that may be used as novel cryoprotectants. Initial efforts to calculate the hydration properties of natural carbohydrates using molecular dynamics simulations were promising, although the parameters and methods must be improved before these calculations are extended to unnatural monosaccharide derivatives.

4.2: Synthesis and IRI Assessment of Fluorinated AFGP8 Analogues and Carbohydrates

Fluorine atoms have been extensively incorporated into biological molecules. A fluorine atom has a similar size to that of a hydroxyl group, which makes the fluorine atom an appropriate replacement for the hydroxyl group in binding studies.[28] For example, Blackburn et al. have observed that the tetrahedral *geminal*-difluoromethylene group (-CF_2) is a good replacement of an oxygen atom in phosphonate and phosphate analogues.[29] Furthermore, Kalinina et al. have incorporated fluorine atoms into synthetic analogues of nucleoside-3-phosphate.[30]

The effect of fluorine atoms on the molecular recognition, structure, and transport properties of biological molecules was examined extensively by Kim and co-workers through the design of highly fluorinated glucose analogues.[31] Their hypothesis was that structural changes that decrease the "polarizability" but maintain the charge distribution and size of a biological molecule would result in enhanced binding to the physiological receptor; a phenomenon termed "polar hydrophobicity".[31] They believed that induced dipole interactions have a larger effect in aqueous solution than in a static environment, such as when the compound is bound to its receptor.[31] It was suggested that fluorine substitution would increase the degree of "polar hydrophobicity", since the C-F bond is very polar but is not polarisable, and that this modification would therefore result in improved transport and recognition of the biological analogue.[31] Compounds that were modified with CF_2 groups replacing CHOH groups did in fact display increased binding,

and transport across the erythrocyte membrane was 10 times greater than for glucose itself. [31, 32] This was attributed to be a result of enhanced affinity for the substrate to the transporter protein.[31, 32] Furthermore, electrostatic interactions between the polarized C-F bond with dipoles in the receptor were expected to occur, while these interactions would be insignificant in aqueous medium.[31] Interestingly, fluorinated compounds are known to cause water molecules to order around the hydrophobic portions of the solute, resulting in a negative entropy of aqueous solution, as in hydrocarbons.[33]

The difluoromethylene group is known to be isopolar and isosteric to oxygen.[34] It is often used as an oxygen replacement because it mimics the polarity of oxygen and is suggested to affect its ability to act as a hydrogen bond acceptor.[35] Fluorines are also an attractive addition to biological molecules because they are chemically inert and have a relatively small size.[33] It is generally accepted that difluoromethylene groups will maintain the overall structure of the carbohydrate, but will affect the hydrogen bonding interactions.[36] The ability of covalent fluorine atoms to form hydrogen bonds is a subject of great debate. There is no question that free fluoride ions are good proton acceptors, forming very strong hydrogen bonds, although the same may not be true of covalently bound fluorine atoms.[37]

Howard et al. have observed that aliphatic C(sp^3)-F fluorine atoms can form stronger hydrogen bonds than olefinic or aromatic C(sp^2)-F fluorine atoms.[38] Despite this observation, aliphatic C(sp^3)-F hydrogen bonds are less than half as strong as C-O hydrogen bonds.[38] In their study of entries in the Cambridge Structural Database System, compounds with bond lengths consistent with optimal covalent F - H hydrogen bonds were very rare.[38] However, the authors suggest that binding sites of receptors and proteins may provide an optimal environment for fluorine hydrogen bonds to form by orientating fluorine atoms directly at the hydrogen bond donor.[38] In a separate study, Dunitz and Taylor examined compounds from the Cambridge Structural Database System and the Brookhaven Protein Data Bank and found that short bond lengths consistent with covalent fluorine hydrogen bonds are very uncommon.[37] When bond lengths were observed that suggest the possible formation of hydrogen bonds, the bonds were very weak.[37] The authors conclude that covalently bonded fluorine very

rarely acts as a hydrogen bond acceptor, and when it does, it is found in exceptional molecular environments.[37] The weak hydrogen bonding capacity of covalently linked fluorine is suggested to be due to its low proton affinity because of its low basicity and tightly held lone pairs and electron shell.[37] Furthermore, it is unable to delocalize its electrons to modify this low affinity.[37] However, weak C-F-H-O hydrogen bonds or bridges have been observed in the crystal structures of some 2-fluoro-2-deoxy pyranosyl fluorides[28, 39] and of calcium 2-fluorobenzoate dehydrate.[40]

Fluorinated carbohydrates have been utilized for several years because fluorine atoms may mediate the biological and chemical properties of the carbohydrate. Glycosyl fluorides are often used as both substrates[41, 42] and inhibitors[34, 41, 42] of carbohydrate enzymatic reactions. As inhibitors, they are used to probe the mechanism and the structure of the active site in enzymatic reactions.[42] The synthesis of fluorinated carbohydrates has been extensively reviewed by Plantier-Royon and Portella.[34] Some noteworthy examples of fluorinated monosaccharides include the preparation of fluorinated D-glucitol and D-mannitol analogues by Giuffredi et al.,[36] and the synthesis of tetrafluorinated glucose and galactose derivatives by Timofte and Linclau[32] (Figure 4.19). Berber et al. have prepared mono- and disaccharides in which a difluoromethylene group replaces the anomeric oxygen (Figure 4.19).[43] In addition to fluorinated carbohydrates, fluorinated glycopeptides have been prepared, such as a fluorinated serine-*O*-glycopeptide by Herpin et al. (Figure 4.19).[44] Fluorine atoms and fluoroalkyl groups are known to increase the lypophilicity of compounds,[41] and fluorinated compounds have been reported to display liquid crystalline behaviour.[45]

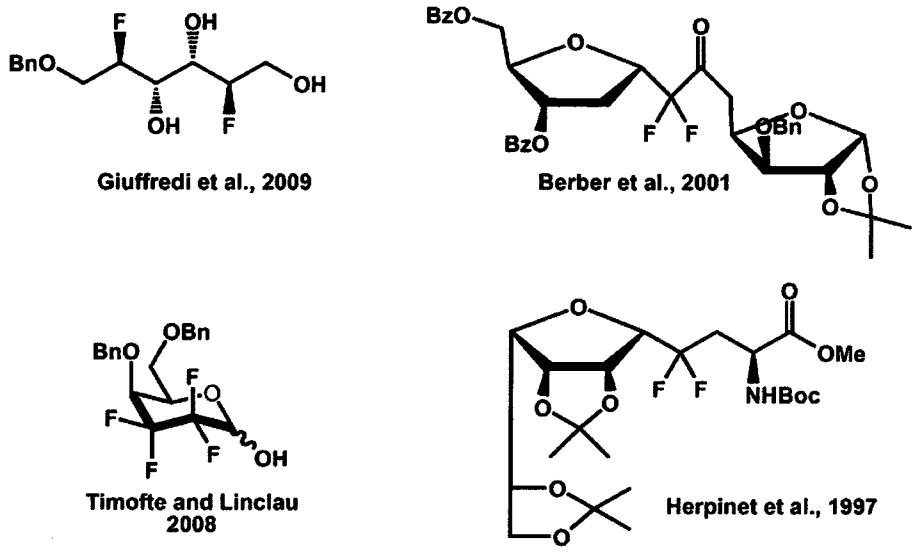

Figure 4.19: Examples of fluorinated carbohydrate analogues prepared by Giuffredi et al.,[36] Berber et al.,[43] Timofte and Linclau,[32] and Herpin et al.[44]

Fluorine atoms were incorporated into an AFGP analogue reported by Quirion and Castelot-Deliencourt-Godefroy in 2006 (Figure 4.2, Image **A**).[46] They reported that these short glycopeptides were able to preserve human embryonic kidney cells, erythrocytes, blood platelets, and skin fibroblasts at physiological and sub-zero temperatures. However, the mechanisms of preservation by these compounds were not investigated, and it is unknown whether they exhibit antifreeze activity through thermal hysteresis or ice-recrystallization inhibition. We realized that similar analogues (Figure 4.20, Image **B**) would be appropriate for examining the role of the CF_2 group on IRI activity. As mentioned above, the *geminal*-difluoromethylene group has been reported to be a good steric mimic of oxygen and of a methylene group,[34] so the conformation of these analogues should be similar to our OGG-Gal analogue (**1**). However, it should be noted that there is a change in anomeric stereochemistry from (**1**) which may affect its conformation. The fluorine atoms are unlikely to form hydrogen bonds with water,[38] so this modification can be considered to be more hydrophobic than an oxygen linkage. We also hypothesized that the reported preservation ability of these compounds may be due to the introduced anomeric hydroxyl group. In order to remove the hydrogen-bond

donating ability of this addition, we decided to synthesize analogues with a small protecting group at this position.

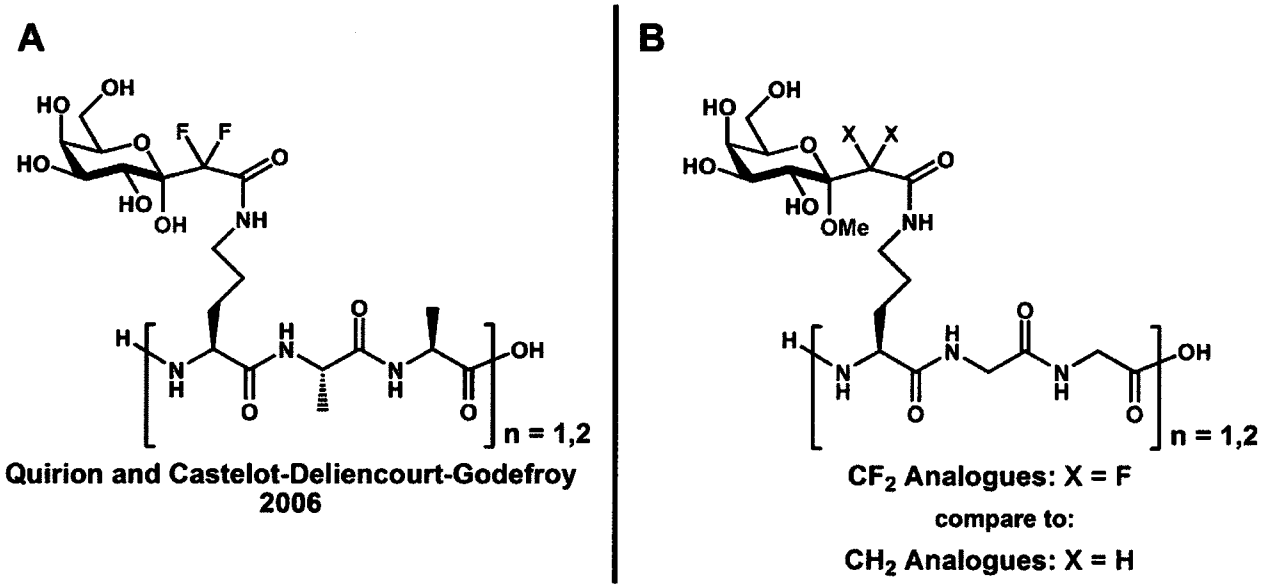

Figure 4.20: Image **A**: Fluorinated AFGP analogues reported by Quirion and Castelot-Deliencourt-Godefroy. Image **B**: Proposed analogues to be synthesized.

The retrosynthesis of the proposed building blocks is shown in Figure 4.21. The glycosylated building block would be obtained by the amide coupling of the amino group of an appropriately protected ornithine to the carboxylic acid portion of a galactose derivative. The *C*-linkage would be installed by an enolate addition strategy onto an appropriately protected lactone. In order to make the fluorinated carbohydrate, a zinc enolate would be used in a Reformatsky reaction, whereas a lithium enolate would be used in the synthesis of the non-fluorinated carbohydrate. This approach will be described in greater detail below.

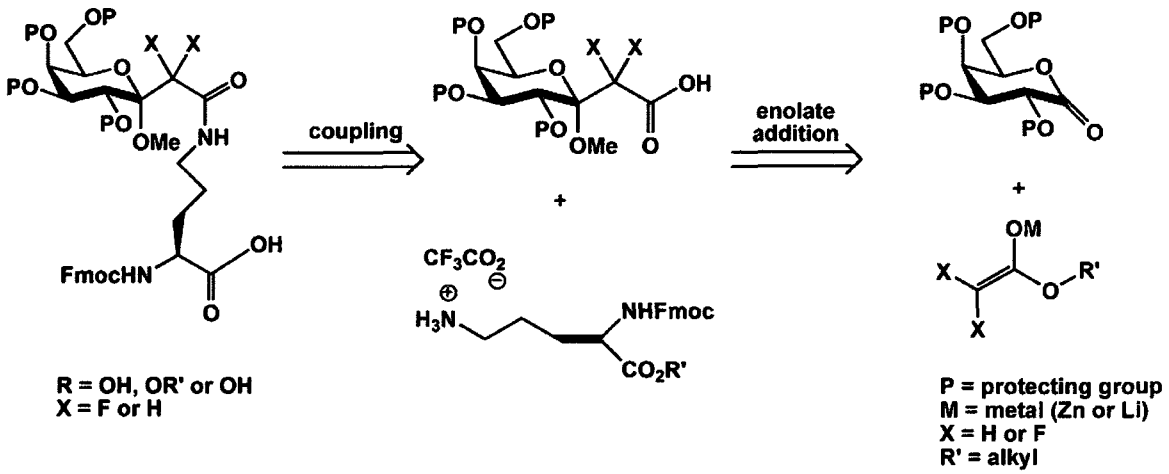

Figure 4.21: Retrosynthesis of proposed analogues involves an enolate addition strategy.

4.2.1: Preparation of a Fluorinated Galactose Derivative Linked to Ornithine

This approach requires the same lactone intermediate (**85**) for both the fluorinated and non-fluorinated compounds. Synthesis of the lactone began from commercially-available β-D-galactose pentaacetate (**48**) (Figure 4.22). The anomeric position was protected as a thio-ether to give (**82**), in order to allow a protecting group exchange from acetates to benzyl groups. Removal of the thio ether by treatment with *N*-bromosuccinamide and oxidation with acetic anhydride and DMSO gave the lactone (**85**) in good yield.

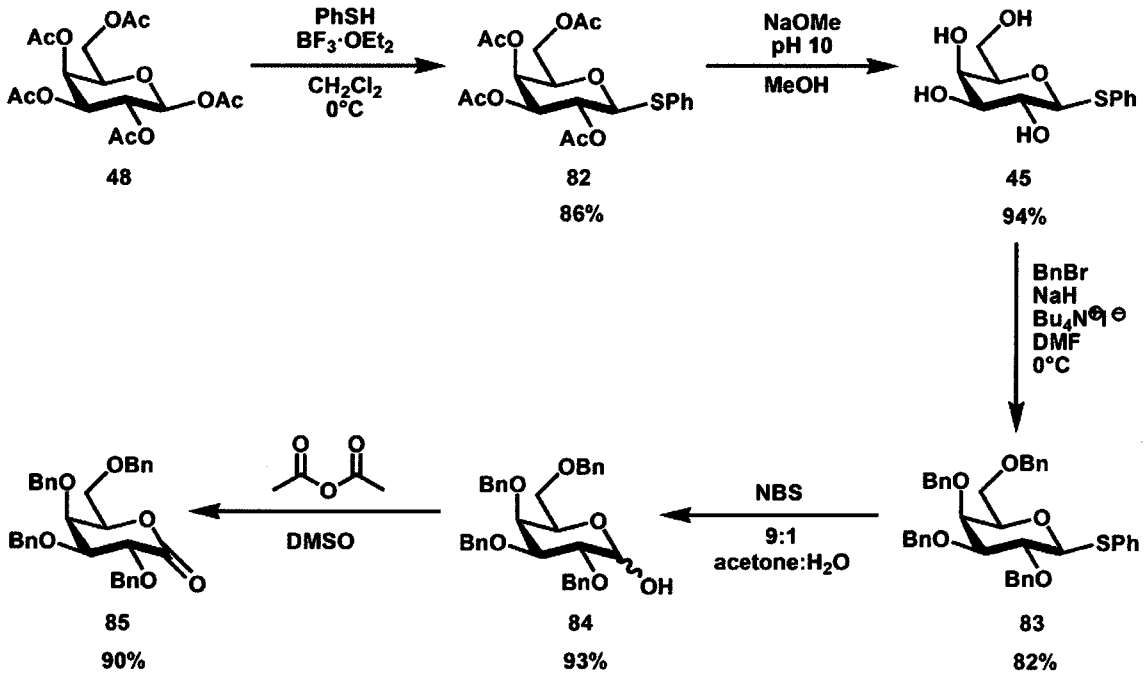

Figure 4.22: Synthesis of benzylated lactone intermediate (**85**)

With the lactone (**85**) in hand, we had the materials to perform the key Reformatsky step to prepare the fluorinated ester. A test Reformatsky reaction was conducted on acetophenone (**86**) before the reaction was attempted on lactone (**85**). The test reaction of acetophenone (**86**) with ethyl bromodifluoroacetate (**87**) gave the product (**88**) in good yield (83%, Figure 4.23) and so we turned our attention to the Reformatsky reaction of the desired lactone (**85**) substrate.

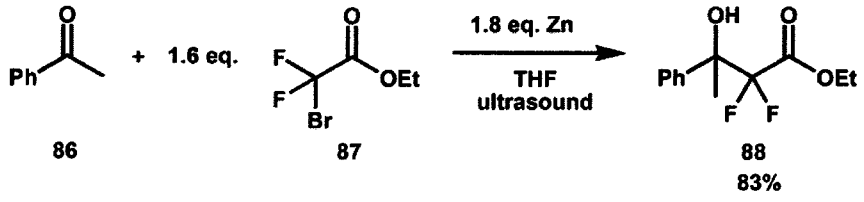

Figure 4.23: Test Reformatsky reaction on acetophenone (**86**) occurs in good yield to give the desired product (**88**)

When the test reaction conditions were repeated using lactone (**85**), only 14% of the desired product (**89**) was obtained, with mainly starting material recovered (Figure 4.24). Several methods of zinc activation, additives, and conditions were explored (Figure 4.24, Table 4.4). Ultrasound was originally used to activate the Zn dust, as reported by Erdik.[47] This method worked very well for the test reaction (Figure 4.23), but did not give the desired product (**89**) in greater than 27% yield (Table 4.4, Entries 1-4). Heating the reaction to reflux was observed to give higher yields than ultrasonic conditions. Using TMSCl to activate the Zn[48] generally gave slightly better results and improved the yield up to 39% (Table 4.4, Entries 5-6). Pre-forming the Zn enolate in a separate flask followed by addition of the lactone resulted in a significant decrease in yield (Table 4.4, Entry 7).

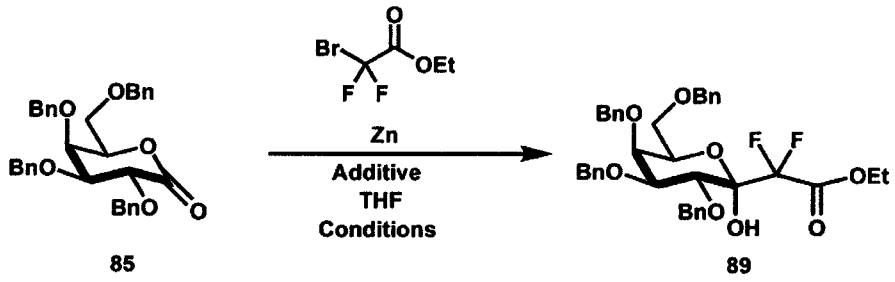

Figure 4.24: Reformatsky reaction to give fluorinated ester (**89**)

Table 4.4: Conditions attempted for Reformatsky reaction on lactone (**85**)

Entry	Lactone (85)	Zn dust	$BrCF_2CO_2Et$ (87)	Additives	Conditions	Yield of (89)
1	1.0 eq.	1.8 eq.	1.6 eq.	--	Ultrasound	14-18%
2	2.5 eq.	1.0 eq.	4.0 eq.	--	Ultrasound	SM rec.
3	1.0 eq.	1.8 eq.	1.6 eq.	--	Ultrasound, then reflux	21-27%
4	1.0 eq.	1.8 eq.	1.6 eq.	0.1 eq. TMSCl	Ultrasound, then reflux	12%
5	1.0 eq.	1.8 eq.	1.6 eq.	0.2 eq. TMSCl	Reflux	39%
6	1.0 eq.	1.8 eq.	1.6 eq.	0.4 eq. TMSCl	Reflux	33-38%
7	1.0 eq.	1.8 eq.	1.6 eq.	0.4 eq. TMSCl	Pre-formed enolate, reflux	10%
8	1.0 eq.	3.0 eq.	1.6 eq.	0.4 eq. TMSCl	Reflux	25%
9	1.0 eq.	2.0 eq.	2.2 eq.	0.5 eq. TMSCl	Reflux	14%
10	1.0 eq.	3.0 eq.	2.0 eq.	1.0 eq. TMSCl	Reflux	22%
11	1.0 eq.	7.0 eq.	2.0 eq.	0.5 eq. TMSCl	Reflux	22-30%
12	1.0 eq.	7.0 eq. (Flame-dried)	2.0 eq.	--	Reflux	17%
13	1.0 eq.	7.0 eq. (HCl-washed)	2.0 eq.	--	Reflux	10%
14	1.0 eq.	7.0 eq. (New bottle)	2.0 eq.	--	Reflux	27%
15	1.0 eq.	7.0 eq.	2.5 eq.	0.5 eq. TMSCl	Reflux	44% + 33% (**90**)
16	1.0 eq.	7.0 eq. (HCl-washed)	2.5 eq.	--	Reflux	23%
17	1.0 eq.	7.0 eq. (HCl-washed)	2.5	0.5 eq. TMSCl	Reflux	39% + 18% SM
18	1.0 eq.	7.0 eq. (HCl-washed)	3.0 eq.	0.5 eq. TMSCl	Reflux	52-62%
19	1.0 eq.	7.0 eq. (HCl- washed)	3.2 eq.	0.5 eq. TMSCl	Reflux	74-81%

Flame-drying the Zn and washing with HCl to remove zinc oxide was also attempted, as was purchasing a new bottle of Zn dust, although these conditions did not

lead to an improvement in yield in the absence of TMSCl (Table 4.4, Entries 12-14, 16). Interestingly, when a large excess of Zn was used in the presence of TMSCl, 44% of the desired product (**89**) was isolated along with a new product (Table 4.4, Entry 15). This product was determined to be the TMS-protected product (**90**) (Figure 4.25). The formation of this side product suggests that the TMSCl is activating the lactone towards enolate addition as well as activating the Zn dust.

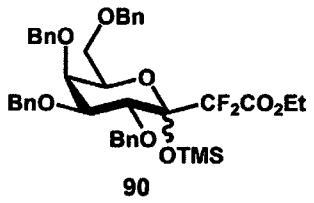

90

Figure 4.25: Side product (**90**) resulting from activation of (**85**) with TMSCl/Zn

Increasing the amount of Zn to 7.0 equivalents with respect to lactone and the amount of ethyl bromodifluoroacetate to 3.0 equivalents gave higher yields of up to 62% (Table 4.4, Entry 18). Finally, the conditions were optimized at 7.0 equivalents of HCl-washed Zn dust, 3.2 equivalents of ethyl bromodifluoroacetate, and 0.5 equivalents of TMSCl with respect to lactone (**85**) (Table 4.4, Entry 19). These conditions gave the desired product consistently in greater than 70% yield.

In all cases, only one diastereomer of the desired product was obtained. The stereochemistry of (**89**) was determined using a ^{1}H-^{19}F HOESY NMR experiment.[49] The spectrum obtained in this experiment is shown in Figure 4.26. The correlations observed are shown in Figure 4.27 which proves that the difluoromethylene group is in the β-position of the carbohydrate. This puts the tertiary hydroxyl group in an anomeric position, where it can be stabilized by the anomeric effect. It should be noted that this will result in a glycopeptide with a β-linkage, whereas our previous *C*-linked analogues all had an α-linkage to the peptide (Figure 2.4).

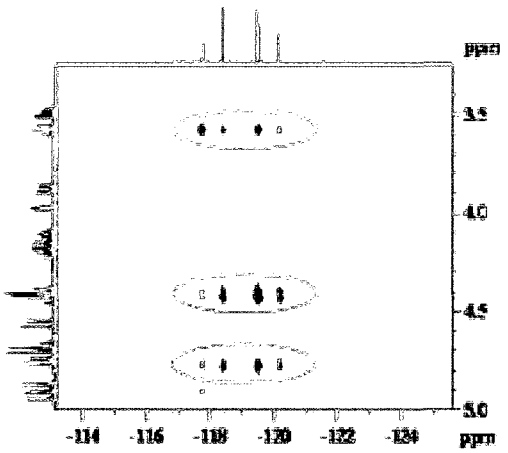

Figure 4.26: ^{1}H - ^{19}F HOESY spectrum of compound (**89**) obtained with the assistance of Dr. Glenn Facey. The ^{19}F spectrum is on the horizontal axis and the ^{1}H spectrum in on the vertical axis.

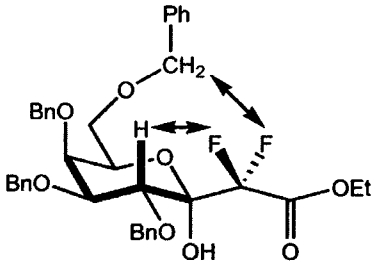

Figure 4.27: Observed ^{1}H-^{19}F correlations determined using a HOESY NMR experiment show that the product (**89**) contains a β-CF_2 group

With the desired product (**89**) in hand, we turned our attention to protection of the tertiary hydroxyl group. Initially, we attempted to remove the anomeric hydroxyl group using Lewis acid catalyzed hydride addition (Figure 4.28). The desired product (**91**) was not obtained, however a side product (**92**) was observed along with recovered starting material. The lack of formation of (**91**) was attributed to the electron withdrawing *geminal* difluoromethylene group, which disfavours formation of the required oxocarbenium ion.

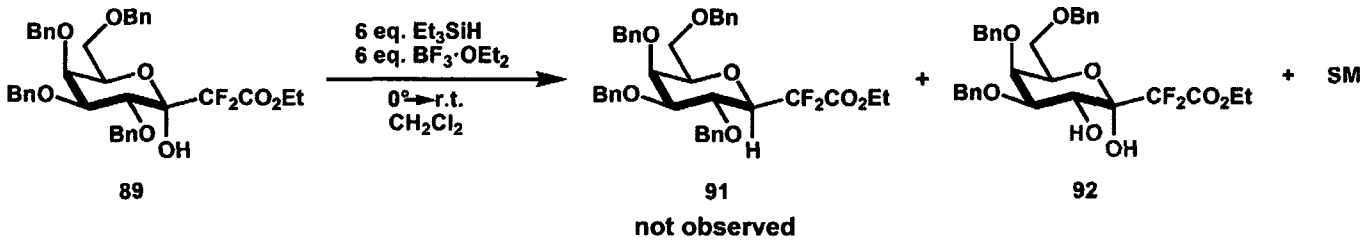

Figure 4.28: Attempted removal of the tertiary hydroxyl group to give to give product (**91**) gave side product (**92**) under Lewis Acid-catalyzed conditions.

This product was characterized using NMR and mass spectrometry, and was determined to be C-2 deprotected product (**92**) (Figure 4.28). The proposed mechanism for its formation is outlined in Figure 4.29. A similar mechanism has been proposed for a selective C-2-debenzylation using iodine that was observed by Cipolla et al. during their synthesis of *C*-glucosides (Figure 4.30).[50]

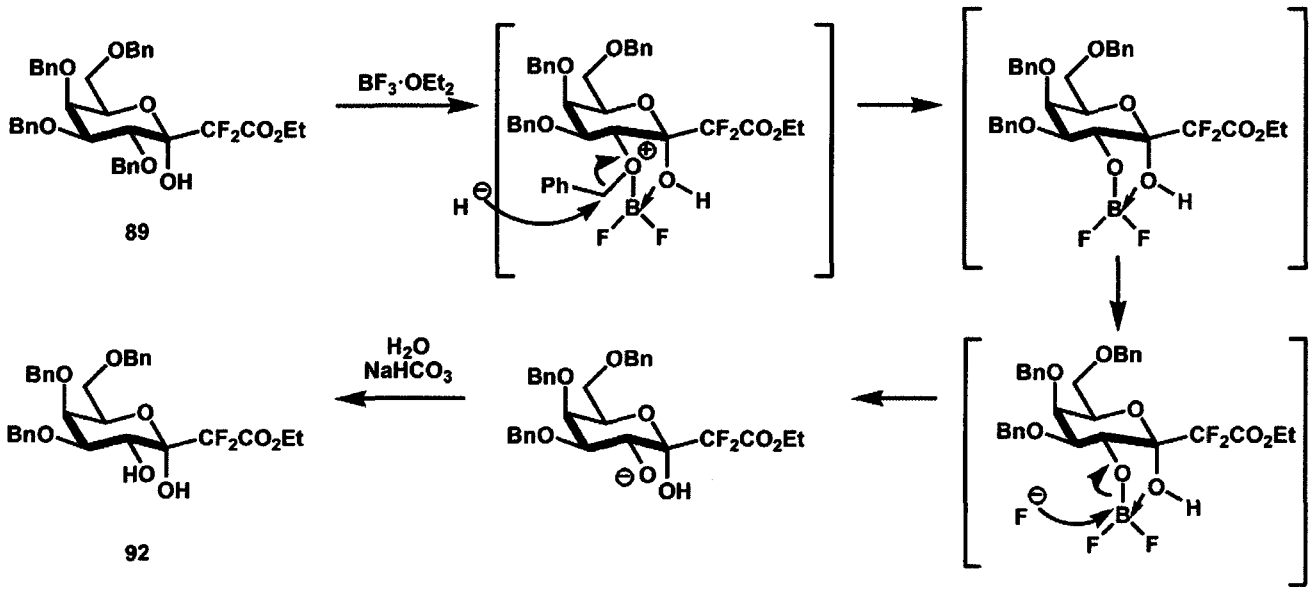

Figure 4.29: Proposed mechanism for the formation of the C-2 de-protected side product (**92**)

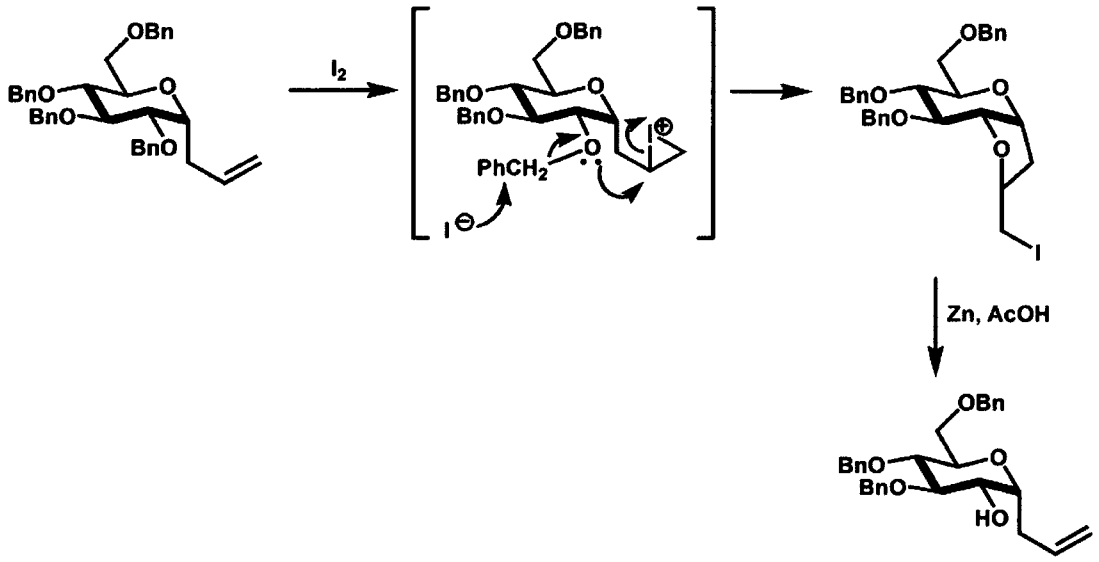

Figure 4.30: Mechanism proposed for C-2-debenzylation observed by Cipolla et al during their synthesis of *C*-glycosides.[50]

At this point we turned our attention to protection of the tertiary hydroxyl group rather than its removal. Conditions to protect the alcohol as a TBS group were unsuccessful, likely due to the steric constraints of putting a large silyl group on a tertiary hydroxyl group. Recovered starting material was the only compound isolated in this reaction (Figure 4.31A). Due to these steric constraints, a relatively small methyl group was chosen as the optimal protecting group. Using MeOH and a Lewis acid, conditions that were reported to work on similar non-fluorinated carbohydrates,[51] gave only recovered starting material and the C-2-debenzylated product (Figure 4.32B). Furthermore, reaction with the strong alkylating agent trimethyloxonium tetrafluoroborate gave only recovered starting material (Figure 4.33C).

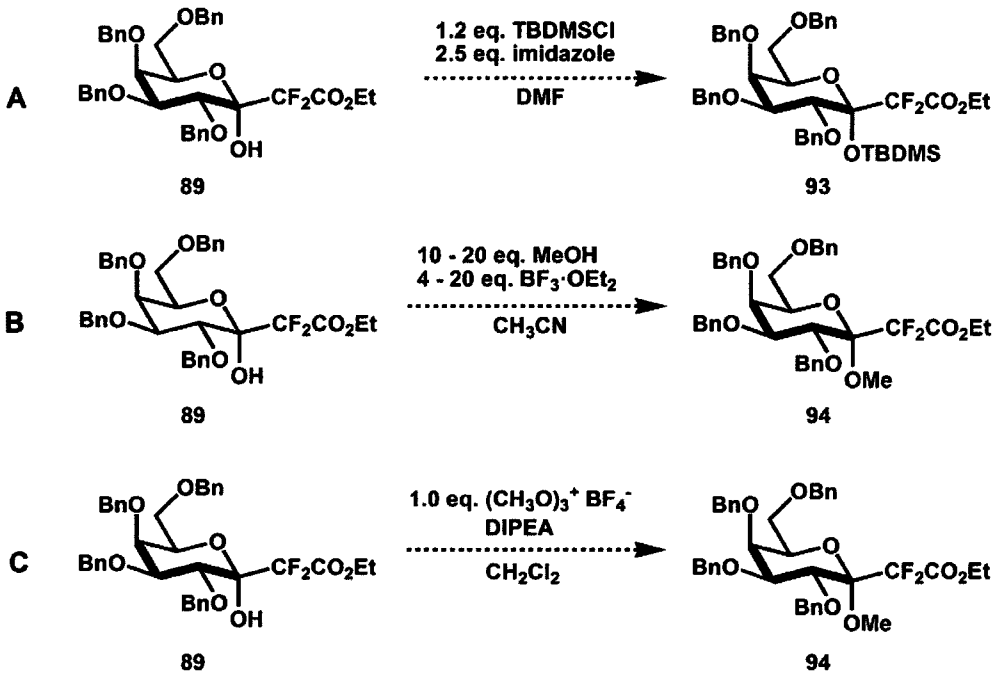

Figure 4.31: Attempted protection of tertiary hydroxyl group of (**89**)

We were originally cautious of using strongly basic conditions due to the potential for anomerization (Figure 4.32). However, we realized that the high electronegativity of fluorine atoms would disfavour the formation of a partial positive charge on the neighbouring anomeric carbon, and that anomerization by this mechanism was quite unlikely.[49] For this reason, basic conditions were employed.

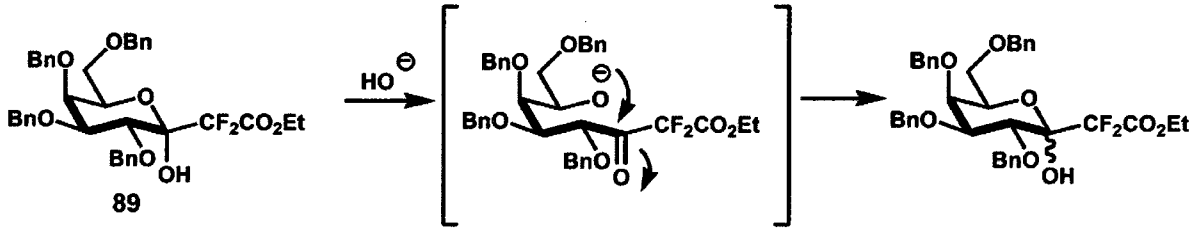

Figure 4.32: Mechanism for possible anomerization of (**89**) under strongly basic conditions.

The first conditions attempted were benzylation conditions that had already been optimized for protection of the galactose thio-ether (**45**). Under these conditions, the desired benzylated product (**95**) was obtained in good yields (Figure 4.33). Furthermore, we were pleased that no anomerization was observed.

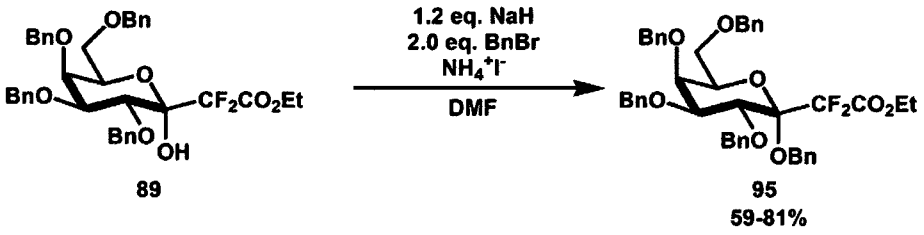

Figure 4.33: Benzylation of tertiary hydroxyl group of (**89**) gives product (**95**)

Once the test benzylation was successful, the methylation was attempted and the desired product (**94**) was consistently obtained in good yields, again with no evidence of anomerization (Figure 4.34A). Saponification of the ethyl ester to give the necessary carboxylic acid (**96**) for coupling to the amide was achieved using a slight excess of sodium hydroxide (Figure 4.34B).

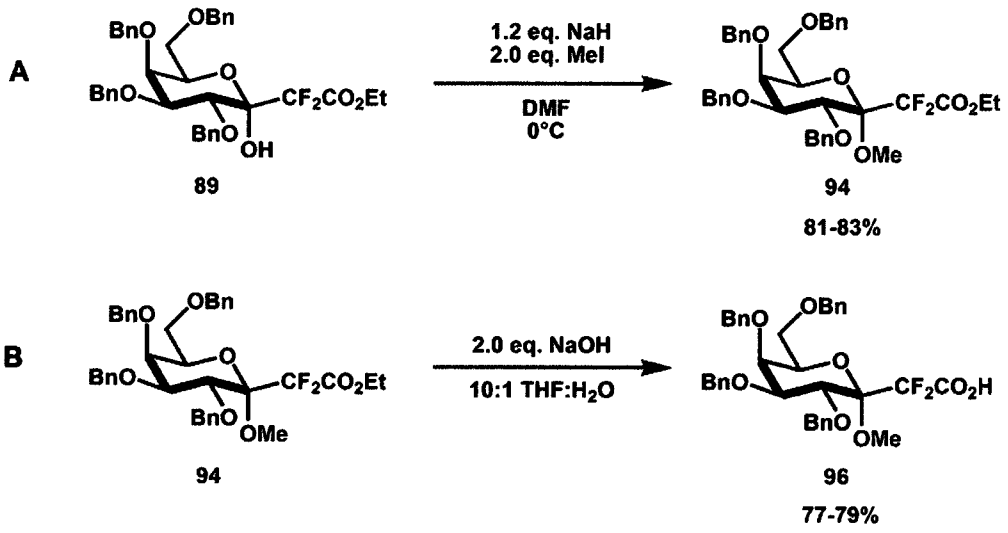

Figure 4.34: Methylation of the tertiary hydroxyl group gives product (**94**) and saponification of the ethyl ester gives product (**96**)

With our desired carboxylic acid in hand, preparation of the required ornithine amino acid coupling partner began from commercially available Fmoc-Orn-Boc (**97**). The free carboxylic acid was protected as a benzyl ester and then the Boc group was removed by treatment with trifluoracetic acid to give a salt (**99**) that was ready for coupling to our fluorinated carboxylic acid (**96**) (Figure 4.35A). The coupling was conducted under standard HBTU conditions[52] and the product was obtained in good yield (Figure 4.35B). The addition of 4Å molecular sieves was found to increase the yield of the reaction.

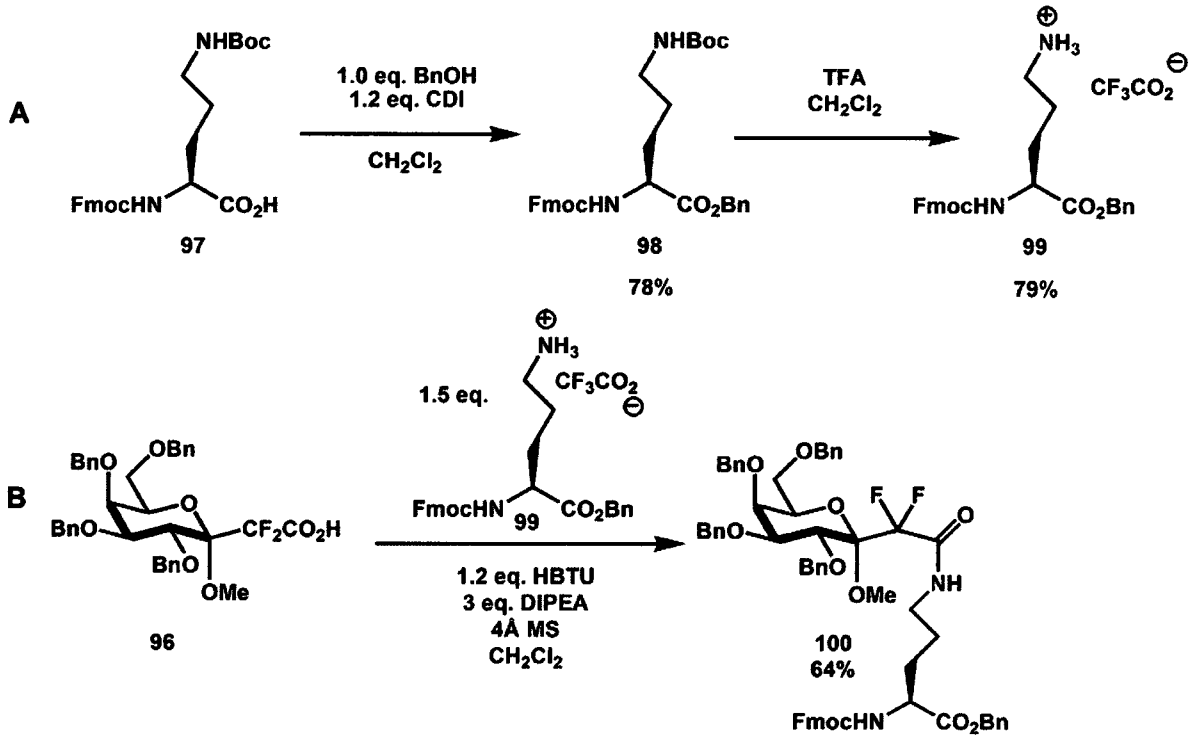

Figure 4.35: Preparation of appropriately protected ornithine derivative (**99**) and coupling to the fluorinated carboxylic acid (**96**) gives product (**100**)

4.2.2: Preparation of a Non-Fluorinated Galactose Derivative Linked to Ornithine

The non-fluorinated control was synthesized from the same lactone intermediate (**85**). Lactone (**85**) could have been treated with the enolate of ethyl acetate to form the ethyl ester (**101**) (Figure 4.36). However, the only ethyl acetate that was on hand was reagent grade and not moisture-free, and traces of water within the ethyl acetate bottle would prevent the desired reaction from occurring. Since the ester would be saponified later in the synthesis, the identity of the ester was unimportant. *Tert*-Butyl acetate was used as an alternate ester source since it was on hand in our laboratory.

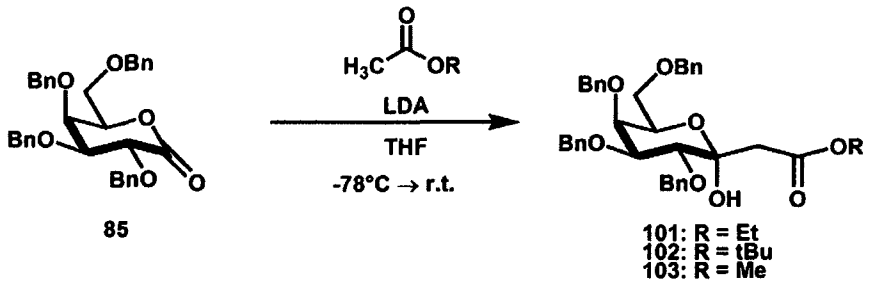

Figure 4.36: Preparation of non-fluorinated esters (**101 – 103**)

Table 4.5: Conditions attempted for enolate addition to the lactone (**85**)

Entry	Lactone (85)	Ester	*n*-BuLi	DIPA	Yield
1	1.0 eq.	1.2 eq. tBuOAc	1.1 eq.	1.2 eq.	26-57% (**102**)
2	1.0 eq.	4.0 eq. tBuOAc	3.9 eq.	4.0 eq.	57-99% (**102**)
3	1.0 eq.	4.0 eq. MeOAc	3.9 eq.	4.0 eq.	59-72% (**103**)

The use of *tert*-butyl acetate gave (**102**) in moderate yields (Table 4.5, Entry 1). A significant improvement in yield was observed when the amount of LDA (generated *in situ*) was raised to 3.9 equivalents (Table 4.5, Entry 2). Problems with the next step of the reaction (Figure 4.37) resulted in a change from *tert*-butyl acetate to methyl acetate, and again the desired product (**103**) was obtained in good yields.

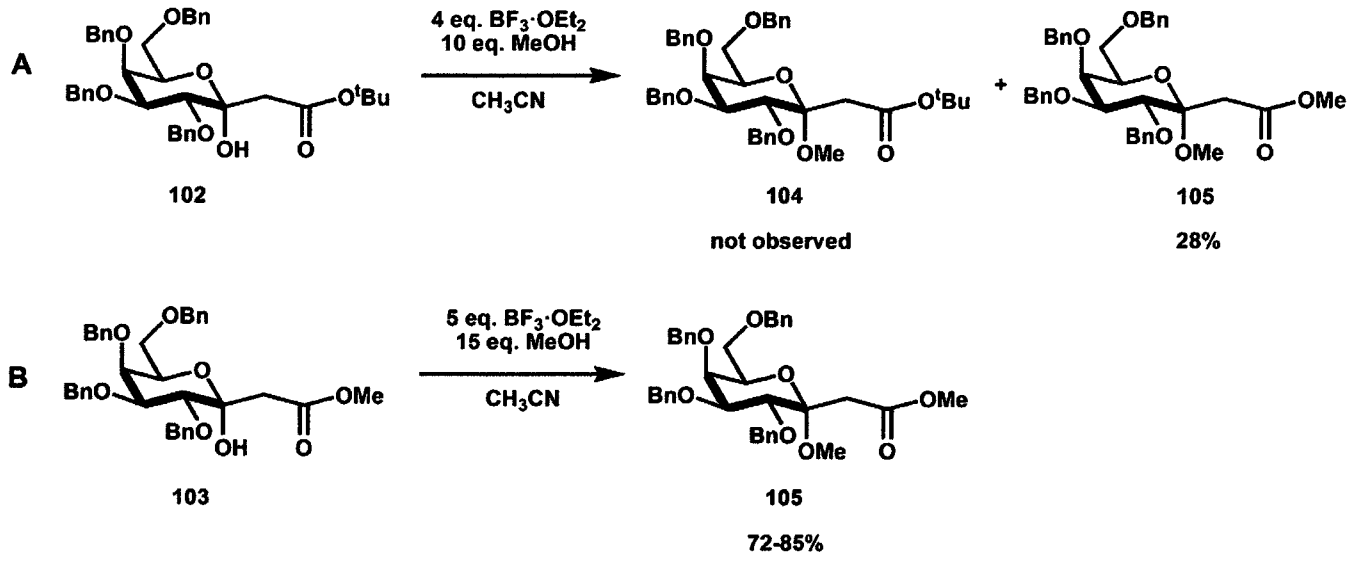

Figure 4.37: Methylation of the tertiary hydroxyl group of the *tert*-butyl and methyl esters (**102**) and (**103**) gives product (**105**)

When the *tert*-butyl ester was treated with Lewis acid and an excess of methanol, the desired product (**104**) was not obtained. Instead, a side product was the only isolated compound (Figure 4.37). Trans-esterification of the *tert*-butyl ester with methanol accounted for the formation of the side product (**105**). For this reason, we switched to the enolate of methyl acetate in the previous step in order to decrease the number of products obtained during the methylation reaction. As seen in Figure 4.37, when the methyl ester (**103**) was treated with methanol and Lewis acid, the desired product (**105**) was obtained in good yield.

When the conditions used for saponification of the fluorinated ester were employed for the non-fluorinated product (**105**), recovered starting material was the only isolated compound. Switching from sodium hydroxide to lithium hydroxide gave the desired carboxylic acid (**106**) in excellent yields (Figure 4.38A). HBTU coupling of the non-fluorinated carboxylic acid (**106**) to the appropriately protected ornithine (**99**) occurred in high yield to give the desired product (**107**) (Figure 4.38B).

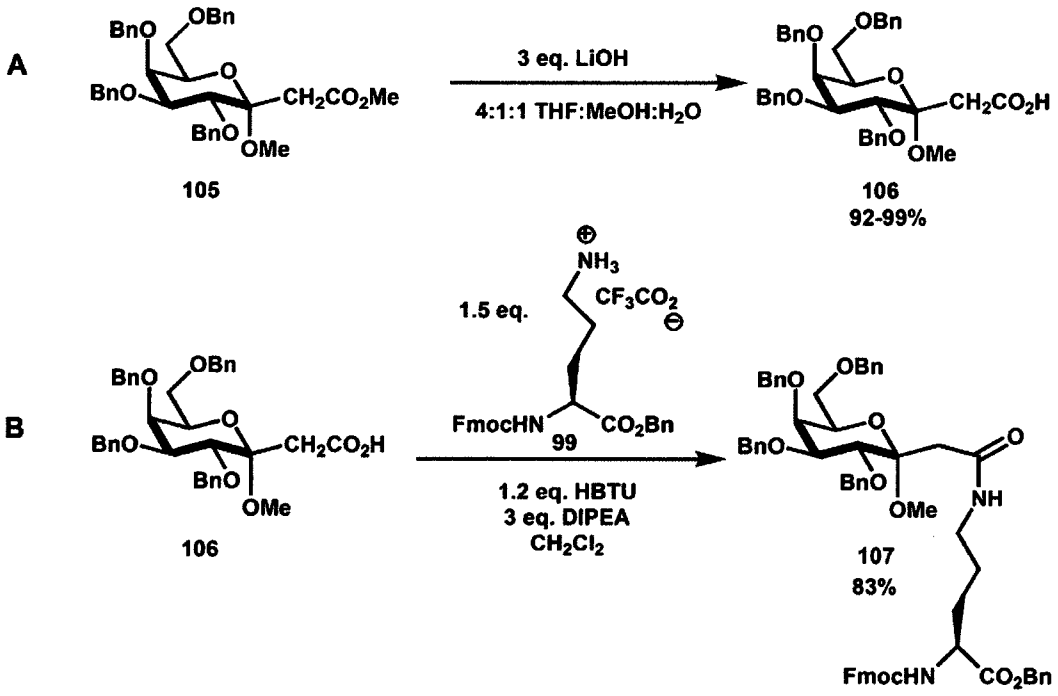

Figure 4.38: Saponification of non-fluorinated methyl ester (**105**) gives carboxylic acid (**106**) which can be coupled to (**99**) to give product (**107**)

4.2.3: Preparation and IRI Testing of a Short Fluorinated Glycopeptide

Once the glycosylated ornithine compounds had been prepared, de-protection of the benzyl esters of (**100**) and (**107**) presented a challenge. Previous work in our laboratory has shown that the benzyl ester can be removed via hydrogenation to give the desired carboxylic acid. However, the benzyl protecting groups on the carbohydrate would also likely be removed under these conditions. Instead, a saponification was attempted (Figure 4.39). Potassium carbonate[53] and lithium hydroxide[54] did not give the desired product and only starting material was recovered under these conditions. However, when we used Kaul et al.'s mild conditions of calcium chloride and sodium hydroxide,[55] the desired products (**108**) and (**109**) were obtained in good yield when 7:3 isopropanol:water was used as the solvent (Figure 4.39).

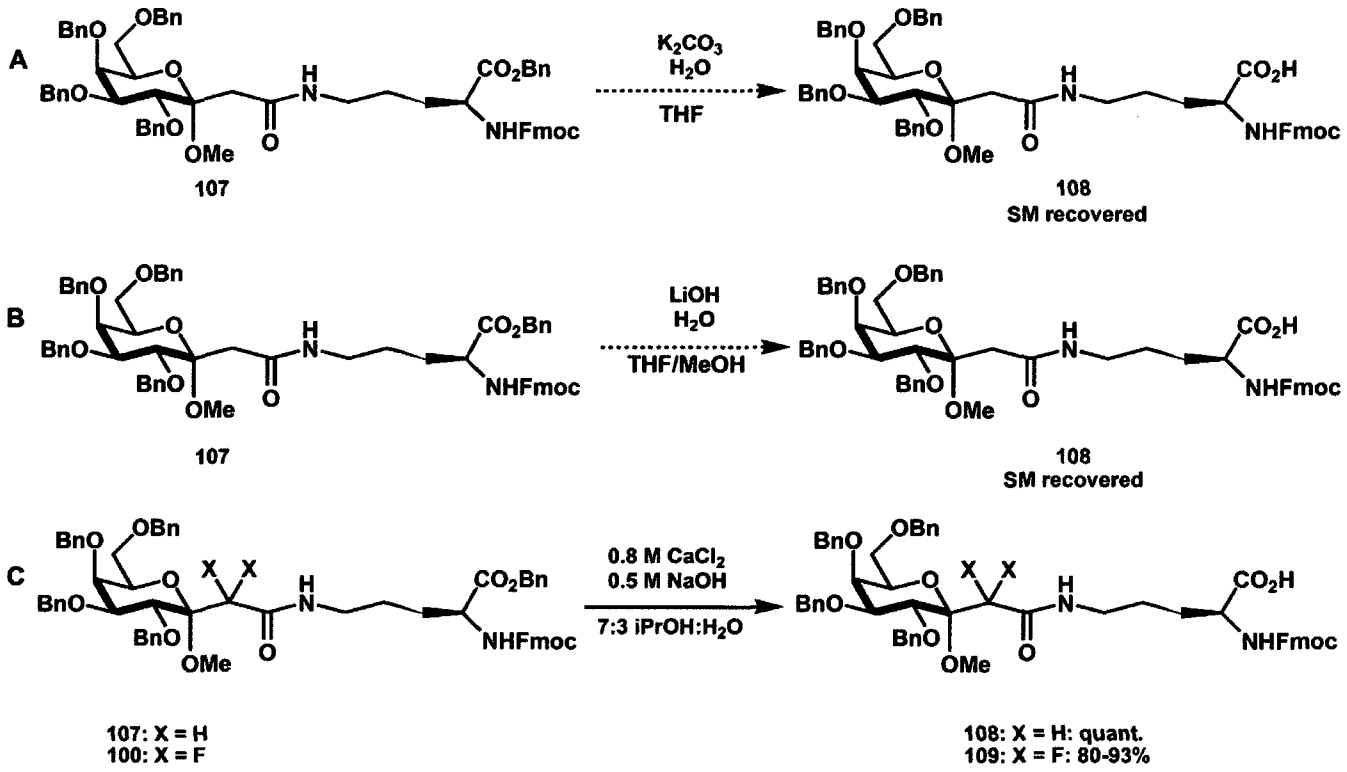

Figure 4.39: Conditions attempted for saponification of benzyl esters to give building blocks (**108**) and (**109**)

With the desired building blocks in hand, solid phase synthesis of a fluorinated tripeptide was conducted as shown in Figure 4.40. This shortened glycopeptide (as compared to OGG-Gal (**1**)) was prepared because tripeptides and hexapeptides were the compounds reported by Quirion et al. to have cryopreservation activity.[46]

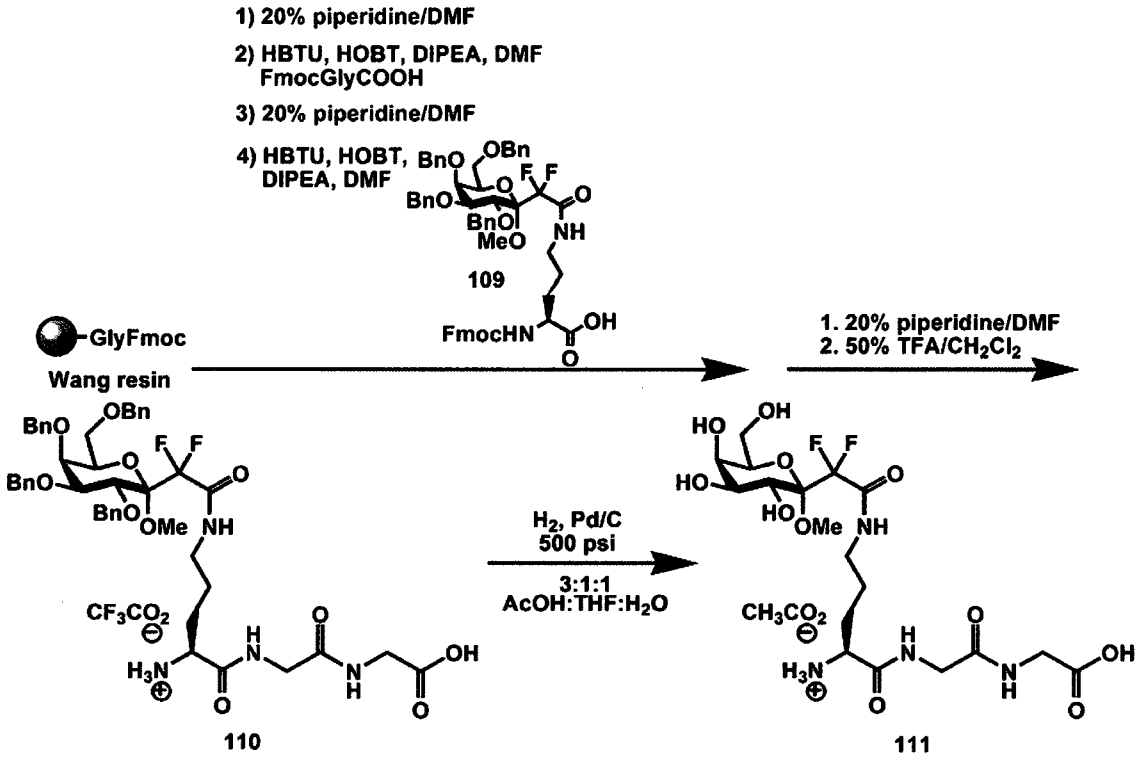

Figure 4.40: Solid phase peptide synthesis of a fluorinated tripeptide (**111**)

The fluorinated tripeptide (**111**) was examined for antifreeze activity as a function of IRI ability and was compared to the native AFGP8 and our AFGP analogue OGG-Gal (**1**). (**111**) was tested without additional purification following the removal of the benzyl groups. For this reason, it was tested at a 10-fold higher concentration than our other AFGP analogues (**1 - 4**) to account for the fact that impurities may have resulted in a lower amount of (**111**) in the solution. Non-specific colligative IRI effects are ruled out by testing our samples in PBS solution, so it is unlikely that the impurities would result in increased IRI activity. Figure 4.41 shows that the fluorinated compound (**111**) did not display any IRI activity, with ice crystals in the fluorinated solution having the same mean grain size as the PBS negative control. It is important to note that although the fluorinated tripeptide (**111**) was tested at a higher concentration than OGG-Gal (**1**), it still appeared to be inactive. Based on this result, we chose not to test compound (**111**) at lower concentrations. This lack of IRI activity may be due to the fact that four

repeating tripeptide units are required for IRI activity, or due to the change in anomeric stereochemistry compared to OGG-Gal (**1**).

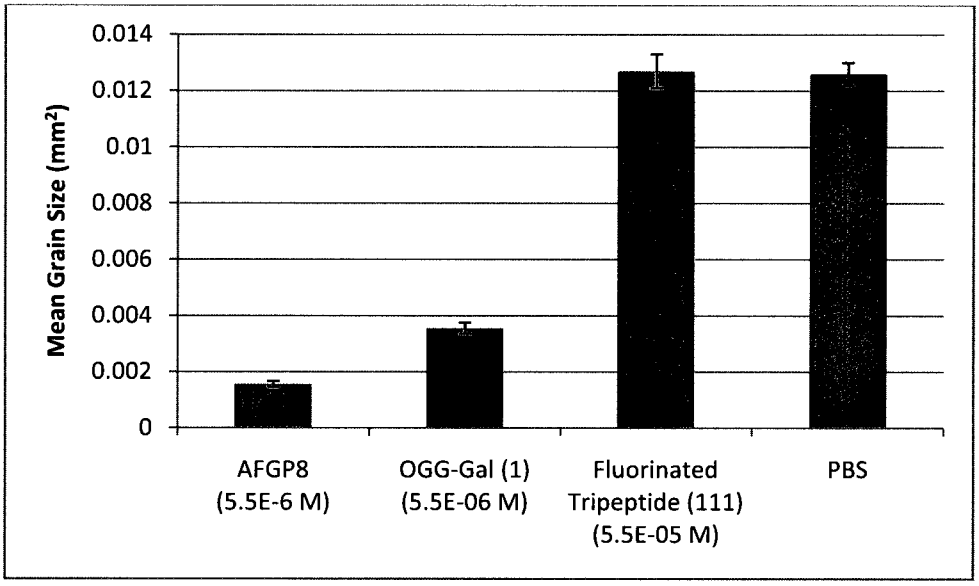

Figure 4.41: Ice-recrystallization inhibition activity of native AFGP8 (positive control), OGG-Gal (**1**), and the fluorinated tripeptide (**111**). The fluorinated tripeptide solution formed ice crystals that were identical in size to those in a PBS solution (negative control).

Unfortunately, the non-fluorinated building block could not be used in solid phase synthesis with the Wang resin used for the fluorinated building block, due to the non-fluorinated compound decomposing under acidic conditions. Strongly acidic trifluoroacetic acid is required to cleave the peptide off of the Wang resin. Since the fluorinated tripeptide did not show any IRI activity, the fluorinated hexapeptide and the non-fluorinated tripeptide were not prepared. Instead, based on our precedent that monosaccharides display moderate IRI activity,[17] we attempted to screen for the IRI activity of several compounds at the monosaccharide level, without their being assembled into glycopeptides.

4.2.4: IRI Assessment of Fluorinated and Non-Fluorinated Monosaccharides

In order to test the monosaccharides for IRI activity, the benzyl protecting groups needed to be removed. The reactions were extremely sensitive to the solvent and the substrate. Compound (**89**) underwent de-benzylation in the presence of palladium over carbon, ethyl acetate, and ethanol to give the desired product (**36**) in good yield (Figure 4.42A). Unfortunately, the hydrogenation conditions also resulted in an unexpected anomerization of the product. The anomers were unable to be separated, so product (**36**) was tested for IRI activity as an anomeric mixture. When compound (**94**) was subjected to hydrogenation conditions, the reaction was extremely sluggish and did not occur until acetic acid[56] was added to the solvent system. Under these conditions the de-benzylation occurred in good yield and without any anomerization to give the desired product (**37**) (Figure 4.42B). De-benzylation of the non-fluorinated monosaccharides (**103**) and (**105**) occurred without difficulty and without any anomerization to give (**38**) and (**39**), respectively (Figure 4.43).

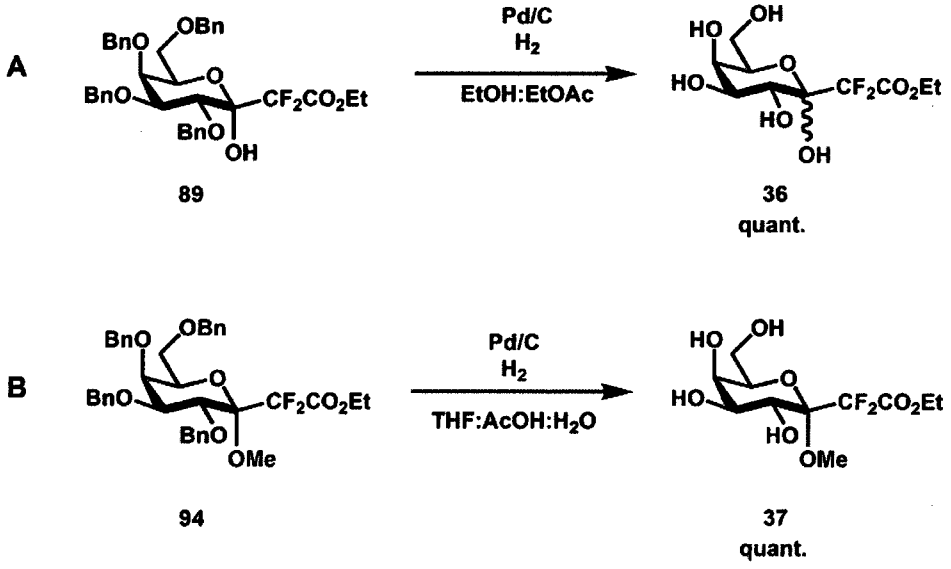

Figure 4.42: Preparation of fluorinated monosaccharides (**36**) and (**37**) for IRI testing.

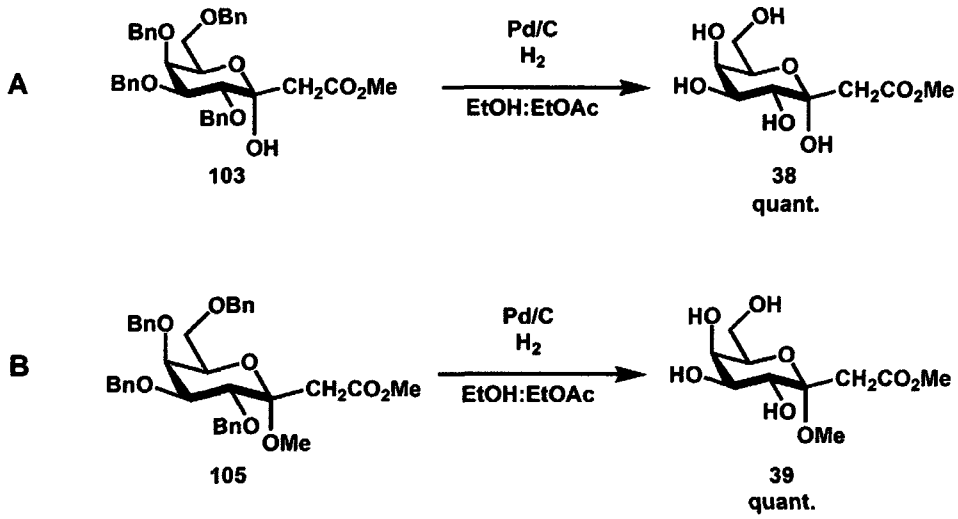

Figure 4.43: Preparation of non-fluorinated monosaccharides (**38**) and (**39**) for IRI testing.

These compounds were then tested for IRI activity, and these results are displayed in Figure 4.44. It is clear from this graph that none of the newly synthesized compounds (**36 – 39**) are as active as galactose (**5**) itself. We see a decrease in activity in going from α-*C*-allyl galactose (**14**) to β-*C*-allyl galactose (**18**), as mentioned previously. It should be noted that the synthesized compounds in this section all contain a β-anomeric linkage to the ester moieties, so we were expecting to see a decrease in activity compared to α-*C*-allyl galactose based on our previous results. The anomeric methoxy group in compounds (**37**) and (**39**) is consistent with the structure of α-methylgalactopyranoside (**32**). By comparing these compounds to (**32**), we were able to determine the effect of the fluorinated and non-fluorinated ester moieties.

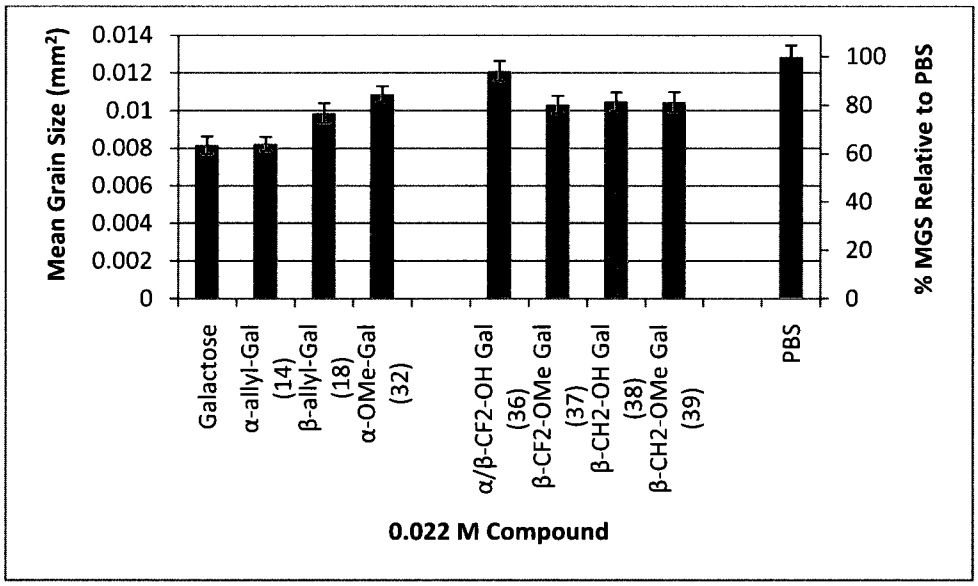

Figure 4.44: IRI activity of galactose (**5**), α-*C*-allyl galactose (**14**), β-*C*-allyl galactose (**18**), α-methyl galactopyranoside (**32**), fluorinated monosaccharides (**36** and **37**), and non-fluorinated control monosaccharides (**38** and **39**). All compounds are relative to the PBS negative control.

Fluorinated product (**36**) has little to no IRI activity, with ice crystals being approximately the same size as in the PBS negative control. This loss in activity may be due to the fact that this compound is an anomeric mixture. This results in a lower actual concentration of the active anomer, although it is not clear at this time whether the alpha or beta anomer is more active. Our previous results have suggested that the alpha anomer generally displays higher RI activity than beta anomers (Figures 3.19 and 3.23). The fluorine atoms do not seem to account for this loss of activity, because fluorinated compound (**37**) has similar activity to α-methygalactopyranoside (**32**). In fact, the ice crystals had statistically identical means in the two solutions, as determined using a Student's T-test Two Sample with Unequal Variance.[16, 17] Since the only structural difference between these compounds is the fluorinated ester, the fluorine atoms do not seem to improve or decrease the IRI activity of monosaccharides. This was confirmed when comparing the activity of fluorinated compounds (**36** and **37**) to non-fluorinated (**38** and **39**). The activity of (**38**) and (**39**) was statistically identical to the activity of fluorinated (**37**), again suggesting that the fluorine atoms have no effect, either positive or negative, on IRI activity of monosaccharides. Furthermore, the methylated anomeric

hydroxyl group of (**39**) did not improve IRI activity compared to the free hydroxyl group of (**38**). There was no statistically significant difference between the mean grain sizes in these solutions. These initial results suggest that fluorine atoms and methoxy groups do not increase the IRI activity of monosaccharides.

As mentioned above, it has been reported that short fluorinated glycopeptides are able to preserve several types of cells at low temperatures.[46] In contrast, our results for the poor IRI activity of fluorinated monosaccharides suggest that these compounds would not be effective cryoprotectants. However, it should be noted that the previously reported fluorinated glycopeptides[46] may be preserving cells by an entirely different mechanism that does not involve ice-recrystallization inhibition. In order to examine this hypothesis, compounds (**36 – 39**) should be subjected to our cryopreservation assay described in the previous chapter to determine whether they are able to protect cells at low temperatures, despite their lack of IRI activity.

4.2.5: Hydration of Fluorinated Carbohydrates and its Role in IRI Activity

As previously stated, fluorine atoms are commonly used in medicinal chemistry as oxygen mimetics and to probe the structure of enzyme active sites. The hydration of fluorine atoms has been studied. Biffinger et al. have observed that fluorine atoms behave like hydrocarbons in that they cause water molecules to become more ordered around themselves.[33] Nishi et al. have examined the different effects of 4-hydroxyproline and 4-fluoroproline on the stability of the collagen triple helix structure.[57] They confirm that fluorine is more hydrophobic than oxygen and therefore has an effect on the hydration of the proline residue.[57] 4-Hydroxyproline was found to be much more effectively hydrated than 4-fluoroproline, suggesting that hydrogen bonds to the fluorine atoms are unlikely to be forming in this solution.[57] The differences in hydration properties between an acetamide group and a trifluoroacetamide group of galactose have been studied by Uedaira et al.[58] They observed that the CH_3 group causes a greater thermal motion of water molecules surrounding itself than the CF_3 group, suggesting that CH_3 causes a greater disruption of water molecules than CF_3.[58] In

general, compounds that cause a large disruption of water molecules are well hydrated, and those that tend to order water molecules are poorly hydrated.

All of these results suggest that fluorine atoms behave as hydrophobic groups and that they cause water molecules to become ordered around themselves, resulting in only a small disruption of the hydrogen bonded network of bulk water. Based upon the model proposed in Chapter 3 in which hydrophobic groups cause a minimal disruption of water molecules within the hydration shell and are therefore poorly hydrated, we would therefore expect fluorinated monosaccharides to display poor IRI activity. This is exactly what we observed for both the fluorinated tripeptide (**111**) and the fluorinated carbohydrate (**36**), both of which were extremely ineffective at inhibiting ice-recrystallization. Fluorinated compound (**37**) and non-fluorinated carbohydrates (**38**) and (**39**) also displayed poor IRI activity, suggesting that they are poorly hydrated. This may be a result of the hydrophobic nature of the CH_2 group at the anomeric position as well as the presence of the electron-withdrawing ester groups. Based upon our results with *N*-acetyl-D-galactosamine, we would expect the ester moiety to be poorly hydrated and therefore to display poor IRI activity.

In order to further examine the effects of hydrophobic groups on IRI activity, the effect of the ester group should be explored with the synthesis of compounds that have different oxidation states and hybridization at that position. All of the results obtained here suggest that hydrophobic fluorine atoms do not lead to an increase in IRI activity. However, Quirion et al. reported that fluorine atoms result in improved cryoprotection of several types of cells.[46] In order to examine this claim, compounds (**111**) and (**36 – 39**) should be tested for cryopreservation ability. Steps are underway to conduct these experiments in the near future.

4.3: Preparation of Compounds to Examine the Potential for Gel Formation and its Effect on IRI Activity

4.3.1: Introduction to Carbohydrate Gelators and Liquid Crystals

Gel systems are known to form in dilute solutions of polymers, proteins, and inorganic substances,[59] but they can also be formed from low-molecular weight organic compounds.[60] The formation of these gels depends on intermolecular forces such as π-π stacking, hydrogen bonding, dipole-dipole, donor-acceptor, hydrophobic interactions, and van der Waals forces.[61-63] Organogelators have potential applications in drug delivery, tissue engineering, medical implants, and they can be used as biocompatible materials.[64, 65]

All gelators can be classified into two forms, which are the non-hydrogen bonding gelators and the hydrogen bonding gelators.[66] Carbohydrate-based systems make up the majority of the hydrogen bonding gelators.[67] The gelation ability and strength of carbohydrate based gelators correlates with the configuration of the sugar and with the substituents on the sugar unit.[62] Gronwald and Shinkai have observed that 4,6-benzylidene acetal-1-α-methylmannopyranoside (Figure 4.45) is able to gelate water at a concentration of 3 weight percent, whereas most carbohydrates are able to gelate only organic solvents.[67] α-methylgalactopyranoside and α-methylmannopyranoside have been observed to be more efficient gelators than their glucose counterparts. In these compounds, sugar molecules were held together by hydrogen bonds between the free hydroxyl groups on the monosaccharides within the gel network.[67] In addition, π-π stacking interactions were observed between the phenyl groups of the benzylidene acetal moieties.[67] Carbohydrate-based low molecular weight gelators have recently been reported in the literature by several groups, including Gronwald and Shinkai,[67] Jung et al.,[60] and Wang et al.[61] (Figure 4.45), among others. These compounds have been observed to form gels in aqueous DMSO, ethanol, and pure water solutions.

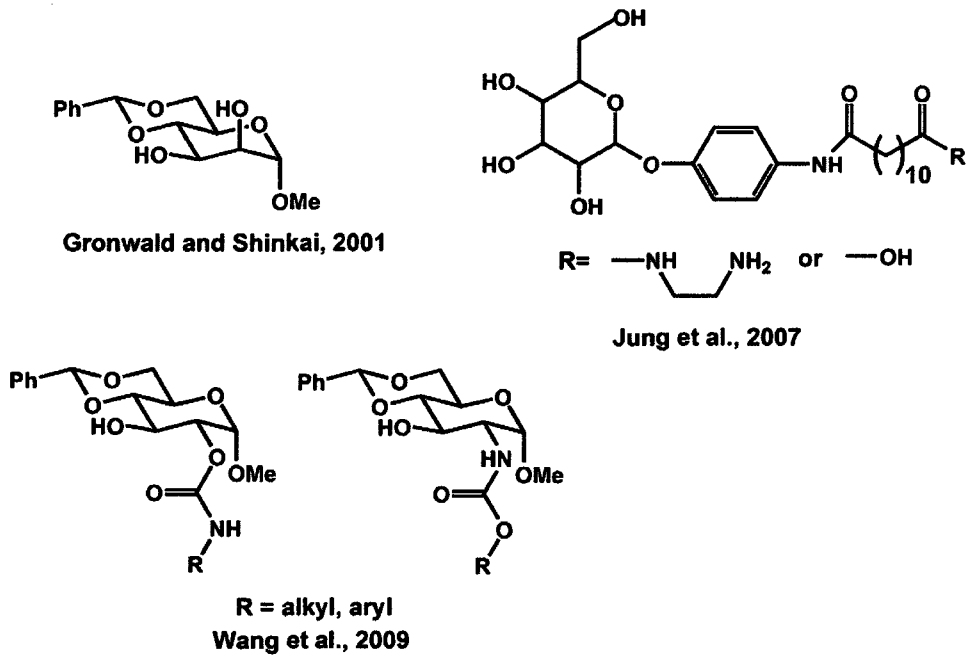

Figure 4.45: Carbohydrate-based gelators reported by Gronwald and Shinkai,[67] Jung et al.,[60] and Wang et al.[61]

Carbohydrates with alkyl and perfluoroalkyl chains have also been reported to exhibit liquid-crystalline behaviour.[45, 68-73] Liquid crystals are compounds that exist in a mesomorphic state with long-range orientational order and some amount of positional order.[74, 75] As early as 1911, Emil Fischer noted that long-chain *n*-alkyl pyranosides display a double melting point.[76] For example, *n*-octyl-1-thio-β-D-glucopyranoside melts at 41.9-43.8 ºC to form a viscous liquid phase, and then further melts to form an isotropic liquid at 125-127 ºC.[68] Alkyl glycosides display these thermotropic liquid crystal phases between room temperature and their melting point.[77]

By definition, liquid crystals are known as mesogens. IUPAC defines a mesogen as "A compound that under suitable conditions of temperature, pressure, and concentration can exist as a mesophase, or, in particular as a liquid crystal phase."[74, 75] There are two types of liquid crystals or mesogens, which are lyotropic and thermotropic.[74] Lyotropic liquid crystal behaviour is a dissolution property, and lyotropic mesophases are formed by dissolving an amphiphilic mesogen in an appropriate solvent.[74, 76] This is characterized by the formation of molecular aggregates or micelles

due to the interaction between the mesogen and the solvent.[74] In contrast, thermotropic liquid crystalline behaviour is a solid-state phenomenon, and thermotropic mesophases are formed by heating a solid or cooling an isotropic liquid.[74] Lyotropic liquid crystals form mesophases in solution, while thermotropic liquid crystals form mesophases in the melt.[78] Many carbohydrate liquid crystals exhibit both thermotropic and lyotrophic behaviour.[69, 76]

The amphiphilic structure of alkyl glycosides is the cause of their lyotropic liquid crystalline behaviour.[76] Usually, carbohydrates form hard crystals that have high melting points due to the large amount of hydrogen bonding between solute molecules.[76] In contrast, hydrocarbons generally form soft crystals with low melting points because they are mainly held together by van der Waals forces.[76] When both these structural components are found in the same molecules, the three-dimensional order of the crystal structure decreases but the molecules remain in ordered clusters.[76] In polar solvents, lyotropic liquid crystals develop an orientation whereby the non-polar tails aggregate together to allow the polar carbohydrate head group to access the solvent.[76] The phase transitions occur with changes in concentration or temperature, and they cause the liquid crystals to pass from a solution, through series of liquid crystal phases, and they may ultimately form a gel.[76]

There are two types of mesophase behaviour.[78] The first is based on "closest packing", in which rod-like molecules in the liquid-crystal phase can pack in an ordered way, forming a more energetically stable structure than remaining in the isotropic phase with random or disordered molecules.[78] The second type is based on "microphase separation", which occurs in amphiphilic liquid crystals containing two incompatible molecular structures within the same molecule that cannot be separated within solution.[78] Alkyl glycosides undergo a microscopic separation and form a series of hydrophilic and lyophilic layers.[78] Carbohydrate-derived liquid crystals are believed to form smectic A crystals in which the carbohydrate head groups hydrogen bond head-to-head to form bilayers, allowing the alkyl groups to pack tail to tail (Figure 4.46).[76, 78] The mesophase is stabilized by van der Waals interactions between the alkyl groups and hydrogen bonding between the carbohydrate head groups.[69] Hydrogen bonding interactions also occur between the bilayers.[69]

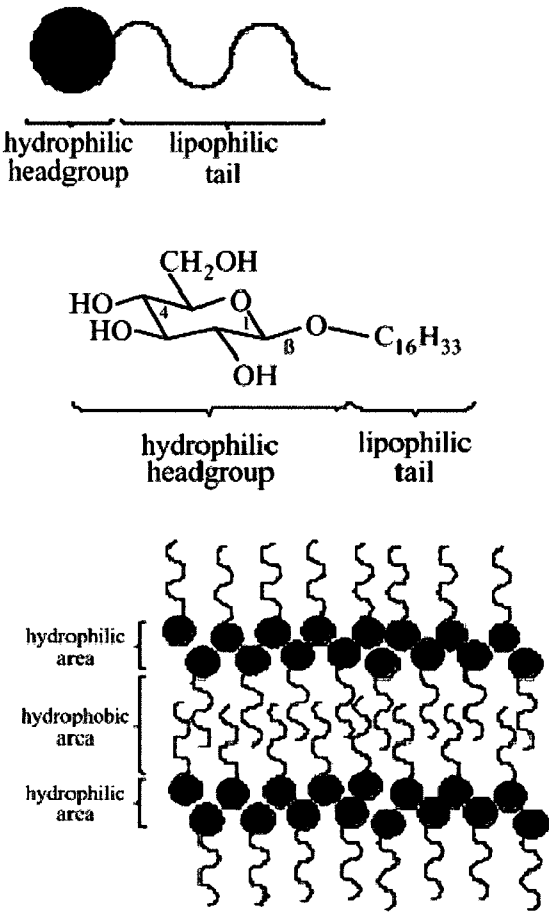

Figure 4.46: Smectic A phase of the amphiphilic glycolipid hexadecyl-β-D-glucopyranoside (image taken from Vill and Hashim, 2002).[78]

Benefits of carbohydrate liquid crystals include the fact that they are easily accessible, non-toxic, and have good solubility in both water and organic solvents.[78] Furthermore, there is a high diversity of structures that may form liquid crystals due to variations in stereochemistry of the sugar hydroxyl groups, the nature of the atom at C-1, the regiochemistry (location of the alkyl group), and the use of constitutional isomers (furanosides or pyranosides).[78, 79] In order to form mesogens, carbohydrates generally require *n*-alkyl chains of six carbons or more, a cyclic carbohydrate moiety, and they must contain some free hydroxyl groups in the carbohydrate component.[76] Hydrogen bonding and van der Waals interactions are also critical for liquid crystal formation.[69, 76]

The stereochemistry of the hydroxyl groups seems to play a role in determining the amount of liquid crystal behaviour that an alkyl glycoside displays. For example, the amount of mesophase behavior of thio-alkyl mannose and glucose derivatives were similar while those for talose derivatives were much lower (Figure 4.47).[69] The authors suggest that in talose, the formation of an intramolecular hydrogen bond between the hydroxyl groups at C-2 and C-4 makes the carbohydrate less able to maintain the hydrogen-bonded network that stabilizes the mesophase structure.[69] This results in a smaller number of hydroxyl groups that are available to form intermolecular hydrogen bonds.[79]

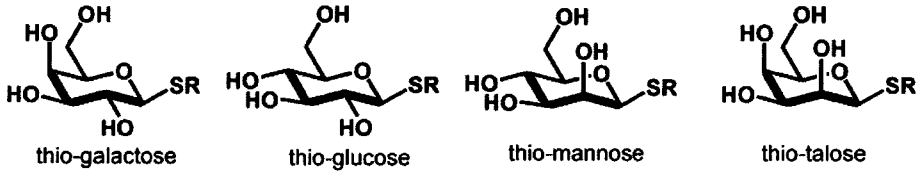

Figure 4.47: Several *n*-alkyl-1-thio-D-glycopyranosides prepared by Galema et al. to study the effect of carbohydrate stereochemistry on liquid crystal properties.[69]

Futhermore, van Doren et al. have suggested that since lyotropic liquid crystals result from the formation of ordered aggregates, the nature of the mesophase at the bulk water interface (at maximum hydration) will be indicative of the morphology of the aggregates.[79] The authors further suggest that at maximum hydration, the effective headgroup size of talose derivatives is smaller than for other hexoses, as is evidenced by talose's smaller hydration number than mannose and glucose.[79] In glucose and mannose, the headgroup is more strongly hydrated which causes the cross-sectional surface area to be enlarged, resulting in micelle formation.[79] Therefore, small differences in carbohydrate stereochemistry have a large effect on the hydration of the carbohydrate headgroups and ultimately on the molecular assembly of the mesophase.[79]

Previous work in our laboratory (Figures 4.48 and 4.49, Trant, Biggs, and Ben, unpublished results) has shown that alkyl chains have an interesting effect on IRI activity, and that there seems to be an optimal chain length. Interestingly, a compound

containing a propyl amide showed greater IRI activity than compounds with either an ethyl or a butyl alkyl chain.

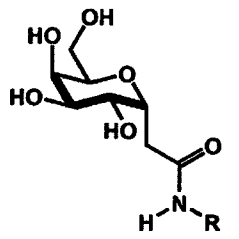

R = Me, Et, Pr, Bu, Bn

Figure 4.48: Compounds previously prepared in our laboratory (Trant, Biggs, and Ben).

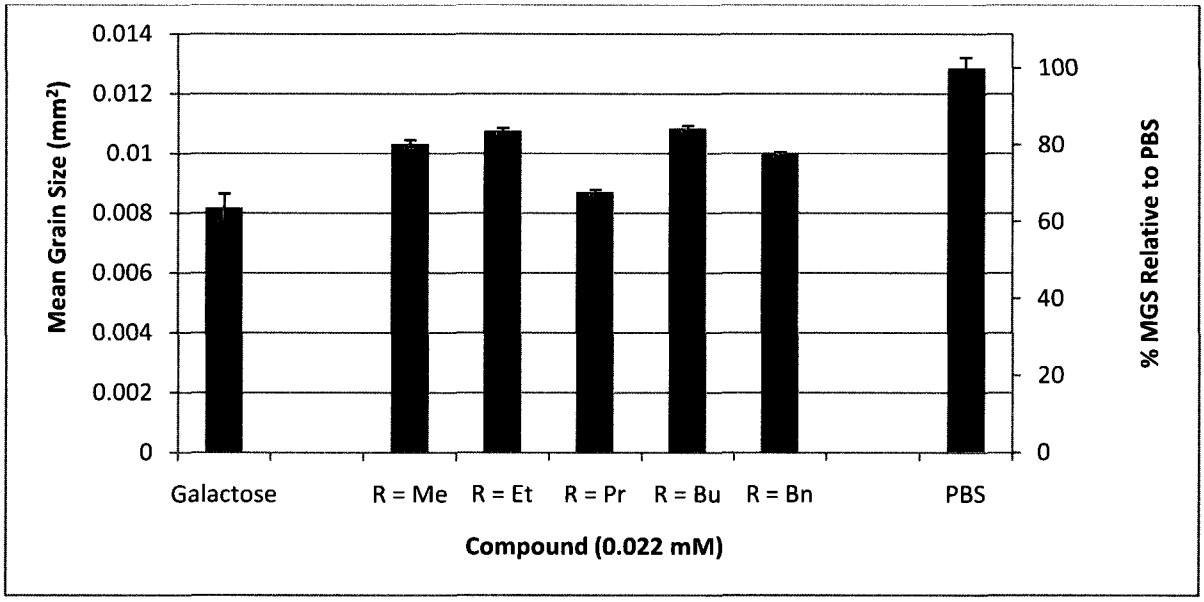

Figure 4.49: IRI activity of glycosyl amides with the general structure seen in Figure 4.48. (Trant, Biggs, and Ben, unpublished results).

4.3.2: Preparation and IRI Activity of Galactose Derivatives with Alkyl Chains

Our hypothesis is that the compounds displayed in Figure 4.48 may be forming gels or mesogens, which are known to form in carbohydrates containing alkyl chains. In

order to examine this further, we proposed the synthesis of several compounds containing saturated alkyl chains at C-1 and C-2 (Figure 4.50). These compounds have structural features similar to known carbohydrate gelators, although we will not assess gel formation within this project. The IRI activity of these compounds was evaluated and we assessed the effect of these alkyl chains on inhibition of ice-recrystallization.

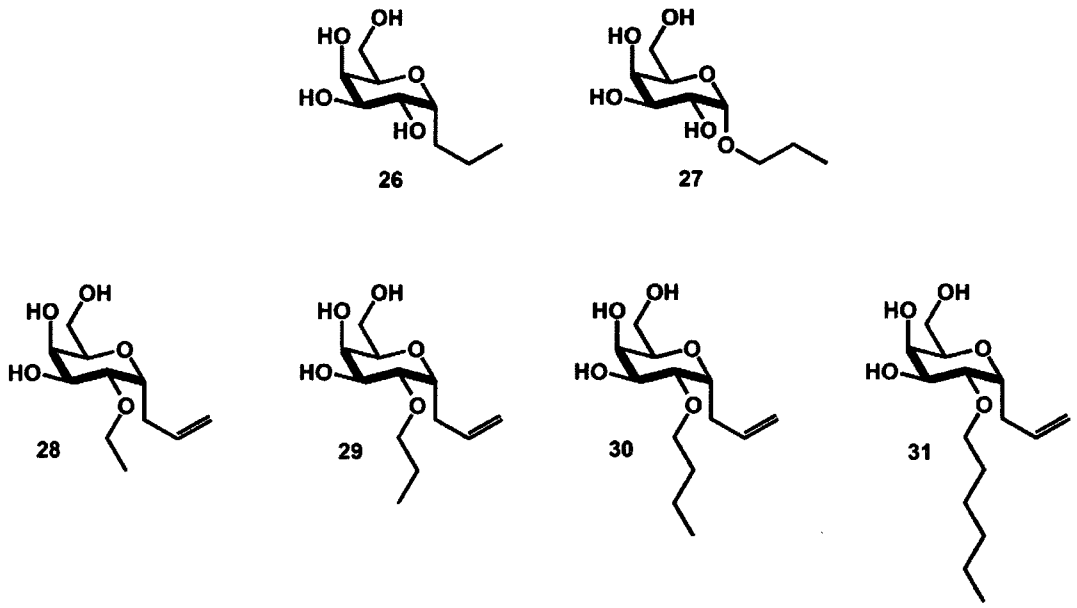

Figure 4.50: Alkylated compounds to examine possible gel or mesophase formation and its effect on IRI activity.

The synthesis of these compounds began with intermediate (**64**), whose formation was described previously (Figure 4.7). This compound was then treated with bromoethane, bromopropane, bromobutane, or bromohexane in order to attain compounds (**112 – 115**), respectively (Figure 4.51). Removal of the protecting groups under acidic conditions gave the desired compounds (**41 – 44**).

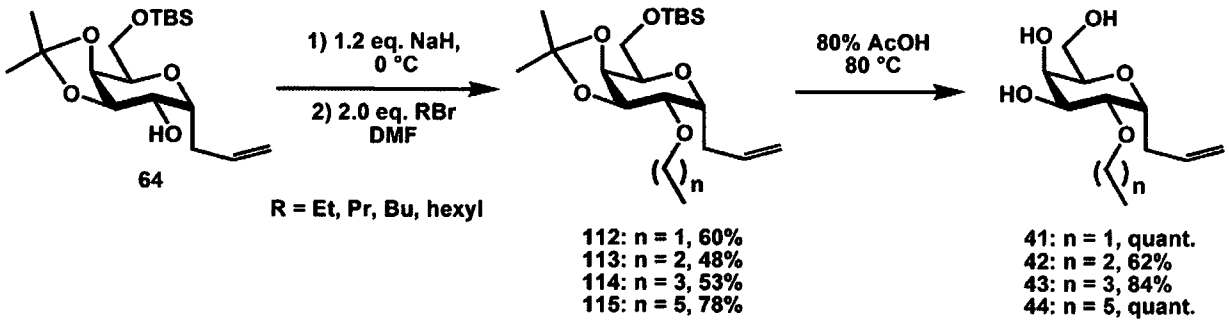

Figure 4.51: Preparation of alkylated compounds (**41** – **44**) from a common intermediate (**64**)

The formation of compounds (**20**) and (**40**) is described in Figures 3.21 and 4.52. The synthesis of α-*O*-propyl galactose derivative (**27**) began with the acetylation of the free hydroxyl groups of (**34**) (Figure 4.52). Hydrogenation gave the acetylated propyl derivative (**117**) which was then de-protected to give the desired product. A similar sequence of reactions gave (**20**) starting from (**14**) and this synthesis was described previously (Figure 3.21).

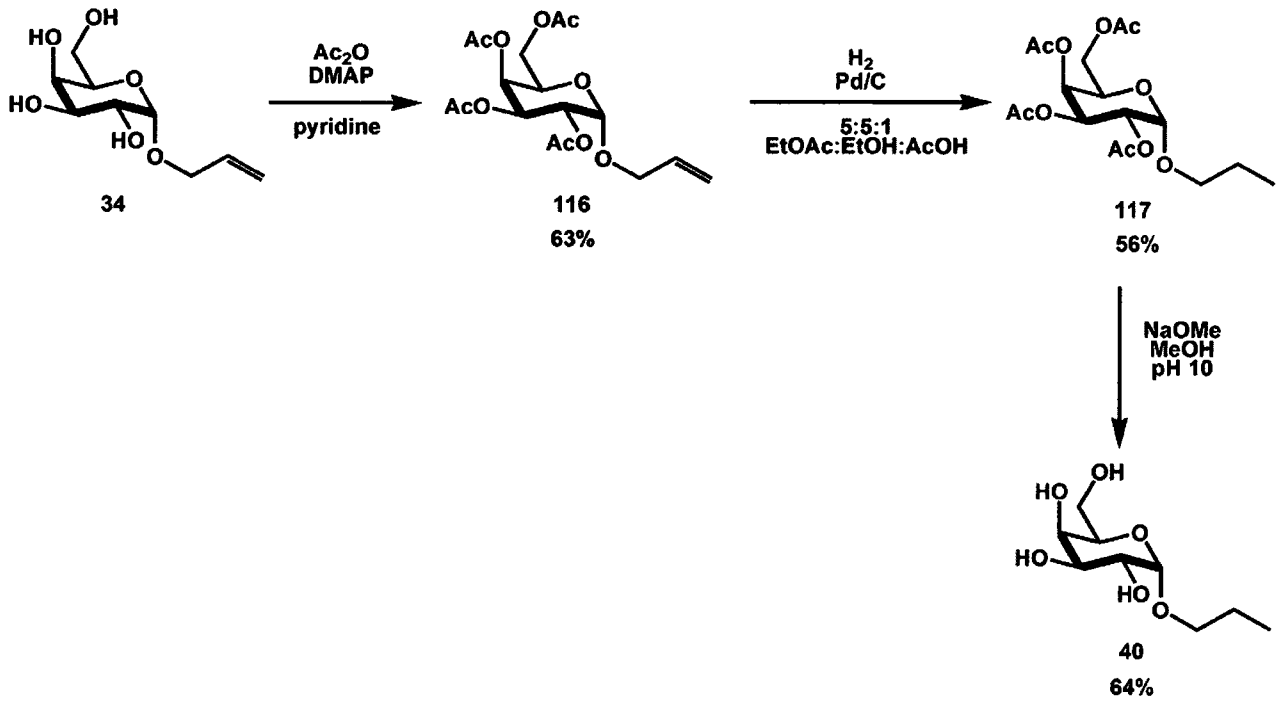

Figure 4.52: α-*O*-propyl galactose (**40**) was prepared from compound (**34**) in three steps.

Figure 4.53 shows the results of the IRI activity assay for these compounds. C-1 alkylated derivatives (**20**) and (**40**) show moderate IRI activity, with these compounds having statistically identical mean grains sizes. In both cases, we observed a decrease in IRI activity relative to galactose (**5**). For the C-2 alkylated compounds (**28, 41 – 44**), we see a steady increase in IRI activity as the length of the alkyl chain is increased. These results suggest that increasing the length of the alkyl chain at C-1 may result in a similar improvement in inhibition of recrystallization, especially in light of previous reports that alkyl chains of six carbons or greater are necessary for liquid-crystalline behavior.[76] We were pleased to see that a solution of compound (**44**) formed ice crystals with a mean grain size that was only 57% the size of those in PBS. This IRI activity is better than any other monosaccharide that we have tested at this concentration, including native galactose (**5**) which forms ice crystals that were 64% the size of those in a PBS solution. These results suggest that long alkyl chains do result in an increase in IRI activity, and this may be due to the formation of gels or liquid crystals in solution.

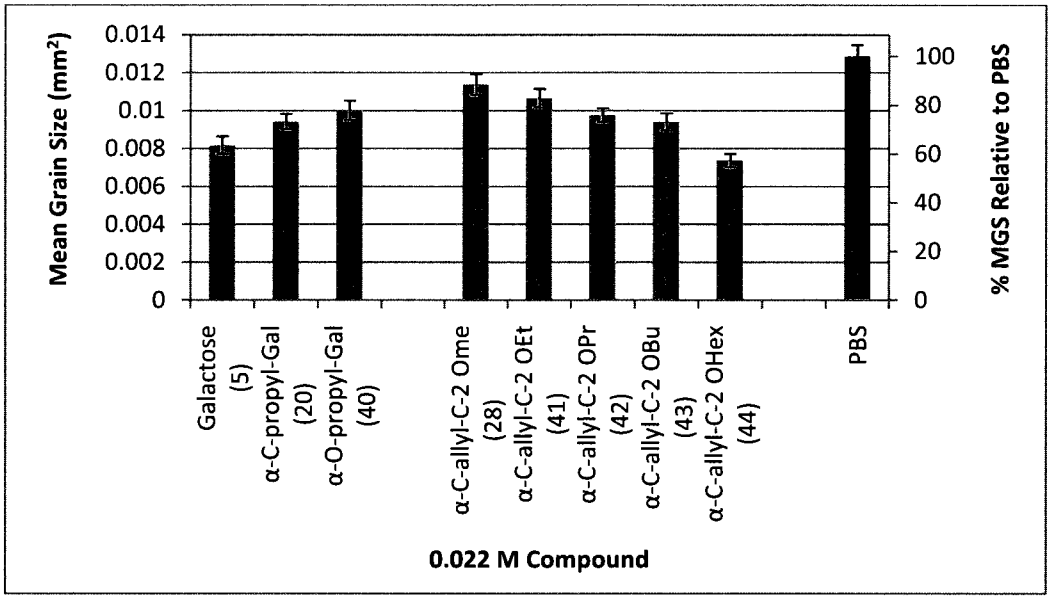

Figure 4.53: IRI activity of C-1 alkylated galactose derivatives (**20**) and (**40**) and C-2 alkylated galactose derivatives (**28** and **41 – 44**)

Both propyl derivatives (**20**) and (**40**) showed a decrease in IRI activity relative to native galactose (**5**). These compounds contain a hydrophobic propyl moiety at the anomeric position, and the decrease in IRI activity is similar to the results seen for the methoxy derivatives (**28**, **41 – 44).** This result provides further support for our proposed model in which hydrophobic groups result in a lesser disruption of the hydrogen bonded network of bulk water, leading to increased ice recrystallization.

Similarly, *C*-allyl galactose derivatives containing an *O*-ethyl (**41**), *O*-propyl (**42**), and *O*-butyl (**43**) at C-2 all showed a significant decrease in IRI activity relative to galactose (**5**), although the moderate IRI activity observed for (**28**) increased with increasing chain length. Again, these compounds contain a hydrophobic group that likely results in ordering of the water molecules around itself, according to our proposed model. These compounds are most likely not forming gels or liquid crystals, because other researchers have noted that an alkyl chain of six carbons or longer is necessary for gel formation.[76] However, we saw an increase in activity for *O*-hexyl galactose derivative (**44**) as compared to galactose (**5**). This compound could be forming a gel or

liquid crystal in solution, as it meets the requirement of having a six-carbon alkyl chain. If this is the case, it suggests that gel formation results in increased IRI activity.

Regardless of whether or not it behaves as a gelator, compound (**44**) was found to be an effective inhibitor of ice-recrystallization despite the long hydrophobic moiety. Therefore, (**44**) does not fit into our proposed model. If this compound is indeed forming a liquid crystal, this would explain why we observe IRI activity despite its hydrophobic tail. Compound (**44**) is likely orienting itself as seen in Figure 4.46, with the hydrophobic tails of adjacent molecules interacting through van der Waals interactions, with the hydrophilic carbohydrate headgroups at the outside. In this orientation, the hydrophilic headgroups are still able to cause a large disturbance of the bulk water molecules surrounding the hydration shell, while the hydrophobic interior of the "sandwich" will repel the polar water molecules. Therefore, the hydroxyl groups on the hydrophilic top face of galactose are unaffected by the hydrophobic tail and are able to disturb the surrounding water as effectively as galactose itself, resulting in effective IRI activity. In fact, compound (**44**) is the most effective monosaccharide at inhibiting ice-recrystallization that we have seen to date, which suggests that gel formation results in increased hydration of the carbohydrate, increased disruption of bulk water, and increased inhibition of ice-recrystallization.

In order to further examine the potential for gel formation and its effect on antifreeze activity, galactose derivatives with longer alkyl chains at C-2 should be prepared. These compounds would have an even higher propensity to form liquid crystals or gels, and if efficient IRI activity is observed this would be additional evidence that gel formation results in inhibition of ice recrystallization. Additionally, longer *O*-alkyl and *S*-alkyl chains should be incorporated at C-1, as these compounds have been known to display liquid crystalline behaviour[69, 80] and these may therefore display effective IRI activity.

4.3.3: Preparation and IRI Activity of Thioglycoside Derivatives

In the final series for this project, we chose to examine the effect of a sulphur atom at the anomeric position. The advantage of this substitution is that the oxidation state of sulphur can be easily modified and therefore its effect on IRI activity can be determined. The *O*-glycosidic linkage of naturally occurring carbohydrates is often replaced with an *S*-glycoside. This modification has been shown to make the carbohydrates less susceptible to enzymatic hydrolysis, however the recognition of the carbohydrate by the biological target is often unaffected.[81-85] For this reason, thioglycosides are often used in enzyme-inhibition studies.

Recently, Singer et al. prepared a series of benzene sulfonamides containing thio, sulfinyl, and sulfonyl glycosides (Figure 4.54).[85] These compounds were tested as inhibitors of carbonic anhydrase isozymes. Their hypothesis was that as the oxidation state of sulphur was raised in these analogues, the compounds would be more likely to form hydrogen bonds to amino acids in the carbonic anhydrase active sites and that this would result in increased inhibition.[85] However, the oxidation state of sulphur seemed to have no effect on the inhibition constant (k_i) of these small molecules.[85]

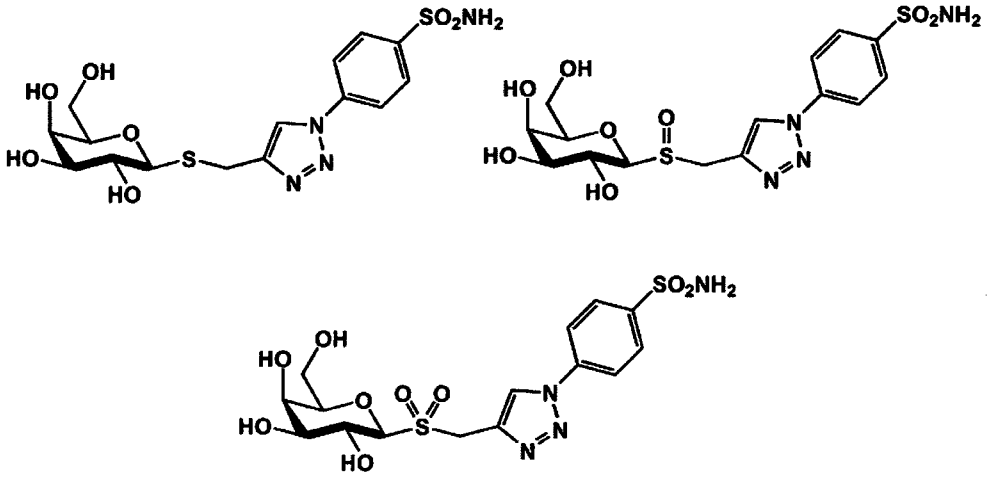

Figure 4.54: Benzene sulfonamides prepared by Singer et al. as small molecule inhibitors of carbonic anhydrase isozymes.[85]

We chose to prepare similar compounds to examine the effect of the oxidation state of sulphur and hydrogen bonding capacity on IRI activity. Furthermore, as mentioned above, thioglycosides often display liquid-crystalline behaviour, [68, 69, 79] and this may result in them displaying efficient IRI activity. The compounds that will be prepared in this series are displayed in Figure 4.55. The synthesis of (**45**) has been previously described (Figure 4.22). Compounds (**46**) and (**47**) were easily prepared from compound (**82**) (Figure 4.56), whose synthesis was described earlier in this chapter (Figure 4.22).

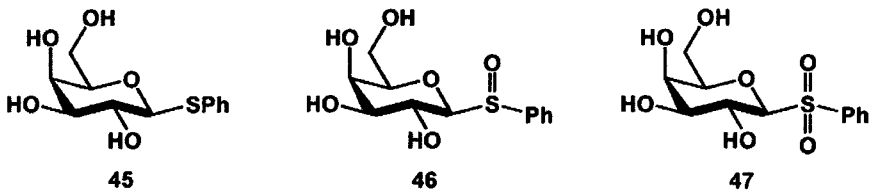

Figure 4.55: *S*-linked galactose derivatives to be prepared and evaluated for IRI activity.

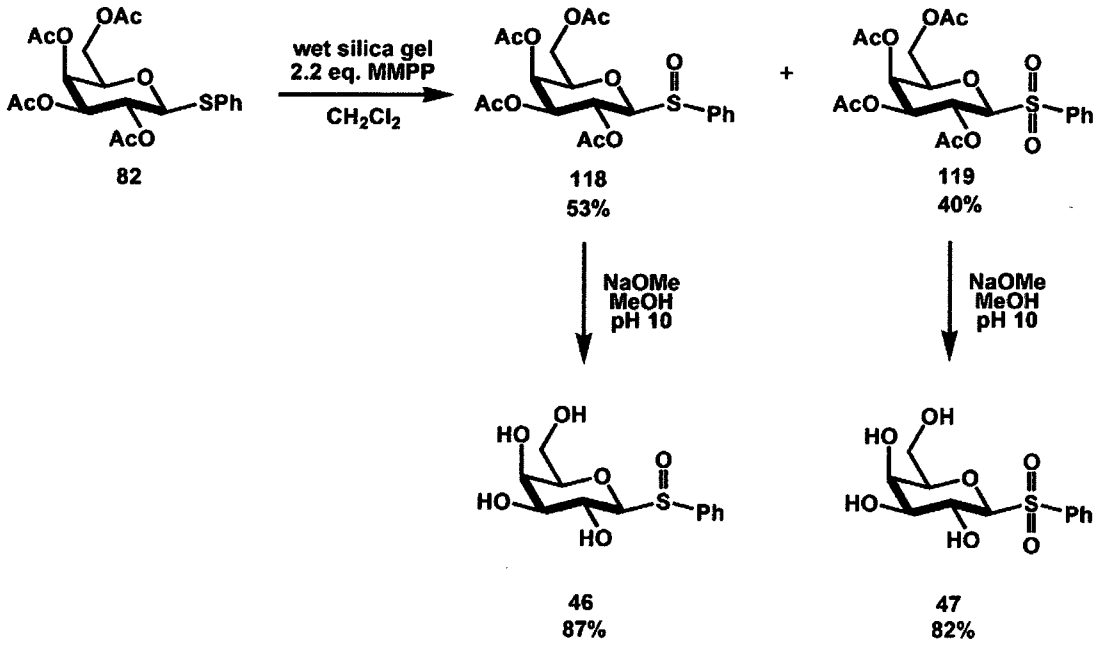

Figure 4.56: Preparation of *S*-linked galactose derivatives (**43** and **44**) from compound (**85**)

The IRI activity of these *S*-linked compounds (**45 – 47**) is shown in Figure 4.57. Other galactose derivatives (**5** and **14**) are shown for comparison. Surprisingly, all of the *S*-linked compounds (**45 – 47**) showed activity that was statistically identical to both galactose (**5**) and *C*-allyl-galactose (**14**). Furthermore, all of the *S*-linked compounds had statistically identical activity[16] to one another. These results suggest that the oxidation state of sulphur does not affect the IRI activity. Even more surprisingly, compounds (**45 – 47**) have their sulphur atoms are in the β-anomeric position, yet they inhibit recrystallization as well as (**5**) and **(14**) which have α-anomeric atoms. These are the first β-linked compounds that that had comparable IRI activity to galactose (**5**) or α-linked derivatives (**14** and **34**).

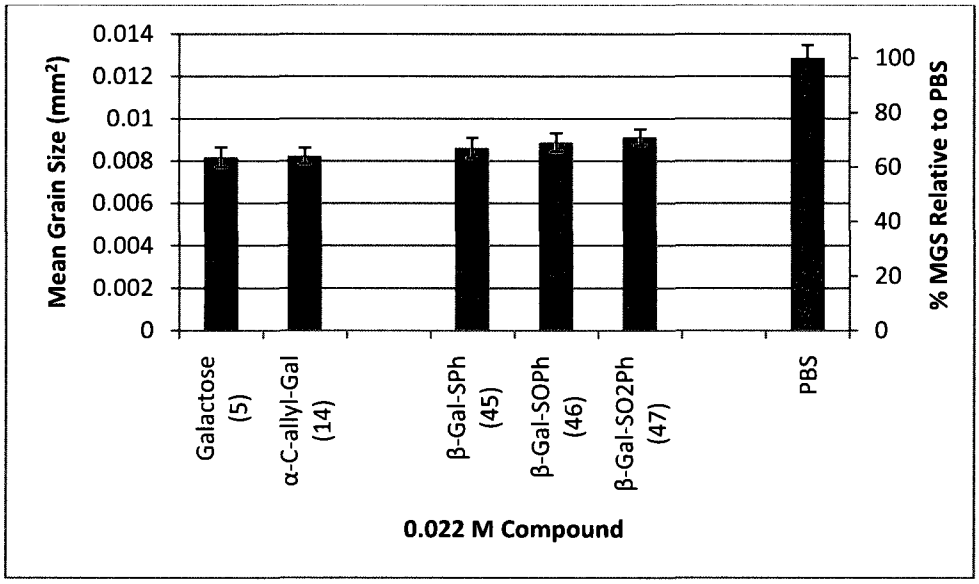

Figure 4.57: IRI activity of *S*-linked galactose derivatives (**45 – 47**) compared to galactose (**5**) and α-*C*-allyl galactose (**14**)

S-linked monosaccharides with various oxidation states showed identical IRI activity. This is consistent with the results of Singer et al. who observed that the oxidation state of sulphur had no effect on the binding of carbohydrates.[85] This suggests that hydrogen bonding interactions are not increased as the oxidation state of sulphur is increased. Therefore, the oxidation state of sulphur does not appear to affect the

hydration of the compound. Interestingly, all *S*-linked analogues examined in this study showed IRI activity comparable to native galactose, despite the β-linkage at the anomeric position. Previous experiments have shown that carbohydrates with *S*-alkyl groups at the anomeric position display liquid crystalline behaviour,[68, 69, 79] although *S*-aryl groups have not been studied. It is possible that the compounds prepared in this study are forming liquid crystals or gels, which would account for their efficient IRI activity. In order to examine this hypothesis, carbohydrates with *S*-alkyl chains of increasing length at the anomeric position should be prepared and evaluated for IRI activity. This work is currently underway in our laboratory. If similar activity to the *S*-aryl compounds (**45 – 47**) is observed, this would provide evidence that the *S*-aryl compounds are forming liquid crystals and this would account for their IRI activity based upon the precedent described earlier in this dissertation

4.4: Summary:

In summary, several compounds containing dramatic structural modifications to the core galactose structure were prepared and evaluated for IRI activity. α/β-methyl galactopyranosides were found to fit well into our observed correlation between the hydration index of a carbohydrate and its IRI activity. The effect of methoxy groups at C-2, C-3, C-4, and C-6 on IRI activity was observed. Methylated derivatives of *C*-allyl galactose were found to display poor IRI activity, regardless of the position of the methoxy group on the carbohydrate. The results are explained as follows, based upon our model of the interaction of carbohydrates with water and ice. Compounds with hydrophobic groups are poorly hydrated and they cause a lesser disruption of the bulk water molecules by causing them to be highly ordered in the region surrounding the hydration shell. A favourable increase in entropy when these ordered water molecules are released into the bulk phase results in a lower energy transfer of water molecules to the QLL of a growing ice crystal, allowing growth and recrystallization to form large ice crystals. Initial attempts to calculate the hydration properties of carbohydrates showed promise, although the parameters must be adjusted before these simulations are applied to unnatural monosaccharide derivatives.

A *geminal* difluoromethylene group at the anomeric position was observed to decrease the amount of IRI activity, likely due to the hydrophobic nature of the fluorine atoms. This suggests that the fluorine atoms are not forming hydrogen bonds in these experiments. These results contradict previous reports that fluorinated compounds can be used as cryoprotectants, and this will need to be explored in the future.

Compounds with alkyl chains at C-1 and C-2 were prepared and evaluated for IRI activity. When the alkyl chain was made up of fewer than five carbons, poor IRI activity was observed. This supports our model that carbohydrates containing hydrophobic groups are poorly hydrated and therefore display low amounts of IRI activity. However, when a compound with a C-2 hexyl chain was assessed, it showed greater IRI activity than galactose itself. Our hypothesis is that this compound is forming a gel or liquid crystal in solution, and the liquid crystalline properties cause it to be more effectively hydrated and result in inhibition of ice-recrystallization.

Thioglycoside monosaccharide derivatives were observed to display efficient IRI activity, although this activity was not affected by the oxidation state of the sulphur atom at the anomeric position. These compounds may also be forming liquid crystals, which would account for their effective IRI activity.

4.5: References:

1. Sonnichsen, F. D.; DeLuca, C. I.; Davies, P. L.; Sykes, B. D., Refined Solution Structure of Type III Antifreeze Protein: Hydrophobic Groups may be Involved in the Energetics of the Protein-Ice Interactions. *Structure* **1996,** 4, 1325-1337.

2. Yang, C.; Sharp, K. A., Hydrophobic Tendency of Polar Group Hydration as a Major Force in Type I Antifreeze Protein Recognition. *PROTEINS: Struct., Funct., Bioinf.* **2005,** 59, 266-274.

3. Baardsnes, J.; Davies, P. L., Contribution of Hydrophobic Residues to Ice Binding By Fish Type III Antifreeze Protein. *Biochim. Biophys. Acta* **2002,** 1601, 49-54.

4. McDonald, S. M.; White, A.; Clancy, P.; Brady, J. W., Binding of an Antifreeze Polypeptide to an Ice/Water Interface via Computer Simulation. *AIChE J.* **1995,** 41, 959-973.

5. Chao, H.; Housten, M. E. J.; Hodges, R. S.; Kay, C. M.; Sykes, B. D.; Loewen, M. C.; Davies, P. L.; Sonnichsen, F. D., A Diminished Role for Hydrogen Bonds in Antifreeze Protein Binding to Ice. *Biochemistry* **1997,** 36, 14652-14660.

6. Karim, O. A.; Haymet, A. D. J., The Ice/Water Interface. *Chem. Phys. Lett.* **1987,** 138, 531-534.

7. Zhang, W.; Laursen, R. A., Structure-Function Relationships in a Type I Antifreeze Polypeptide: The Role of Threonine Methyl and Hydroxyl Groups in Antifreeze Activity. *J. Biol. Chem.* **1998,** 273, 34806-34812.

8. Bar, M.; Celik, Y.; Fass, D.; Braslavsky, I., Interactions of β-Helical Antifreeze Protein Mutants with Ice. *Cryst. Growth & Design* **2008,** 8, 2954-2963.

9. Graether, S. P.; DeLuca, C. I.; Baardsnes, J.; Hill, G. A.; Davies, P. L.; Jia, Z., Quantitative and Qualitative Analysis of Type III Antifreeze Protein Structure. *J. Biol. Chem.* **1999,** 274, 11842-11847.

10. Czechura, P.; Tam, R. Y.; Dimitrijevic, E.; Murphy, A. V.; Ben, R. N., The Importance of Hydration for Inhibiting Ice Recrystallization with *C*-Linked Antifreeze Glycoproteins. *J. Am. Chem. Soc.* **2008,** 130, 2928-2929.

11. Yang, X.; Gerczei, T.; Glover, L.; Correll, C. C., Crystal Structures of Restriction-Inhibitor Complexes with Implications for RNA Recognition and Base Flipping. *Nat. Struct. Biol.* **2001,** 8, 968-973.

12. Galema, S. A.; Hoiland, H., Stereochemical Aspects of Hydration of Carbohydrates in Aqueous Solutions. 3. Density and Ultrasound Measurements. *J. Phys. Chem.* **1991,** 95, 5321-5326.

13. Dashnau, J. L.; Sharp, K. A.; Vanderkooi, J. M., Carbohydrate Intramolecular Hydrogen Bonding Cooperativity and Its Effect on Water Structure. *J. Phys. Chem. B* **2005,** 109, 24152-24159.

14. Park, T.-J.; Weiwer, M.; Yuan, X.; Baytas, S. N.; Munoz, E. M.; Murugesan, S.; Linhardt, R. J., Glycosylation in Room Temperature Ionic Liquid Using Unprotected and Unactivated Donors. *Carbohydrate Res.* **2007,** 342, 614-620.

15. Bornaghi, L. F.; Poulsen, S.-A., Microwave-Accelerated Fischer Glycosylation. *Tetrahedron Lett.* **2005,** 46, 3485-3488.

16. Ruxton, G. D., The Unequal Variance t-Test is an Underused Alternative to Student's t-Test and the Mann-Whitney U Test. *Behav. Ecol.* **2006,** 17, 688-690.

17. Tam, R. Y.; Ferreira, S. S.; Czechura, P.; Chaytor, J. L.; Ben, R. N., Hydration Index - A Better Parameter for Explaining Small Molecule Hydration in Inhibition of Ice Recrystallization. *J. Am. Chem. Soc.* **2008,** 130, 17494-17501.

18. Chevallier, O. P.; Migaud, M. E., Investigation of Acetyl Migrations in Furanosides. *Beilstein J. Org. Chem.* **2006,** 2, 14-1 to 14-6.

19. Mastihubova, M.; Biely, P., Lipase-Catalysed Preparation of Acetates of 4-Nitrophenyl beta-D-Xylopyranoside and their Use in Kinetic Studies of Acetyl Migration. *Carbohydrate Res.* **2004,** 339, 1353-1360.

20. Ishido, Y.; Sakairi, N.; Sekiya, M.; Nakazaki, N., Regioselective *O*-Deacylation of Fully Acylated Glycosides and 1,2-*O*-Isopropylidinealdofuranose Derivatives with Hydrazine Hydrate. *Carbohydrate Res.* **1981,** 97, 51-79.

21. Caffarena, E. R.; Grigera, J. R., On the Hydrogen Bond Structure of Water at Different Densities. *Physica A* **2004,** 342, 34-39.

22. Cheetham, N. W. H.; Lam, K., Molecular Dynamics Simulations of Glycosides in Aqueous Solution. *Carbohydrate Res.* **1996,** 282, 13-23.

23. Behler, J.; Price, D. W.; Drew, M. G. B., Water Structuring Properties of Carbohydrates, Molecular Dynamics Studies on 1,5-Anhydro-D-Fructose. *Phys. Chem. Chem. Phys.* **2001,** 3, 588-601.

24. Dashnau, J. L.; Nucci, N. V.; Sharp, K. A.; Vanderkooi, J. M., Hydrogen Bonding and the Cryoprotective Properties of Glycerol/Water Mixtures. *J. Phys. Chem. B* **2006,** 110, 13670-13677.

25. Lemieux, R. U., How Water Provides the Impetus for Molecular Recognition in Aqueous Solution. *Acc. Chem. Res.* **1996,** 29, 373-380.

26. Nutt, D. R.; Smith, J. C., Dual Function of the Hydration Layer around an Antifreeze Protein Revealed by Atomistic Molecular Dynamics Simulations. *J. Am. Chem. Soc.* **2008,** 130, 13066-13073.

27. Glinski, J.; Burakowski, A., Is the Hydration Number of a Non-Electrolyte Additive with Length and Constituents of the Solute Molecule? *Eur. Phys. J. Spec. Topics* **2008,** 154, 275-279.

28. Street, I. P.; Armstrong, C. R.; Withers, S. G., Hydrogen Bonding and Specificity. Fluorodeoxy Sugars as Probes of Hydrogen Bonding in the Glycogen Phosphorylase-Glucose Complex. *Biochemistry* **1986,** 25, 6021-6027.

29. Blackburn, G. M.; Kent, D. E.; Kolkmann, F., The Synthesis and Metal Binding Characteristics of Novel, Isopolar Phosphonate Analogues of Nucleotides. *J. Chem. Soc. Perk. Trans. 1* **1984,** 1984, 1119-1125.

30. Kalinina, I.; Gautier, A.; Salcedo, C.; Valnot, J.-Y.; Piettre, S. R., Second-Generation Synthesis of Protected Phosphonothiodifluoromethylene Analogues of Nucleoside-3'-Phosphates. *Tetrahedron* **2004,** 60, 4895-4900.

31. Kim, H. W.; Rossi, P.; Shoemaker, R. K.; DiMagno, S. G., Structure and Transport Properties of a Novel, Heavily-Fluorinated Carbohydrate Analogue. *J. Am. Chem. Soc.* **1998,** 120, 9082-9083.

32. Timofte, R. S.; Linclau, B., Enantioselective Synthesis of Tetrafluorinated Glucose and Galactose. *Org. Lett.* **2008,** 10, 3673-3676.

33. Biffinger, J. C.; Kim, H. W.; DiMagno, S. G., The Polar Hydrophobicity of Fluorinated Compounds. *ChemBioChem* **2004,** 5, 622-627.

34. Plantier-Royon, R.; Portella, C., *C*-Difluoromethylene-Containing, *C*-Trifluoromethyl and *C*-Perfluoroalkyl Carbohydrates. Synthesis by Carbohydrate Transformation or Building Block Methods. *Carbohydrate Res.* **2000,** 327, 119-146.

35. Brigaud, T.; Lefebvre, O.; Plantier-Royon, R.; Portella, C., Mixed Organofluorine - Organosilicon Chemistry. 6. Synthesis of gem-Difluoro-*C*-Glycosides and *C*-Disaccharides from Acylsilanes and Trifluoromethyltrimethylsilane. An Exploratory Study. *Tetrahedron Lett.* **1996,** 37, (34), 6115-6116.

36. Giuffredi, G. T.; Purser, S.; Sawicki, M.; Thomspon, A. L.; Gouverneur, V., Asymmetric De Novo Synthesis of Fluorinated D-Glucitol and D-Mannitol Analogues. *Tetrahedron: Asymmetry* **2009,** 20, 910-920.

37. Dunitz, J. D.; Taylor, R., Organic Fluorine Hardly Ever Accepts Hydrogen Bonds. *Chem. Eur. J.* **1997,** 1, 89-98.

38. Howard, J. A. K.; Hoy, V. J.; O'Hagen, D.; Smith, G. T., How Good is Fluorine as a Hydrogen Bond Acceptor? *Tetrahedron* **1996,** 52, 12613-12622.

39. Withers, S. G.; Street, I. P.; Rettig, S. J., The Preferred Conformation of 2-Fluoro-2-Deoxy beta-D-Mannopyranosyl Fluoride. An X-Ray Crystallographic and 2-Dimensional Proton Nuclear Magnetic Resonance Study. *Can. J. Chem.* **1986,** 64, 232-236.

40. Karipides, A.; Miller, C., Crystal Structure of Calcium 2-Fluorobenzoate Dihydrate: Indirect Calcium---Fluorine Binding through a Water-Bridged Outer-Sphere Intermolecular Hydrogen Bond. *J. Am. Chem. Soc.* **1984,** 106, 1494-1495.

41. Miethchen, R., Modified Natural Substances - Fluorinated and Fluoroalkylated Monosaccharides and Inositols. *J. Fluorine Chem.* **2004,** 125, 895-901.

42. Williams, S. J.; Withers, S. G., Glycosyl Fluorides in Enzymatic Reactions. *Carbohydrate Res.* **2000,** 327, 27-46.

43. Berber, H.; Brigaud, T.; Lefebvre, O.; Plantier-Royon, R.; Portella, C., Reactions of Difluoroenoxysilanes with Glycosyl Donors: Synthesis of Difluoro-*C*-Glycosides and Difluoro-*C*-Disaccharides. *Chem. Eur. J.* **2001,** 7, (4), 903-909.

44. Herpin, T. F.; Motherwell, W. B.; Weibel, J.-M., Two Free Radical Routes for the Preparation of Novel Difluoromethylene-Linked Serine-*O*-Glycopeptide Analogues. *J. Chem. Soc. Chem. Comm.* **1997,** 1997, 923-924.

45. Miethchen, R.; Hein, M., Liquid Crystals Based on Fluorinated Carbohydrates. *Carbohydrate Res.* **2000,** 327, 169-183.

46. Quirion, J.-C.; Castelot-Deliencourt-Godefroy, G. Gem Difluorinated *C*-Glycopeptides, their Preparation and their Use for the Preservation of Biological Materials and/or in Cryosurgery. WO 2006/059227 A1, June 8 2006, 2006.

47. Erdik, E., Use of Activation Methods for Organozinc Reagents. *Tetrahedron* **1987,** 43, 2203-2212.

48. Picotin, G.; Miginiac, P., Activation of Zinc by Trimethylchlorosilane: An Improved Procedure for the Preparation of beta-Hydroxy Esters from Ethyl Bromoacetate and Aldehydes or Ketones (Reformatsky Reaction). *J. Org. Chem.* **1987,** 52, 4796-4798.

49. Cuenca, A. B.; D'Hooge, F.; Gouge, V.; Castelot-Deliencourt, G.; Oulyadi, H.; Leclerc, E.; Jubault, P.; Pannecoucke, X.; Quirion, J.-C., Addition of Ethyl Bromodifluoroacetate to Lactones: Reactivity and Stereoselectivity. *Synlett* **2005,** 2005, (17), 2627-2630.

50. Cipolla, L.; Lay, L.; Nicotra, F., New and Easy Access to *C*-Glycosides of Glucosamine and Mannosamine. *J. Org. Chem.* **1997,** 62, 6678-6681.

51. Schweizer, F.; Otter, A.; Hindsgaul, O., Synthesis of Sugar-Fused GABA-Analogues. *Synlett* **2001,** 2001, 1743-1746.

52. Rodriquez, M.; Terracciano, S.; Cini, E.; Settembrini, G.; Bruno, I.; Bifulco, G.; Taddei, M.; Gomez-Paloma, L., Total Synthesis, NMR Solution Structure, and Binding Model of the Potent Histone Deacetylase Inhibitor FR235222. *Angew. Chem. Int. Ed.* **2006,** 45, 423-427.

53. Huffman, W. F.; Hall, R. F.; Grant, J. A.; Holden, K. G., Nuclear Analogues of beta-Lactam Antibiotic. 4. Total Synthesis of Bisnorisopenicillins from Antibacterially Active Monocyclic beta-Lactam Precursors. *J. Med. Chem.* **1978,** 21, 413-415.

54. Bastianns, H. M. M.; van der Baan, J. L.; Ottenheijm, H. C. J., Flexible and Convergent Total Synthesis of Cyclotheonamide B. *J. Org. Chem.* **1997,** 62, 3880-3889.

55. Kaul, R.; Surprenant, S.; Lubell, W. D., Systematic Study of the Synthesis of Macrocyclic Dipeptide beta-Turn Mimics Possessing 8-, 9-, and 10- Membered Rings by Ring-Closing Metathesis. *J. Org. Chem.* **2005,** 70, 3838-3844.

56. Rajanikanth, B.; Seshadri, R., A Facile Synthesis of Nojirimycin. *Tetrahedron Lett.* **1989,** 30, 755-758.

57. Nishi, Y.; Uchiyama, S.; Doi, M.; Nishiuchi, Y.; Nakazawa, T.; Ohkubo, T.; Kobayashi, Y., Different Effects of 4-Hydroxyproline and 4-Fluoroproline on the Stability of Collagen Triple Helix. *Biochemistry* **2005,** 44, 6034-6042.

58. Uedaira, H.; Okouchi, S.; Tsuda, S.; Uedaira, H., Hydration of Glucose and Galactose Derivatives. *Bull. Chem. Soc. Jpn.* **2001,** 74, 1857-1861.

59. van Esch, J. H.; Feringa, B. L., New Functional Materials Based on Self-Assembling Organogels: From Serendipity towards Design. *Angew. Chem. Int. Ed.* **2000,** 39, 2263-2266.

60. Jung, J. H.; Rim, J. A.; Cho, E. J.; Lee, S. J.; Jeong, I. Y.; Kameda, N.; Masuda, M.; Shimizu, T., Stabilization of an Asymmetric Bolaamphiphilic Sugar-Based Crown Ether Hydrogel by Hydrogen Bonding Interaction and its Sol-Gel Transcription. *Tetrahedron* **2007,** 63, 7449-7456.

61. Wang, G.; Cheuk, S.; Yang, H.; Goyal, N.; Reddy, P. V. N.; Hopkinson, B., Synthesis and Characterization of Monosaccharide-Derived Carbamates as Low-Molecular-Weight Gelators. *J. Am. Chem. Soc.* **2009,** DOI: 10.1021/la804337g.

62. Friggeri, A.; Gronwald, O.; van Bommel, K. J. C.; Shinkai, S.; Reinhoudt, D. N., Charge-Transfer Phenomena in Novel, Dual-Component, Sugar-Based Organogels. *J. Am. Chem. Soc.* **2002,** 124, 10754-10758.

63. Kobayashi, H.; Friggeri, A.; Koumoto, K.; Amaike, M.; Shinkai, S.; Reinhoudt, D. N., Molecular Design of "Super" Hydrogelators: Understanding the Gelation Process of Azobenzene-Based Sugar Derivatives in Water. *Org. Lett.* **2002,** 4, 1423-1426.

64. Vemula, P. K.; Li, J.; John, G., Enzyme Catalysis: Tool to Make and Break Amygdalin Hydrogelators from Renewable Resources: A Delivery Model for Hydrophobic Drugs. *J. Am. Chem. Soc.* **2006,** 128, 8932-8938.

65. Nie, X.; Wang, G., Synthesis and Self-Assembling Properties of Diacetylene-Containing Glycolipds. *J. Org. Chem.* **2006,** 71, 4734-4741.

66. Luboradzki, R.; Gronwald, O.; Ikeda, M.; Shinkai, S.; Reinhoudt, D. N., An Attempt to Predict the Gelation Ability of Hydrogen-bond-based Gelators Utilizing a Glycoside Library. *Tetrahedron* **2000,** 56, 9595-9599.

67. Gronwald, O.; Shinkai, S., Sugar-Integrated Gelators of Organic Solvents. *Chem. Eur. J.* **2001,** 7, (20), 4328-4334.

68. van Doren, H. A.; van der Geest, R.; Kellogg, R. M.; Wynberg, H., Synthesis and Liquid Crystalline Properties of the *n*-Alkyl 1-Thio-alpha-D-Glucopyranosides, a New Homologous Series of Carbohydrate Mesogens. *Carbohydrate Res.* **1989,** 194, 71-77.

69. Galema, S. A.; Engberts, J. B. F. N.; Van Doren, H. A., Synthesis, Purification and Liquid Crystalline Behavior of Several Alkyl 1-Thio-D-Glycopyranosides. *Carbohydrate Res.* **1997,** 303, 423-434.

70. Zur, C.; Miller, A. O.; Miethchen, R., Amphiphilic and Mesogenic Carbohydrates IX. Perfluoroalkyl Substituted Monosaccharides: a New Group of Amphiphilic Liquid Crystals. *Liq. Cryst.* **1998,** 24, 695-699.

71. Auzely, R.; Benvegnu, T.; Mackenzie, G.; Haley, J. A.; Goodby, J. W.; Plusquellec, D., Synthesis and Liquid-Crystalline Properties of Novel Archaeal Diether-Type Glycolipds Possessing One or Two Furanosyl Units. *Carbohydrate Res.* **1998,** 314, 65-77.

72. Bault, P.; Gode, P.; Goethals, G.; Goodby, J. W.; Haley, J. A.; Kelly, S. M.; Mehl, G. H.; Ronco, G.; Villa, P., Liquid Crystalline Derivatives of Galactose and Galactitol: Dependence of Thermotropic Mesomorphism on Carbohydrate Form. *Liq. Cryst.* **1998,** 25, 31-45.

73. Goodby, J. W.; Haley, J. A.; Mackenzie, G.; Watson, M. J.; Plusquellec, D.; Ferrieres, V., Amphitropic Liquid-Crystalline Properties of Some Novel Alkyl Furanosides. *J. Mater. Chem.* **1995,** 5, 2209-2220.

74. Baron, M., Definitions of Basic Terms Relating to Low-Molar-Mass and Polymer Liquid Crystals. *Pure Appl. Chem.* **2001,** 73, 845-895.

75. Baron, M.; Stepto, R. F. T., Definitions of Basic Terms Relating to Polymer Liquid Crystals. *Pure Appl. Chem.* **2002,** 74, 493-509.

76. Jeffrey, G. A., Carbohydrate Liquid Crystals. *Acc. Chem. Res.* **1986,** 19, 168-173.

77. Jeffrey, G. A.; Bhattacharjee, S., Carbohydrate Liquid-Crystals. *Carbohydrate Res.* **1983,** 115, 53-58.

78. Vill, V.; Hashim, R., Carbohydrate Liquid Crystals: Structure-Property Relationship of Thermotropic and Lyotropic Glycolipids. *Curr. Opin. Colloid Interface Sci.* **2002,** 7, 395-409.

79. van Doren, H. A.; Galema, S. A.; Engberts, J. B. F. N., Unexpected Formation of Vesicular Aggregates in Aqueous Solutions of *n*-Octyl 1-Thio-alpha-D-Talopyranoside. Marked Effects of Intramolecular Hydrogen Bonding. *Langmuir* **1995,** 11, 687-688.

80. Chong, T. T.; Hashim, R.; Bryce, R. A., Molecular Dynamics Simulation of Monoalkyl Glycoside Micelles in Aqueous Solution: Influence of Carbohydrate Headgroup Stereochemistry. *J. Phys. Chem. B* **2006,** 110, 4978-4984.

81. Driguez, H., Thiooligosaccharides as Tools for Structural Biology. *ChemBioChem* **2001,** 2, 311-318.

82. Witczak, Z. J.; Sun, J.; Mielguj, R., Synthesis of L-Fucopyranosyl-4-Thiodisaccharides From Levoglucosenone and their Inhibitory Activity on alpha-L-Fucosidase. *Bioorg. Med. Chem. Lett.* **1995,** 5, 2169-2174.

83. Pachamuthu, K.; Schmidt, R. R., Synthetic Route to Thiooligosaccharides and Thioglycopeptides. *Chem. Rev.* **2006,** 106, 160-187.

84. Witczak, Z. J.; Chhabra, R.; Chen, H.; Xie, X.-Q., Thiosugars II. A Novel Approach to Thiodisaccharides. The Synthesis of 3-Deoxy-4-Thiocellobiose From Levoglucosenone. *Carbohydrate Res.* **1997,** 301, 167-175.

85. Singer, M.; Lopez, M.; Bornahi, L. F.; Innocenti, A.; Vullo, D.; Supuran, C. T.; Poulsen, S.-A., Inhibition of Carbonic Anhydrase Isozymes with Benzene Sulfonamides Incorporating Thio, Sulfinyl, and Sulfonyl Glycoside Moieties. *Bioorg. Med. Chem. Lett.* **2009,** 19, 2273-2276.

Chapter 5 : Exploring the Nature of the Ice-Water Interface Using CARS

5.1: Introduction

5.1.1: Introduction to Microscopy:

Several spectroscopic and microscopic methods exist to examine living cells, tissues, and biological interfaces. The compound microscope was invented by Zacharias and Hans Janssen in 1590,[1] although it was not used to examine biological specimens for several years. Anton von Leeuwenhoek constructed over 500 microscopes with advanced lenses and used them to identify bacteria, protozoa, and spermatozoa.[1] This popularized the use of microscopes for explorations in science. The technology was advanced in the 18th century by Robert Hooke, who added fine and coarse adjustments to the microscope, enabling him to coin the word "cell" through his examination of the structure of cork.[1]

One of the main advantages of optical and light microscopy is that they are non-invasive. However, stains are often used to achieve specific visualization of cellular components, which minimizes the non-invasiveness of the experiment.[2] In addition, many samples are unable to be stained. In order to circumvent this problem, microscopy techniques which allow contrast of cellular components without the requirement for a chromophore-containing stain were sought. For example, phase-contrast microscopy takes advantages of differences in the refractive index of components, enhancing light and dark regions in the cell.[3] An alternate technique, differential contrast microscopy, uses two polarized light beams to create contrast between cellular components, also taking advantage of slight refractive index differences.[2, 3]

In addition to achieving spatial resolution to allow researchers to focus on certain areas of the sample, chemical selectivity is also important when examining biological samples.[4] This can be achieved using fluorescence or vibrational microscopy. The development of fluorescent probes, as well as the discovery of tools such as the green

fluorescent protein for cell labelling, has resulted in the wide use of fluorescence microscopy.[2] One common technique is confocal laser scanning fluorescence microscopy.[2] However, there are some disadvantages associated with this technique. Adding fluorophores to samples allows for effective chemical selectivity, however, their large size can result in major physiological changes to the sample which may result in misleading observations.[2] Furthermore, the fluorophore often has a low survival time under excitation conditions, and both the fluorophore and the sample can undergo "photobleaching" by the laser.[2] This limits the amount of viable observation time.

Both contrast and chemical selectivity can be achieved through the use of vibrational microscopy, a non-invasive technique making use of the intrinsic properties of a sample's molecules. Two common vibrational techniques are infrared absorption and Raman scattering microscopy, both of which permit direct chemical imaging of unstained samples.[2, 4] Infrared (IR) microscopy requires long excitation wavelengths, which results in low optical spatial resolution. Furthermore, the broad water absorption in IR microscopy makes examination of aqueous solutions difficult. Spontaneous Raman spectroscopy uses a shorter wavelength, and the excitation lasers operate in the visible spectral range. Although this technique is often used to study material and biological samples, it has some drawbacks like any other technique. High average power, high excitation intensities, and long integration times must be used.[2] These may not be tolerated by the sample, especially in dynamic living systems. In addition, the Stokes-shifted fluorescence is visualized in the same spectral range as the weaker Raman signal, causing complications from background fluorescence.[2] These techniques lack the sensitivity required for rapid examination of biological materials.[5]

5.1.2: Introduction to CARS Spectroscopy:

Many of these challenges can be addressed by the use of Coherent Anti-Stokes Raman Scattering (CARS) microscopy. CARS spectroscopy was first reported in the 1960's,[6] and the first report of a CARS microscope was published in 1982.[7] The theory behind this technique will be discussed below. This technique generates molecule-specific contrast based on their vibrational spectra, and sample staining is not

necessary.[2] The efficiency is orders-of-magnitude greater than in spontaneous Raman microscopy, and the signal is enhanced for weak concentrations, resulting in improvement over conventional Raman methods.[8] The main difference between spontaneous Raman spectroscopy and CARS is that CARS is a coherent process, where the molecular vibrations oscillate in phase, resulting in constructive interference.[9] The CARS signal is therefore proportional to the square of the concentration of the vibrational modes, whereas spontaneous Raman spectroscopy has an incoherent signal and a linear dependence on concentration.[9]

CARS is a four-wave mixing process in which two laser beams, a pump beam, and a Stokes beam induce a polarization $\mathbf{P}^{(3)}$ in the sample, which gives rise to an anti-Stokes radiation.[2, 4, 5] The pump field $E_p(\omega_p)$, the Stokes field $Es(\omega_s)$, and the probe field $E_{pr}(\omega_{pr})$ interact with the sample to generate an anti-Stokes field E_{as} with a frequency of $\omega_{as} = \omega_p + \omega_{pr} - \omega_s$.[2, 4] Often the pump and probe fields are obtained from the same laser, so the equation simplifies to $\omega_{as} = 2\omega_p - \omega_s$.[2] A schematic description of CARS is shown in Figure 5.1.

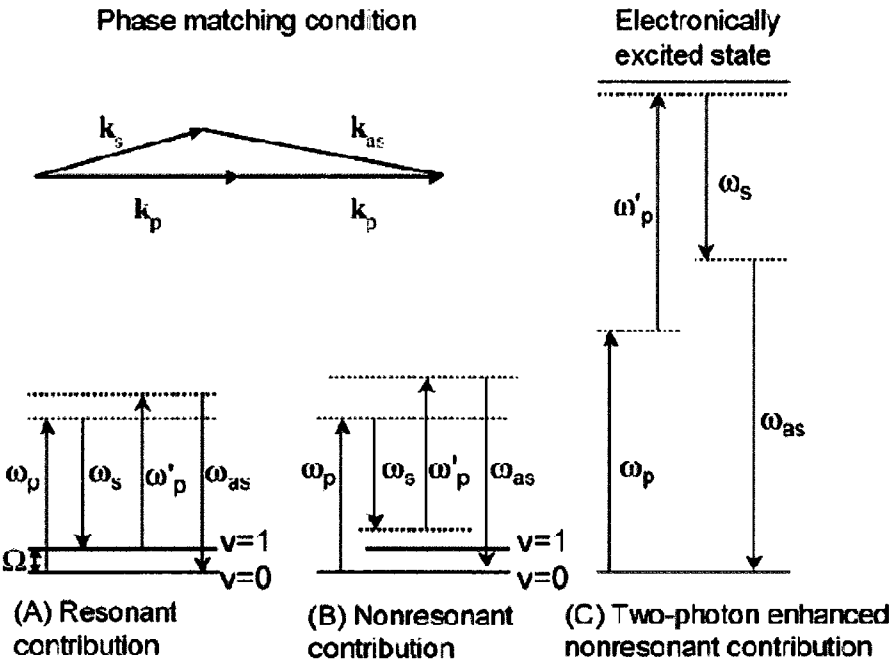

Figure 5.1: Energy diagram of CARS (taken from Cheng and Xie, 2004).[4] Image A: Resonance CARS signal. Image B: Non-resonant CARS from an electronic contribution. Image C: Electronic contribution enhanced by a two-photon resonance of the pump beam associated with an excited electronic state. The phase matching condition requires that $| \Delta k | \cdot l \ll \pi$, where l is the interaction length, $\Delta k = k_{as} - (2k_p - k_s)$, and k_{as}, k_p, and k_s are the wave vectors of the anti-Stokes, pump, and Stokes fields, respectively.[2]

Based on this description of the CARS process, one can derive the main features of CARS microscopy. The vibrational resonances of $\chi^{(3)}$ provide the contrast mechanism. When the frequency difference between the pump and Stokes beams ($\omega_p - \omega_s$) matches the vibrational frequency of the sample Ω, then the $\chi_R^{(3)}$ resonance results in a significant enhancement of the CARS signal.[2] The strong signal is obtained as long as constructive interference is maintained between the beams within the interaction volume, where the phase-matching condition is met (Figure 5.16).[2] In order to plot the distribution of a species with vibrational frequency Ω, the difference ($\omega_p - \omega_s$) is tuned to match Ω and the laser beam is scanned over the signal while the CARS signal is monitored.[2] Vibrational contrast is achieved from the enhanced signal when the frequency difference is tuned to a Raman-active vibrational band.[4] The signal

generation is a third-order non-linear process, requiring high excitation intensities which are obtained in the focal volume of the focused laser beam, which ultimately allows for three-dimensional imaging.[2]

In CARS, $\omega_p > \omega_s$, so ω_{as} is always higher than the excitation frequency.[2] This means that any background fluorescence and spontaneous Raman signals are observed at lower frequencies than the excitation, so these signals do not interfere with detection of the CARS signal.[2] However, a non-resonant background is observed, and this can limit the image contrast and spectral selectivity.[4] Other problems with this technique include the requirement for advanced laser excitation sources that have high peak power and moderate average power.[4] In recent years, several advanced laser sources and methods overcoming these challenges have been developed.[4]

Initially, following the discovery of this microscopic method, high-resolution of the samples was not achieved. Improvements in the technique have allowed for high spatial resolution and three-dimensional sectioning of samples. Using near-infrared laser pulses that are generated by a titanium:sapphire laser has led to an improvement in the signal-to-noise ratio.[9] Spectral resolution can also be achieved when there is a greater degree of control over the optical phase resulting from femtosecond (fs) laser pulses.[10] A simple method of gaining this control is to use a quadratic spectral phase variation.[10] This is a linear variation of the pulse frequencies, called "chirp". When the degree of chirp is controlled, higher spectral resolution can be attained using broad-band fs laser pulses.[10] This method is called spectral focussing.[10]

CARS spectroscopy has widespread application in both biology and material science.[2] CARS was used to observe water diffusion in *Dictyostelium* cells.[11] Observation of lipids is well-suited to CARS microscopy due to their good detectability. Live animal experiments have been conducted, where the C-H stretching vibrations of fatty acids in mice[5] and in *C. Elegans* nematodes[12] have been monitored. The high resolution and chemical specificity have made CARS ideal to observe the vibrational properties of porphyrin microcrystals, and repulsive and attractive interactions of colloidal particles during glass formation.[13]

5.1.3: Structure of Liquid Water:

The molecular structure of water and ice has been extensively studied using various methods and techniques. Raman spectroscopy has been used in several studies, often in combination with other methods.

Walrafen and coworkers examined liquid water in the temperature range of 10 – 95 ºC using Raman spectroscopy.[14, 15] They observed the existence of an isosbestic point at 3460 cm^{-1}, which is a frequency at which two absorption spectra cross.[14, 15] This point provides evidence for an equilibrium between two forms of water.[15] The authors suggest that these two forms of water are hydrogen-bonded and non-hydrogen-bonded water molecules.[14, 15] In other words, water consists of both non-hydrogen bonded monomeric water molecules, and water molecules that form a hydrogen-bonded lattice.[15] These experiments provide support for a two-state "flickering-cluster" or "mixture" model, in which hydrogen-bonded clusters of water molecules are in equilibrium with closely packed but non-hydrogen-bonded water molecules.[16-18] This model fits the properties of liquid water quite well, but is unable to fully describe the properties of supercooled water and ice. In order to overcome this discrepancy, Sceats and Rice have proposed a "random network" model of water which contains several different species of water molecules with differing hydrogen-bond angles.[19, 20]

An intermediate model has been developed by Stanley and Teixeira, which is termed the "percolation model".[21] In this model, each water molecule is assigned to one of five species based on the number of hydrogen bonds (from zero to four) that it forms.[21, 22] The spatial positions of these species are not random but are correlated, such that the four-bonded molecules form discrete regions or "patches" within the hydrogen-bonded network.[21] The patches of four-bonded water molecules occur with greater frequency due to increased hydrogen bonding until these patches "percolate", or form an infinite cluster at the glass transition temperature.[23] These patches of tetra-bonded water have a structure similar to that of ice, although they are technically in the liquid state.[21] This model describes the hydrogen-bonded network of water as being gel-like over short time scales.[21, 22]

A detailed examination of the Raman spectrum of liquid water was performed by Carey and Korenowski using a high-pressure Raman cell.[24] They observed all of the Raman peaks of water as a function of temperature between 22 and 400 ºC (Table 5.1).[24] The peak at 162 cm^{-1} is due to O-O stretching along the O-H - - O (hydrogen bond) direction, and its frequency decreases with increasing temperature.[24] This is likely due to a weakening of hydrogen bonds as the temperature is increased. All three liberational peaks decrease in frequency with increasing temperature, since the liberational force constants decrease as hydrogen bonding is decreased.[24] The three liberations are the same as the three rotations that a water molecule would have in the gas phase.[24]

Table 5.1: Water molecular translational, liberational, OH bending, and OH stretching Raman peaks as a function of temperature at constant pressure of 256 barr (adapted from Carey and Korenowski)[24]

Raman Peak	**Temperature (ºC)**								
(cm^{-1})	**22**	**30**	**50**	**70**	**90**	**100**	**200**	**300**	**400**
Translational	65	66	67	68	69	69	69	67	63
	162	157	149	142	138	134	123	113	105
Liberational	430	425	370	334	302	271	243	243	240
	650	665	613	577	547	500	465	478	481
	795	802	767	751	719	701	690	693	701
OH Bending	1581	1581	1591	1585	1575	1575	1597	1584	1588
	1641	1642	1641	1640	1641	1640	1634	1636	1639
OH	3051	3028	3054	3050	3050	3048	3053	--	--
Stretching	3233	3242	3254	3265	3282	3291	3312	3322	3314
	3393	3386	3393	3390	3389	3385	3391	3439	3486
	3511	3484	3499	3490	3489	3478	3454	3485	3522
	3628	3626	3624	3619	3615	3600	3539	3561	3586
	--	--	--	--	--	--	3654	3658	3658

There are two OH bending modes which arise from different levels of hydrogen bonding, and both these modes remained relatively constant at all temperatures studied.[24] Several OH stretching modes are observed, which are believed to arise from varying amounts of hydrogen bonding.[24] The intensities change as the temperature is increased and the tetrahedral hydrogen bonded network of water is destroyed, although the frequencies were observed to be essentially temperature independent.[24] The researchers also used this data to determine the hydrogen bond strength in liquid water, and calculated the energy of hydrogen bond in water to be 2.53 kcal/mol.[24]

Green et al. observed a low frequency shoulder in the O-H stretching Raman spectrum that can be used as a probe of the in-phase collective motions of water.[25] As the temperature of water is decreased to -46 ºC, the relative intensity of the shoulder increased until it approached that of ice.[25] This suggests that clusters of water molecules with similar hydrogen-bonding energies form as the water is supercooled towards the glass transition temperature.[25]

5.1.4: Structure of Supercooled water:

D'Arrigo et al. have examined the Raman scattering in the O-H stretching band of normal and supercooled water across a temperature range of -24 to 90 ºC between 2600-4000 cm^{-1}.[22] At temperatures greater than 20 ºC, two temperature-independent contributions were observed.[22] An additional contribution arose at temperatures below 20 ºC, which was attributed to an enhanced Raman signal corresponding to the O-H stretching band.[22] This was proposed to be due to a heterophase fluctuation, where small clusters of ice were constantly forming and being destroyed.[22] This contribution appears at low temperatures and becomes relevant upon supercooling. The overall intensity of the O-H band around 3150 cm^{-1} remained relatively constant at temperatures between 20 and 90 ºC and then increased as the temperature was lowered down to -24 ºC (see Figure 5.2).[22] The authors suggest the existence of "open" (tetrahedral) and "closed" water molecules[22] that are similar to the hydrogen-bonded and non-hydrogen-bonded water molecules proposed by Walrafen et al.[14, 15] The

authors also confirmed the existence of the isosbestic point at temperatures above 20 ºC, as described above by Walrafen and coworkers.[14, 15, 22]

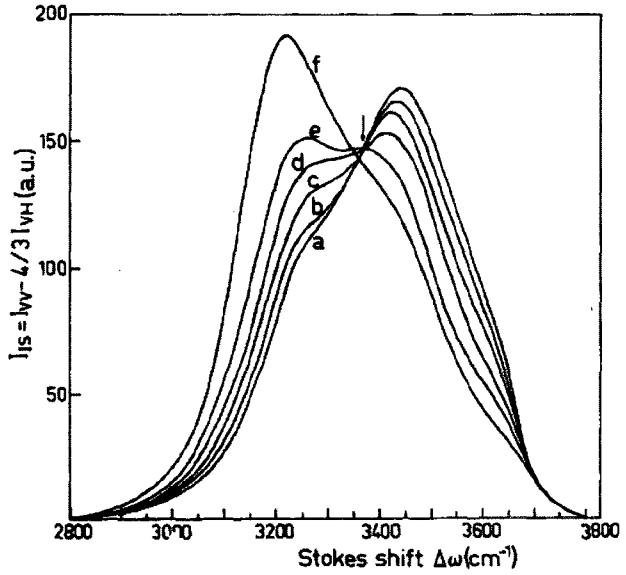

Figure 5.2: Raman spectra of the OH stretching region of water at several temperatures (taken from D'Arrigo et al., 1981).[22] Legend: a: T=95 ºC, b: T=80 ºC, c: T=60 ºC, d: T=40 ºC, e: T=20 ºC, f: T= -24 ºC. The arrow indicates the isosbestic point.[22]

Supercooled water at temperatures down to -20 ºC has been studied using Raman spectroscopy in the hindered translational region of 20 - 400 cm^{-1}.[26] The authors observed an increase in intensity of the hindered translational band at 190 cm^{-1} upon supercooling, which suggests an increase in the number of four-coordinated water molecules.[26] This would result in restricted translational movement. The peak positions were found to be temperature dependent, with an increase in frequency as the temperature was decreased.[26] This suggests that the hydrogen-bonded oxygen-oxygen distance was decreasing with decreasing temperature.[26] Furthermore, a non-linear dependence of the bandwidth on temperature suggests there is a limiting local water structure at lower temperatures.[26] The width of the peak at 190 cm^{-1} decreases with decreasing temperature, suggesting that structural disorder in liquid water is responsible for the width of this peak.[26]

Aliotta et al. examined the depolarized quasi-electric and inelastic light scattering in normal and supercooled bulk water down to -27 ºC using depolarized Rayleigh and low frequency Raman scattering data.[27] The quasi-elastic component showed fine structure, and both "fast" and "slow" contributions were observed.[27] These contributions are due to the decrease in local order due to center of gravity correlations, resulting from strong intermolecular hydrogen bonds.[27] The presence of the fast contribution is due to the dynamics of the hydrogen bonds.[27] The slow contribution is observed at temperatures below 10 ºC, due to the formation of more extended polyhedron structures.[27] These results suggest that liquid water, particularly that in the supercooled phase, is made up of locally ordered correlated patches based on hydrogen bonding.[27]

Hare and Sorenson used Raman spectroscopy to study bulk water that was supercooled down to -33 ºC.[23] They observed that the depolarization ratio and peak intensities were temperature dependent, which are believed to fit a two-state model in which both states have frequency dependent depolarization ratios.[23] Their results suggest that the water spectrum approaches that of an amorphous solid as the temperature is cooled towards the glass transition temperature.[23] This similarity is believed to be due to the increase in the percolation of four-bonded water molecules as the temperature is cooled, supporting the percolation model proposed by Stanley and Teixeira.[21, 23]

5.1.5: Structure of Ice:

Much of the current understanding of the structure of liquid and supercooled water has been aided by experiments to discover the structure of ice. There are two common forms of ice, known as hexagonal ice Ih and cubic ice Ic (Figure 5.3).[28] Hexagonal ice forms when liquid water freezes at atmospheric pressure. In this form of ice, the oxygen atoms make up a "wurtzite" lattice, which is a hexagonal form of the diamond lattice.[28] Ice Ic has the oxygen atoms arranged in a diamond lattice. Cubic ice cannot be formed by simply cooling hexagonal ice, but can be obtained when water vapours are condensed at temperatures below -80 ºC.[28] Both of these forms of ice are "disordered", meaning that each oxygen atom has two closer neighbouring hydrogen

atoms, and two other neighbouring hydrogen atoms that are farther away.[28] Several other forms of ice can be obtained at pressures other than atmospheric pressure.

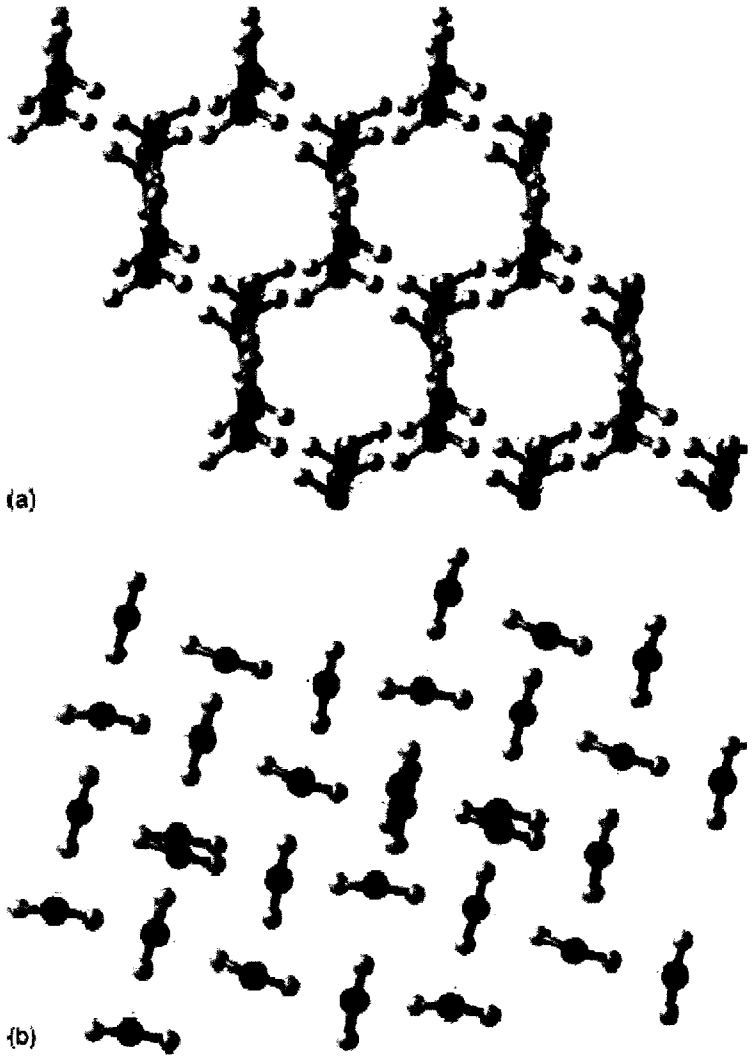

Figure 5.3: Structures of ice at 1 atm determined using *ab initio* techniques, taken from Oganov and Glass. [29] (a) = Ice Ih and (b) = Ice Ic

In 1977, Whalley examined the infrared and Raman spectra of ice Ih and Ic, and assigned the O-H stretching bands.[30] In this experiment, the spectra were so similar that they were indistinguishable at the accuracy level used.[30] Sivakumar et al. have

observed that the Raman and infrared spectra of polycrystalline ice I and low density amorphous solid water are also very similar.[31]

Recently, Saito and Ohmine used two-dimensional (2D)-Raman spectroscopy to examine the structures of liquid water, ice Ih, and amorphous ice.[32] This technique was observed to be sensitive to the nonlinear anharmonic dynamics and local hydrogen bonded structure of water, and was also very sensitive to the anisotropy of the hydrogen bonded network structure of ice Ih.[32] Hydrogen bond stretching bands are observed with the polarization direction parallel to the *c* axis, and the liberational motions are observed with the polarization directions parallel to the *a* axis.[32] Hydrogen bonding stretching motions were decreased in amorphous ice as compared to crystalline ice Ih, resulting in a significant difference in their Raman spectra.[32]

When comparing liquid water to ice Ih, a strong peak arising from hydrogen bonding stretching is observed in ice Ih, whereas the intensities of the hydrogen bonding bending and liberational peaks were very weak.[32] The lower frequency bands are also very weak because the hydrogen bonded network is nearly frozen and does not rearrange.[32]

X-ray Raman based Extended X-ray Absorption Fine Structure (EXAFS) was recently used to examine the nearest-neighbour oxygen distances in water and ice.[33] Measuring the distance between neighbouring water molecules was believed to be a good method of observing the local structural differences between liquid water and ice.[33] Changes were observed in the amplitudes, frequencies, and phases of the spectra which were attributed to small differences in local ordering due to neighbouring oxygen atoms.[33] A larger difference in the O-O distribution in liquid water compared to ice was observed by a reduction in the amplitude for water.[33] The nearest neighbour oxygen distances in water were found to be more asymmetric than in ice, with a longer distance between the oxygen atoms but a shorter peak position.[33]

Li and coworkers examined the structure of ice Ic using inelastic neutron-scattering spectroscopy.[34, 35] Two molecular optic bands were observed, suggesting that there exists two different strengths of hydrogen bonds.[34, 35] These different hydrogen

bonds are distributed at random through the ice lattice.[34] They proposed a network of strong and weak hydrogen bonds (Figure 5.4) which is similar to the percolation model, although in the percolation model the hydrogen bonds are either present or absent.[34] The strong and weak bonds will have different bond energies, which will affect the heat capacity of liquid water.[34]

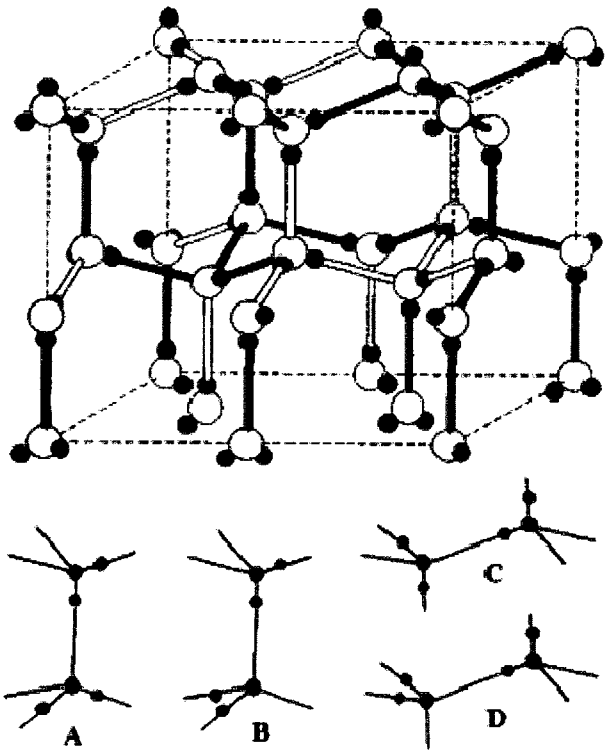

Figure 5.4: A section of the ice Ih lattice (taken from Li and Ross, 1993).[34] Solid lines represent a strong bond and the pair of thin lines represents a weak bond. Four possible orientations of molecule pairs are shown. In the ice Ih lattice, A and B are oriented along the c-axis and C and D are in the basal plane. Ice Ic contains only C and D types of molecule pairs.[34]

5.1.6: Ice-Water Interface:

The solid-liquid interface layer of ice crystals has been studied using Raman and Rayleigh scattering.[36] This is possible because the intensity of the Rayleigh scattering of the interface layer is nearly 500 times larger than the scattering resulting from bulk water.[36] The Raman spectra suggests that the interface layer of a growing ice crystal is

water-like.[36] None of the characteristic Raman peaks corresponding to ice were observed. The distance between two hydrogen-bonded water molecules is believed to be the same as in bulk water.[36] Slight differences from the spectra of bulk water are suggested to be due to an increase in the number of strong hydrogen bonds relative to weak hydrogen bonds.[36] In other words, when put into the perspective of the D'Arrigo two component model,[22] the amount of "open" or tetra-bonded water is increased in the interface layer relative to the "closed" water.[36] Other observations were that the water molecules in the interface have a slightly higher average number of hydrogen bonds than in bulk water.[36]

Using molecular dynamics simulations, the ice/water interface at 240 K was simulated by Karim and Haymet.[37] Discrete, definite regions of bulk water, bulk solid, and the interface were observed in the simulation.[37] The interface was stable for at least 100 picoseconds (ps), and its width was that of three to four layers of water molecules, which corresponded to 10-15 Å.[37] Patches of solid-like and liquid-like molecules were undergoing dynamical rearrangements within the interface.[37]

5.1.6.1: Studies on the Quasi-Liquid Layer:

The existence of a liquid-like layer on the surface of ice crystals was first proposed by Michael Faraday in the 19th century.[38] He observed that two growing ice crystals will adhere and freeze together when placed in close contact, and that this phenomenon was more rapid when there was a water film between two ice surfaces.[38] Early experiments on this liquid-like layer have been extensively reviewed by Jellinek.[39] Much of our understanding of this so-called "quasi-liquid layer" (QLL) has come in the past three decades.

Beaglehole and Nason measured the ellipticity coefficient for light reflected from the basal and prism faces of ice crystals.[40] Through this experiment, they observed a "water-like layer" at temperatures below the bulk freezing point.[40] The thickness of this layer was dependent on the orientation of the crystal and the temperature.[40] Furukawa and coworkers have used experimental techniques and computer simulations to study

the properties of the quasi-liquid layer at the surface of ice crystals.[41, 42] They observed that the properties of the QLL are similar to bulk water, and they also observed that the thickness of the layer was dependent on surface temperature and the crystal orientation.[41] They further observed differences in the thickness on the two faces of the ice crystal.[41] These experiments were confirmed by computer simulations.[42] Examination of the simulation interfaces showed that the water molecules in the QLL are more disordered than the crystalline arrangement that is observed deeper into the ice phase.[42] Surface melting was observed to occur on both faces of the growing ice crystal and the thickness of the QLL differed on the different ice crystal faces.[42]

Computer simulations were also performed by Karim and Haymet in an effort to model the QLL.[37] They observed that the QLL is quite broad, approximately 15 Å thick in this simulation.[37] Hydrogen bonding and well-oriented water molecules led to greater order in the ice crystal than in the QLL.[37] Additionally, the diffusion constant of water is larger in the interface layer than in bulk water.[37]

There is considerable disagreement regarding the actual thickness of the QLL. Different experiments yield very different measurements.[43] For example, the calculated or estimated thickness differs based on temperature, which crystal face is being examined, and which measurement method is being used.[43] Furthermore, examining the QLL against water vapour or air gives a different result than when a polycrystalline ice sample is used.[43] Impurities in the ice crystal that are expelled into the QLL during melting are also believed to affect the thickness.[43]

To address these issues, Sadtchenko and Ewing grew a polycrystalline ice film on the face of a germanium prism and measured the sample using attenuated total reflection spectroscopy.[43] The authors note that there are actually two QLL's that should be taken into account.[43] The first is between the ice and the substrate, termed QLL_{is}, and the second is between ice and vapour, called the QLL_{iv}.[43] The QLL spectra could be deconvoluted out of the ice spectra, allowing for several observations to be made. First, the QLL is negligible at -28 ºC, however, it is quite thick at the ice triple (melting) point.[43] The QLL spectrum could not be distinguished from that of bulk water over the entire extinction range, confirming that the QLL is very much like bulk water.[43] The

average thickness observed in this experiment was 2 nm, which corresponds to seven layers of water molecules.[43] The spectrum of the QLL changed as the temperature was lowered.[43] Between 0 and -1 ºC, the properties of the QLL were very similar to liquid water.[43] However, at temperatures below -1 ºC, the spectrum showed more difference from that of bulk water.[43] The QLL disappeared almost entirely below -10 ºC, where only one layer of water molecules was detected.[43]

Raman spectroscopy was also used to study the water and ice interfaces.[44] In this method, the extent of hydrogen bonding in the QLL was monitored by examining the shape of the O-H stretching band.[44] Analyzing the spectra revealed that the surface of liquid water has the lowest amount of hydrogen bonding, followed by the ice surface, then the bulk water, and bulk ice has the most.[44] The addition of sodium halide salts was found to disrupt the hydrogen bond network of bulk water, but they have an even greater effect on the ice surface.[44] Sodium chloride is known to be excluded during freezing, resulting in a concentrated salt solution and pure ice at the ice surface and in the QLL.[44] The change in the QLL spectrum upon the addition of salts was attributed to either the disruption of hydrogen bonding within the QLL or the formation of a liquid salt solution at the ice surface.[44] Similar results were seen when HCl and HNO_3 were added to the solution.[44] The change in the spectra may be a result in increased hydrogen bonding to the dissociated hydronium ions at the surface.[44] Different amounts of hydrogen bonding were observed at the air-ice interface than at the air-water interface, in both the presence and absence of solutes (NaCl or HCl).[44] These results suggest that the QLL cannot always be treated as being identical to bulk water.[44] The effect of impurities on the QLL was also examined by Rempel et al.[45] They propose that the presence of a liquid-like interface along the boundaries of adjacent ice crystals provides a path for diffusion, since solid-state diffusion through single ice grains is very slow.[45]

Based upon the results to date, a thermodynamic model of quasi-liquid formation was proposed by Henson et al.[46] In this model, the introduction of a liquid at the interface minimizes the surface free energy.[46] This is not due to a modification of the free energies of the liquid or solid phases, but due to the addition of a surface configurational entropy term by the interaction of the liquid with the ice lattice.[46] The

enthalpy and entropy of sublimation and vaporization do not change, so the QLL remains thermodynamically equivalent to the bulk water.[46]

5.1.7: Raman Studies of Biological Antifreezes:

Raman spectroscopy has also been used to study antifreeze glycoproteins in liquid and frozen solutions.[47] The spectra were obtained from 2600-3800 cm^{-1} because aside from a C-H stretching band at 2950 cm^{-1}, the glycoprotein bands occur at frequencies below 2000 cm^{-1}.[47] The Raman spectra of pure water, and of 1% solutions of AFGP4 and AFGP8 at -0.3 ºC were almost identical (Figure 5.5).[47] The only difference was the presence of a small band at 2948 cm^{-1} in the antifreeze solutions, arising from symmetric C-H stretching.[47] Similarly, the Raman spectra of pure ice and ice crystals frozen from 1% solutions of AFGP4 and AFGP8 were nearly identical (Figure 5.6).[47]

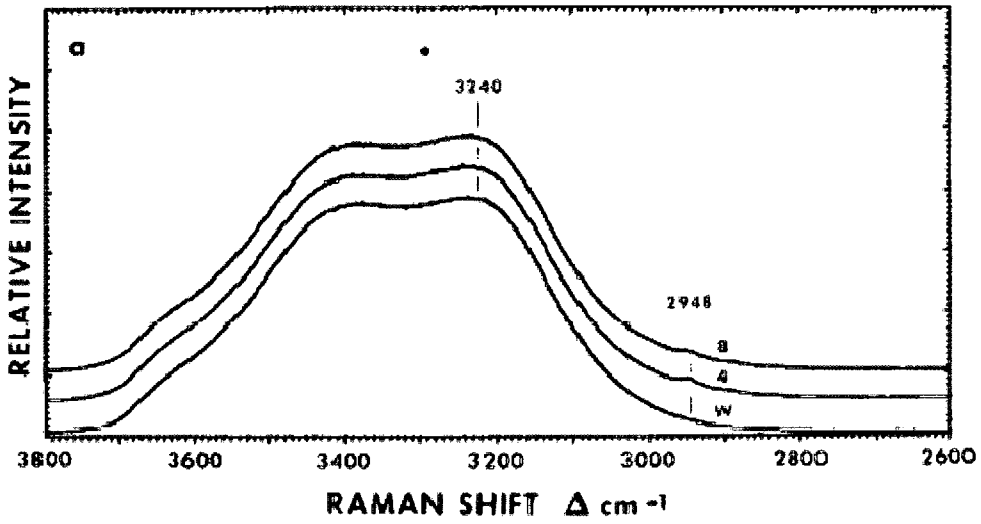

Figure 5.5:[47] Raman spectra at -0.3 ºC for water (Curve W) and 1% solutions of AFGP4 (Curve 4) and AFGP8 (Curve 8) (taken from Tomimatsu et al.)[47]

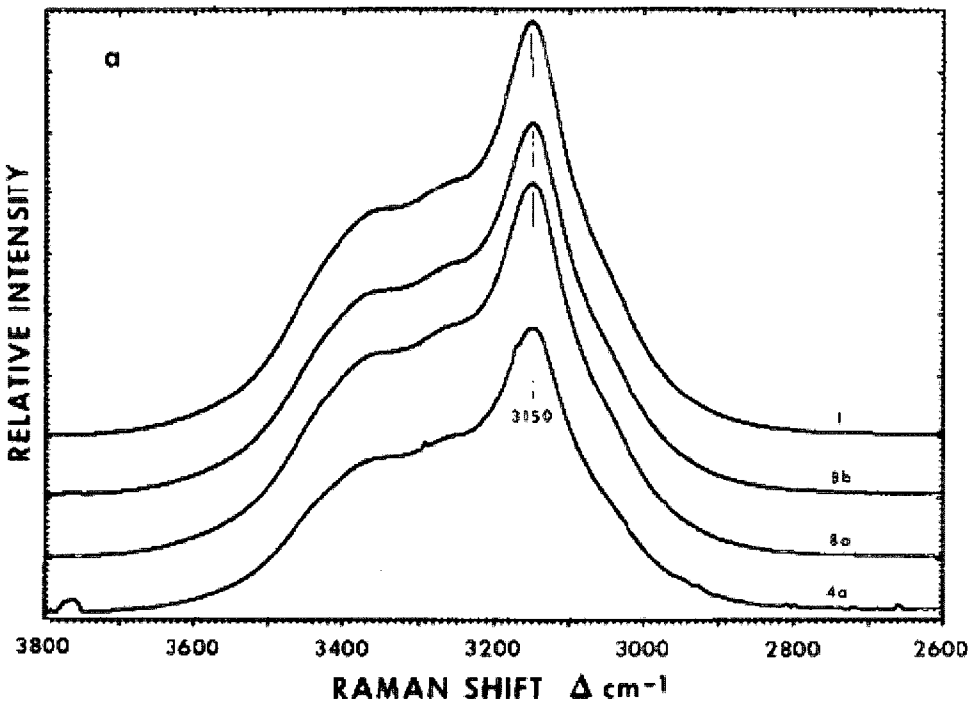

Figure 5.6:[47] Raman spectra at -5.0 ºC of ice from pure water (Curve 1) and from 1% solutions of AFGP4 (Curve 4a) and AFGP8 (Curves 8a and 8b) (taken from Tomimatsu et al.)[47]

The fact that the Raman spectra in the OH stretching region of pure ice was identical to the antifreeze solutions suggests that the AFGPs do not affect the properties of bulk ice.[47] This is consistent with the observation that AFGPs do not alter the melting point of ice.[47] The authors also propose that the structuring of water around the antifreezes is unlikely as this would be visualized in differences in the spectra of pure ice and frozen antifreeze solutions.[47]

The Raman spectra of frozen 5% solutions of AFGP4 and AFGP8 were also examined by subtracting the spectral features arising from water and fluorescence background.[47] Bands attributed to α-helical, β-polypeptide, and random coil conformations were observed.[47] Differences were observed between the spectra of AFGP4 and AFGP8 in a band around 1400 cm^{-1} which is characteristic of COH bending of the carbohydrate hydroxyl groups.[47] These differences may be due to differences in

the hydrogen bonding of the hydroxyl groups within the two antifreezes.[47] The vibrational modes, which are sensitive to structure and conformation, also differed between the two antifreezes.[47] These conformational changes may have affected the affinity of the hydroxyl groups for ice.[47]

The authors also observed a difference in the affinity of the antifreezes for ice while preparing the ice crystals from each solution.[47] AFGP4 was not excluded from the growing ice crystals at all, and was therefore evenly distributed throughout the ice.[47] In contrast, under certain conditions AFGP8 was completely excluded from the ice phase, suggesting that there was a difference in the affinity of the two antifreezes for the ice-water interface.[47] Since AFGP4 is known to have stronger antifreeze activity than the smaller AFGP8, this interfacial affinity may be important in the mechanism of action of antifreeze glycoproteins.[47]

The interaction of antifreeze glycoproteins with the ice-water interface was further studied by Uda et al. using attenuated total reflection (ATR)-FTIR spectroscopy.[48] The backbone conformation of a mixture of AFGP4-6 adsorbed at the ice-water interface was examined.[48] Similar to the observations of Sadtchenko and Ewing, the spectrum of the QLL and that of pure water were almost identical, indicating that the QLL contains mainly liquid with a negligible solid component.[43, 48] The QLL thickness was very low at -14 ºC, and it increased in thickness as the temperature was increased.[48] Interestingly, the absolute thickness of the QLL for the AFGP/D_2O sample studied here was three times larger than for a pure D_2O film.[48] This result suggested that there was an increase in the amount of AFGP molecules that are solvated into the QLL relative to the adsorbed molecules.[48] An alternate explanation is that the AFGP molecules that are not strongly bound to the ice surface can be released into the QLL as it increases in thickness.[48] If this is the case, the proteins interact with the QLL more strongly than with the ice lattice, and the dominant interfacial interaction is the QLL solvating the AFGP surface.[48]

The α-helical content of the AFGP increased upon freezing, but not upon supercooling of the solution.[48] This confirms that the structural changes are due to an AFGP-ice interaction. Furthermore, the amount of AFGP with an α-helical conformation

decreased as the QLL increased in thickness, which is likely due to the adsorbed AFGP molecules dissolving into the QLL.[48] The AFGP molecules are not incorporated into the growing ice lattice, so they must remain in the QLL and the increase in the α-helical signal is likely due to AFGP molecules interacting with the ice crystals (those that are adsorbed at the interface).[48] This change in conformation confirms that the AFGP molecules are highly flexible and undergo a conformational change to allow protein-ice interactions.[48] In an α-helical conformation, the protein develops many absorption sites and this maximizes the interaction with ice crystals.[48] These observations suggest that the structure and function of the AFGPs are correlated to the amount of QLL available at the ice surface.[48]

5.2: CARS Observations of Water and Antifreeze Solutions at Room Temperature and Sub-Zero Temperatures:

Water is vitally important to biological systems. By mass, it comprises approximately 80% of most living cells.[49] It has been shown that water is not an inert solvent, but is actively involved in biological mechanisms.[50] Water has been called the "lubricant of life", because its existence surrounding biological molecules is crucial for biological processes.[51] Water plays a role in acid-base reactions and in enzyme catalysis.[50] Hydrogen bonding is extremely important in creating some order within liquid water, and hydrogen bonds also form between water and polar hydrophilic solutes.[50] The concept of hydrophobic hydration has also been proposed when water is in the presence of non-polar hydrophobic solutes.[50] There is considerable evidence that the motions and structure of water surrounding biological systems ("bound water") is different from that of bulk water.[49-51]

The diffusion of water through permeable membranes within biological systems is extremely important.[52] Maintenance of an osmotic balance within cells by transport of water is a requirement for cell survival. In addition, water regulation is of fundamental importance during cryopreservation, where cells will die if they are not able to restore an osmotic balance. As mentioned earlier in this dissertation, the formation of extracellular

ice causes problems during freezing protocols if the cells are not able to lose water at a fast enough rate to prevent intracellular freezing.[53, 54]

Despite the vast number of Raman studies on water, supercooled water, ice, and/or biological antifreezes, to the best of our knowledge CARS spectroscopy has not been used to monitor these samples. The advantage of using CARS to examine these samples is that we can easily modify the experimental setup to incorporate live cells and tissues. This may aid our understanding of the nature of the ice-water interface in the presence of live cells. Furthermore, the effect of biological antifreezes on the ice-water interface can be explored by monitoring the OH-stretching region of the CARS spectrum. Using live cells, we can observe the role of biological antifreezes on water and ice surrounding biological samples. Our goals are to determine whether the CARS spectra of liquid and frozen solutions of water and antifreezes are similar to the Raman spectra previously observed for these species. For example, we will evaluate whether the CARS signal becomes narrower and sharper for ice with respect to liquid water, due to the strengthening hydrogen bonds. Secondly, we hope to determine whether the OH stretching region in frozen antifreeze solutions is different from that of pure ice. By looking for differences between these samples, we can observe the effect of biological antifreezes on ice and the ice-water interface. Once we have established the CARS spectra for these solutions at various temperatures, we can extend the experimental setup to include live cells to determine the effect of these solutions on the cells. The use of a CARS microscope attached to a cryostage will allow us to realize these experimental goals.

5.2.1: Using CARS to Study the Differences between Water, Supercooled Water, and Ice

To initiate this project, we obtained the CARS spectra for water, supercooled water, and ice. The spectrum of supercooled water was taken after the cryostage had been cooled to -10 ºC. At this temperature, the water remains supercooled in the absence of an ice nucleation source. In our experimental setup, we had unexpected difficulties getting the sample to nucleate, since our cryostage was unable to go below -

10 ºC. Eventually we discovered that when we used a sapphire cover slip and an external nucleation source, we were able to induce freezing. When a piece of dry ice was placed on the side of the stage away from the sample, the sample immediately froze, allowing us to obtain the spectrum of ice. These spectra can be seen in Figure 5.7.

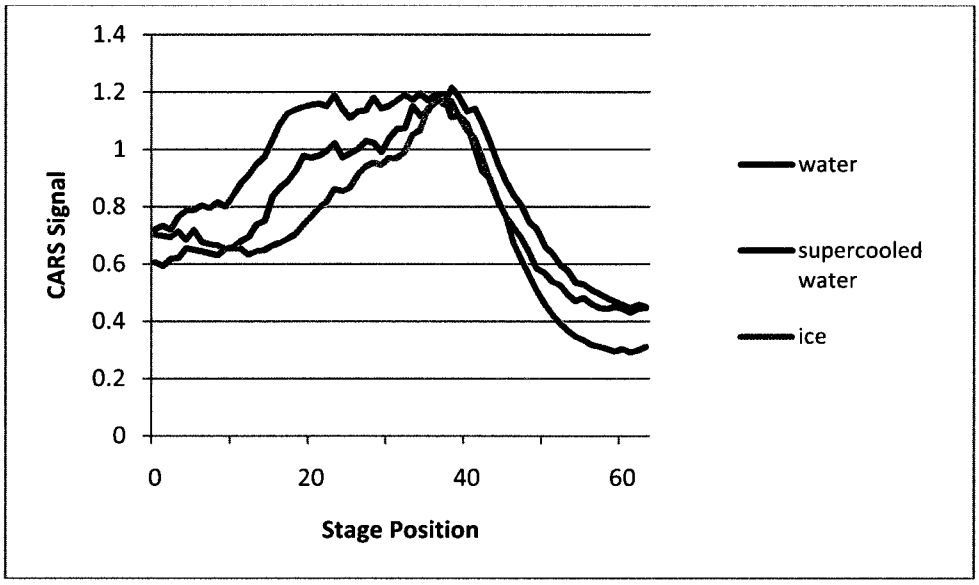

Figure 5.7: CARS spectra of the OH stretching region of water, supercooled water, and ice. The x-axis represents the stage position, which is an indirect measurement of the Raman excitation frequency. The blue curve represents distilled water at 20 ºC, the red curve represents supercooled water at -10 ºC, and the green curve is of ice at -10 ºC following ice nucleation.

The shape of the curves representing water and supercooled water are similar. The intensity of the water spectrum is slightly higher on the left side of the graph, which is opposite to the results obtained by D'Arrigo et al where the supercooled water displayed an increased intensity over water.[22] As expected, we saw a sharpening and narrowing of the spectra associated with ice as compared to both water and supercooled water, likely due to the stronger O-H bonds in ice.

5.2.2: Examination of the Effect of Biological Antifreezes on the Ice-Water Interface During Freezing.

With these results in hand, we sought to determine whether differences were seen when the CARS spectra of a 1 mM solution of AFGP8 in distilled water were obtained. These results can be seen in Figure 5.8. As observed for distilled water, the liquid and supercooled AFGP8 solutions give CARS spectra that are nearly identical, although the liquid AFGP8 solution was higher in intensity. Furthermore, the shape of both the liquid and supercooled AFGP8 spectra are nearly identical to the curves obtained for water and supercooled water, respectively. The curve corresponding to a frozen AFGP8 solution is sharper and narrower than the curve from the liquid samples, likely due to the formation of strong intramolecular hydrogen bonds within the frozen sample. This strong hydrogen bonding results in restricted motion of the water molecules within ice compared to liquid. Interestingly, the shape of the curve for the frozen AFGP8 solution is slightly different from that of ice, with a significant increase in the intensity of the CARS signal being observed on the left side of the spectrum for frozen AFGP8. This may be due to the interaction of AFGP8 with ice, although additional experiments would be necessary to confirm this result.

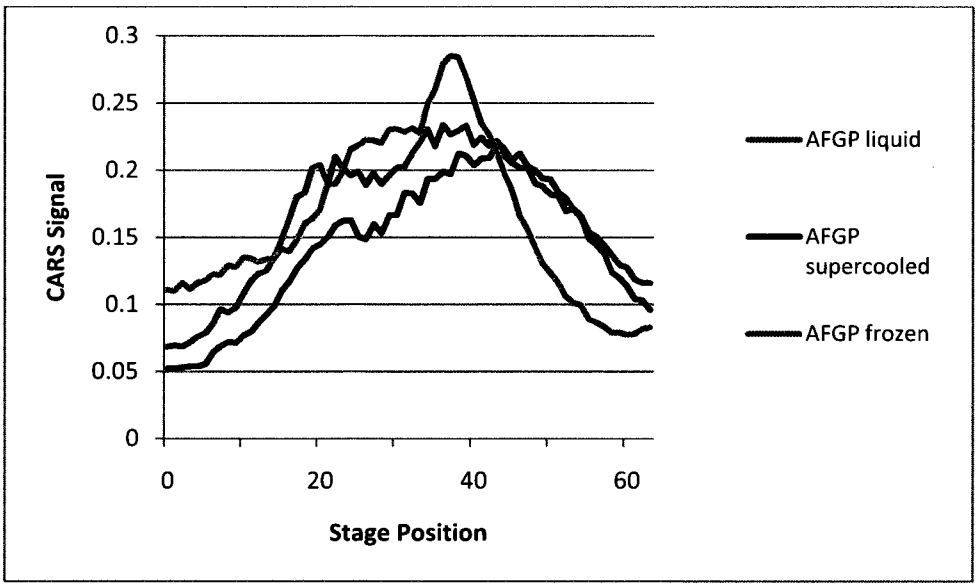

Figure 5.8: CARS spectra of a 1.0 mM AFGP8 solution at various temperatures. The blue curve represents a liquid AFGP solution at 20 ºC, the red curve represents a supercooled solution at -10 ºC, and the green curve is of a frozen solution at -10 ºC following ice nucleation.

A similar experiment was done with a 1.0 mM solution of AFP I in distilled water. The spectra for liquid, supercooled, and frozen AFP solutions are shown in Figure 5.9. Again, the shapes of the spectra for liquid and supercooled AFP solutions were nearly identical in shape. In this case, we observed an increase in intensity of the CARS signal for the supercooled AFP solution relative to the liquid AFP solution. This is similar to the results obtained by D'Arrigo et al. when examining liquid and supercooled solutions of water.[22] Again, the frozen AFP displays a sharper and narrower curve than either liquid or supercooled AFP. The increase in CARS signal intensity for the frozen solution was again observed on the left side of the graph, although it was not as pronounced as for the frozen AFGP8 solution.

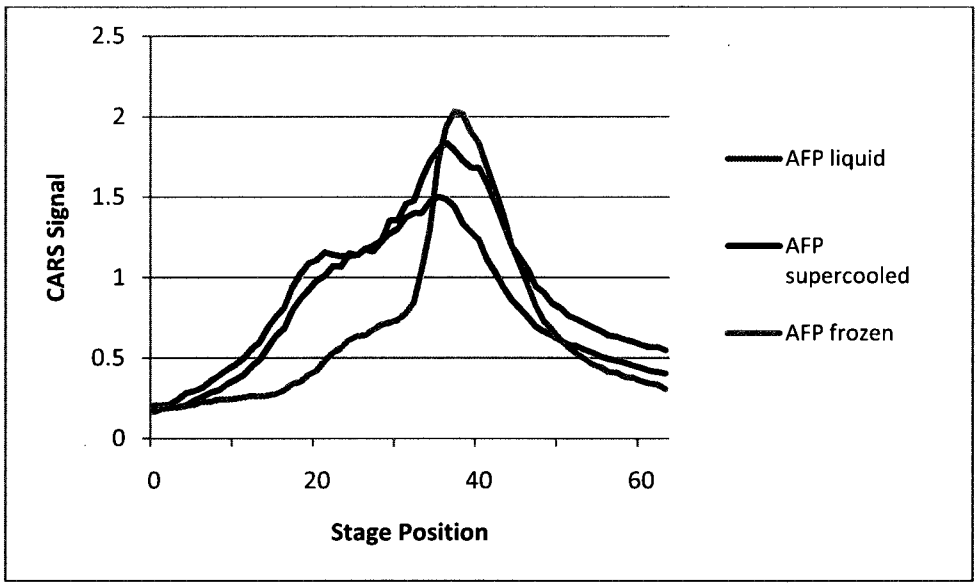

Figure 5.9: CARS spectra of a 1.0 mM AFP I solution at various temperatures. The blue curve represents a liquid AFP solution at 20 ºC, the red curve represents a supercooled AFP solution at -10 ºC, and the green curve is of a frozen solution at -10 ºC following ice nucleation.

At this point in our experiments, we turned our attention to studying the ice-water interface. Initially, we were unable to inhibit ice growth long enough to obtain any images or CARS data of the ice-water interface. This was the case even when a solution of AFGP8 was used. We realized that AFP I has a larger thermal hysteretic gap than AFGP8, and that we might be able to hold a solution of AFP I within this TH gap long enough to inhibit ice growth and observe the ice-water interface. Gratifyingly, when we used a solution of AFP I in distilled water, ice growth was inhibited by the antifreeze protein and several images of the ice-water interface were obtained. An example is shown in Figure 5.10. This image confirms the usefulness of biological antifreezes in stabilizing the ice-water interface and this technique can be used in the future for further interface studies.

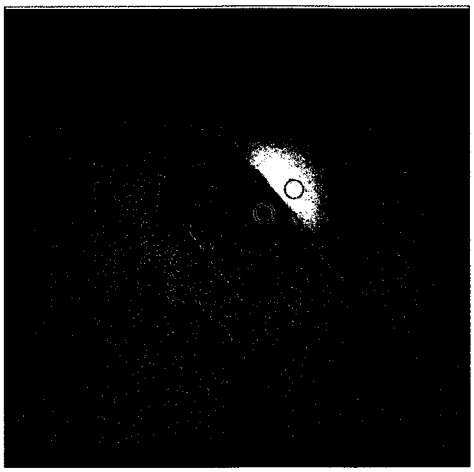

Figure 5.10: The ice-water interface. Ice is observed on the left side of the image and water is observed on the right. The blue and red circles correspond to areas used to obtain CARS spectra for the water and ice.

The CARS spectra of the two sides of the ice-water interface are shown in Figure 5.11. The results are similar to those seen in Figure 5.7, in which the spectrum of ice is much sharper and narrower than for water. However, this is an exciting result because the spectra could be obtained for both water and ice from a single image. This graph suggests that we will be able to monitor the ice-water interface in the presence of living cells, and we will be able to obtain CARS spectra from every area of the image.

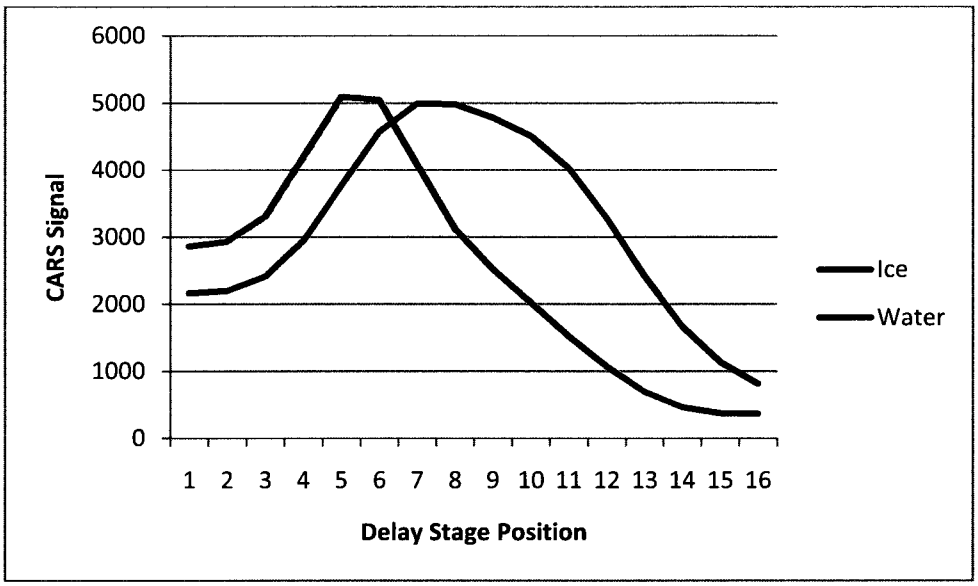

Figure 5.11: CARS spectra of ice and water taken from areas near the ice-water interface from a single CARS image.

Using the AFP I solution, we were able to obtain a series of images of the ice water interface across a wide range of frequencies. These images are shown in Figure 5.12. These images could not be obtained for a distilled water solution, because the ice-water interface did not remain long enough to be imaged before the entire sample froze.

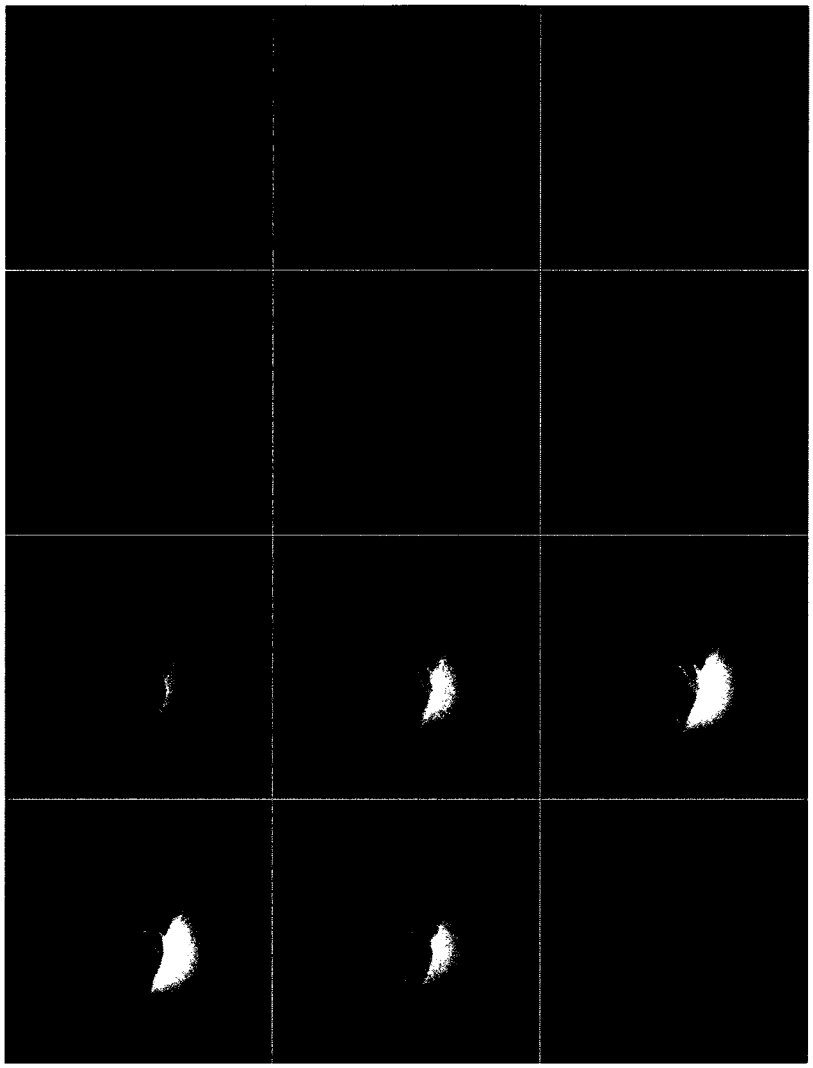

Figure 5.12: The ice-water interface of an AFP I solution taken across several frequencies. Ice is on the left hand side and water is on the right.

These initial results demonstrate that we can use CARS to observe differences between water, ice, and supercooled water. However, as expected the results obtained are very similar to those reported in the literature using Raman spectroscopy. The ability of biological antifreezes to stabilize the ice-water interface is an exciting result and will allow for further investigation of this interface. The benefits of CARS will likely be realized when live cell samples are used. Unfortunately, time constraints have not allowed us to extend these experiments to live cells at this time. Now that the experimental setup has been optimized, live cells can be used in future experiments,

where we hope to examine how modifications in the structure of AFPs and AFGPs affect the stabilization of the interface and whether they enhance membrane stabilization of living cells.

5.3: Summary:

CARS microscopy was examined as a method to examine the ice-water interface. It was observed that AFP I is able to inhibit ice growth long enough for the ice-water interface to be studied using spectroscopy and microscopy. These initial experiments took longer than expected as many challenges were encountered and many adjustments needed to be made to the experimental setup. Now that our experimental setup has been optimized, these experiments will be extended to biological systems where we will examine the ice-water interface in the presence of biological tissues as well as the effect of biological antifreezes on biological membranes. Initial studies with live cells have showed promise that we will be able to realize our experimental goals in the future.

5.4: References:

1. Kriss, T. C.; Kriss, V. M., History of the Operating Microscope: From Magnifying Glass to Microneurosurgery. *Neurosurgery* **1998,** 42, 899-907.

2. Muller, M.; Zumbusch, A., Coherent Anti-Stokes Raman Scattering Microscopy. *ChemPhysChem* **2007,** 8, 2156-2170.

3. Purves, W. K.; Sadava, D.; Orians, G. H.; Heller, H. C., *Life: The Science of Biology*. 6th ed.; W.H. Freeman and Company: Sunderland, Massachusetts, 2001.

4. Yang, C.; Sharp, K. A., Hydrophobic Tendency of Polar Group Hydration as a Major Force in Type I Antifreeze Protein Recognition. *PROTEINS: Struct., Funct., Bioinf.* **2005,** 59, 266-274.

5. Evans, C. L.; Potma, E. O.; Puoris'haag, M.; Cote, D.; Lin, C. P.; Xie, X. S., Chemical Imaging of Tissue In Vivo with Video-Rate Coherent Anti-Stokes Raman Scattering Microscopy. *Proc. Nat. Acad. Sci. USA* **2005,** 102, 16807-16812.

6. Kim, H. W.; Rossi, P.; Shoemaker, R. K.; DiMagno, S. G., Structure and Transport Properties of a Novel, Heavily-Fluorinated Carbohydrate Analogue. *J. Am. Chem. Soc.* **1998,** 120, 9082-9083.

7. Duncan, M. D.; Reintjes, J.; Manuccia, T. J., Scanning Coherent Anti-Stokes Raman Microscope. *Opt. Lett.* **1982,** 7, 350-352.

8. Begley, R. F.; Harvery, A. B.; Byer, R. L., Coherent Anti-Stokes Raman Spectroscopy. *Appl. Phys. Lett.* **1974,** 25, 387-390.

9. Zumbusch, A.; Holtom, G. R.; Xie, X. S., Three-Dimensional Vibrational Imaging by Coherent Anti-Stokes Raman Scattering. *Phys. Rev. Lett.* **1999,** 82, 4142-4145.

10. Pegoraro, A. F.; Ridsdale, A.; Moffatt, D. J.; Jia, Y.; Pezacki, J. P.; Stolow, A., Optimally Chirped Multimodal CARS Microscopy Based on a Single Ti:sapphire Oscillator. *Opt. Express* **2009,** 17, 2984-2996.

11. Potma, E. O.; de Boeij, W. P.; van Haastert, P. J. M.; Wiersma, D. A., Real-Time Visualization of Intracellular Hydrodynamics in Single Living Cells. *Proc. Nat. Acad. Sci. USA* **2001,** 98, 1577-1582.

12. Burkacky, O.; Zumbusch, A.; Brackmann, C.; Enejder, A., Dual-Pump Coherent Anti-Stokes-Raman Scattering Microscopy. *Opt. Lett.* **2006,** 31, 3656-3658.

13. Kaufman, L. J.; Weitz, D. A., Direct Imaging of Repulsive and Attractive Colloidal Glasses. *J. Chem. Phys.* **2006,** 125, 074716-1 - 074716-11.

14. Walrafen, G. E., Raman Spectral Studies of the Effects of Temperature on Water Structure. *J. Chem. Phys.* **1967,** 47, 114-126.

15. Walrafen, G. E.; Hokmabadi, M. S.; Yang, W.-H., Raman Isosbestic Points From Liquid Water. *J. Chem. Phys.* **1986,** 85, 6964-6969.

16. Hagler, A. T.; Scheraga, H. A.; Nemethy, G., Structure of Liquid Water. Statistical Thermodynamic Theory. *J. Phys. Chem.* **1972,** 76, 3229-3243.

17. Lentz, B. R.; Hagler, A. T.; Scheraga, H. A., Structure of Liquid Water. II. Improved Statistical Thermodynamic Treatment and Implications of a Cluster Model. *J. Phys. Chem.* **1974,** 78, 1531-1550.

18. Nemethy, G.; Scheraga, H. A., Structure of Water and Hydrophobic Bonding in Proteins. I. A Model for the Thermodynamic Properties of Liquid Water. *J. Chem. Phys.* **1962,** 36, 3382-3400.

19. Sceats, M. G.; Rice, S. A., The Water-Water Pair Potential Near the Hydrogen Bonded Equilibrium Configuration. *J. Chem. Phys.* **1980,** 72, 3236-3247.

20. Sceats, M. G.; Rice, S. A., The Entropy of Liquid Water From the Random Network Model. *J. Chem. Phys.* **1980,** 72, 3260-3262.

21. Stanley, H. E.; Teixeira, J., Interpretation of the Unusual Behavior of H_2O and D_2O at Low Temperatures: Tests of a Percolation Model. *J. Chem. Phys.* **1980,** 73, 3404-3422.

22. D'Arrigo, G.; Maisano, G.; Mallamace, F.; Migliardo, P.; Wanderlingh, F., Raman Scattering and Structure of Normal and Supercooled Water. *J. Chem. Phys.* **1981,** 75, 4264-4270.

23. Hare, D. E.; Sorenson, C. M., Raman Spectroscopic Study of Bulk Water Supercooled to - 33 °C. *J. Chem. Phys.* **1990,** 93, 25-33.

24. Carey, D. M.; Korenowski, G. M., Measurement of the Raman Spectrum of Liquid Water. *J. Chem. Phys.* **1998,** 108, 2669-2675.

25. Green, J. L.; Lacey, A. R.; Sceats, M. G., Spectroscopic Evidence for Spatial Correlations of Hydrogen Bonds in Liquid Water. *J. Phys. Chem.* **1986,** 90, 3958-3964.

26. Krisnamurthy, S.; Bansil, R.; Wiafe-Akenten, J., Low-Frequency Raman Spectrum of Supercooled Water. *J. Chem. Phys.* **1983,** 79, 5863-5870.

27. Aliotta, F.; Vasi, C.; Maisano, G.; Majolino, D.; Mallamace, F.; Migliardo, P., Role of the H Bond and Cooperative Effects in Normal and Supercooled Water Studied By Anisotropic Low Frequency Light Scattering. *J. Chem. Phys.* **1986,** 84, 4731-4738.

28. Lee, C.; Vanderbilt, D.; Laasonen, K., Ab Initio Studies on the Structural and Dynamical Properties of Ice. *Phys. Rev. B Cond. Matt.* **1993,** 47, 4863-4872.

29. Oganov, A. R.; Glass, C. W., Crystal Structure Prediction Using Ab Initio Evolutionary Techniques: Principles and Applications. *J. Chem. Phys.* **2006,** 124, 244704-1 - 244704-15.

30. Whalley, E., A Detailed Assignment of the O-H Stretching Bands of Ice I. *Can. J. Chem.* **1977,** 55, 3429-3441.

31. Sivakumar, T. C.; Schuh, D.; Sceats, M. G.; Rice, S. A., The 2500-4000 cm^{-1} Raman and Infrared Spectra of Low Density Amorphous Solid Water and of Polycrystalline Ice I. *Chem. Phys. Lett.* **1977,** 48, 212-218.

32. Saito, S.; Ohmine, I., Fifth-Order Two-Dimensional Raman Spectroscopy of Liquid Water, Crystalline Ice Ih and Amorphous Ices: Sensitivity to Anharmonic Dynamics and Local Hydrogen Bond Network Structure. *J. Chem. Phys.* **2006,** 125, (084506-1 - 084506-12).

33. Bergmann, U.; Di Cicco, A.; Wernet, P.; Principi, E.; Glatzel, P.; Nilsson, A., Nearest-Neighbour Oxygen Distances in Liquid Water and Ice Observed by X-Ray Raman Based Extended X-Ray Absorption Fine Structure. *J. Chem. Phys.* **2007,** 127, 174504-1 - 174504-5.

34. Li, J.; Ross, D. K., Evidence for Two Kinds of Hydrogen Bond in Ice. *Nature* **1993,** 365, 327-329.

35. Li, J. C.; Bennington, S. M.; Ross, D. K., Further Evidence for the Existence of Two Kinds of H-Bonds in Ice Ih. *Phys. Lett. A* **1994,** 192, 295-300.

36. Halter, P. U.; Bilgram, J. H.; Kanzig, W., Properties of the Solid-Liquid Interface Layer of Growing Ice Crystals: A Raman and Rayleigh Scattering Study. *J. Chem. Phys.* **1988,** 89, 2622-2629.

37. Karim, O. A.; Haymet, A. D. J., The Ice/Water Interface. *Chem. Phys. Lett.* **1987,** 138, 531-534.

38. Farady, M., Note on Regelation. *Proc. Roy. Soc. London* **1860,** 10, 440-450.

39. Jellinek, H. H. G., Liquid-Like (Transition) Layer on Ice. *J. Colloid. Interface Sci.* **1967,** 25, 192-205.

40. Beaglehole, D.; Nason, D., Transition Layer on the Surface of Ice. *Surf. Sci.* **1980,** 96, 357-363.

41. Furukawa, Y.; Yamamoto, M.; Kuroda, T., Ellipsometric Study of the Quasi-Liquid Layer at the Surface of Ice Crystal. Terra Scientific Publishing Company: Tokyo, 1989; pp 647-650.

42. Inada, T.; Modak, P. R., Growth Control of Ice Crystals By Poly(Vinyl Alcohol) and Antifreeze Protein in Ice Slurries. *Chem. Eng. Sci.* **2006,** 61, 3149-3158.

43. Sadtchenko, V.; Ewing, G. E., Interfacial Melting of Thin Ice Films: An Infrared Study. *J. Chem. Phys.* **2002,** 116, 4686-4697.

44. Kahan, T. F.; Reid, J. P.; Donaldson, D. J., Spectroscopic Probes of the Quasi-Liquid Layer on Ice. *J. Phys. Chem. A* **2007,** 111, 11006-11012.

45. Rempel, A. W.; Waddington, E. D.; Wettlaufer, J. S.; Worster, M. G., Possible Displacement of the Climate Signal in Ancient Ice by Premelting and Anomalous Diffusion. *Nature* **2001,** 411, 568-571.

46. Henson, B. F.; Voss, L. F.; Wilson, K. R.; Robinson, J. M., Thermodynamic Model of Quasiliquid Formation on H_2O Ice: Comparison with Experiment. *J. Chem. Phys.* **2005,** 123, 144707-1 - 144707-7.

47. Tomimatsu, Y.; Scherer, J. R.; Yeh, Y.; Feeney, R. E., Raman Spectra of a Solid Antifreeze Glycoprotein and Its Liquid and Frozen Aqueous Solutions. *J. Biol. Chem.* **1976,** 251, 2290-2298.

48. Jung, J. H.; Rim, J. A.; Cho, E. J.; Lee, S. J.; Jeong, I. Y.; Kameda, N.; Masuda, M.; Shimizu, T., Stabilization of an Asymmetric Bolaamphiphilic Sugar-Based Crown Ether Hydrogel by Hydrogen Bonding Interaction and its Sol-Gel Transcription. *Tetrahedron* **2007,** 63, 7449-7456.

49. Cooke, R.; Kuntz, I. D., The Properties of Water in Biological Systems. *Ann. Rev. Biophys. Bioeng.* **1974,** 3, 95-126.

50. Tait, M. J.; Franks, F., Water in Biological Systems. *Nature* **1971,** 230, 91-94.

51. Nandi, N.; Bhattacharyya, K.; Bagchi, B., Dielectric Relaxation and Solvation Dynamics of Water in Complex Chemical and Biological Systems. *Chem. Rev.* **2000,** 100, 2013-2045.

52. Latour, L. L.; Svoboda, K.; Mitra, P. P.; Sotak, C. H., Time-Dependent Diffusion of Water in a Biological Model System. *Proc. Nat. Acad. Sci. USA* **1994,** 91, 1229-1233.

53. Mazur, P., Principles of Cryobiology. In *Life in the Frozen State*, 1 ed.; Fuller, B.; Lane, N.; Benson, E. E., Eds. CRC Press: 2004; pp 3-66.

54. Karlsson, J. O. M.; Toner, M., Long-Term Storage of Tissues by Cryopreservation: Critical Issues. *Biomaterials* **1996,** 17, 243-256.

Chapter 6: General Conclusions and Future Directions

6.1: Summary and General Conclusions

This dissertation has described the role of carbohydrates in biological systems and has reviewed the literature regarding the hydration of carbohydrates. In addition, our current understanding of biological antifreezes (antifreeze proteins and antifreeze glycoproteins) has arisen from several experiments, and these experiments have been discussed. Thermal hysteresis (TH) and ice-recrystallization inhibition (IRI) activity have been defined and described. The cryopreservation of cells and the role of ice-recrystallization in causing cell damage were reviewed.

The broad goals of this thesis were to develop a greater understanding of the mechanism of ice-recrystallization and the factors affecting recrystallization inhibitors through synthesis of novel carbohydrate derivatives and examination of the ice-water interface. Furthermore, the relationship between hydration of carbohydrates and their ability to inhibit ice-recrystallization, as well as the relationship between IRI activity and cryopreservation, needed to be explored.

Specifically, the goals of the dissertation were as follows:

1) Evaluate carbohydrates for antifreeze activity and determine whether IRI activity is linked to the hydration of the carbohydrates.
2) Observe through *in vitro* cell-based assays whether IRI activity can be correlated to cytotoxicity and/or cryopreservation ability of carbohydrates.
3) Determine whether *C*-linked monosaccharides display IRI activity and whether the anomeric stereochemistry affects IRI activity levels.
4) Test carbohydrates containing amine and acetamide moieties for IRI activity
5) Synthesize several monosaccharides containing drastic structural modifications (methoxy groups, alkyl groups, and *geminal*-difluoromethylene groups) and assess their IRI activity.

6) Examine the nature of the ice-water interface using CARS.

Through the successful fulfillment of these goals, several observations and conclusions were made. Mono- and disaccharides were observed to display moderate IRI activity in the absence of a peptide component, and the IRI activity was related to the hydration of the carbohydrates. Partial molar compressibilities, hydration numbers, and hydration indices of carbohydrates were compared to their IRI activity, and the hydration index (hydration number divided by partial molar volume) was found to be the best predictor of IRI activity.

A series of *in vitro* cell-based experiments with human embryonic liver cells allowed us to examine the ability of carbohydrates to prevent cell death at physiological and sub-zero temperatures. High concentrations (200 and 500 mM) of carbohydrates were observed to cause more cell death at 37 ºC than lower concentrations, but higher concentrations were also more effective at preventing cell death at subzero temperatures. This suggests that a balance between cytotoxicity and cryotoxicity is required, such as is the case with the known cryoprotectant DMSO. A 220 mM solution of galactose was found to be as effective at preventing cell death following freeze-thaw as a 5% solution of DMSO. In addition, an exciting correlation between IRI activity and cryoprotection ability was observed, and this suggests that we can use a compound's hydration and IRI activity to design novel cryoprotectants for cells and tissues.

Some *C*- and *S*-linked compounds were found to be as effective at inhibiting ice-recrystallization as native *O*-linked monosaccharides, suggesting that the nature of the atom at C-1 is not important in conferring IRI activity. However, the anomeric stereochemistry seems to play a role with α-linked compounds generally showing increased activity over β-linked compounds, and this has been linked to the hydration of the compound.

Galactosamine and glucosamine showed greater IRI activity than *N*-acetyl-D-galactosamine and *N*-acetyl-D-glucosamine, respectively. It has been proposed that amine groups disrupt the three dimensional structure of water more than acetamide groups and therefore that galactosamine is more effectively hydrated than *N*-acetyl-D-

galactosamine. This provides support for our hypothesis that hydration of the carbohydrate is correlated to the ability of the carbohydrate to inhibit ice recrystallization.

Several compounds containing dramatic structural modifications to the core galactose structure were prepared and evaluated for IRI activity. α/β-methyl galactopyranoside was found to fit well into our observed correlation between the hydration index of a carbohydrate and its IRI activity, confirming that the hydration index is a better predictor of IRI activity than hydration numbers.

The effect of methoxy groups at C-2, C-3, C-4, and C-6 on IRI activity was observed. Methylated derivatives of *C*-allyl galactose were found to display poor IRI activity, regardless of the position of the methoxy group on the carbohydrate. A model for the interaction of carbohydrates with water and ice and the resulting effect on ice recrystallization was proposed. In this model, compounds that are well hydrated cause a large disruption of the water molecules in the bulk surrounding the carbohydrate's hydration shell. More energy is required to transfer these poorly-ordered disrupted water molecules to the QLL of a growing ice crystal, so the recrystallization of ice is inhibited.

This model was extended to hydrophobic compounds in the following way. Compounds with hydrophobic groups are poorly hydrated and they cause a lesser disruption of the bulk water molecules by causing them to be highly ordered in the region surrounding the hydration shell. This ordering results in a lower energy transfer of water molecules to the QLL of a growing ice crystal, allowing growth and recrystallization to form large ice crystals. Initial attempts to calculate the hydration properties of carbohydrates using molecular dynamics simulations were attempted and showed promise, although the parameters must be adjusted before these simulations are applied to unnatural monosaccharide derivatives.

A *geminal* difluoromethylene group at the anomeric position was observed to decrease the amount of IRI activity, likely due to their hydrophobic nature. This suggests that the fluorine atoms are not forming hydrogen bonds in these experiments.

Compounds with alkyl chains at C-1 and C-2 were prepared and evaluated for IRI activity. When the alkyl chain was made up of fewer than five carbons, poor IRI activity was observed. This supports our model that carbohydrates containing hydrophobic groups are poorly hydrated and therefore display low amounts of IRI activity. However, when a compound with a C-2 hexyl chain was assessed, it showed greater IRI activity than galactose itself. This compound may be forming a gel or liquid crystal in solution, and the liquid crystalline properties cause it to be more effectively hydrated and result in inhibition of ice-recrystallization.

CARS microscopy was examined as a method to examine the ice-water interface. The CARS spectra of water, supercooled water, and ice as well as solutions of AFP I and AFGP8 were observed to be similar to their Raman spectra. It was observed that AFP I is able to inhibit ice growth long enough for the ice-water interface to be studied using spectroscopy and microscopy.

6.2: Future Directions

The relationships between IRI activity, carbohydrate hydration, and carbohydrate cryoprotective ability need to be further explored through the IRI testing of additional commercially available and novel synthesized carbohydrates. Furthermore, it must be determined if the relationship between IRI activity and cryoprotective ability extends to other non-carbohydrate compounds such as glycerol and other poly-alcohols.

The enhanced IRI activity of α-*C*-allyl galactose needs to be further examined through the IRI testing of similar compounds such as galactose-derivatives with a vinyl group and a homo-allylic group at the anomeric position. Synthesis and evaluation of carbohydrates with anomeric aryl groups will allow one to determine whether π-π stacking interactions affect IRI activity.

The relationship between carbohydrate hydration and IRI activity will be greater understood if the hydration properties of unnatural carbohydrates such as α-*C*-allyl

galactose and α-*O*-allyl galactose are determined through molecular dynamics simulations. Initial efforts towards this end suggest that this is an attainable goal.

The role of the acetamide and amino group can be further examined through the preparation of carbohydrates with ester groups. Moving the amino and acetamide groups to other positions of the carbohydrate as well as the preparation of deoxy galactose derivatives are also important studies which are currently underway in our laboratory. The effect of the nature of the counter ion of the acetamide moiety on IRI activity should be explored through experiments that switch the chloride counter ion for alternate counter ions.

The fluorinated compounds prepared in this dissertation must be evaluated for cytotoxicity and cryopreservation ability in order to determine if the reported preservation ability of fluorinated AFGP analogues is due to a mechanism other than IRI activity. Furthermore, other efficient inhibitors of ice-recrystallization such as α-*C*-allyl galactose and α-*O*-allyl galactose should be evaluated for cryoprotective ability to confirm our observations that IRI activity is correlated to cryoprotective ability.

Finally, the potential relationship between liquid crystal formation and IRI activity needs to be explored. Firstly, the alkylated compounds reported in this dissertation should be evaluated for liquid crystal or gel formation. Secondly, known carbohydrate gelators and liquid crystals should be prepared and evaluated for IRI activity.

Chapter 7: Experimental

Table of Contents

7.1: General Experimental

All anhydrous reactions were performed in flame-dried or oven-dried glassware under a positive pressure of dry argon or nitrogen. Air or moisture-sensitive reagents and anhydrous solvents were transferred with oven-dried syringes or cannulae. All flash chromatography was performed with E. Merck silica gel 60 (230-400 mesh) or Silicycle Ultrapure SiliaFlash ® F60 (230-400 mesh). Analytical thin layer chromatography (TLC) was performed with 0.2 mm pre-coated silica gel plates 60 F_{254} (E. Merck). Preparatory thin layer chromatography was performed using Silicycle Glass Backed TLC Extra Hard Layer, 60 Å. Components were visualized by illumination with a short-wavelength ultra-violet light and/or staining (ceric ammonium molybdate stain solution).

All solvents used for reactions were distilled unless aqueous systems. Tetrahydrofuran (THF) and diethyl ether were distilled from sodium/benzophenone under nitrogen. Dichloromethane, triethylamine, benzene and diisopropylethylamine (DIPEA) were distilled from calcium hydride. *N,N*-dimethylformamide (DMF) was stored

over activated molecular sieves. *n*-Butyl-lithium was titrated according to the method of Burchat et al immediately prior to using to determine the concentration in solution.[1]

Solid-phase peptide synthesis (SPPS) was performed using Fmoc-Gly-Wang resin (Novabiochem). SPPS reactions were monitored using both Ninhydrin (Kaiser) and 2,4,6-trinitrobenzenesulfonic acid (TNBS) tests to detect the existence of free amino groups. The ninhydrin test was performed by adding two drops of a mixture solution (5 g of ninhydrin in 100 mL ethanol, 80 g liquefied phenol in 20 mL ethanol, and 2 mL of 0.001 M aqueous potassium cyanide to 98 mL of pyridine) to a sampling of resin and heating to 120 ºC. A dark blue solution indicated the existence of free amino groups. TNBS test was performed by adding one drop of a mixture solution (10% diisopropylethyl amine in DMF and 1% 2,4,6-trinitrobenzenesulfonic acid in DMF) to a sampling of resin. A resulting red resin indicated the existence of free amino groups.

^{1}H (300, 400 or 500 MHz), ^{13}C (75, 100 or 125 MHz), and ^{19}F NMR (282, 376, or 470 MHz) spectra were obtained at ambient temperature on a Bruker Avance 300, Bruker Avance 400, or Bruker Avance 500 spectrometer. Deuterated chloroform ($CDCl_3$) or deuterated methanol (CD_3OD) were used for NMR experiments, unless otherwise stated. Chemical shifts are reported in ppm downfield from TMS and corrected using the solvent residual signal as a reference.[2] Splitting patterns are designated as follows: s, singlet; d, doublet; t, triplet; q, quartet; m, multiplet and br, broad. Low resolution mass spectroscopy (MS) was performed on a Micromass Quatro-LC Electrospray spectrometer with a pump rate of 20 µL/min using electrospray ionization (ESI). Infrared absorption spectra (IR) were recorded on a Shimadzu FTIR-8400S spectrometer as a neat film from 4000 cm^{-1} to 650 cm^{-1}.

7.2: Compound Preparation Procedures and Experimental Data

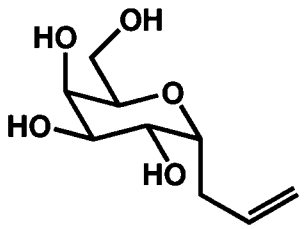

1-*C*-allyl-α-D-Galactopyranoside (14):
To a solution of β-D-galactose pentaacetate (8.0 g, 21 mmol) in distilled CH_3CN (80 mL), allyltrimethylsilane (6.5 mL, 41 mmol) and boron trifluoride diethyl etherate (7.7 mL, 62 mmol) were added dropwise and the reaction mixture was stirred for 27 hours. The solvent was evaporated and the product was extracted with dichloromethane (CH_2Cl_2), washed with water, saturated $NaHCO_3$ solution, dried over magnesium sulfate and concentrated. Flash column chromatography (3:1 hexanes:EtOAc) afforded the product (**49**) (6.0 g, 79%, 9:1 α: β mixture) as a colourless oil. The mixture was separated after the next step.

To a solution of (**49**) (5.0 g, 13 mmol) in MeOH (30 mL) was added a pre-mixed solution of Na in MeOH (100 mL, pH 10). The reaction was left stirring overnight at room temperature. Amberlite® IR-120H ion-exchange resin was added to neutralize the reaction mixture. The resin was filtered through a plug of cotton and the solvent was removed under reduced pressure. The α-anomer was re-crystallized out from MeOH and Et_2O to give white crystals (2.3 g, 84%).

^{1}H NMR (400 MHz, *CD_3OD)* δ ppm 5.88 (tdd, *J* = 17.2, 10.2, 7.0 Hz, 1H), 5.14-5.02 (m, 2H), 3.99 (td, *J* = 10.1, 4.9 Hz, 1H), 3.95 (dd, *J* = 3.2, 2.2 Hz, 1H), 3.89 (dd, *J* = 8.7, 5.2 Hz, 1H), 3.78-3.66 (m, 4H), 2.49-2.34 (m, 2H)

All spectral data was in accordance with the literature.[3]

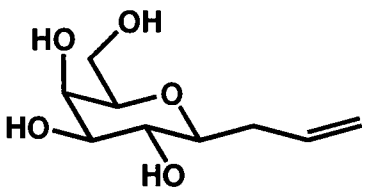

1-*C*-allyl-β-D-Galactopyranoside (18):
To a solution of (**52**) (80 mg, 0.22 mmol) in MeOH (5 mL) was added a pre-mixed solution of Na in MeOH (15 mL, pH 10). The reaction was left stirring overnight at room temperature. Amberlite® IR-120H ion-exchange resin was added to neutralize the reaction mixture. The resin was filtered through a plug of cotton and the solvent was removed under reduced pressure to give a solid (40 mg, 91%). The product was filtered through neutral alumina to remove trace impurities.

^{1}H NMR (400 MHz, *CD_3OD*) δ ppm 5.98 (tdd, *J* = 17.2, 10.2, 6.9 Hz, 1H), 5.12-5.00 (m, 2H), 3.87 (dd, *J* = 1.1, 2.6 Hz, 1H), 3.73-3.64 (m, 2H), 3.45-3.39 (m, 3H), 3.16-3.11 (m, 1H), 2.63-2.57 (m, 1H), 2.29-2.21 (m, 1H)

^{13}C NMR (100 MHz, CD_3OD) δ 136.70, 116.71, 81.34, 80.18, 76.46, 72.29, 70.89, 62.75, 37.18;

HRMS calcd for $C_9H_{16}O_5$ $(M+Na)^+$ 227.0895, found 227.0884.

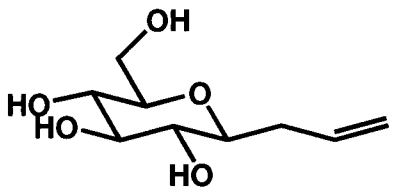

1-*C*-allyl-β-D-Glucopyranoside (19)
To a solution of (**55**) (50 mg, 0.13 mmol) in MeOH (5 mL) was added a pre-mixed solution of Na in MeOH (15 mL, pH 10). The reaction was left stirring overnight at room temperature. Amberlite® IR-120H ion-exchange resin was added to neutralize the

reaction mixture. The resin was filtered through a plug of cotton and the solvent was removed under reduced pressure to give a solid (20 mg, 74%). The product was filtered through neutral alumina to remove trace impurities.

^{1}H NMR (400 MHz, *CD_3OD*) δ ppm 6.02-5.92 (m, 1H), 5.12-5.01 (m, 2H), 3.83 (dd, *J* = 2.3, 11.9 Hz, 1H), 3.63 (dd, *J*=5.5, 11.9 Hz, 1H), 3.34-3.16 (m, 4H), 3.11-3.07 (m, 1H), 2.61-2.54 (m, 1H), 2.26-2.18 (m, 1H)

^{13}C NMR (100 MHz, *CD_3OD*) δ 136.33, 116.97, 81.61, 80.59, 79.82, 74.85, 71.95, 63.08, 37.04;

HRMS calcd for $C_9H_{16}O_5$ $(M+Na)^+$ 227.0895, found 227.0886.

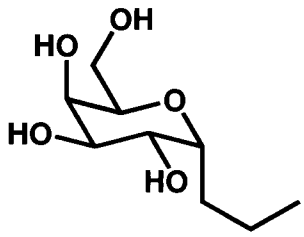

1-*C*-propyl-α-D-galactopyranoside (20):
To a solution of compound (**57**) (0.12 g, 0.32 mmol) in MeOH (3 mL) was added a pre-mixed solution of Na in MeOH (10 mL, pH 10). The reaction was left stirring overnight at room temperature. Amberlite® IR-120H ion-exchange resin was added to neutralize the reaction mixture. The resin was filtered through a plug of cotton and the solvent was removed under reduced pressure to give a white solid (46 mg, 70%). Preparative thin layer chromatography (4:1:1:1 EtOAc:CH_3CN:MeOH:H_2O) gave pure product.

^{1}H NMR (400 MHz, *CD_3OD)* δ ppm 3.97-3.89 (m, 3H), 3.76 (dt, *J* = 8.9, 8.7, 2.5 Hz, 1H), 3.70-3.64 (m, 3H), 1.71-1.61 (m, 1H), 1.59-1.49 (m, 2H), 1.37-1.29 (m, 1H), 0.96 (t, *J* = 7.2 Hz, 3H)

^{13}C NMR (100 MHz, *CD_3OD)* δ ppm 75.77, 73.85, 71.99, 70.32, 70.31, 62.31, 28.09, 20.06, 14.36

Accurate Mass (ESI): Calcd for $C_9H_{18}O_5Na$ $(M+Na)^+$ 229.105, found 229.132 ± 0.014

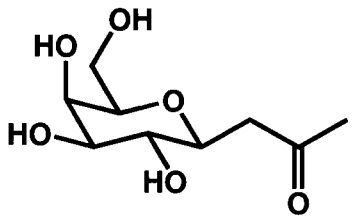

1-(2-propanone)-β-D-galactopyranoside (23) (procedure adapted from Bragnier and Scherrmann[4]):

To a solution of galactose (0.50 g, 2.8 mmol) in 18 mL of a 2:1 H_2O:THF solution was added $NaHCO_3$ (0.93 g, 11 mmol) and 2,4-pentanedione (0.57 mL, 5.6 mmol). A reflux condenser was attached and the solution was heated to 85 ºC for 24 hours. The solution was neutralized with Amberlite® IR-120H ion-exchange resin. The beads were filtered off and the filtrate was extracted with CH_2Cl_2. The aqueous layer was concentrated *in vacuo* to give a solid (0.57 g, 93%).

^{1}H NMR (400 MHz, *CD_3OD)* δ ppm 3.95 (d, *J* = 3.1 Hz, 1H), 3.75-3.61 (m, 5H), 3.44 (t, *J* = 9.6 Hz, 1H), 3.02 (dd, *J* = 16.7, 3.0 Hz, 1H), 2.73 (dd, *J* = 16.7, 9.2 Hz, 1H), 2.26 (s, 3H)

All spectral data was in accordance with the literature.[4]

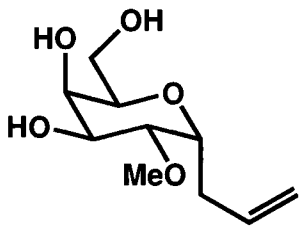

1-*C*-allyl-2-*O*-methyl-α-D-galactopyranoside (28):

Compound (**65**) (0.17 g, 0.46 mmol) was dissolved in 20 mL of 80% AcOH (v/v in H_2O). The reaction was stirred at 80 °C for 1.5 hours. The solvent was evaporated off and the product was dried *in vacuo* to give the product as a white solid (0.10 g, quant.). Recrystallization from MeOH and Et_2O gave a pure product.

^{1}H NMR (400 MHz, *CD_3OD)* δ ppm 5.88 (tdd, *J* = 17.2, 10.2, 7.0 Hz, 1H), 5.12 (ddd, *J* = 17.1, 3.9, 1.5 Hz, 1H), 5.06-5.02 (m, 1H), 4.19-4.12 (m, 1H), 3.90 (d, *J* = 3.0 Hz, 1H), 3.75-3.65 (m, 4H), 3.55 (dd, *J* = 9.0, 5.3 Hz, 1H), 3.44 (s, 3H), 2.50-2.42 (m, 1H), 2.30-2.26 (m, 1H)

^{13}C NMR (100 MHz, *CD_3OD*): δ ppm 136.65, 116.98, 79.99, 73.90, 73.69, 70.65, 70.36, 62.15, 58.73, 30.95

Accurate Mass (ESI): Calcd for $C_{10}H_{18}O_5Na$ $(M+Na)^+$ 241.105, found 241.139 ± 0.014

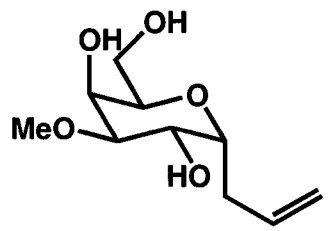

1-C-allyl-3-O-methyl-α-D-galactopyranoside (29) (procedure adapted from Blom et al5):

To a solution of (**68**) (0.70 g, 1.5 mmol) in 20 mL DMF was added sodium hydride (74 mg, 60% dispersion in mineral oil, 1.9 mmol). The suspension was stirred for 1 hour to allow deprotonation, and then methyl iodide (96 µL, 1.5 mmol) was added and the reaction was allowed to warm to room temperature overnight. The reaction was quenched with NH_4Cl. The solvent was removed *in vacuo* (water aspirator on rotary evaporator) and the product was extracted with EtOAc, washed with H_2O and brine, dried with $MgSO_4$, filtered, and concentrated. Flash chromatography (3:1 hexanes:EtOAc) gave the methylated intermediate (**69**) as an oil (0.35 g, 49%).

To a solution of the methylated intermediate (**69**) (0.12 g, 0.26) in 5 mL MeOH was added a pre-mixed solution of Na in MeOH (15 mL, pH 10). The reaction was left stirring overnight at room temperature. Amberlite® IR-120H ion-exchange resin was added to neutralize the reaction mixture. The resin was filtered through a plug of cotton and the solvent was removed under reduced pressure to give a solid (40 mg, 75%). Preparative thin layer chromatography (4:1:1:1 EtOAc:CH_3CN:MeOH:H_2O) gave pure product.

^{1}H NMR (400 MHz, *CD_3OD)* δ 5.88 (tdd, *J* = 17.2, 10.2, 7.0 Hz, 1H), 5.15-5.10 (m, 1H), 5.05-5.03 (m, 1H), 4.15 (dd, *J* = 3.1, 1.4 Hz, 1H), 4.01-3.85 (m, 3H), 3.75-3.65 (m, 3H), 3.45 (s, 3H), 2.49-2.36 (m, 2H)

^{13}C NMR (100 MHz, *CD_3OD*): δ ppm 136.72, 116.92, 81.75, 75.83, 73.92, 68.50, 66.56, 61.98, 57.26, 31.00

MS (ESI): Calcd for $C_{10}H_{18}O_5$ $(M+Na)^+$ 241.11, found 240.9, $(2M+Na)^+$ 459.49, found 459.3

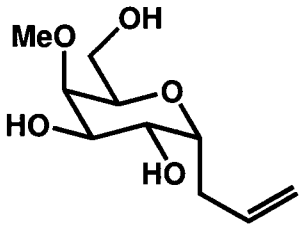

1-C-allyl-4-*O*-methyl-α-D-galactopyranoside (30) (procedure adapted from Blom et al[5] and Xie et al[6]):

To a solution of compound (**73**) (0.43 g, 0.86 mmol) in 20 mL DMF at 0 °C was added sodium hydride (40 mg, 60% dispersion in mineral oil, 1.0 mmol). The suspension was stirred for 1 hour to allow deprotonation, and then methyl iodide (0.11 mL, 1.7 mmol) was added and the reaction was allowed to warm to room temperature overnight. The reaction was quenched with saturated NH_4Cl and concentrated *in vacuo* to remove the DMF (using a water aspirator attached to a rotary evaporator). The product was extracted with EtOAc, washed with H_2O and brine, dried with $MgSO_4$, filtered, and concentrated. Flash chromatography (3:1 petroleum ether:EtOAc) gave the product (**74**) as an oil (0.34 g, 77%).

A solution of methylated intermediate (**74**) (0.10 g, 0.20 mmol) in 5 mL CH_2Cl_2 was cooled to -78 ºC in a dry ice:acetone bath. Boron trichloride (0.98 mL, 1.0 M solution in CH_2Cl_2, 0.98 mmol) was added and the solution was stirred for 3 hours, and then quenched with 4 mL of a 1:1 MeOH:CH_2Cl_2 solution. Preparative thin layer chromatography (4:1:1:1 EtOAc:CH_3CN:MeOH:H_2O) gave the product as a white solid (3.6 mg, 10%).

^{1}H NMR (400 MHz, *CD_3OD)* δ ppm 5.85 (tdd, *J* = 17.2, 10.2, 7.0 Hz, 1H), 5.12 (ddd, *J* = 17.2, 3.6, 1.5 Hz, 1H), 5.03 (tdd, *J* = 10.2, 2.2, 1.1, Hz, 1H), 3.98-3.92 (m, 1H), 3.88-3.84 (m, 3H), 3.76 (dd, *J* = 7.0, 3.7 Hz, 1H), 3.67 (t, *J* = 3.5 Hz, 2H), 3.47 (s, 3H), 2.44-2.30 (m, 2H)

^{13}C NMR (100 MHz, *CD_3OD*): δ ppm 136.54, 117.06, 78.62, 75.19, 72.96, 72.93, 70.81, 70.75, 60.47, 32.92

MS (ESI): Calcd for $C_{10}H_{18}O_5$ $(M+Na)^+$ 241.11, found 241.3, $(M+K)^+$ 257.08, found 257.3

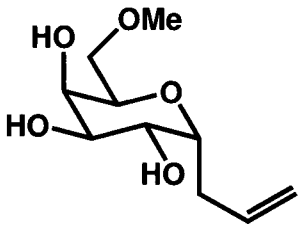

1-C-allyl-6-*O*-methyl-α-D-galactopyranoside (31) (procedure adapted from Blom et al[5]):

To a solution of compound (**77**) (0.26 g, 0.78 mmol) in 15 mL DMF was added sodium hydride (38 mg, 60% dispersion in mineral oil, 0.94 mmol). The suspension was stirred for 1 hour to allow deprotonation, and then methyl iodide (49 µL, 0.78 mmol) was added and the reaction was allowed to warm to room temperature overnight. The reaction was quenched with NH_4Cl. The solvent was removed *in vacuo* (water aspirator on rotary evaporator) and the product was extracted with EtOAc, washed with H_2O and brine, dried with $MgSO_4$, filtered, and concentrated. Flash chromatography (3:1 hexanes:EtOAc) gave the methylated intermediate (**78**) as an oil (0.15 g, 56%).

To a solution of the methylated intermediate (**78**) (0.15 g, 0.44) in 5 mL MeOH was added a pre-mixed solution of Na in MeOH (15 mL, pH 10). The reaction was left stirring overnight at room temperature. Amberlite® IR-120H ion-exchange resin was added to neutralize the reaction mixture. The resin was filtered through a plug of cotton and the solvent was removed under reduced pressure to give a solid (0.1 g, quant.). Preparative thin layer chromatography (4:1:1:1 EtOAc:CH_3CN:MeOH:H_2O) gave pure product.

^{1}H NMR (400 MHz, *CD_3OD)* δ 5.88 (tdd, *J* = 17.2, 10.2, 7.0 Hz, 1H), 5.12 (ddd, *J* = 17.1, 3.4, 1.4 Hz, 1H), 5.06-5.03 (m, 1H), 4.15 (d, *J* = 2.8 Hz, 1H), 4.00-3.95 (m, 2H), 3.74-3.67 (m, 3H), 3.45 (s, 3H), 2.47-2.38 (m, 2H)

^{13}C NMR (100 MHz, *CD_3OD*): δ ppm 136.70, 116.95, 81.72, 75.84, 73.89, 68.49, 66.54, 61.98, 57.26, 30.98

Accurate Mass (ESI): Calcd for $C_{10}H_{18}O_5Na$ $(M+Na)^+$ 241.105, found 241.123 ± 0.014

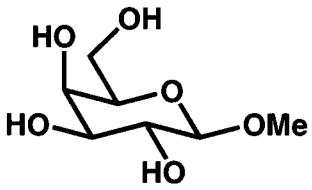

β-methylgalactopyranoside (32) (procedure adapted from Bornaghi and Poulsen[7]):

To a solution of galactose (5.0 g, 28 mmol) in 50 mL MeOH was added Amberlite® IR-120H ion-exchange resin (5.0 g). The reaction was refluxed for 48 hours, at which point the resin was filtered off and the product was concentrated *in vacuo*. (**32**) was obtained by recrystallization from MeOH and Et_2O as white crystals.

^{1}H NMR (400 MHz, *CD_3OD)* δ ppm 4.13 (d, *J* = 7.1 Hz, 1H), 3.83 (dd, *J* = 3.0, 1.0 Hz, 1H), 3.79-3.70 (m, 2H), 3.53 (s, 3H), 3.52-3.46 (m, 3H)

^{13}C NMR (100 MHz, *CD_3OD)* δ ppm 106.03, 76.66, 75.00, 72.51, 70.32, 62.49, 57.26

MS (ESI): Calcd for $C_7H_{14}O_6$ $(M+NH_4)^+$ 217.1, found 217.1, $(2M+Na)^+$ 411.2, found 411.3

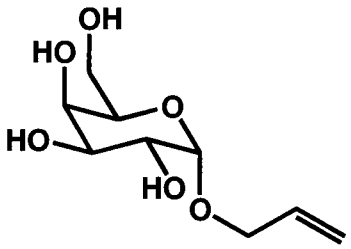

1-*O*-allyl-α-D-Galactopyranoside (34) (procedure adapted from Goebel et al[8]):
Allyl alcohol (70 mL) and boron trifluoride diethyl etherate (0.28 mL, 2.2 mmol) were added to a flask containing galactose (5.9 g, 33 mmol). The reaction was heated to reflux for 3 hours, and then concentrated *in vacuo* to remove the solvent. The product was recrystallized from MeOH and Et_2O to give a white solid (6.4 g, 88%)

^{1}H NMR (400 MHz, *CD_3OD*) δ ppm 5.99-5.83 (m, 1H), 5.14-5.00 (m, 2H), 4.01-3.94 (m, 2H), 3.91-3.86 (m, 1H), 3.78-3.66 (m, 4H), 2.50-2.33 (m, 2H)

All spectral data was in accordance with the literature.[9]

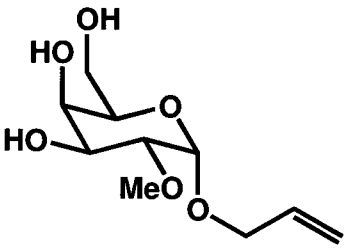

1-*O*-allyl-2-*O*-methyl-α-D-Galactopyranoside (35) (procedure adapted from Czechura et al[10]):
Compound **81** (0.13 g, 0.34 mmol) was dissolved in 20 mL of 80% acetic acid (v/v in H_2O). The reaction was stirred at 80 °C for 3 hours. The solvent was evaporated off and the product was dried *in vacuo* to give the product as a white solid (80 mg, quant.).

Preparative thin layer chromatography (4:1:1:1 EtOAc:CH_3CN:MeOH:H_2O) gave a pure product.

^{1}H NMR (400 MHz, *CD_3OD)* δ ppm 6.00-5.92 (m, 1H), 5.32 (ddd, *J* = 17.2, 3.3, 1.6 Hz, 1H), 5.19 (ddd, *J* = 10.3, 2.9, 1.4 Hz, 1H), 5.06 (d, *J* = 3.7 Hz, 1H), 4.26-4.16 (m, 3H), 4.07-4.01 (m, 1H), 3.99-3.96 (m, 1H), 3.86 (dd, *J* = 3.5, 1.0 Hz, 1H), 3.82 (dd, *J* = 9.9, 3.4 Hz, 1H), 3.51 (dd, *J* = 9.9, 3.7 Hz, 1H), 3.47 (s, 3H)

^{13}C NMR (100 MHz, *CD_3OD*): δ ppm 135.44, 117.81, 96.84, 79.38, 70.95, 70.41, 69.74, 69.37, 65.12, 58.60

Accurate Mass (ESI): Calcd for $C_{10}H_{18}O_6$ Na $(M+Na)^+$ 257.100, found 257.117 ± 0.0143

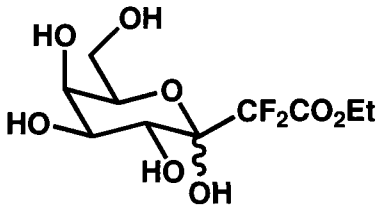

1-α-hydroxyl-1-β-(ethyl-2,2,-difluoroacetate)-D-galactopyranoside (36) (procedure adapted from Motawia et al[11]):

To a solution of (**89**) (94 mg, 0.14 mmol) in 6 mL 99% EtOH and 6 mL EtOAc was added palladium over carbon (19 mg, 20% by mass). N_2 was bubbled through the mixture for 10 minutes, and then H_2 was bubbled through for 30 minutes. An H_2 balloon was attached and the reaction was stirred under an H_2 atmosphere for 5.5 hours. The product was filtered over celite using a scintered glass funnel, washed with EtOAc and EtOH, and concentrated *in vacuo* to give a white powder (43 mg, quant.). Preparatory thin layer chromatography (6:1:1:1 EtOAc:CH_3CN:MeOH:H_2O) gave a pure product as an anomeric mixture.

^{1}H NMR (400 MHz, *CD_3OD)* δ ppm 4.37-4.28 (m, 2H), 4.12 (ddd, *J* = 11.5, 8.8, 6.3 Hz, 1H), 3.94 (dt, *J* = 6.2, 1.2 Hz, 1H), 3.75-3.57 (m, 3H), 1.33 (t, *J* = 7.1 Hz, 3H)

^{13}C NMR (100 MHz, *CD_3OD)* δ ppm 164.21, 163.79, 114.37, 110.16, 97.63, 82.11, 77.72, 75.87, 73.54, 72.54, 72.14, 70.34, 68.65, 64.22, 64.11, 64.03, 62.23, 14.28, 14.21

^{19}F NMR (400 MHz, *CD_3OD)* δ ppm -115.63, -115.66, -116.23, -116.31, -116.34, -116.92, -117.05, -117.41, -117.53, -117. 58, -118.21, -118.27

Accurate Mass (ESI): Calcd for $C_{10}H_{16}O_8F_2Na$ $(M+Na)^+$ 325.071, found 325.130 ± 0.017

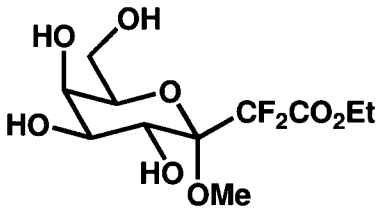

1-α-*O*-methyl-1-β-(ethyl-2,2,-difluoroacetate)-D-galactopyranoside (37) (procedure adapted from Rajanikanth and Seshadri[12]):

To a solution of (**94**) (0.13 g, 0.19 mmol) in 10 mL THF with 1 drop glacial acetic acid was added palladium over carbon (19 mg, 20% by mass). N_2 was bubbled through the mixture for 10 minutes, and then H_2 was bubbled through for 30 minutes. An H_2 balloon was attached and the reaction was stirred under an H_2 atmosphere for 3 hours. At this point, the reaction was not complete by TLC. 2 mL of a 33% AcOH (glacial in water) was added, and the reaction was stirred under an H_2 atmosphere for 48 hours. The product was filtered over celite using a scintered glass funnel, washed with EtOAc and EtOH, and concentrated *in vacuo* to give a white powder (61 mg, quantitative). Preparatory thin layer chromatography (4:1:1:1 EtOAc:CH_3CN:MeOH:H_2O) gave a pure product.

^{1}H NMR (400 MHz, *CD_3OD)* δ ppm 4.32-4.28 (m, 2H), 3.92 (dd, *J* = 10.7, 1.9 Hz, 2H), 3.79-3.67 (m, 4H), 3.53 (dd, *J* = 3.6, 1.3 Hz, 3H), 1.34 (t, *J* = 7.1 Hz, 3H)

^{13}C NMR (100 MHz, *CD_3OD)* δ ppm 164.24, 99.63, 74.98, 72.27, 70.47, 69.48, 64.08, 51.46, 14.12

^{19}F NMR (400 MHz, *CD_3OD)* δ ppm -113.42, -114.13, -116.78, -117.47

MS (ESI): Calcd for $C_{11}H_{18}O_8F_2Na$ $(M+Na)^+$ 339.087, found 339.124 ± 0.017

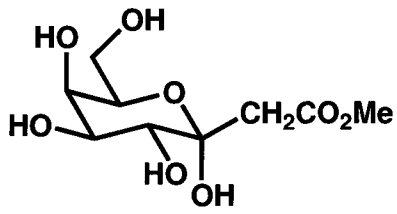

1-α-hydroxyl-1-β-ethyl acetate-D-galactopyranoside (38) (procedure adapted from Motawia et al[11]) :

To a solution of (**103**) (0.12 g, 0.20 mmol) in 8 mL 99% EtOH and 8 mL EtOAc was added palladium over carbon (approx. 40 mg). N_2 was bubbled through the mixture for 10 minutes, and then H_2 was bubbled through for 30 minutes. An H_2 balloon was attached and the reaction was stirred under an H_2 atmosphere for 3 days. The product was filtered over celite using a scintered glass funnel, washed with EtOAc and EtOH, and concentrated *in vacuo* to give a white powder (50 mg, quant.). Preparatory thin layer chromatography (6:1:1:1 EtOAc:CH_3CN:MeOH:H_2O) gave a pure product.

^{1}H NMR (400 MHz, *CD_3OD)* δ 3.94 (dt, *J* = 6.5, 1.2 Hz, 1H), 3.88 (dd, *J* = 3.2, 1.1 Hz, 1H), 3.74 (dd, *J* = 9.7, 3.3 Hz, 1H), 3.67 (s, 3H), 3.69-3.60 (m, 4H), 2.84 (d, *J* = 14.9 Hz, 1H), 2.71 (d, *J* = 14.9 Hz, 1H)

^{13}C NMR (100 MHz, *CD_3OD)* δ ppm 173.53, 98.53, 72.82, 72.59, 72.12, 71.08, 62.51, 52.35, 42.64

Accurate Mass (ESI): Calcd for $C_{10}H_{16}O_8Na$ $(M+Na)^+$ 275.074, found 275.128 ± 0.014

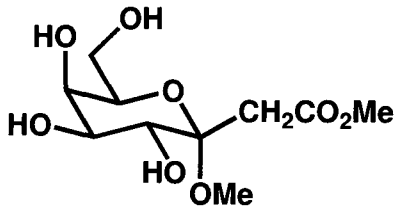

1-α-*O*-methyl-1-β-ethyl acetate-D-galactopyranoside (39) (procedure adapted from Motawia et al[11]):

To a solution of (**104**) (0.10 mg, 0.16 mmol) in 10 mL 99% EtOH and 10 mL EtOAc was added palladium over carbon (approx. 20 mg). N_2 was bubbled through the mixture for 10 minutes, and then H_2 was bubbled through for 30 minutes. An H_2 balloon was attached and the reaction was stirred for 5 hours. The product was filtered over celite using a sintered glass funnel, washed with EtOAc and EtOH, and concentrated *in vacuo* to give a white powder (43 mg, quant.). Preparatory thin layer chromatography (6:1:1:1 EtOAc:CH_3CN:MeOH:H_2O) gave a pure product.

^{1}H NMR (400 MHz, *CD_3OD)* δ ppm 3.92 (d, *J* = 11.5 Hz, 1H), 3.86 (d, *J* = 9.7 Hz, 1H), 3.73-3.69 (m, 3H), 3.66 (s, 3H), 3.64-3.63 (m, 1H), 3.33 (s, 3H), 2.91 (d, *J* = 13.9 Hz, 1H), 2.69 (d, *J* = 13.9 Hz, 1H)

^{13}C NMR (100 MHz, *CD_3OD)* δ ppm 171.81, 101.28, 73.76, 72.60, 72.25, 71.01, 62.79, 52.28, 48.66, 38.87

Accurate Mass (ESI): Calcd for $C_{10}H_{18}O_8Na$ $(M+Na)^+$ 289.090, found 289.106 ± 0.014

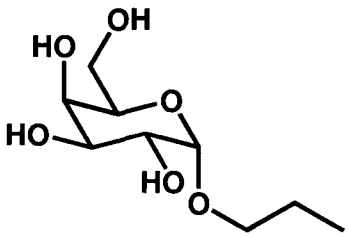

1-*O*-propyl-α-D-galactopyranoside (40):
To a solution of compound (**117**) (0.10 g, 0.26 mmol) in MeOH (3 mL) was added a pre-mixed solution of Na in MeOH (10 mL, pH 10). The reaction was left stirring overnight at room temperature. Amberlite® IR-120H ion-exchange resin was added to neutralize the reaction mixture. The resin was filtered through a plug of cotton and the solvent was removed under reduced pressure to give a white solid (36 mg, 64%). Preparative thin layer chromatography (4:1:1:1 EtOAc:CH_3CN:MeOH:H_2O) gave pure product.

^{1}H NMR (400 MHz, *CD_3OD)* δ ppm 4.80 (d, *J* = 3.2 Hz, 1H), 3.88-3.87 (m, 1H), 3.81 (dt, *J* = 6.1, 0.7 Hz, 1H), 3.74 (t, *J* = 3.2 Hz, 2H), 3.72-3.65 (m, 3H), 3.41 (td, *J* = 9.6, 6.5 Hz, 1H), 1.70-1.60 (m, 2H), 0.96 (t, *J* = 7.4 Hz, 3H)

^{13}C NMR (100 MHz, *CD_3OD)* δ ppm 100.30, 72.34, 71.58, 71.10, 70.79, 70.33, 62.75, 23.78, 11.05

Accurate Mass (ESI): Calcd for $C_9H_{18}O_6Na$ $(M+Na)^+$ 245.100, found 245.112 ± 0.014

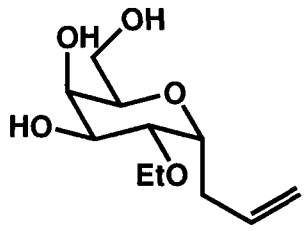

1-*C*-allyl-2-*O*-ethyl-α-D-galactopyranoside (41)
Compound (**112**) (0.20 g, 0.52 mmol) was dissolved in 20 mL of 80% AcOH (v/v in H_2O). The reaction was stirred at 80 °C for 1.5 hours. The solvent was evaporated and the product was dried *in vacuo* to give a white solid (0.12 g, quant.). Preparative thin layer chromatography (4:1:1:1 EtOAc:CH_3CN:MeOH:H_2O) gave a pure product.

^{1}H NMR (400 MHz, *CD_3OD)* δ ppm 5.82 (tdd, *J* = 17.2, 10.2, 7.0 Hz, 1H), 5.10 (ddd, *J* = 17.2, 3.6, 1.5 Hz, 1H), 5.04 (tdd, *J* = 10.2, 2.2, 1.1 Hz, 1H), 4.46 (dd, *J* = 11.6, 8.7 Hz, 1H), 4.15 (dd, *J* = 11.8, 3.4 Hz, 1H), 4.11 (dd, *J* = 9.9, 4.9 Hz, 1H), 3.93-3.89 (m, 2H), 3.79 (dd, *J* = 8.0, 3.1 Hz, 1H), 3.69-3.56 (m, 3H), 2.42-3.37(m, 1H), 2.34-2.28 (m, 1H), 2.03 (s, 3H), 1.20 (t, *J* = 7.02 Hz, 3H)

^{13}C NMR (100 MHz, *CD_3OD*): δ ppm 136.51, 117.04, 78.51, 72.91, 72.25, 70.26, 69.71, 67.33, 64.11, 32.05, 15.97

MS (ESI): Calcd for $C_{11}H_{20}O_5$ $(M+Na)^+$ 255.12, found 255.15, $(2M+Na)^+$ 487.25 found 487.26

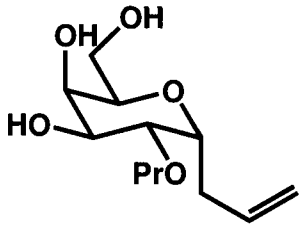

1-C-allyl-2-*O*-propyl-α-D-galactopyranoside (42)
Compound (**113**) (0.14 g, 0.35 mmol) was dissolved in 10 mL of 80% AcOH (v/v in H_2O). The reaction was stirred at 80 °C for 3 hours. The solvent was evaporated and the product was dried *in vacuo* to give a white solid (50 mg, 62%). Preparative thin layer chromatography (4:1:1:1 EtOAc:CH_3CN:MeOH:H_2O) gave a pure product.

^{1}H NMR (400 MHz, *CD_3OD)* δ ppm 5.93-5.81 (m, 1H), 5.11 (tdd, *J* = 17.1, 3.4, 1.7 Hz, 1H), 5.09-5.02 (m, 1H), 4.14 (ddd, *J* = 15.3, 9.6, 4.1 Hz, 1H), 3.92 (dd, *J* = 3.1, 1.9 Hz, 1H), 3.76-3.45 (m, 6H), 2.51-2.43 (m 1H), 2.36-2.30 (m, 1H), 2.03 (s, 1H) 1.64-1.56 (m, 2H), 0.95 (t, *J* = 7.42 Hz, 3H)

^{13}C NMR (100 MHz, *CD_3OD*): δ ppm 136.75, 116.91, 78.52, 74.17, 73.93, 73.73, 70.70, 70.30, 62.03, 31.34, 24.40, 11.03

MS (ESI): Calcd for $C_{12}H_{22}O_5$ $(M+Na)^+$ 269.14, found 269.13, $(2M+Na)^+$ 515.29 found 515.29

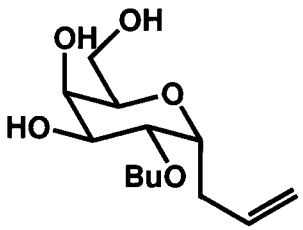

1-*C*-allyl-2-*O*-butyl-α-D-galactopyranoside (43)
Compound (**114**) (0.17 g, 0.41 mmol) was dissolved in 20 mL of 80% AcOH (v/v in H_2O). The reaction was stirred at 80 °C for 3 hours. The solvent was evaporated and

the product was dried *in vacuo* to give a white solid (90 mg, 84%). Preparative thin layer chromatography (4:1:1:1 EtOAc:CH_3CN:MeOH:H_2O) gave a pure product.

^{1}H NMR (400 MHz, *CD_3OD)* δ ppm 5.87 (tdd, *J* = 17.1, 10.2, 7.0 Hz, 1H), 5.10 (dtd, *J* = 9.0, 4.0, 3.8, 1.8 Hz, 1H), 5.05-5.02 (m, 1H), 4.14-4.09 (m, 1H), 3.92 (dd, *J* = 3.2, 1.8 Hz, 1H), 3.76-3.51 (m, 7H), 2.45-2.42 (m, 1H), 2.35-2.30 (m, 1H), 1.59-1.454 (m, 2H), 1.44-1.38 (m, 2H), 0.94 (t, *J* = 7.36 Hz, 3H)

^{13}C NMR (100 MHz, *CD_3OD*): δ ppm 136.75, 116.95, 78.55, 74.18, 73.93, 71.77, 70.70, 70.31, 62.04, 33.41, 31.36, 20.43, 14.30

MS (ESI): Calcd for $C_{13}H_{24}O_5$ $(M+Na)^+$ 283.15, found 283.16, $(2M+Na)^+$ 543.31 found 543.35

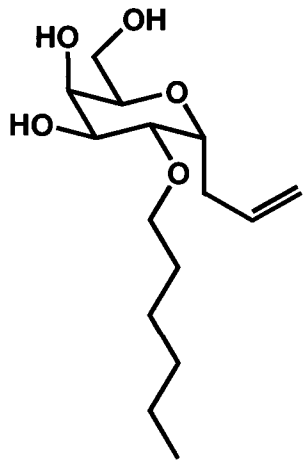

1-*C*-allyl-2-*O*-hexyl-α-D-galactopyranoside (44)

Compound (**115**) (0.25 g, 0.57 mmol) was dissolved in 10 mL of 80% acetic acid (v/v in H_2O). The reaction was stirred at 80 °C for 3 hours. The solvent was evaporated off and the product was dried *in vacuo* to give the product as a white solid (0.17 g, quant.). Preparative thin layer chromatography (4:1:1:1 EtOAc:CH_3CN:MeOH:H_2O) gave a pure product.

^{1}H NMR (400 MHz, *CD_3OD)* δ ppm 5.93-5.81 (m, 1H), 5.13-5.17 (m, 1H), 5.06-5.02 (m, 1H), 4.14-4.09 (m, 1H), 3.92 (dd, *J* = 3.2, 1.7 Hz, 1H), 3.82-3.50 (m, 7H), 2.51-2.43 (m, 1H), 2.36-2.29 (m, 1H), 1.62-1.55 (m, 2H), 1.43-1.27 (m, 6H), 0.91 (t, *J* = 6.9 Hz, 3H)

^{13}C NMR (100 MHz, *CD_3OD*): δ ppm 136.76, 116.90, 78.56, 74.20, 73.96, 72.09, 70.71, 70.32, 62.04, 32.88, 31.36, 31.23, 27.01, 23.73, 14.41

MS (ESI): Calcd for $C_{15}H_{28}O_5$ $(M+Na)^+$ 311.18, found 311.21, $(2M+Na)^+$ 599.37, found 599.43

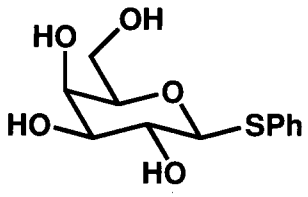

Phenyl-1-thio-β-D-galactopyranoside (45) (procedure adapted from Belot et al)[13]:

Compound (**82**) (4.0 g, 9.5 mmol) was dissolved in a pre-mixed solution of Na in MeOH (pH 10) overnight. Amberlite® IR-120H ion-exchange resin was added to neutralize the reaction mixture. The resin was filtered through a plug of cotton and the solvent was removed under reduced pressure to give a white solid (2.4 g, 94%).

^{1}H NMR (400 MHz, *CD_3OD*) δ ppm 7.56-7.54 (m, 2H), 7.31-21 (m, 3H), 4.58 (d, *J* = 9.7 Hz, 1H), 3.90 (dd, *J* = 3.3, 0.8 Hz, 1H), 3.73 (dq, *J* = 11.5, 6.1 Hz, 2H), 3.61 (t, *J* = 9.4 Hz, 1H), 3.56 (ddd, *J* = 6.6, 5.3, 0.9 Hz, 1H), 3.50 (dd, *J* = 9.2, 3.3 Hz, 1H)

All spectral data was in accordance with the published data.[14]

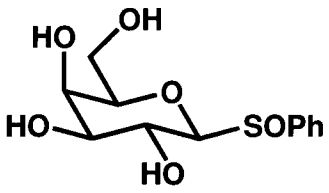

1-(phenyl sulfoxide)-β-D-galactopyranoside (46):
To a solution of compound (**118**) (0.60 g, 1.3 mmol) in MeOH (10 mL) was added a pre-mixed solution of Na in MeOH (50 mL, pH 10). The reaction was left stirring overnight at room temperature. Amberlite® IR-120H ion-exchange resin was added to neutralize the reaction mixture. The resin was filtered through a plug of cotton and the solvent was removed under reduced pressure to give a white solid (0.33 g, 87%). Preparative thin layer chromatography (100% EtOAc) gave pure product as a mixture of sulfoxide diastereomers.

^{1}H NMR (400 MHz, *CD_3OD)* δ ppm 7.65 (ddd, *J* = 5.2, 4.0, 2.1 Hz, 2H), 7.55 (dd, *J* = 5.2, 1.8 Hz, 3H), 7.50 (dd, *J* = 6.4, 1.7 Hz, 3H), 7.41 (ddd, *J* = 7.3, 2.7, 0.9 Hz, 2H), 4.71 (d, *J* = 3.7 Hz, 1H), 4.13 (d, *J* = 7.3 Hz, 1H), 3.88 (d, *J* = 3.3 Hz, 1H), 3.83 (dd, *J* = 3.0, 1.0 Hz, 1H), 3.77 (ddd, *J* = 6.6, 5.5, 2.9 Hz, 3H), 3.73-3.70 (m, 3H), 3.53 (s, 3H), 3.51-3.47 (m, 2H), 3.40 (s, 3H)

^{13}C NMR (100 MHz, *CD_3OD)* δ ppm 135.19, 131.70, 130.38, 129.14, 128.91, 125.25, 123.93, 104.64, 100.11, 75.27, 75.00, 73.61, 71.13, 70.90, 70.14, 69.69, 68.93, 68.87, 61.41, 61.11, 55.90, 54.25

MS (ESI): Calcd for $C_{12}H_{16}O_6S$ $(M+NH_4)^+$ 306.1, found 306.4, $(M+Na)^+$ 311.1, found 311.4

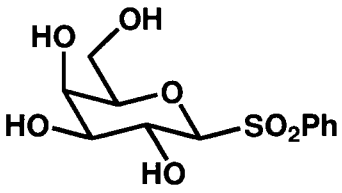

1-(phenyl sulfone)-β-D-galactopyranoside (47):
To a solution of compound (**119**) (0.27 g, 0.57 mmol) in MeOH (10 mL) was added a pre-mixed solution of Na in MeOH (50 mL, pH 10). The reaction was left stirring overnight at room temperature. Amberlite® IR-120H ion-exchange resin was added to neutralize the reaction mixture. The resin was filtered through a plug of cotton and the solvent was removed under reduced pressure to give a white solid (0.14 g, 82%). The product was re-crystallized from MeOH and Et_2O to give white crystals.

^{1}H NMR (400 MHz, *CD_3OD)* δ ppm 7.97 (td, *J* = 8.6, 1.7 Hz, 2H), 7.75-7.71(m, 1H), 7.63-7.59 (m, 2H), 4.36 (d, *J* = 9.5 Hz, 1H), 3.91 (t, *J* = 9.4 Hz, 1H), 3.85 (s, *J* = 3.2 Hz, 1H), 3.63-3.61 (m, 2H), 3.54 (ddd, *J* = 7.3, 6.4, 2.1 Hz, 2H)

^{13}C NMR (100 MHz, *CD_3OD)* δ ppm 138.33, 135.29, 130.77, 130.75, 130.05, 93.75, 81.35, 75.72, 69.86, 68.21, 62.19

MS (ESI): Calcd for $C_{12}H_{16}O_7S$ $(M+NH_4)^+$ 322.1, found 322.1, $(M+Na)^+$ 327.1, found 327.1

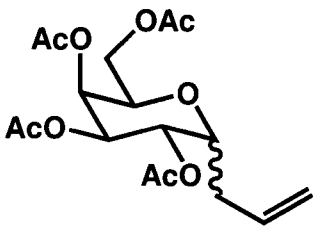

1-*C*-allyl-2,3,4,6-tetra-*O*-acetyl-D-α/β-galactopyranoside (49) (procedure adapted from BeMiller et al[15]):

To a solution of β-D-galactose pentaacetate (3.0 g, 7.7 mmol) in anhydrous nitromethane (30 mL), allyltrimethylsilane (3.7 mL, 23 mmol) and boron trifluoride diethyl etherate (2.8 mL, 23 mmol) were added dropwise and the reaction mixture was stirred for 27 hours. The solvent was evaporated and the product was extracted with CH_2Cl_2, washed with water, saturated $NaHCO_3$ solution, dried over $MgSO_4$ and concentrated. R_f = 0.63 in 1:1 hexanes: EtOAc. Flash column chromatography (3:1 hexanes:EtOAc) afforded an α: β mixture (2.0 g, 70%) as a colourless oil.

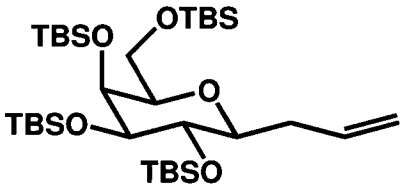

1-*C*-Allyl-2,3,4,6-tetra-*O*-tertbutyldimethylsilyl-β-D-galactopyranoside (51) (prepared according to Ben et al[16]):

To separate the anomeric mixture, (**49**) was de-acetylated to afford (**50**) (95%) and then TBS protected as follows. A solution of (**50**) (0.47 g, 2.3 mmol) in CH_2Cl_2 (20 mL) was cooled to 0 °C. TBSOTf (prepared according to Corey et al[17]) and 2,6-lutidine were added dropwise. The reaction mixture was stirred for 3 hours and monitored by TLC. The product was extracted with CH_2Cl_2 and washed with 10% HCl, saturated $NaHCO_3$, brine, dried over $MgSO_4$ and concentrated. Flash column chromatography (1:1 hexanes:CH_2Cl_2, R_f = 0.63) afforded the product (0.84 g, 55%) as well as the alpha anomer (0.14 g, 9%), both as colourless oils.

^{1}H NMR: (400 MHz, *$CDCl_3$*) δ ppm 5.92 (dddd, *J* = 16.0, 10.3, 7.61, 5.8 Hz, 1H), 5.08-4.98 (m, 2H), 4.08 (s, 1H), 3.78 (t, *J* = 8.7 Hz, 1H), 3.61 (dd, *J* = 6.8, 3.6 Hz, 2H), 3.54 (dd, *J* = 8.9, 1.7 Hz, 1H), 3.31 (t, *J* = 7.0 Hz, 1H), 3.12 (dt, *J* = 9.6, 9.6, 2.3 Hz, 1H), 2.56 (dd, *J* = 14.6, 7.6 Hz, 1H), 2.13-2.03 (m, 1H), 0.90 (dd, *J* = 17.4, 4.4 Hz, 36H), 0.16-0.01 (m, 24H)

^{13}C NMR: (100 MHz, *$CDCl_3$*) δ 136.35, 115.76, 81.34, 78.94, 78.07, 72.12, 71.95, 61.47, 36.35, 27.00, 26.45, 26.07, 25.82, 25.71, 19.33, 18.63, 18.22, 18.09, -2.06, -2.94, -3.26, -3.69, -4.09, -4.56, -5.24, -5.35

MS (ESI): calcd for $C_{37}H_{72}O_5Si_4$ $(M+H)^+$ 661.5, found 661.6.

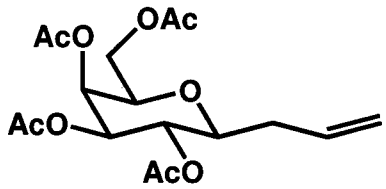

1-*C*-Allyl 2,3,4,6-tetra-*O*-acetyl-β-D-galactopyranoside (52) (procedure adapted from Ben et al[16]):

To a solution of (**51**) (0.30 g, 0.45 mmol) in 25 mL THF, tetrabutylammonium fluoride (0.53 g, 2.04 mmol) was added. The reaction mixture was stirred for 3 hours, at which point dimethylaminopyridine (0.55 g, 4.5 mmol) and acetic anhydride (5 mL) were added. The reaction mixture was stirred for an additional 18 hours. The product was extracted with ethyl acetate, washed with 10% HCl, saturated $NaHCO_3$, water, brine, dried over $MgSO_4$, and concentrated. The product (0.10 g, 60%) was obtained as a colourless oil.

^{1}H NMR (400 MHz, $CDCl_3$) δ ppm 5.82 (tdd, *J* = 17.1, 10.4, 6.8 Hz, 1H), 5.41 (dd, *J* = 3.4, 1.1 Hz, 1H), 5.15-5.06 (m, 3H), 5.00 (dd, *J* = 10.1, 3.4 Hz, 1H), 4.14 (dd, *J* = 11.2, 6.7 Hz, 1H), 4.05 (dd, *J* = 11.3, 6.7 Hz, 1H), 3.85 (dt, *J* = 6.7, 1.2 Hz, 1H), 3.46 (td, *J* = 9.6, 5.8 Hz, 1H), 2.36-2.30 (m, 2H), 2.15 (s, 3H), 2.03 (s, 3H), 2.03 (s, 3H), 1.97 (s, 3H)

^{13}C NMR (100 MHz, $CDCl_3$) δ 170.41, 170.29, 170.22, 169.70, 133.25, 117.38, 77.75, 74.07, 72.20, 69.22, 67.70, 61.56, 36.03, 20.82, 20.70, 20.68, 20.62

All spectral data was consistent with that reported in the literature.[18]

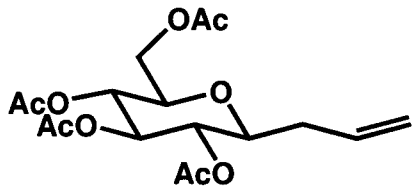

1-*C*-Allyl-2,3,4,6-tetra-*O*-acetyl-β-D-glucopyranoside (55) (procedure adapted from Horton and Miyake[19]:

A round bottom flask containing glucose pentaacetate (2.0 g, 5.1 mmol) was cooled to 0 °C in an ice bath and HBr (13 mL, 30% in AcOH) was added. The solution was stirred for 3 hours, and then diluted with CH_2Cl_2. The product was washed several times with H_2O until pH 7 was reached, and then washed with brine. The organic layers were dried with $MgSO_4$, filtered, and concentrated to give a white solid (**54**) (2.1 g, 97%) that was stored in the freezer under Ar atmosphere overnight and used directly for the next reaction.

Allyl magnesium bromide (50 mL, 1.0 M solution in Et_2O) was diluted with 50 mL THF and heated to 40 °C. A solution of glucosyl bromide (**54**) (1.7 g, 4.2 mmol) was dissolved in 15 THF and cannulated into the Grignard solution slowly (over 1.5 hours). The solution was warmed to 60 °C for 5 hours, and then cooled to room temperature. H_2O (10 mL) and 12 M HCl (5 mL) were slowly added until the solution reached pH 1. The aqueous layer was neutralized with saturated $NaHCO_3$, washed with Et_2O, and dried *in vacuo* overnight. The flask was flushed with N_2 and acetic anhydride (60 mL) and NaOAc (2 g) were added. The solution was warmed to 100 °C, at which point the reaction was violently exothermic and much of the material was ejected from the flask. The remaining product was retained at 100 °C for 3 hours and then cooled to room temperature. The product was concentrated, dissolved in CH_2Cl_2, washed with H_2O,

$NaHCO_3$, and brine, dried over $MgSO_4$, filtered, and concentrated. Flash chromatography (3:1 hexanes:EtOAc) gave the product (0.24 g, 15%).

^{1}H NMR (400 MHz, CDCl3) δ ppm 5.80 (dddd, *J* = 14.9, 13.7, 9.6, 6.8 Hz, 1H), 5.15 (t, *J* = 9.4 Hz, 1H), 5.11-5.03 (m, 3H), 4.90 (t, *J* = 9.6 Hz, 1H), 4.22 (dd, *J* = 12.3, 5.0 Hz, 1H), 4.08 (dd, *J* = 12.3, 2.4 Hz, 1H), 3.61 (ddd, *J* = 10.0, 5.0, 2.4 Hz, 1H), 3.48 (ddd, *J* = 9.8, 7.1, 4.2 Hz, 1H), 2.36-2.22 (m, 2H), 2.06 (s, 3H), 2.01 (s, 3H), 2.00 (s, 3H), 1.98 (s, 3H)

All spectral data was consistent with that reported in the literature.[10]

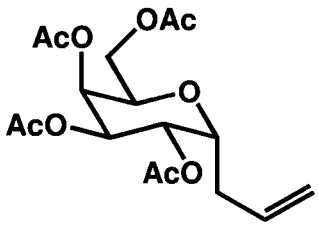

1-*C*-allyl-2,3,4,6-tetra-*O*-acetyl-α-D-galactopyranoside (56):
To a solution of (**14**) (0.50 g, 2.5 mmol) in 15 mL pyridine was added acetic anhydride (15 mL) and dimethylaminopyridine (30 mg). The reaction was stirred under an N_2 atmosphere overnight. The product was diluted with CH_2Cl_2, washed with $CuSO_4$ solution to remove the pyridine, washed with H_2O, dried with $MgSO_4$, filtered, and concentrated *in vacuo*. Flash chromatography (3:1 hexanes:EtOAc) gave pure product (0.70 g, 77%).

^{1}H NMR (400 MHz, CDCl3) δ ppm 5.76 (dt, *J* = 16.9, 6.8 Hz, 1H), 5.42 (s, 1H), 5.25 (ddd, *J* = 12.4, 9.3, 4.1 Hz, 2H), 5.16-5.13 (m, 2H), 4.31 (td, *J* = 9.9, 4.8 Hz, 1H), 4.21 (dd, *J* = 12.5, 9.1 Hz, 1H), 4.10 (q, *J* = 5.3, 4.9 Hz, 2H), 2.52-2.44 (m, 1H), 2.28 (td, *J* = 15.1, 5.6 Hz, 1H), 2.13 (s, 3H), 2.08 (s, 3H), 2.05 (s, 3H), 2.03 (s, 3H)

All data was in accordance with the literature.[10]

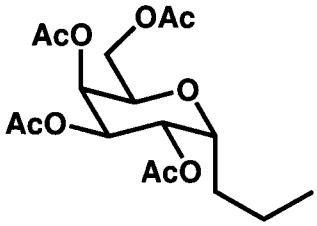

1-*C*-propyl- 2,3,4,6-*O*-acetyl-α-D-galactopyranoside (57):
To a solution of compound (**56**) (0.25 g, 0.67 mmol) in 5 mL EtOAc and 5 mL EtOH was added palladium over carbon (30 mg). N_2 was bubbled through the suspension for 10 minutes, followed by H_2 for 50 minutes. A H_2 balloon was attached and the reaction was left stirring overnight. Thin layer chromatography showed that the reaction was not complete, so 1 mL of a 33% AcOH solution (1 mL glacial acetic acid in 2 mL H_2O) was added and H_2 was bubbled through for 6 hours. TLC indicated that the reaction was complete, and the reaction was filtered over celite and concentrated *in vacuo*. The product was obtained as a white solid (0.12 g, 48%).

^{1}H NMR (400 MHz, *$CDCl_3$):* δ ppm 5.41 (dd, *J* = 3.1, 2.5 Hz, 1H), 5.27 (dd, *J* = 9.5, 5.1 Hz, 1H), 5.20 (dd, *J* = 9.5, 3.3 Hz, 1H), 4.22 (ddd, *J* = 10.9, 8.0, 3.0 Hz, 2H), 4.08 (dd, *J* = 11.1, 5.4 Hz, 1H), 4.05-4.02 (m, 1H), 2.13 (s, 3H), 2.08 (s, 3H), 2.05 (s, 3H), 2.03 (s, 3H), 1.75-1.65 (m, 1H), 1.51-1.25 (m, 3H), 0.95 (t, *J* = 7.2 Hz, 3H)

^{13}C NMR (100 MHz, *$CDCl_3$*): δ ppm 170.56, 170.15, 170.01, 169.89, 71.96, 68.46, 68.04, 67.88, 67.72, 61.56, 27.64, 20.80, 20.72, 20.71, 20.67, 18.53, 13.79

MS (ESI): Calcd for $C_{17}H_{26}O_9$ $(M+Na)^+$ 397.15, found 397.12, $(M+K)^+$ 413.12, found 413.17

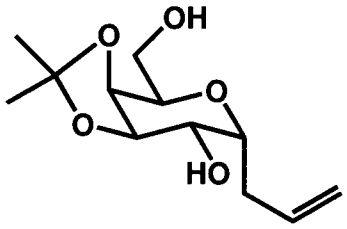

1-C-allyl-3,4-O-isopropylidene-α-D-galactopyranoside (63) (procedure adapted from Czechura et al10):
To a solution of (**14**) (1.1 g, 5.3 mmol) in 20 mL distilled CH_3CN was added 2,2-dimethoxy propane (3.3 mL, 26 mmol) and p-toluene sulfonic acid (50 mg). The reaction was placed on a rotary evaporator set at 230 torr in a 45 ℃ water bath for approximately 1 hour and monitored by TLC. One drop of triethylamine was added to neutralize the reaction, and the product was concentrated *in vacuo.* Flash chromatography (8:1 hexanes:EtOAc, R_f = 0.50) gave an oil (0.80 g, 59%).

^{1}H NMR (400 MHz, *$CDCl_3$*) δ ppm 5.86 (tdd, *J* = 17.2, 10.2, 7.0 Hz, 1H), 5.18 (ddd, *J* = 17.2, 3.3, 1.5 Hz, 1H), 5.11 (tdd, *J* = 10.2, 2.1, 1.1 Hz, 1H), 4.31 (dq, *J* = 7.3, 2.6 Hz, 2H), 4.09-4.04 (m, 2H), 3.84 (tdd, *J* = 10.4, 4.7, 3.0 Hz, 2H), 3.73 (ddd, *J* = 11.5, 9.3, 4.4 Hz, 1H), 2.47-2.36 (m, 2H), 2.17 (dd, *J* = 9.3, 3.2 Hz, 1H), 2.03 (d, *J* = 4.5 Hz, 1H), 1.49 (s, 3H), 1.34 (s, 3H)

All spectral data was in accordance with the literature.[10]

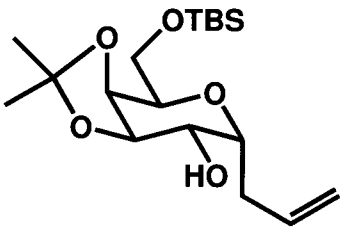

1-*C*-allyl-3,4-*O*-isopropylidene-6-*O*-*tert*-butyldimethylsilyl-α-D-galactopyranoside (64) (procedure adapted from Czechura et al[10]):
To a solution of (**63**) (0.80 g, 3.3) in 12 mL CH_2Cl_2 was added pyridine (12 mL), dimethylaminopyridine (16 mg), and tert-butyldimethylsilyl chloride (0.59 g, 3.9 mmol).

The reaction was stirred overnight, and then diluted with CH_2Cl_2, washed with 10% HCl to remove the pyridine, washed with H_2O, dried over $MgSO_4$, filtered, and concentrated. Flash chromatography (3:1 hexanes:EtOAc, R_f = 0.55) gave the product as an oil (1.0 g, 88%).

^{1}H NMR (400 MHz, *$CDCl_3$*) δ ppm 5.86 (tdd, *J* = 17.1, 10.2, 7.0 Hz, 1H), 5.16 (ddd, *J* = 17.2, 3.4, 1.5 Hz, 1H), 5.09 (ddd, *J* = 10.2, 2.0, 1.0 Hz, 1H), 4.39 (dd, *J* = 7.2, 1.9 Hz, 1H), 4.22 (dd, *J* = 7.2, 3.2 Hz, 1H), 4.01 (ddt, *J* = 6.0, 4.8, 2.1 Hz, 2H), 3.80-3.70 (m, 3H), 2.38-2.34 (m, 2H), 1.95 (d, *J* = 4.2 Hz, 1H), 1.48 (s, 3H), 1.33 (s, 3H), 0.89 (s, 9H), 0.06 (d, *J* = 1.1 Hz, 6H)

All spectral data was consistent with that reported in the literature.[10]

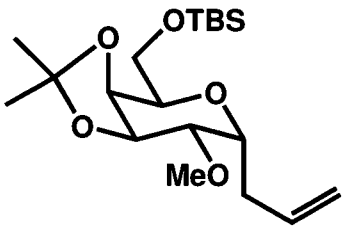

1-*C*-allyl-2-*O*-methyl-3,4-*O*-isopropylidene-6-*O*-tert-butyldimethylsilyl-α-D-galactopyranoside (65) (procedure adapted from Blom et al[5]):

To a suspension of sodium hydride (48 mg, 60% dispersion in mineral oil, 1.2 mmol) in 10 mL DMF at 0 °C was cannulated a solution of (**64**) (0.36 g, 1.0 mmol) in 10 mL DMF. The suspension was stirred for 1 hour to allow deprotonation, and then methyl iodide (0.13 mL, 2.0 mmol) was added and the reaction was allowed to warm to room temperature overnight. The reaction was quenched with saturated NH_4Cl and EtOAc and H_2O was added. The product was washed with water several times to remove the DMF. The product was then extracted with EtOAc, washed with H_2O and brine, dried with $MgSO_4$, filtered, and concentrated. Flash chromatography (3:1 hexanes:EtOAc, R_f = 0.80) gave the product as an oil (0.31 g, 84%).

^{1}H NMR (400 MHz, *$CDCl_3$)* δ ppm 5.87-5.74 (m, 1H), 5.11 (ddd, *J* = 17.1, 3.4, 1.5 Hz, 1H), 5.06 (tdd, *J* = 10.2, 2.0, 1.0 Hz, 1H), 4.37 (dd, *J* = 7.2, 1.7 Hz, 1H), 4.29 (dd, *J* = 7.2, 3.4 Hz, 1H), 4.00 (dt, *J* = 7.4, 7.4, 2.9 Hz, 1H), 3.91 (ddd, *J* = 7.8, 5.8, 1.7 Hz, 1H), 3.73 (ddd, *J* = 15.3, 9.5, 7.0 Hz, 2H), 3.44 (s, 3H), 3.24 (t, *J* = 3.2 Hz, 1H), 2.35 (ddt, *J* = 7.3, 2.3 Hz, 2H), 1.49 (s, 3H), 1.33 (s, 3H), 0.89 (s, 9H), 0.06 (d, *J* = 1.7 Hz, 6H)

^{13}C NMR (100 MHz, *$CDCl_3$)*: δ ppm 134.58, 117.13, 109.01, 78.26, 71.98, 71.34, 70.67, 69.57, 62.43, 58.39, 34.50, 27.08, 25.87, 24.65, 18.31, -5.35, -5.49

MS (ESI): Calcd for $C_{19}H_{36}O_5Si$ $(M+Na)^+$ 395.22, found 395.32, $C_{19}H_{36}O_6Si$ $(M+K)^+$ 411.20, found 411.33

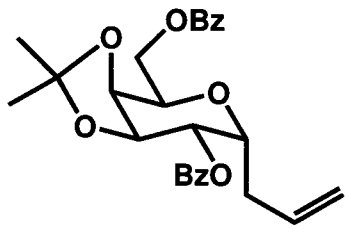

1-*C*-allyl-2,6-*O*-benzoyl-3,4-*O*-isopropylidene-α-D-galactopyranoside (66)

(procedure adapted from Mandal and Misra[20]):

To a solution of (**63**) (1.0 g, 4.9 mmol) in 10 mL dry CH_2Cl_2 was added pyridine (2.0 mL, 24 mmol) and benzoyl chloride (1.7 mL, 15 mmol). An N_2 balloon was attached and the reaction was stirred overnight. The product was diluted with CH_2Cl_2, washed with $CuSO_4$ to remove the pyridine, washed with H_2O, dried with $MgSO_4$, filtered, and concentrated *in vacuo*. Flash chromatography (3:1 hexanes:EtOAc, R_f = 0.57) gave pure product (1.9 g, 84%).

^{1}H NMR (400 MHz, *$CDCl_3$)* δ ppm 8.10-8.03 (m, 4H), 7.70-7.66 (m, 1H), 7.62-7.43 (m, 5H), 5.80 (tdd, *J* = 17.1, 10.2, 7.0 Hz, 1H), 5.32 (t, *J* = 3.1 Hz, 1H), 5.06-5.01 (m, 2H),

4.56 (d, *J* = 6.3 Hz, 2H), 4.47 (dd, *J* = 7.3, 3.2 Hz, 1H), 4.43 (dd, *J* = 7.3, 1.7 Hz, 1H), 4.39 (dd, *J* = 6.2, 1.7 Hz, 1H), 4.34 (ddd, *J* = 7.9, 6.7, 3.0 Hz, 1H), 2.45 (ddd, *J* = 14.4, 7.9, 6.7 Hz, 1H), 2.30 (td, *J* = 14.2, 6.9 Hz, 1H), 1.56 (s, 3H), 1.36 (s, 3H)

^{13}C NMR (100 MHz, *$CDCl_3$*): δ ppm 166.35, 165.30, 134.52, 133.66, 133.49, 133.37, 133.03, 130.56, 130.16, 129.74, 129.69, 129.35, 128.86, 128.61, 128.46, 128.35, 117.83, 110.34, 72.35, 72.11, 70.04, 68.18, 64.48, 35.20, 26.63, 24.62

MS (ESI): Calcd for $C_{26}H_{28}O_7$ $(M+NH_4)^+$ 470.22, found 470.29, $C_{26}H_{28}O_7$ $(M+Na)^+$ 475.17, found 475.24, $C_{26}H_{28}O_7$ $(M+K)^+$ 491.15, found 491.23

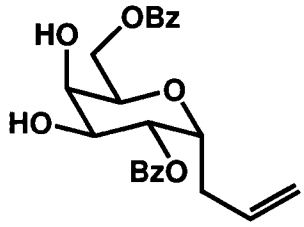

1-*C*-allyl-2,6-*O*-benzoyl-α-D-galactopyranoside (67) (procedure adapted from Mandal and Misra[20]):

A solution of (**66**) (1.9 g, 4.1 mmol) in 40 mL 80% AcOH (v/v in H_2O) was stirred at 80 ºC for 3 hours. The solvent was evaporated off and the product was dried *in vacuo.* Flash chromatography (2:1 hexanes:EtOAc) gave pure product (1.3 g, 72%).

^{1}H NMR (400 MHz, *$CDCl_3$)* δ ppm 8.06 (ddd, *J* = 8.5, 2.8, 1.3 Hz, 4H), 7.62-7.58 (m, 2H), 7.48-7.43 (m, 4H), 5.84-5.73 (m, 1H), 5.39 (dd, *J* = 8.5, 5.2 Hz, 1H), 5.10 (dd, *J* = 17.1, 1.5 Hz, 1H), 4.99 (dd, *J* = 10.3, 1.4 Hz, 1H), 4.67 (dd, *J* = 11.7, 4.9 Hz, 1H), 4.57 (dd, *J* = 11.7, 7.3 Hz, 1H), 4.42-4.39 (m, 1H), 4.16-4.13 (m, 2H), 4.07 (ddd, *J* = 8.5, 4.2, 2.3 Hz, 1H), 3.06 (d, *J* = 5.8 Hz, 1H), 2.84 (d, *J* = 4.3 Hz, 1H), 2.60-2.52 (m, 1H), 2.44-2.38 (m, 1H)

^{13}C NMR (100 MHz, *$CDCl_3$*): δ ppm 166.79, 166.73, 133.59, 133.57, 133.23, 129.84, 129.77, 129.34, 128.55, 128.39, 117.61, 72.84, 71.34, 70.11, 69.35, 68.72, 63.08, 31.23

MS (ESI): Calcd for $C_{23}H_{24}O_7$ $(M+Na)^+$ 435.14, found 435.26, $C_{26}H_{28}O_7$ $(M+K)^+$ 451.12, found 451.24, $C_{26}H_{28}O_7$ $(2M+Na)^+$ 847.29, found 847.50

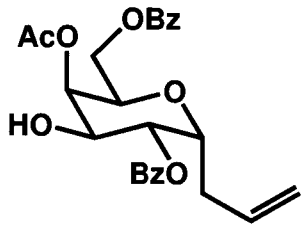

1-*C*-allyl-2,6-*O*-benzoyl-4-*O*-acetyl-α-D-galactopyranoside (68) (procedure adapted from Mandal and Misra[20]):

A solution of (**67**) (0.50 g, 1.2 mmol) in 20 mL 80 benzene was added triethyl ortho acetate (5.6 mL, 31 mL) and *p*-toluene sulfonic acid (8.0 mg, 0.040 mmol). The reaction was stirred at room temperature for 1 hour, and then triethylamine (1.0 mL) was added and the reaction was concentrated *in vacuo*. The residue was dissolved in 60% AcOH (v/v in H_2O) and the reaction was stirred for 20 minutes. The solution was concentrated (water aspirator on rotary evaporator) and CH_2Cl_2 was added. The product was extracted with CH_2Cl_2, washed with saturated $NaHCO_3$ and water, dried with $MgSO_4$, filtered, and concentrated. R_f = 0.23 in 3:1 hexanes:EtOAc. Flash chromatography (1:1 hexanes:EtOAc) gave pure product (0.37 g, 67%).

^{1}H NMR (400 MHz, *$CDCl_3$)* δ ppm 8.08-8.04 (m, 4H), 7.61-7.54 (m, 2H), 7.48-7.42 (m, 4H), 5.77 (tdd, *J* = 17.1, 10.2, 6.8 Hz, 1H), 5.46 (t, *J* = 3.5 Hz, 1H), 5.36 (dd, *J* = 7.2, 3.9 Hz, 1H), 5.08 (ddd, *J* = 17.1, 4.9, 1.6 Hz, 1H), 4.97 (dd, *J* = 10.2, 1.5 Hz, 1H), 4.78 (dd, *J* = 11.5, 8.1 Hz, 1H), 4.45-4.36 (m, 2H), 4.27 (d, *J* = 6.7 Hz, 1H), 2.97 (br s, 1H), 2.55-2.48 (m, 1H), 2.39-2.32 (m, 1H), 2.16 (s, 3H), 2.06 (d, *J* = 13.3 Hz, 1H)

^{13}C NMR (100 MHz, *CDCl$_3$*): δ ppm 170.47, 166.35, 166.16, 133.55, 133.49, 133.44, 133.28, 133.20, 133.11, 129.83, 129.73, 129.71, 129.26, 128.55, 128.34, 117.67, 72.23, 70.25, 69.73, 69.11, 67.65, 61.93, 32.20, 20.87

MS (ESI): Calcd for $C_{25}H_{26}O_8$ $(M+Na)^+$ 477.15, found 477.29, $C_{25}H_{26}O_8$ $(2M+Na)^+$ 931.93, found 931.58

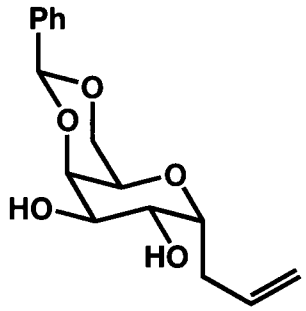

1-*C*-allyl-4,6-*O*-benzylidene acetyl-α-D-galactopyranoside (70) (procedure adapted from Blom et al[5]):

To a solution of compound (**14**) (1.0 g, 4.9 mmol) in 20 mL DMF in a flame-dried flask was added benzaldehyde dimethyl acetal (0.74 mL, 4.9 mmol) and *p*-toluene sulfonic acid (0.080 g, 0.49 mmol). The reaction was stirred under an N_2 atmosphere overnight. The solution was concentrated *in vacuo*, and the product was re-crystallized from MeOH and Et_2O to give white crystals (0.80 g, 56%).

^{1}H NMR (400 MHz, *CDCl$_3$*) δ ppm 7.50 (dd, *J* = 6.6, 3.1 Hz, 2H), 7.41-7.35 (m, 3H), 5.92-5.80 (m, 1H), 5.54 (s, 1H), 5.16-5.08 (m, 2H), 4.31 (ddd, *J* = 11.5, 5.8, 3.6 Hz, 1H), 4.26 (d, *J* = 3.3 Hz, 1H), 4.23 (d, *J* = 1.3 Hz, 1H), 4.15 (dd, *J* = 9.9, 6.0 Hz, 1H), 4.05 (dd, *J* = 12.5, 1.8 Hz, 1H), 3.77 (dd, *J* = 9.9, 3.9 Hz, 1H), 3.59 (d, *J* = 0.8 Hz, 1H), 2.55-2.49 (m, 1H), 2.39-2.32 (m, 1H)

All spectral data was consistent with that reported in the literature.[21]

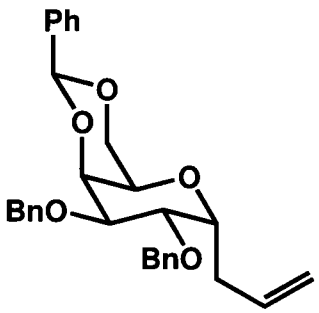

1-*C*-allyl-2,3-*O*-benzyl-4,6-*O*-benzylidene acetyl-α-D-galactopyranoside (71) (procedure adapted from Boulineau and Wei[22]):

A solution of compound (**70**) (0.87 g, 3.0 mmol) in 20 mL DMF in a flame-dried flask was cooled to 0 ºC in an ice bath. Sodium hydride (0.36 g, 8.9 mmol, 60% dispersion in mineral oil) was added and the suspension was stirred for 15 minutes to allow deprotonation. Benzyl bromide (1.1 mL, 8.9 mmol) was added and the solution was allowed to warm to room temperature overnight. The reaction was quenched with saturated NH_4Cl and EtOAc and H_2O were added. The product was washed with water several times to remove the DMF. The product was then extracted with EtOAc, washed with H_2O and brine, dried with $MgSO_4$, filtered, and concentrated. Flash chromatography (gradient: 100% petroleum ether to 1:1 petroleum ether: EtOAc) gave the product (1.1 g, 74%).

^{1}H NMR (400 MHz, *$CDCl_3$*) δ ppm 7.55-7.52 (m, 2H), 7.41-7.25 (m, 13H), 5.87-5.77 (m, 1H), 5.48 (s, 1H), 5.11-5.04 (m, 2H), 4.82 (d, *J* = 11.6 Hz, 2H), 4.77 (d, *J* = 1.9 Hz, 3H), 4.64 (d, *J* = 11.6 Hz, 1H), 4.32 (ddd, *J* = 11.2, 6.0, 3.6 Hz, 1H), 4.25-4.21 (m, 2H), 4.18 (dd, *J* = 12.3, 1.5 Hz, 1H), 3.98 (dd, *J* = 12.4, 1.8 Hz, 1H), 3.76 (dd, *J* = 9.8, 3.6 Hz, 1H), 3.43 (d, *J* = 0.9 Hz, 1H), 2.54-2.48 (m, 1H), 2.37 (ddd, *J* = 15.5, 11.3, 7.4 Hz, 1H)

All spectral data was consistent with that reported in the literature.[21]

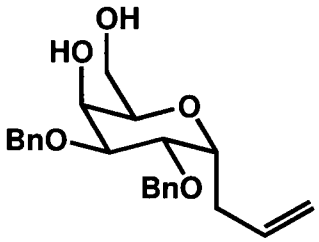

1-*C*-allyl-2,3-*O*-benzyl-α-D-galactopyranoside (72) (procedure adapted from Blom et al[5]):

To a solution of compound (**71**) (1.1 g, 2.2 mmol) in 30 mL MeOH was added (S)-10-camphor sulfonic acid (0.33 g, 1.1 mmol). 10 mL CH_2Cl_2 was added to encourage dissolution of (**71**). The reaction was stirred overnight, and then 1.0 mL triethylamine was added and the solution was concentrated *in vacuo*. Flash chromatography (1:1 hexanes:EtOAc) gave the product (0.36 g, 42%).

^{1}H NMR (400 MHz, *$CDCl_3$)* δ ppm 7.38-7.28 (m, 10H), 5.79 (tdd, *J* = 16.8, 10.2, 6.9 Hz, 1H) 5.10 (tdd, *J* = 7.3, 2.8, 1.7 Hz, 2H), 4.76-4.61 (m, 4H), 4.15 (td, *J* = 10.7, 5.5 Hz, 1H), 4.08 (dd, *J* = 3.4, 1.9 Hz, 1H), 3.98 (dd, *J* = 9.1, 5.7 Hz, 1H), 3.90 (dd, *J* = 11.4, 6.7 Hz, 1H), 3.74-3.66 (m, 3H), 2.45-2.40 (m, 3H)

^{13}C NMR (100 MHz, *$CDCl_3$*): δ ppm 138.25, 137.83, 134.69, 128.56, 128.42, 128.00, 127.79, 127.77, 127.74, 117.11, 77.56, 75.66, 73.36, 73.28, 72.52, 70.57, 68.27, 62.73, 29.92

MS (ESI): Calcd for $C_{23}H_{28}O_5$ $(M+NH_4)^+$ 402.32, found 402.29, $(M+Na)^+$ 407.18, found 407.23, $(2M+Na)^+$ 791.37, found 791.47

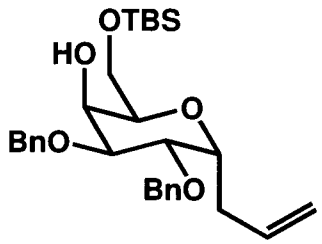

1-*C*-allyl-2,3-*O*-benzyl-6-*O*-*tert*-butyldimethylsilyl-α-D-galactopyranoside (73)

(procedure adapted from Czechura et al[10]):
To a solution of (**72**) (0.36 g, 0.94 mmol) in 15 mL CH_2Cl_2 was added pyridine (15 mL), tert-butyldimethylsilyl chloride (0.17 g, 1.1 mmol), and dimethylamino pyridine (15 mg). The reaction was stirred under an N_2 atmosphere overnight and then diluted with CH_2Cl_2, washed with 10% HCl to remove the pyridine, washed with H_2O, dried over $MgSO_4$, filtered, and concentrated. Flash chromatography (3:1 hexanes:EtOAc, R_f = 0.29) gave the product as an oil (0.43 g, 92%).

^{1}H NMR (400 MHz, *$CDCl_3$):* δ ppm 7.38-7.27 (m, 10H), 5.81 (tdd, *J* = 17.1, 10.2, 6.9 Hz, 1H), 5.12-5.04 (m, 2H), 4.77-4.70 (m, 3H), 4.61 (d, *J* = 11.7 Hz, 1H), 4.11-4.08 (m, 2H), 3.99 (dd, *J* = 9.1, 5.7 Hz, 1H), 3.87 (dd, *J* = 10.0, 6.8 Hz, 1H), 3.69 (ddd, *J* = 12.4, 9.5, 4.4 Hz, 2H), 3.62-3.59 (m, 1H), 2.68 (br s, 1H), 2.42 (t, *J* = 7.2 Hz, 2H), 0.89 (s, 9H), 0.06 (s, 6H)

^{13}C NMR (100 MHz, *$CDCl_3$*): δ ppm 138.44, 138.22, 134.99, 128.47, 128.37, 127.82, 127.72, 127.71, 127.68, 116.71, 78.04, 76.01, 73.68, 73.31, 72.38, 70.70, 67.30, 62.49, 29.93, 25.90, 18.31, -5.41, -5.47

MS (ESI): Calcd for $C_{29}H_{42}O_5Si$ $(M+Na)^+$ 521.27, found 521.43, $(M+K)^+$ 537.24, found 537.42, $(2M+Na)^+$ 1019.55, found 1019.86, $(2M+K)^+$ 1035.52, found 1035.85

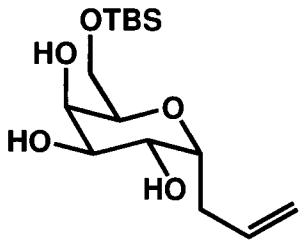

1-*C*-allyl-6-*O*-tert-butyldimethylsilyl-α-D-galactopyranoside (75):
To a solution of compound (**14**) (1.0 g, 4.9 mmol) in 15 mL CH_2Cl_2 was added pyridine (15 mL), *tert*-butyldimethylsilyl chloride (0.89 g, 5.9 mmol), and dimethylaminopyridine (20 mg). The reaction was stirred under an N_2 atmosphere overnight and then diluted with CH_2Cl_2, washed with 10% HCl to remove the pyridine, washed with H_2O, dried over $MgSO_4$, filtered, and concentrated. Flash chromatography (3:1 hexanes:EtOAc) gave the product as an oil (0.95 g, 61%).

^{1}H NMR (400 MHz, *$CDCl_3$*) δ ppm 5.84 (tdd, *J* = 17.0, 10.1, 6.8 Hz, 1H), 5.15-5.07 (m, 2H), 4.19-4.14 (m, 2H), 4.02 (dd, *J* = 8.8, 5.5 Hz, 1H), 3.87 (dq, *J* = 10.6, 4.9 Hz, 2H), 3.69-3.66 (m, 2H), 3.06 (s, 1H), 2.40 (ddd, *J* = 10.6, 7.8, 6.3 Hz, 2H), 2.19 (br s, 1H), 1.57 (br s, 1H), 0.90 (s, 9H), 0.09 (d, *J* = 1.3 Hz, 6H)

^{13}C NMR (100 MHz, *$CDCl_3$*): δ ppm 134.77, 116.90, 74.49, 71.20, 70.53, 69.92, 69.48, 63.58, 29.68, 25.81, 25.74, 25.64, 18.19, -5.52, -5.55

MS (ESI): Calcd for $C_{15}H_{30}O_5Si$ $(M+Na)^+$ 341.18, found 341.28, $(2M+Na)^+$ 659.95, found 659.57

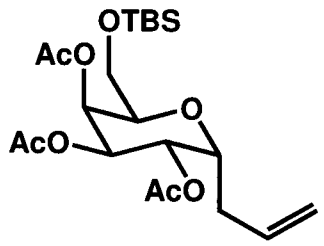

1-*C*-allyl-2,3,4-*O*-acetyl-6-*O*-*tert*-butyldimethylsilyl-α-D-galactopyranoside (76): To a solution of compound (**75**) (0.95 g, 3.0 mmol) in 20 mL pyridine was added acetic anhydride (20 mL) and dimethylaminopyridine (50 mg). The reaction was stirred under an N_2 atmosphere overnight. The product was diluted with CH_2Cl_2, washed with $CuSO_4$ to remove the pyridine, washed with H_2O, dried with $MgSO_4$, filtered, and concentrated *in vacuo*. Flash chromatography (3:1 hexanes:EtOAc, R_f = 0.54) gave pure product (1.2 g, 89%).

^{1}H NMR (400 MHz, *$CDCl_3$):* δ ppm 5.77 (tdd, *J* = 17.0, 10.1, 6.8 Hz, 1H), 5.49 (dd, *J* = 3.3, 1.7 Hz, 1H), 5.32 (dd, *J* = 10.4, 5.8 Hz, 1H), 5.22 (dd, *J* = 10.4, 3.4 Hz, 1H), 5.17-5.07 (m, 2H), 4.33-4.27 (m, 1H), 3.87-3.83 (m, 1H), 3.62 (dd, *J* = 9.8, 6.0 Hz, 1H), 3.53 (dd, *J* = 9.8, 7.5 Hz, 1H), 2.57-2.49 (m, 1H), 2.32-2.25 (m, 1H), 2.12 (s, 3H), 2.04 (s, 3H), 2.00 (s, 3H), 0.85 (s, 9H), 0.01 (d, *J* = 6.1 Hz, 6H)

^{13}C NMR (100 MHz, *$CDCl_3$*): δ ppm 170.19, 170.04, 169.96, 133.63, 117.48, 72.54, 70.05, 68.46, 68.40, 67.92, 60.79, 30.23, 25.74, 20.82, 20.73, 18.13, -5.59, -5.69

MS (ESI): Calcd for $C_{21}H_{36}O_8Si$ $(M+Na)^+$ 467.21, found 467.30, $C_{26}H_{28}O_7$ $(M+K)^+$ 483.18, found 483.29

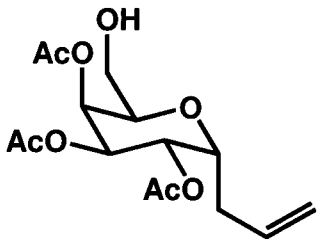

1-*C*-allyl-2,3,4-*O*-acetyl-α-D-galactopyranoside (77) (procedure adapted from Czechura et al[10]):

To a solution of compound (**76**) (0.52 g, 1.0 mmol) in 19 mL distilled THF was added 1 mL glacial acetic acid and tetrabutylammonium fluoride (0.32 g, 1.2 mmol). The reaction was left stirring overnight and then quenched with saturated $NaHCO_3$. The product was extracted with EtOAc, washed with $NaHCO_3$, water, and brine, dried with $MgSO_4$, filtered, and concentrated. Flash chromatography (1:1 hexanes:EtOAc) gave the product as an oil (0.26 g, 79%).

^{1}H NMR (400 MHz, *$CDCl_3$):* δ ppm 5.75 (tdd, *J* = 17.0, 10.2, 6.9 Hz, 1H), 5.41-5.37 (m, 1H), 5.32 (dd, *J* = 10.1, 5.7 Hz, 1H), 5.22 (dd, *J* = 10.1, 3.3 Hz, 1H), 5.12 (t, *J* = 13.5 Hz, 2H), 4.29 (dt, *J* = 10.3, 5.1 Hz, 1H), 3.89 (t, *J* = 6.2 Hz, 1H), 3.65 (dd, *J* = 11.5, 7.3 Hz, 1H), 3.45 (dd, *J* = 11.6, 5.3 Hz, 1H), 2.55-2.47 (m, 1H), 2.29 (td, *J* = 15.0, 5.2 Hz, 1H), 2.13 (s, 3H), 2.04 (s, 3H), 2.00 (s, 3H)

^{13}C NMR (100 MHz, *$CDCl_3$*): δ ppm 170.89, 170.02, 169.91, 133.37, 117.90, 72.09, 70.32, 68.60, 68.34, 68.09, 60.88, 30.44, 20.79, 20.71, 20.68

MS (ESI): Calcd for $C_{15}H_{22}O_8$ $(M+NH_4)^+$ 348.17, found 348.25, $C_{15}H_{22}O_8$ $(M+Na)^+$ 353.12 found 353.19, $C_{25}H_{26}O_8$ $(2M+Na)^+$ 683.65, found 683.40

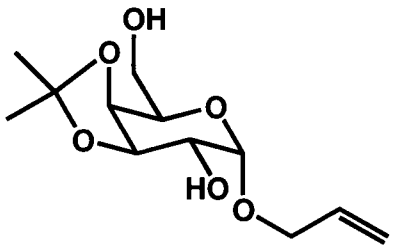

1-*O*-allyl-3,4-*O*-isopropylidene-α-D-galactopyranoside (79):
To a solution of (**34**) (2.0 g, 9.1 mmol) in 40 mL distilled acetonitrile was added 2,2-dimethoxy propane (4.5 mL, 36 mmol) and *p*-toluene sulfonic acid (0.10 g). The reaction was placed on a rotary evaporator set at 230 torr in a 45 °C water bath for approximately 1 hour and monitored by TLC. One drop of triethylamine was added to neutralize the reaction, and the product was concentrated *in vacuo*. Flash chromatography (9:1 hexanes:EtOAc) gave an oil (0.55 g, 23%).

^{1}H NMR (400 MHz, *$CDCl_3$*) δ ppm 5.91 (dddd, *J* = 17.2, 10.4, 6.1, 5.4 Hz, 1H), 5.31 (qd, *J* = 17.2, 1.6 Hz, 1H), 5.23 (ddd, *J* = 10.4, 2.7, 1.3 Hz, 1H), 4.95 (d, *J* = 3.9 Hz, 1H), 4.29-4.23 (m, 3H), 4.11-4.05 (m, 2H), 3.93 (ddd, *J* = 11.8, 6.3, 3.2 Hz, 1H), 3.84-3.78 (m, 2H), 2.36 (d, *J* = 7.0 Hz, 1H), 2.26 (dd, *J* = 9.3, 3.3 Hz, 1H), 1.50 (s, 3H), 1.35 (s, 3H)

All spectra data was in accordance with the literature.[23]

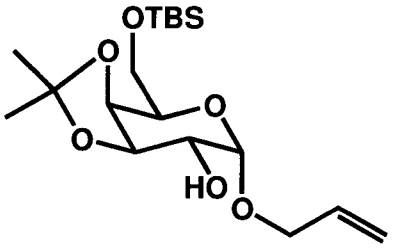

1-*O*-allyl-3,4-*O*-isopropylidene-6-*O*-*tert*-butyldimethylsilyl-α-D-galactopyranoside (80):
To a solution of (**79**) (0.55 g, 2.1) in 10 mL CH_2Cl_2 was added pyridine (10 mL), dimethylaminopyridine (10 mg), and *tert*-butyldimethylsilyl chloride (0.38 g, 2.5 mmol).

The reaction was stirred overnight, and then diluted with CH_2Cl_2, washed with 10% HCl to remove the pyridine, washed with H_2O, dried over $MgSO_4$, filtered, and concentrated. Flash chromatography (3:1 hexanes:EtOAc) gave the product as an oil (0.56 g, 71%).

^{1}H NMR (400 MHz, *$CDCl_3$*) δ ppm 5.92 (dddd, *J* = 16.7, 10.4, 6.2, 5.3 Hz, 1H), 5.29 (qd, *J* = 17.2, 1.6 Hz, 1H), 5.21 (ddd, *J* = 10.4, 2.7, 1.2 Hz, 1H), 4.89 (d, *J* = 3.9 Hz, 1H), 4.29-4.18 (m, 3H), 4.04 (qdd, *J* = 10.6, 6.2, 1.3 Hz, 2H), 3.87-3.76 (m, 3H), 2.23 (d, *J* = 7.4 Hz, 1H), 1.50 (s, 3H), 1.34 (s, 3H), 0.90 (s, 9H), 0.08 (s, 6H)

All spectra data was in accordance with the literature.[24]

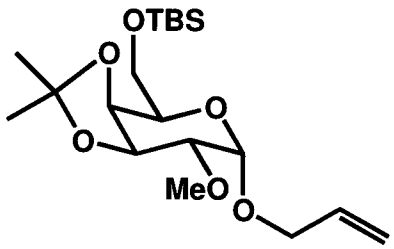

1-*O*-allyl-2-*O*-methyl-3,4-*O*-isopropylidene-6-*O*-*tert*-butyldimethylsilyl-α-D-galactopyranoside (81) (procedure adapted from Blom et al[5]):

To a solution of compound (**80**) (0.56 g, 1.5 mmol) in 20 mL DMF at 0 °C was added sodium hydride (72 mg, 60% dispersion in mineral oil, 1.8 mmol). The suspension was stirred for 1 hour to allow deprotonation, and then methyl iodide (0.19 mL, 3.0 mmol) was added and the reaction was allowed to warm to room temperature overnight. The reaction was quenched with saturated NH_4Cl and concentrated *in vacuo* to remove the DMF (using a water aspirator attached to the rotary evaporator). The product was extracted with EtOAc, washed with H_2O and brine, dried with $MgSO_4$, filtered, and concentrated. Flash chromatography (3:1 hexanes:EtOAc) gave the product as an oil (0.35 g, 49%).

^{1}H NMR (400 MHz, *$CDCl_3$*) δ ppm 5.94 (dddd, *J* = 17.0, 10.4, 6.5, 5.3 Hz, 1H), 5.33-5.20 (m, 2H), 4.97 (d, *J* = 3.6 Hz, 1H), 4.27-4.17 (m, 3H), 4.06-4.01 (ddd, *J* = 6.5, 4.4, 3.3 Hz, 2H), 3.87 (dd, *J* = 10.1, 6.3 Hz, 1H), 3.80 (dd, *J* = 10.1, 6.7 Hz, 1H), 3.51 (s, 3H), 3.36 (dd, *J* = 7.7, 3.6 Hz, 1H), 1.52 (s, 3H), 1.33 (s, 3H), 0.90 (s, 9H), 0.08 (d, *J* = 1.2 Hz, 6H)

^{13}C NMR (100 MHz, *$CDCl_3$*): δ ppm 133.57, 118.22, 109.00, 95.05, 79.49, 75.80, 73.20, 68.16, 68.14, 62.38, 58.56, 28.40, 26.37, 25.83, -5.34, -5.45

MS (ESI): Calcd for $C_{19}H_{36}O_6Si$ $(M+NH_4)^+$ 406.26, found 406.35, $C_{19}H_{36}O_6Si$ $(M+Na)^+$ 411.22, found 411.29

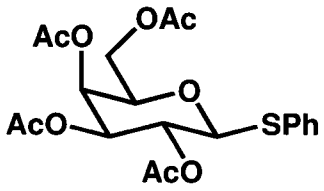

1-thio-phenyl-2,3,4,6-tetra-*O*-acetyl-β-D-galactopyranoside (82) (procedure adapted from Ohlsson and Magnusson[25]):

To a solution of 10 g (26 mmol) of galactose pentaacetate in 40 mL dry CH_2Cl_2 at 0 °C was added benzene thiol (7.3 mL, 72 mmol) followed by dropwise addition of boron trifluoride diethyl etherate (9.0 mL, 712 mmol). The reaction was stirred at room temperature overnight. CH_2Cl_2 was added to dilute the reaction mixture. The mixture was washed three times with 2M NaOH and three times with brine. The CH_2Cl_2 solution was dried with $MgSO_4$, filtered, and concentrated. Purification using flash chromatography (1:1 hexanes:ethyl acetate, R_f = 0.33) yielded a white solid (9.7g, 86% yield).

^{1}H NMR (400 MHz, *$CDCl_3$*) δ ppm 7.53-7.51 (m, 2H), 7.33-7.31 (m, 3H), 5.42 (dd, *J* = 3.3, 0.9 Hz, 1H), 5.24 (t, *J* = 10.0 Hz, 1H), 5.05 (dd, *J* = 10.0, 3.4 Hz, 1H), 4.72 (d, *J* = 10.0 Hz, 1H), 4.20 (dd, *J* = 11.3, 7.0 Hz, 1H), 4.12 (dd, *J* = 11.4, 6.2 Hz, 1H), 3.96-3.93 (m, 1H), 2.12 (s, 3H), 2.10 (s, 3H), 2.05 (s, 3H), 1.97 (s, 3H)

All spectral data was in accordance with the published data.[26]

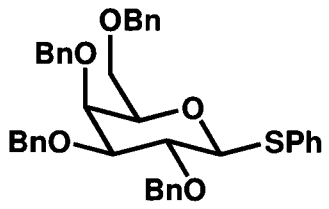

1-thio-phenyl-2,3,4,6-tetra-*O*-benzyl-β-D-galactopyranoside (83) (procedure adapted from Boulineau and Wei[22]):

To a flame-dried flask under N_2 atmosphere was added NaH (1.9 g, 78.3 mmol) and tertbutylammonium iodide (0.48 g, 1.3 mmol). The flask was cooled to 0 °C and 40 mL of DMF was added. A solution of (**45**) (3.6 g, 13 mmol) in 40 mL DMF was cannulated into the NaH suspension. 30 mL DMF was added to restore stirring, and benzyl bromide (9.2 mL, 78 mmol) was added. The reaction mixture was allowed to warm to room temperature overnight. MeOH was added to quench the reaction. A small amount of EtOAc was added and the organic layer was washed several times with water to remove the DMF. The organic layer was dried with $MgSO_4$, filtered, and concentrated *in vacuo*. R_f = 0.83 in 1:1 hexanes: EtOAc. The product was re-crystallized from MeOH to yield white crystals (6.8 g, 82%).

^{1}H NMR (400 MHz, *$CDCl_3$*) δ ppm 7.56-7.54 (m, 2H), 7.38-7.24 (m, 20H), 7.17-7.16 (m, 3H), 4.96 (d, *J* = 11.5 Hz, 1H), 4.78-4.68 (m, 4H), 4.62 (dd, *J* = 15.9, 10.6 Hz, 2H), 4.44 (q, *J* = 11.7 Hz, 2H), 3.98 (d, *J* = 2.6 Hz, 1H), 3.93 (t, *J* = 9.5 Hz, 1H), 3.65-3.58 (m, 4H)

All spectral data was in accordance with the published data.[25]

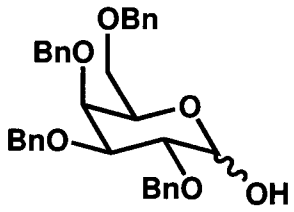

2,3,4,6-Tetra-*O*-benzyl-α,β-D-galactopyranose. (84) (procedure adapted from Bleriot et al[27]):

To a solution of (**83**) (3.0 g, 4.8 mmol) in 100 mL 9:1 acetone:water was added *N*-bromosuccinamide (NBS) (1.7 g, 9.5 mmol). The reaction was stirred for 4 hours with four additional additions of *N*-bromosuccinamide (0.90 g each). The reaction was quenched with saturated $NaHCO_3$ solution. EtOAc was added and the product was extracted with EtOAc and washed with water and brine. The organic layer was dried over $MgSO_4$, filtered, and concentrated. Flash chromatography (2:1 hexanes:EtOAc, R_f = 0.23) yielded the product as a clear colourless oil (anomeric mixture) (2.4 g, 93%).

^{1}H NMR (400 MHz, *$CDCl_3$*) δ ppm 7.39-7.25 (m, 20H), 5.28 (d, *J* = 3.6 Hz, 1H), 4.95-4.90 (m, 2H), 4.84-4.65 (m, 5H), 4.59 (dd, *J* = 11.5, 7.3 Hz, 1H), 4.43 (dd, *J* = 11.9, 6.8 Hz, 3H), 4.16 (t, *J* = 6.3 Hz, 1H), 4.04 (dd, *J* = 9.9, 3.6 Hz, 1H), 3.97 (d, *J* = 2.7 Hz, 1H), 3.89 (t, *J* = 2.8 Hz, 1H), 3.76 (dd, *J* = 9.6, 7.5 Hz, 1H), 3.60-3.47 (m, 3H)

All spectral data was in accordance with the published data.[28]

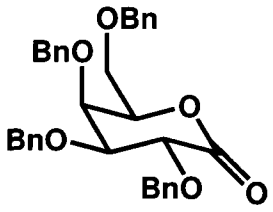

2,3,4,6-Tetra-*O*-benzyl-D-galactonolactone (85) (procedure adapted from Kuzuhara and Fletcher[29]):

Compound (**84**) (1.6 g, 3.0 mmol) was dissolved in 35 mL anhydrous DMSO and stirred for 15 minutes at room temperature. Acetic anhydride (distilled and stored over molecular sieves, 4.6 mL, 49 mmol) was added and the reaction was stirred at room temperature under a nitrogen atmosphere overnight. The product was extracted with CH_2Cl_2 and the organic layer was washed with H_2O, dried over $MgSO_4$, filtered, and concentrated *in vacuo*. R_f = 0.40 in 3:1 hexanes:EtOAc. Flash chromatography (gradient 3:1 to 1:1 hexanes:EtOAc) yielded the product as a clear colourless oil (1.5 g, 90%).

^{1}H NMR (400 MHz, *$CDCl_3$*) δ ppm 7.43-7.22 (m, 20H), 5.18 (d, *J* = 11.0 Hz, 1H), 4.93 (d, *J* = 11.3 Hz, 1H), 4.80-4.67 (m, 3H), 4.61 (d, *J* = 11.3 Hz, 1H), 4.48 (q, *J* = 11.7 Hz, 3H), 4.34 (ddd, *J* = 8.0, 5.6, 1.6 Hz, 1H), 4.16 (t, *J* = 1.9 Hz, 1H), 3.88 (dd, *J* = 9.6, 2.2 Hz, 1H), 3.73-3.64 (m, 2H)

All spectral data was in accordance with the published data.[30]

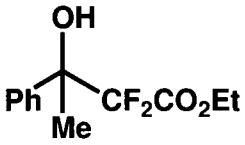

Ethyl 2,2-difluoro-3-hydroxy-3-phenylbutanoate (88):

A suspension of Zn (0.20 g, 3.1 mmol) in 5 mL dry THF was sonicated for 30 minutes to activate the Zn.[31] A solution of acetophenone (0.20 mL, 1.7 mmol) and ethylbromodifluoroacetate (0.34 mL, 2.7 mL) in 3 mL THF was cannulated into the Zn suspension and washed with 2 mL THF. The reaction was sonicated for 1.5 hours and then stirred at room temperature for 3 hours. Saturated NH_4Cl solution was added to quench the reaction. R_f = 0.77 in 1:1 hexanes:EtOAc. The product was extracted with EtOAc and the organic layer was washed with water and brine, dried over $MgSO_4$, filtered, and concentrated *in vacuo* to give an oily solid (0.33 g, 83%).

^{1}H NMR (400 MHz, *$CDCl_3$*) δ ppm 7.53-7.51 (m, 2H), 7.39-7.33 (m, 3H), 4.16 (q, *J* = 7.2 Hz, 1H), 3.13 (s, 1H), 1.75 (t, *J* = 1.5 Hz, 3H), 1.12 (t, *J* = 7.2 Hz, 3H)

All spectral data was in accordance with the published data.[32]

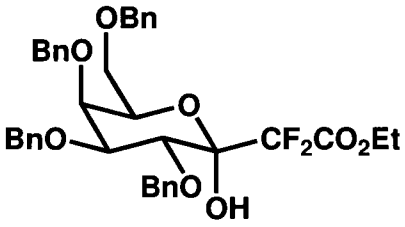

1-α-hydroxy-1-β-(ethyl-2,2,-difluoroacetate)-2,3,4,6,-*O*-benzyl-D-galactopyranoside (89) (procedure adapted from Cuenca et al[33]):

Zn was activated by washing with 2% HCl, H_2O, EtOH, and Et_2O and dried under high vacuum for one hour. To a flame-dried flask under N_2 atmosphere was added activated Zn (1.0 g, 16 mmol), 15 mL THF, and TMSCl to further activate the zinc[34] (0.14 mL,

1.13 mmol). The mixture was stirred for 1 hour. A solution of (**85**) (1.2 g, 2.3 mmol) and ethyl bromodifluoroacetate (0.93 mL, 7.2 mmol) in 15 mL THF was cannulated into the Zn suspension and washed with 5 mL THF. The reaction was refluxed for 30 hours under a nitrogen atmosphere, cooled to room temperature, and quenched with saturated NH_4Cl solution (10 mL). The product was extracted with EtOAc and the organic layer was washed was brine, dried over $MgSO_4$, filtered, and concentrated *in vacuo*. Flash chromatography (3:1 hexanes:EtOAc, R_f = 0.27) yielded the product as a clear colourless oil (1.2 g, 79%).

^{1}H NMR (400 MHz, *$CDCl_3$*) δ ppm 7.35-7.27 (m, 20H), 4.92 (dd, *J* = 16.6, 10.8 Hz, 1H), 4.78-4.68 (m, 3H), 4.58 (d, *J* = 11.5 Hz, 1H), 4.47-4.40 (m, 3H), 4.24-4.15 (m, 3H), 4.12 (m, 1H), 3.99 (dd, *J* = 2.6, 1.0 Hz, 1H), 3.89 (dd, *J* = 9.6, 2.7 Hz, 1H), 3.55 (ddd, *J* = 14.8, 9.2, 6.7 Hz, 2H), 1.20 (t, *J* = 7.1 Hz, 3H)

^{13}C NMR (100 MHz, *$CDCl_3$*) δ ppm 162.81, 138.62, 138.09, 137.79, 137.76, 128.43, 128.39, 128.31, 128.24, 128.18, 127.81, 127.75, 127.77, 127.75, 127.70, 127.52, 127.49, 96.42 (td, J = 13.3, 5.7 Hz), 80.69, 75.30, 74.55, 74.44, 73.57, 73.43, 72.75, 71.22, 68.13, 63.10, 13.77

^{19}F NMR (400 MHz, *$CDCl_3$*) δ ppm -117.72, -118.39, -119.42, -120.11

IR: 350.56, 3064.68, 3029.96, 2875.67, 2867.95, 2840.95, 1751.24, 1496.66, 1452.30, 1365.51, 1311.50, 1209.28, 1145.64, 1099.351027.99, 1010.63, 914.20, 856.34, 734.83, 696.25

MS (ESI): Calcd for $C_{38}H_{40}O_8F_2$ $(M+NH_4)^+$ 680.3, found 680.4, $(M+Na)^+$ 685.3, found 685.4

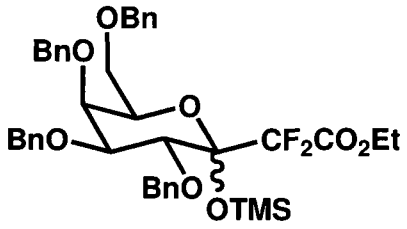

1-α-*O*-trimethylsilyl-1-β-(ethyl-2,2,-difluoroacetate)-2,3,4,6,-*O*-benzyl-D-galactopyranoside (90)

Zn was activated by washing with 2% HCl, H_2O, EtOH, and Et_2O and dried under high vacuum for one hour. To a flame-dried flask under N_2 atmosphere was added activated Zn (0.66 g, 10.2 mmol), 8 mL THF, and TMSCl to further activate the zinc[34] (90 µL, 0.73 mmol). The mixture was stirred for 0.5 hours. A solution of (**85**) (0.78 g, 1.5 mmol) and ethyl bromodifluoroacetate (0.47 mL, 3.6 mmol) in 12 mL THF was cannulated into the Zn suspension and washed with 5 mL THF. The reaction was refluxed for 18 hours under a nitrogen atmosphere, cooled to room temperature, and quenched with saturated NH_4Cl solution (10 mL). The product was extracted with EtOAc and the organic layer was washed was brine, dried over $MgSO_4$, filtered, and concentrated *in vacuo*. Flash chromatography (3:1 hexanes:EtOAc, R_f = 0.62) yielded the product as a clear colourless oil (0.35 g, 33%) as well as compound (**89**) (0.42 g, 44%).

^{1}H NMR (400 MHz, *$CDCl_3$*) δ ppm 7.33-7.24 (m, 20H), 4.95 (d, *J* = 11.3 Hz, 1H), 4.90 (d, *J* = 10.6 Hz, 1H), 4.77-4.69 (m, 3H), 4.55-4.41 (m, 3H), 4.38-4.30 (m, 4H), 4.15 (qd, *J* = 10.7, 7.1 Hz, 1H), 4.04 (qd, *J* = 10.7, 7.1 Hz, 1H), 3.97-3.96 (m, 1H), 3.90 (ddd, *J* = 8.1, 5.2, 0.9 Hz, 1H), 3.81-3.78 (m, 2H), 3.63 (t, *J* = 8.7 Hz, 1H), 3.48 (dd, *J* = 9.1, 5.2 Hz, 1H), 1.34 (t, *J* = 7.2 Hz, 4H), 1.15 (t, *J* = 7.1 Hz, 2H), 1.10 (t, *J* = 7.1 Hz, 3H), 0.25 (s, 6H), 0.16 (s, 9H)

^{13}C NMR (100 MHz, *$CDCl_3$*) δ ppm 162.52, 138.93, 138.75, 138.29, 137.86, 128.42, 128.36, 128.11, 127.98, 127.84, 127.79, 127.66, 127.64, 127.60, 127.36, 127.21, 113.09 (t, *J* = 262.2 Hz), 97.82, 80.31, 75.61, 74.65, 74.48, 74.13, 73.56, 72.67, 70.70, 68.00, 63.21, 63.16, 62.76, 60.32, 14.60, 13.75, 13.69, 1.71, 1.21

MS (ESI): Calcd for $C_{41}H_{48}O_8F_2Si$ $(M+NH_4)^+$ 752.3 found 752.5, $(M+Na)^+$ 757.3, found 757.4

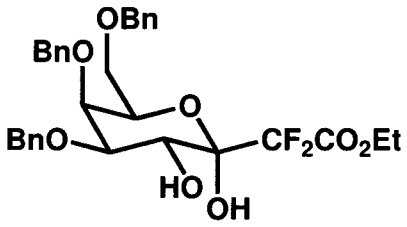

1-α-hydroxy-1-β-(ethyl-2,2,-difluoroacetate)-3,4,6,-*O*-benzyl-D-galactopyranoside (92) (procedure adapted from Turnbull and Moore[35]):

A solution of compound (**89**) (0.16 g, 0.24 mmol) in 30 mL dry CH_2Cl_2 was cooled to 0 ℃. Triethylsilane (0.23 mL, 1.5 mmol) and boron trifluoride diethyl etherate (0.18 mL, 1.5 mmol) were added and the reaction was warmed to room temperature overnight. The reaction was quenched with saturated $NaHCO_3$, extracted with CH_2Cl_2, and washed with water. The product was dried with $MgSO_4$, filtered, and concentrated *in vacuo*. Flash chromatography (3:1 hexanes:EtOAc, R_f = 0.42) gave the product as an oil (0.09 g, 65%).

^{1}H NMR (400 MHz, *$CDCl_3$*): δ ppm 7.37-7.27 (m, 15H), 4.88 (d, *J* = 11.5 Hz, 1H), 4.74 (d, *J* = 11.8 Hz, 1H), 4.67 (d, *J* = 11.8 Hz, 1H), 4.54 (dd, *J* = 14.3, 10.6 Hz, 2H), 4.46 (q, *J* = 11.8 Hz, 2H), 4.28-4.24 (m, 3H), 4.13 (t, *J* = 6.6 Hz, 1H), 3.96 (s, *J* = 1.6 Hz, 1H), 3.73 (dd, *J* = 9.6, 2.7 Hz, 1H), 3.55 (ddd, *J* = 15.2, 9.3, 6.6 Hz, 1H), 1.24 (t, *J* = 7.1 Hz, 3H)

^{13}C NMR (100 MHz, *$CDCl_3$*): δ ppm 163.10, 138.45, 137.91, 137.70, 128.51, 128.40, 128.17, 127.86, 127.81, 127.62, 127.51, 112.03 (dd, *J* = 263.7, 260.0 Hz) 96.33 (dd, *J* = 26.8, 25.1 Hz), 79.83, 74.40, 73.44, 73.06, 72.65, 71.38, 68.25, 67.21, 63.29, 13.73

^{19}F NMR (400 MHz, *$CDCl_3$*): δ ppm -117.01, -117.70, -121.28, -121.97

IR: 3369.41, 2921.96, 2852.52, 1758.96, 1724.24, 1647.10, 1633.59, 1533.30, 1496.66, 1452.30, 1372.22, 1313.43, 1276.79, 1217.00, 1149.50, 1097.42, 1070.42, 1026.06,736.76, 698.28

MS (ESI): Calcd for $C_{31}H_{34}O_8F_2$ $(M+NH_4)^+$ 590.3, found 590.4, $(M+Na)^+$ 595.2, found 595.3

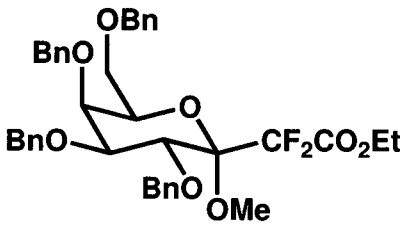

1-α-*O*-methyl-1-β-(ethyl-2,2,-difluoroacetate)-2,3,4,6,-*O*-benzyl-D-galactopyranoside (94) (procedure adapted from Schweizer et al[36]):
To a flame-dried flask under N_2 atmosphere was added NaH (69 mg, 2.9 mmol). The flask was cooled to 0℃ and 20 mL of DMF was added. A solution of (**89**) (1.6 g, 2.4 mmol) in 20 mL DMF was cannulated into the NaH suspension and washed with 20 mL DMF. The reaction was stirred for 30 minutes, and then methyl iodide (0.30 mL, 4.8 mmol) was added. The reaction mixture was allowed to warm to room temperature overnight. Saturated NH_4Cl was added to quench the reaction. A small amount of EtOAc was added and the organic layer was washed several times with water to remove the DMF. The organic layer was dried with $MgSO_4$, filtered, and concentrated *in vacuo*. Flash chromatography (3:1 hexanes:ethyl acetate, R_f = 0.54) yielded the product as a colourless oil (1.3 g, 81%).

^{1}H NMR (400 MHz, *$CDCl_3$*) δ ppm 7.33-7.21 (m, 20H), 4.94 (t, *J* = 11.1 Hz, 2H), 4.68 (d, *J* = 3.9 Hz, 2H), 4.64 (d, *J* = 10.5 Hz, 1H), 4.55 (d, *J* = 11.5 Hz, 1H), 4.51 (d, *J* = 11.7 Hz, 1H), 4.44 (d, *J* = 11.7 Hz, 1H) 4.29 (dd, *J* = 9.5, 1.1 Hz, 1H), 4.07-3.99 (m, 4H), 3.80 (t, *J* = 6.4 Hz, 1H), 3.66-3.63 (m, 2H), 3.52 (d, *J* = 2.4 Hz, 3H), 1.13 (t, *J* = 7.1 Hz, 3H)

^{13}C NMR (100 MHz, *$CDCl_3$*): δ ppm 174.00, 138.72, 138.29, 138.16, 137.87, 128.48, 128.48, 128.24, 128.07, 127.86, 127.73, 127.71, 127.59, 127.52, 127.36, 98.64 (t, *J* = 23.1 Hz), 81.02, 75.44, 74.93, 74.50, 74.08, 73.70, 72.89, 71.89, 68.49, 62.96, 51.33, 13.67

^{19}F NMR (400 MHz, *$CDCl_3$*): δ ppm -111.32, -112.03, -115.14, -115.47

MS (ESI): Calcd for $C_{39}H_{42}O_8F_2$ $(M+NH_4)^+$ 694.3, found 694.5, $(M+Na)^+$ 699.3, found 699.4

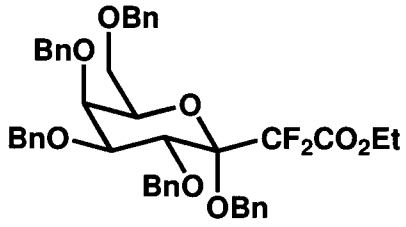

1-α-*O*-benzyl-1-β-(ethyl-2,2,-difluoroacetate)-2,3,4,6,-*O*-benzyl-D-galactopyranoside (95) (procedure adapted from Boulineau and Wei[22]):

To a flame-dried flask under N_2 atmosphere was added NaH (5 mg, 0.22 mmol) and tertbutylammonium iodide (7 mg, 0.018 mmol). The flask was cooled to 0 °C and 10 mL of DMF was added. A solution of compound (**89**) (0.12 g, 0.18 mmol) in 10 mL DMF was cannulated into the NaH suspension and washed with 5 mL DMF. The reaction was stirred for 30 minutes, and then benzyl bromide (43 µL, 0.36 mmol) was added. The reaction mixture was allowed to warm to room temperature overnight. The solvent was removed *in vacuo*, using toluene to co-evaporate. The product was extracted with EtOAc, washed with water and brine, dried with $MgSO_4$, filtered, and concentrated *in vacuo*. R_f = 0.39 in 7:1 hexanes:EtOAc. Flash chromatography (10:1 hexanes:EtOAc) gave the product as an oil (80 mg, 59%).

^{1}H NMR (400 MHz, *$CDCl_3$*) δ ppm 7.34-7.24 (m, 25H), 5.00 (d, *J* = 11.1 Hz, 1H), 4.94 (d, *J* = 11.6 Hz, 1H), 4.97 (dd, *J* = 23.0, 11.3 Hz, 1H), 4.78 (d, *J* = 12.1 Hz, 1H), 4.68-4.55

(m, 4H), 4.45 (q, *J* = 11.8 Hz, 2H), 4.33 (dd, *J* = 9.8, 1.7 Hz, 1H), 4.02 (dd, *J* = 9.8, 2.6 Hz, 1H), 3.96-3.91 (m, 3H), 3.77 (t, *J* = 6.8 Hz, 1H), 3.62 (d, *J* = 6.1 Hz, 2H), 1.06 (t, *J* = 7.2 Hz, 3H)

^{13}C NMR (100 MHz, *$CDCl_3$*): δ ppm 193.29, 138.84, 138.68, 138.28, 137.96, 128.42, 128.40, 128.34, 128.23, 127.99, 127.76, 127.71, 127.67, 127.51, 127.37, 127.21, 127.15, 127.05, 100.01, 80.30, 75.25, 74.39, 74.05, 73.91, 73.51, 72.50, 72.10, 68.58, 62.90,13.63

^{19}F NMR (400 MHz, *$CDCl_3$*): δ ppm -111.66, -112.36, -114.92, -115.62

IR: 3031.89, 2923.88, 2854.45, 1766.67, 1496.66, 1454.23, 1371.29, 1307.65, 1215.07, 1191.93, 1149.50, 1103.21, 1062.70, 1027.99, 916.12, 734.83, 698.18

MS (ESI): Calcd for $C_{45}H_{46}O_8F_2$ $(M+NH_4)^+$ 770.4, found 770.5, $(M+Na)^+$ 775.3, found 775.5

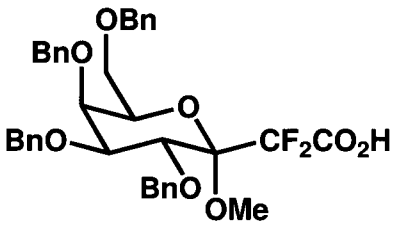

1-α-*O*-methyl-1-β-(2,2,-difluoroacetic acid)-2,3,4,6,-*O*-benzyl-D-galactopyranoside (96):

Compound (**94**) (1.1 g, 1.6 mmol) was dissolved in 60 mL THF. To this solution was added a solution of NaOH (0.13 g, 3.3 mmol) in 6 mL H_2O. The reaction was stirred overnight and then CH_2Cl_2 and 10% HCl were added. The organic layer was washed with 10% HCl, and then the aqueous layer was extracted with CH_2Cl_2. The combined organic fractions were dried with $MgSO_4$, filtered, and concentrated *in vacuo* to give a white solid (0.83 g, 78%). No additional purification was required.

^{1}H NMR (400 MHz, *$CDCl_3$)* δ ppm 8.25 (s, 1H), 7.35-7.27 (m, 20H), 5.02 (s, *J* = 10.5 Hz, 1H), 4.95 (d, *J* = 11.6 Hz, 1H) 4.76-4.69 (m, 3H), 4.58 (d, *J* = 11.6 Hz, 1H), 4.47 (q, *J* = 11.8 Hz, 2H), 4.34 (dd, *J* = 9.9, 2.1 Hz, 1H), 4.06 (dd, *J* = 9.9, 2.6 Hz, 1H), 3.99 (dd, *J* = 2.5, 1.1 Hz, 1H), 3.83-3.81 (m, 1H), 3.63 (d, *J* = 6.4 Hz, 2H), 3.42 (d, *J* = 2.2 Hz, 3H)

^{13}C NMR (100 MHz, *$CDCl_3$*): δ ppm 163.27, 138.23, 137.75, 137.58, 136.62, 128.52, 128.46, 128.33, 128,31, 128.00, 127.89, 127.86, 127.82, 127.70, 127.58, 113.80 (t, *J* = 267.5 Hz), 98.81 (dd, *J* = 25.8, 21.5 Hz), 80.38, 75.79, 75.60, 74.63, 73.98, 73.98, 73.65, 72.86, 72.30, 51.16

^{19}F NMR (400 MHz, *$CDCl_3$*): δ ppm -109.25, -109.97, -111.27, -111.99

MS (ESI): Calcd for $C_{37}H_{38}O_8F_2$ $(M+NH_4)^+$ 666.3, found 666.5, $(M+Na)^+$ 671.1, found 671.4

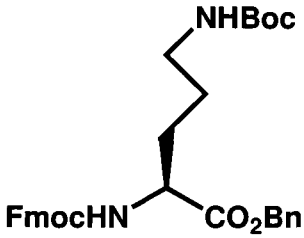

5-*tert*-Butoxycarbonylamino-(2*S*)-(9H-fluoren-ylmethoxycarbonylamino)pentanoic acid benzyl ester [Fmoc-Orn(Boc)-OBn] (98):

To a solution of Fmoc-Orn-Boc (5.0 g., 11 mmol) in 90 mL dry CH_2Cl_2 was added carbonyl diimidazole (2.0 g, 12 mmol). The reaction was stirred for 40 minutes, and then benzyl alcohol (1.1 mL, 11 mmol) was added. The reaction was stirred at room temperature overnight. CH_2Cl_2 and H_2O were added and the product was extracted with CH_2Cl_2, washed with saturated NH_4Cl and H_2O, dried with $MgSO_4$, filtered, and concentrated *in vacuo*. Flash chromatography (25:1 CH_2Cl_2:MeOH) gave the product as a white solid (4.7 g, 78%).

^{1}H NMR (400 MHz, *CD_3OD)* δ ppm 7.79 (d, *J* = 7.5 Hz, 2H), 7.65 (dd, *J* = 7.5, 2.0 Hz, 2H), 7.40-7.27 (m, 10H), 5.14 (q, *J* = 12.3 Hz, 2H), 4.37-4.31 (m, 2H), 4.21-19 (m, 2H), 3.03 (t, *J* = 6.8 Hz, 2H), 1.90-1.81 (m, 1H), 1.72-1.62 (m, 1H), 1.57-1.45 (m, 2H), 1.42 (s, 9H)

All spectral data was in accordance with the literature.[37]

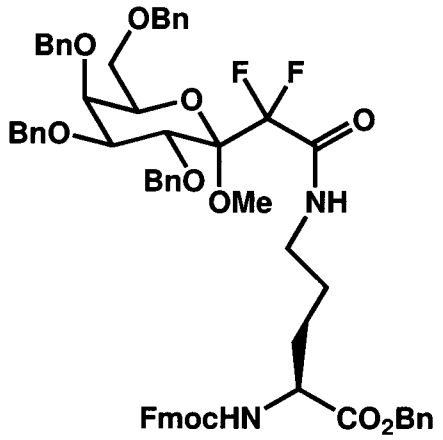

(S-) benzyl-2-(((9H-fluoren-9-yl)methoxy)carbonylamino)-5-(2,2-difluoro-2-((2R,3S,5S)-3,4,5-tris(benzyloxy)-6-(benzyloxymethyl)-2-methoxy-tetrahydro-2-H-pyran-2-yl)acetamido)pentanoate (100) (procedure adapted from Czechura et al[10]): To a solution of fully protected amino acid derivative (**98**) (4.7 g, 8.3 mmol) in 23 mL of CH_2Cl_2, 23 mL of TFA was added. The reaction was stirred for 3 hours and then concentrated under reduced pressure. The syrup was re-dissolved in a 1:1 mixture of toluene and CH_2Cl_2, concentrated, then re-crystallized from diethyl ether to afford a white solid (**99**).

To a solution of (**96**) (0.44 g, 0.68 mmol) in 25 mL dry CH_2Cl_2 was added activated 4Å molecular sieves and HBTU (0.32 g, 0.81 mmol). The reaction was stirred for 15 minutes, and (**99**) (0.55 g, 1.0 mmol) and distilled diisopropylethylamine (0.36 mL, 2.0 mmol) were added. The reaction was stirred at room temperature under an N_2 atmosphere overnight. CH_2Cl_2 and H_2O were added, and the product was extracted with

CH_2Cl_2, washed with H_2O and brine, dried with $MgSO_4$, filtered, and concentrated *in vacuo*. R_f = 0.27 in 95:5 CH_2Cl_2:MeOH. Flash chromatography (95:5 then 98:2 CH_2Cl_2:MeOH) gave the product as an oil (0.47 g, 64%).

^{1}H NMR (400 MHz, *$CDCl_3$)* δ ppm 7.75 (d, *J* = 7.7 Hz, 2H), 7.57 (d, *J* = 7.2 Hz, 2H), 7.40-7.18 (m, 28H), 6.68 (t, *J* = 5.4 Hz, 1H), 5.28 (d, *J* = 8.3 Hz, 1H), 5.18-5.11 (m, 2H), 4.93 (d, *J* = 11.0 Hz, 1H), 4.79 (q, *J* = 10.1 Hz, 2H), 4.72 (q, *J* = 11.6 Hz, 2H), 4.50-4.36 (m, 5H), 4.26-4.18 (m, 2H), 3.93 (d, *J* = 8.6 Hz, 2H), 3.80 (t, *J* = 6.4 Hz, 1H), 3.65 (s, 1H), 3.61-6.54 (m, 2H), 3.48 (d, *J* = 2.7 Hz, 3H), 3.00 (dt, *J* = 12.3, 6.2 Hz, 1H), 2.76 (dt, *J* = 12.7, 6.4 Hz, 1H), 1.63-1.59 (m, 1H), 1.45-1.36 (m, 1H), 1.27-1.11 (m, 3H)

^{13}C NMR (100 MHz, *$CDCl_3$*): δ ppm 171.90, 162.49, 155.90, 143.82, 143.62, 141.27, 138.35, 138.16, 137.92, 137.67, 135.12, 128.60, 128.58, 128.51, 128.45, 128.41, 128.27, 128.14, 128.09, 127.88, 127.77, 127.71, 127.67, 127.56, 127.48, 127.04, 124.99, 124.96, 119.95, 116.76, 114.18 (dd, *J* = 263.4, 260.2 Hz), 111.56, 107.75, 98.36 (dd, *J* = 26.3, 22.4 Hz), 80.49, 76.28, 75.51, 74.64, 74.45, 73.39, 73.17, 71.66, 68.44, 67.22, 66.87, 63.61, 53.48, 51.51, 47.11, 38.82, 29.52, 24.90

^{19}F NMR (400 MHz, *$CDCl_3$*): δ ppm -110.02, -110.81, -112.50, -113.21

MS (ESI): Calcd for $C_{64}H_{64}N_2O_{11}F_2$ $(M+Na)^+$ 1097.4, found 1097.5

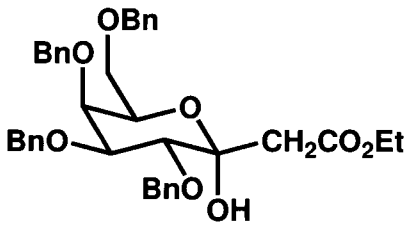

1-α-hydroxyl-1-β-ethyl acetate-2,3,4,6,-*O*-benzyl-D-galactopyranoside (101) (procedure adapted from Schweizer et al[36]):

To a solution of distilled diisopropylamine (0.14 mL, 0.96 mmol) in 10 mL dry THF at 0 °C was added *n*-butyllithium (0.37 mL, 0.88 mmol, 2.4 M solution). The reaction flask was cooled to -78 °C (acetone/dry ice bath) and ethyl acetate (0.14 mL, 1.6 mmol) was added. A solution of (**85**) (0.43 g, 0.80 mmol) in 10 mL dry THF was cannulated into the flask with the pre-formed enolate and washed with 5 mL THF. The reaction was allowed to warm to room temperature under an N_2 atmosphere overnight. Saturated NH_4Cl was added to quench the reaction and the product was extracted with EtOAc, washed with water and brine, dried with $MgSO_4$, filtered, and concentrated *in vacuo*. Flash chromatography (5:1 hexanes:ethyl acetate) gave the product as an oil (70 mg, 14%) and recovered starting material (0.15 g, 35%).

^{1}H NMR (400 MHz, *$CDCl_3$)* δ ppm 7.40-7.28 (m, 20H), 5.40 (d, *J* = 1.4 Hz, 1H), 5.01 (d, *J* = 11.4 Hz, 1H), 4.95 (d, *J* = 11.4 Hz, 1H), 4.77 (d, *J* = 3.6 Hz, 2H), 4.69 (d, *J* = 11.5 Hz, 1H), 4.62 (d, *J* = 11.4 Hz, 1H), 4.46 (q, *J* = 11.8, Hz, 2H), 4.21-4.18 (m, 1H), 4.17-4.05 (m, 4H), 3.81 (dd, *J* = 9.8, 1.3 Hz, 1H), 3.61 (dd, *J* = 9.2, 7.8 Hz, 1H), 3.49 (dd, *J* = 9.3, 5.6 Hz, 1H), 2.84 (d, *J* = 15.6 Hz, 1H), 2.37 (d, *J* = 15.5 Hz, 1H), 1.20 (t, *J* = 7.1 Hz, 3H)

^{13}C NMR (100 MHz, *$CDCl_3$)*: δ ppm 172.54, 138.79, 138.41, 128.54, 128.38, 128.34, 128.32, 128.17, 127.77, 127.75, 127.64, 127.55, 127.50, 97.61, 80.39, 78.33, 75.20, 74.75, 74.64, 73.33, 72.55, 70.11, 68.60, 60.93, 40.53, 13.97

MS (ESI): Calcd for $C_{38}H_{42}O_8F_2$ $(M+NH_4)^+$ 644.3, found 644.5, $(M+Na)^+$ 649.3, found 649.5

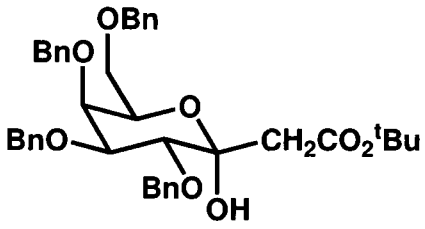

1-α-hydroxyl-1-β-*tert*-butyl acetate-2,3,4,6,-*O*-benzyl-D-galactopyranoside (102) (procedure adapted from Schweizer et al[36]):

To a solution of distilled diisopropylamine (0.79 mL, 5.6 mmol) in 10 mL dry THF at 0 ℃ was added *n*-butyllithium (2.4 mL, 5.4 mmol, 2.3 M solution). The reaction flask was cooled to -78 ℃ (acetone/dry ice bath) and *tert*-butyl acetate (0.75 mL, 5.6 mmol) was added. A solution of (**85**) (0.75 g, 1.4 mmol) in 10 mL dry THF was cannulated into the flask with the pre-formed enolate and washed with 5 mL THF. The reaction was allowed to warm to room temperature under an N_2 atmosphere overnight. Saturated NH_4Cl was added to quench the reaction and the product was extracted with EtOAc, washed with water and brine, dried with $MgSO_4$, filtered, and concentrated *in vacuo*. Flash chromatography (3:1 hexanes:ethyl acetate, R_f = 0.40) gave the product as an oil (0.91 g, 99%).

^{1}H NMR (400 MHz, *$CDCl_3$)* δ ppm 7.37-7.27 (m, 20H), 5.50 (d, *J* = 1.4 Hz, 1H), 4.99 (d, *J* = 11.4 Hz, 1H), 4.94 (d, *J* = 11.4 Hz, 1H), 4.77 (d, *J* = 13.8 Hz, 1H), 4.74 (d, *J* = 13.9 Hz, 1H), 4.69 (dd, *J* = 10.5, 6.6 Hz, 1H), 4.61 (d, *J* = 11.4 Hz, 1H), 4.49 (d, *J* = 11.7 Hz, 1H), 4.41 (d, *J* = 11.7 Hz, 1H), 4.20-4.17 (m, 1H), 4.10 (dd, *J* = 9.9, 2.8 Hz, 1H), 4.03 (dd, *J* = 2.7, 1.2 Hz, 1H), 3.78 (dd, *J* = 9.9, 1.4 Hz, 1H), 3.61 (dd, *J* = 9.3, 7.6 Hz, 1H), 3.48 (dd, *J* = 9.3, 5.6 Hz, 1H), 2.78 (d, *J* = 15.3 Hz, 1H), 2.31 (d, *J* = 15.3 Hz, 1H), 1.40 (s, 9H)

All spectral data was in accordance with the literature.[38]

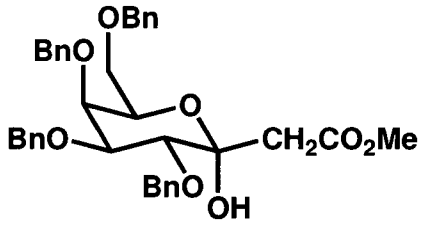

1-α-hydroxyl-1-β-methyl acetate-2,3,4,6,-*O*-benzyl-D-galactopyranoside (103) (procedure adapted from Schweizer et al[36]):

To a solution of distilled diisopropylamine (2.0 mL, 14 mmol) in 40 mL dry THF at 0 °C was added *n*-butyllithium (5.7 mL, 14 mmol, 2.4 M solution). The reaction flask was cooled to -78 °C (acetone/dry ice bath) and methyl acetate (1.1 mL, 14 mmol) was added. A solution of (**85**) (1.9 g, 3.6 mmol) in 20 mL dry THF was cannulated into the flask with the pre-formed enolate and washed with 10 mL THF. The reaction was allowed to warm to room temperature under an N_2 atmosphere overnight. Saturated NH_4Cl was added to quench the reaction and the product was extracted with CH_2Cl_2, washed with water and brine, dried with $MgSO_4$, filtered, and concentrated *in vacuo.* Flash chromatography (3:1 hexanes:ethyl acetate, R_f = 0.27) gave the product as an oil (1.6 g, 72%).

^{1}H NMR (400 MHz, *$CDCl_3$)* δ ppm 7.39-7.27 (m, 20H), 5.30 (d, *J* = 1.3 Hz, 1H), 5.00 (d, *J* = 11.5 Hz, 1H), 4.94 (d, *J* = 11.4 Hz, 1H), 4.77 (d, *J* = 15.6 Hz, 1H), 4.74 (d, *J* = 15.7 Hz, 1H), 4.68 (d, *J* = 11.5 Hz, 1H), 4.61 (d, *J* = 11.5 Hz, 1H), 4.44 (q, *J* = 11.8 Hz, 2H), 4.19-4.16 (m, 1H), 4.10 (dd, *J* = 9.8, 2.7 Hz, 1H), 4.04 (d, *J* = 1.0 Hz, 1H), 3.80 (dd, *J* = 9.8, 1.2 Hz, 1H), 3.63 (s, 3H), 3.59 (dd, *J* = 9.2, 7.9 Hz, 1H), 3.48 (dd, *J* = 9.3, 5.6 Hz, 1H), 2.81 (d, *J* = 15.6 Hz, 1H), 2.35 (d, *J* = 15.6 Hz, 1H)

All spectral data was in accordance with the literature.[36]

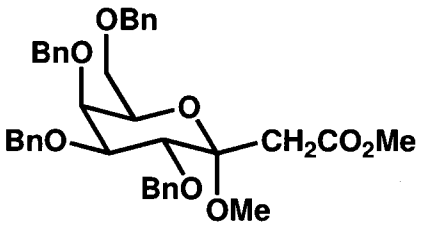

1-α-*O*-methyl-1-β-methyl acetate-2,3,4,6,-*O*-benzyl-D-galactopyranoside (105) (procedure adapted from Schweizer et al[36]):
To a solution of (**103**) (0.79 g, 1.3 mmol) in 30 mL CH_3CN under an N_2 atmosphere was added MeOH (0.78 mL, 19 mmol) and boron trifluoride diethyl etherate (0.81 mL, 6.5 mmol). The reaction was stirred at room temperature for 2 days. The product was extracted with CH_2Cl_2 and washed with H_2O, dried with $MgSO_4$, filtered, and concentrated *in vacuo*. Flash chromatography (3:1 hexanes:EtOAc, R_f = 0.39) yielded a colourless oil (0.69 g, 85%).

^{1}H NMR (400 MHz, *$CDCl_3$)* δ ppm 7.35-7.20 (m, 20H), 4.99 (dd, *J* = 11.3, 4.5 Hz, 2H), 4.76-4.70 (m, 3H), 4.55 (d, *J* = 11.6 Hz, 1H), 4.46 (q, *J* = 11.8 Hz, 2H), 4.35 (d, *J* = 9.9 Hz, 1H), 4.05 (dd, *J* = 9.8, 2.5 Hz, 1H), 3.99 (s, 1H), 3.76 (t, *J* = 6.6 Hz, 1H), 3.62-3.52 (m, 2H), 3.48 (s, 3H), 3.29 (s, 3H), 2.84 (d, *J* = 13.8 Hz, 1H), 2.72 (d, *J* = 13.7 Hz, 1H)

^{13}C NMR (100 MHz, *$CDCl_3$*): δ ppm 169.31, 139.12, 138.56, 138.48, 138.00, 128.40, 128.39, 128.34, 128.12, 127.75, 127.72, 127.53, 127.49, 127.43, 127.39, 127.27, 100.41, 80.81, 78.00, 75.44, 74.57, 74.25, 73.52, 72.58, 70.67, 68.75, 51.65, 48.40, 37.84

MS (ESI): Calcd for $C_{38}H_{42}O_8$ $(M+NH_4)^+$ 644.3, found 644.4, $(M+Na)^+$ 649.3, found 649.4

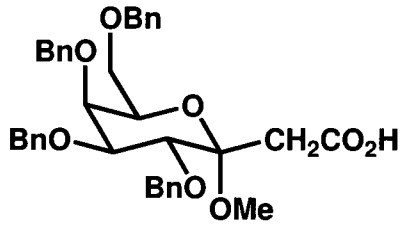

1-α-*O*-methyl-1-β-acetic acid-2,3,4,6,-*O*-benzyl-D-galactopyranoside (106) :

(procedure adapted from Bastiaans et al[39]):

Compound (**105**) (0.69 g, 1.0 mmol) was dissolved in 20 mL THF and 5 mL MeOH. To this solution was added a solution of LiOH (70 mg, 3.1 mmol) in 5 mL H_2O. The reaction was stirred overnight and then CH_2Cl_2 and 10% HCl were added. The organic layer was washed with 10% HCl, and then the aqueous layer was extracted with CH_2Cl_2. The combined organic fractions were dried with $MgSO_4$, filtered, and concentrated *in vacuo* to give a white solid (0.62 g, 99%). No additional purification was required.

^{1}H NMR (400 MHz, *$CDCl_3$)* δ ppm 7.35-7.25 (m, 20H), 4.97 (dd, *J* = 11.2, 3.5 Hz, 2H), 4.75 (d, *J* = 11.8 Hz, 3H), 4.57 (d, *J* = 11.6 Hz, 1H), 4.45 (q, *J* = 11.8 Hz, 2H), 4.13 (d, *J* = 9.8 Hz, 1H), 4.04 (dd, *J* = 9.8, 2.6 Hz, 1H), 3.97 (d, *J* = 1.5 Hz, 1H), 3.84 (t, *J* = 6.4 Hz, 1H), 3.56-3.53 (m, 2H), 3.28 (s, 3H), 2.86 (d, *J* = 15.9 Hz, 1H), 2.78 (d, *J* = 15.9 Hz, 1H)

^{13}C NMR (100 MHz, *$CDCl_3$)*: δ ppm 169.93, 138.42, 138.10, 137.67, 137.06, 128.92, 128.51, 128.47, 128.44, 128.30, 128.07, 127.88, 127.79, 127.77, 127.75, 127.62, 127.55, 99.67, 80.36, 78.43, 75.97, 74.57, 74.32, 73.59, 72.79, 71.30, 68.59, 48.97, 39.93

MS (ESI): Calcd for $C_{37}H_{40}O_8$ $(M+Na)^+$ 635.3, found 635.4

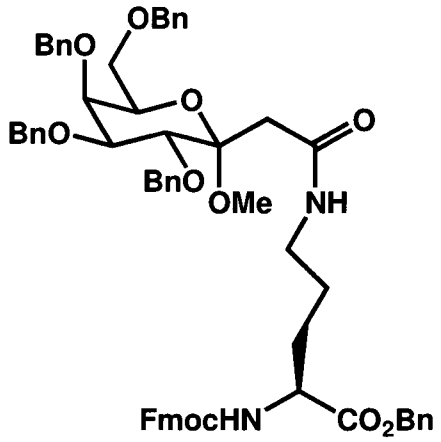

(S-) benzyl-2-(((9H-fluoren-9-yl)methoxy)carbonylamino)-5-(2-((2R,3S,5S)-3,4,5-tris(benzyloxy)-6-(benzyloxymethyl)-2-methoxy-tetrahydro-2-H-pyran-2-yl)acetamido)pentanoate (107) (procedure adapted from Czechura et al[10]):
To a solution of (**106**) (0.34 g, 0.56 mmol) in 20 mL dry CH_2Cl_2 was added activated 4Å molecular sieves and HBTU (0.26 g, 0.67 mmol). The reaction was stirred for 15 minutes, and (**99**) (0.45 g, 0.83 mmol) and distilled diisopropylethylamine (0.29 mL, 1.7 mmol) were added. The reaction was stirred at room temperature under an N_2 atmosphere overnight. CH_2Cl_2 and H_2O were added, and the product was extracted with CH_2Cl_2, washed with H_2O and brine, dried with $MgSO_4$, filtered, and concentrated *in vacuo*. R_f = 0.40 95:5 CH_2Cl_2:MeOH. Flash chromatography (95:5 then 98:2 CH_2Cl_2:MeOH) gave the product as an oil (0.52 g, 91%).

^{1}H NMR (400 MHz, *$CDCl_3$)* δ ppm 7.75 (d, *J* = 7.5 Hz, 2H), 7.58 (dd, *J* = 6.6, 4.91 Hz, 2H), 7.40-7.17 (m, 28H), 6.88 (t, *J* = 5.6 Hz, 1H), 5.32-5.29 (m, 1H), 5.14 (s, 2H), (d, *J* = 10.6 Hz, 1H), 4.84 (d, *J* = 10.5 Hz, 1H), 4.74 (d, *J* = 1.9 Hz, 2H), 4.69 (d, *J* = 10.6 Hz, 1H), 4.49-4.33 (m, 4H), 4.33-4.18 (m, 3H), 4.04 (d, *J* = 9.4 Hz, 1H), 3.95 (d, *J* = 10.1 Hz, 2H), 3.82 (t, *J* = 6.4 Hz, 1H), 3.57 (quintet, *J* = 9.2 Hz, 2H), 3.21 (s, 3H), 3.04-3.02 (m, 1H), 2.83 (d, *J* = 15.8 Hz, 1H), 2.71 (d, *J* = 15.8 Hz, 1H), 2.53-2.51 (m, 1H), 1.63-1.58 (m, 3H), 1.41-1.31 (m, 1H), 1.22-1.12 (m, 21H)

^{13}C NMR (100 MHz, *$CDCl_3$)*: δ ppm 172.10, 168.86, 155.93, 143.92, 143.72, 141.29, 141.27, 138.47, 138.33, 137.78, 137.72, 135.27, 128.84, 128.62, 128.49, 128.46, 128.34, 128.28, 128.25, 128.24, 127.91, 127.779, 127.74, 127.70, 127.67, 127.52,

127.07, 125.14, 125.05, 100.32, 80.43, 77.80, 76.11, 74.80, 73.50, 72.86, 70.61, 68.61, 67.14, 66.99, 53.86, 48.46, 47.13, 40.53, 38.54, 29.61, 25.62

MS (ESI): Calcd for $C_{64}H_{66}N_2O_{11}$ $(M+Na)^+$ 1061.5, found 1061.5

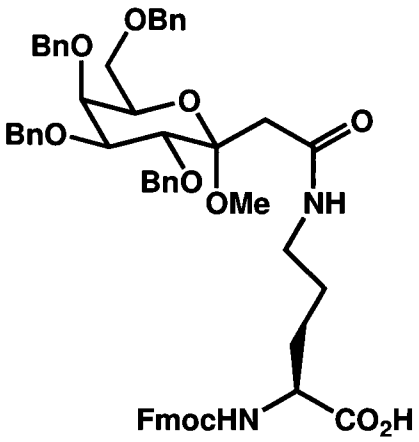

(S-)-2-(((9H-fluoren-9-yl)methoxy)carbonylamino)-5-(2-((2R,3S,5S)-3,4,5-tris(benzyloxy)-6-(benzyloxymethyl)-2-methoxy-tetrahydro-2-H-pyran-2-yl)acetamido)pentanoate (108) (procedure adapted from Kaul et al[40]):
To a solution of (**107**) (0.30 g, 0.29 mmol) in 35 mL isopropanol was added a solution of NaOH (0.16 g, 4.0 mmol to generate a 0.08 M solution upon dilution) and $CaCl_2$ (3.7 g, 33 mmol to generate a 0.66 M solution upon dilution) in 15 mL H_2O. The reaction was left stirring overnight. EtOAc, H_2O, and 10% HCl were added and the layers were separated. The aqueous layer was acidified with 10% HCl and extracted with EtOAc. The combined organic layers were washed with brine, dried with $MgSO_4$, filtered, and concentrated *in vacuo*. Preparative thin layer chromatography (70:2.5:1.25:1.25 v/v/v/v EtOAc, CH_3CN, MeOH, H_2O, R_f = 0.64) gave give a white solid (0.30 g, 100%).

^{1}H NMR (400 MHz, *acetone-d6)* δ ppm 7.85 (d, *J* = 7.6 Hz, 2H), 7.71 (dd, *J* = 7.3, 2.9 Hz, 2H), 7.44-7.20 (m, 25H), 7.05 (t, *J* = 5.1 Hz, 1H), 5.09-4.83 (m, 3H), 4.76 (dd, *J* = 11.2, 3.0 Hz, 2H), 4.64 (d, *J* = 10.8 Hz, 2H), 4.54 (s, 2H), 4.36-4.16 (m, 5H), 4.04 (dd, *J* = 9.9, 2.5 Hz, 1H), 3.90 (t, *J* = 6.3 Hz, 1H), 3.70 (ddd, *J* = 20.7, 9.5, 6.3 Hz, 2H), 3.21 (s,

3H), 3.12 (td, J = 13.3, 6.3 Hz, 1H), 2.95-2.85 (m, 2H), 2.62 (d, J = 14.6 Hz, 2H), 1.79-1.75 (m, 1H), 1.62-1.56 (m, 1H), 1.48-1.41 (m, 2H)

^{13}C NMR (100 MHz, *acetone-d6*): δ ppm 173.09, 170.00, 168.47, 141.23, 139.23, 139.10, 138.67, 128.28, 128.23, 128.12, 128.07, 128.03, 127.66, 127.51, 127.48, 127.35, 127.23, 127.11, 126.49, 125.38, 125.33, 100.62, 80.31, 78.04, 75.24, 74.99, 74.26, 72.84, 71.88, 70.98, 69.14, 66.31, 47.46, 47.16, 40.42, 38.41, 26.09

MS (ESI): Calcd for $C_{57}H_{60}N_2O_{11}$ $(M+Na)^+$ 971.4, found 971.4

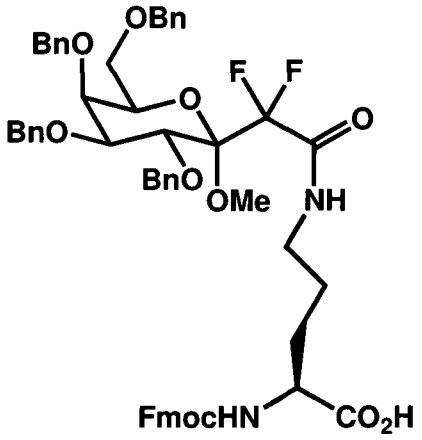

(S)-2-(((9H-fluoren-9-yl)methoxy)carbonylamino)-5-(2,2-difluoro-2-((2R,3S,5S)-3,4,5-tris(benzyloxy)-6-(benzyloxymethyl)-2-methoxy-tetrahydro-2H-pyran-2-yl)acetamido)pentanoic acid (109) (procedure adapted from Kaul et al[40]):
To a solution of (**100**) (0.27 g, 0.25 mmol) in 35 mL isopropanol was added a solution of NaOH (0.16 g, 4.0 mmol to generate a 0.08 M solution upon dilution) and $CaCl_2$ (3.7 g, 33 mmol to generate a 0.66 M solution upon dilution) in 15 mL H_2O. The reaction was left stirring overnight. EtOAc, H_2O, and 10% HCl were added and the layers were separated. The aqueous layer was acidified with 10% HCl and extracted with EtOAc. The combined organic layers were washed with brine, dried with $MgSO_4$, filtered, and concentrated *in vacuo*. Preparative thin layer chromatography (70:10:5:5 v/v/v/v EtOAc, CH_3CN, MeOH, H_2O, R_f = 0.71) gave a pink solid (0.20 g, 80%).

^{1}H NMR (400 MHz, *acetone-d6)* δ ppm 7.85 (d, *J* = 7.5 Hz, 2H), 7.69 (t, *J* = 7.0 Hz, 2H) 7.44-7.20 (m, 25H), 4.97 (d, *J* = 11.3 Hz, 1H), 4.84 (td, *J* = 10.5, 8.2 Hz, 3H), 4.72 (d, *J* = 11.8 Hz, 1H), 4.64 (d, *J* = 12.0 Hz, 2H), 4.54 (q, *J* = 12.0 Hz, 2H), 4.30-4.18 (m, 5H), 4.03 (ddd, *J* = 13.4, 7.4, 4.0 Hz, 1H), 3.93 (t, *J* = 6.3 Hz, 1H), 3.73-3.66 (m, 2H), 3.47 (s, 3H), 1.82-1.77 (m, 1H), 1.65-1.48 (m, 4H), 1.29-1.19 (m, 2H)

^{13}C NMR (100 MHz, *acetone-d6*): δ ppm 173.43, 164.07, 158.00, 146.08, 145.93, 143.07, 140.06, 140.99, 140.69, 140.47, 130.12, 130.03, 129.75, 129.70, 129.66, 129.50, 129.47, 129.40, 129.34, 129.28, 128.93, 127.15, 127.07, 121.78, 116.79 (dd, *J* = 264.7, 262.3 Hz), 100.19 (t, *J* = 22.7 Hz), 82.39, 77.81, 76.45, 76.41, 76.24, 76.14, 74.76, 74.04, 73.77, 70.72, 70.02, 68.12, 65.51, 55.77, 52.56, 52.53, 48.98, 40.60, 27.27, 23.00, 22.98

^{19}F NMR (400 MHz, *acetone-d6*): δ ppm -109.66, -110.38, -112.54, -113.25

MS (ESI): Calcd for $C_{57}H_{58}N_2O_{11}F_2$ $(M+NH_4)^+$ 1002.4, found 1002.5, $(M+Na)^+$ 1007.4, found 1007.4

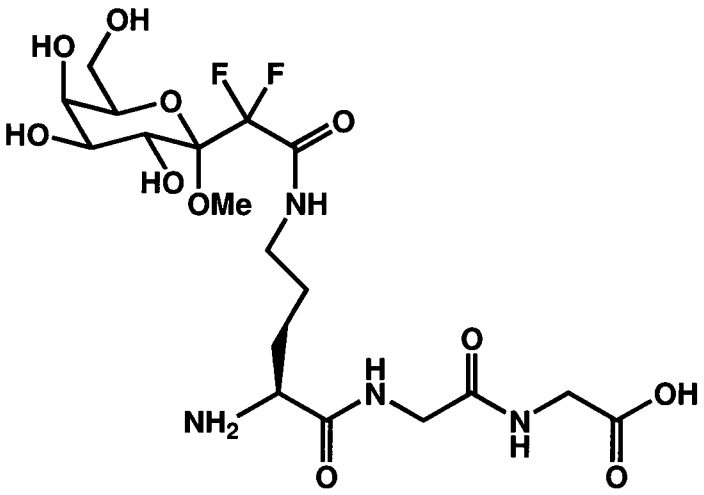

This polypeptide was prepared by linear solid-phase synthesis starting from Fmoc-Gly-Wang resin with loading capacity of 0.6-0.65 mmol/g. The resin was first swollen with DMF for 1 hr. A solution of 20% piperidine in DMF was added and the reaction was stirred for 2 hours. The resin was washed with DMF. Kaiser and TNBS tests were

positive. The beads were washed three times with DMF. For the coupling reaction performed with Fmoc-Gly-OH, a premixed solution of Fmoc-Gly-OH (94 mg, 5.0 eq), HBTU (143 mg, 1.2 eq.), HOBT (43 mg, 1.0 eq.) and DIPEA (0.11 mL, 2.0 eq.) in DMF was added to the solid-phase synthesizer. The coupling reaction was run for 1 hour, and then the solution was drained. The addition of the premixed solution of Fmoc-Gly-OH, HBTU, and DIPEA was repeated and stirred for 1 hour. At this time, negative results were obtained for the Kaiser and TNBS tests. The beads were washed with DMF, re-suspended in DMF, and left stirring overnight. The beads were treated with a 20% solution of piperidine for 30 minutes. The solution was drained and the beads were again treated with 20% piperidine in DMF for 30 minutes before draining and washing with DMF. Kaiser and TNBS tests were positive. For the coupling reactions performed with building block (**109**), a premixed solution of (**109**) (0.10 g, 1.6 eq.), HBTU (47 mg, 1.2 eq.), HOBT (14 mg, 1.0 eq.) and DIPEA (36 µL, 2 eq.) in DMF was added to the solid-phase synthesizer. The reaction mixture was allowed to stir for 24 hours until negative Kaiser and TNBS test results were obtained. Following the last coupling reaction, the Fmoc protecting group was removed with a solution of 20% piperidine in DMF. The resin was washed successively with DMF and CH_2Cl_2, and dried for 2 hours. The resin was treated with 50% TFA in a solution of CH_2Cl_2 for 45 minutes, drained and treated with a 50% solution of TFA in CH_2Cl_2 for 45 minutes. The solution was filtered and the resin was washed with CH_2Cl_2. All filtrate was collected and concentrated under reduced pressure to give (**110**). This product was then dissolved in a 3:1:1 solution of AcOH:THF:H_2O. Palladium over carbon was added and N_2 was bubbled through for 15 minutes. H_2 was bubbled through the solution for 4.5 hours and then an H_2 balloon was attached and the reaction was left stirring overnight. The palladium was removed by filtering over Celite, and the filtrate was concentrated to give a white solid (**111**).

^{1}H NMR (400 MHz, *CD_3OD*) δ ppm 7.98 (s, 1H), 3.14 (m, 3H), 3.00 (s, 3H), 2.86 (s, 3H), 1.99 (s, 7H), 1.79 (td, J = 11.3, 5.7 Hz, 3H), 1.70 (dd, J = 10.4, 5.4 Hz, 1H), 1.34 (m, 2H), 0.90 (t, J = 6.8 Hz, 1H)

MS (ESI): Calcd for $C_{18}H_{31}O_{11}N_4F_2$ $(M+H)^+$ 517.2, found 517.4

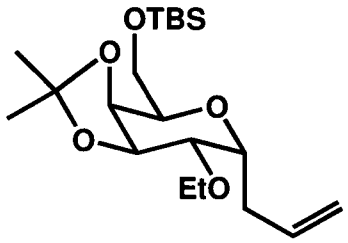

1-*C*-allyl-2-*O*-ethyl-3,4-*O*-isopropylidene-6-*O*-*tert*-butyldimethylsilyl-α-D-galactopyranoside (112)

To a solution of compound (**64**) (0.31 g, 0.87 mmol) in 20 mL DMF at 0 ºC was added tert butylammonium iodide (32 mg, 0.087 mmol) and sodium hydride (42 mg, 60% dispersion in mineral oil, 1.0 mmol). The suspension was stirred for 1 hour to allow deprotonation, and then bromoethane (0.13 mL, 1.7 mmol) was added and the reaction was allowed to warm to room temperature overnight. The reaction was quenched with saturated NH_4Cl and EtOAc and H_2O was added. The product was washed with water several times to remove the DMF. The product was then extracted with EtOAc, washed with H_2O and brine, dried with $MgSO_4$, filtered, and concentrated. R_f = 0.74 in 3:1 petroleum ether:EtOAc. Flash chromatography (3:1 hexanes:EtOAc) gave the product as an oil (0.20 g, 60%) and recovered starting material (50 mg, 16%).

^{1}H NMR (400 MHz, *$CDCl_3$)* δ ppm 5.82-5.74 (m, 1H), 5.10 (ddd, *J* = 17.2, 3.5, 1.5 Hz, 1H), 5.05 (tdd, *J* = 10.2, 2.2, 1.1 Hz, 1H), 4.37 (dd, *J* = 7.2, 1.7 Hz, 1H), 4.28 (dd, *J* = 7.2, 3.3 Hz, 1H), 3.99 (dt, *J* = 7.3, 2.8 Hz, 1H), 3.94 (ddd, *J* = 7.9, 5.8, 1.7 Hz, 1H), 3.77-3.67 (m, 3H), 3.48 (qd, *J* = 9.3, 7.0 Hz, 1H), 3.33 (t, *J* = 3.1 Hz, 1H), 2.38-2.33 (m, 2H), 1.48 (s, 3H), 1.33 (s, 3H), 1.20 (t, *J* = 7.0 Hz, 3H), 0.89 (s, 9H), 0.06 (d, *J* = 1.6 Hz, 6H)

^{13}C NMR (100 MHz, *$CDCl_3$*): δ ppm 134.73, 117.00, 108.97, 76.34, 72.00, 71.86, 70.74, 69.57, 66.06, 62.48, 34.78, 27.05, 25.90, 24.63, 18.36, 15.56, -5.32, -5.45

MS (ESI): Calcd for $C_{20}H_{38}O_5Si$ $(M+Na)^+$ 409.24, found 409.19, $(M+K)^+$ 425.21, found 425.18

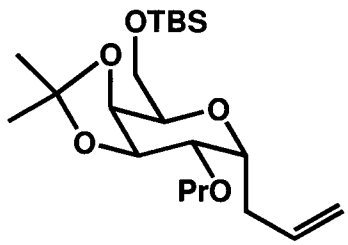

1-*C*-allyl-2-*O*-propyl-3,4-*O*-isopropylidene-6-*O*-*tert*-butyldimethylsilyl-α-D-galactopyranoside (113)

To a solution of compound (**64**) (0.26 g, 0.73 mmol) in 20 mL DMF at 0 ºC was added tert butylammonium iodide (27 mg, 0.073 mmol) and sodium hydride (35 mg, 60% dispersion in mineral oil, 0.87 mmol). The suspension was stirred for 1 hour to allow deprotonation, and then bromopropane (0.13 mL, 1.5 mmol) was added and the reaction was allowed to warm to room temperature overnight. The reaction was quenched with saturated NH_4Cl and EtOAc and H_2O was added. The product was washed with water several times to remove the DMF. The product was then extracted with EtOAc, washed with H_2O and brine, dried with $MgSO_4$, filtered, and concentrated. Flash chromatography (3:1 hexanes:EtOAc) gave the product as an oil (0.14 g, 48%).

^{1}H NMR (400 MHz, *$CDCl_3$)* δ ppm 5.79 (tdd, *J* = 17.1, 10.2, 7.0 Hz, 1H), 5.09 (dd, *J* = 17.2, 1.7 Hz, 1H), 5.05 (dd, *J* = 10.2, 0.9 Hz, 1H), 4.37 (dd, *J* = 7.3, 1.5 Hz, 1H), 4.29 (dd, *J* = 7.3, 3.2 Hz, 1H), 3.99 (dt, *J* = 7.3, 2.8 Hz, 1H), 3.94 (ddd, *J* = 7.8, 5.9, 1.6 Hz, 1H), 3.77-3.70 (m, 2H), 3.59 (td, *J* = 9.0, 6.5 Hz, 1H), 3.38 (td, *J* = 9.0, 6.5 Hz, 1H), 3.32 (t, *J* = 3.0 Hz, 1H), 2.37-2.33 (m, 2H), 1.58 (dd, *J* = 14.0, 6.8 Hz, 2H), 1.48 (s, 3H), 1.33 (s, 3H), 0.92 (t, *J* = 7.1 Hz, 3H), 0.89 (s, 9H), 0.06 (d, *J* = 1.6 Hz, 6H)

^{13}C NMR (100 MHz, $CDCl_3$): δ ppm 134.74, 117.00, 108.99, 76.39, 72.34, 72.00, 71.59, 70.83, 69.66, 62.49, 34.91, 29.70, 26.99, 25.89, 24.59, 23.27, 18.35, 10.68, -5.32, -5.44

MS (ESI): Calcd for $C_{21}H_{40}O_5Si_1$ $(2M+NH_4)^+$ 818.6, found 818.4

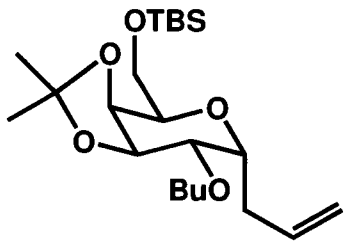

1-*C*-allyl-2-*O*-butyl-3,4-*O*-isopropylidene-6-*O*-*tert*-butyldimethylsilyl-α-D-galactopyranoside (114)

To a solution of compound (**64**) (0.28 g, 0.78 mmol) in 20 mL DMF at 0 ºC was added tert butylammonium iodide (29 mg, 0.078 mmol) and sodium hydride (37 mg, 60% dispersion in mineral oil, 0.94 mmol). The suspension was stirred for 1 hour to allow deprotonation, and then bromobutane (0.17 mL, 1.6 mmol) was added and the reaction was allowed to warm to room temperature overnight. The reaction was quenched with saturated NH_4Cl and EtOAc and H_2O was added. The product was washed with water several times to remove the DMF. The product was then extracted with EtOAc, washed with H_2O and brine, dried with $MgSO_4$, filtered, and concentrated. Flash chromatography (3:1 hexanes:EtOAc) gave the product as an oil (0.17 g, 53%) and recovered SM (30 mg, 11%).

^{1}H NMR (400 MHz, *$CDCl_3$)* δ ppm 5.84-5.73 (m, 1H), 5.09 (ddd, *J* = 17.2, 3.5, 1.5 Hz, 1H), 5.05 (tdd, *J* = 10.3, 2.1, 1.1 Hz, 1H), 4.36 (dd, *J* = 7.3, 1.6 Hz, 1H), 4.28 (dd, *J* = 7.3, 3.2 Hz, 1H), 3.99 (dt, *J* = 7.3, 2.8 Hz, 1H), 3.94 (ddd, *J* = 7.8, 5.8, 1.7 Hz, 1H), 3.67-3.61 (m, 3H), 3.41 (td, *J* = 9.2, 6.4 Hz, 1H), 3.31 (t, *J* = 3.0 Hz, 1H), 2.35 (ddt, *J* = 7.3, 2.6, 1.2 Hz, 2H), 1.54 (ddd, *J* = 12.0, 9.2, 6.8 Hz, 2H), 1.48 (s, 3H), 1.41-1.35 (m, 2H), 1.33 (s, 3H), 0.91 (t, *J* = 7.4 Hz, 3H), 0.89 (s, 9H), 0.06 (d, *J* = 1.5 Hz, 6H)

^{13}C NMR (100 MHz, *$CDCl_3$*): δ ppm 134.75, 117.00, 108.99, 76.70, 72.00, 71.58, 70.82, 70.48, 69.65, 62.49, 34.91, 32.14, 26.99, 25.89, 24.60, 19.37, 18.35, 13.89, -5.33, -5.44

MS (ESI): Calcd for $C_{22}H_{46}O_5Si$ $(M+Na)^+$ 437.27, found 437.22, $(M+K)^+$ 453.24, found 453.22

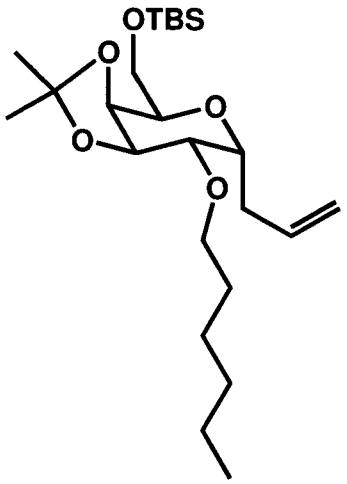

1-*C*-allyl-2-*O*-hexyl-3,4-*O*-isopropylidene-6-*O*-*tert*-butyldimethylsilyl-α-D-galactopyranoside (115)

To a solution of compound (**64**) (0.26 g, 0.73 mmol) in 20 mL DMF at 0 ºC was added tert butylammonium iodide (27 mg, 0.073 mmol) and sodium hydride (35 mg, 60% dispersion in mineral oil, 0.87 mmol). The suspension was stirred for 1 hour to allow deprotonation, and then bromohexane (0.20 mL, 1.5 mmol) was added and the reaction was allowed to warm to room temperature overnight. The reaction was quenched with saturated NH_4Cl and EtOAc and H_2O was added. The product was washed with water several times to remove the DMF. The product was then extracted with EtOAc, washed with H_2O and brine, dried with $MgSO_4$, filtered, and concentrated. Flash chromatography (3:1 hexanes:EtOAc) gave the product as an oil (0.25 g, 78%) and recovered starting material (30 mg, 12%).

^{1}H NMR (400 MHz, *$CDCl_3$)* δ 5.84-5.74 (m, 1H), 5.12-5.11 (m, 1H), 5.05 (ddd, *J* = 10.2, 2.2, 1.2 Hz, 1H), 4.37 (dd, *J* = 7.3, 1.6 Hz, 1H), 4.29 (dd, *J* = 7.3, 3.2 Hz, 1H), 3.99 (dt, *J* = 7.3, 2.8 Hz, 1H), 3.94 (ddd, *J* = 7.9, 5.8, 1.7 Hz, 1H), 3.77-3.68 (m, 2H), 3.62 (td, *J* = 9.1, 6.5 Hz, 1H), 3.41 (td, *J* = 9.1, 6.5 Hz, 1H), 3.31 (t, *J* = 3.0 Hz, 1H), 2.35 (ddt, *J* = 7.4, 2.4, 1.3 Hz, 2H), 1.59-1.51 (m, 2H), 1.48 (s, 3H), 1.33 (s, 3H), 1.32-1.22 (m, 6H), 0.90-0.88 (m, 12H), 0.06 (d, *J* = 1.7 Hz, 6H)

^{13}C NMR (100 MHz, *$CDCl_3$*): δ ppm 134.75, 116.99, 108.99, 76.38, 71.96, 71.57, 70.82, 70.78, 69.65, 62.47, 34.91, 31.63, 30.00, 26.99, 25.88, 25.82, 24.59, 24.59, 22.60, 18.34, 14.04, -5.33, -5.45

MS (ESI): Calcd for $C_{24}H_{46}O_5Si$ $(M+Na)^+$ 465.30, found 465.25, $(M+K)^+$ 481.28, found 481.24

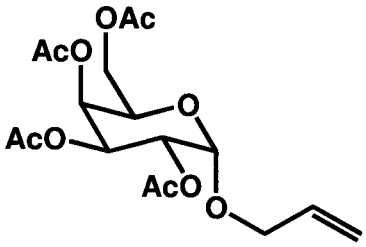

1-*O*-allyl-2,3,4,6-*O*-acetyl-α-D-galactopyranoside (116):
To a solution of compound (**34**) (0.50 g, 2.5 mmol) in 15 mL pyridine was added acetic anhydride (15 mL) and dimethylaminopyridine (30 mg). The reaction was stirred overnight, and then diluted with EtOAc. The product was washed with $CuSO_4$ to remove the pyridine, and then washed with brine. Flash chromatography (2:1 petroleum ether:EtOAc) gave the product as an oil (0.57 g, 63%).

^{1}H NMR (400 MHz, *$CDCl_3$):* δ ppm 5.85 (ddd, *J* = 22.4, 10.8, 5.6 Hz, 1H), 5.43 (d, *J* = 3.1 Hz, 1H), 5.37-5.34 (m, 1H), 5.28 (d, *J* = 17.2 Hz, 1H), 5.20 (d, *J* = 10.4 Hz, 1H), 5.12 (q, *J* = 3.8 Hz, 2H), 4.22 (t, *J* = 6.6 Hz, 1H), 4.16 (dd, *J* = 13.0, 5.2 Hz, 1H), 4.07 (d, *J* = 6.6 Hz, 2H), 4.00 (dd, *J* = 13.0, 6.1 Hz, 1H), 2.12 (s, 3H), 2.06 (s, 3H), 2.03 (s, 3H), 1.96 (s, 3H)

This compound has been previously reported in the literature.[41]

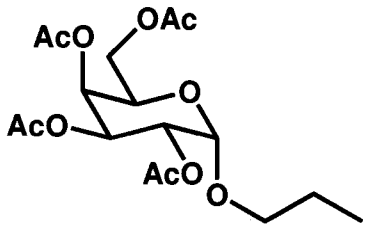

1-*O*-propyl-2,3,4,6-*O*-acetyl-α-D-galactopyranoside (117):
To a solution of compound (**116**) (0.18 g, 0.46 mmol) in 5 mL EtOAc and 5 mL EtOH was added palladium over carbon (30 mg). N_2 was bubbled through the suspension for 10 minutes, followed by H_2 for 50 minutes. A H_2 balloon was attached and the reaction was left stirring overnight. Thin layer chromatography showed that the reaction was not complete, so 1 mL of a 33% AcOH solution (1 mL glacial acetic acid in 2 mL H_2O) was added and H_2 was bubbled through for 6 hours. TLC indicated that the reaction was complete, and the reaction was filtered over celite and concentrated *in vacuo*. The product was obtained as a white solid (0.100 g, 56%).

^{1}H NMR (400 MHz, *$CDCl_3$):* δ ppm 5.45 (dd, *J* = 3.4, 1.3 Hz, 1H), 5.35 (ddd, *J* = 12.0, 3.4, 1.5 Hz, 1H), 5.10 (qd, *J* = 5.1, 3.7 Hz, 2H), 4.23-4.21 (m, 1H), 4.09 (dd, *J* = 6.6, 2.1 Hz, 2H), 3.64 (td, *J* = 9.8, 6.6 Hz, 1H), 3.39 (td, *J* = 9.8, 6.6 Hz, 1H), 2.14 (s, 3H), 2.07 (s, 3H), 2.04 (s, 3H), 1.98 (s, 3H), 1.64-1.59 (m, 2H), 0.93 (t, *J* = 7.4 Hz, 3H)

^{13}C NMR (100 MHz, *$CDCl_3$*): δ ppm 170.42, 170.41, 170.24, 170.02, 96.06, 70.26, 68.27, 68.14, 67.67, 66.12, 61.80, 22.57, 20.76, 20.68, 20.64, 10.53

MS (ESI): Calcd for $C_{17}H_{26}O_{10}$ $(M+Na)^+$ 413.14, found 413.12, $(M+K)^+$ 429.12, found 429.11

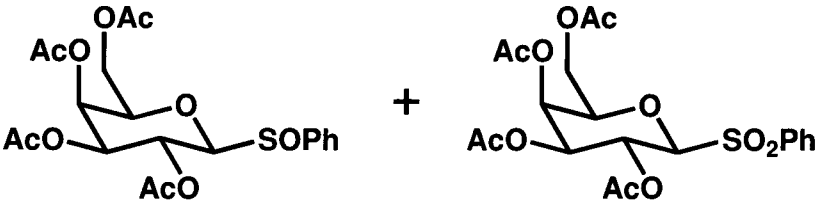

1-(phenyl sulfoxide)-2,3,4,6-tetra-*O*-acetyl-*β* -D-galactopyranoside (118) and 1-(phenyl sulfone)-2,3,4,6-tetra-*O*-acetyl-*β* -D-galactopyranoside (119) (procedure adapted from Ali and Stevens[42]):

To a flame-dried round bottom flask was added silica gel (5.0 g). H_2O (3 mL) was added via syringe while vigorous stirring was maintained. Once the solid was free-flowing, MMPP (0.78 g, 1.6 mmol) and CH_2Cl_2 (25 mL) was added. A solution of (**82**) (0.64 g, 1.4 mmol) in 5 mL CH_2Cl_2 was cannulated into the suspension and washed with 2 mL CH_2Cl_2. The reaction was stirred at room temperature for 2 hours, at which point additional MMPP (0.78 g) was added. The reaction was stirred for 4 hours, and then filtered on a sintered glass funnel and washed with CH_2Cl_2. The products were concentrated *in vacuo* and flash chromatography (1:2 hexanes:EtOAc) gave the sulfone (**119**, R_f = 0.28) (0.27 g, 40%) and the sulfoxide (**118**, R_f = 0.15) (0.36 g, 53%, mixture of sulfoxide diastereomers) as white solids.

1-(phenyl sulfoxide)-2,3,4,6-tetra-*O*-acetyl-*β* -D-galactopyranoside (118)

^{1}H NMR (400 MHz, *$CDCl_3$)* δ ppm 7.75-7.72 (m, 2 H), 7.68-7.66 (m, 2H), 7.56-7.52 (m, 6H), 5.55 (t, *J* = 9.86 Hz, 1H), 5.51 (dd, *J* = 13.95, 5.85 Hz, 1H), 5.35 (ddd, *J* = 5.80, 3.29, 0.91 Hz, 2H), 5.08 (ddd, *J* = 11.05, 9.97, 3.30 Hz, 2H), 4.36 (d, *J* = 9.86 Hz, 1H), 4.26 (d, *J* = 9.79 Hz, 1H), 4.06-3.85 (m, 6H), 2.09 (s, 3H), 2.07 (s, 3H), 2.02 (s, 3H), 1.99 (s, 3H), 1.98 (s, 6H), 1.97 (s, 3H), 1.93 (s, 3H)

^{13}C NMR (100 MHz, *$CDCl_3$)* δ ppm 170.21, 170.11, 169.97, 169.88, 169.62, 168.93, 139.30, 138.85, 131.61, 131.52, 128.76, 128.70, 125.91, 125.82, 92.37, 90.26, 75.27, 74.94, 71.96, 71.52, 66.82, 66.72, 64.99, 64.50, 61.17, 60.99, 20.74, 20.71, 20.59, 20.54, 20.51, 20.42

MS (ESI): Calcd for $C_{20}H_{24}O_{10}S$ $(M+NH_4)^+$ 474.1, found 474.5, $(M+Na)^+$ 479.1, found 479.4

1-(phenyl sulfone)-2,3,4,6-tetra-O-acetyl-β -D-galactopyranoside (119)

^{1}H NMR (400 MHz, *$CDCl_3$)* δ ppm 7.95 (dd, *J* = 8.2, 1.0 Hz, 2H), 7.70 (t, *J* = 7.5 Hz, 1H), 7.58 (t, *J* = 7.8 Hz, 2H), 5.43 (t, *J* = 9.8 Hz, 1H), 5.30 (d, *J* = 3.1 Hz, 1H), 5.03 (dd, *J* = 9.9, 3.2 Hz, 1H), 4.50 (d, *J* = 9.7 Hz, 1H), 4.11-4.04 (m, 2H), 3.97-3.91 (m, 1H), 2.13 (s, 3H), 1.97 (s, 3H), 1.95 (s, 3H), 1.88 (s, 3H)

All spectral data was in accordance with the literature.[43]

7.3: Methods and Materials for Assessing Antifreeze Activity

7.3.1: Assessing Thermal Hysteresis (TH) and Dynamic Ice-Shaping (DIS) Activities

TH and DIS activities of carbohydrates were studied using a Clifton nanoliter osmometer (Clifton Technical Physics). The compound being tested was dissolved in distilled water to form a 10 mg/mL solution. Then, a drop (sub-microliter) of solution was introduced into an oil (microscope immersion oil)-filled cylindrical well on an aluminum plate. The solution was flash frozen at -40 °C and then nucleated by slow warming to acquire a stable single ice crystal. The melting and freezing points of the solution were determined by changing the temperature of the system at a constant rate of 10 mOsmol (0.0186 °C) per 15 seconds.

7.3.2: Assessing Ice-Recrystallization Inhibition (IRI) Activity

The RI activities were measured using a recrystallization inhibition assay developed by Horwath et al.[44] A 10 µL solution of compound in PBS was dropped from a height of two meters through a shielding tube to a polished aluminum block, which was pre-cooled to -80 °C on dry ice. The "splat cooling" of the solution produced an ice wafer about 1 cm in diameter and 20 µm in thickness. The wafer was then quickly moved onto a microscope cover glass and transferred into a cold chamber, which was dried with continuous air flow to avoid moisture condensing on the ice wafer. The sample was annealed at -6 °C for 30 minutes before the size of the ice grains was photographed using a microscope equipped with an LMPlanF1 20x/0.40 objective. The temperature of the cold chamber was controlled by a Series 800 temperature controller (Alpha Omega Instruments). For each sample drop, three photographs were taken from different areas of the ice wafer. The drop was repeated two additional times to give a total of nine pictures per sample. The size of ice grains was calculated by taking the surface area of twelve random ice grains in each photograph using Domain Recognition Software following the procedure of Jackman et al.[45]

7.4: Methods and Materials for Assessing In Vitro Cytotoxicity

7.4.1: Cell Culture

WRL 68 human embryonic liver cells (ATCC, CL-48) were cultured in Eagle's Minimum Essential Media (MEM) (ATCC, 30-2003) supplemented with 10% fetal bovine serum (FBS) (ATCC, 30-2020) and 1% penicillin-streptomycin (GIBCO, 15140). Cells were incubated in a 37 ºC incubator supplied with 5% CO_2. Passage 89 to 104 of WRL 68 cells were used in our study.

All cells were trypsinized with trypsin-EDTA solution (0.25% trypsin, 1mM EDTA·4Na) (GIBCO, 25200) and incubated in half area 96 well plates with density of around 5 x 10^3 cells/well until they reached 100 % confluence for experiments.

7.4.2: MTT Assay (conducted by Louise Guolla and Liz von Moos)

The MTT assay kit was purchased from Sigma (TOX-1) and the *in vitro* toxicology assay was performed according to the product information sheet (available online: http://www.sigmaaldrich.com/etc/medialib/docs/Sigma/Bulletin/tox1bul.Par.0001.File.tmp/tox1bul.pdf). All experiments were repeated three times and 12 parallel wells were used for each condition. For the MTT assay performed at physiological temperatures, cells were treated with different concentrations of compound in culture media and incubated for 18 hours before MTT assays were performed.

After incubating cells with the compound being tested, plates were centrifuged at 1500 rpm for three minutes before the culture medium was replaced with 50 µL MTT (Sigma, M5655) solution (5 mg/mL) in Hank's Balanced Salt Solution (HBSS, Invitrogen). Then, plates were incubated at 37 ºC with 5% CO_2 for three hours. To each well was added with another 50 µL MTT solubilization solution (10% Triton X-100 plus 0.1 N HCl in isopropanol) and each well was aspirated until all the formazan precipitates were dissolved. The absorbance of each well was read at a wavelength of 570 nm with a multiwell plate reader (AD 340C Absorbance Detector, Beckman Coulter, Inc.). Viable cells are those that are able to convert tetrazolium bromide into formazan (Figure 7.1).

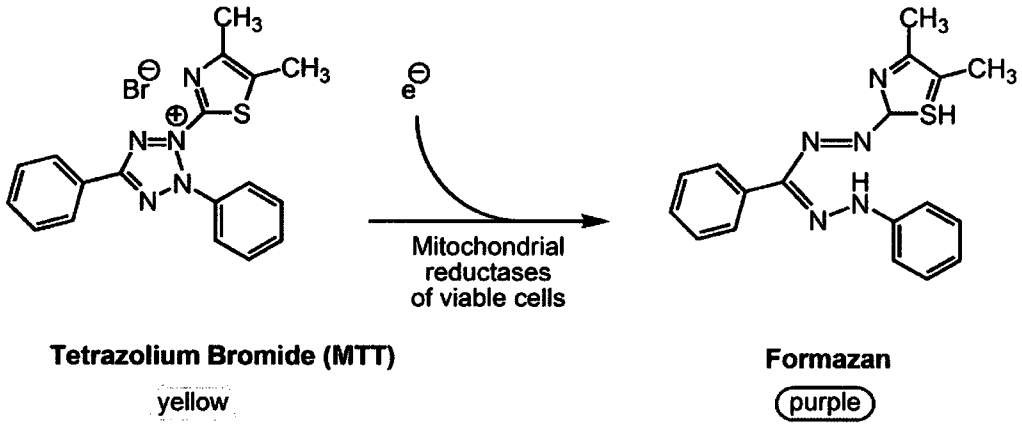

Figure 7.1: Basis for the MTT cell viability assay. Viable cells are able to convert tetrazolium bromide into formazan.

7.4.3: Cryopreservation and Thawing (conducted by Liz von Moos and Luke Wu)

WRL 68 cells were cultured and trypsinized as described above. Cells were diluted with culture media and counted using a hemacytometer. Aliquots containing $1x10^7$ cells were added to 15 mL centrifuge tubes and cells were pelleted by centrifugation for 10 min at 2000 rpm. The supernatant was removed and the cells were re-suspended in 1.5 mL HTK supplemented with sugar to a concentration of 22, 200 or 500 mM with or without DMSO at a concentration of 5 %. HTK supplemented with DMSO to a concentration of 5 or 10 % served as the positive controls. Cell suspensions were transferred to 1.8 mL cryogenic vials and placed in to a "Mr. Frosty" freezing container. The container was placed in an ultra-cold freezer (-80°C) for 24 h. According to the manufacturer, "Mr. Frosty" provides a sample cooling rate of approximately 1°C /min. Samples were then stored in the vapour phase of liquid nitrogen (-150 °C) in a Dewar for 7 days. Following storage, samples were rapidly thawed in a 37 °C water bath with gentle agitation. Thawed samples were transferred to 15 mL centrifuge tubes and slowly diluted to 3mL by dropwise addition of cell culture medium. After 3 min samples were further diluted to 9mL. Cells were pelleted by centrifugation for 10 min at 2000 rpm. The supernatant was decanted and the pellet re-suspended in 5 mL Eagle's Minimal Essential Medium (MEM) cell culture medium. Centrifuge tubes were stored in a 37°C water bath until flow cytometry was conducted, approximately 2 hours.

7.4.4: Flow Cytometry (conducted by Luke Wu)

After cryopreservation and thawing as described above, the cell count was determined using a hemacytometer. An aliquot containing 1 x 10^6 cells was transferred to a 15 mL centrifuge tube and diluted with to 1mL with cell culture media containing 10% FBS. Cells were pelleted by centrifugation for 10 min at 300g and 4°C. The supernatant was removed and the pellet was re-suspended in 1mL Annexin-V binding buffer and 100 µL of the sample was transferred to a flow cytometry tube. Subsequently, 5µL 7-Actinomycin D (7AAD) (BD Pharmingen) and 4µL Annexin V-PE (PE) (BD Pharmingen) were added and samples were incubated for 20 min in the dark. Following incubation, samples were diluted to 500µL with 1x Annexin-V binding buffer. Flow cytometry analysis on 10,000 cells was carried out on a BD LSR flow cytometer using Cell quest software (Becton Dickinson). Annexin V-PE was measured on FL-2 while 7-AAD was measured on FL-3. Viable cells were those that were both Annexin V-negative (reflecting the absence of apoptosis) and 7AAD-negative (reflecting the absence of necrosis). Compensation was set from single stain experiments with 7-AAD and Annexin-V. Aliquots from non-cryopreserved samples labelled with equivalent fluorochromes were used to set the control gate excluding 99% 7AAD+ cells. Time between thawing and analysis by flow cytometry was 2 h. All trials were performed at least in duplicate.

7.5: Student's t-Test

Both MTT assay results and RI activities were analyzed using the "Student's t-Test: Two Samples with Unequal Variance" to statistically evaluate whether a significant difference exists between two samples. The standards used for student's t-test are two-tailed test and two-sample assuming equal variances. Significant difference is believed to exist between two groups of data when the calculated t value exceeds the tabulated value for P = 0.05 or the calculated P value is smaller than 0.05.

To compare the means of two treatments (with the number of replicates of n_1 and n_2), the student's t-test was performed as follows:

1. Calculate the mean ($\bar{x}_1$, $\bar{x}_2$) and variance (σ_1^2, σ_2^2) of each treatment.
2. Calculate the square root of the variance of the difference between two means.

$$\sigma_d = \sqrt{\frac{\sigma_1^2}{n_1} + \frac{\sigma_2^2}{n_2}}$$

3. Calculate t value.

$$t = \frac{\bar{x}_1 - \bar{x}_2}{\sigma_d}$$

4. Look up the tabulated t value at the degree of freedom of ($n_1 + n_2 - 2$) and P = 0.05.
5. Compare the calculated t value with the tabulated t value. If the calculated value exceeds the tabulated value, there is significant difference between the two treatments with 95% confidence.

This test is incorporated into Microsoft Excel 2007, and a Two-Sample Unequal Variance Student's T-test was performed using this program.

7.6: Error bar determination:

Error bars for IRI activity were calculated by dividing the standard error of the mean (SEM) for each sample by the average mean grain size (MGS) for the PBS negative control on the day of testing. An ANOVA confirmed that the error between samples was considerably larger than the error within samples.

Error bars for cell viability at 37 ºC and -80 ºC reflect the standard error of the mean (SEM) for that sample. Again, ANOVAs confirmed that the error between samples was considerably larger than the error within samples. In all cases, the error bars reflect the measured value plus and minus the error for that sample.

7.7: Computational Methods for Hydration Number Calculation (conducted by Christopher Rowley):

All molecular dynamics simulations were performed using Amber 9.[46] The carbohydrates were solvated in an orthorhombic box of TIP3P water molecules.[47] The simulation cells of the solvated carbohydrates had volumes of approximately 50 Å[48] and contained roughly 3000 water molecules. The GLYCAM 04 force field[48] was used to model the natural carbohydrates. Partial atomic charges for carbohydrates that did not have existing parameters in the GLYCAM force field were assigned by constraining the charges of the carbohydrate ring to the GLYCAM charges for galactose, then using the RESP procedure[49] to fit charges for the remaining atoms. The simulations were equilibrated for 100 ps before a 1 ns production run at 300 K.

Average hydration numbers were calculated using snapshots from the production MD trajectory at 1 ps intervals. A solvent water molecule was designated as hydrogen bonding with the solute if the O···H distance was less than 3.0 Å and the O–H···O angle was greater than 120º.

7.8: CARS (conducted with assistance from Andy Ridsdale and Doug Moffatt):

A depiction of the optical arrangement is given in Figure 7.2. A Spectra Physics Tsunami Ti:Sapphire laser system produced pulses of 60 fs at 80 MHz with 550mW total average power. In most cases the laser was operated at a center wavelength of 800 nm. A Faraday isolator was used to avoid back reflections into the laser. The pulse train was sent through a prism compressor optimized for shortest pulse duration at the input to the PCF. The Ti:Sa beam was split by a 50:50 beam splitter into a pump and Stokes arm. The pump proceeded to the sample via a variable time delay stage and its average power was controlled by a variable neutral-density filter. The remaining 250 mW of power was directed to a PCF (NL-1.4.775-945, Crystal Fiber) which was previously shown to generate pulses in the near infrared.[50] The fiber also generated light in the visible range which was filtered before the Stokes and pump were

recombined. Typical powers before the microscope scan head were 12 mW in the Stokes and, depending on the sample, 40 to 150 mW in the pump. To control the chirp in the simplest possible way, we used fixed length blocks of glass: one 3 cm block of SF6 glass was placed in the pump arm and a 5 cm block of SF6 glass was placed in the Stokes arm to achieve nearly matched chirps. It is straightforward to implement an optical scheme wherein the degree of pulse chirp is continuously variable, such as by making use of prism or grating based zero dispersion line. This should permit continuous tuning of the effective CARS spectral resolution from ≈ 5 - 400 cm^{-1}. The power in the Stokes arm dropped to about 7 mW with the glass in place while the power in the pump remained unchanged (the glass blocks were AR coated for 800 nm). Note that these powers were attenuated by about a factor of ≈2 through the microscope system before reaching the back aperture of the objective.

All imaging was performed on a modified Olympus Fluoview 300 (FV300) laser scanning system and IX71 inverted microscope. A 40X 1.15 NA UAPO water immersion lens with a cover slip correction collar was used as the objective and a 0.55 NA long working distance condenser lens for collection in the forward direction. The efficiency of collection in this configuration was insensitive to small adjustments of the focus of the collecting lens. Fluorescence signal was collected through the objective lens (epi-detection). A 400 - 700 nm filter (E700sp, Chroma Technology Vermont USA) was used to discriminate TPF, SHG, sum frequency generation (SFG) and anti-Stokes signals from the pump and Stokes beams. To discriminate forward propagating second-harmonic and CARS signals, additional band-pass filters were used. For imaging, light was directed to photomultiplier tubes (PMT) with enhanced red sensitivity (Hamamatsu R3896). For low temperature experiments, the microscope was attached to a Linkam cryostage (model 100-OI) and a Linkam controller (model PE 94).

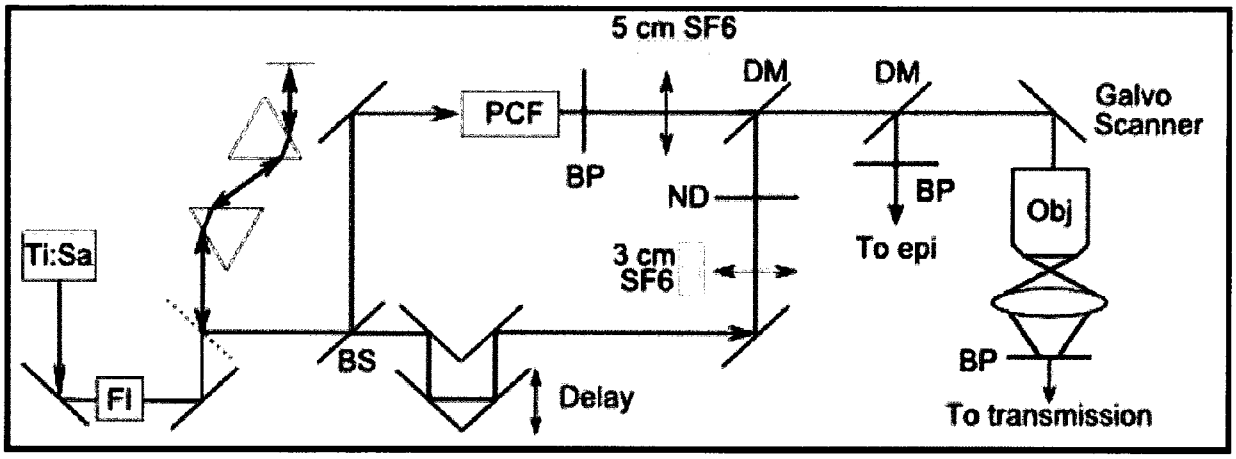

Figure 7.2: Multimodal CARS microscopy optical arrangement. Pulses from the Ti:Sa oscillator are sent through a Faraday isolator (FI) followed by a prism compressor. A 50:50 beam splitter (BS) divided the incoming light. One arm was sent through a photonic crystal fiber (PCF) and bandpass filter (BP) before being recombined on a dichroic mirror (DM). The other half was sent through a time delay arm that included a neutral density filter (ND). In both the pump and Stokes paths, glass (SF6) could be added to control the chirp. The recombined beam was sent into the FV300 microscope. Inside the FV300, there were more dichroic mirrors and filters to separate the signals from the excitation light. Note that the epi-detected fluorescence signals were collected inside the microscope.

7.8: References:

1. Burchat, A. F.; Chong, J. M.; Nielson, N., Titration of Alkyllithiums with a Simple Reagent to a Blue Endpoint. *J. Organomet. Chem.* **1997,** 542, 281-283.

2. Gottlieb, H. E.; Kotlyar, V.; Nudelman, A., NMR Chemical Shifts of Common Laboratory Solvents as Trace Impurities. *J. Org. Chem.* **1997,** 62, 7512-7515.

3. Mari, S.; Canada, F. J.; Jimenez-Barbero, J.; Bernardi, A.; Marcou, G.; Motto, I.; Velter, I.; Nicotra, F.; Ferla, B. L., Synthesis and Conformational Analysis of Galactose-Derived Bicyclic Scaffolds. *Eur. J. Org. Chem.* **2006,** 2006, 2925-2933.

4. Bragnier, N.; Scherrmann, M.-C., One-Step Synthesis of beta-*C*-Glycosidic Ketones in Aqueous Media: The Case of 2-Acetamido Sugars. *Synthesis* **2005,** 2005, 0814-0818.

5. Blom, P.; Ruttens, B.; Van Hoof, S.; Hubrecht, I.; Van der Eycken, J., A Convergent Ring-Closing Metathesis Approach to Carbohydrate-Based Macrolides with Potential Antibiotic Activity. *J. Org. Chem.* **2005,** 70, 10109-10112.

6. Witczak, Z. J.; Chhabra, R.; Chen, H.; Xie, X.-Q., Thiosugars II. A Novel Approach to Thiodisaccharides. The Synthesis of 3-Deoxy-4-Thiocellobiose from Levoglucosenone. *Carbohydrate Res.* **1997,** 301, 167-175.

7. Singer, M.; Lopez, M.; Bornahi, L. F.; Innocenti, A.; Vullo, D.; Supuran, C. T.; Poulsen, S.-A., Inhibition of Carbonic Anhydrase Isozymes with Benzene Sulfonamides Incorporating Thio, Sulfinyl, and Sulfonyl Glycoside Moieties. *Bioorg. Med. Chem. Lett.* **2009,** 19, 2273-2276.

8. Goebel, M.; Nothofer, H.-G.; Rob, G.; Ugi, I., A Facile Synthesis of Per-*O*-Alkylated Glycono-delta-Lactones from Per-*O*-alkylated Glycopyranosides and a Novel Ring Contraction for Pyranoses. *Tetrahedron* **1997,** 53, (9), 3123-3134.

9. Fang, T. T.; Bendiak, B., The Stereochemical Dependence of Unimolecular Dissociation of Monosaccharide-Glycoaldehyde Anions in the Gas Phase: A Basis for Assignment of the Stereochemistry and Anomeric Configuration of Monosaccharides in Oligosaccharides by Mass Spectrometry via a Key Discriminatory Product Ion of Disaccharide Fragmentation, m/z 221. *J. Am. Chem. Soc.* **2007,** 129, 9721-9736.

10. Czechura, P.; Tam, R. Y.; Dimitrijevic, E.; Murphy, A. V.; Ben, R. N., The Importance of Hydration for Inhibiting Ice Recrystallization with *C*-Linked Antifreeze Glycoproteins. *J. Am. Chem. Soc.* **2008,** 130, 2928-2929.

11. Motawia, M. S.; Olsen, C. E.; Denyer, K.; Smith, A. M.; Moller, B. L., Synthesis of 4'-*O*-Acetyl-Maltose and alpha-D-Galactopyranosyl-(1-->4)-D-Glucopyranose for Biochemical Studies of Amylose Biosynthesis. *Carbohydrate Res.* **2001,** 330, 309-318.

12. Rajanikanth, B.; Seshadri, R., A Facile Synthesis of Nojirimycin. *Tetrahedron Lett.* **1989,** 30, 755-758.

13. Belot, F.; Otter, A.; Fukuda, M.; Hindsgaul, O., Efficient Synthesis of Two HNK-1 Related Pentasaccharides. *Synlett* **2003,** 2003, 1315-1318.

14. Janczuck, A. J.; Zhang, W.; Andreana, P. R.; Warrick, J.; Weng, P. G., The Synthesis of Deoxy-alpha-Gal Epitope Derivatives for the Evaluation of an Anti-alpha-Gal Antibody Binding. *Carbohydrate Res.* **2002,** 337, 1247-1259.

15. BeMiller, J. N.; Yadav, M. P.; Kalabokis, V. N.; Myers, R. W., *N*-Substituted (beta-D-Galactopyranosylmethyl)amines, and *C*-beta-D-Galactopyranosylformamides, and Related Compounds. *Carbohydrate Res.* **1990,** 200, 111-126.

16. Ben, R. N.; Eniade, A. A.; Hauer, L., Synthesis of a *C*-linked Antifreeze Glycoprotein (AFGP) Mimic: Probes for Investigating the Mechanism of Action. *Organic Letters* **1999,** 1, 1759-1762.

17. Corey, E. J.; Cho, H.; Rucker, C.; Hua, D. H., Studies with Trialkylsilyltriflates: New Syntheses and Applications. *Tetrahedron Lett.* **1981,** 22, 3455-3458.

18. Praly, J.-P.; Chen, G.-R.; Gola, J.; Hetzer, G., C-C Bond Formation with Acetylated 1-Chloroglycopyranos-1-yl Radicals, 2: Stereocontrolled Access to Higher Sugars (Non-1-en-4-ulopuranosyl Derivatives) and Glycomimetics [3-(Beta-D-Glycopyranosyl)-1-propenes and (3Z)-4,8-Anhydro-nona-1,3-dienitols]. *Eur. J. Org. Chem.* **2000,** 2000, 2831-2838.

19. Horton, D.; Miyake, T., Stereoselective Syntheses of *C*-(D-glucopyranosyl)alkenes. *Carbohydrate Res.* **1988,** 184, 221-229.

20. Mandal, P. K.; Misra, A. K., Concise Synthesis of Two Pentasaccharides Corresponding to the alpha-Chain Oligosaccharides of *Neisseria gonorrhoeae* and *Neisseria meningitidis*. *Tetrahedron* **2008,** 64, 8685-8691.

21. Zou, W.; Shao, H.; Wu, S.-H., Intramlecular Aldol Cyclization of C-4-Ulopyranosyl-2'-Oxoalkanes Controlled by Steric Effects. Asymmetric Synthesis of Substituted 8-Oxabicyclo[3.2.1]Octanones and -Octenones and Cyclopentenones. *Carbohydrate Res.* **2004,** 339, 2475-2485.

22. Boulineau, F. P.; Wei, A., Mirror-Image Carbohydrates: Synthesis of the Unnatural Enantiomer of a Blood Group Trisaccharide. *J. Org. Chem.* **2004,** 69, 3391-3399.

23. He, D.-Y.; Li, Z.-J.; Cai, M.-S., Synthesis of an Intermediate Fragment of the Capsular Polysaccharides of *Klebsiella* Type 8. *Carbohydrate Res.* **1993,** 239, 267-271.

24. Oka, T.; Fujiwara, K.; Murai, A., Synthesis of Both Enantiomers of the BC-ring Part of Ciguatoxin. *Tetrahedron* **1996,** 52, 12091-12110.

25. Ohlsson, J.; Magnusson, G., Galabiosyl Donors; Efficient Synthesis from 1,2,3,4,6-Penta-*O*-Acetyl-beta-D-Galactopyranose. *Carbohydrate Res.* **2000,** 329, 49-55.

26. Weng, S.-S.; Lin, Y.-D.; Chen, C.-T., Highly Diastereoselective Thioglycosylation of Functionalized Peracetylated Glycosides Catalyzed by MoO_2Cl_2. *Org. Lett.* **2006,** 8, 5633-5636.

27. Bleriot, Y.; Untersteller, E.; Fritz, B.; Sinay, P., Total Synthesis of Calditol: Structural Clarification of this Typical Component of Archaea Order *Sulfolobales*. *Chem. Eur. J.* **2002,** 8, 240-246.

28. Misra, A. K.; Agnihotri, G., Chloramine-T-Mediated Chemoselective Hydrolysis of Thioglycosides into Glycosyl Hemiacetals Under Neutral Conditions. *Carbohydrate Res.* **2004,** 339, 885-890.

29. Kuzuhara, H.; Fletcher, H. G. J., Syntheses with Partially Benzylated Sugars. VIII. Substitution at C-5 in an Aldose. The Synthesis of 5-*O*-Methyl-D-glucofuranose Derivatives. *J. Org. Chem.* **1967,** 32, 2531-2534.

30. Dondoni, A.; Scherrmann, M.-C., Thiazole-Based Synthesis of Formyl *C*-Glycosides. *J. Org. Chem.* **1994,** 59, 6404-6412.

31. Erdik, E., Use of Activation Methods for Organozinc Reagents. *Tetrahedron* **1987,** 43, 2203-2212.

32. Ocampo, R.; Dolbier, W. R., Jr.; Paredes, R., Synthesis of 1,1-Difluoroalkenes Via alpha,alpha-Difluoro-beta-Lactones. *J. Fluorine Chem.* **1998,** 88, 41-50.

33. Cuenca, A. B.; D'Hooge, F.; Gouge, V.; Castelot-Deliencourt, G.; Oulyadi, H.; Leclerc, E.; Jubault, P.; Pannecoucke, X.; Quirion, J.-C., Addition of Ethyl Bromodifluoroacetate to Lactones: Reactivity and Stereoselectivity. *Synlett* **2005,** 2005, (17), 2627-2630.

34. Picotin, G.; Miginiac, P., Activation of Zinc by Trimethylchlorosilane: An Improved Procedure for the Preparation of beta-Hydroxy Esters from Ethyl Bromoacetate and Aldehydes or Ketones (Reformatsky Reaction). *J. Org. Chem.* **1987,** 52, 4796-4798.

35. Turnbull, P.; Moore, H. W., Regioselective Synthesis Of Highly Substituted Napthols. *J. Org. Chem.* **1995,** 60, 644-649.

36. Schweizer, F.; Otter, A.; Hindsgaul, O., Synthesis of Sugar-Fused GABA-Analogues. *Synlett* **2001,** 2001, 1743-1746.

37. Larionov, O. V.; Meijere, A. d., Enantioselective Total Syntheses of Belactosin A, Belactosin C, and Its Homoanalogue. *Org. Lett.* **2004,** 6, 2153-2156.

38. Orsini, F.; Teodoro, E. D., A New Co(0) Complex Mediated Synthesis of *C*-Glycoside Analogues. *Tetrahedron:Asymmetry* **2003,** 14, 2521-2528.

39. Bastiaans, H. M. M.; van der Baan, J. L.; Ottenheijm, H. C. J., Flexible and Convergent Total Synthesis of Cyclotheonamide B. *J. Org. Chem.* **1997,** 62, 3880-3889.

40. Kaul, R.; Surprenant, S.; Lubell, W. D., Systematic Study of the Synthesis of Macrocyclic Dipeptide beta-Turn Mimics Possessing 8-, 9-, and 10- Membered Rings by Ring-Closing Metathesis. *J. Org. Chem.* **2005,** 70, 3838-3844.

41. Konstantinovic, S.; Dimitrijevic, B.; Teodorovic, A.; Gojkovic, S.; Pavolic, V.; Radulovic, V., $SnCl_4$ Induced Formation of C3-C11 Alkenyl Galactopyranosides as Precursors for Unsaturated Neutral Bolaforms. *J. Serb. Chem. Soc.* **2005,** 70, 925-929.

42. Ali, M. H.; Stevens, W. C., A Facile and Selective Procedure for Oxidation of Sulfides to Sulfoxides on Silica Gel Supported Magnesium Monoperosyphthalate (MMPP) in Dichloromethane. *Synthesis* **1997,** 7, 764-768.

43. Agnihotri, G.; Misra, A. K., Fast Oxidation of Thioglycosides to Glycosyl Sulfones Using $KMnO_4/CuSO_4$-$5H_2O$ Under Neutral Reaction Conditions. *Carbohydrate Res.* **2006,** 341, 275-280.

44. Horwath, K. L.; Easton, C. M.; Poggioli Jr., G. J.; Myers, K.; Schnorr, I. L., Tracking the Profile of a Specific Antifreeze Protein and its Contribution to the Thermal Hysteresis Activity in Cold Hardy Insects. *Eur. J. Entomol.* **1996,** 93, 419-433.

45. Jackman, J.; Noestheden, M.; Moffat, D.; Pezacki, J. P.; Findlay, S.; Ben, R. N., Assessing Antifreeze Activity of AFGP 8 Using Domain Recognition Software. *Biochem. Biophys. Res. Commun.* **2007,** 354, 340-344.

46. Case, D. A.; Thomas E. Cheatham, I.; Darden, T.; Gohlke, H.; Luo, R.; Kenneth M. Merz, J.; Onufriev, A.; Simmerling, C.; Wang, B.; Woods, R. J., The Amber Biomolecular Simulation Programs. *J. Comp. Chem.* **2005,** 26, 1668- 1688.

47. Jorgenson, W. L.; Chandrasekhar, J.; Madura, J. D.; Impey, R. W.; Klein, M. L., Comparison of Simple Potential Functions for Simulating Liquid Water. *J. Chem. Phys.* **1983,** 79, 926-935.

48. Basma, M.; Sundara, S.; Calgan, D.; Vernali, T.; Woods, R. J., Solvated Ensemble Averaging in the Calculation of Partial Atomic Charges. *J. Comp. Chem.* **2001,** 22, 1125-1137.

49. Bayly, C. I.; Cieplak, P.; Cornell, W. D.; Kollman, P. A., A Well-Behaved Electrostatic Potential Based Method Using Charge Restraints for Deriving Atomic Charges: The RESP Model. *J. Phys. Chem.* **1993,** 97, 10269-10280.

50. Hilligsoe, K. M.; Andersen, T. V.; Paulsen, H. N.; Nielsen, C. K.; Molmer, K.; Keiding, S.; Kristiansen, R.; Hansen, K. P.; Larsem, J. J., Supercontinuum Generation in a Photonic Crystal Fiber with Two Zero Dispersion Wavelengths. *Opt. Express* **2004,** 12, 1045-1054.

Appendix 1

^{1}H and ^{13}C NMR Spectra

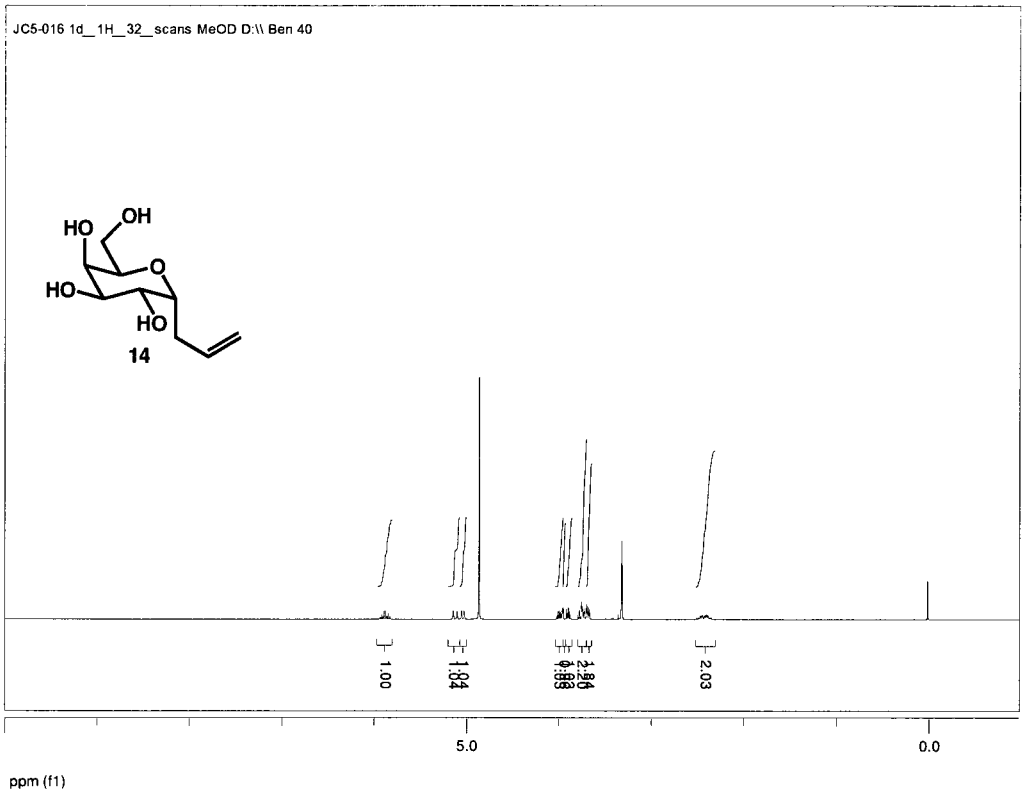
JC5-016 1d_1H_32_scans MeOD D:\\ Ben 40
HO
OH
O
HO
HO
14
1.00
1.94
2.03
5.0
0.0
ppm (f1)

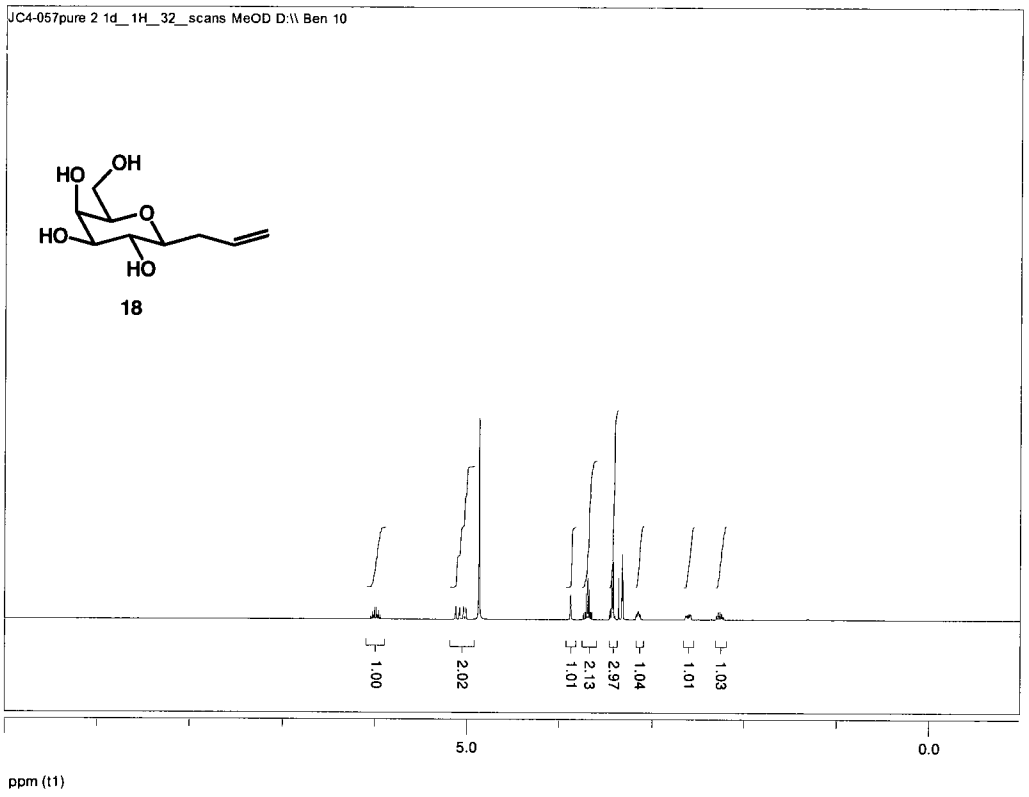
JC4-057pure 2 1d__1H__32__scans MeOD D:\\ Ben 10
HO
OH
O
HO
HO
18
1.00
2.02
1.01
2.13
2.97
1.04
1.01
1.03
5.0
0.0
ppm (t1)

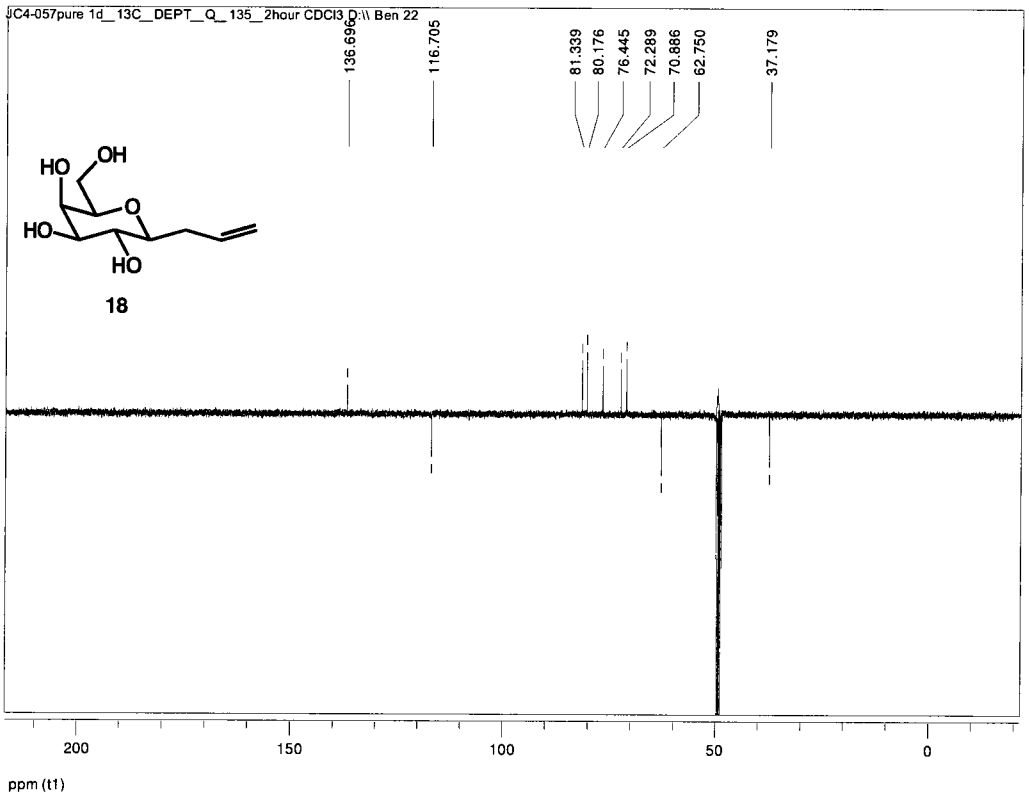
JC4-057pure 1d__13C__DEPT__Q__135__2hour CDCl3 D:\\ Ben 22
136.696
116.705
81.339
80.176
76.445
72.289
70.886
62.750
37.179
HO
OH
O
HO
HO
18
200
150
100
50
0
ppm (t1)

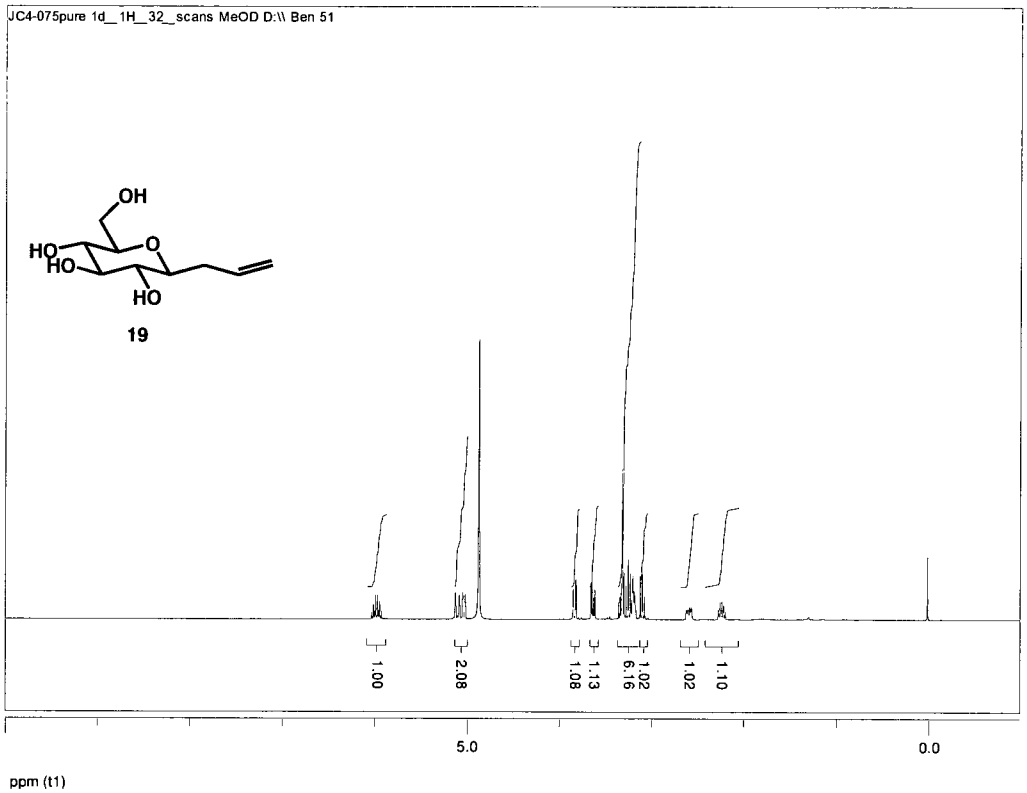
JC4-075pure 1d__1H__32__scans MeOD D:\\ Ben 51
OH
HO
HO
O
HO
19
1.00
2.08
1.08
1.13
6.16
1.02
1.02
1.10
5.0
0.0
ppm (t1)

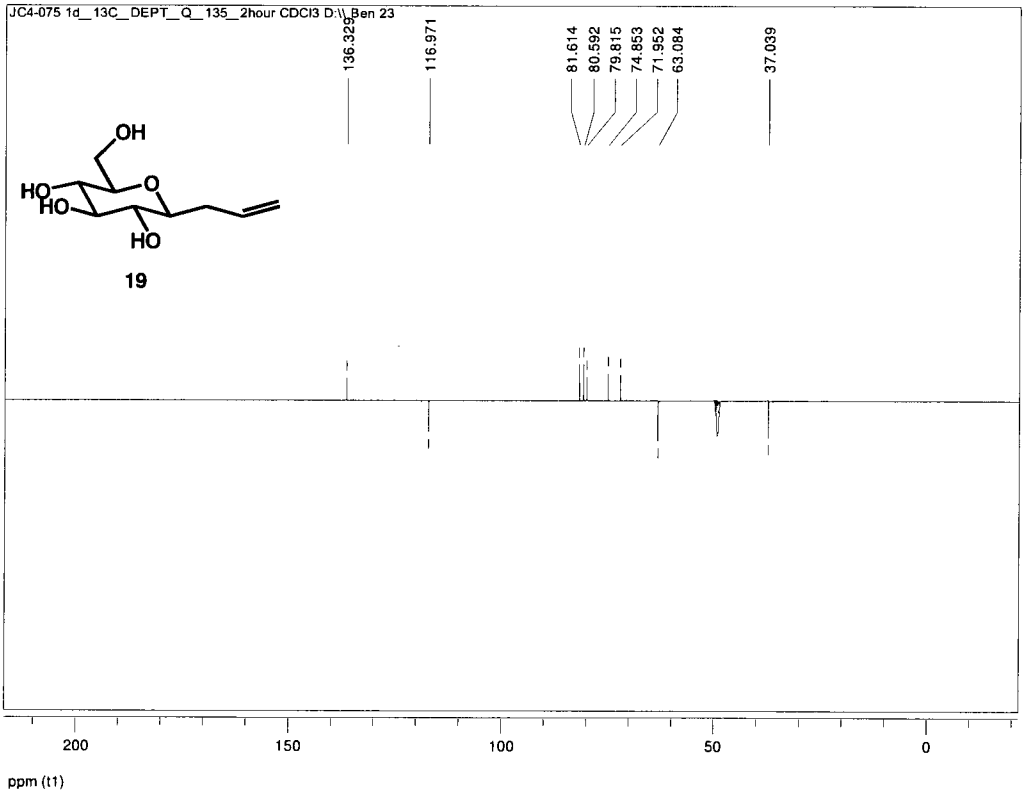
JC4-075 1d__13C__DEPT__Q__135__2hour CDCl3 D:\\ Ben 23
136.329
116.971
81.614
80.592
79.815
74.853
71.952
63.084
37.039
OH
HO
HO
O
HO
19
200
150
100
50
0
ppm (t1)

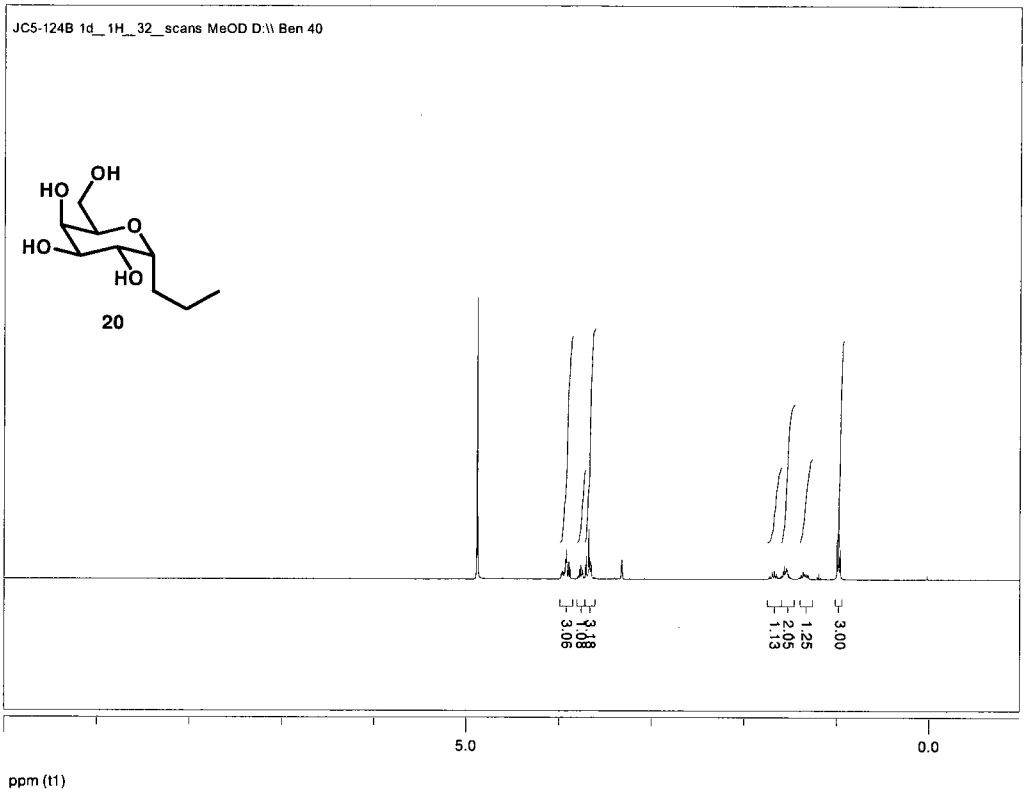
JC5-124B 1d_ 1H_ 32_ scans MeOD D:\\ Ben 40
HO
OH
O
HO
HO
20
3.90
3.88
3.86
1.13
2.05
1.25
3.00
5.0
0.0
ppm (t1)

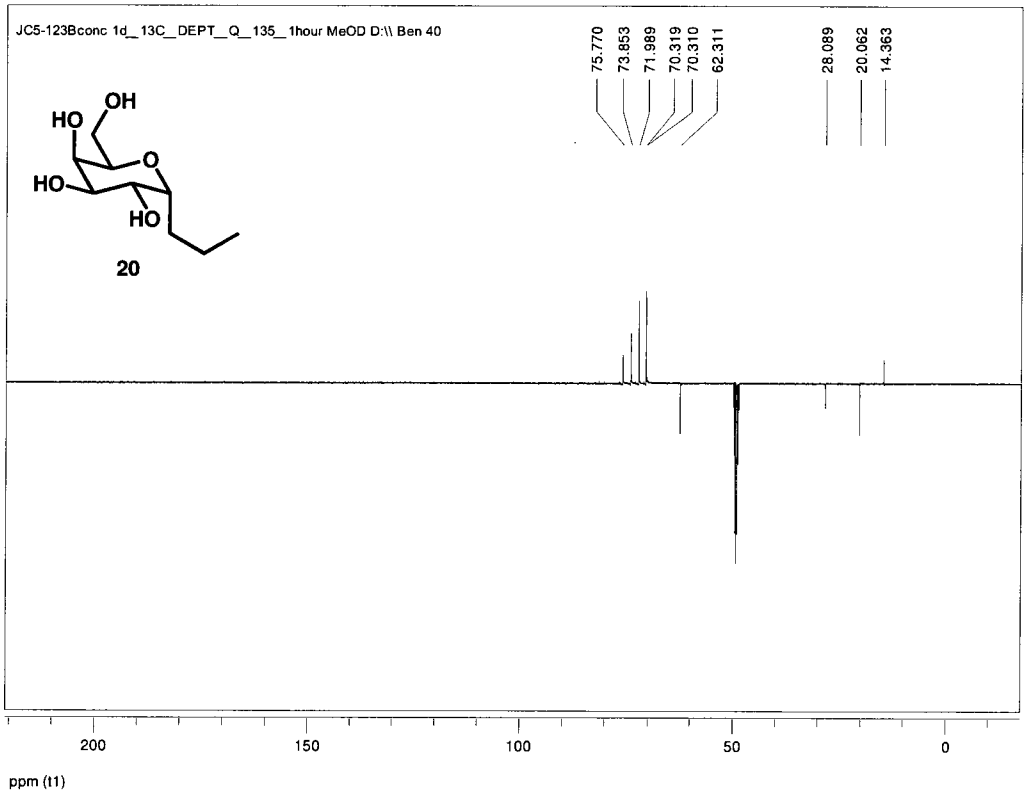
JC5-123Bconc 1d_ 13C_ DEPT_ Q_ 135_ 1hour MeOD D:\\ Ben 40
HO
OH
O
HO
HO
20
75.770
73.853
71.989
70.319
70.310
62.311
28.089
20.062
14.363
200
150
100
50
0
ppm (t1)

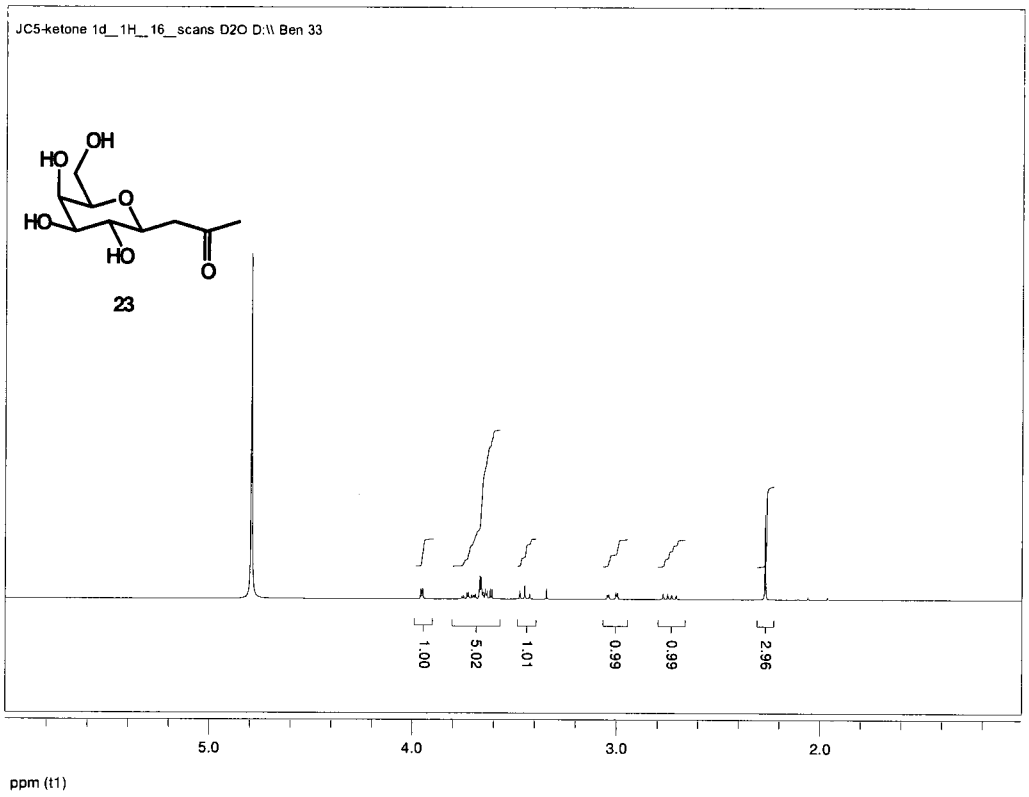
JC5-ketone 1d__1H__16__scans D2O D:\\ Ben 33
OH
HO
O
HO
HO
O
23
1.00
5.02
1.01
0.99
0.99
2.96
5.0
4.0
3.0
2.0
ppm (t1)

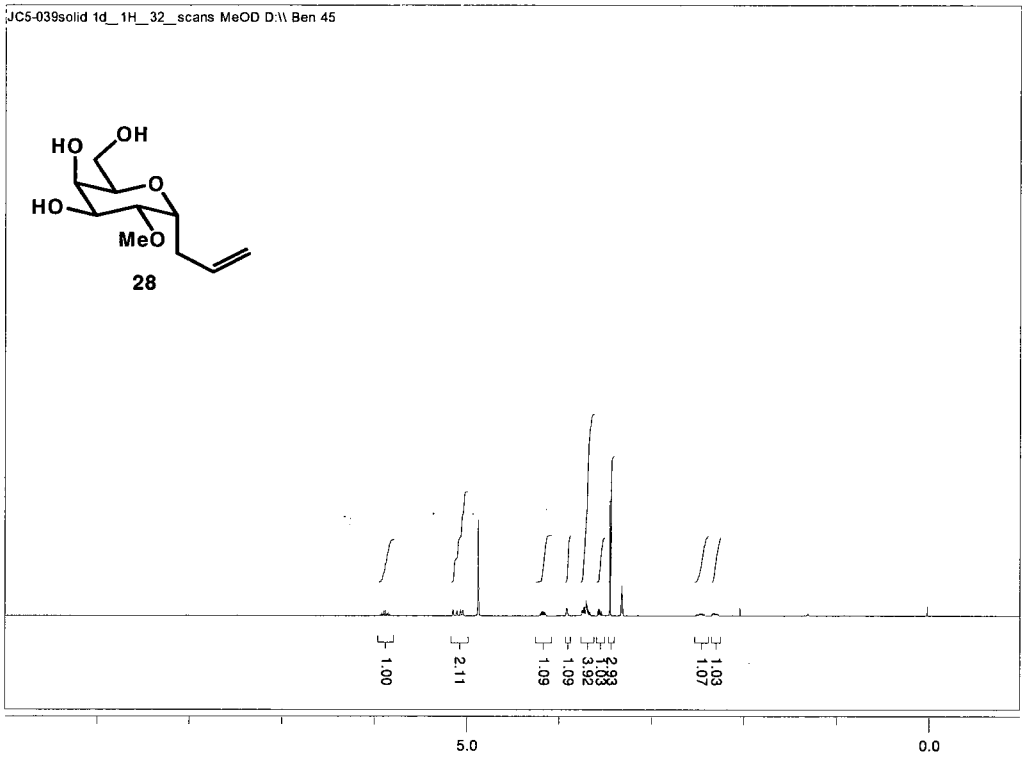
JC5-039solid 1d__1H__32__scans MeOD D:\\ Ben 45
HO
OH
O
HO
MeO
28
1.00
2.11
1.09
1.09
3.92
1.03
1.07
5.0
0.0
ppm (t1)

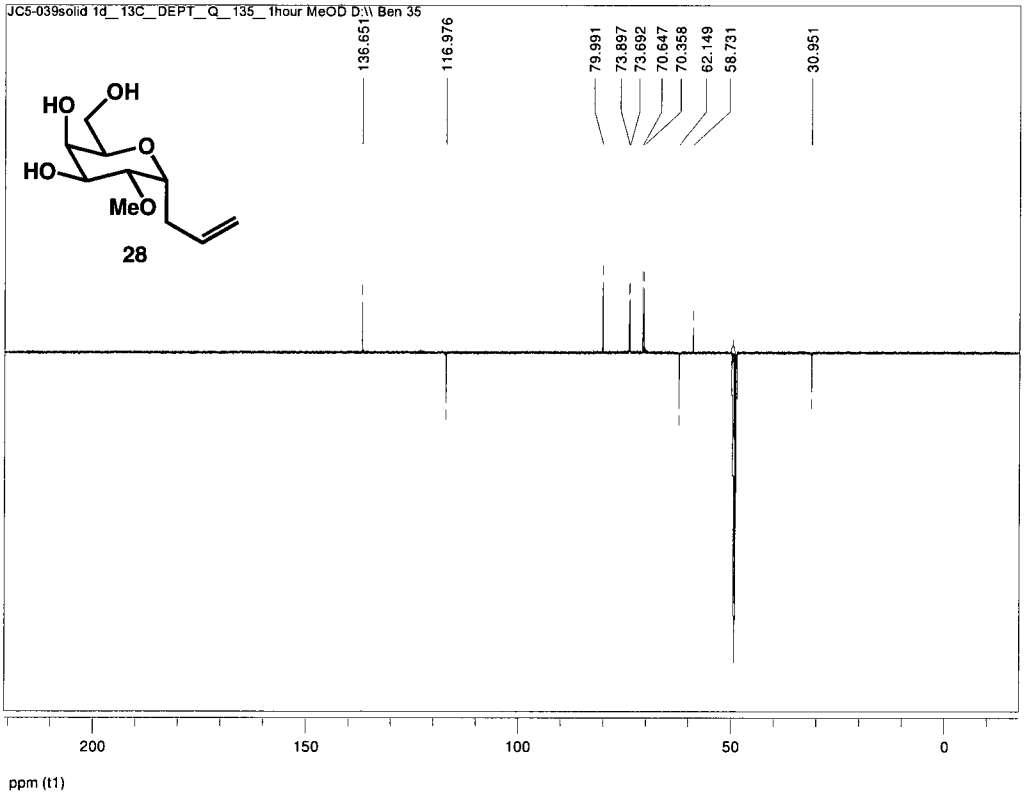
JC5-039solid 1d__13C__DEPT__Q__135__1hour MeOD D:\\ Ben 35
136.651
116.976
79.991
73.897
73.692
70.647
70.358
62.149
58.731
30.951
HO
OH
O
HO
MeO
28
200
150
100
50
0
ppm (t1)

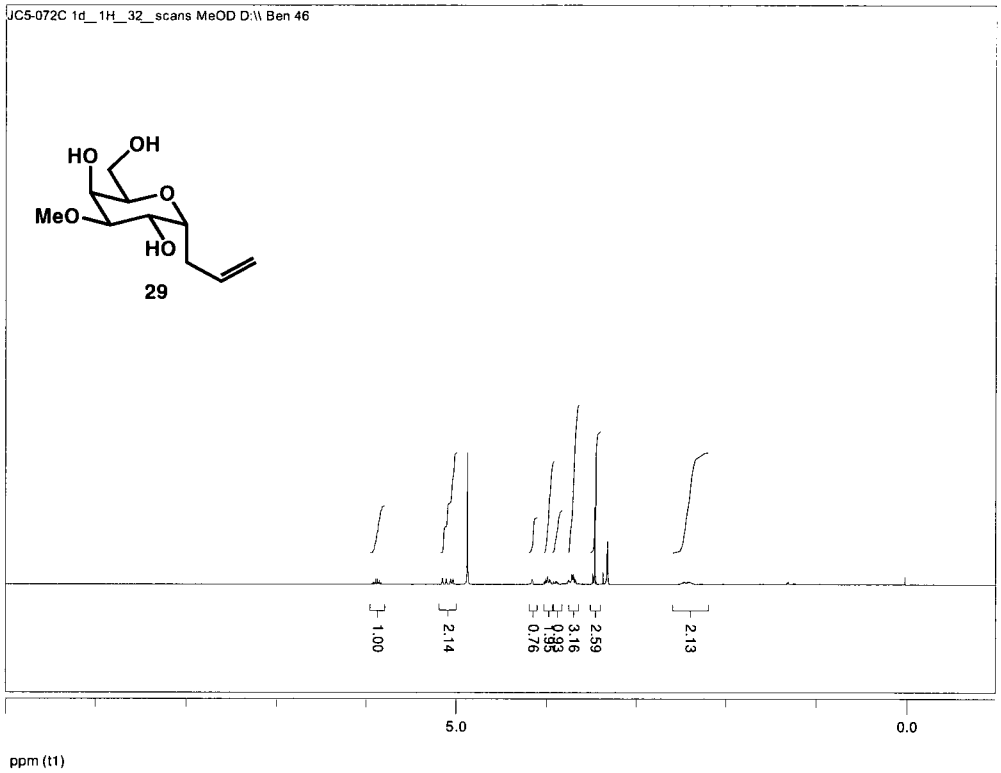
JC5-072C 1d__1H__32__scans MeOD D:\\ Ben 46
HO
OH
O
MeO
HO
29
1.00
2.14
0.76
1.93
1.95
3.16
2.59
2.13
5.0
0.0
ppm (t1)

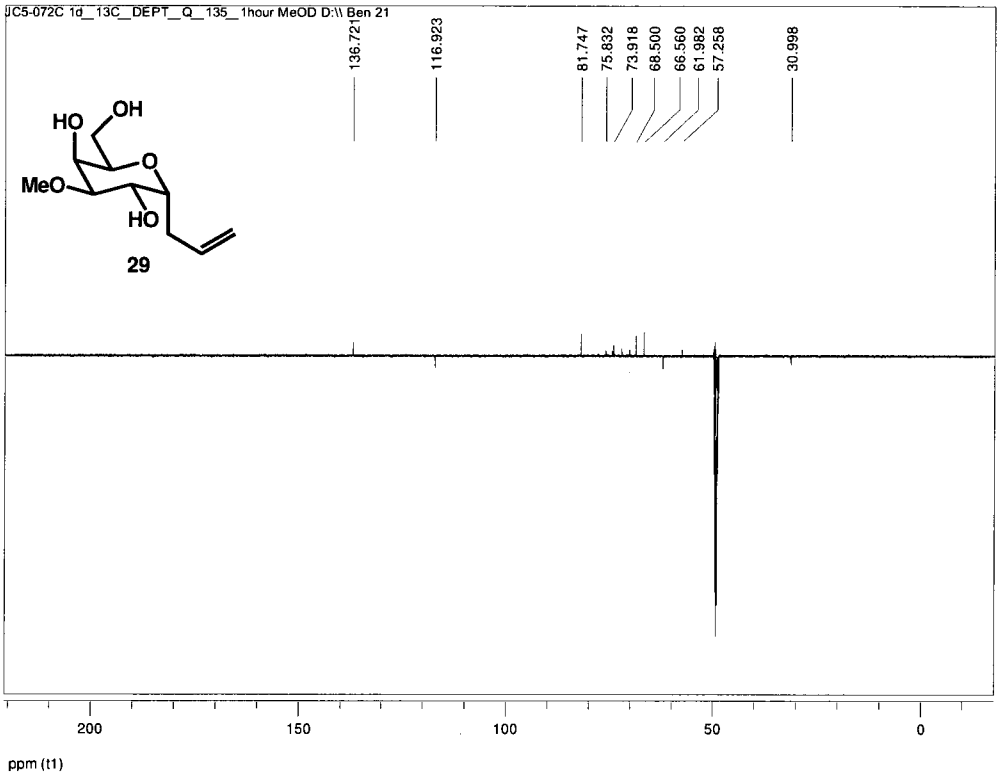
JC5-072C 1d__13C__DEPT__Q__135__1hour MeOD D:\\ Ben 21
136.721
116.923
81.747
75.832
73.918
68.500
66.560
61.982
57.258
30.998
HO
OH
O
MeO
HO
29
200
150
100
50
0
ppm (t1)

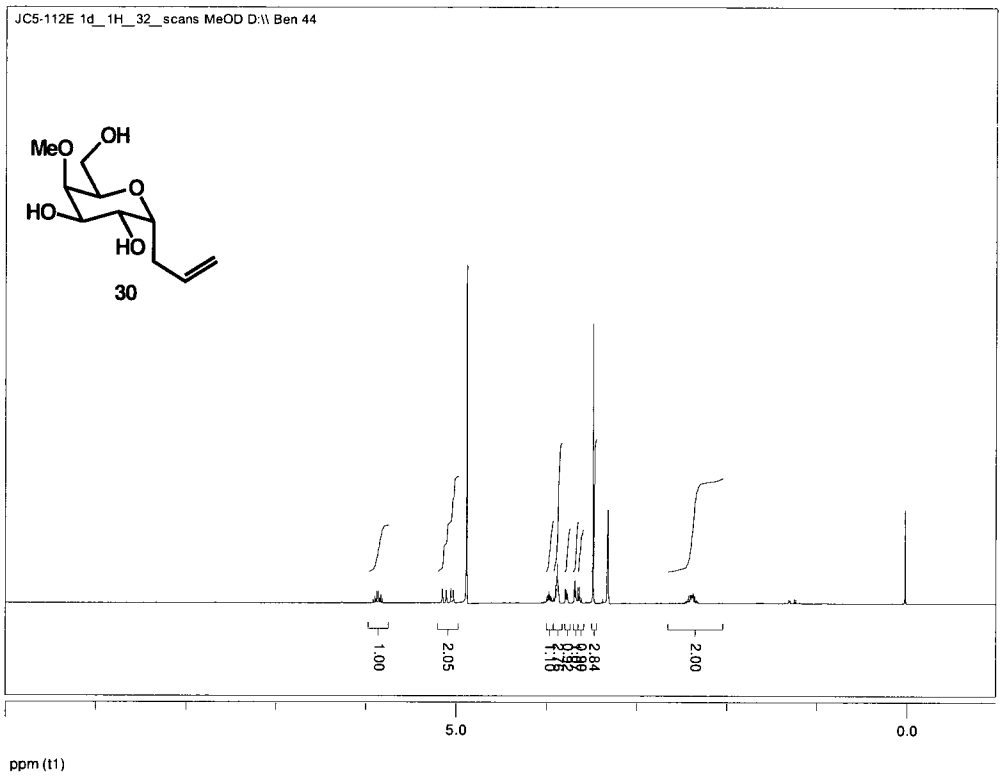
JC5-112E 1d__1H__32__scans MeOD D:\\ Ben 44
MeO
OH
O
HO
HO
30
1.00
2.05
2.84
2.00
5.0
0.0
ppm (t1)

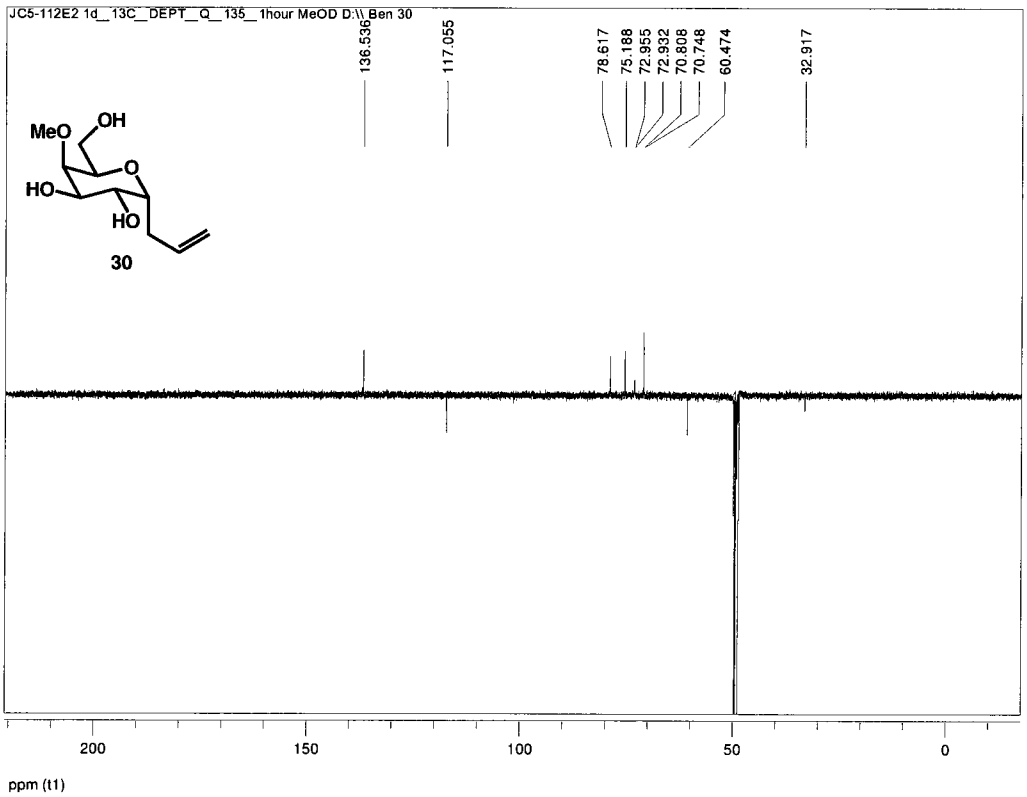
JC5-112E2 1d__13C__DEPT__Q__135__1hour MeOD D:\\ Ben 30
136.536
117.055
78.617
75.188
72.955
72.932
70.808
70.748
60.474
32.917
MeO
OH
O
HO
HO
30
200
150
100
50
0
ppm (t1)

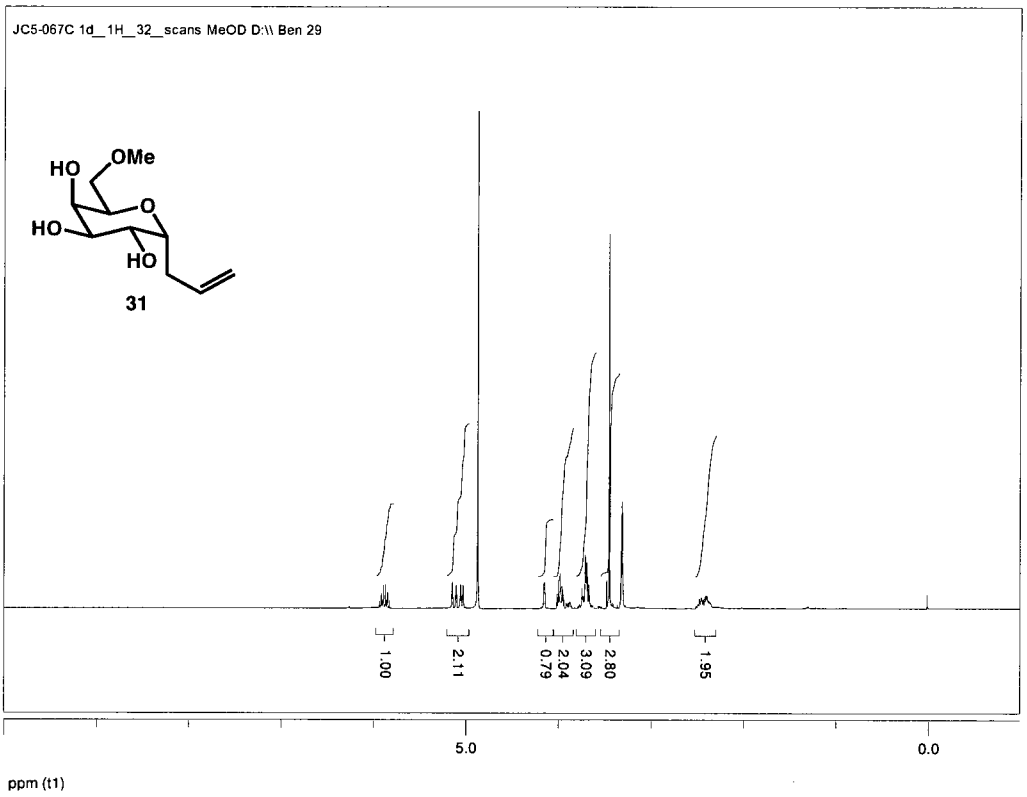
JC5-067C 1d__1H__32__scans MeOD D:\\ Ben 29
HO
OMe
O
HO
HO
31
1.00
2.11
0.79
2.04
3.09
2.80
1.95
5.0
0.0
ppm (t1)

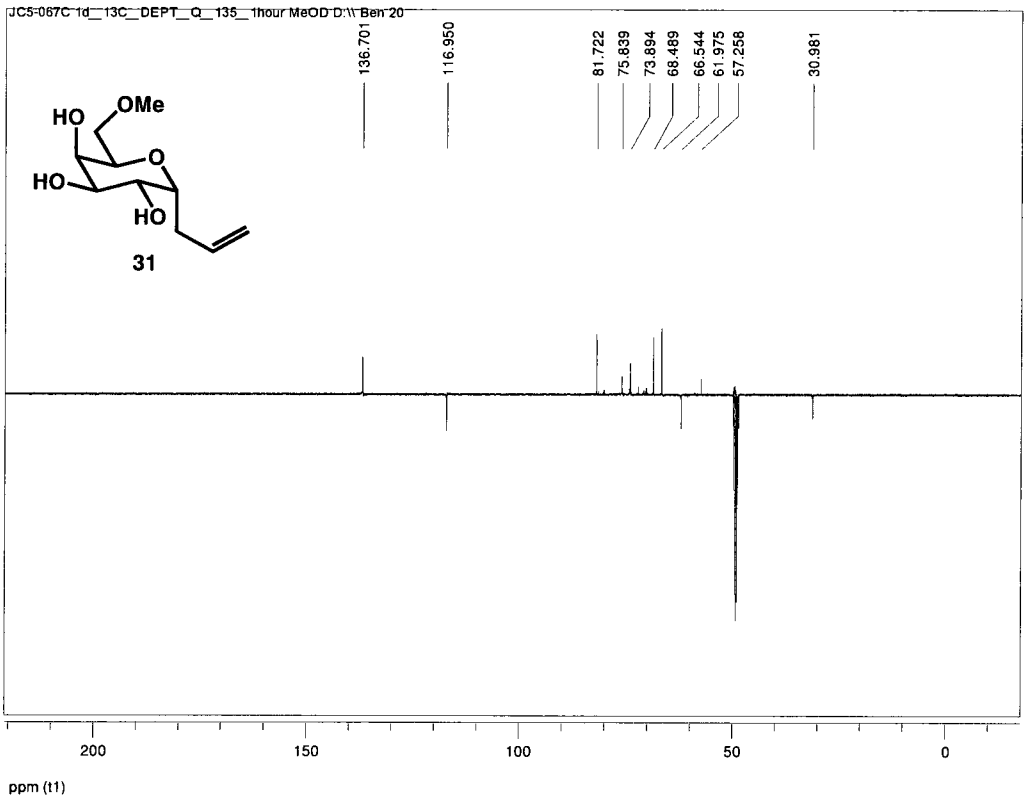
JC5-067C 1d__13C__DEPT__Q__135__1hour MeOD D:\\ Ben 20
136.701
116.950
81.722
75.839
73.894
68.489
66.544
61.975
57.258
30.981
HO
OMe
O
HO
HO
31
200
150
100
50
0
ppm (t1)

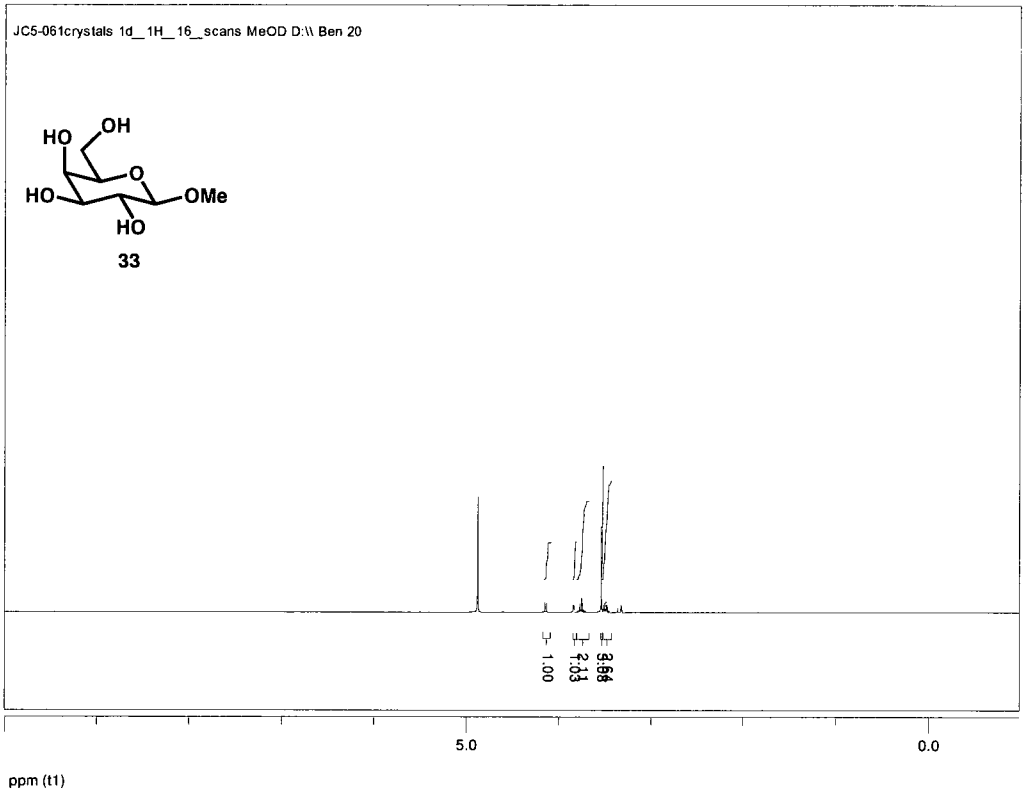
JC5-061crystals 1d__1H__16__scans MeOD D:\\ Ben 20
HO
OH
O
HO
OMe
HO
33
1.00
2.11
7.03
3.84
3.88
5.0
0.0
ppm (t1)

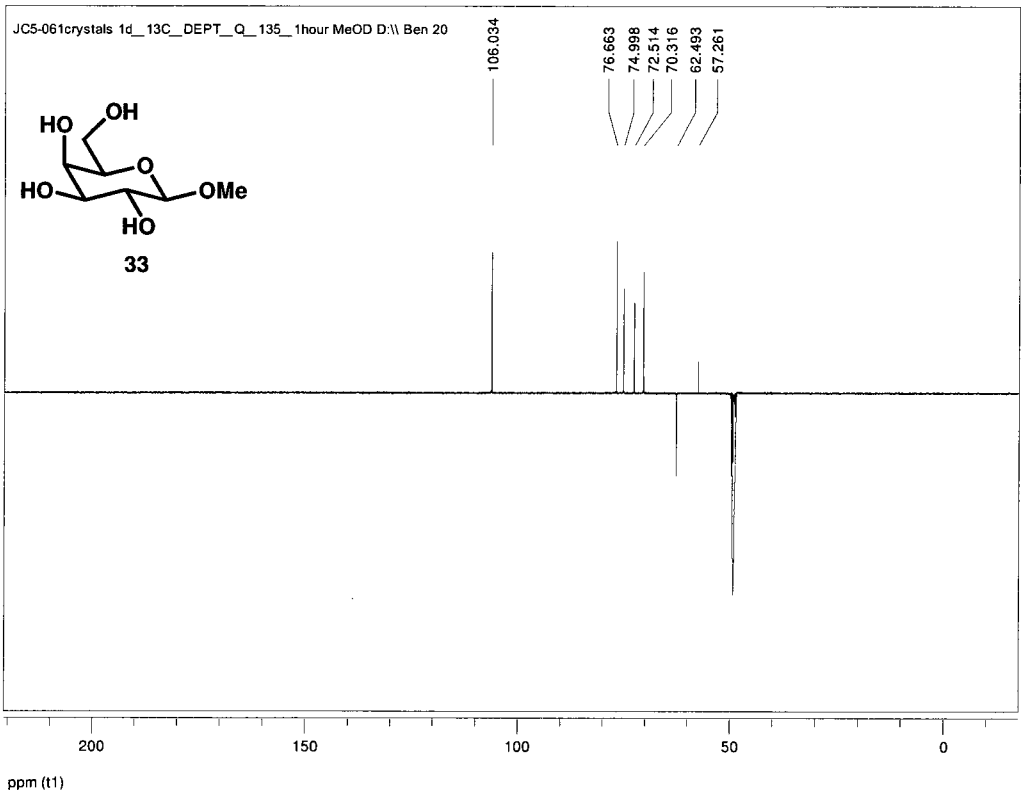
JC5-061crystals 1d__13C__DEPT__Q__135__1hour MeOD D:\\ Ben 20
106.034
76.663
74.998
72.514
70.316
62.493
57.261
HO
OH
O
HO
OMe
HO
33
200
150
100
50
0
ppm (t1)

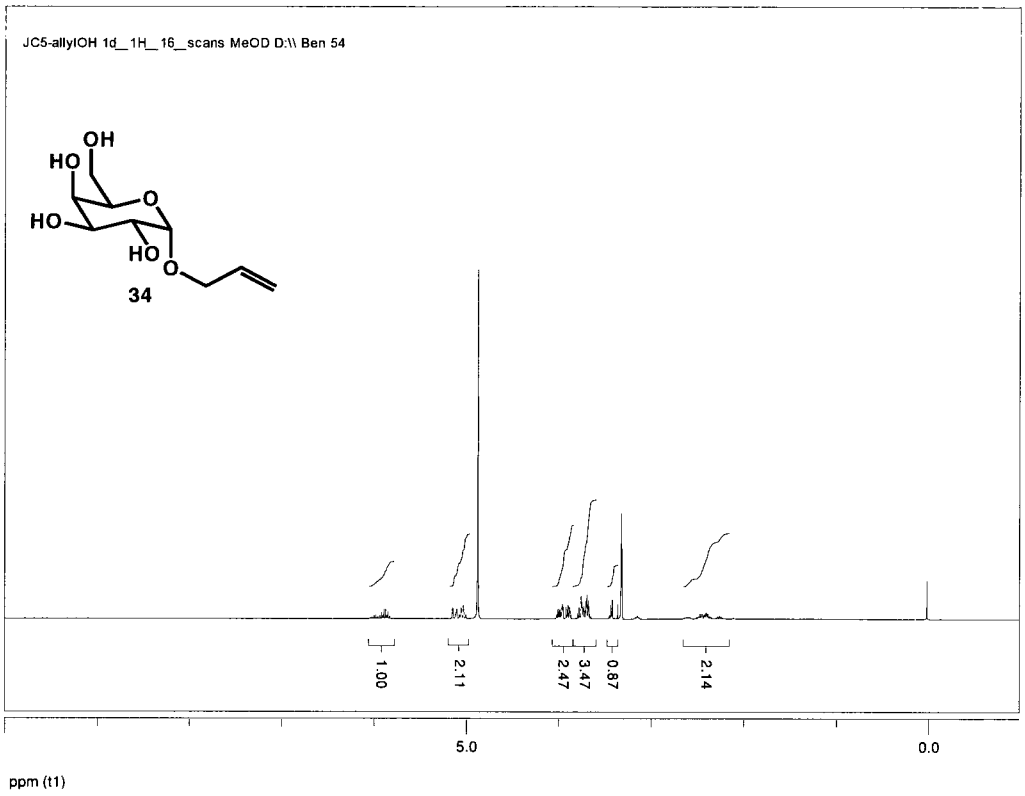
JC5-allylOH 1d_1H_16_scans MeOD D:\\ Ben 54
OH
HO
O
HO
HO
O
34
1.00
2.11
2.47
3.47
0.87
2.14
5.0
0.0
ppm (t1)

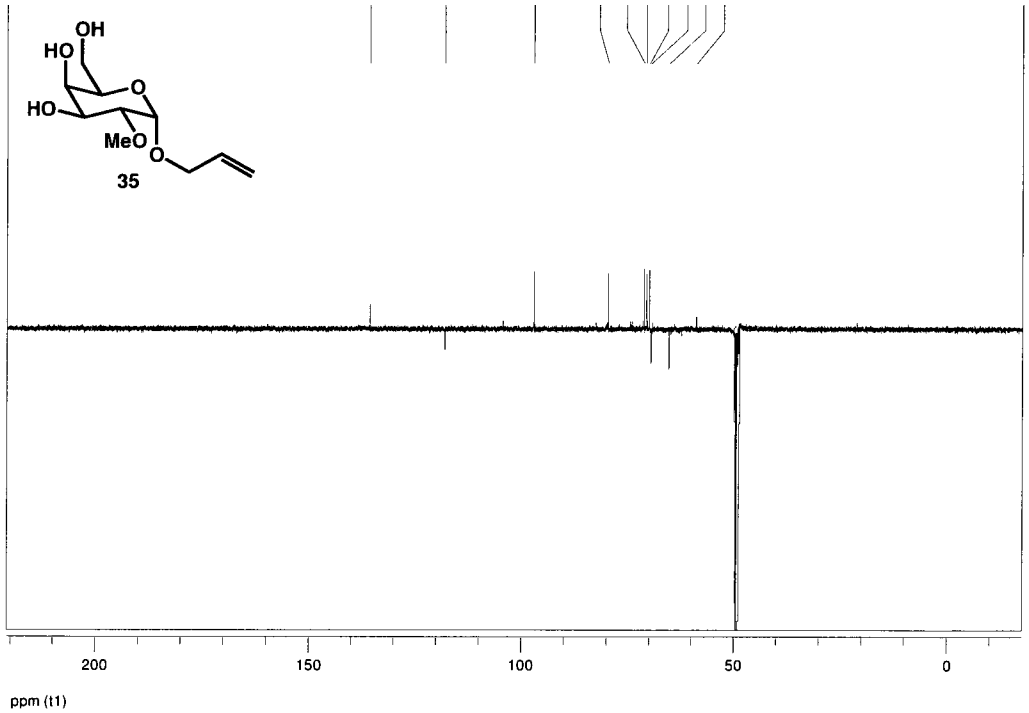
OH
HO
O
HO
MeO
O
35
200
150
100
50
0
ppm (t1)

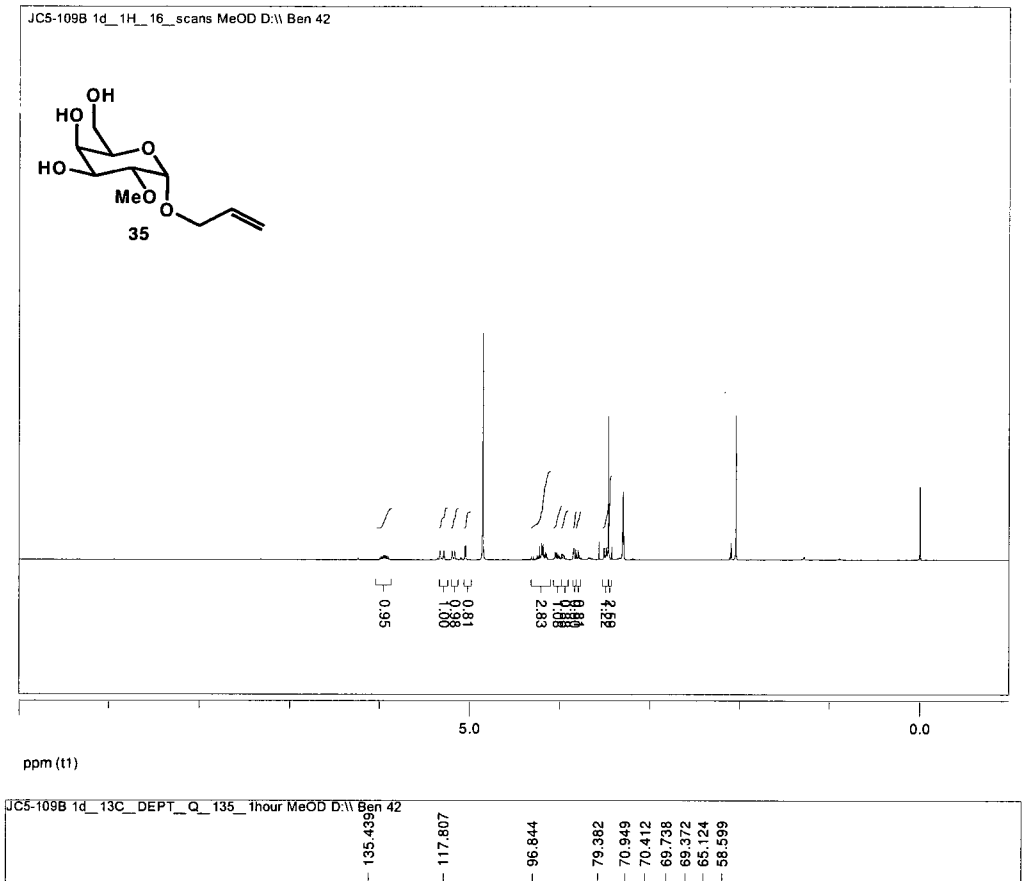
JC5-109B 1d__1H__16__scans MeOD D:\\ Ben 42
OH
HO
O
HO
MeO
O
35
0.95
1.00
0.88
1.81
2.83
2.82
5.0
0.0
ppm (t1)

JC5-109B 1d__13C__DEPT__Q__135__1hour MeOD D:\\ Ben 42
135.439
117.807
96.844
79.382
70.949
70.412
69.738
69.372
65.124
58.599

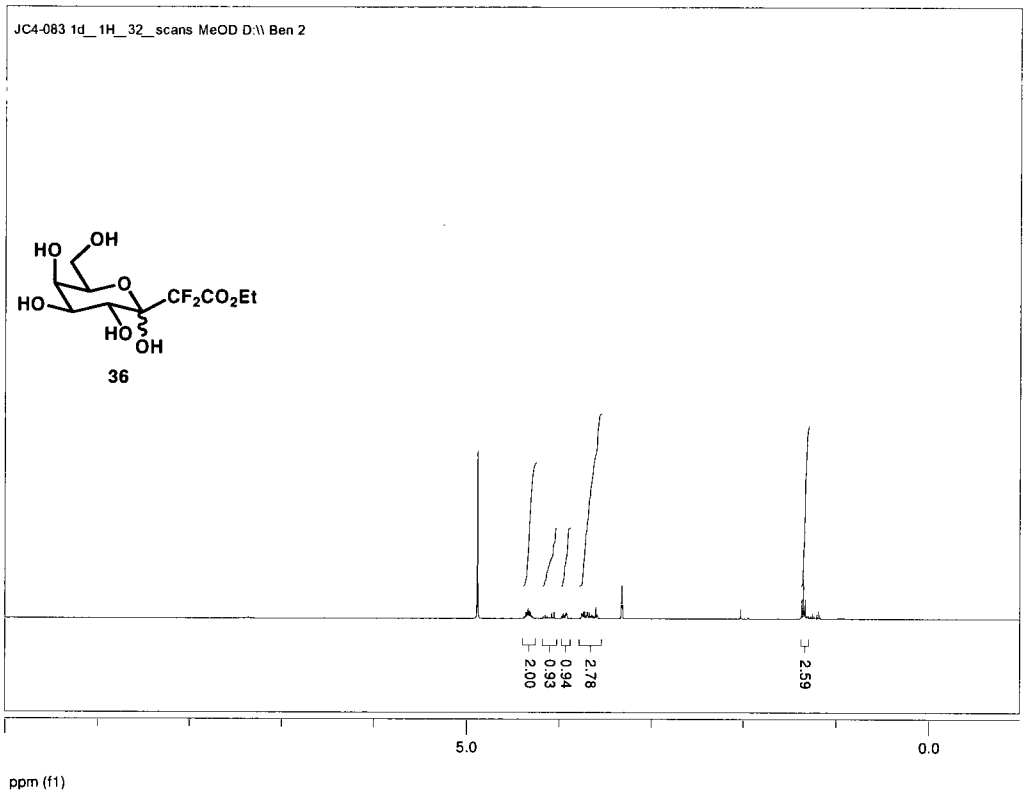
JC4-083 1d__1H__32__scans MeOD D:\\ Ben 2
HO
OH
O
HO
CF2CO2Et
HO
OH
36
2.00
0.93
0.94
2.78
2.59
5.0
0.0
ppm (f1)

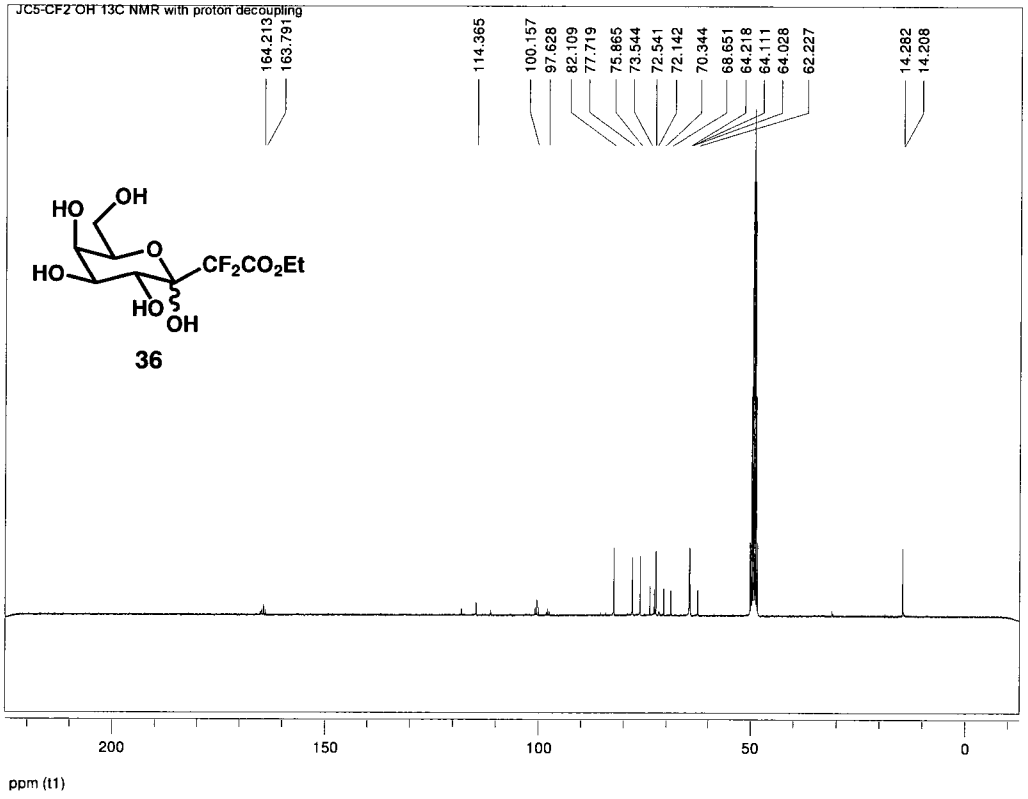
JC5-CF2 OH 13C NMR with proton decoupling
164.213
163.791
114.365
100.157
97.628
82.109
77.719
75.865
73.544
72.541
72.142
70.344
68.651
64.218
64.111
64.028
62.227
14.282
14.208
HO
OH
O
HO
CF2CO2Et
HO
OH
36
200
150
100
50
0
ppm (t1)

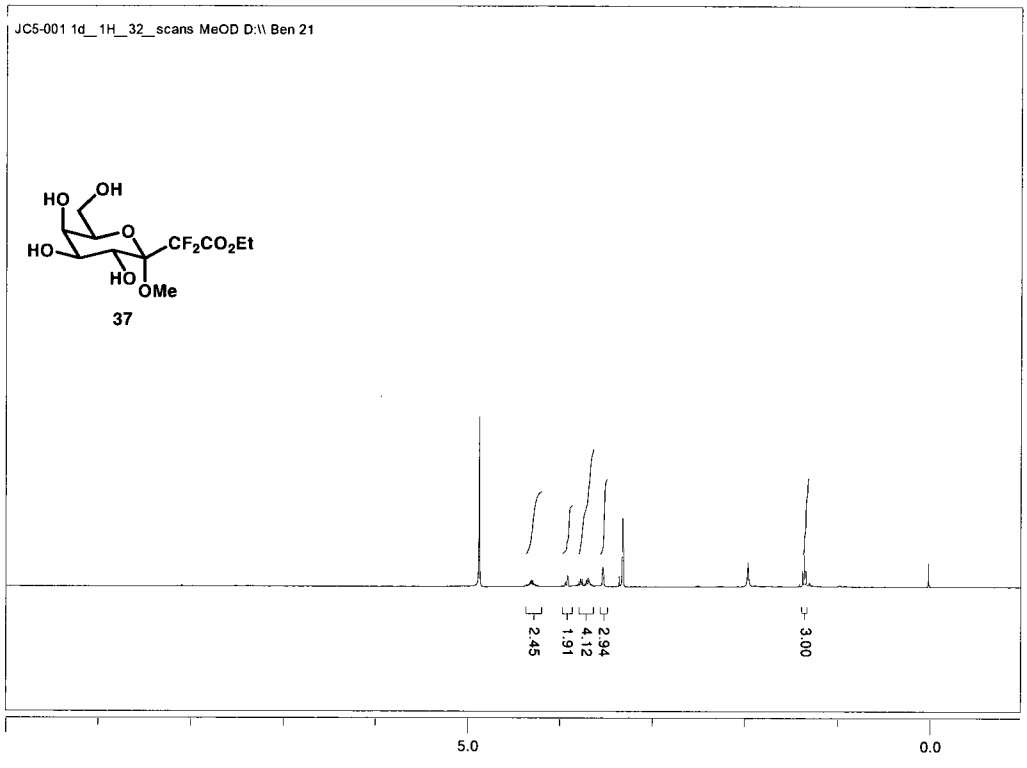
JC5-001 1d__1H__32__scans MeOD D:\\ Ben 21
HO
OH
O
HO
CF2CO2Et
HO
OMe
37
2.45
1.91
4.12
2.94
3.00
5.0
0.0
ppm (t1)

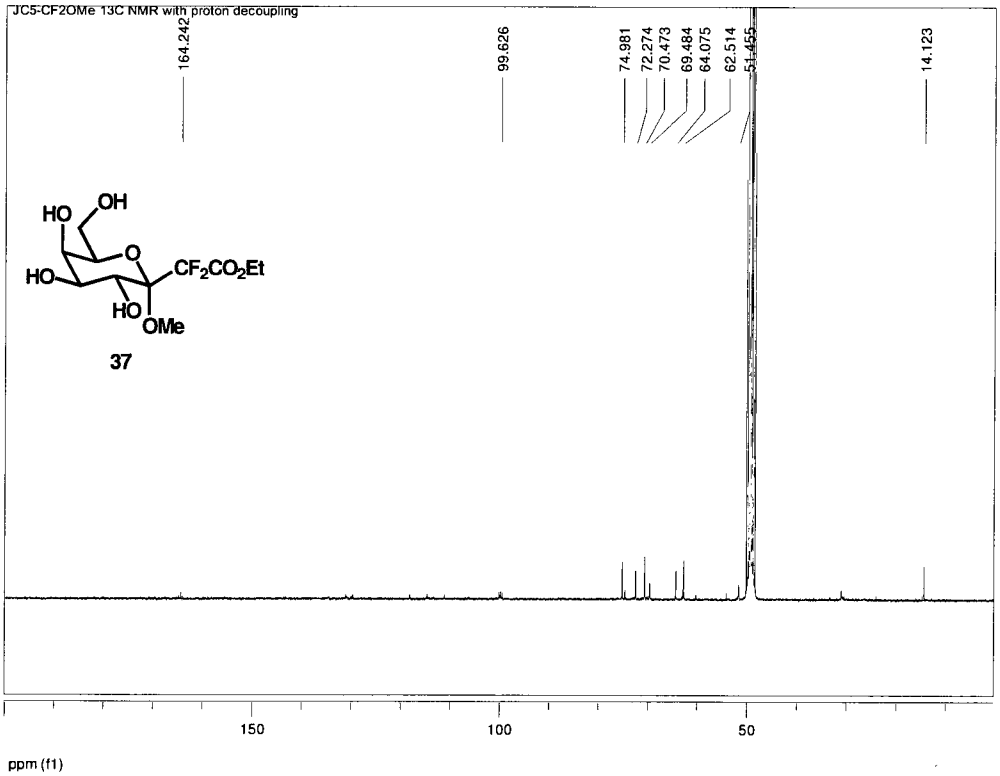
JC5-CF2OMe 13C NMR with proton decoupling
164.242
99.626
74.981
72.274
70.473
69.484
64.075
62.514
51.455
14.123
HO
OH
O
HO
CF2CO2Et
HO
OMe
37
150
100
50
ppm (f1)

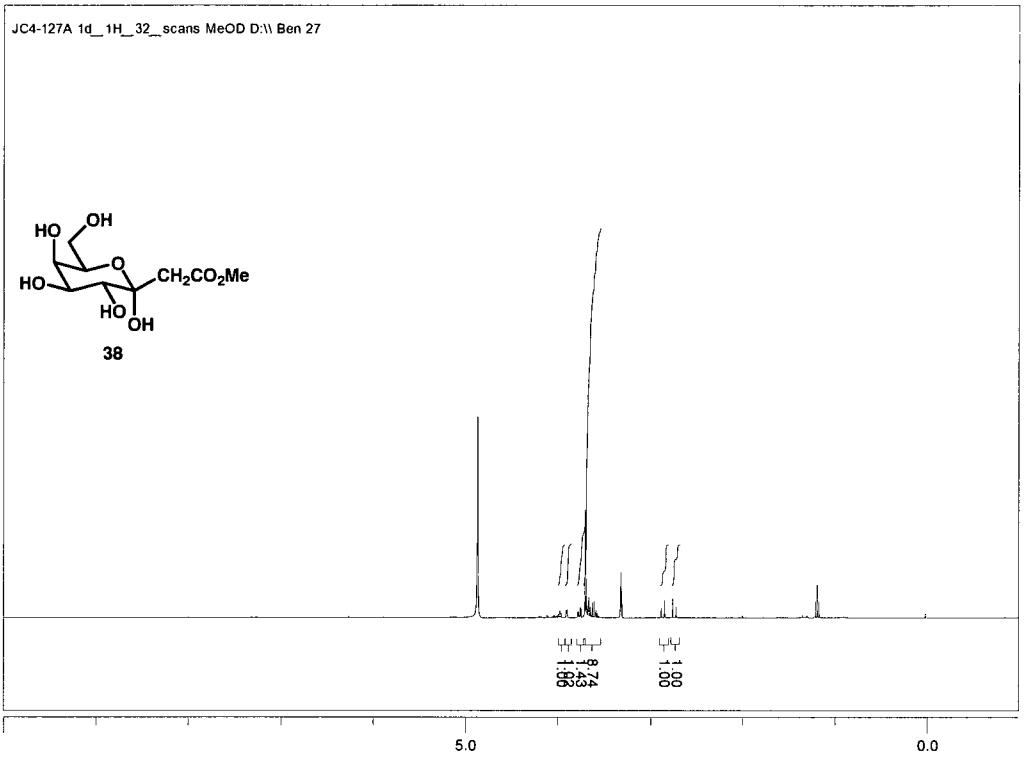
JC4-127A 1d__1H__32__scans MeOD D:\\ Ben 27
HO
OH
O
HO
CH2CO2Me
HO
OH
38
1.00
1.00
8.74
1.43
1.00
5.0
0.0
ppm (f1)

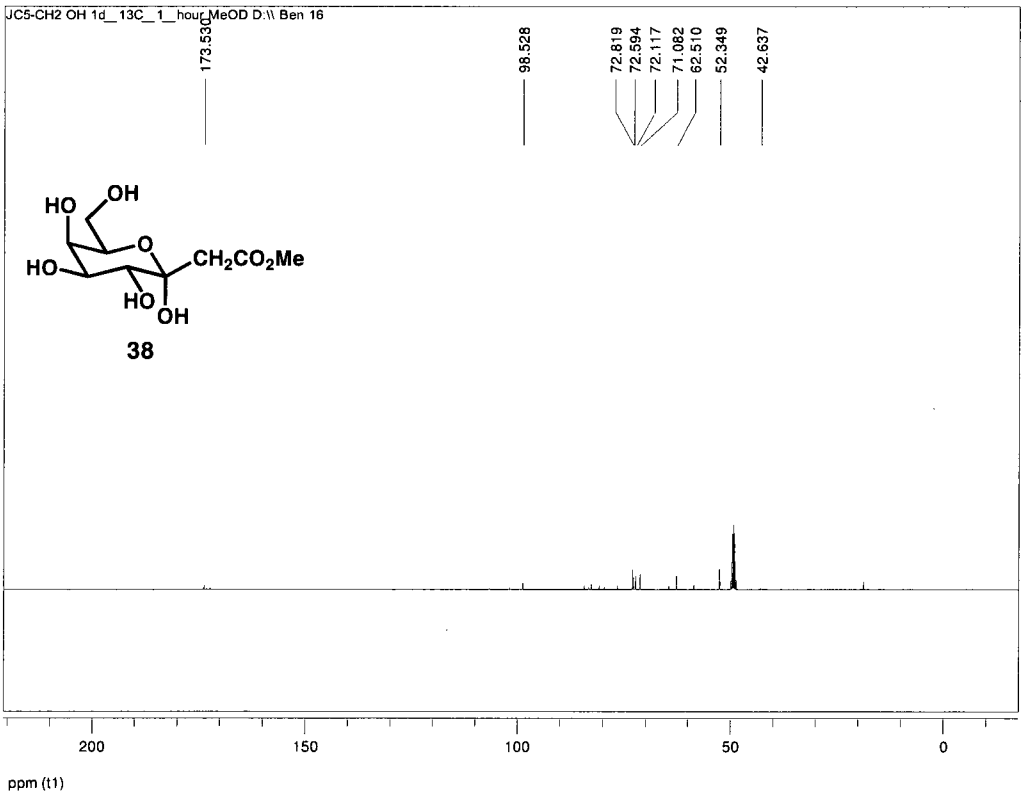
JC5-CH2 OH 1d__13C__1__hour MeOD D:\\ Ben 16
173.530
98.528
72.819
72.594
72.117
71.082
62.510
52.349
42.637
HO
OH
O
HO
CH2CO2Me
HO
OH
38
200
150
100
50
0
ppm (t1)

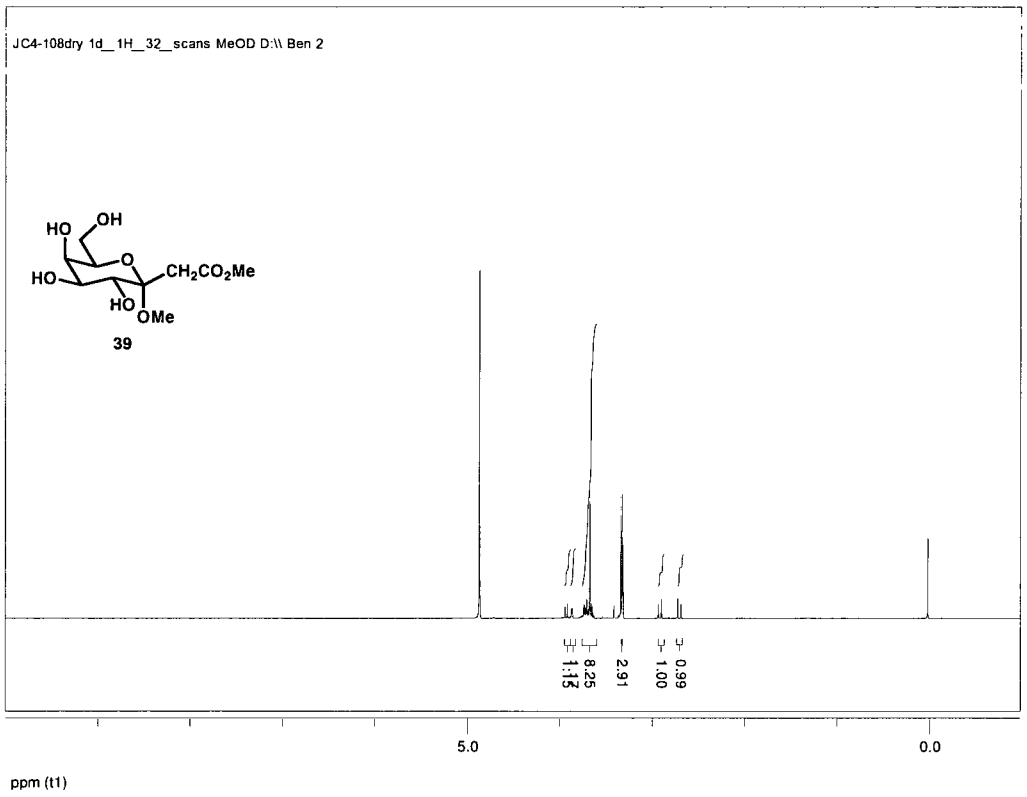
JC4-108dry 1d__1H__32__scans MeOD D:\\ Ben 2
HO
OH
O
HO
CH2CO2Me
HO
OMe
39
1.13
8.25
2.91
1.00
0.99
5.0
0.0
ppm (t1)

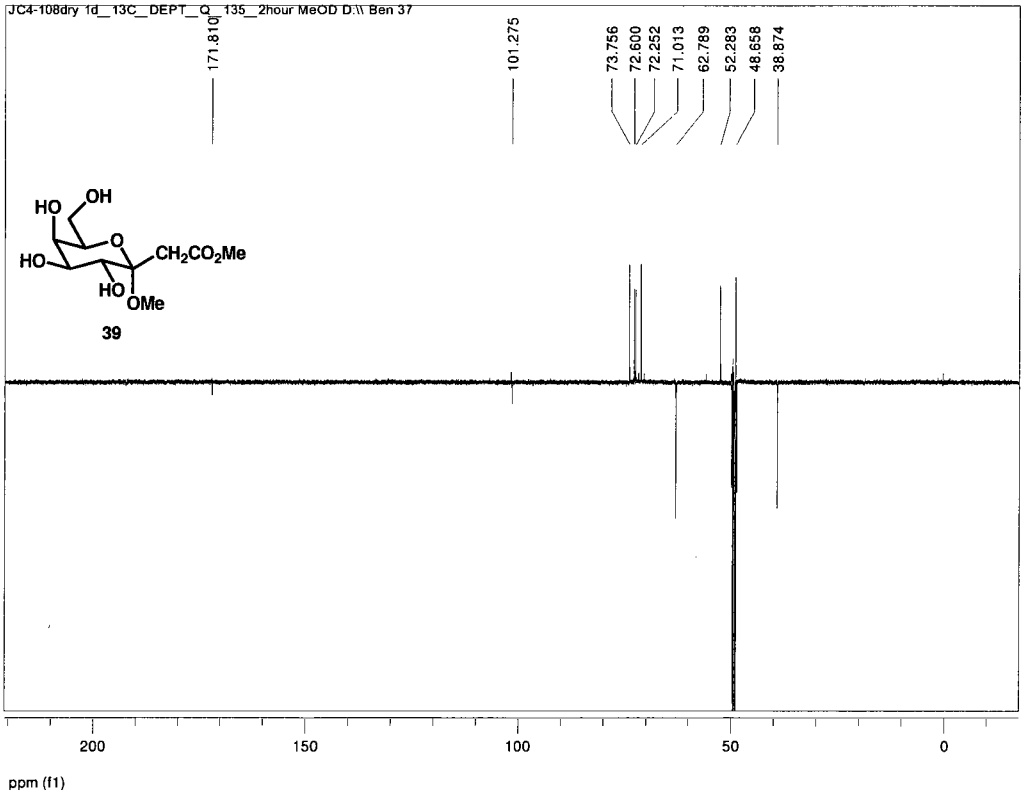
JC4-108dry 1d__13C__DEPT__Q__135__2hour MeOD D:\\ Ben 37
171.810
101.275
73.756
72.600
72.252
71.013
62.789
52.283
48.658
38.874
HO
OH
O
HO
CH2CO2Me
HO
OMe
39
200
150
100
50
0
ppm (f1)

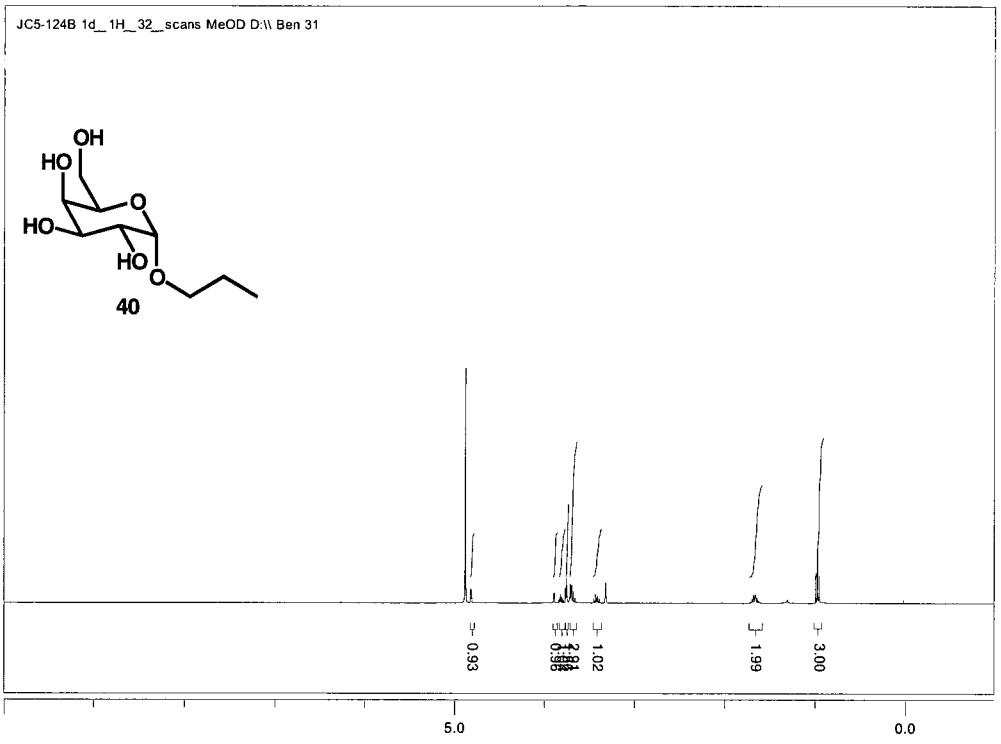
JC5-124B 1d__1H__32__scans MeOD D:\\ Ben 31
OH
HO
O
HO
HO
O
40
0.93
1.02
1.99
3.00
5.0
0.0
ppm (t1)

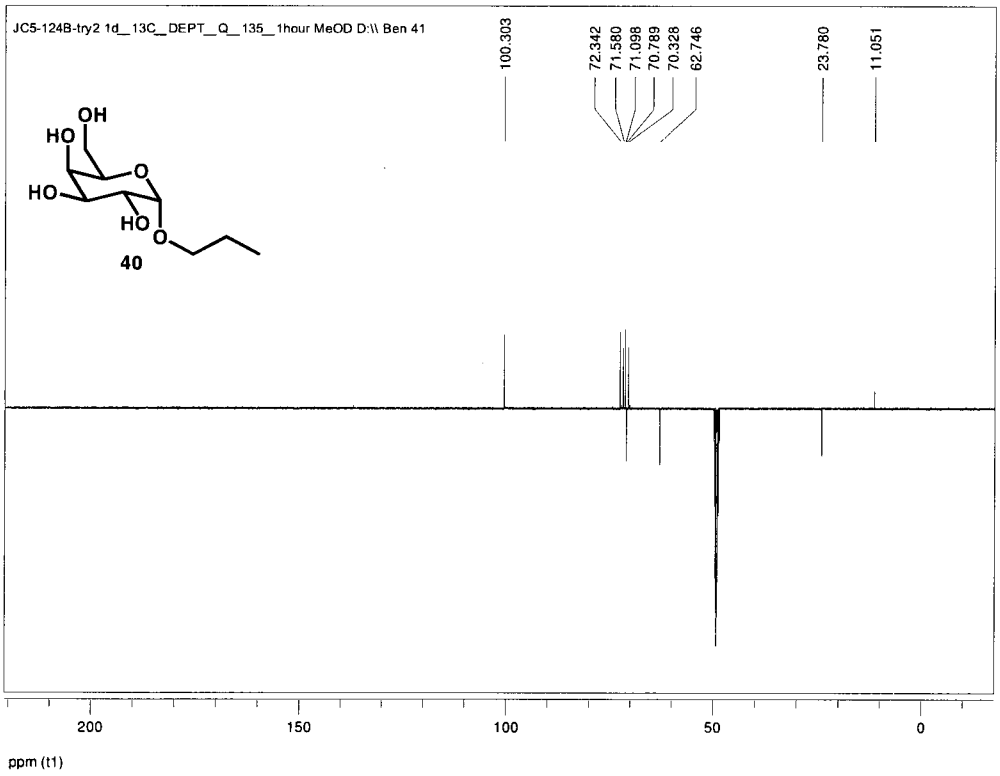
JC5-124B-try2 1d__13C__DEPT__Q__135__1hour MeOD D:\\ Ben 41
OH
HO
O
HO
HO
O
40
100.303
72.342
71.580
71.098
70.789
70.328
62.746
23.780
11.051
200
150
100
50
0
ppm (t1)

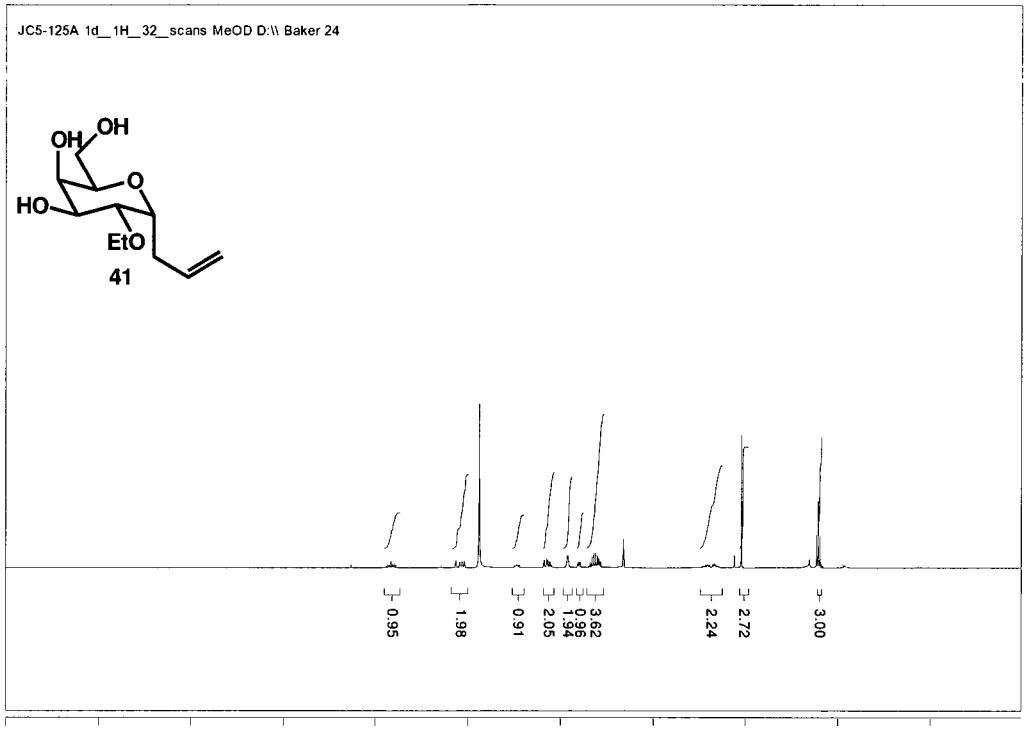
JC5-125A 1d__1H__32__scans MeOD D:\\ Baker 24
OH
OH
O
HO
EtO
41
0.95
1.98
0.91
2.05
1.94
0.96
3.62
2.24
2.72
3.00

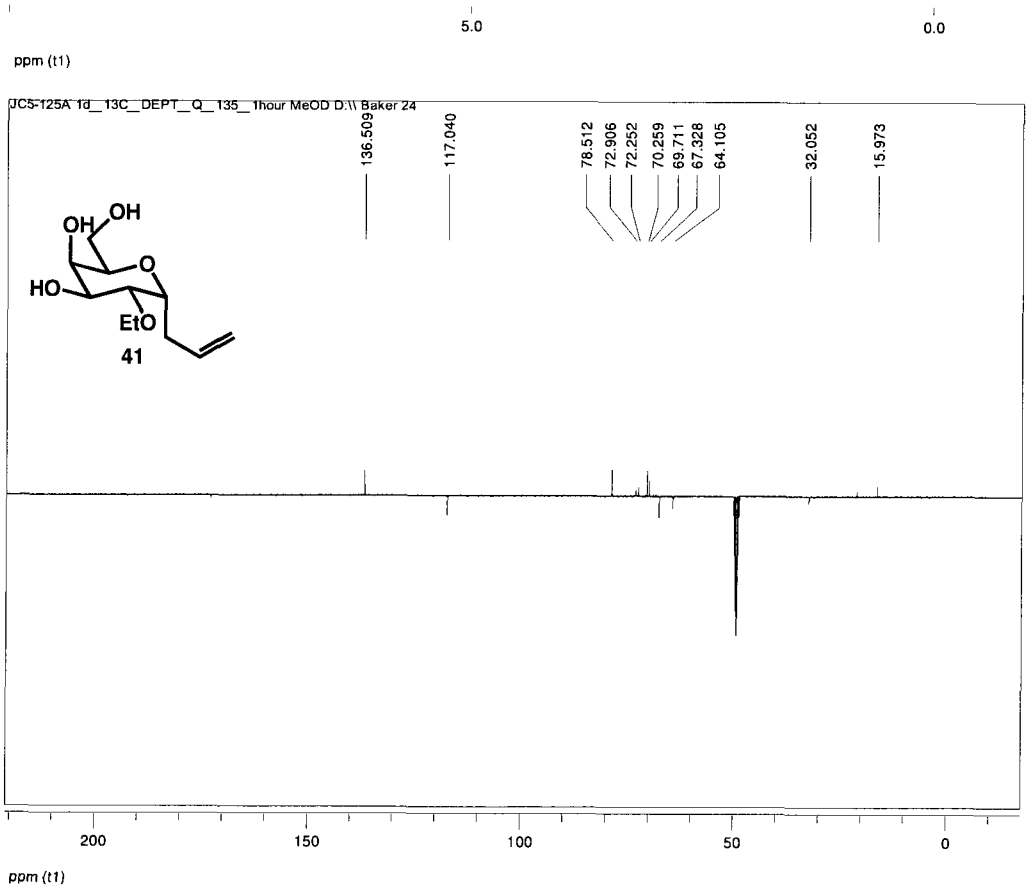
5.0
0.0
ppm (t1)
JCS-125A 1d_13C_DEPT_Q_135_1hour MeOD D:\\ Baker 24
136.509
117.040
78.512
72.906
72.252
70.259
69.711
67.328
64.105
32.052
15.973
OH
OH
O
HO
EtO
41
200
150
100
50
0
ppm (t1)

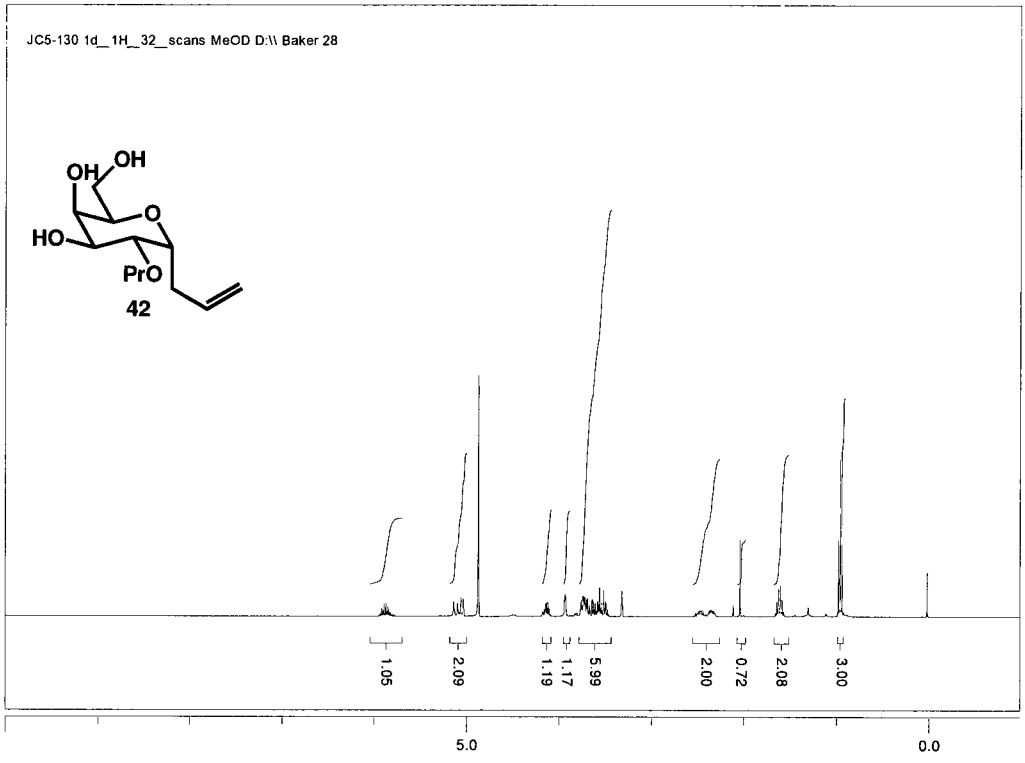
JC5-130 1d__1H__32__scans MeOD D:\\ Baker 28
OH
OH
O
HO
PrO
42
1.05
2.09
1.19
1.17
5.99
2.00
0.72
2.08
3.00
5.0
0.0
ppm (t1)

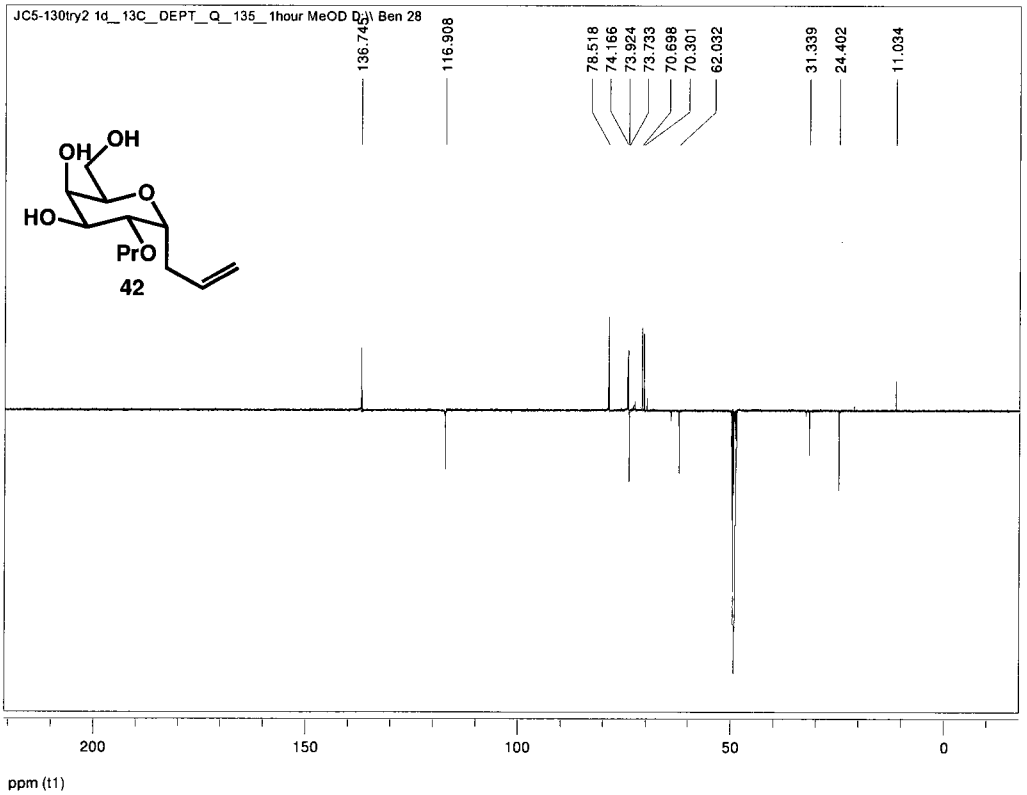
JC5-130try2 1d__13C__DEPT__Q__135__1hour MeOD D:\\ Ben 28
136.745
116.908
78.518
74.166
73.924
73.733
70.698
70.301
62.032
31.339
24.402
11.034
OH
OH
O
HO
PrO
42
200
150
100
50
0
ppm (t1)

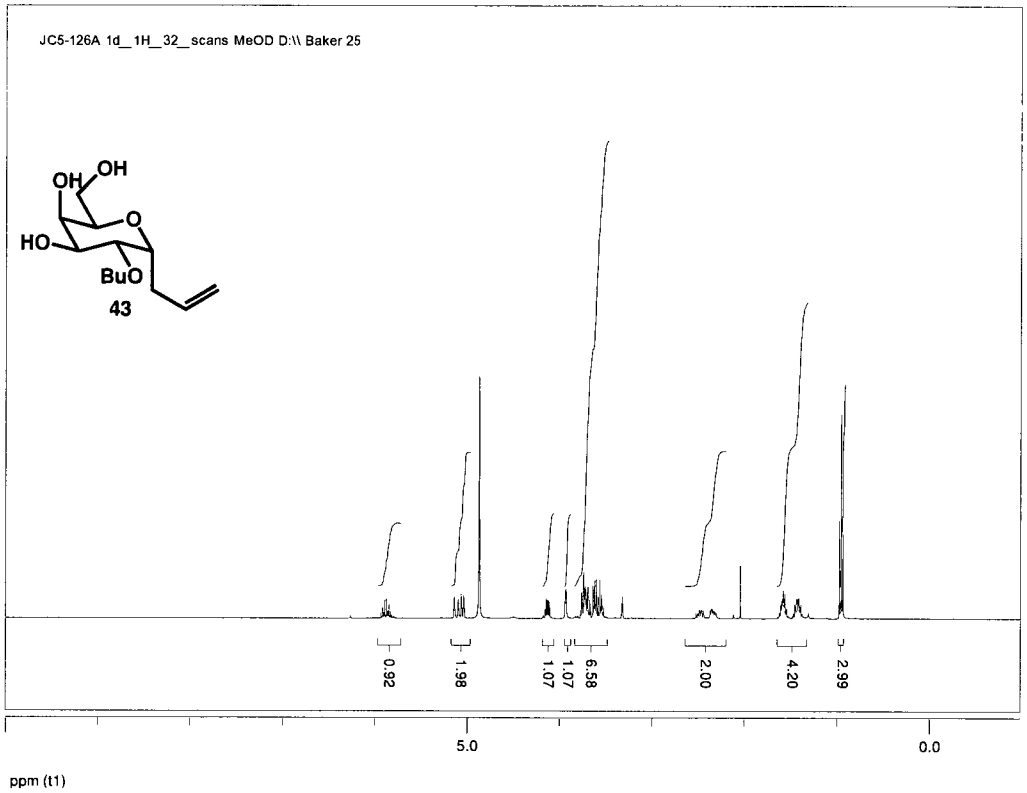
JC5-126A 1d__1H__32__scans MeOD D:\\ Baker 25
OH
OH
O
HO
BuO
43
0.92
1.98
1.07
1.07
9.58
2.00
4.20
2.99
5.0
0.0
ppm (t1)

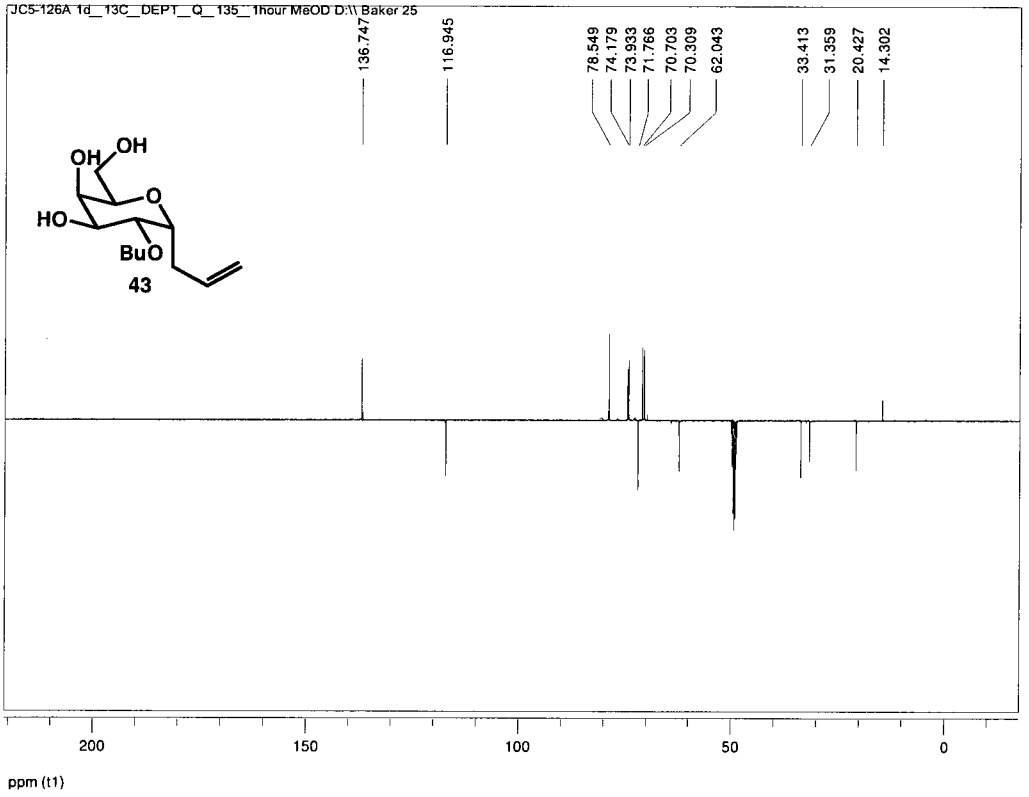
JC5-126A 1d__13C__DEPT__Q__135__1hour MeOD D:\\ Baker 25
136.747
116.945
78.549
74.179
73.933
71.766
70.703
70.309
62.043
33.413
31.359
20.427
14.302
OH
OH
O
HO
BuO
43
200
150
100
50
0
ppm (t1)

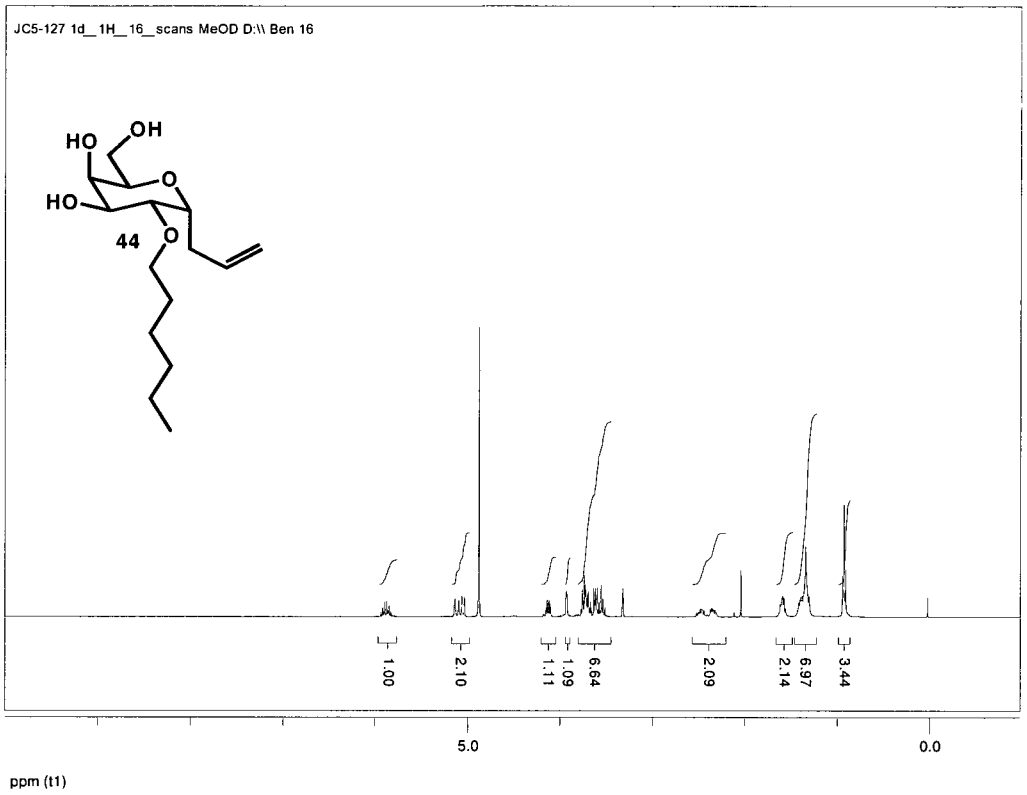
JC5-127 1d__1H__16__scans MeOD D:\\ Ben 16
HO
OH
HO
O
44
O
1.00
2.10
1.11
1.09
9.64
2.09
2.14
9.67
3.44
5.0
0.0
ppm (t1)

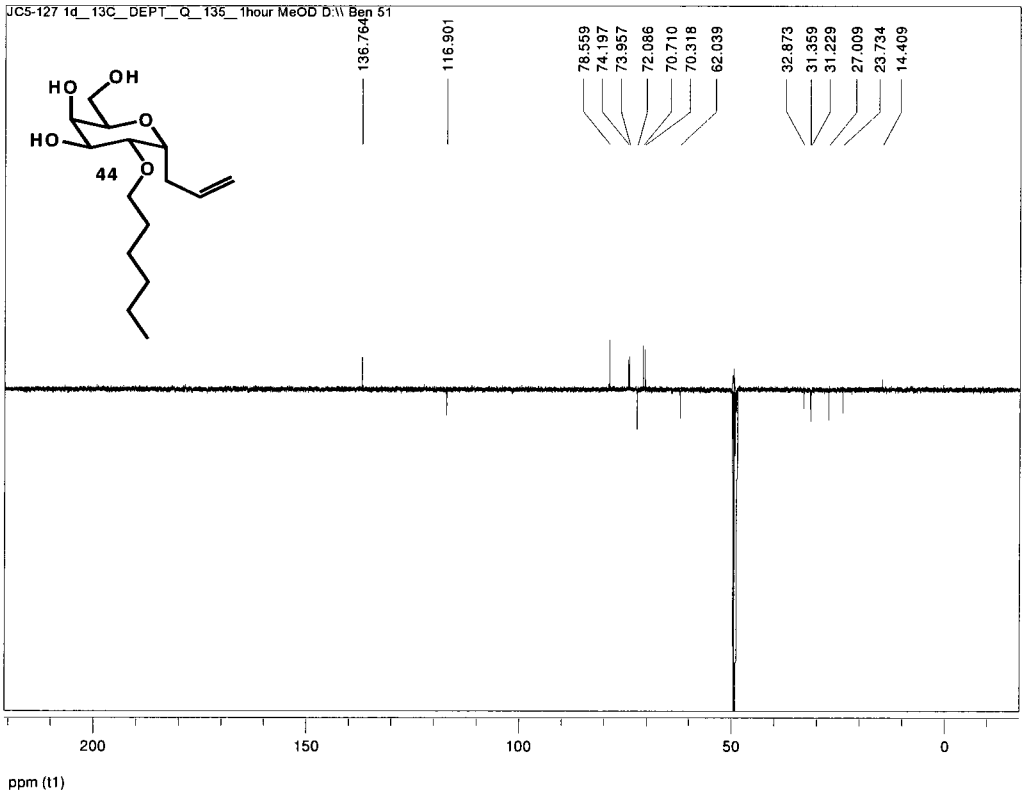
JC5-127 1d__13C__DEPT__Q__135__1hour MeOD D:\\ Ben 51
HO
OH
HO
O
44
O
136.764
116.901
78.559
74.197
73.957
72.086
70.710
70.318
62.039
32.873
31.359
31.229
27.009
23.734
14.409
200
150
100
50
0
ppm (t1)

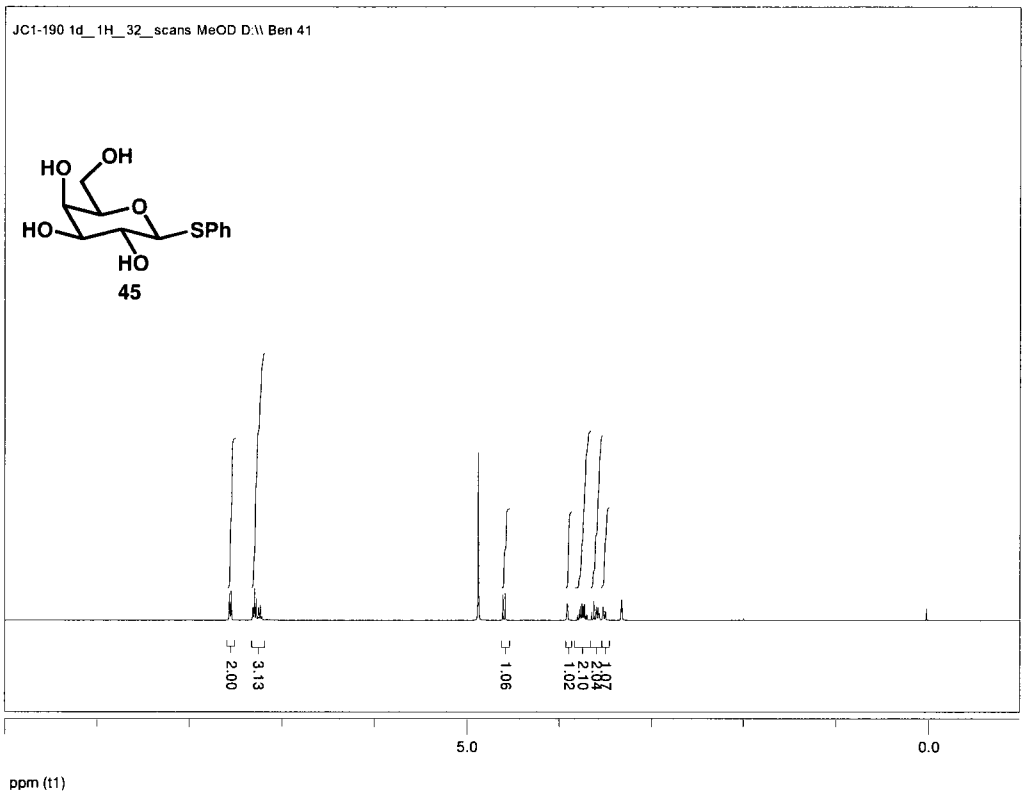
JC1-190 1d__1H__32__scans MeOD D:\\ Ben 41
HO
OH
O
HO
SPh
HO
45
2.00
3.13
1.06
1.02
2.10
5.0
0.0
ppm (t1)

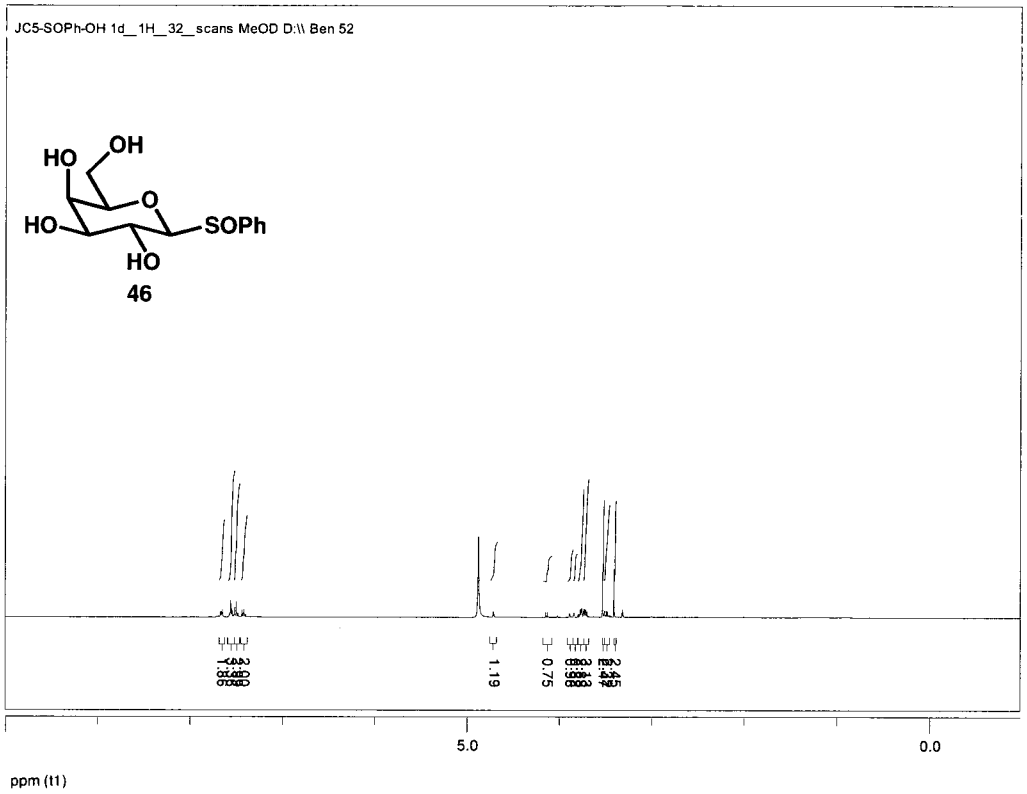
JC5-SOPh-OH 1d__1H__32__scans MeOD D:\\ Ben 52
HO
OH
O
HO
SOPh
HO
46
1.19
0.75
5.0
0.0
ppm (t1)

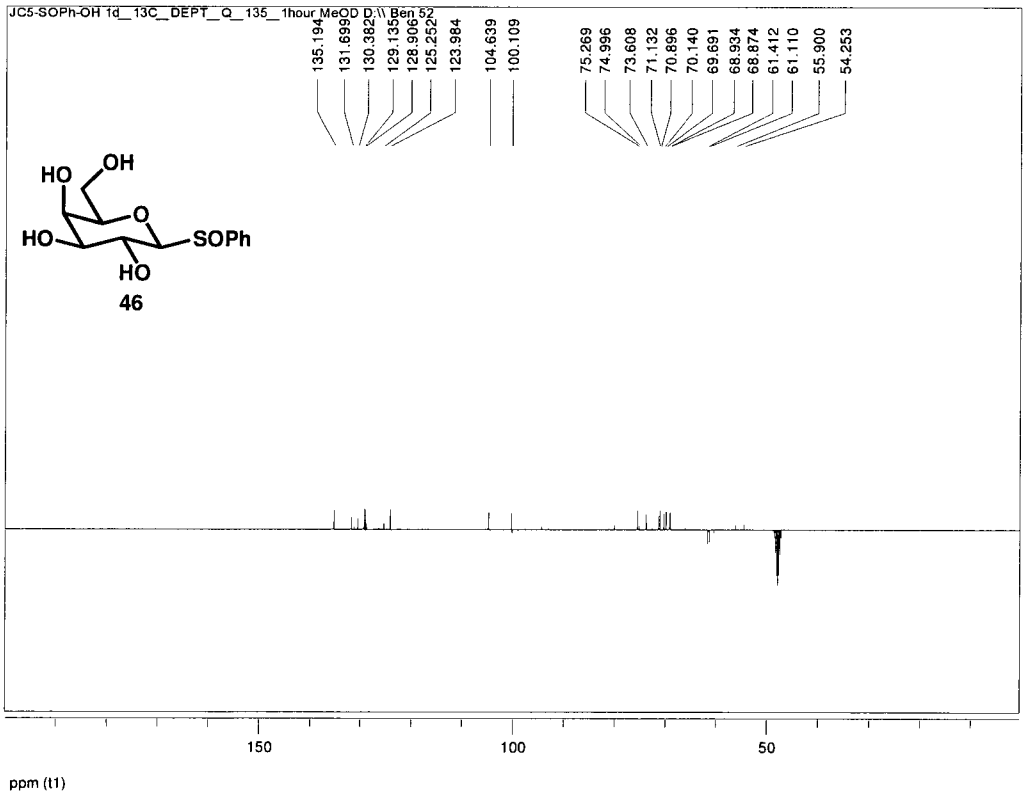
JC5-SOPh-OH 1d__13C__DEPT__Q__135__1hour MeOD D:\\ Ben 52
135.194
131.699
130.382
129.135
128.906
125.252
123.984
104.639
100.109
75.269
74.996
73.608
71.132
70.896
70.140
69.691
68.934
68.874
61.412
61.110
55.900
54.253
HO
OH
O
HO
SOPh
HO
46
150
100
50
ppm (t1)

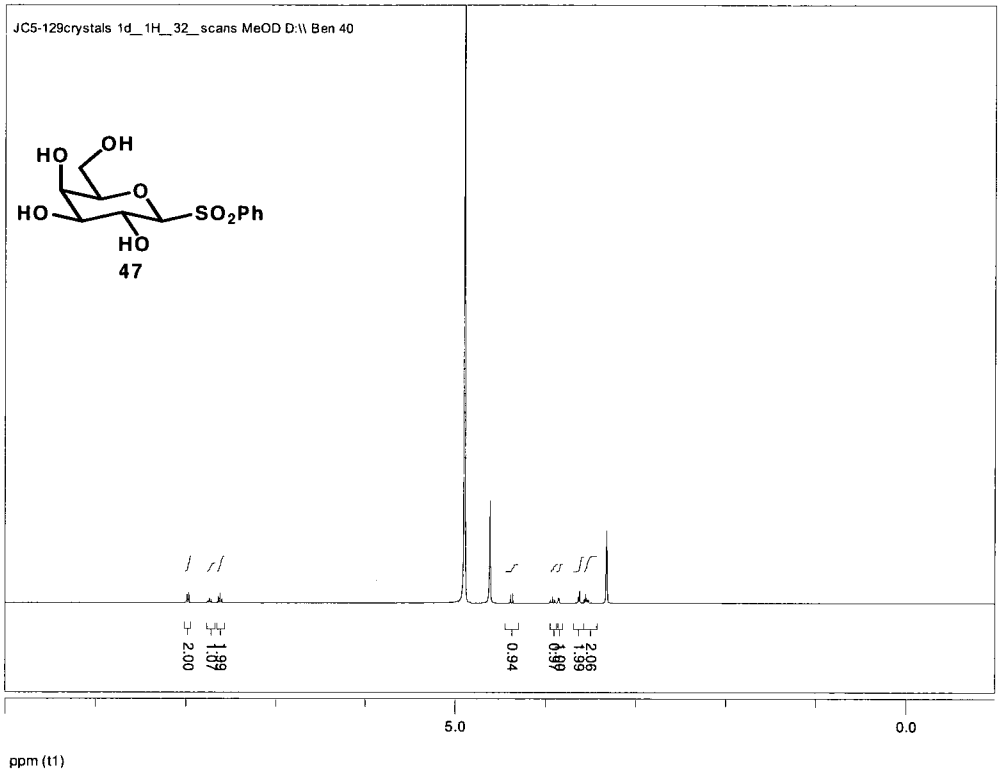
JC5-129crystals 1d__1H__32__scans MeOD D:\\ Ben 40
HO
OH
O
HO
SO2Ph
HO
47
2.00
1.07
0.94
0.99
1.99
2.06
5.0
0.0
ppm (t1)

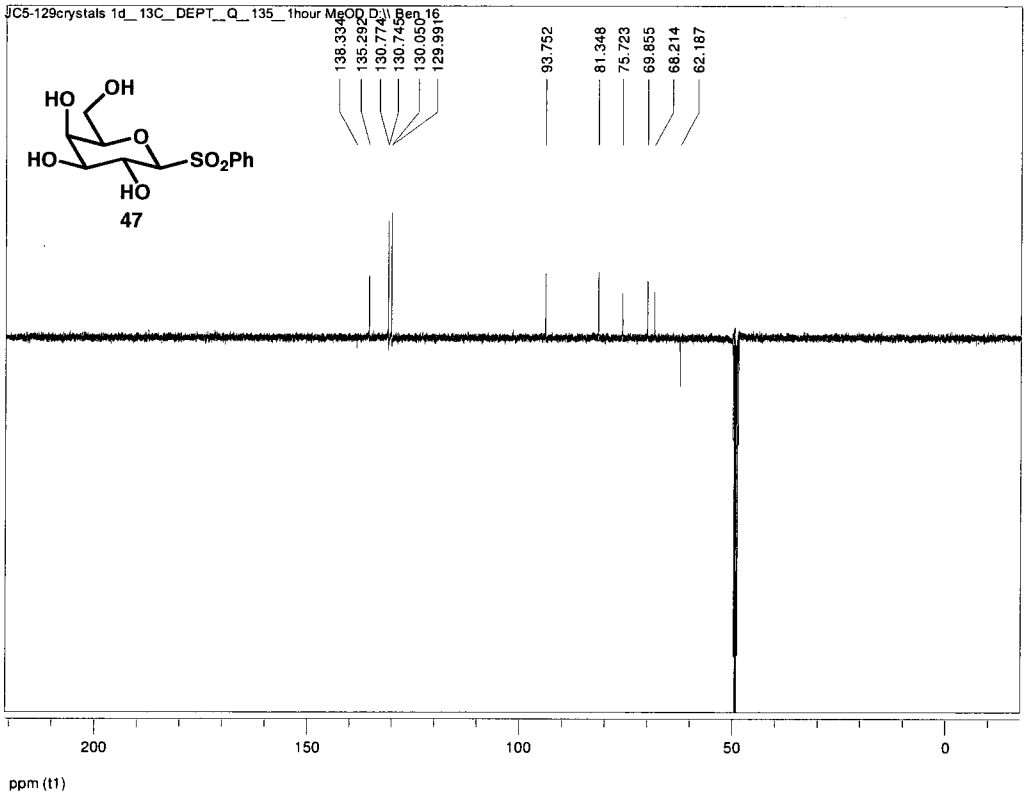
JC5-129crystals 1d__13C__DEPT__Q__135__1hour MeOD D:\\ Ben 16
138.334
135.292
130.774
130.745
130.050
129.991
93.752
81.348
75.723
69.855
68.214
62.187
HO
OH
O
HO
SO2Ph
HO
47
200
150
100
50
0
ppm (t1)

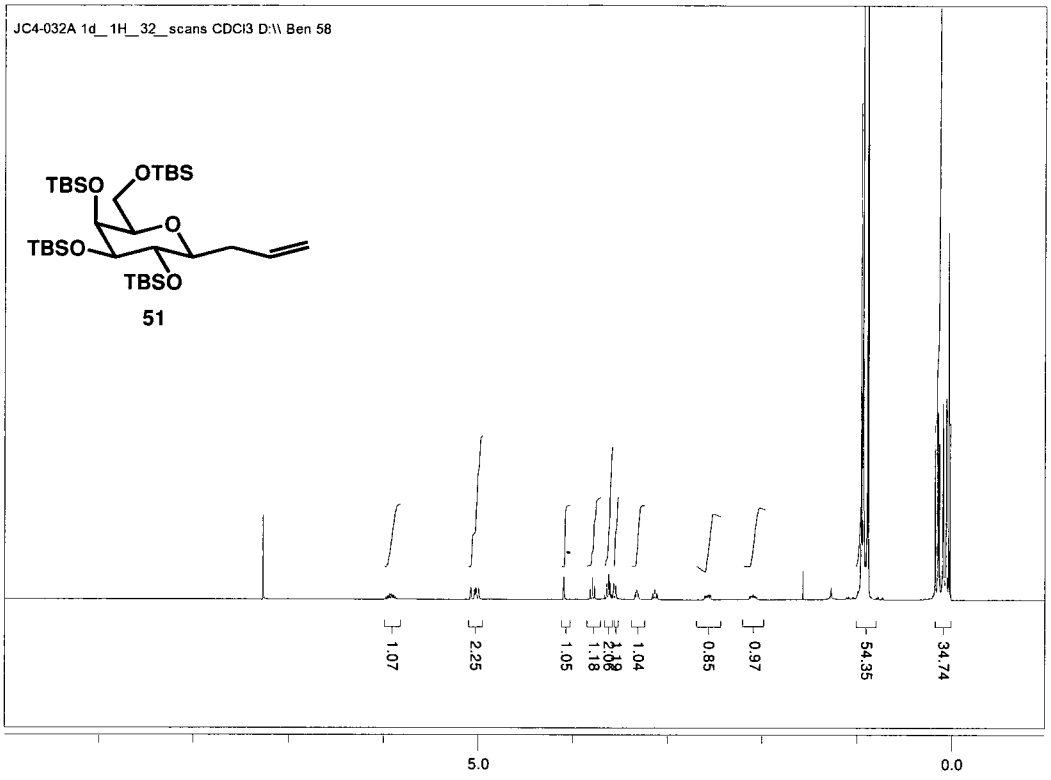
JC4-032A 1d__1H__32__scans CDCl3 D:\\ Ben 58
TBSO
OTBS
O
TBSO
TBSO
51
1.07
2.25
1.05
1.18
1.04
0.85
0.97
54.35
34.74
5.0
0.0
ppm (t1)

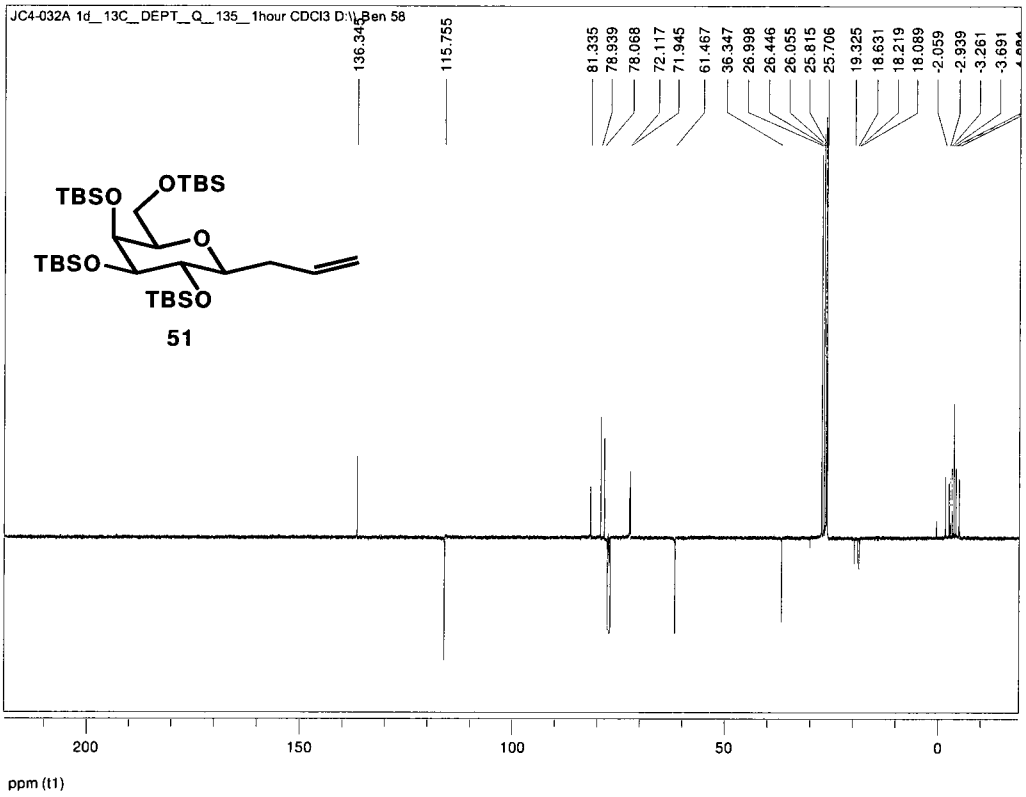
JC4-032A 1d__13C__DEPT__Q__135__1hour CDCl3 D:\\ Ben 58
136.345
115.755
81.335
78.939
78.068
72.117
71.945
61.467
36.347
26.998
26.446
26.055
25.815
25.706
19.325
18.631
18.219
18.089
-2.059
-2.939
-3.261
-3.691
TBSO
OTBS
O
TBSO
TBSO
51
200
150
100
50
0
ppm (t1)

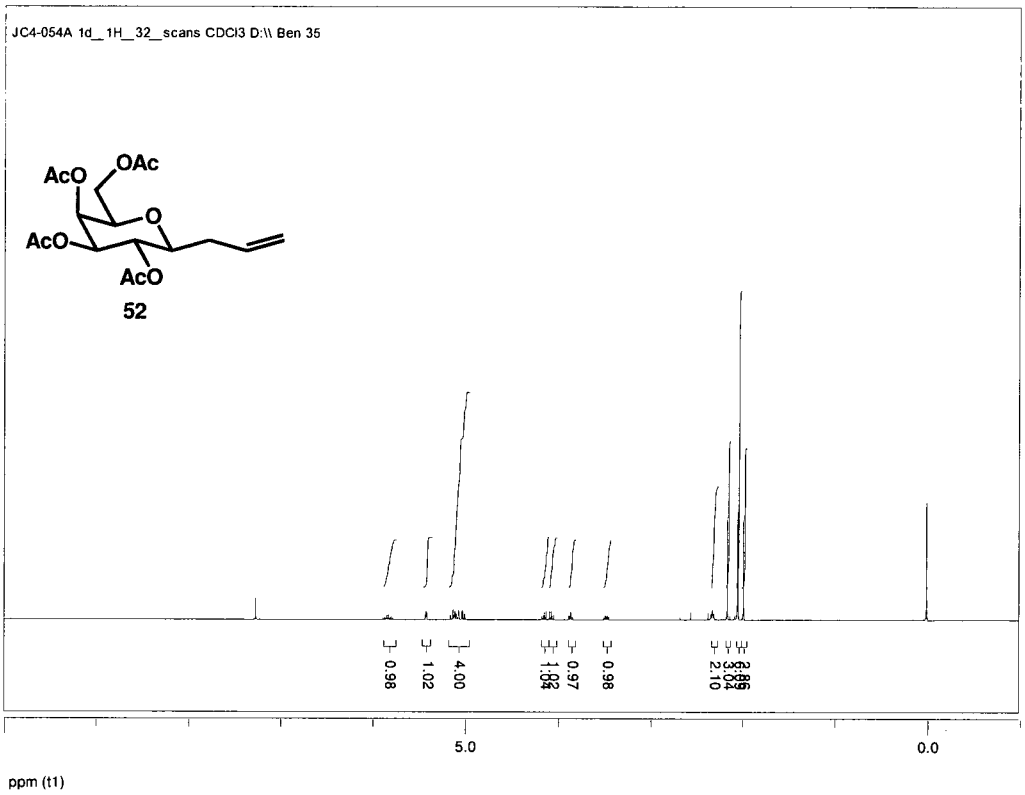
JC4-054A 1d__1H__32__scans CDCl3 D:\\ Ben 35
AcO
OAc
O
AcO
AcO
52
0.98
1.02
4.00
1.02
0.97
0.98
2.10
3.04
2.86
5.0
0.0
ppm (t1)

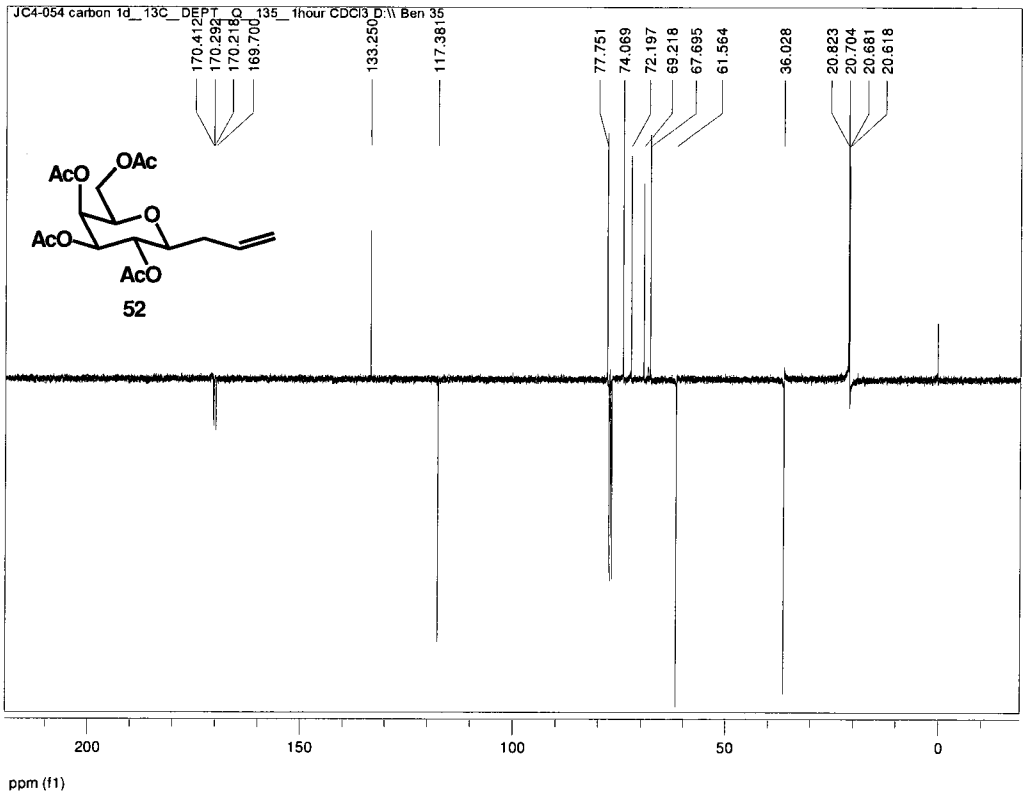
JC4-054 carbon 1d__13C__DEPT__135__1hour CDCl3 D:\\ Ben 35
170.412
170.292
170.218
169.700
133.250
117.381
77.751
74.069
72.197
69.218
67.695
61.564
36.028
20.823
20.704
20.681
20.618
AcO
OAc
O
AcO
AcO
52
200
150
100
50
0
ppm (f1)

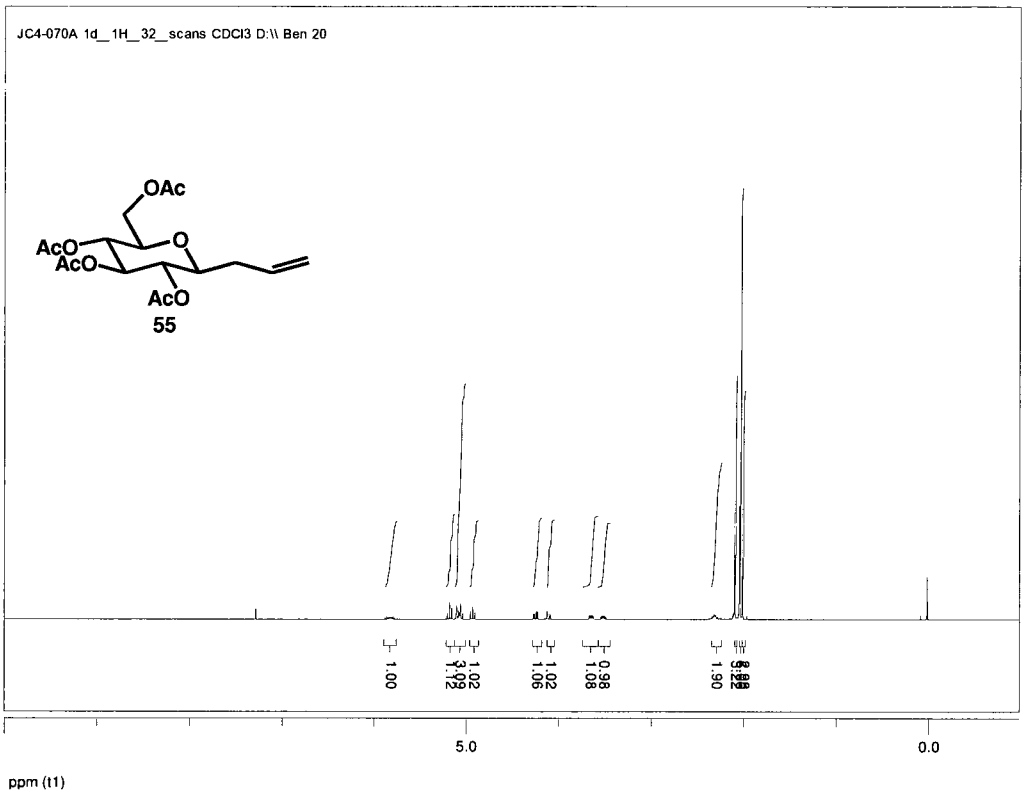
JC4-070A 1d__1H__32__scans CDCl3 D:\\ Ben 20
OAc
AcO
AcO
O
AcO
55
1.00
3.09
1.12
1.02
1.06
0.98
1.08
1.90
5.0
0.0
ppm (t1)

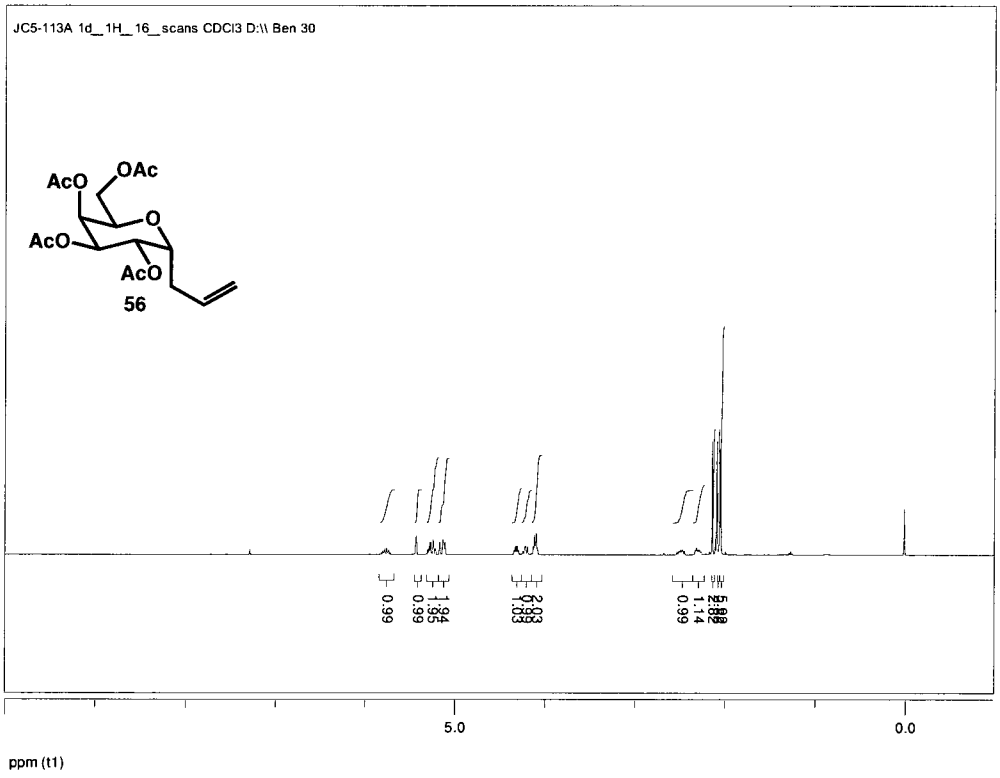
JC5-113A 1d__1H__16__scans CDCl3 D:\\ Ben 30
AcO
OAc
AcO
O
AcO
56
0.99
0.99
1.94
1.95
2.03
1.03
0.99
1.14
5.0
0.0
ppm (t1)

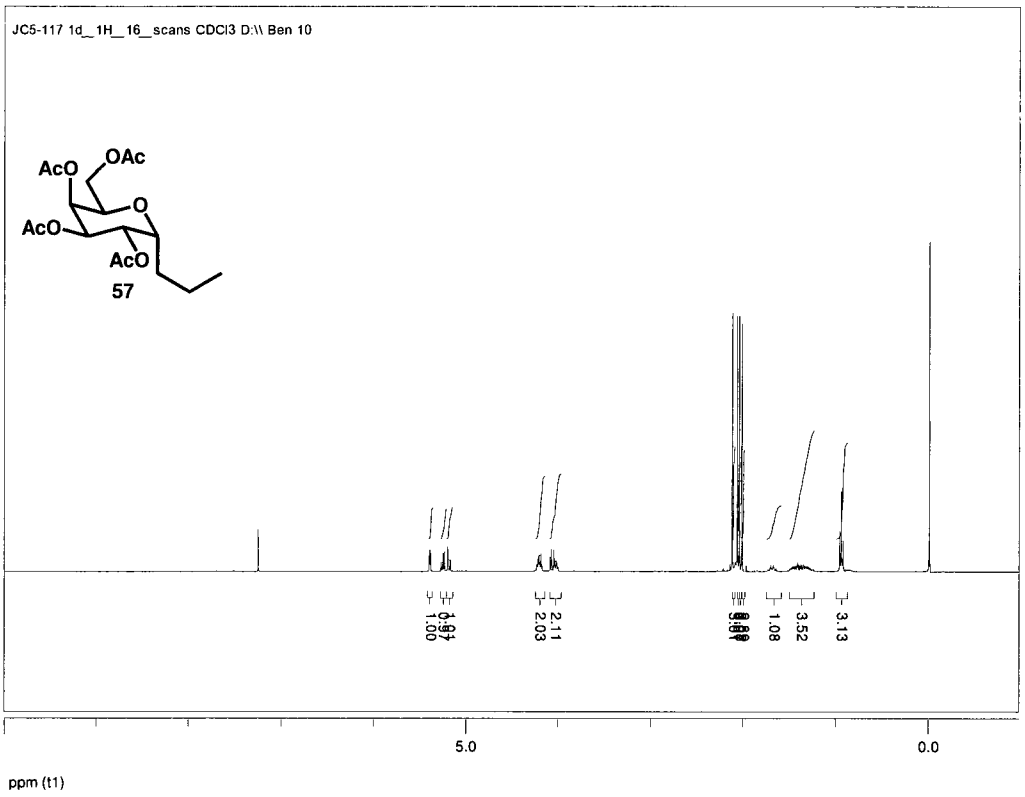
JC5-117 1d_1H_16_scans CDCl3 D:\\ Ben 10
AcO
OAc
O
AcO
AcO
57
1.00
0.97
2.03
2.11
1.08
3.52
3.13
5.0
0.0
ppm (t1)

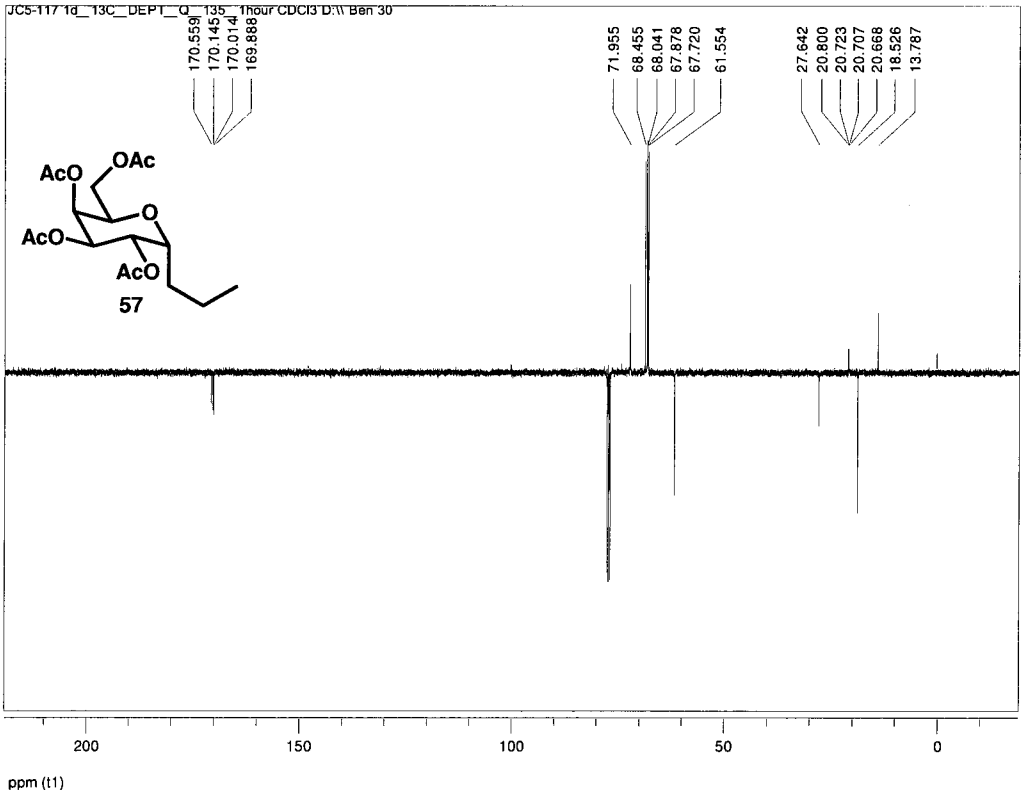
JC5-117 1d_13C_DEPT_Q_135_1hour CDCl3 D:\\ Ben 30
170.559
170.145
170.014
169.888
71.955
68.455
68.041
67.878
67.720
61.554
27.642
20.800
20.723
20.707
20.668
18.526
13.787
AcO
OAc
O
AcO
AcO
57
200
150
100
50
0
ppm (t1)

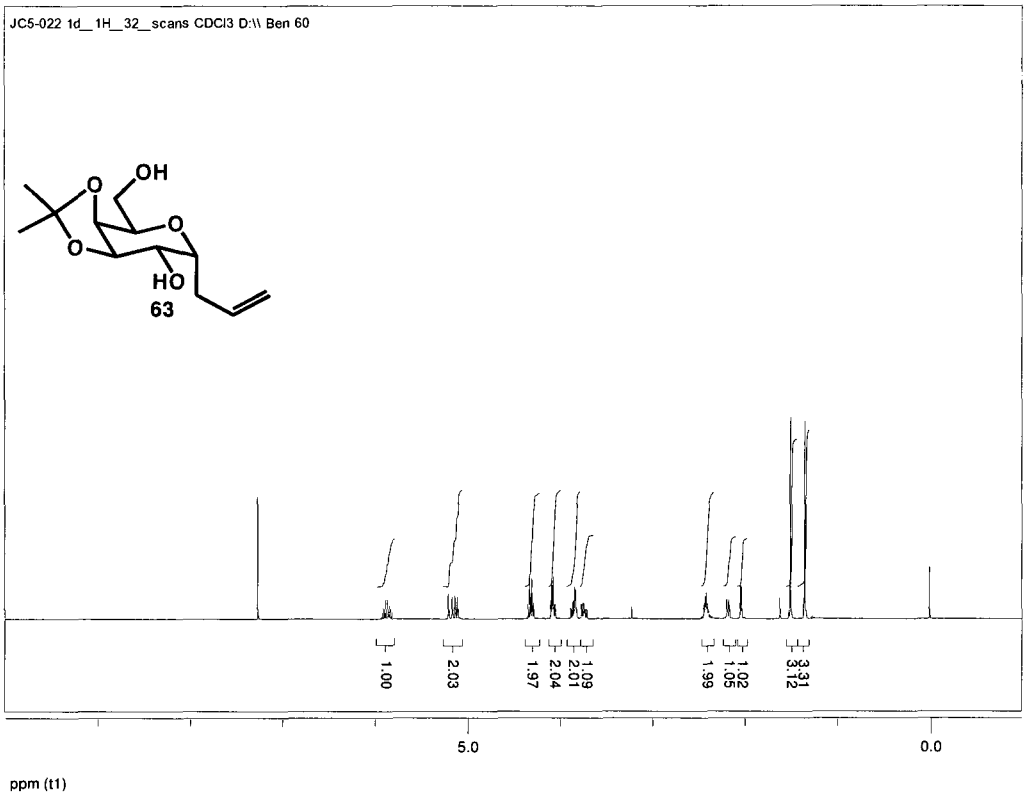
JC5-022 1d__1H__32__scans CDCl3 D:\\ Ben 60
OH
O
O
O
HO
63
1.00
2.03
1.97
2.04
2.01
1.09
1.99
1.02
1.05
3.31
3.12
5.0
0.0
ppm (t1)

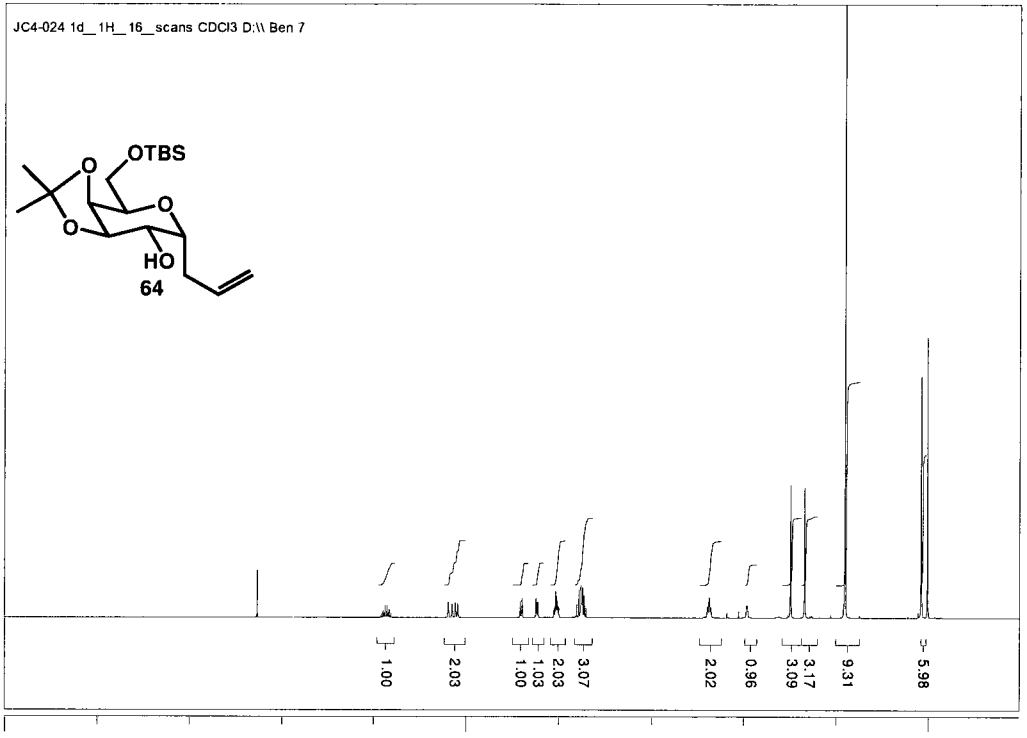
JC4-024 1d__1H__16__scans CDCl3 D:\\ Ben 7
OTBS
O
O
O
HO
64
1.00
2.03
1.00
1.03
2.03
3.07
2.02
0.96
3.09
3.17
9.31
5.98

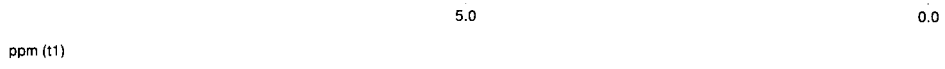
5.0
0.0
ppm (t1)

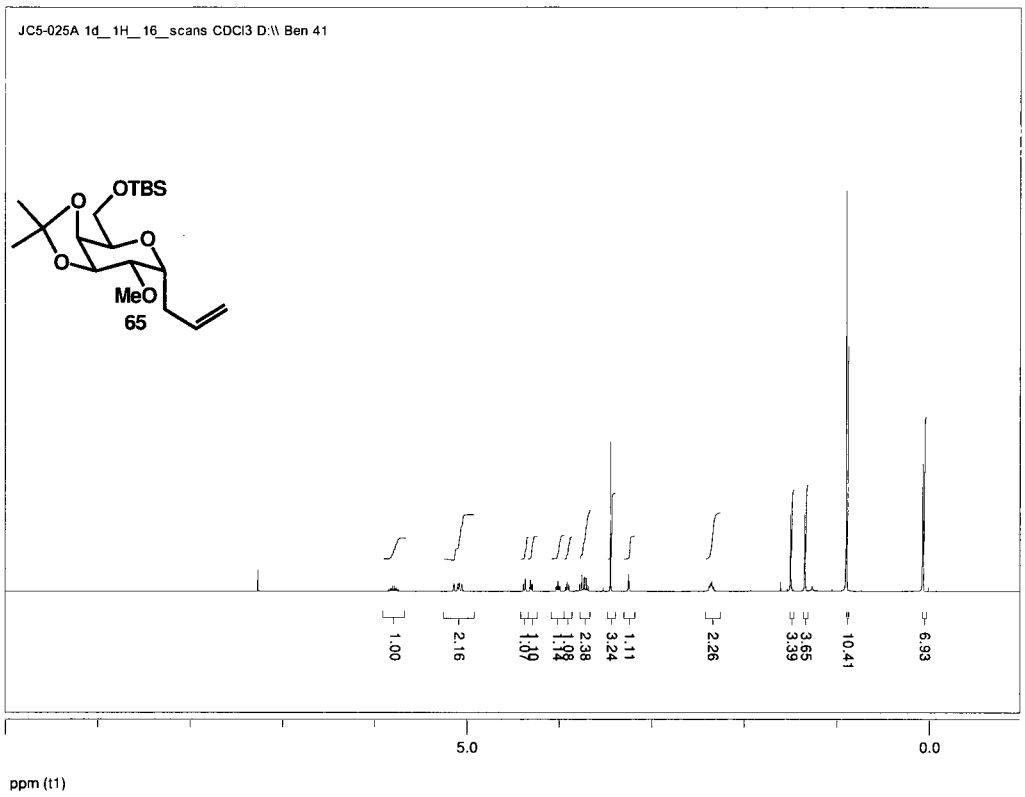
JC5-025A 1d__1H__16__scans CDCl3 D:\\ Ben 41
OTBS
MeO
65
1.00
2.16
1.07
1.19
1.08
1.14
2.38
3.24
1.11
2.26
3.39
3.65
10.41
6.93
5.0
0.0
ppm (t1)

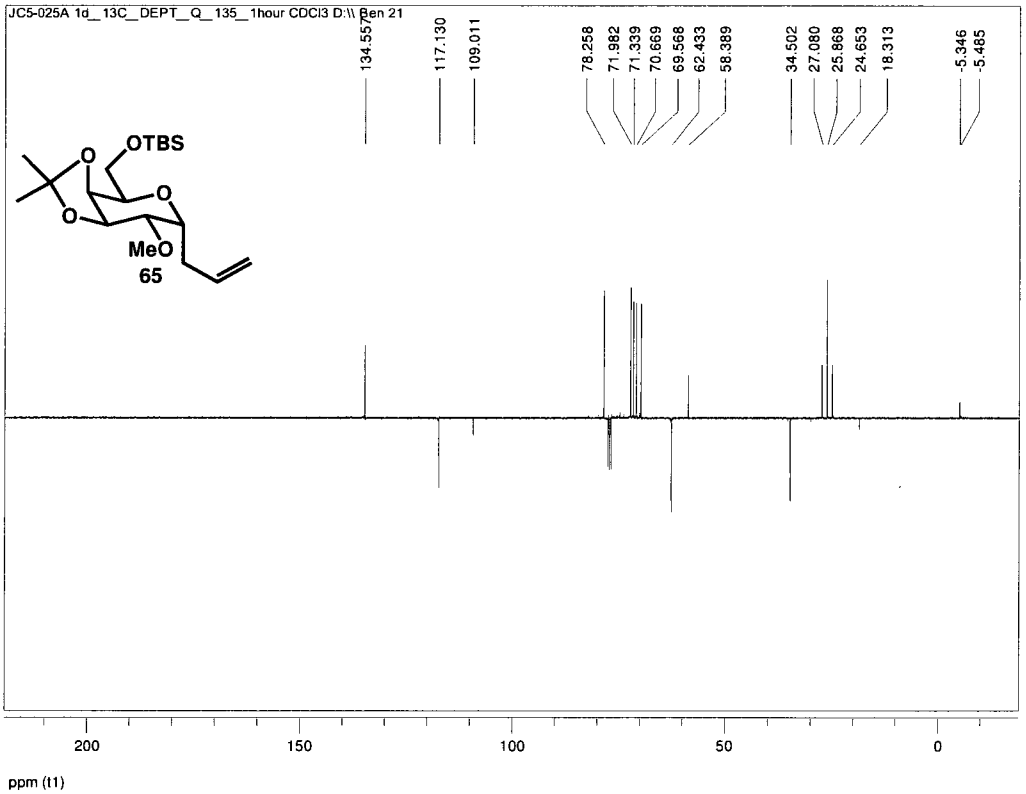
JC5-025A 1d__13C__DEPT__Q__135__1hour CDCl3 D:\\ Ben 21
134.557
117.130
109.011
78.258
71.982
71.339
70.669
69.568
62.433
58.389
34.502
27.080
25.868
24.653
18.313
-5.346
-5.485
OTBS
MeO
65
200
150
100
50
0
ppm (t1)

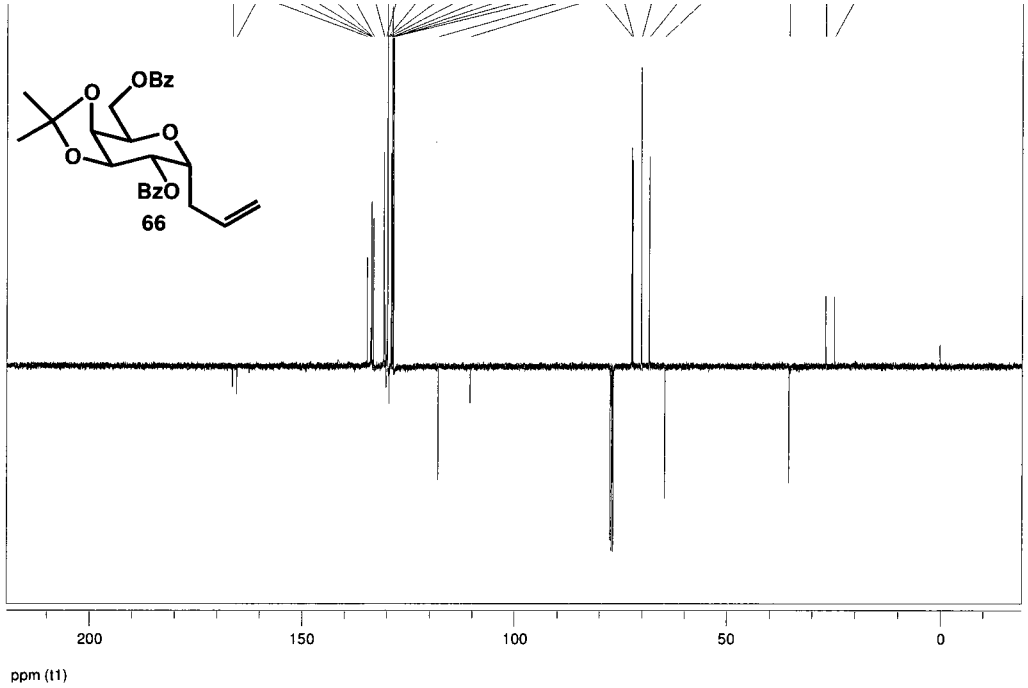
OBz
O
O
O
BzO
66
200
150
100
50
0
ppm (t1)

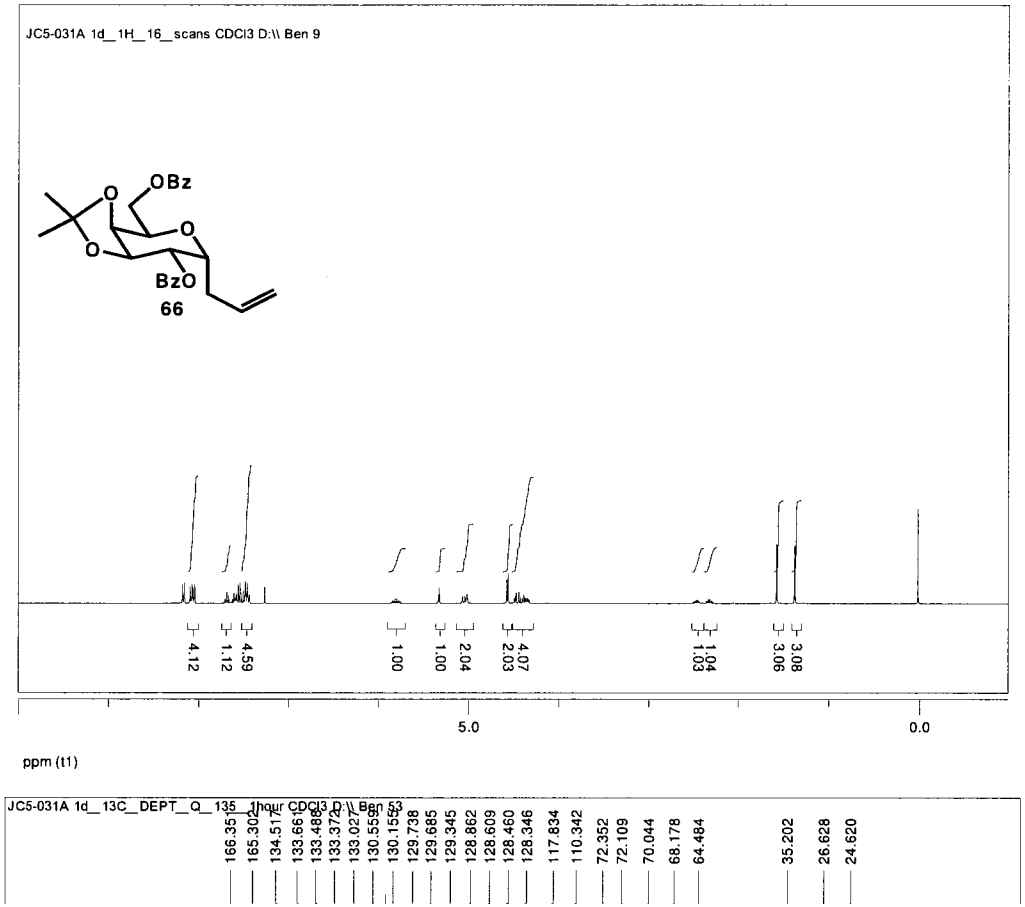
JC5-031A 1d__1H__16__scans CDCl3 D:\\ Ben 9
OBz
O
O
O
BzO
66
4.12
1.12
4.59
1.00
1.00
2.04
2.03
4.07
1.03
1.04
3.06
3.08
5.0
0.0
ppm (t1)

JC5-031A 1d__13C__DEPT__Q__135__1hour CDCl3 D:\\ Ben 53
166.351
165.302
134.517
133.661
133.488
133.372
133.027
130.559
130.155
129.738
129.685
129.345
128.862
128.609
128.460
128.346
117.834
110.342
72.352
72.109
70.044
68.178
64.484
35.202
26.628
24.620

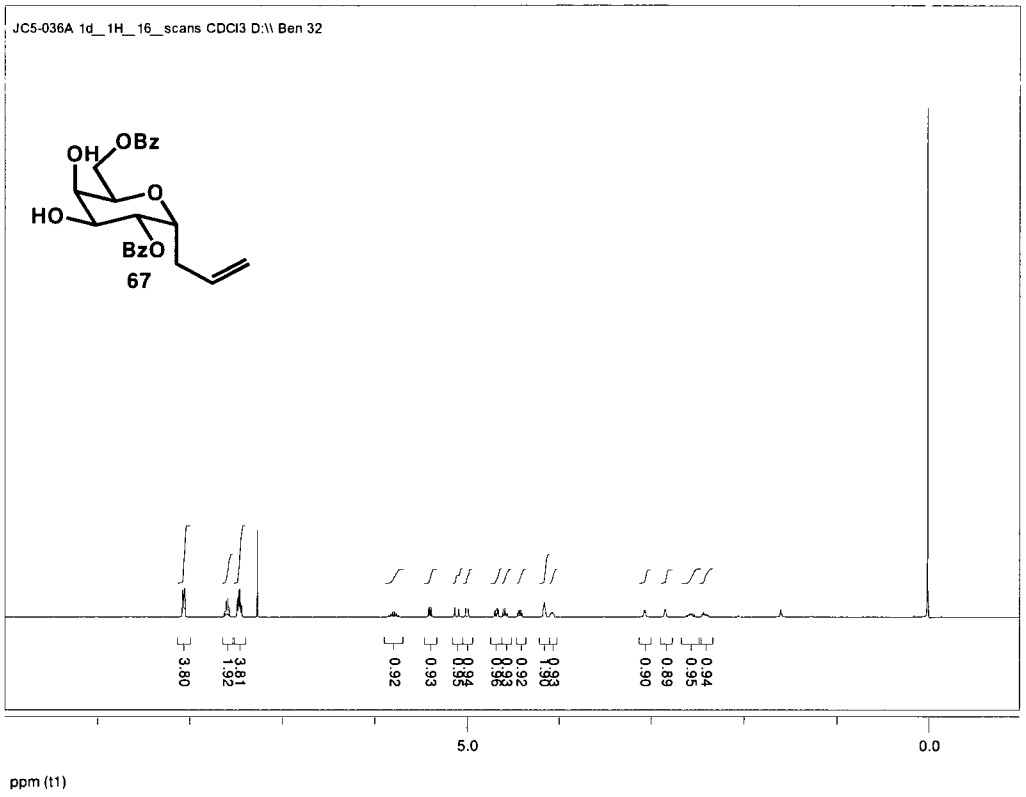
JC5-036A 1d__1H__16__scans CDCl3 D:\\ Ben 32
OH
OBz
O
HO
BzO
67
3.80
1.92
3.81
0.92
0.93
0.95
0.94
0.92
0.92
1.00
1.03
0.90
0.89
0.95
0.94
5.0
0.0
ppm (t1)

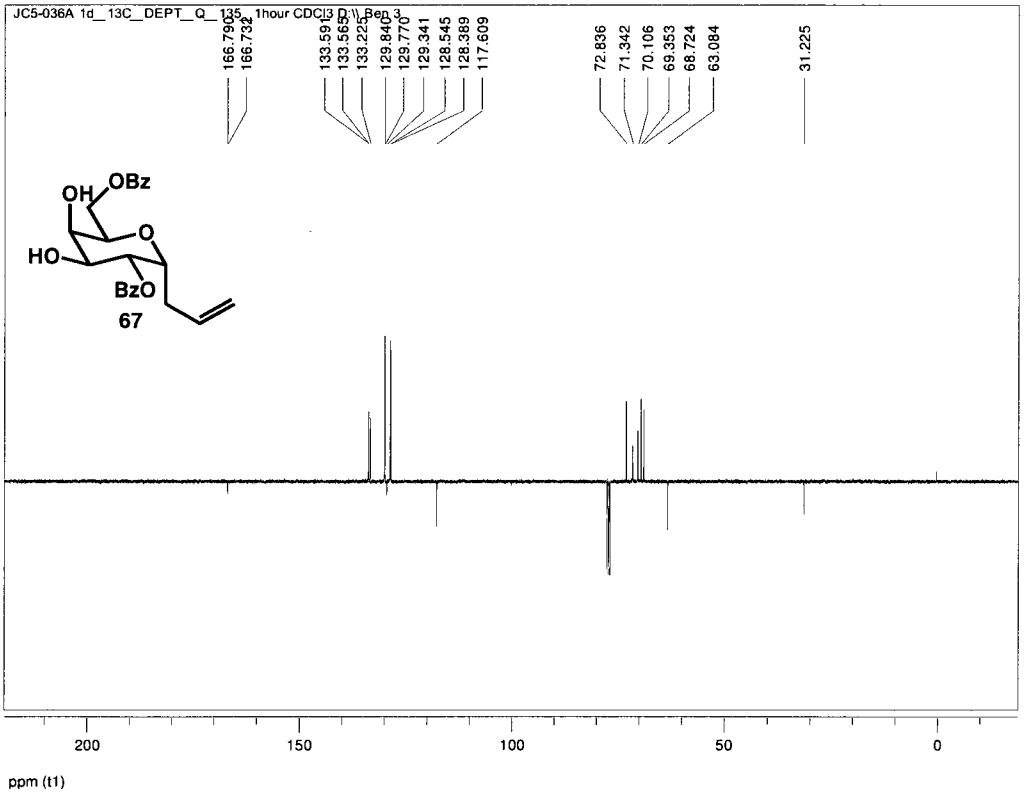
JC5-036A 1d__13C__DEPT__Q__135__1hour CDCl3 D:\\ Ben 3
166.790
166.732
133.591
133.565
133.225
129.840
129.770
129.341
128.545
128.389
117.609
72.836
71.342
70.106
69.353
68.724
63.084
31.225
OH
OBz
O
HO
BzO
67
200
150
100
50
0
ppm (t1)

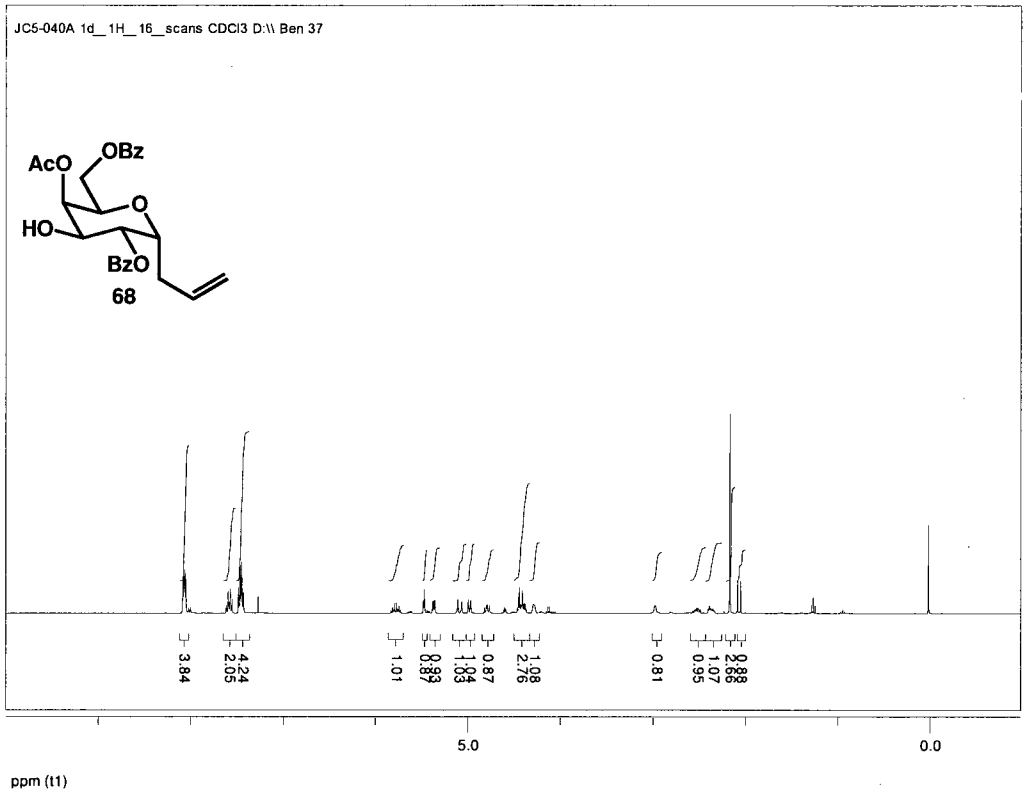
JC5-040A 1d__1H__16__scans CDCl3 D:\\ Ben 37
AcO
OBz
O
HO
BzO
68
3.84
4.24
2.05
1.01
0.83
0.87
1.04
0.87
1.08
2.76
0.81
0.95
1.07
2.88
2.66
5.0
0.0
ppm (t1)

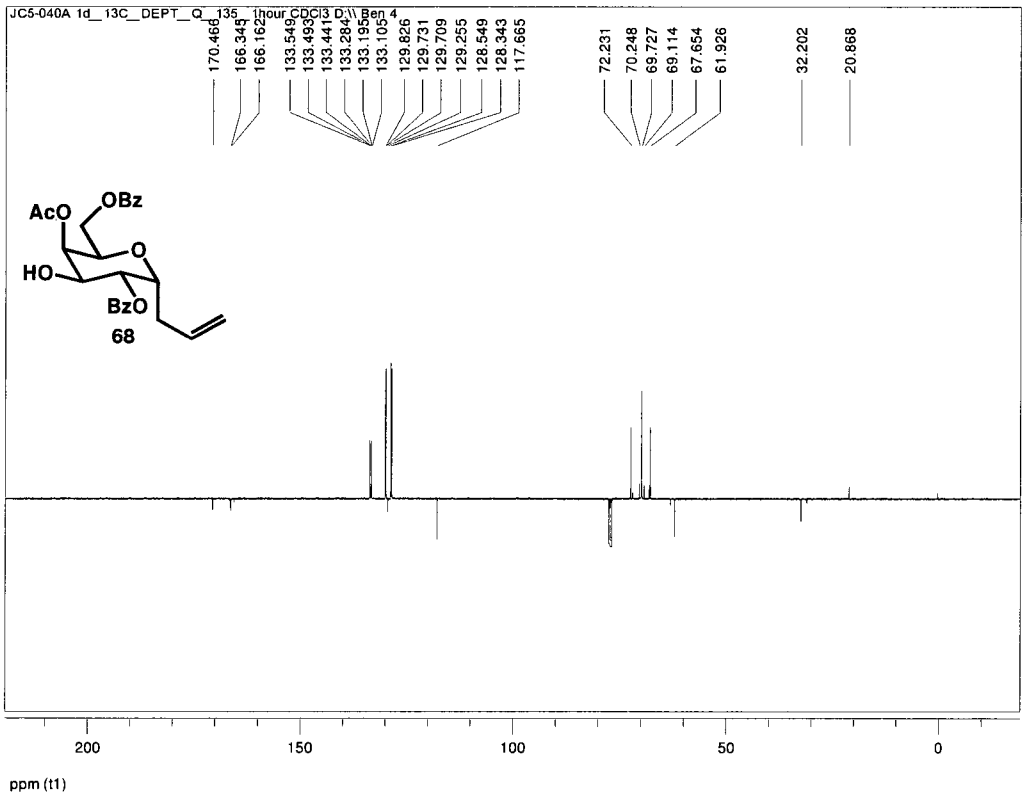
JC5-040A 1d__13C__DEPT__Q__135__1hour CDCl3 D:\\ Ben 4
170.468
166.345
166.162
133.545
133.496
133.441
133.284
133.195
133.105
129.826
129.731
129.709
129.255
128.549
128.343
117.665
72.231
70.248
69.727
69.114
67.654
61.926
32.202
20.868
AcO
OBz
O
HO
BzO
68
200
150
100
50
0
ppm (t1)

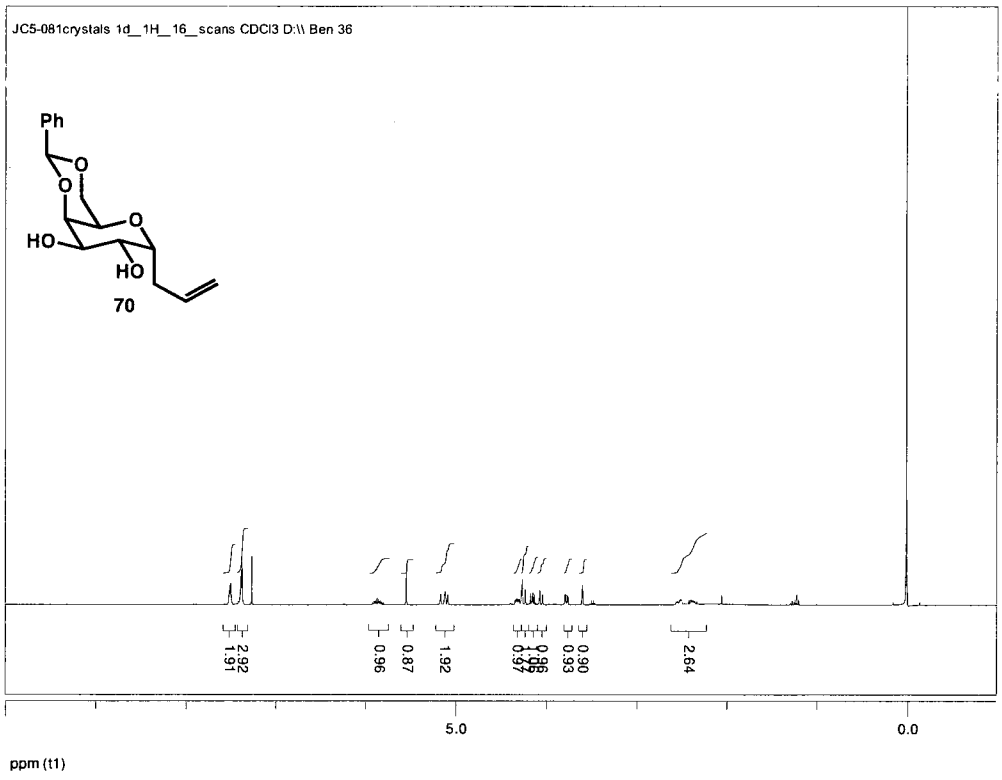
JC5-081crystals 1d_1H_16_scans CDCl3 D:\\ Ben 36
Ph
O
O
O
HO
HO
70
2.92
1.91
0.96
0.87
1.92
0.97
0.93
0.90
2.64
5.0
0.0
ppm (t1)

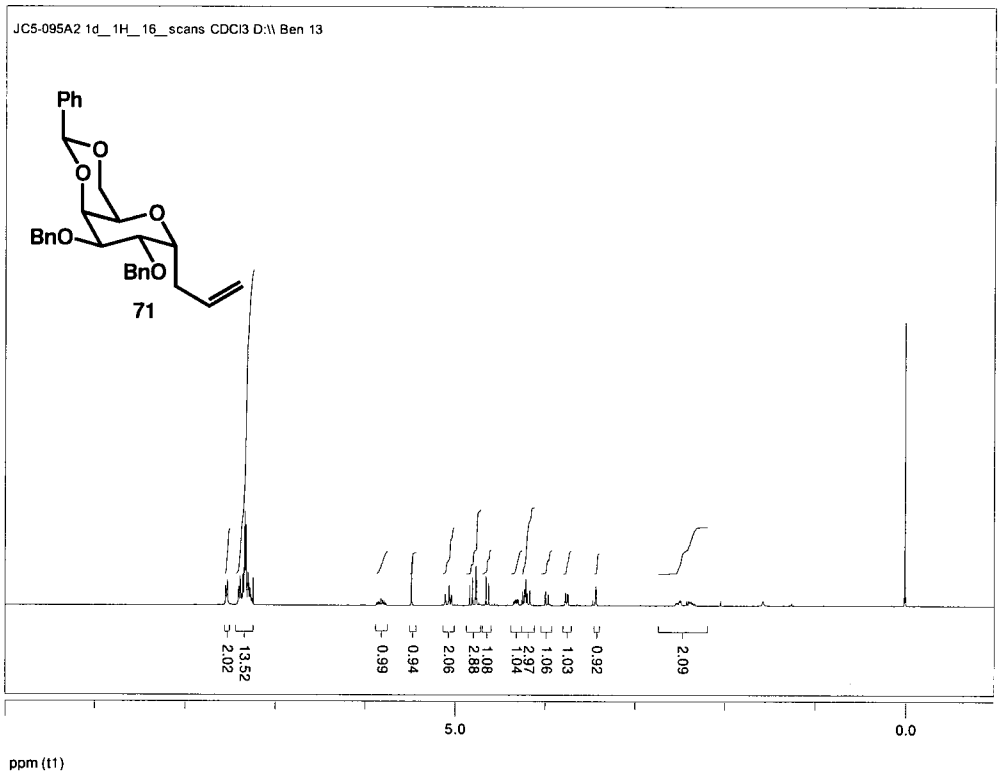
JC5-095A2 1d__1H__16__scans CDCl3 D:\\ Ben 13
Ph
O
O
O
BnO
BnO
71
2.02
13.52
0.99
0.94
2.06
2.88
1.08
2.97
1.04
1.06
1.03
0.92
2.09
5.0
0.0
ppm (t1)

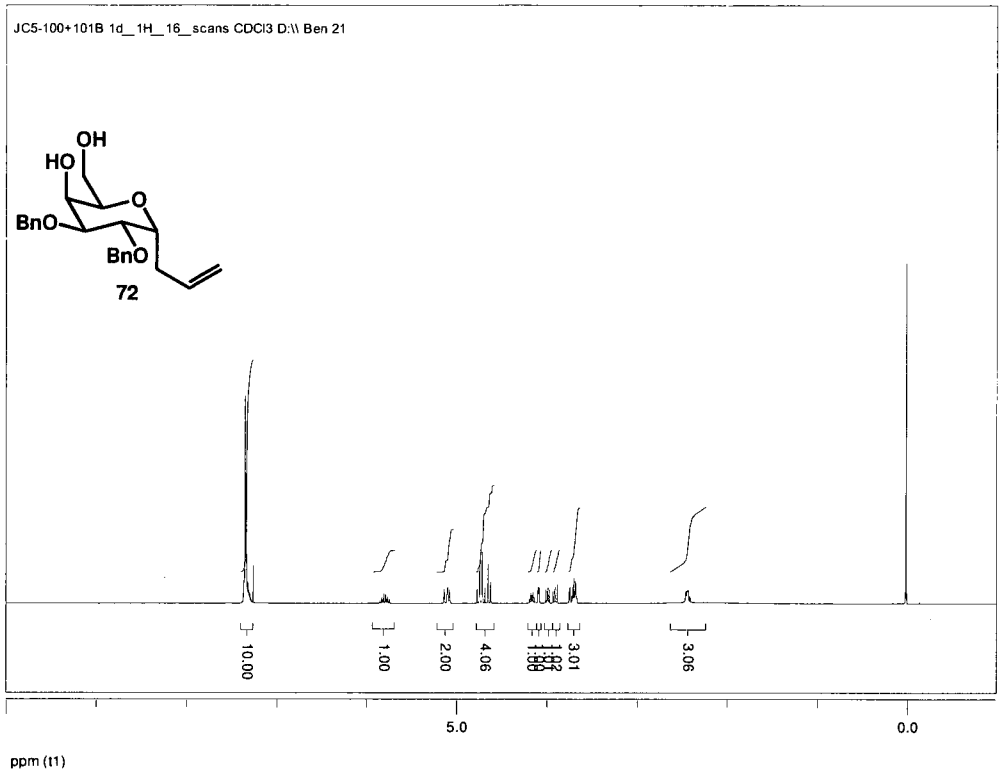
JC5-100+101B 1d__1H__16__scans CDCl3 D:\\ Ben 21
OH
HO
O
BnO
BnO
72
10.00
1.00
2.00
4.06
3.01
3.06
5.0
0.0
ppm (t1)

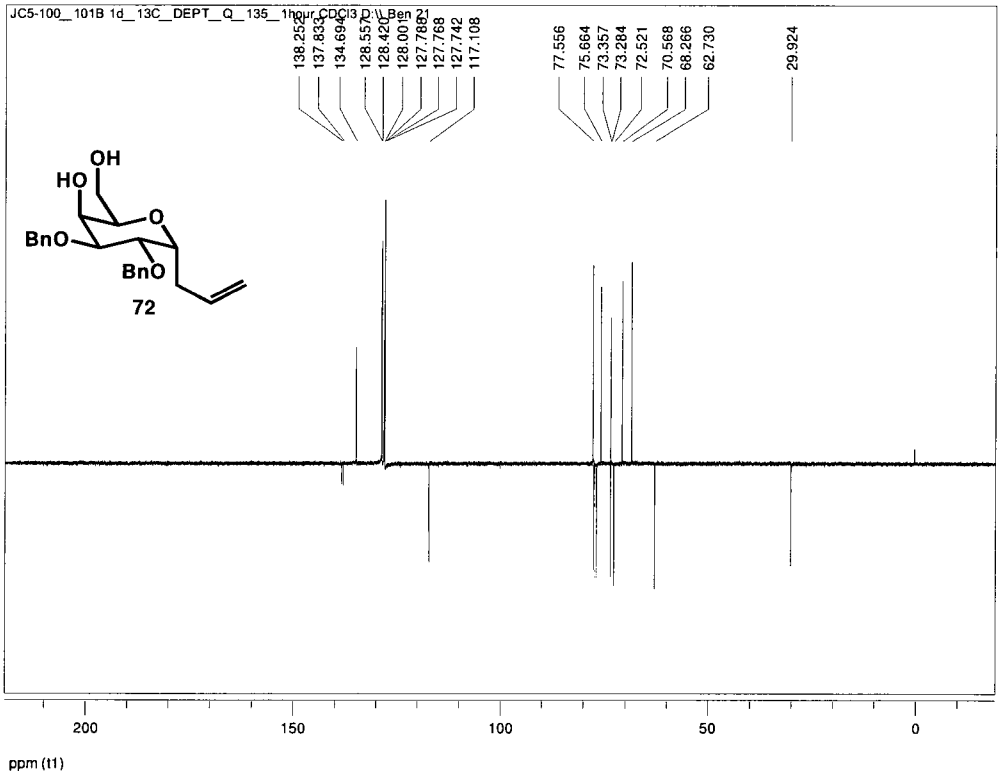
JC5-100__101B 1d__13C__DEPT__Q__135__1hour__CDCl3 D:\\ Ben 21
138.252
137.833
134.694
128.557
128.420
128.001
127.788
127.768
127.742
117.108
77.556
75.664
73.357
73.284
72.521
70.568
68.266
62.730
29.924
OH
HO
O
BnO
BnO
72
200
150
100
50
0
ppm (t1)

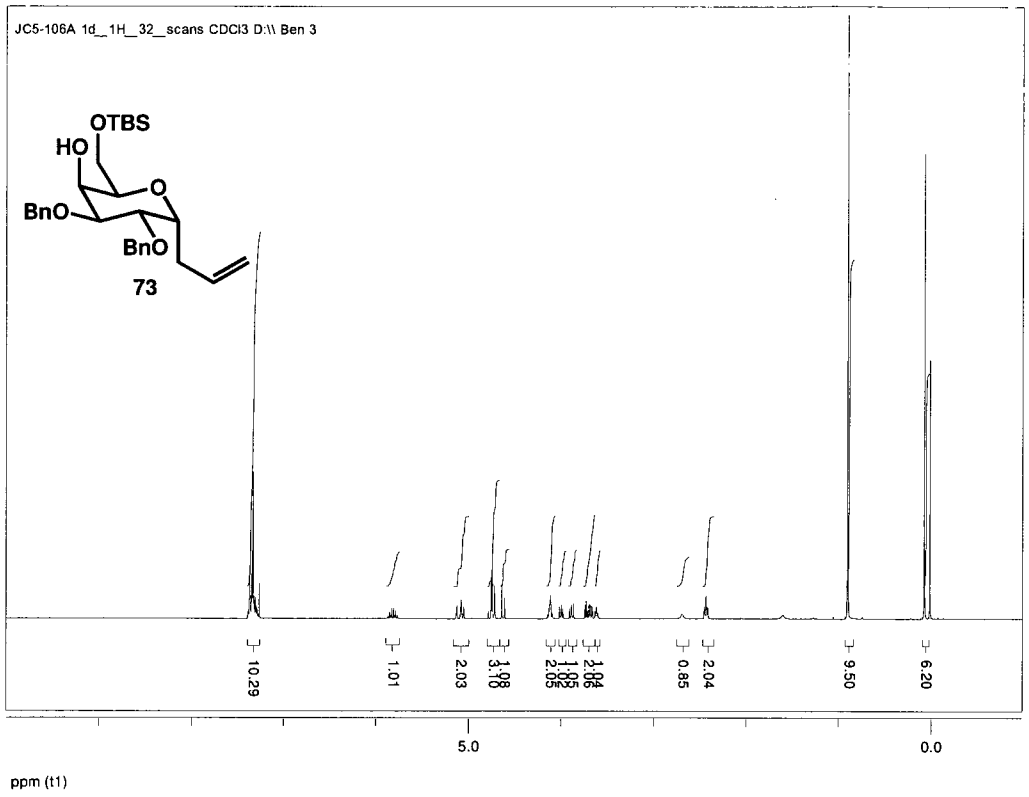
JC5-106A 1d__1H__32__scans CDCl3 D:\\ Ben 3
OTBS
HO
O
BnO
BnO
73
10.29
1.01
2.03
3.10
2.05
0.85
2.04
6.50
6.20
5.0
0.0
ppm (t1)

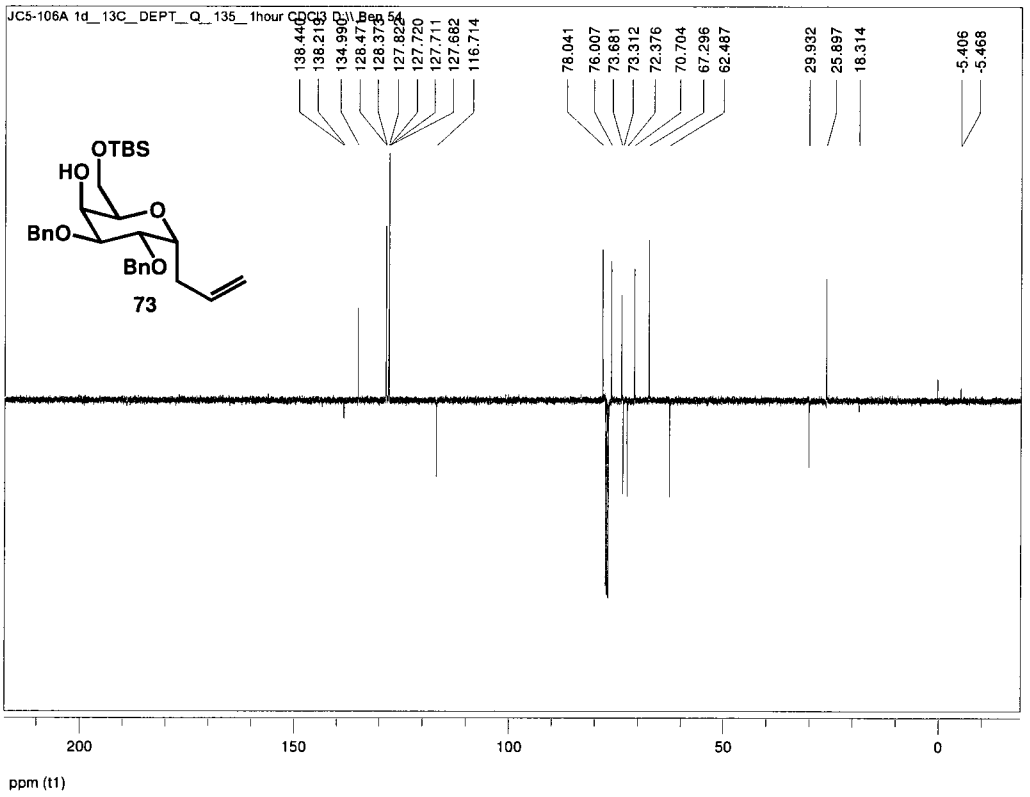
JC5-106A 1d__13C__DEPT__Q__135__1hour CDCl3 D:\\ Ben 54
138.440
138.219
134.990
128.473
128.373
127.822
127.720
127.711
127.682
116.714
78.041
76.007
73.681
73.312
72.376
70.704
67.296
62.487
29.932
25.897
18.314
-5.406
-5.468
OTBS
HO
O
BnO
BnO
73
200
150
100
50
0
ppm (t1)

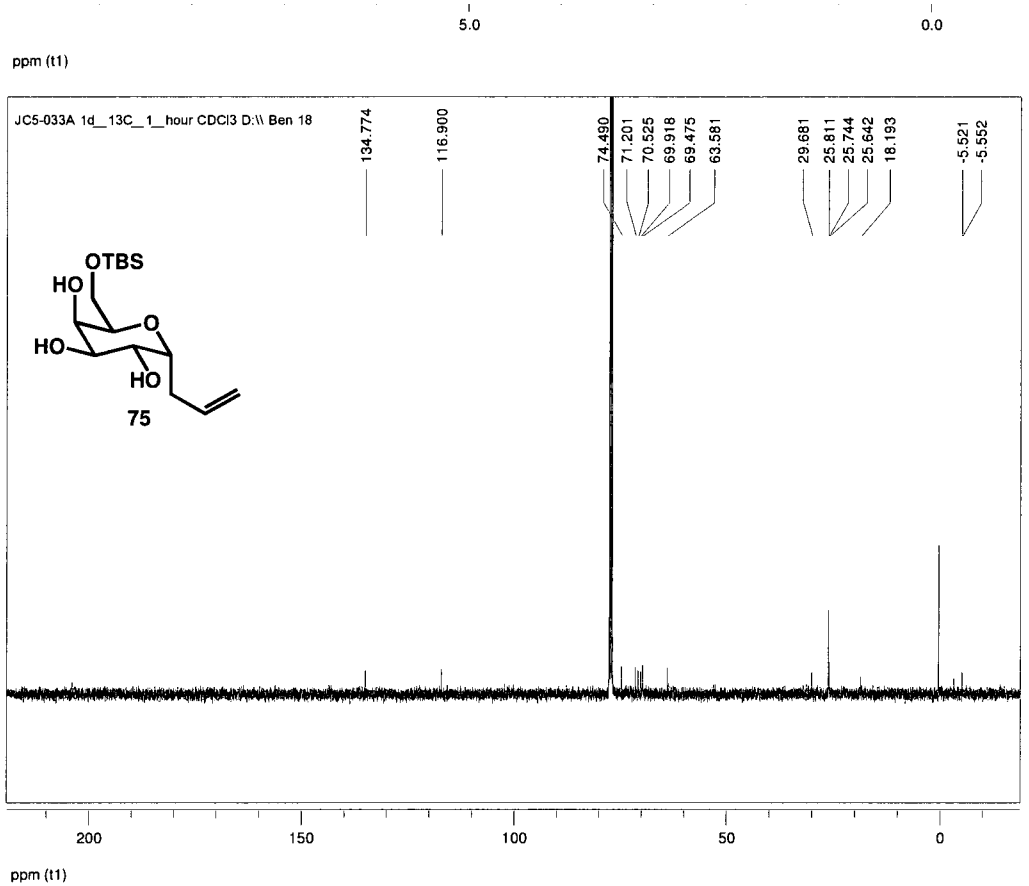
5.0
0.0
ppm (t1)
JC5-033A 1d_13C_1_hour CDCl3 D:\\ Ben 18
134.774
116.900
74.490
71.201
70.525
69.918
69.475
63.581
29.681
25.811
25.744
25.642
18.193
-5.521
-5.552
OTBS
HO
O
HO
HO
75
200
150
100
50
0
ppm (t1)

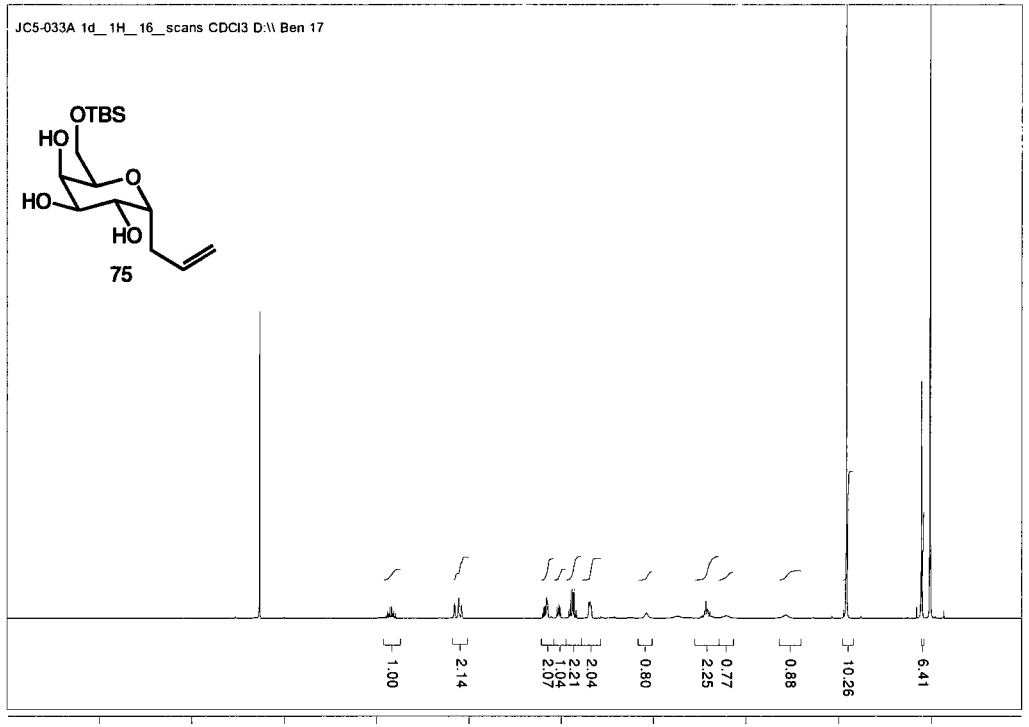
JC5-033A 1d__1H__16__scans CDCl3 D:\\ Ben 17
OTBS
HO
O
HO
HO
75
1.00
2.14
1.04
2.21
2.07
2.04
0.80
0.77
2.25
0.88
10.26
6.41

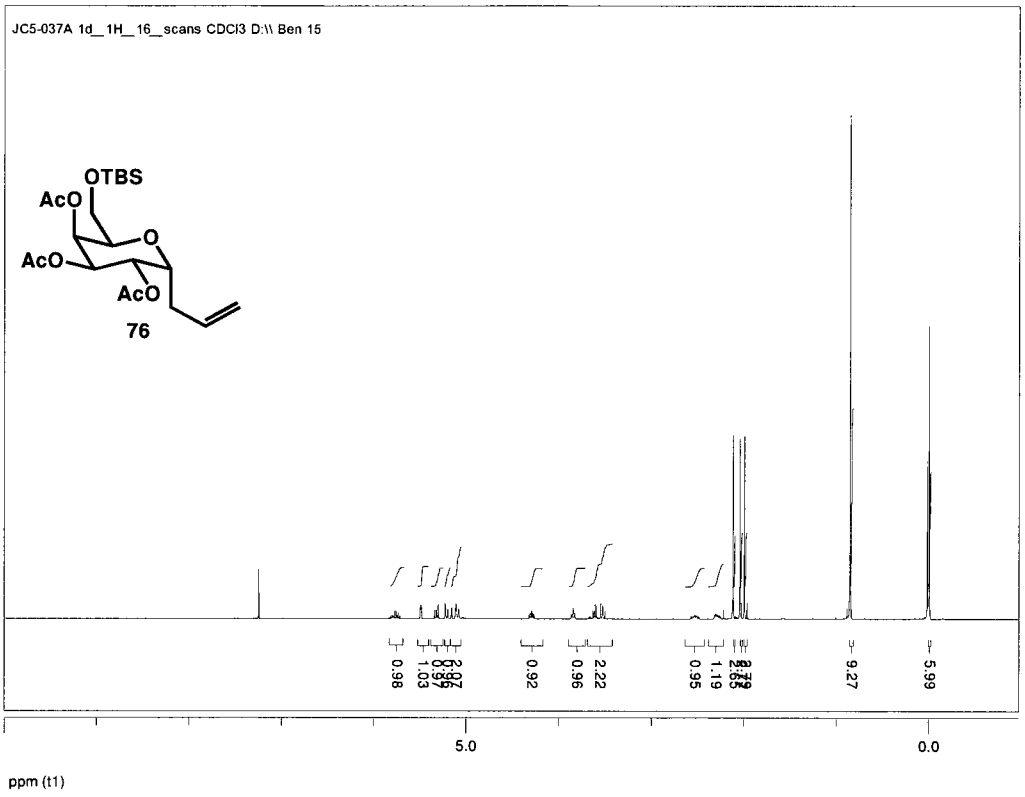
JC5-037A 1d__1H__16__scans CDCl3 D:\\ Ben 15
OTBS
AcO
AcO
AcO
O
76
0.98
1.03
2.07
0.92
0.96
2.22
0.95
1.19
6.27
5.69
5.0
0.0
ppm (t1)

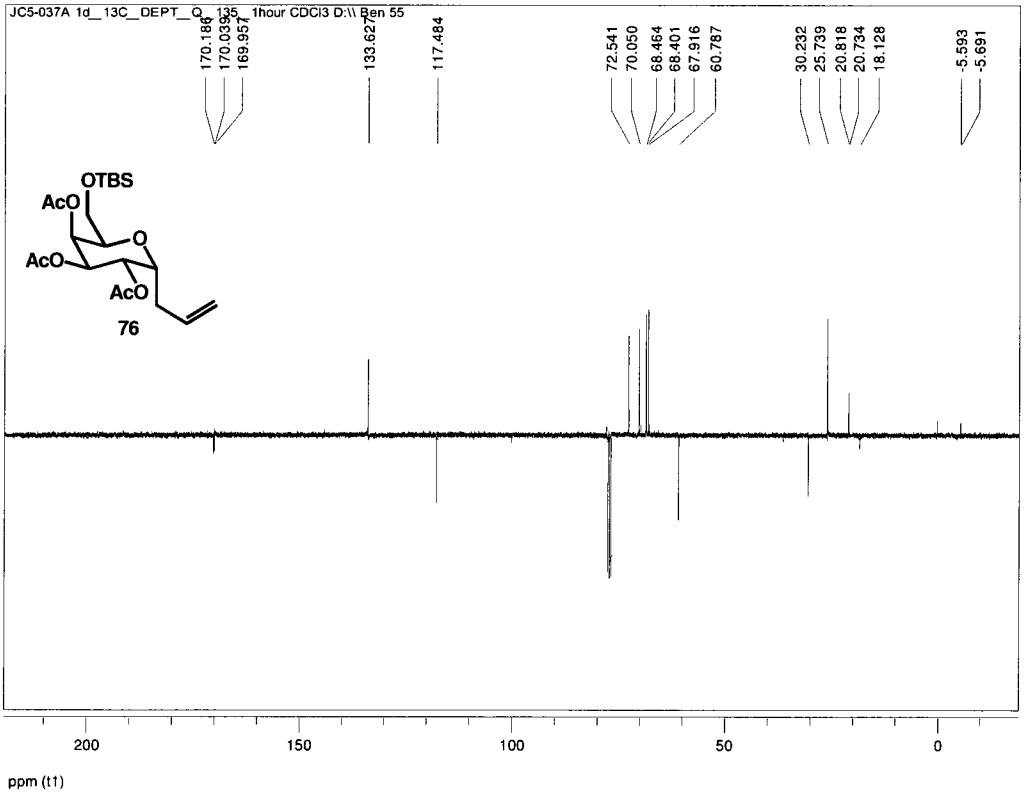
JC5-037A 1d__13C__DEPT__Q__135__1hour CDCl3 D:\\ Ben 55
170.186
170.039
169.957
133.627
117.484
72.541
70.050
68.464
68.401
67.916
60.787
30.232
25.739
20.818
20.734
18.128
-5.593
-5.691
OTBS
AcO
AcO
AcO
O
76
200
150
100
50
0
ppm (t1)

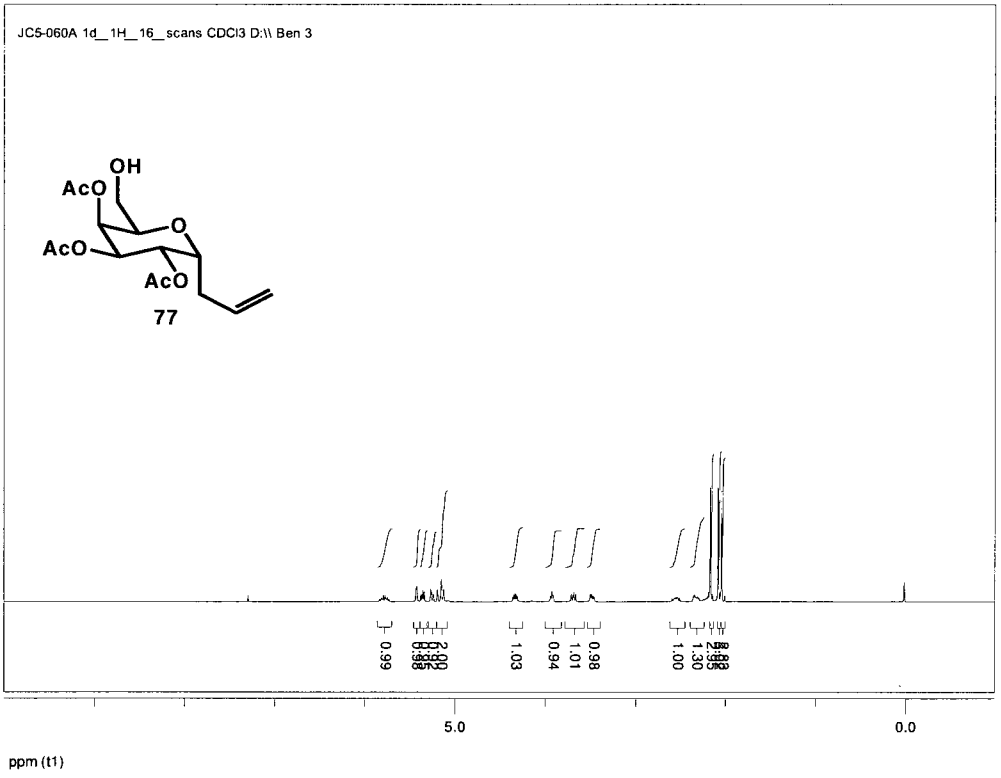
JC5-060A 1d__1H__16__scans CDCl3 D:\\ Ben 3
OH
AcO
O
AcO
AcO
77
0.99
2.00
1.03
0.94
1.01
0.98
1.00
1.30
5.0
0.0
ppm (t1)

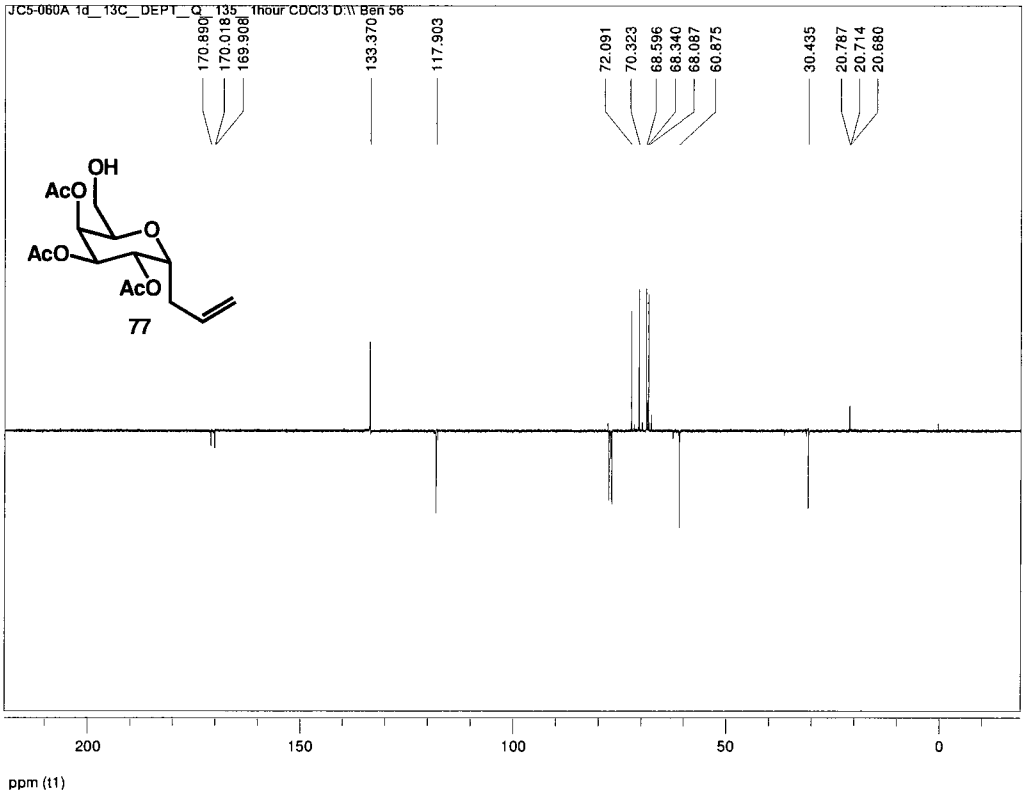
JC5-060A 1d__13C__DEPT__Q__135__1hour CDCl3 D:\\ Ben 56
170.890
170.018
169.908
133.370
117.903
72.091
70.323
68.596
68.340
68.087
60.875
30.435
20.787
20.714
20.680
OH
AcO
O
AcO
AcO
77
200
150
100
50
0
ppm (t1)

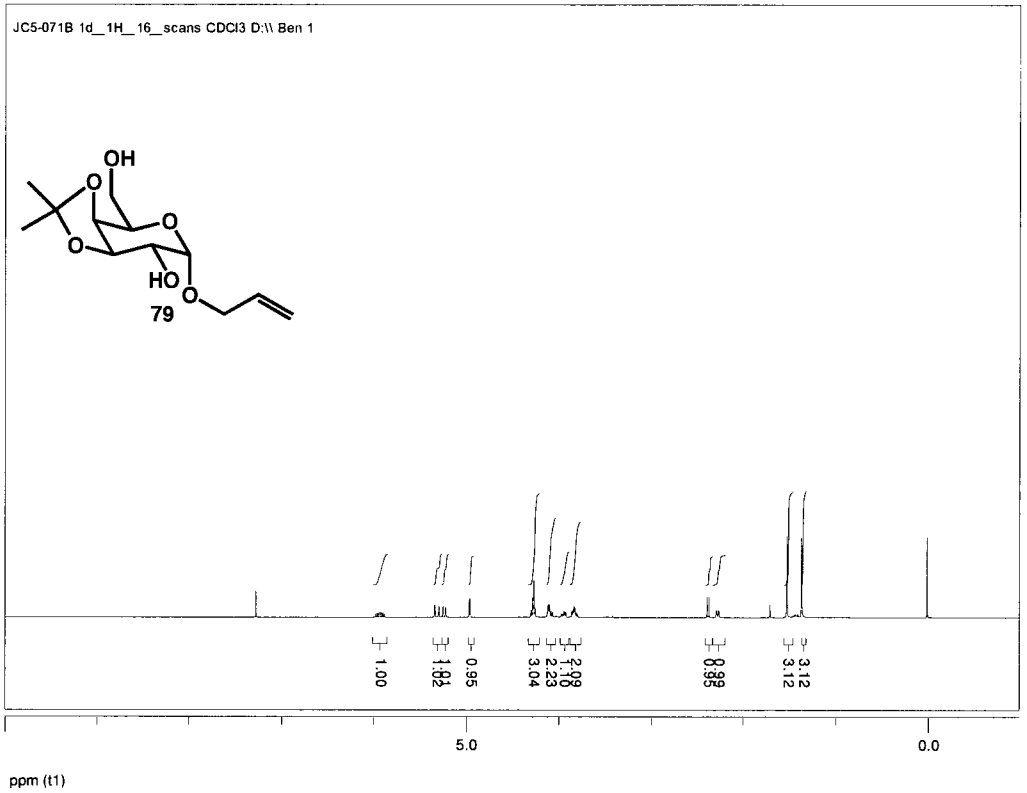
JC5-071B 1d__1H__16__scans CDCl3 D:\\ Ben 1
OH
O
O
O
HO
O
79
1.00
1.82
0.95
3.04
2.23
0.99
3.12
5.0
0.0
ppm (t1)

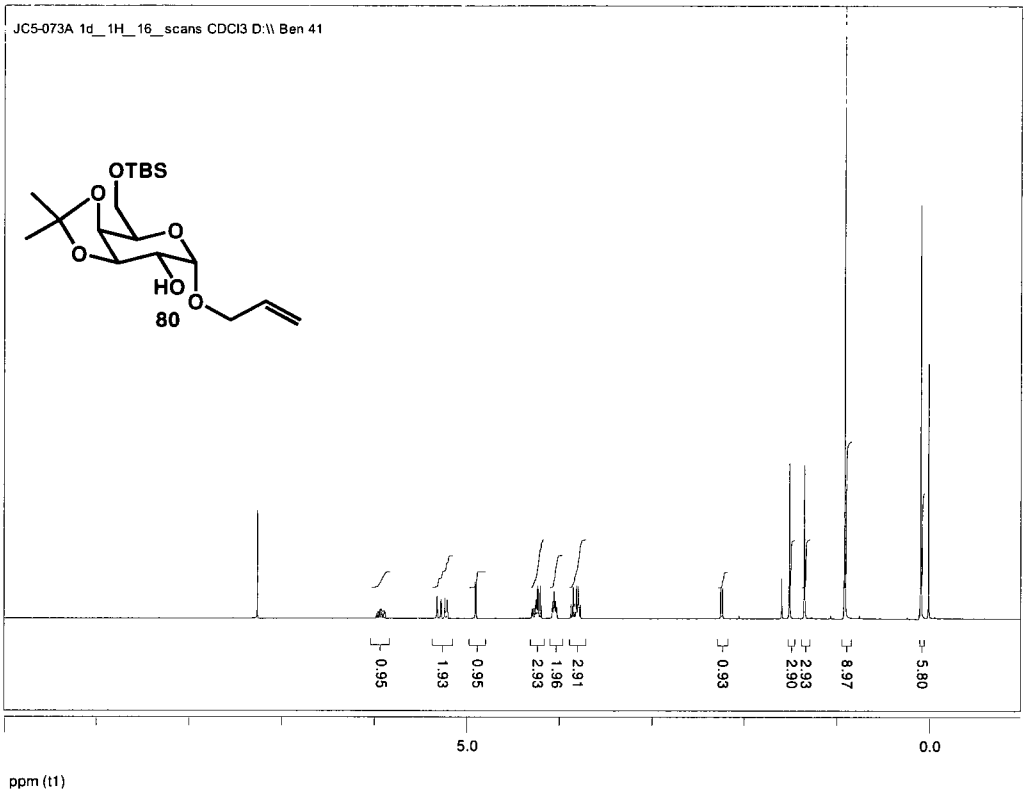
JC5-073A 1d__1H__16__scans CDCl3 D:\\ Ben 41
OTBS
O
O
O
HO
O
80
0.95
1.93
0.95
2.93
1.96
2.91
0.93
2.90
2.93
8.97
5.80
5.0
0.0
ppm (t1)

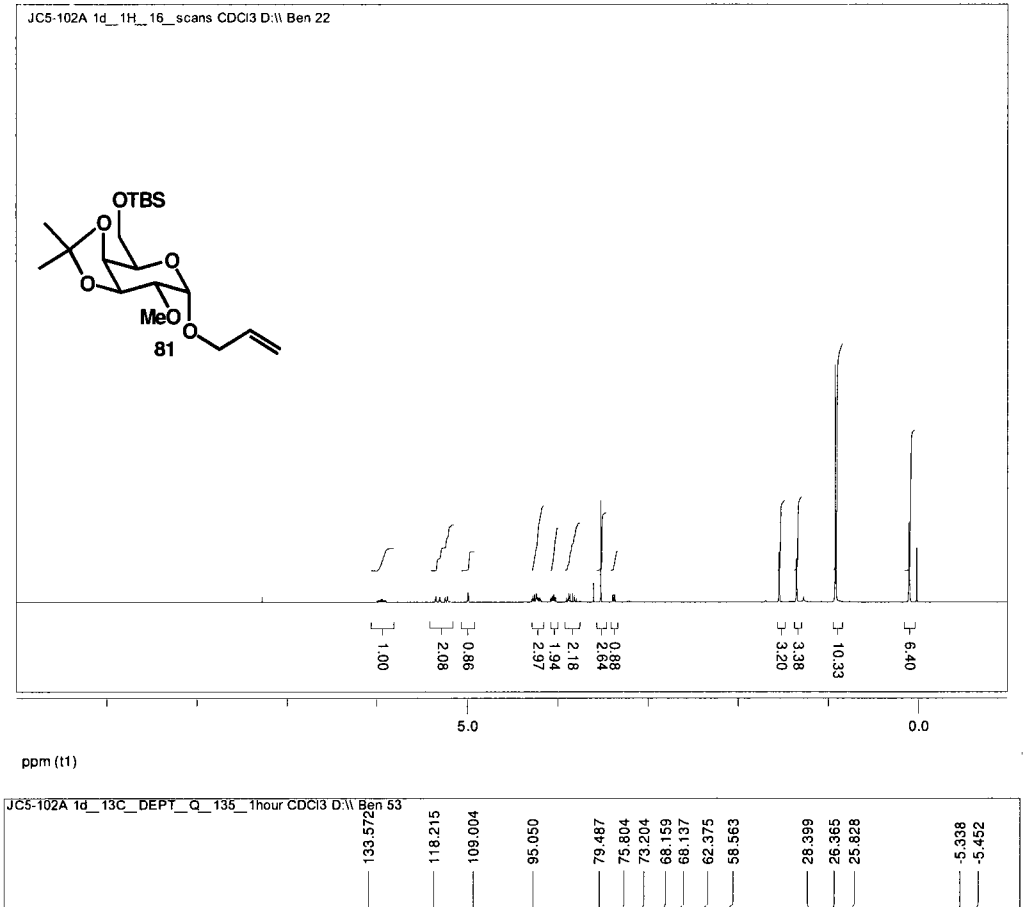
JC5-102A 1d__1H__16__scans CDCl3 D:\\ Ben 22
OTBS
O
O
O
O
MeO
O
81
1.00
2.08
0.86
2.97
1.94
2.18
2.64
0.88
3.20
3.38
10.33
6.40
5.0
0.0
ppm (t1)

JC5-102A 1d__13C__DEPT__Q__135__1hour CDCl3 D:\\ Ben 53
133.572
118.215
109.004
95.050
79.487
75.804
73.204
68.159
68.137
62.375
58.563
28.399
26.365
25.828
-5.338
-5.452

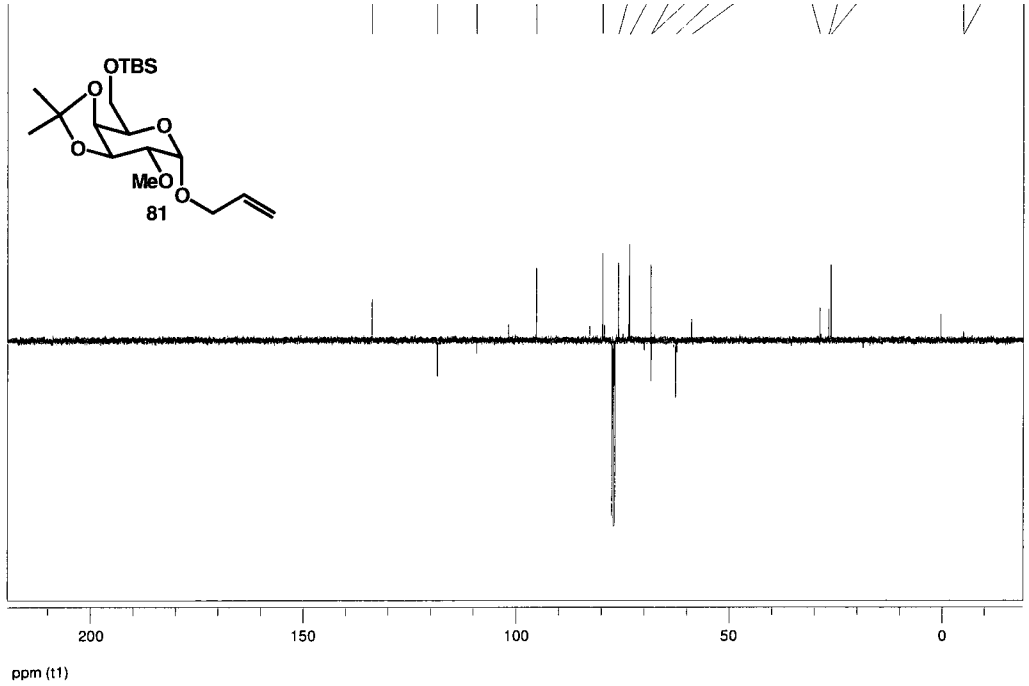
OTBS
O
O
O
MeO
O
81
200
150
100
50
0
ppm (t1)

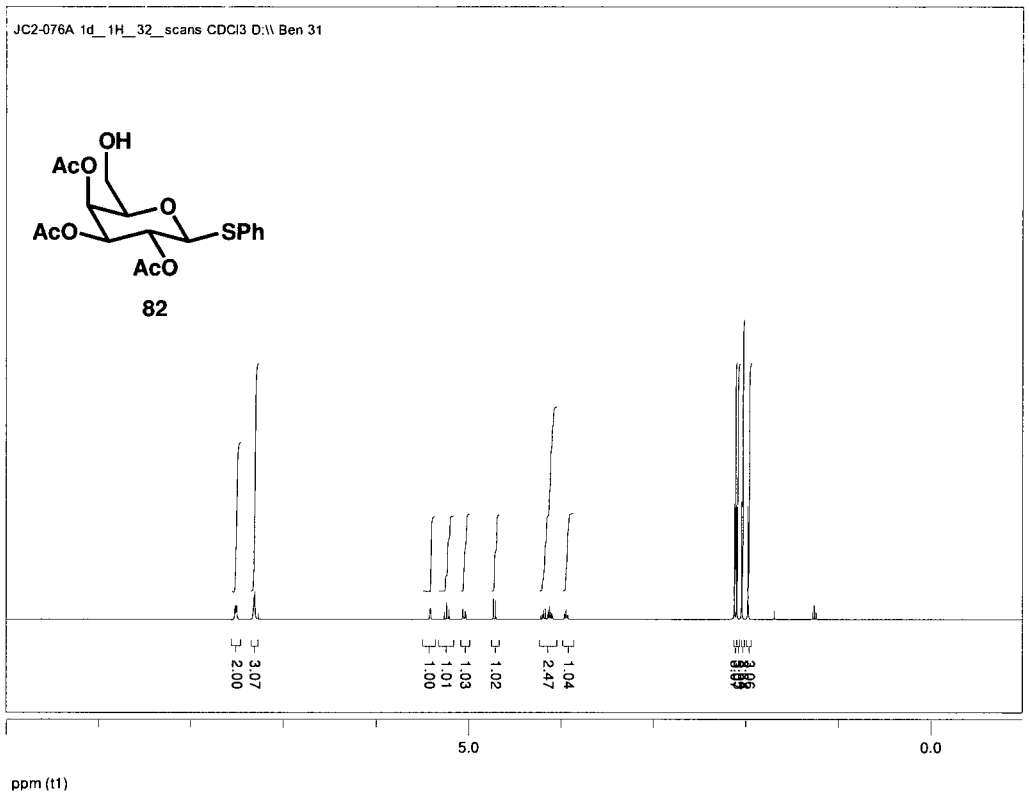
JC2-076A 1d__1H__32__scans CDCl3 D:\\ Ben 31
OH
AcO
O
AcO
SPh
AcO
82
2.00
3.07
1.00
1.01
1.03
1.02
2.47
1.04
5.0
0.0
ppm (t1)

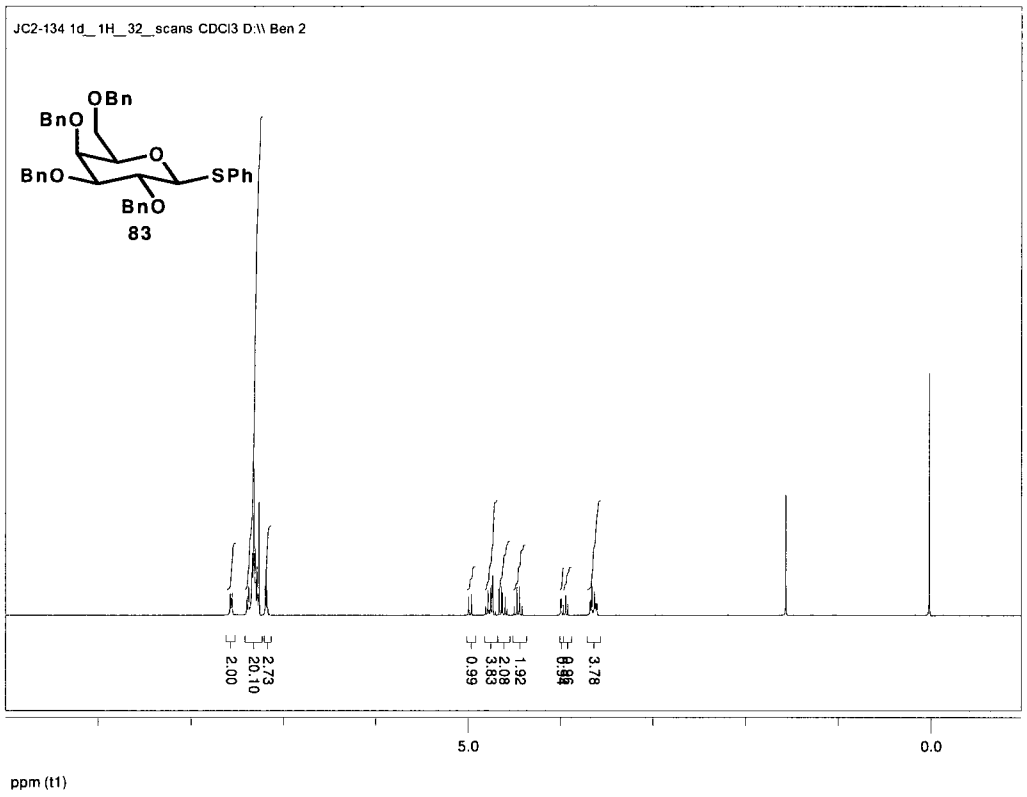
JC2-134 1d_1H_32_scans CDCl3 D:\\ Ben 2
OBn
BnO
O
BnO
SPh
BnO
83
2.00
20.10
2.73
0.99
3.83
2.08
1.92
3.78
5.0
0.0
ppm (t1)

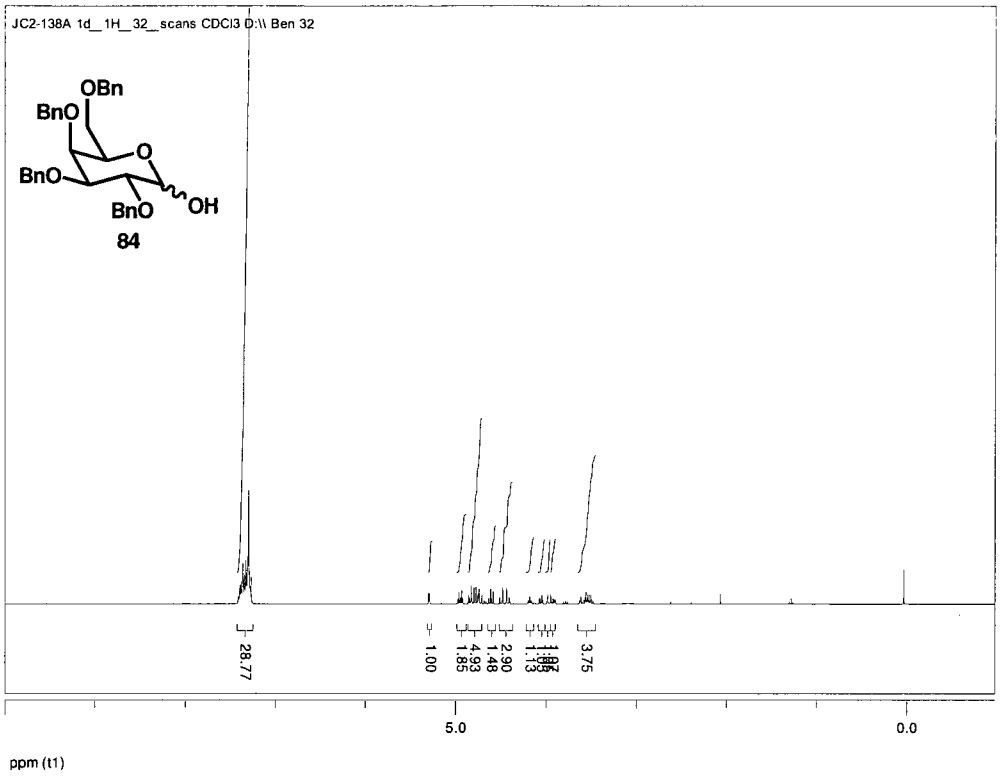
JC2-138A 1d__1H__32__scans CDCl3 D:\\ Ben 32
OBn
BnO
O
BnO
OH
BnO
84
28.77
1.00
4.93
1.85
1.48
2.90
1.13
3.75
5.0
0.0
ppm (t1)

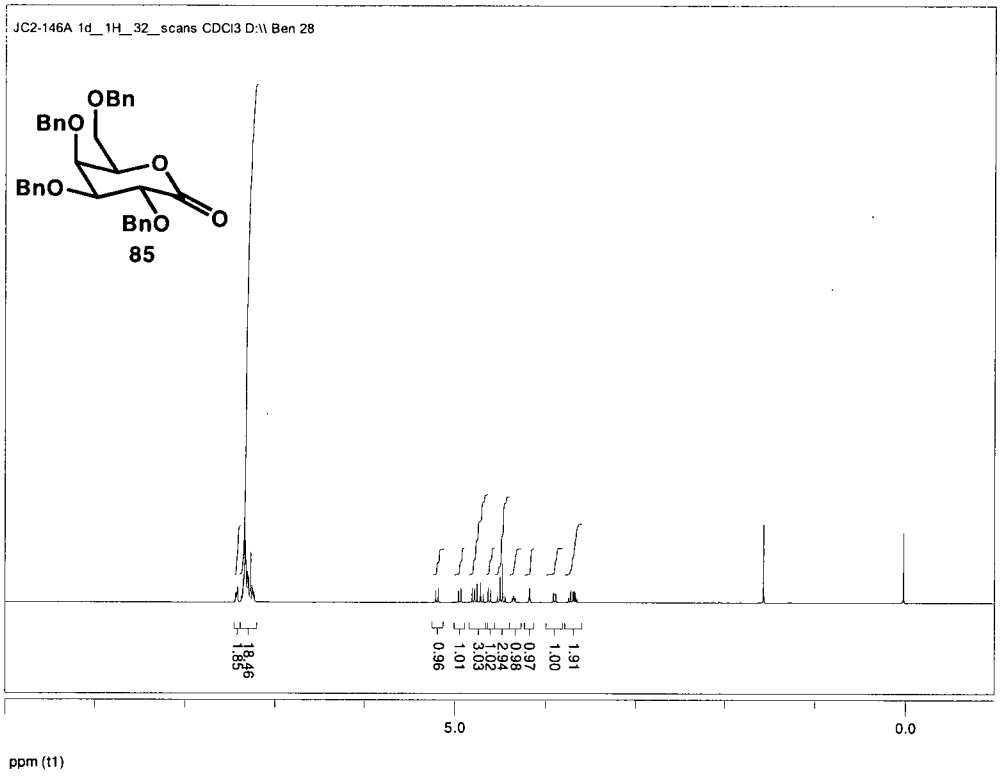
JC2-146A 1d__1H__32__scans CDCl3 D:\\ Ben 28
OBn
BnO
BnO
BnO
O
O
85
18.46
1.85
0.96
1.01
3.03
1.02
2.94
0.98
0.97
1.00
1.91
5.0
0.0
ppm (t1)

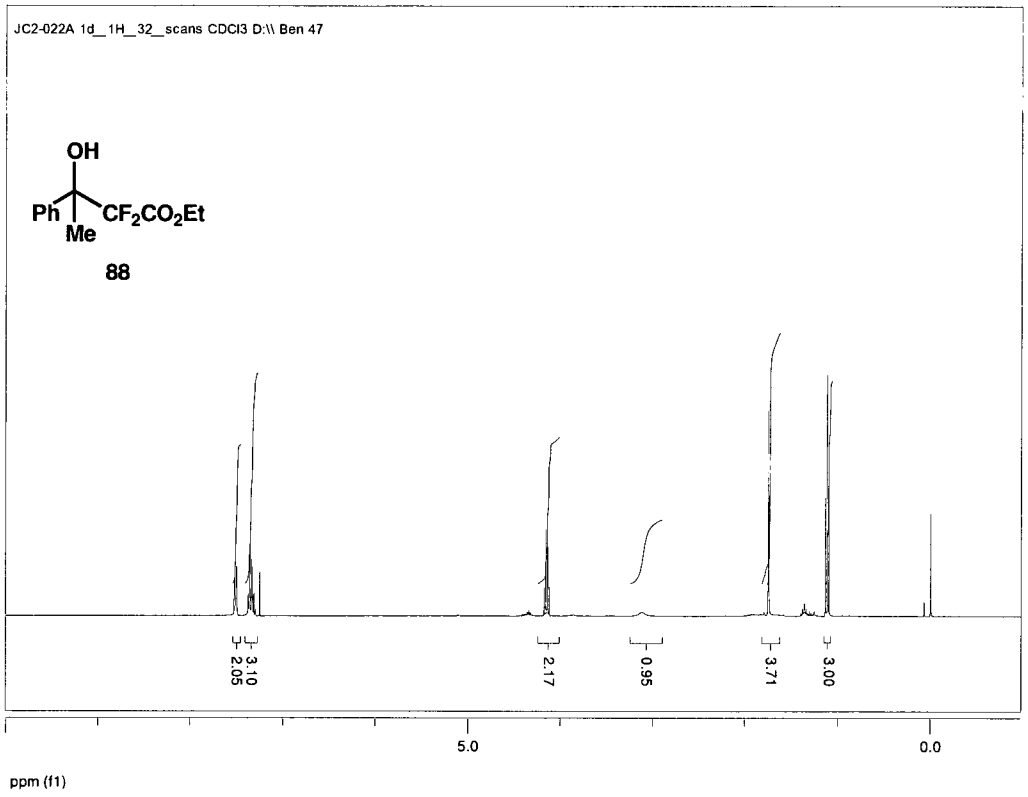
JC2-022A 1d__1H__32__scans CDCl3 D:\\ Ben 47
OH
Ph
CF2CO2Et
Me
88
3.10
2.05
2.17
0.95
3.71
3.00
5.0
0.0
ppm (f1)

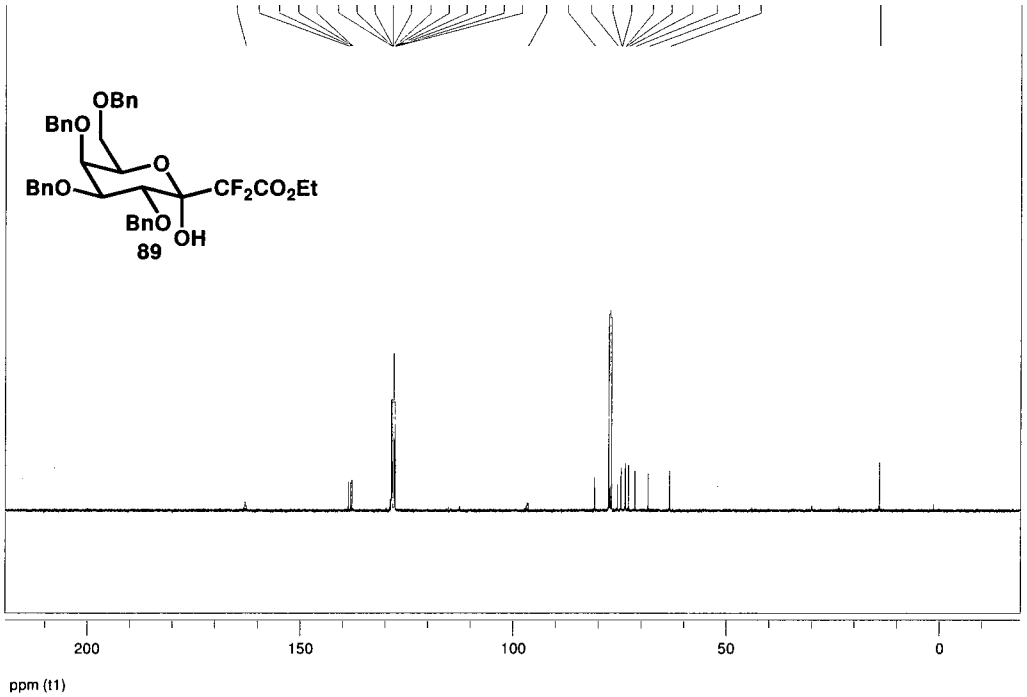
OBn
BnO
O
BnO
CF2CO2Et
BnO
OH
89
200
150
100
50
0
ppm (t1)

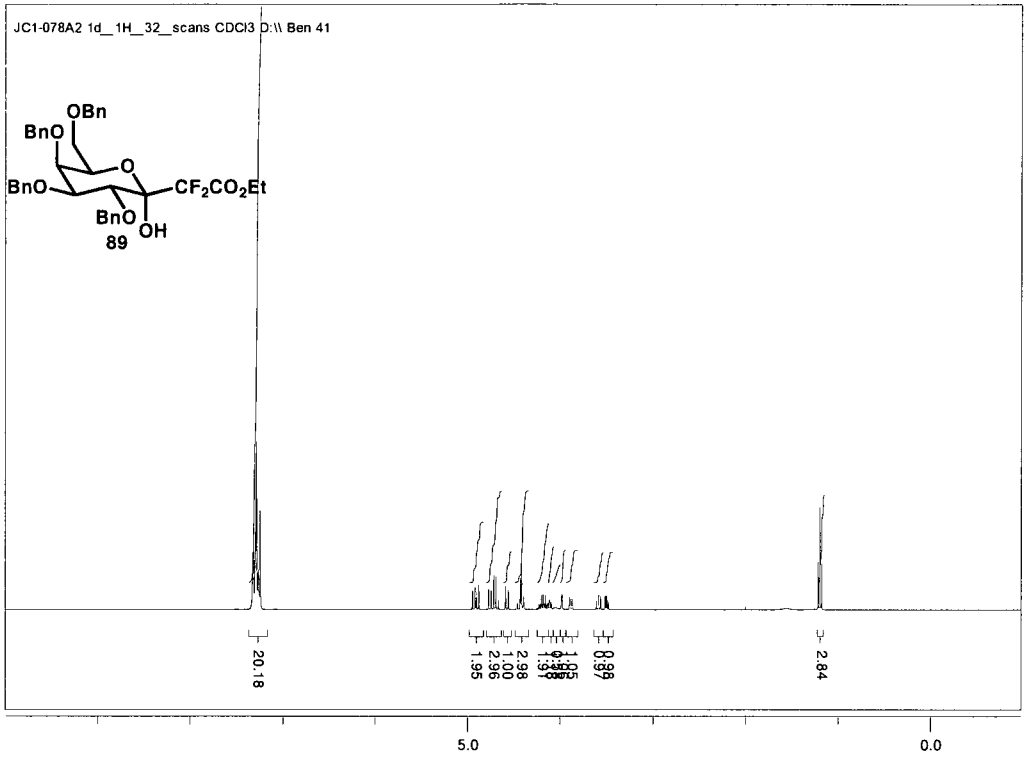
JC1-078A2 1d__1H__32__scans CDCl3 D:\\ Ben 41
OBn
BnO
O
BnO
CF2CO2Et
BnO
OH
89
20.18
1.95
2.96
1.00
2.98
0.98
2.84
5.0
0.0
ppm (t1)

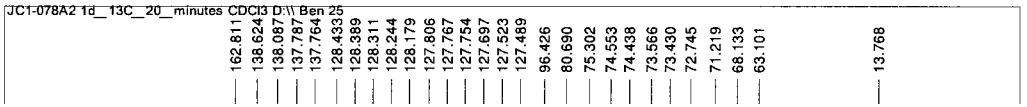
JC1-078A2 1d__13C__20__minutes CDCl3 D:\\ Ben 25
162.811
138.624
138.087
137.787
137.764
128.433
128.389
128.311
128.244
128.179
127.806
127.767
127.754
127.697
127.523
127.489
96.426
80.690
75.302
74.553
74.438
73.566
73.430
72.745
71.219
68.133
63.101
13.768

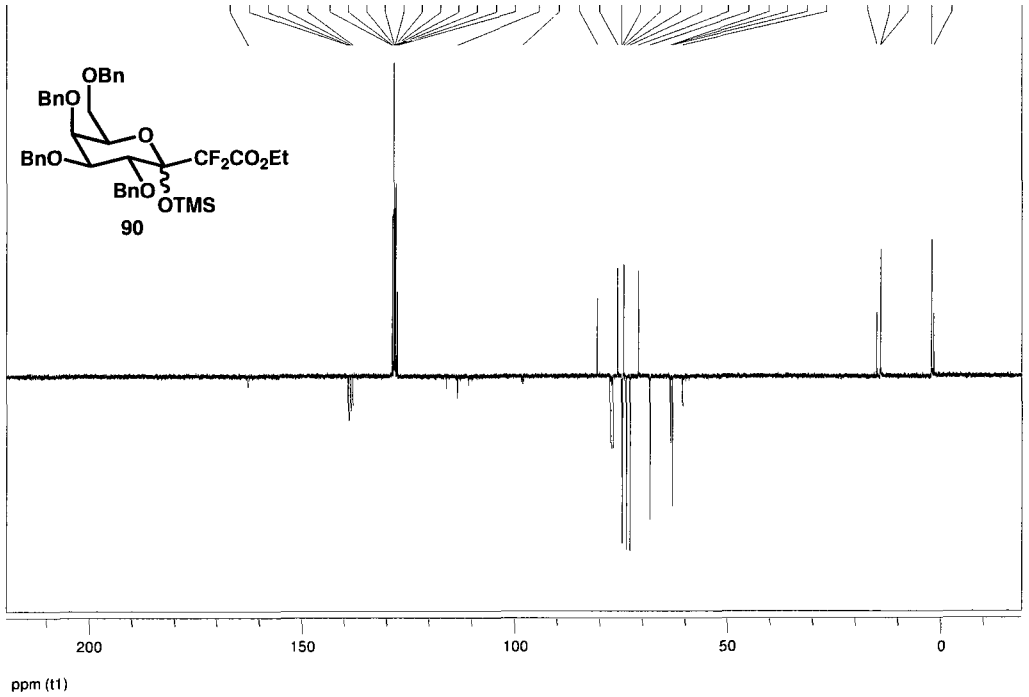
OBn
BnO
O
BnO
CF2CO2Et
BnO
OTMS
90
200
150
100
50
0
ppm (t1)

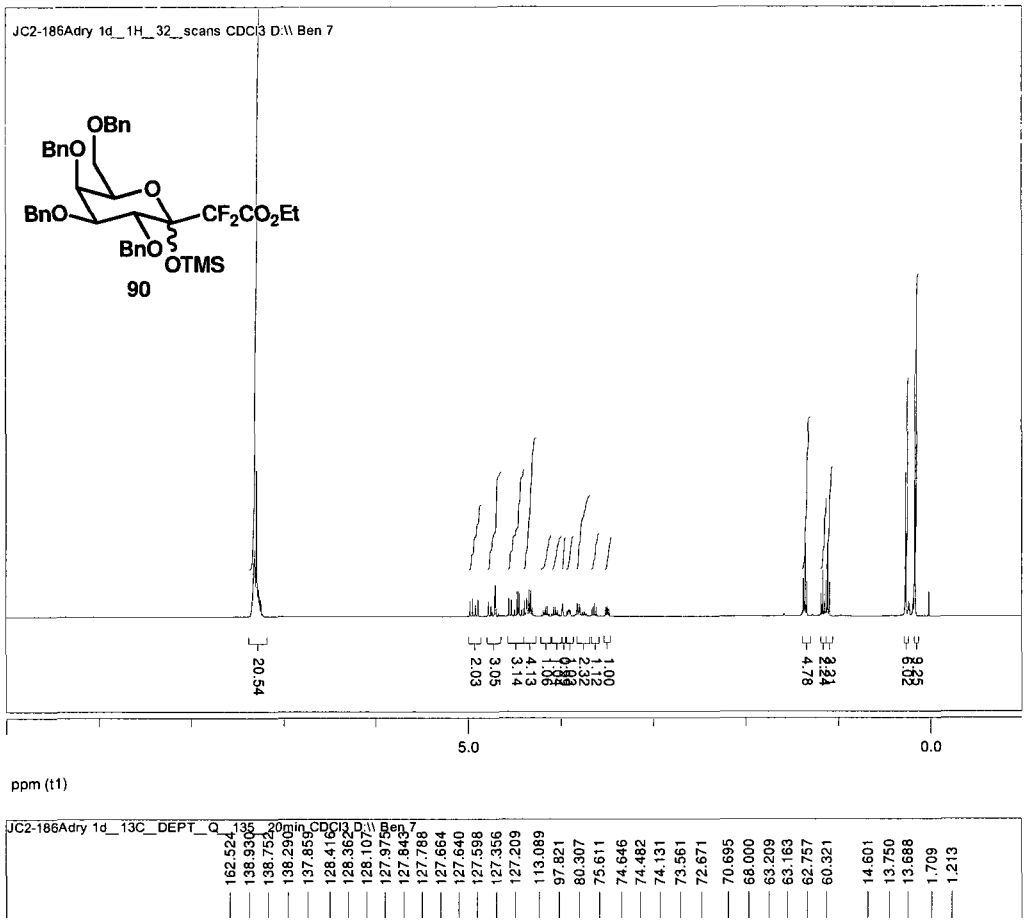
JC2-186Adry 1d__1H__32__scans CDCl3 D:\\ Ben 7
OBn
BnO
O
BnO
CF2CO2Et
BnO
OTMS
90
20.54
2.03
3.05
3.14
4.13
2.32
1.00
4.78
6.02
5.0
0.0
ppm (t1)
JC2-186Adry 1d__13C__DEPT__Q__135__20mg__CDCl3 D:\\ Ben 7
162.524
138.930
138.752
138.290
137.859
128.416
128.362
128.107
127.975
127.843
127.788
127.664
127.640
127.598
127.356
127.209
113.089
97.821
80.307
75.611
74.646
74.482
74.131
73.561
72.671
70.695
68.000
63.209
63.163
62.757
60.321
14.601
13.750
13.688
1.709
1.213

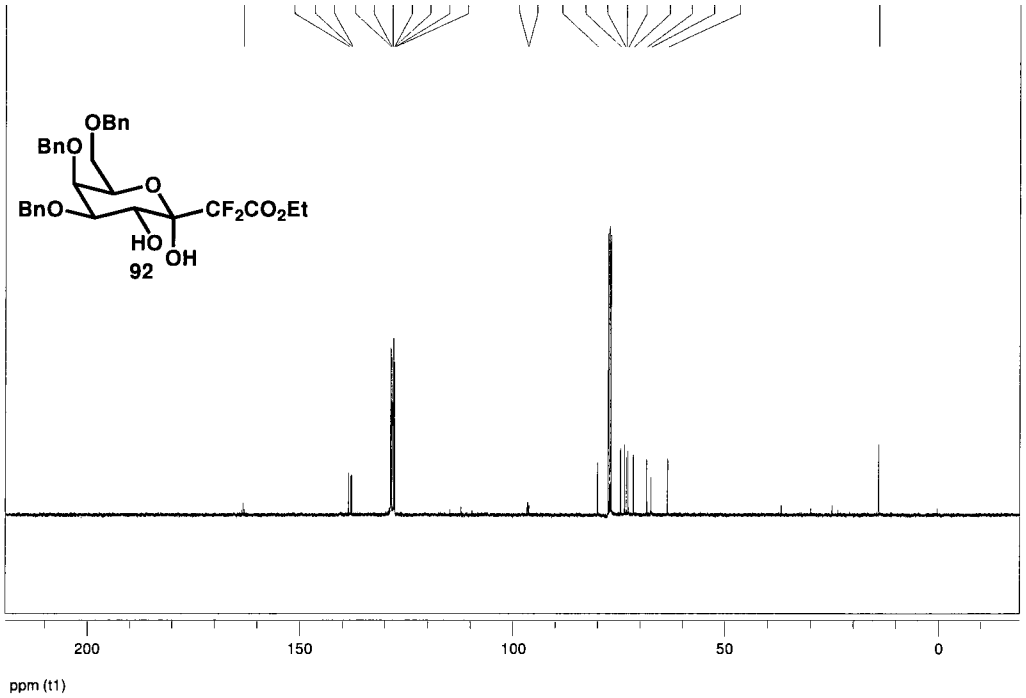
OBn
BnO
O
BnO
CF2CO2Et
HO
OH
92
200
150
100
50
0
ppm (t1)

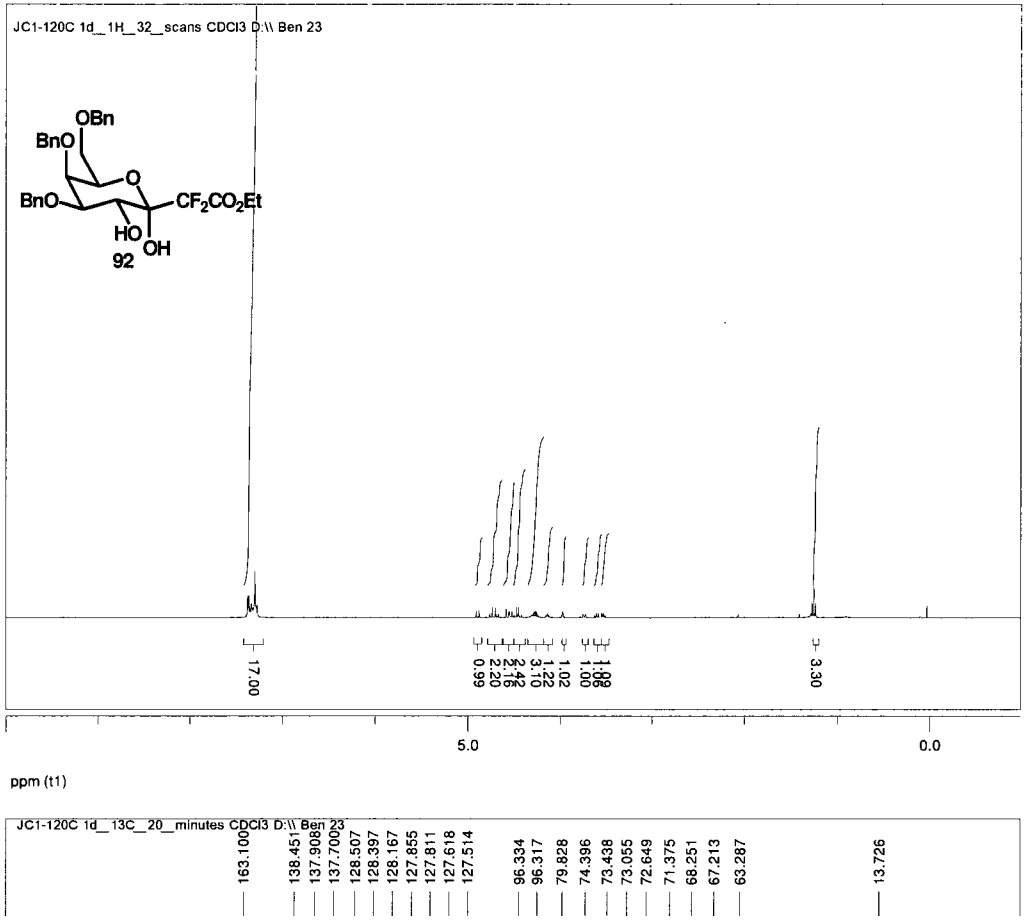
JC1-120C 1d__1H__32__scans CDCl3 D:\\ Ben 23
OBn
BnO
O
BnO
CF2CO2Et
HO
OH
92
17.00
0.99
2.20
2.16
2.42
3.10
1.22
1.20
1.00
3.30
5.0
0.0
ppm (t1)
JC1-120C 1d__13C__20__minutes CDCl3 D:\\ Ben 23
163.100
138.451
137.908
137.700
128.507
128.397
128.167
127.855
127.811
127.618
127.514
96.334
96.317
79.828
74.396
73.438
73.055
72.649
71.375
68.251
67.213
63.287
13.726

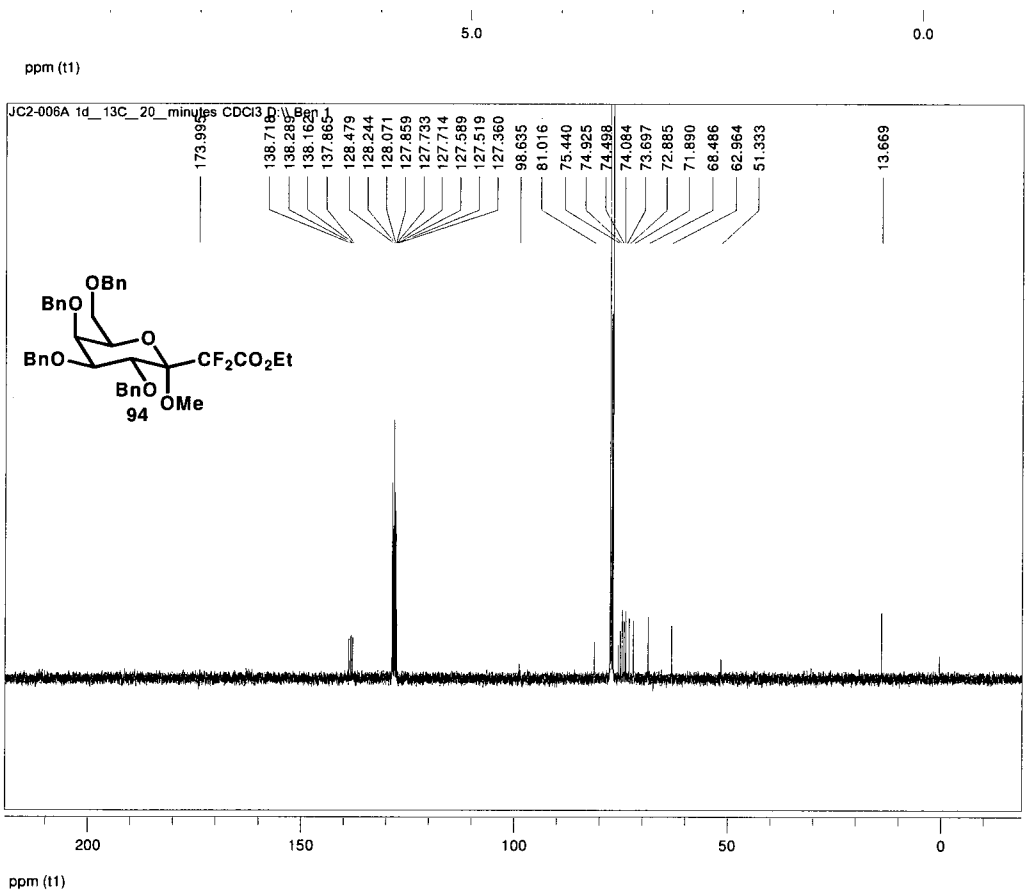
5.0
0.0
ppm (t1)
JC2-006A 1d__13C__20__minutes CDCl3 D:\\ Ben 1
173.995
138.718
138.285
138.162
137.865
128.479
128.244
128.071
127.859
127.733
127.714
127.589
127.519
127.360
98.635
81.016
75.440
74.925
74.498
74.084
73.697
72.885
71.890
68.486
62.964
51.333
13.669
OBn
BnO
O
BnO
CF2CO2Et
BnO
OMe
94
200
150
100
50
0
ppm (t1)

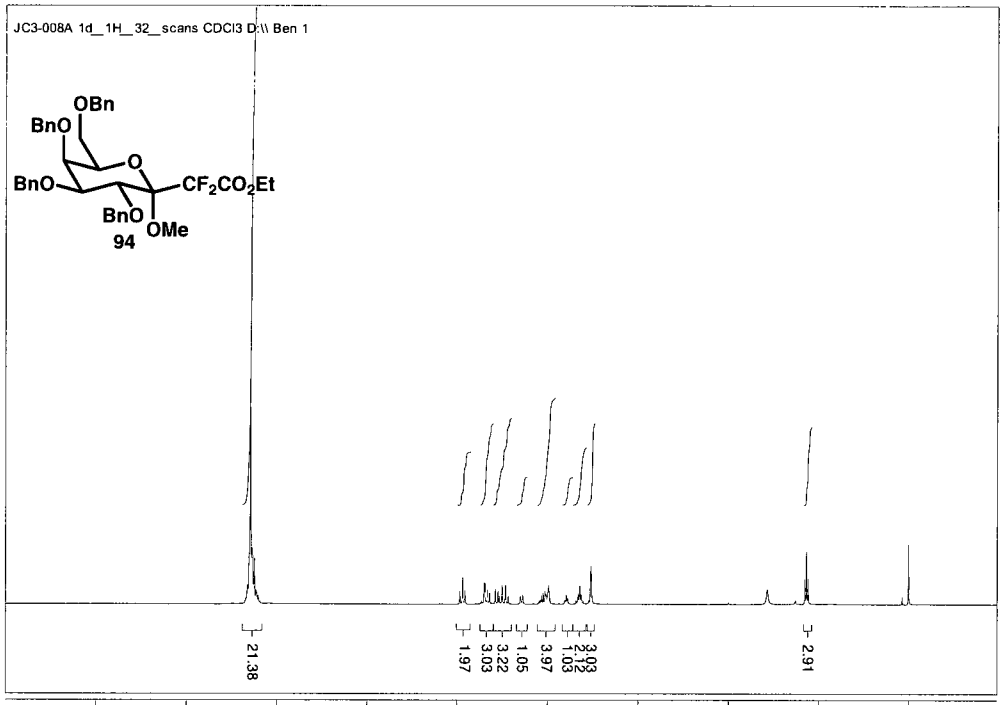
JC3-008A 1d_1H_32_scans CDCl3 D:\\ Ben 1
OBn
BnO
O
BnO
CF2CO2Et
BnO
OMe
94
21.38
1.97
3.03
3.22
1.05
3.97
3.03
3.12
1.03
2.91

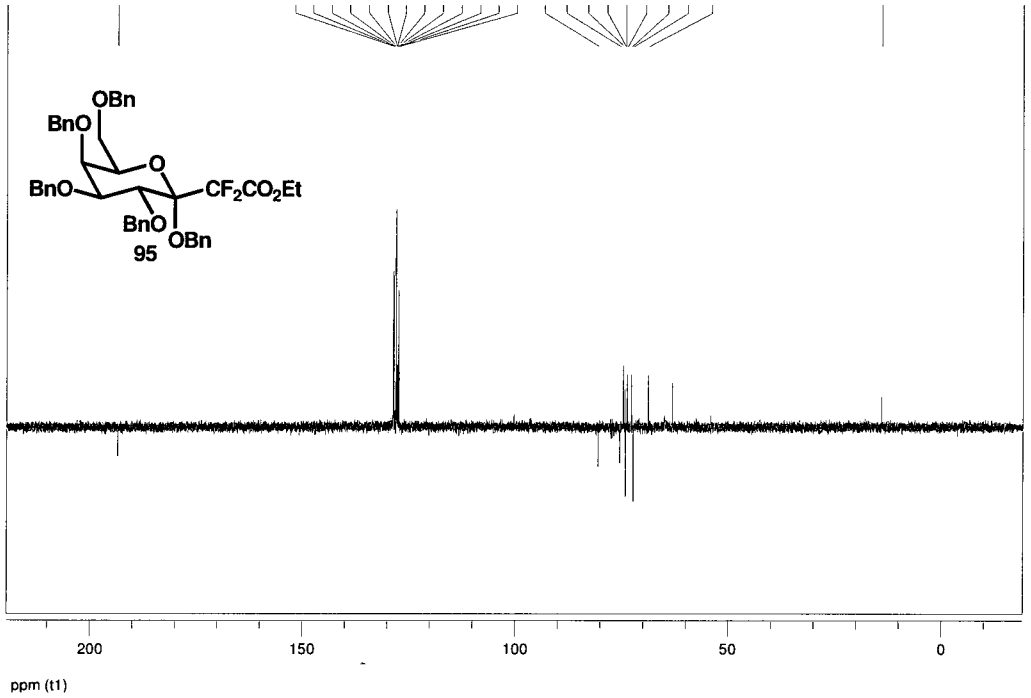
OBn
BnO
O
BnO
CF2CO2Et
BnO
OBn
95
200
150
100
50
0
ppm (t1)

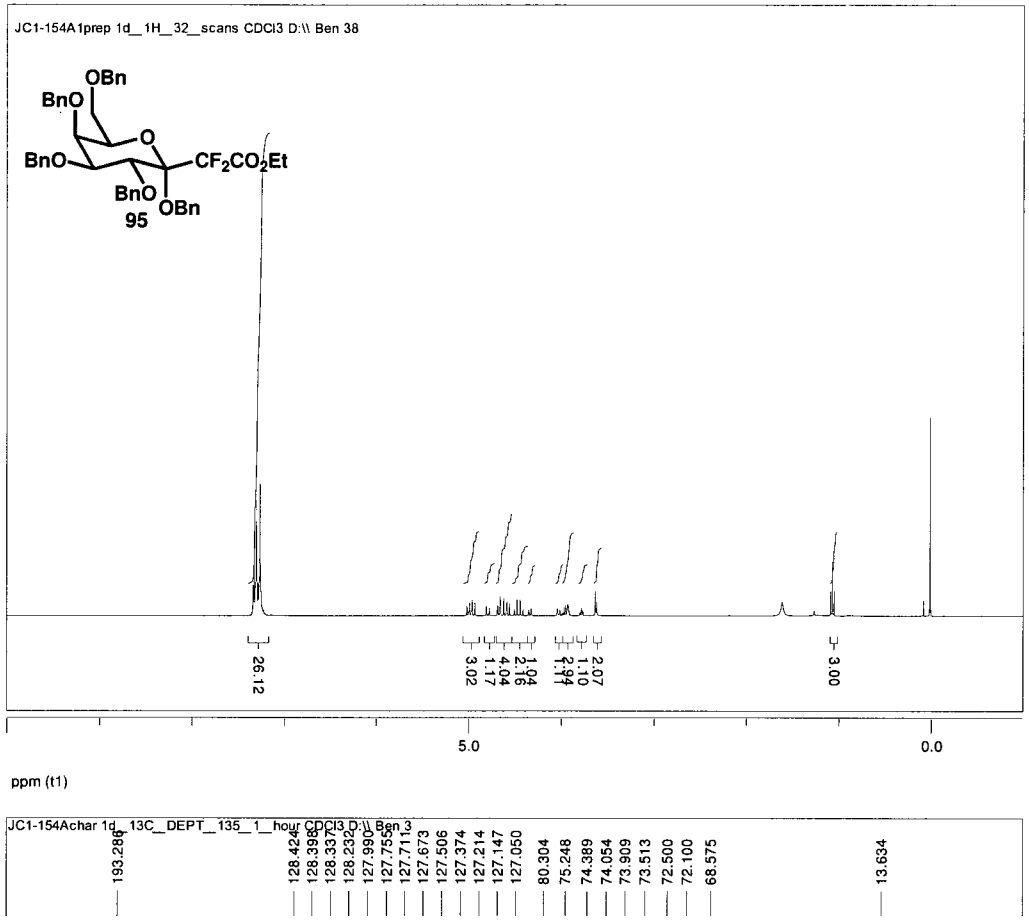
JC1-154A1prep 1d__1H__32__scans CDCl3 D:\\ Ben 38
OBn
BnO
O
BnO
CF2CO2Et
BnO
OBn
95
26.12
3.02
1.17
4.04
2.06
1.04
2.64
1.10
2.07
3.00
5.0
0.0
ppm (t1)
JC1-154Achar 1d__13C__DEPT__135__1__hour CDCl3 D:\\ Ben 3
193.286
128.424
128.398
128.337
128.232
127.990
127.755
127.711
127.673
127.506
127.374
127.214
127.147
127.050
80.304
75.248
74.389
74.054
73.909
73.513
72.500
72.100
68.575
13.634

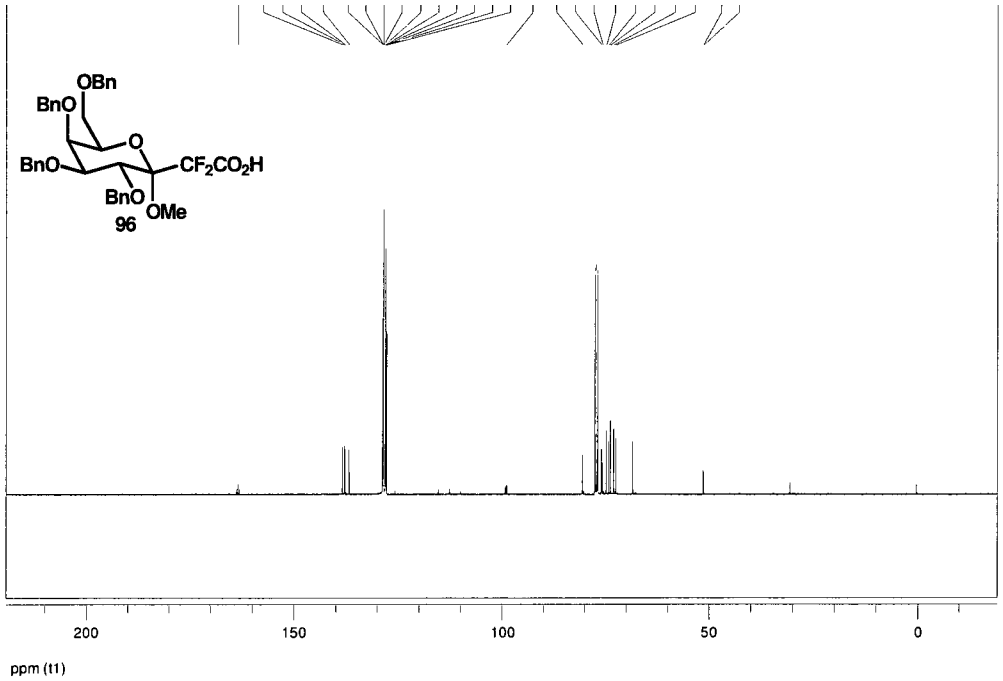
OBn
BnO
O
BnO
CF2CO2H
BnO
OMe
96
200
150
100
50
0
ppm (t1)

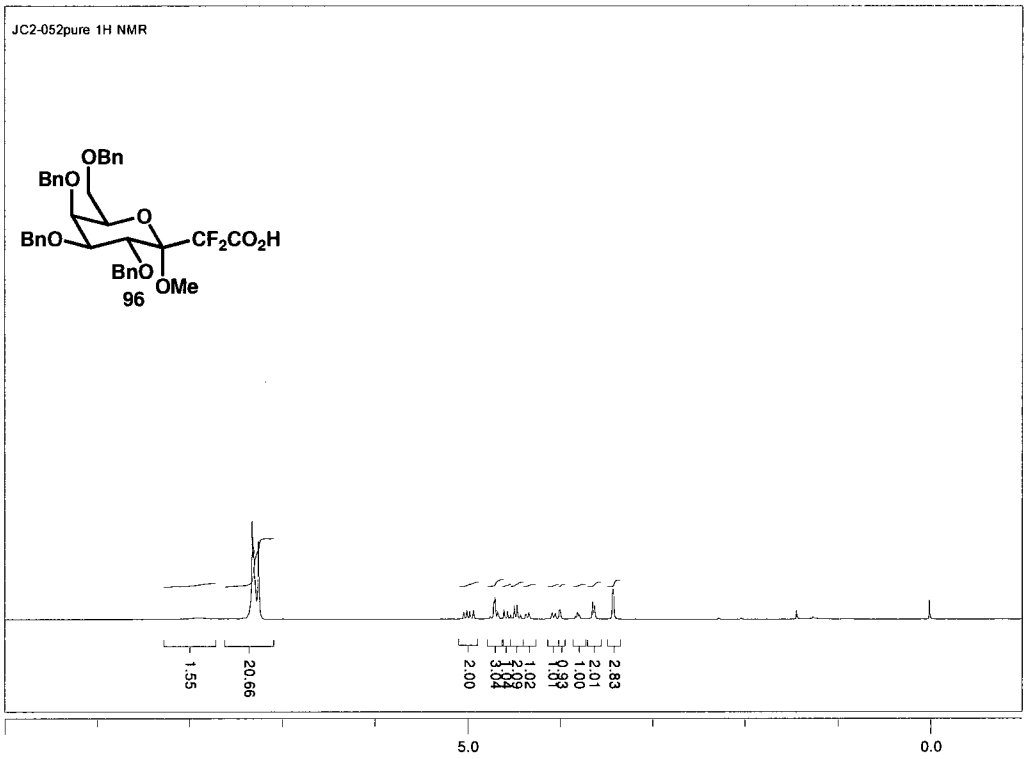
JC2-052pure 1H NMR
OBn
BnO
O
BnO
CF2CO2H
BnO
OMe
96
1.55
20.66
2.00
1.02
1.00
2.01
2.83
5.0
0.0
ppm (t1)

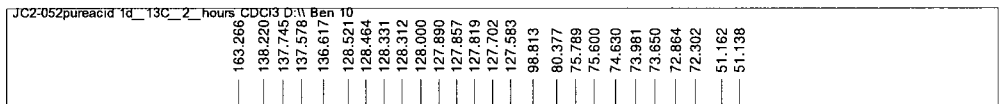
JC2-052pureacid 1d__13C__2__hours CDCl3 D:\\ Ben 10
163.266
138.220
137.745
137.578
136.617
128.521
128.464
128.331
128.312
128.000
127.890
127.857
127.819
127.702
127.583
98.813
80.377
75.789
75.600
74.630
73.981
73.650
72.864
72.302
51.162
51.138

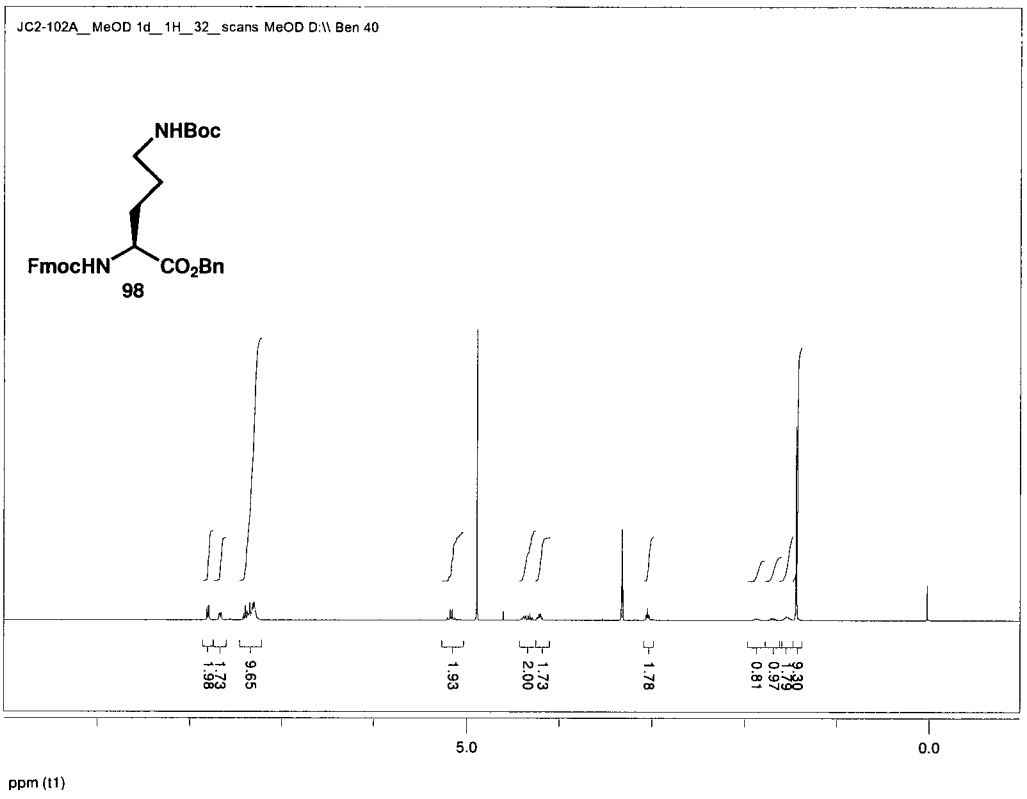
JC2-102A__MeOD 1d__1H__32__scans MeOD D:\\ Ben 40
NHBoc
FmocHN
CO2Bn
98
1.73
1.98
9.65
1.93
1.73
2.00
1.78
0.81
0.97
1.79
9.30
5.0
0.0
ppm (t1)

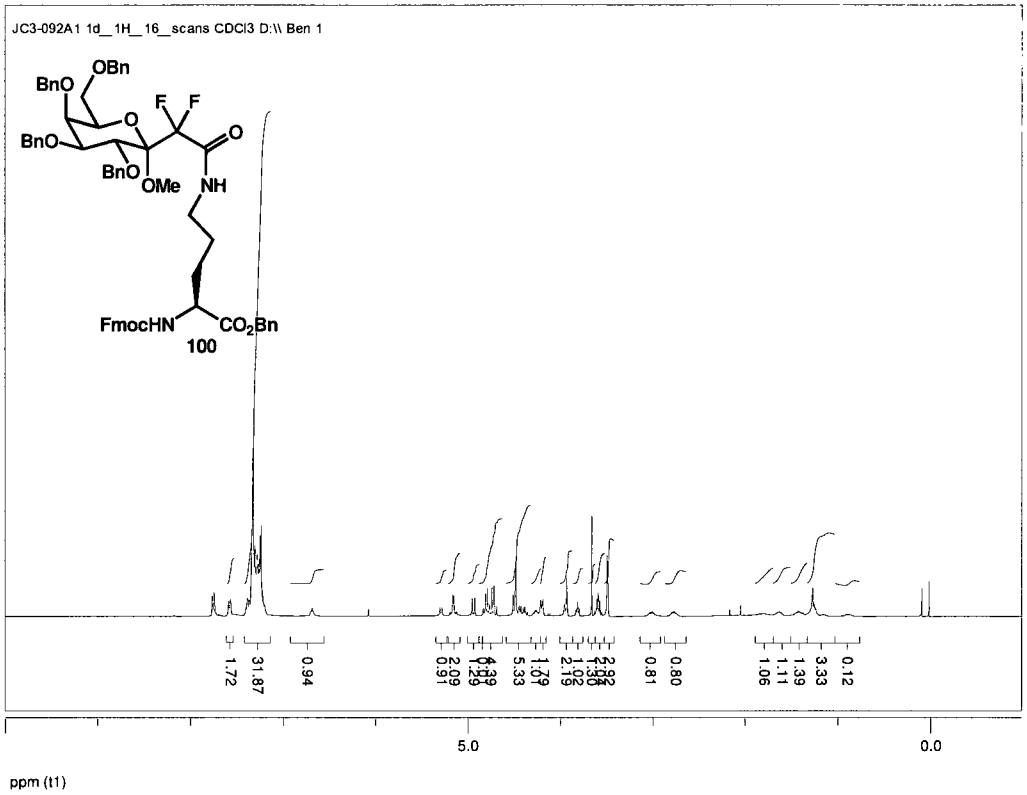
JC3-092A1 1d__1H__16_scans CDCl3 D:\\ Ben 1
BnO
OBn
F
F
O
BnO
BnO
OMe
NH
FmocHN
CO2Bn
100
1.72
31.87
0.94
0.91
2.09
5.33
1.07
0.81
0.80
1.06
1.11
1.39
3.33
0.12
5.0
0.0
ppm (t1)

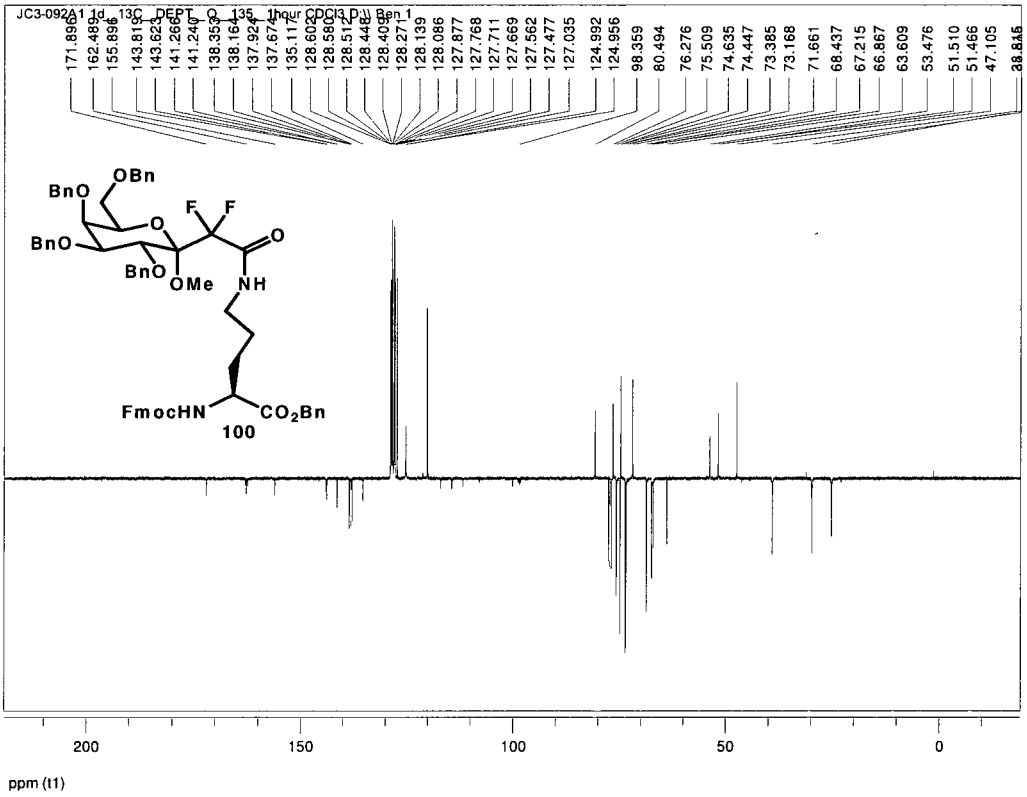
JC3-092A1 1d__13C_DEPT_O_135_1hour CDCl3 D:\\ Ben 1
171.895
162.489
155.896
143.813
143.623
141.265
141.245
138.354
138.164
137.924
137.674
135.117
128.602
128.582
128.511
128.444
128.405
128.271
128.139
128.086
127.877
127.768
127.711
127.669
127.562
127.477
127.035
124.992
124.956
98.359
80.494
76.276
75.509
74.635
74.447
73.385
73.168
71.661
68.437
67.215
66.867
63.609
53.476
51.510
51.466
47.105
BnO
OBn
F
F
O
BnO
BnO
OMe
NH
FmocHN
CO2Bn
100
200
150
100
50
0
ppm (t1)

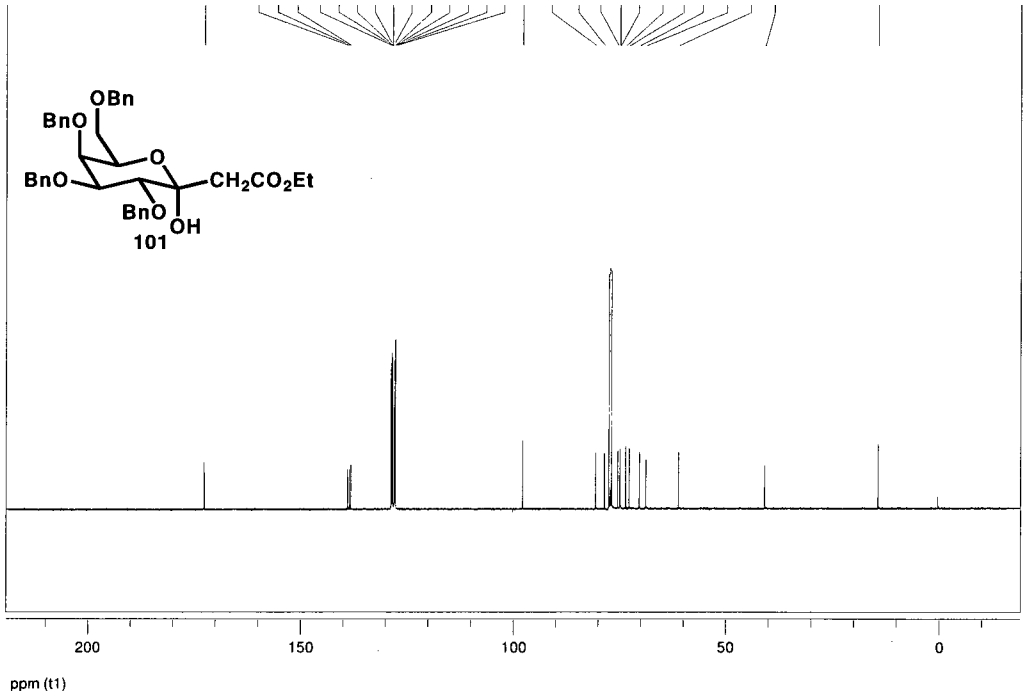
OBn
BnO
O
BnO
CH2CO2Et
BnO
OH
101
200
150
100
50
0
ppm (t1)

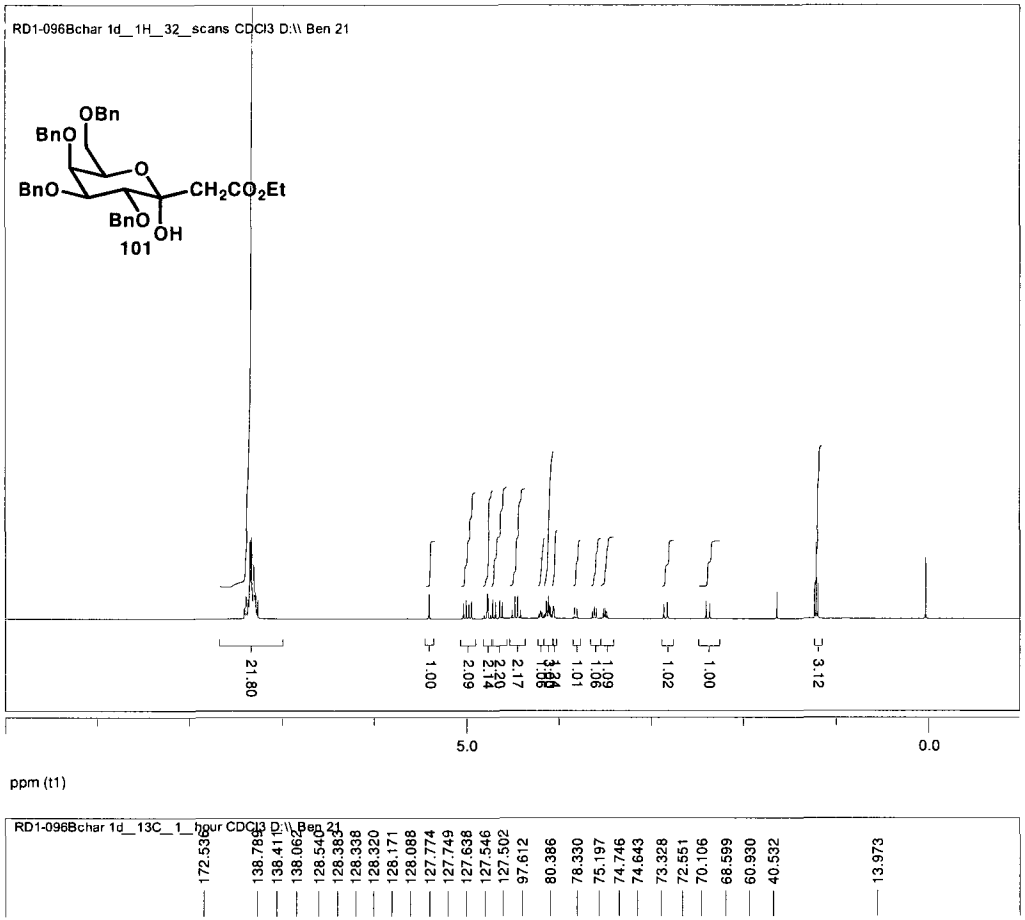
RD1-096Bchar 1d__1H__32__scans CDCl3 D:\\ Ben 21
OBn
BnO
O
BnO
CH2CO2Et
BnO
OH
101
21.80
1.00
2.09
2.14
2.20
2.17
1.01
1.09
1.06
1.02
1.00
3.12
5.0
0.0
ppm (t1)
RD1-096Bchar 1d__13C__1__hour CDCl3 D:\\ Ben 21
172.536
138.789
138.411
138.062
128.540
128.383
128.338
128.320
128.171
128.088
127.774
127.749
127.638
127.546
127.502
97.612
80.386
78.330
75.197
74.746
74.643
73.328
72.551
70.106
68.599
60.930
40.532
13.973

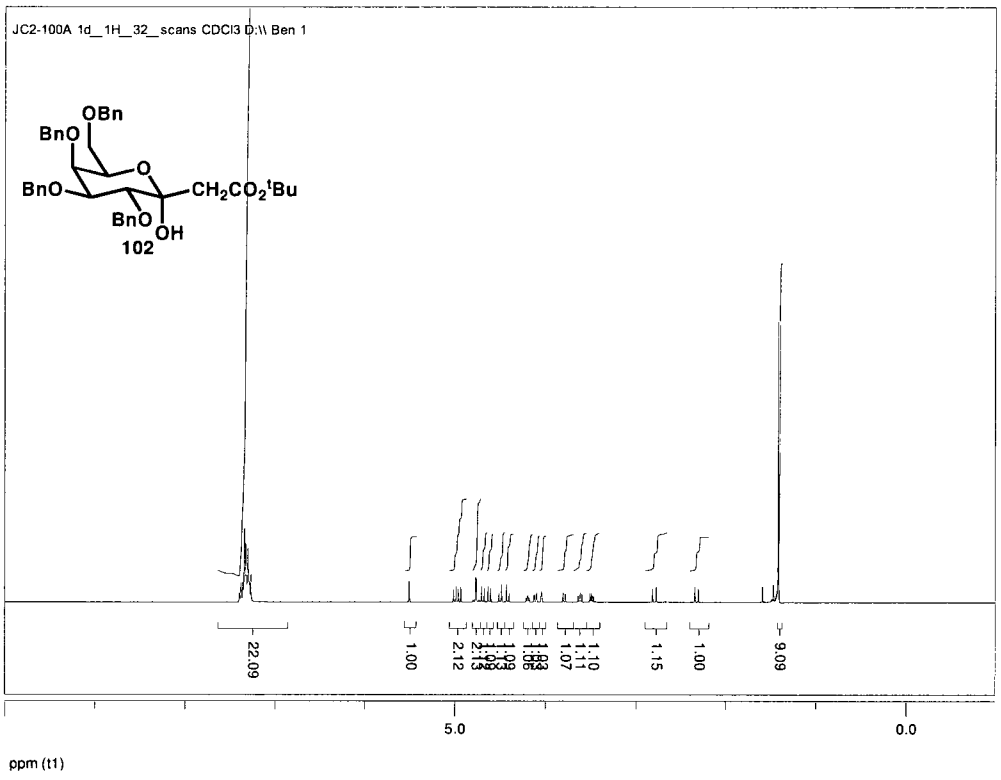
JC2-100A 1d__1H__32__scans CDCl3 D:\\ Ben 1
OBn
BnO
O
BnO
CH2CO2tBu
BnO
OH
102
22.09
1.00
2.12
1.15
1.00
9.09
5.0
0.0
ppm (t1)

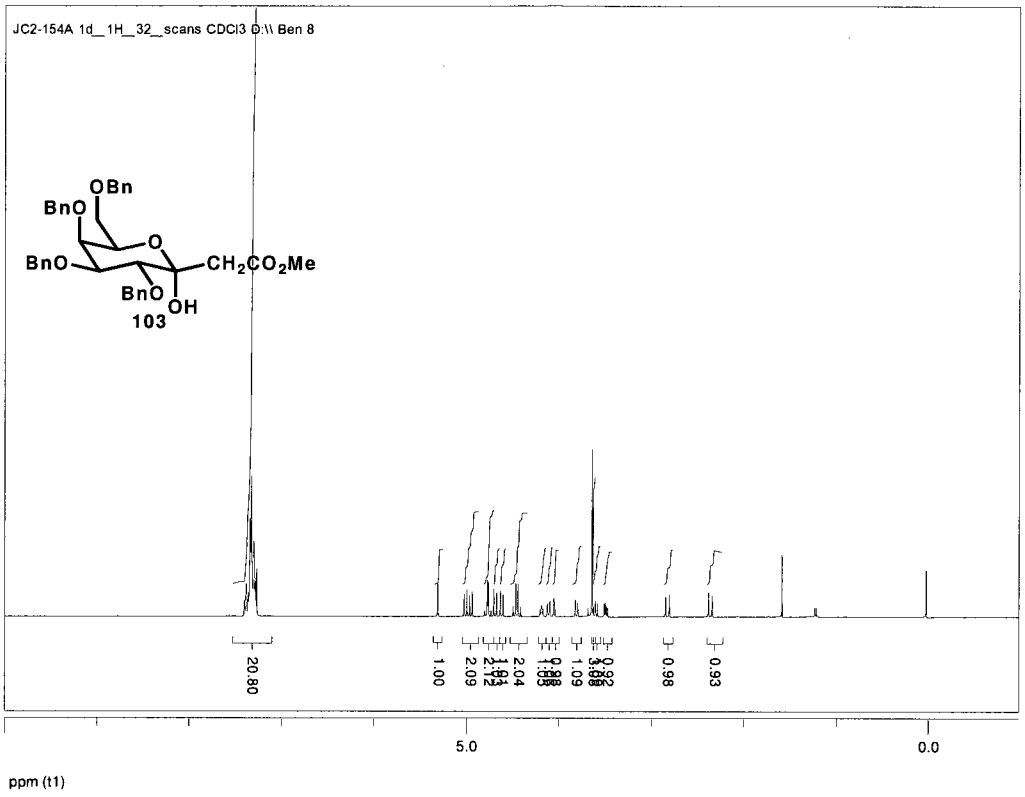
JC2-154A 1d__1H__32__scans CDCl3 D:\\ Ben 8
OBn
BnO
O
BnO
CH2CO2Me
BnO
OH
103
20.80
1.00
2.09
2.04
1.09
0.98
0.93
5.0
0.0
ppm (t1)

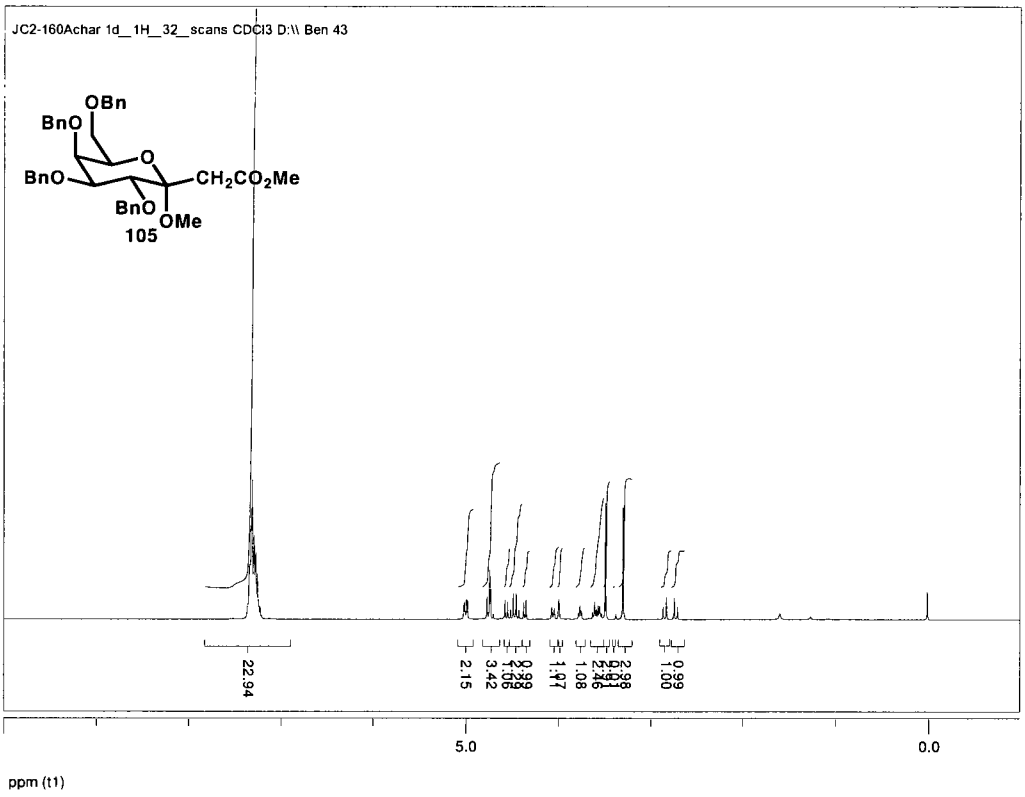
JC2-160Achar 1d__1H__32__scans CDCl3 D:\\ Ben 43
OBn
BnO
BnO
O
CH2CO2Me
BnO
OMe
105
22.94
2.15
3.42
1.08
1.00
5.0
0.0
ppm (t1)

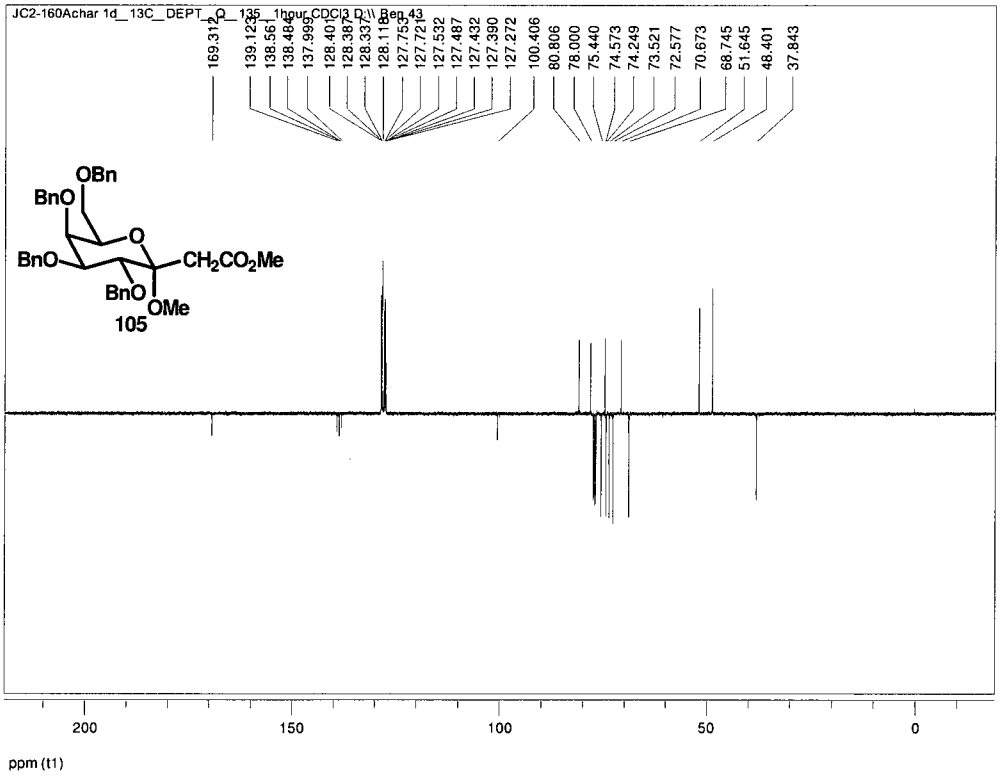
JC2-160Achar 1d__13C__DEPT__O__135__1hour CDCl3 D:\\ Ben 43
169.312
139.123
138.561
138.484
137.999
128.401
128.387
128.337
128.118
127.753
127.721
127.532
127.487
127.432
127.390
127.272
100.406
80.806
78.000
75.440
74.573
74.249
73.521
72.577
70.673
68.745
51.645
48.401
37.843
OBn
BnO
BnO
O
CH2CO2Me
BnO
OMe
105
200
150
100
50
0
ppm (t1)

ppm (t1)

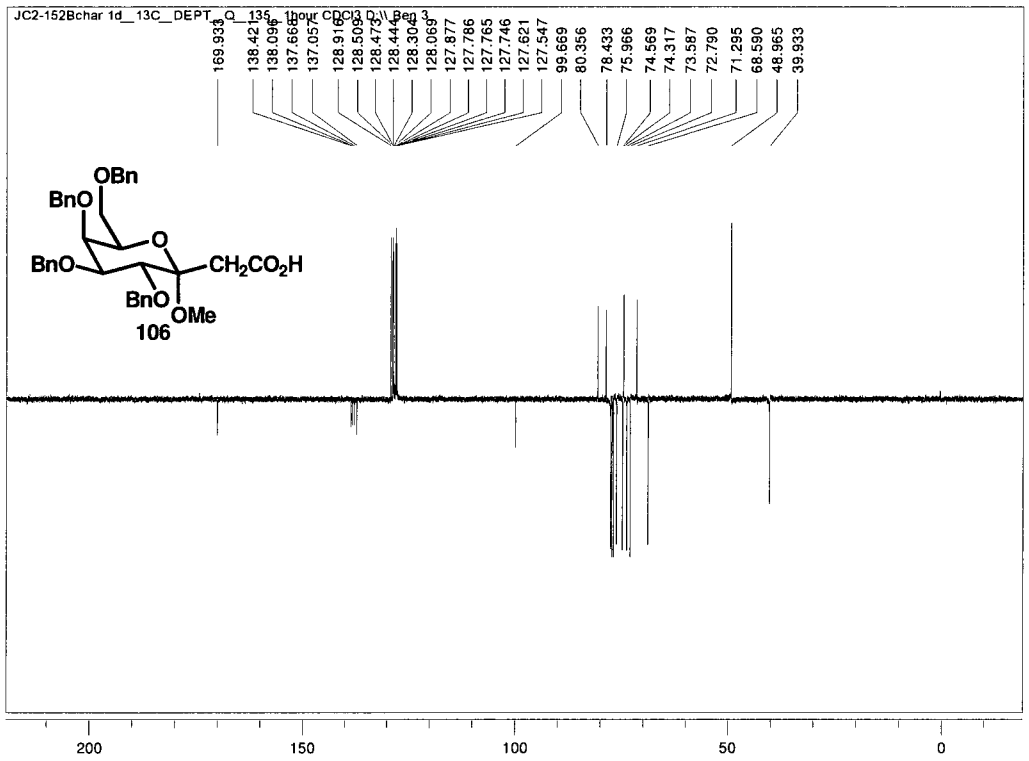
JC2-152Bchar 1d__13C__DEPT__Q__135__1hour CDCl3 D:\\ Ben 3
169.933
138.421
138.096
137.668
137.057
128.916
128.509
128.473
128.444
128.304
128.069
127.877
127.786
127.765
127.746
127.621
127.547
99.669
80.356
78.433
75.966
74.569
74.317
73.587
72.790
71.295
68.590
48.965
39.933
OBn
BnO
O
BnO
CH2CO2H
BnO
OMe
106
200
150
100
50
0
ppm (t1)

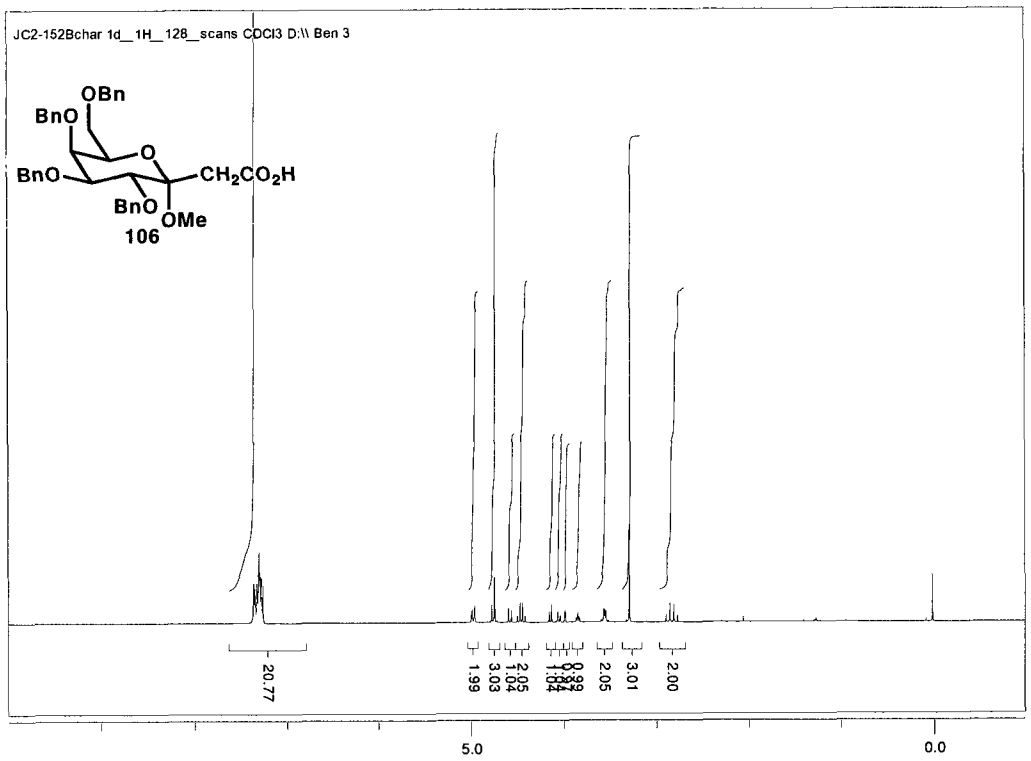
JC2-152Bchar 1d__1H__128__scans CDCl3 D:\\ Ben 3
OBn
BnO
O
BnO
CH2CO2H
BnO
OMe
106
20.77
1.99
3.03
2.05
1.04
2.05
3.01
2.00
5.0
0.0

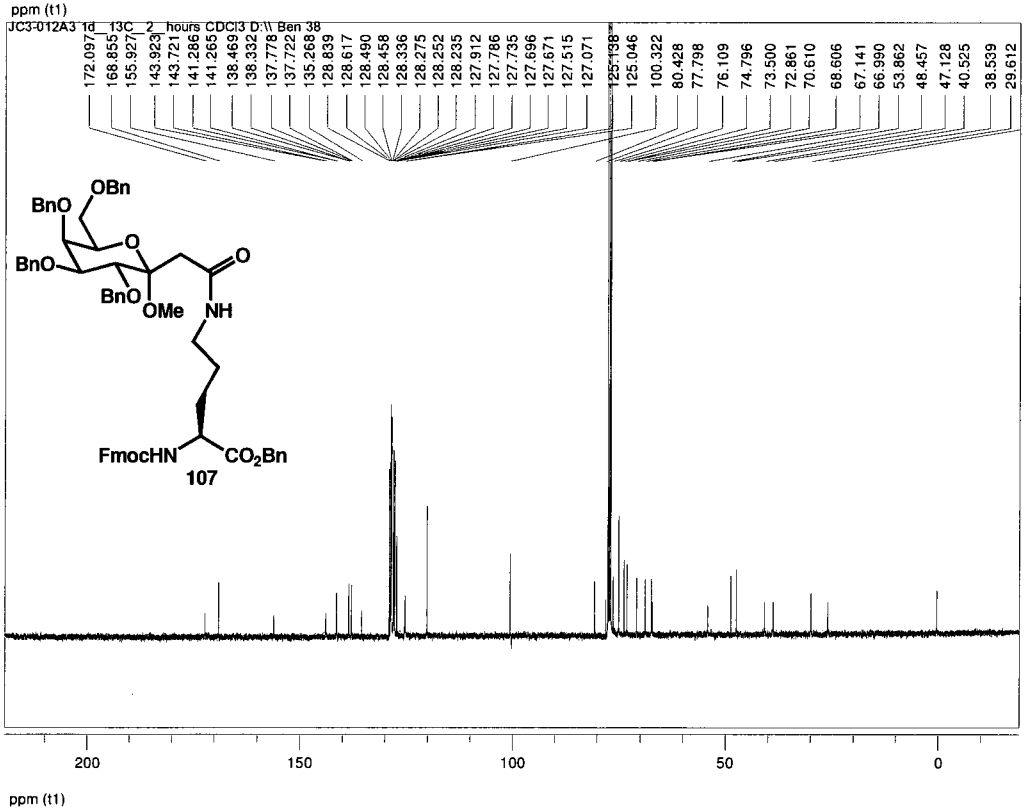
ppm (t1)
JC3-012A3 1d 13C 2 hours CDCl3 D:\\ Ben 38
172.097
168.855
155.927
143.923
143.721
141.286
141.265
138.469
138.332
137.778
137.722
135.269
128.839
128.617
128.490
128.458
128.336
128.275
128.252
128.235
127.912
127.786
127.735
127.696
127.671
127.515
127.071
125.138
125.046
100.322
80.428
77.798
76.109
74.796
73.500
72.861
70.610
68.606
67.141
66.990
53.862
48.457
47.128
40.525
38.539
29.612
OBn
BnO
O
BnO
O
BnO
OMe
NH
FmocHN
CO2Bn
107
200
150
100
50
0
ppm (t1)

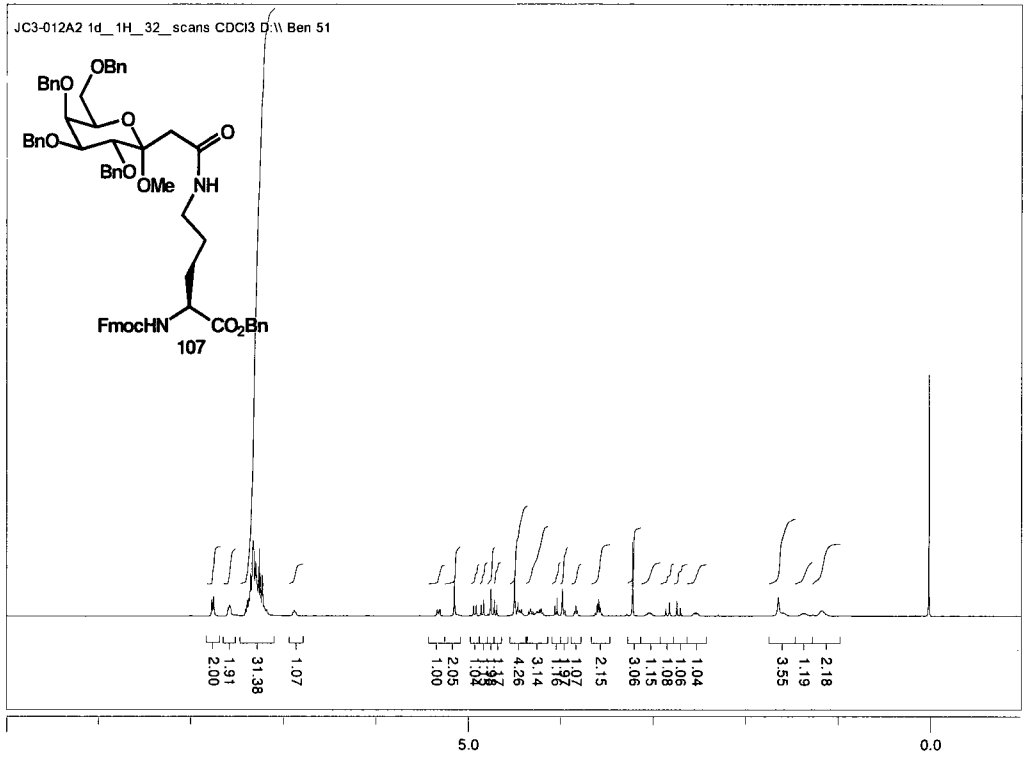
JC3-012A2 1d__1H__32__scans CDCl3 D:\\ Ben 51
OBn
BnO
O
BnO
O
BnO
OMe
NH
FmocHN
CO2Bn
107
2.00
1.91
31.38
1.07
1.00
2.05
4.26
3.14
2.15
3.06
1.15
1.08
1.06
1.04
3.55
1.19
2.18
5.0
0.0

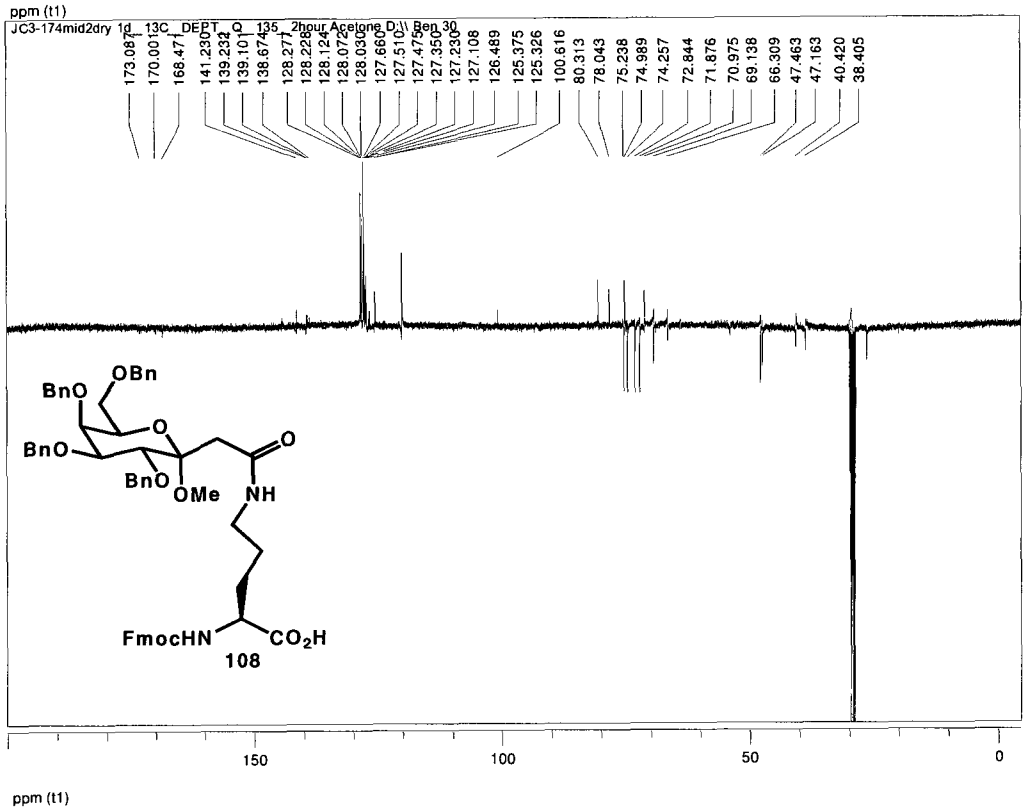
ppm (t1)
JC3-174mid2dry 1d 13C DEPT Q 135 2hour Acetone D:\ Ben 30
173.087
170.001
168.471
141.230
139.232
139.101
138.674
128.277
128.225
128.124
128.072
128.030
127.660
127.510
127.475
127.350
127.230
127.108
126.489
125.375
125.326
100.616
80.313
78.043
75.238
74.989
74.257
72.844
71.876
70.975
69.138
66.309
47.463
47.163
40.420
38.405
BnO
OBn
O
BnO
O
BnO
OMe
NH
FmocHN
CO2H
108
150
100
50
0
ppm (t1)

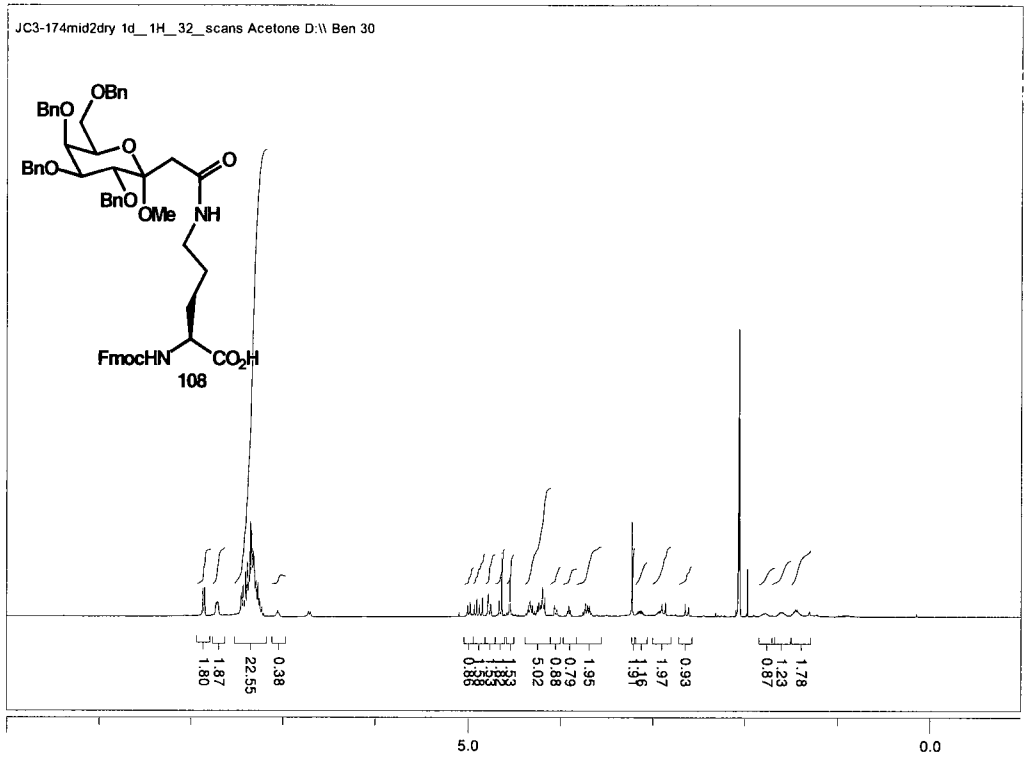
JC3-174mid2dry 1d__1H__32__scans Acetone D:\\ Ben 30
BnO
OBn
O
BnO
O
BnO
OMe
NH
FmocHN
CO2H
108
1.80
1.87
22.55
0.38
5.02
0.88
0.79
1.95
1.97
0.93
0.87
1.23
1.78
5.0
0.0

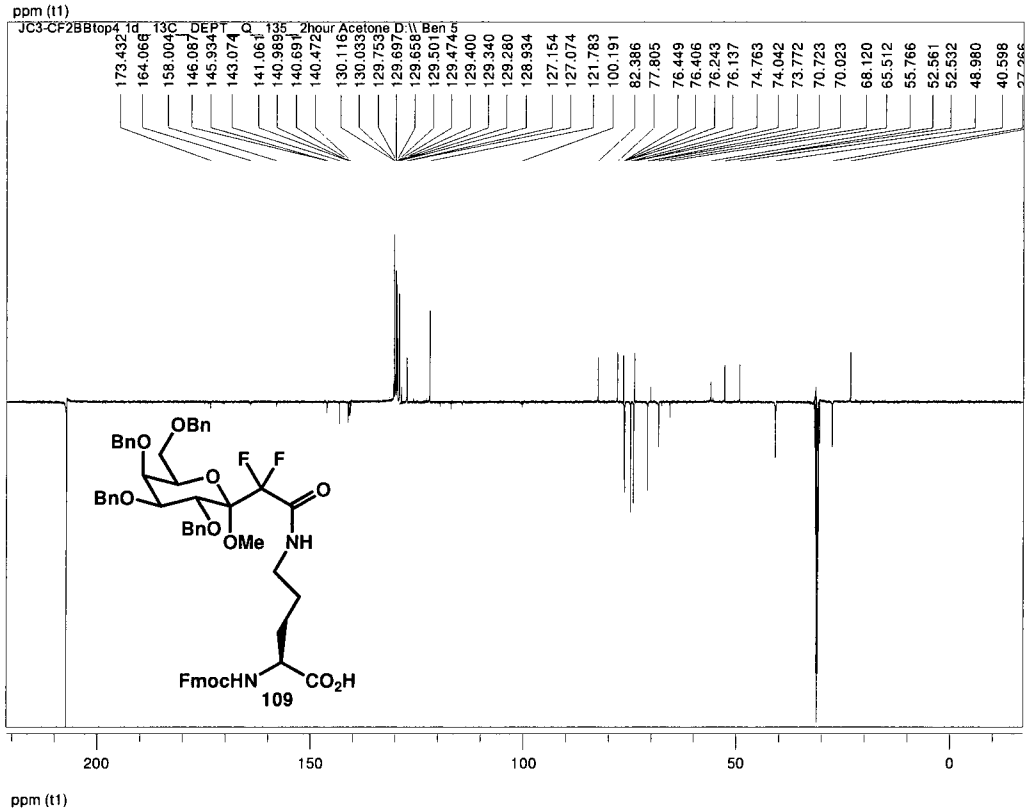
ppm (t1)
JC3-CF2BBtop4_1d 13C DEPT Q 135 2hour Acetone D:\\ Ben
173.432
164.068
158.004
146.087
145.934
143.074
141.061
140.989
140.691
140.472
130.116
130.039
129.753
129.697
129.658
129.501
129.474
129.400
129.340
129.280
128.934
127.154
127.074
121.783
100.191
82.386
77.805
76.449
76.406
76.243
76.137
74.763
74.042
73.772
70.723
70.023
68.120
65.512
55.766
52.561
52.532
48.980
40.598
BnO
OBn
O
F
F
O
BnO
BnO
OMe
NH
FmocHN
CO2H
109
200
150
100
50
0
ppm (t1)

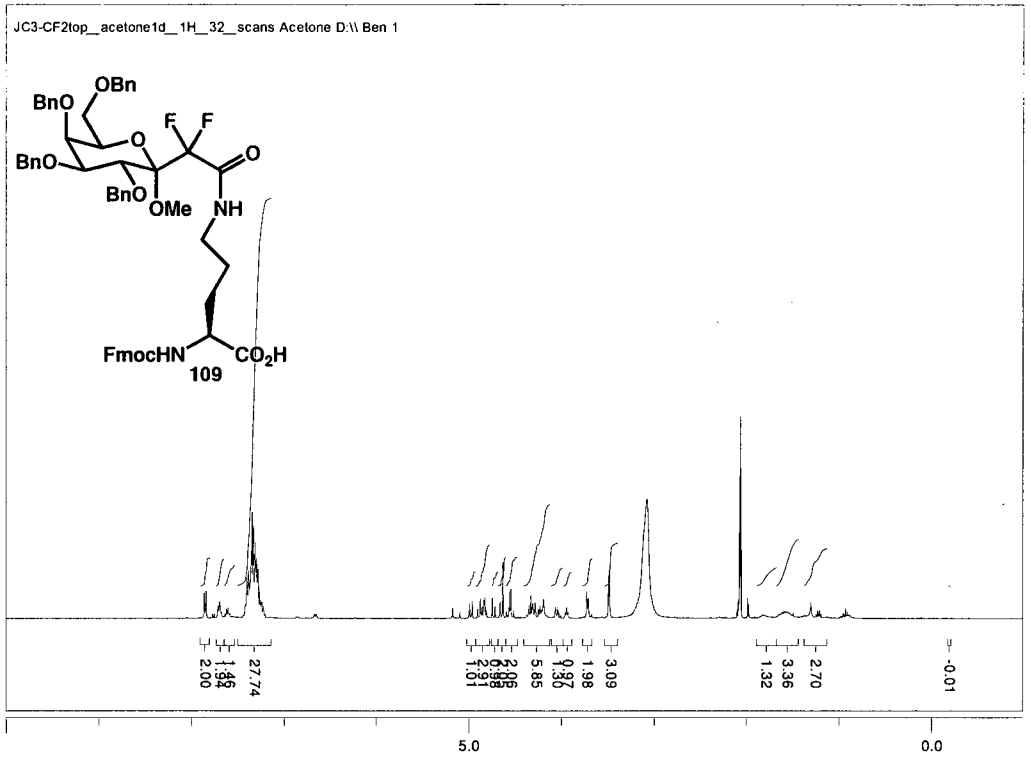
JC3-CF2top_acetone1d_1H_32_scans Acetone D:\\ Ben 1
OBn
BnO
F
F
O
BnO
O
BnO
OMe
NH
FmocHN
CO2H
109
2.00
1.46
1.94
27.74
1.01
5.85
9.87
1.98
3.09
1.32
3.36
2.70
-0.01
5.0
0.0

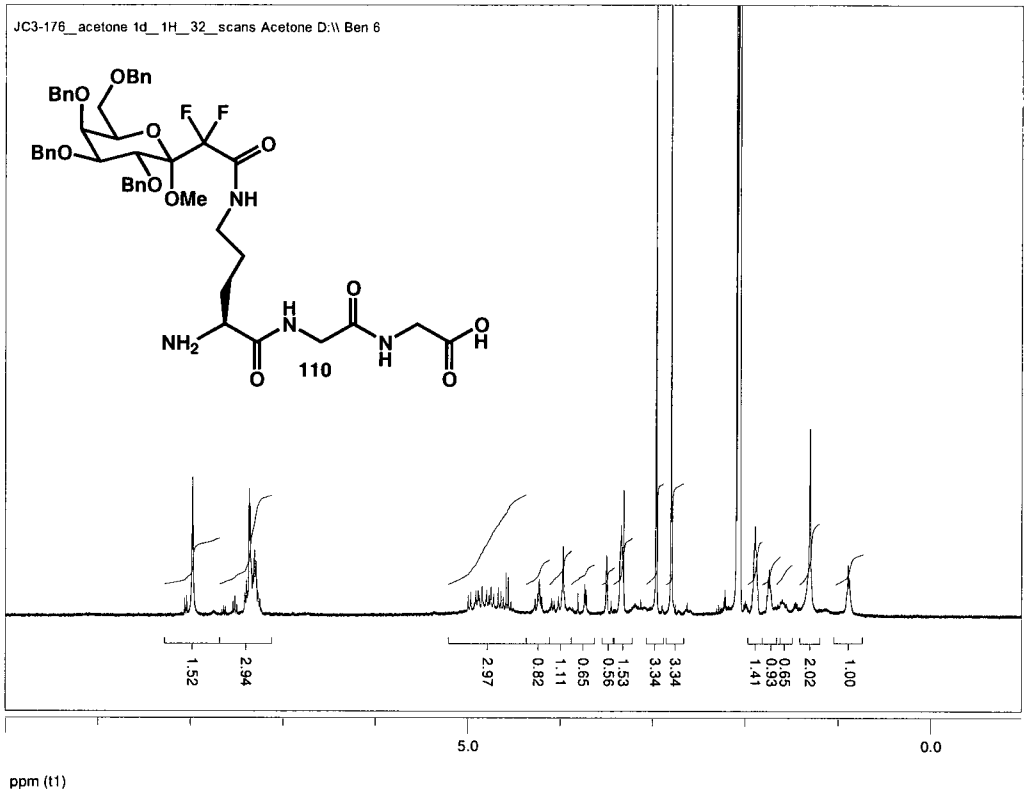
JC3-176_acetone 1d_1H_32_scans Acetone D:\\ Ben 6
BnO
OBn
BnO
BnO
OMe
O
F
F
O
NH
NH2
H
N
O
N
H
O
H
O
O
110
1.52
2.94
2.97
0.82
1.11
0.65
0.56
1.53
3.34
3.34
1.41
0.93
0.65
2.02
1.00
5.0
0.0
ppm (t1)

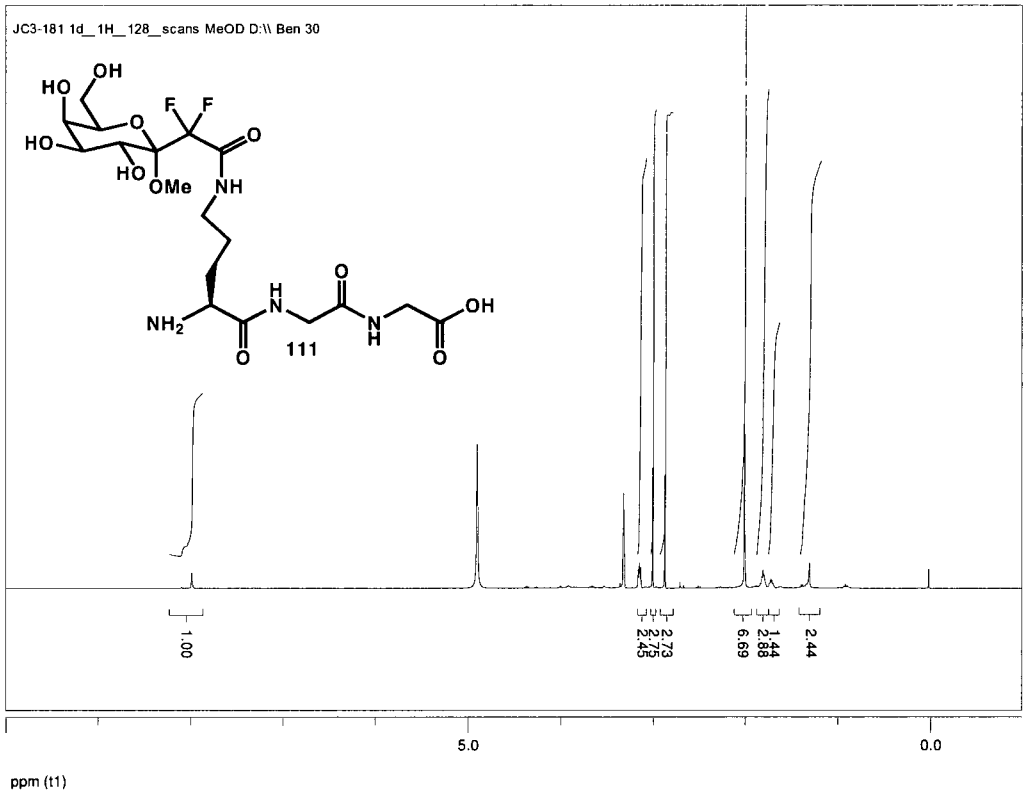
JC3-181 1d__1H__128__scans MeOD D:\\ Ben 30
HO
OH
HO
O
F
F
O
HO
OMe
NH
NH2
H
N
O
N
H
OH
O
O
111
1.00
2.45
2.75
2.73
6.69
2.88
1.44
2.44
5.0
0.0
ppm (t1)

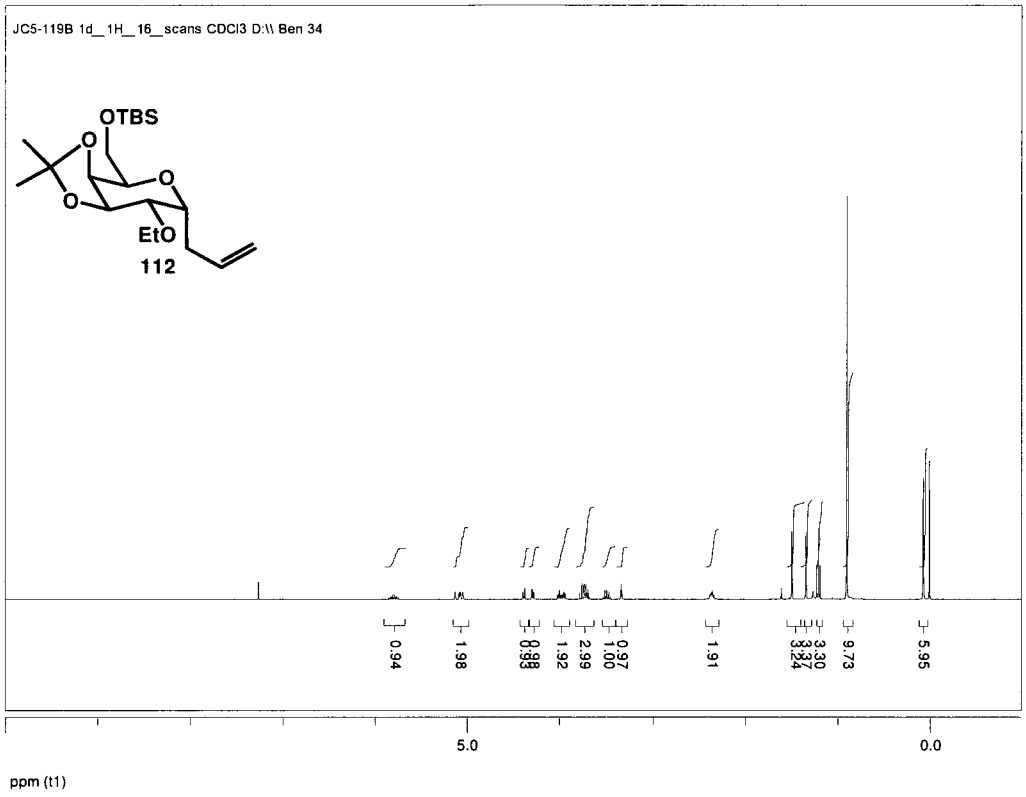
JC5-119B 1d__1H__16__scans CDCl3 D:\\ Ben 34
OTBS
O
O
O
EtO
112
0.94
1.98
0.98
0.88
1.92
2.99
1.00
0.97
1.91
3.27
3.24
3.30
9.73
5.96
5.0
0.0
ppm (t1)

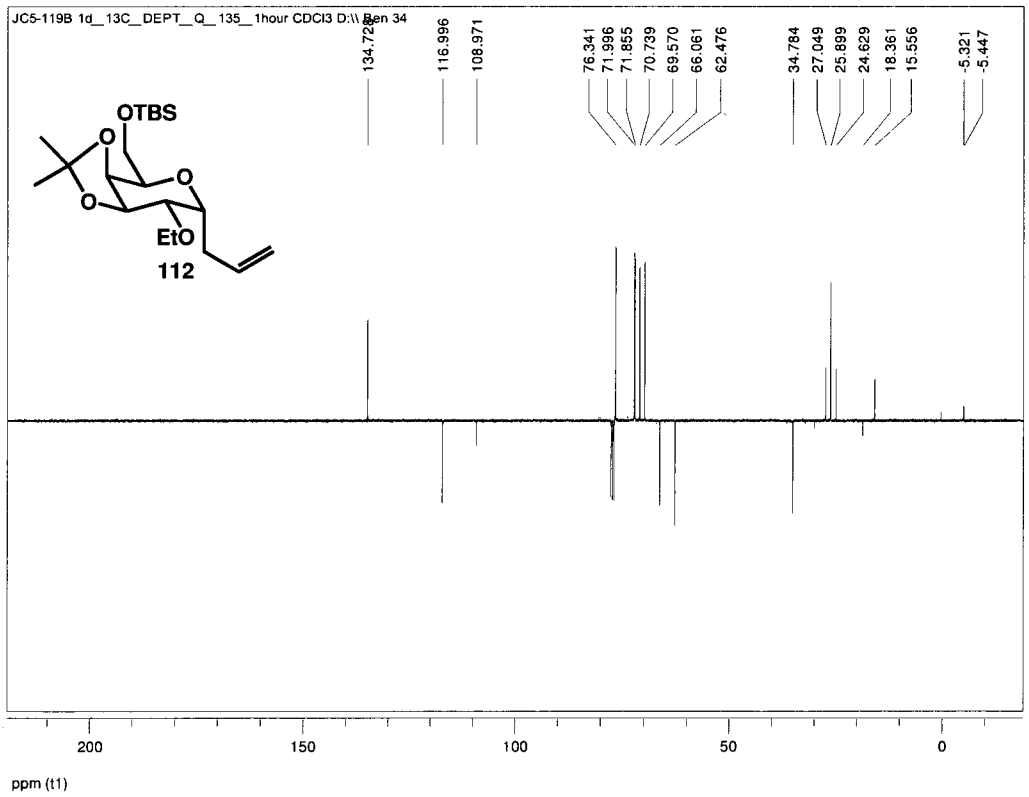
JC5-119B 1d__13C__DEPT__Q__135__1hour CDCl3 D:\\ Ben 34
OTBS
O
O
O
EtO
112
134.728
116.996
108.971
76.341
71.996
71.855
70.739
69.570
66.061
62.476
34.784
27.049
25.899
24.629
18.361
15.556
-5.321
-5.447
200
150
100
50
0
ppm (t1)

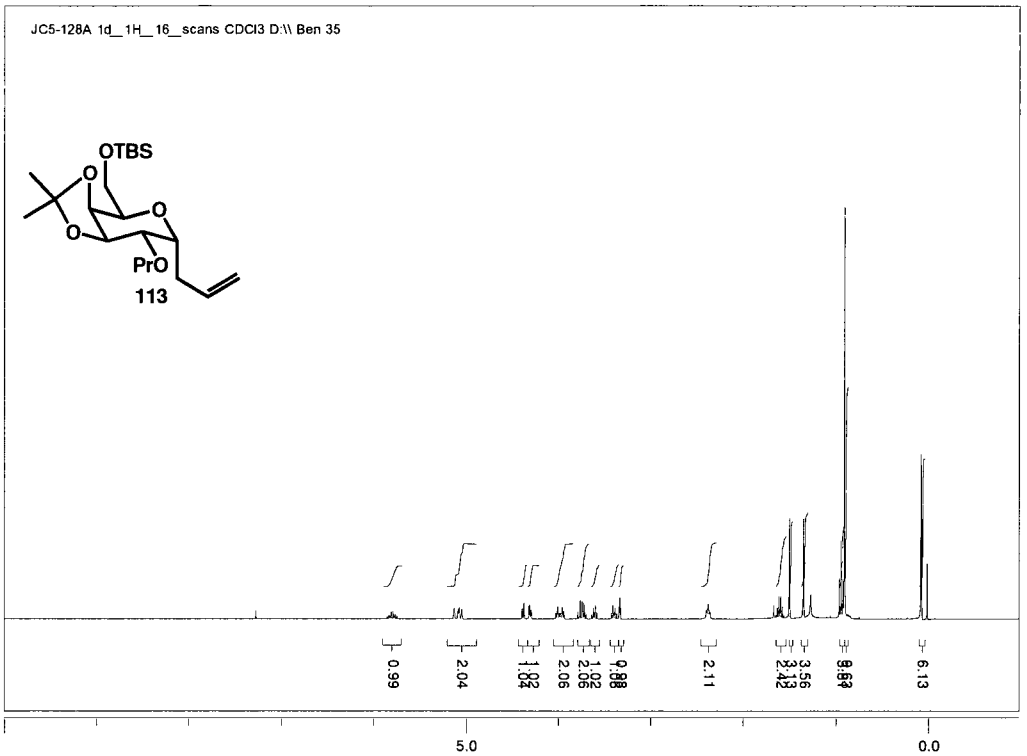
JC5-128A 1d__1H__16__scans CDCl3 D:\\ Ben 35
OTBS
O
O
O
O
PrO
113
0.99
2.04
2.06
2.11
3.56
6.13
5.0
0.0
ppm (t1)

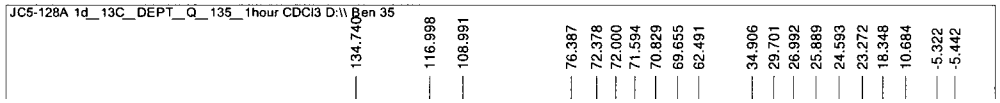
JC5-128A 1d__13C__DEPT__Q__135__1hour CDCl3 D:\\ Ben 35
134.740
116.998
108.991
76.387
72.378
72.000
71.594
70.829
69.655
62.491
34.906
29.701
26.992
25.889
24.593
23.272
18.348
10.684
-5.322
-5.442

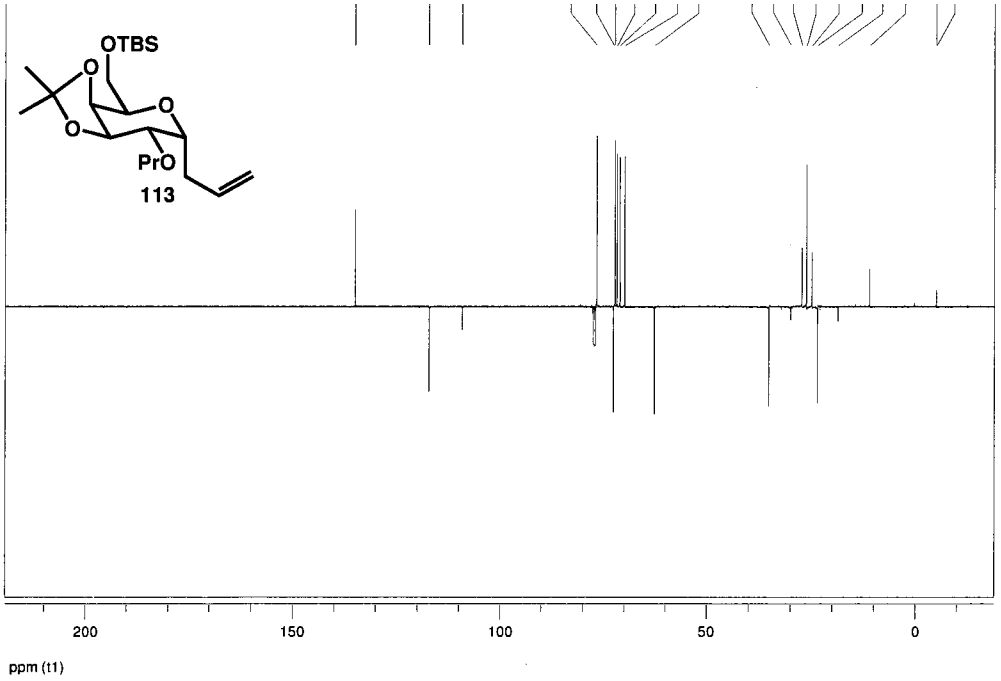
OTBS
O
O
O
PrO
113
200
150
100
50
0
ppm (t1)

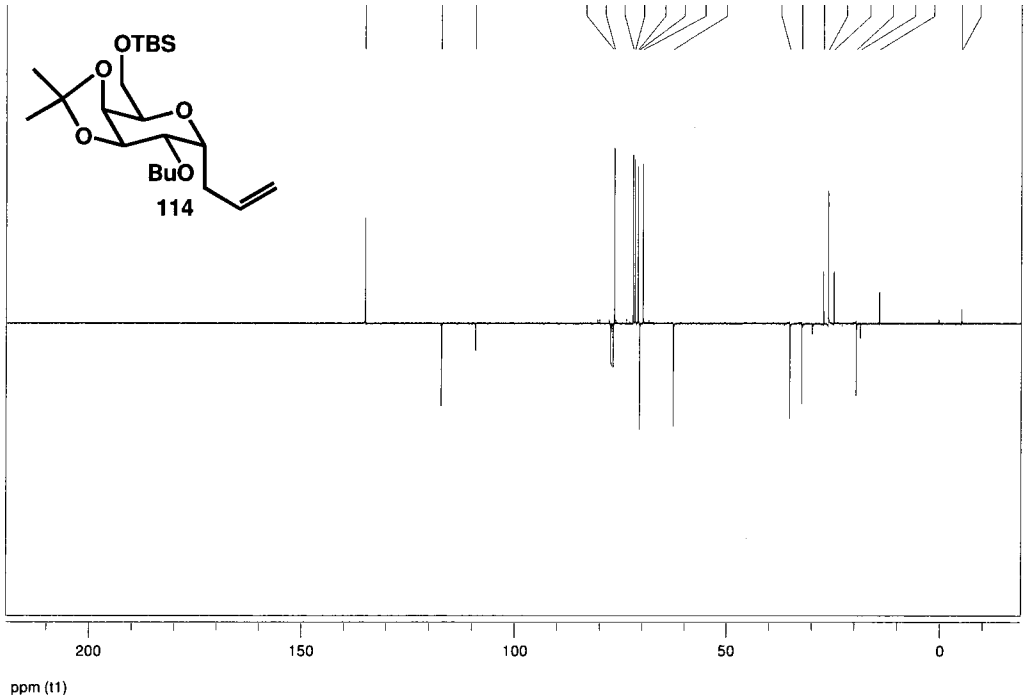
OTBS
O
O
O
BuO
114
200
150
100
50
0
ppm (t1)

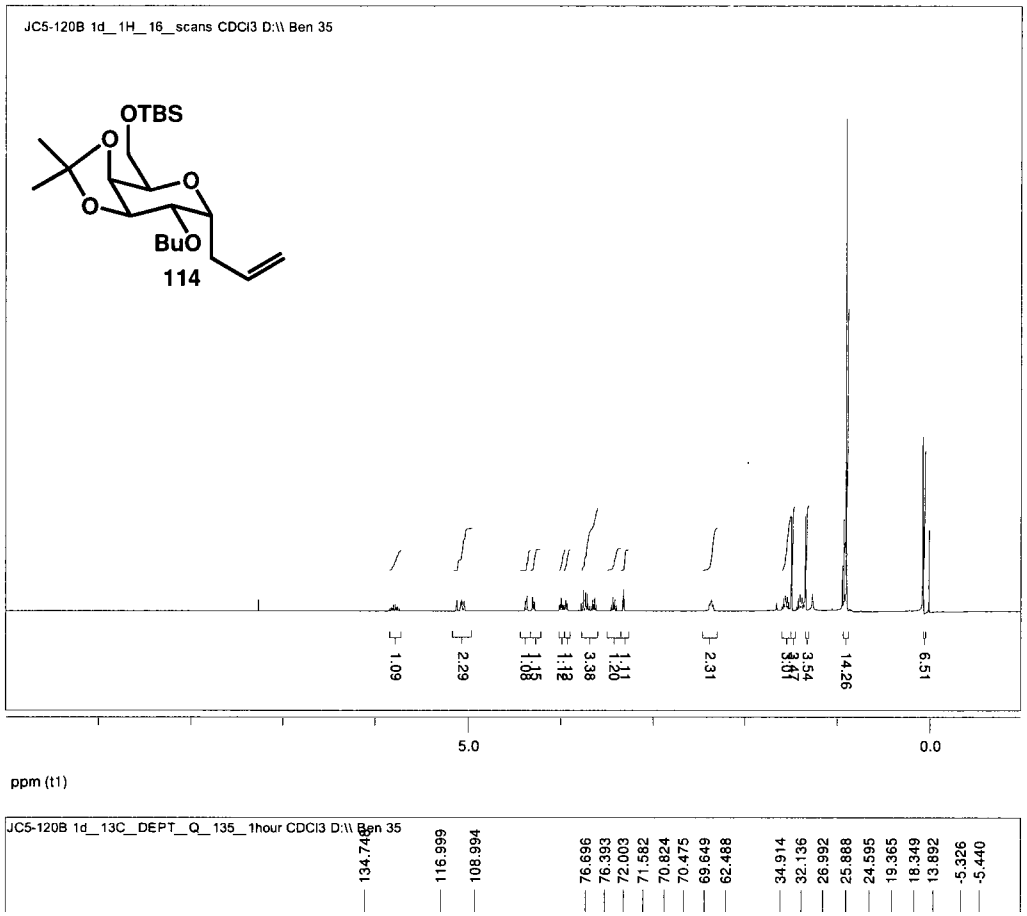
JC5-120B 1d__1H__16__scans CDCl3 D:\\ Ben 35
OTBS
O
O
O
BuO
114
1.09
2.29
1.15
1.12
3.38
1.11
1.20
2.31
3.54
14.26
6.51
5.0
0.0
ppm (t1)

JC5-120B 1d__13C__DEPT__Q__135__1hour CDCl3 D:\\ Ben 35
134.748
116.999
108.994
76.696
76.393
72.003
71.582
70.824
70.475
69.649
62.488
34.914
32.136
26.992
25.888
24.595
19.365
18.349
13.892
-5.326
-5.440

ppm (t1)

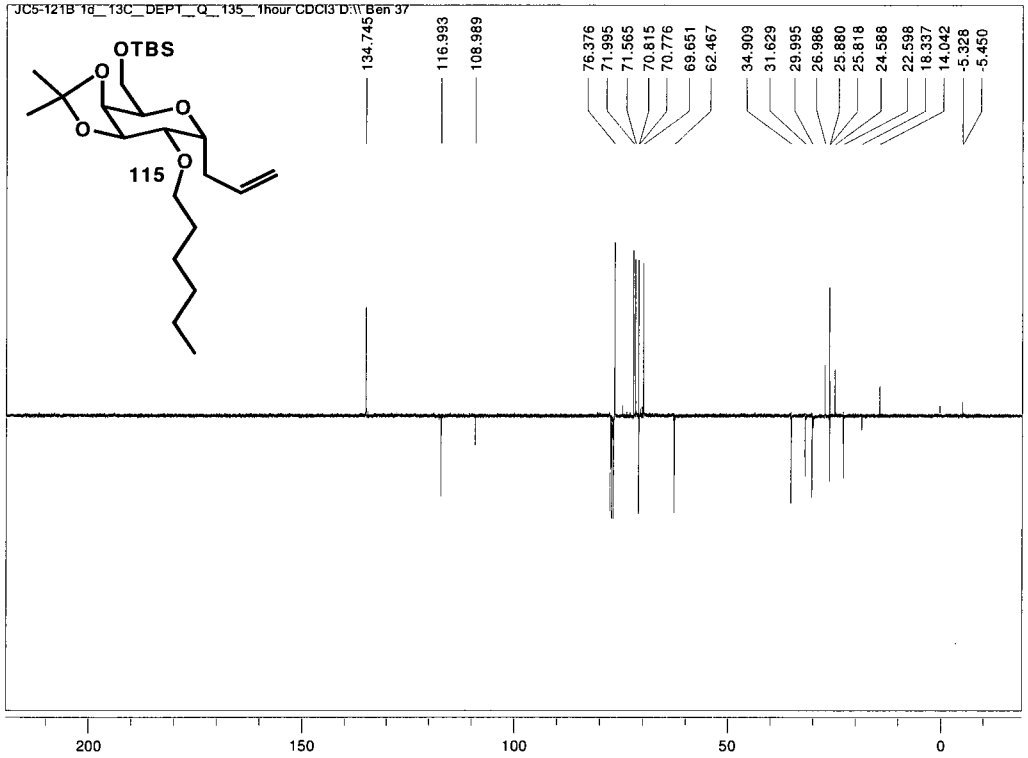
JC5-121B 1d__13C__DEPT__Q__135__1hour CDCl3 D:\\ Ben 37
OTBS
O
O
O
O
115
134.745
116.993
108.989
76.376
71.995
71.565
70.815
70.776
69.651
62.467
34.909
31.629
29.995
26.986
25.880
25.818
24.588
22.598
18.337
14.042
-5.328
-5.450
200
150
100
50
0

ppm (t1)

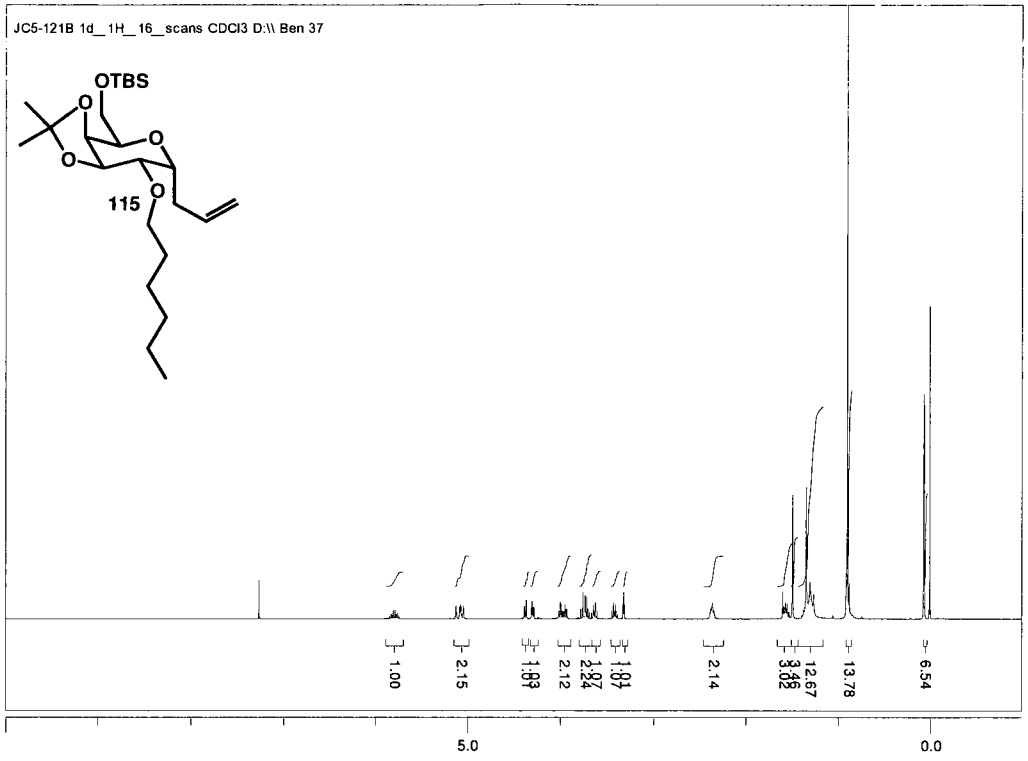
JC5-121B 1d__1H__16__scans CDCl3 D:\\ Ben 37
OTBS
O
O
O
O
115
1.00
2.15
1.83
2.12
2.24
1.97
1.91
2.14
3.46
3.02
12.67
13.78
6.54
5.0
0.0

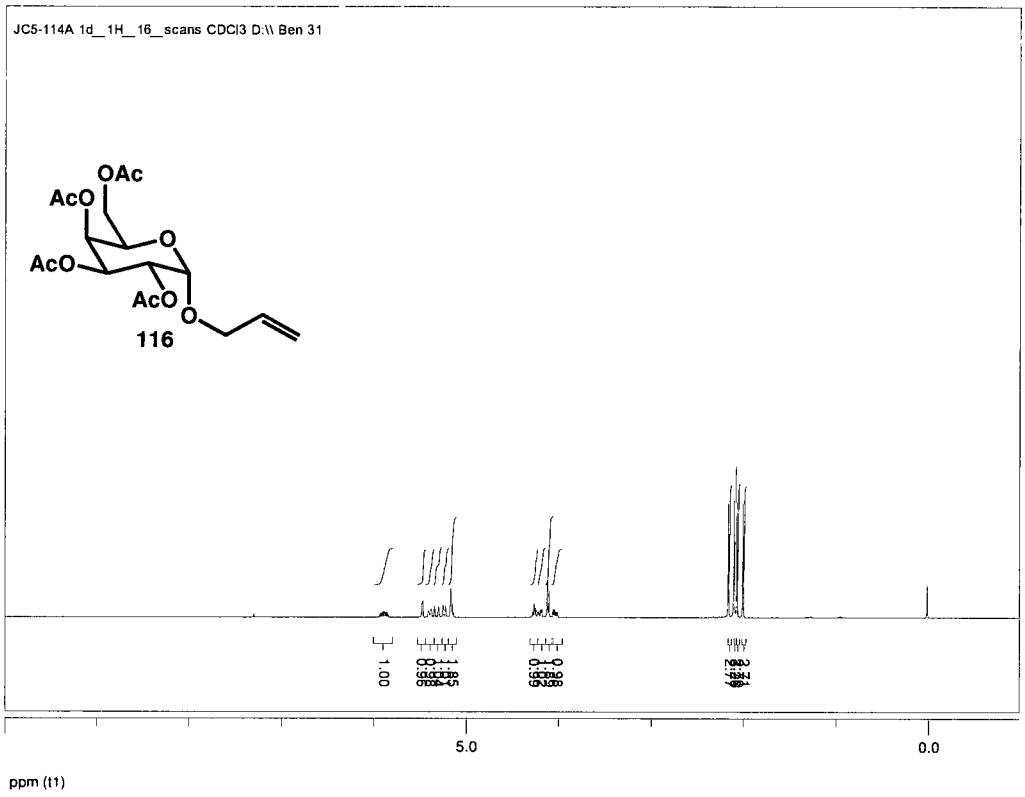
JC5-114A 1d__1H__16__scans CDCl3 D:\\ Ben 31
OAc
AcO
O
AcO
AcO
O
116
1.00
5.0
0.0
ppm (t1)

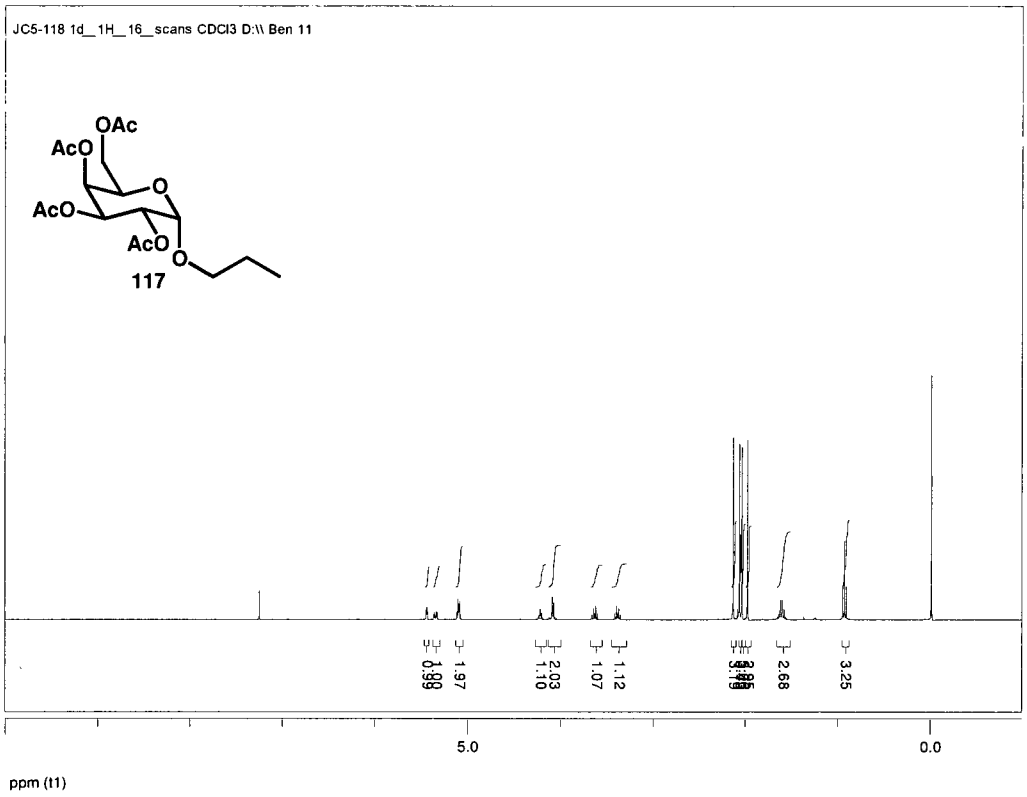
JC5-118 1d__1H__16_scans CDCl3 D:\\ Ben 11
OAc
AcO
AcO
AcO
O
O
117
0.99
1.97
2.03
1.10
1.07
1.12
2.68
3.25
5.0
0.0
ppm (t1)

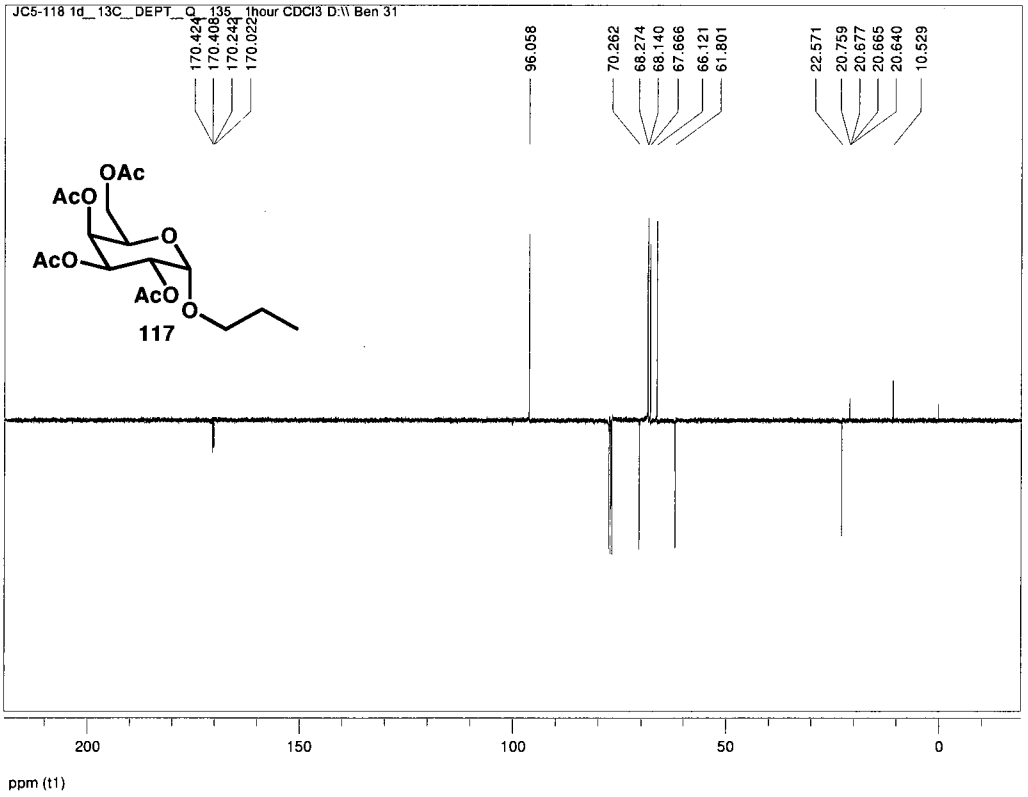
JC5-118 1d__13C__DEPT__Q__135__1hour CDCl3 D:\\ Ben 31
170.424
170.408
170.244
170.022
96.058
70.262
68.274
68.140
67.666
66.121
61.801
22.571
20.759
20.677
20.665
20.640
10.529
OAc
AcO
AcO
AcO
O
O
117
200
150
100
50
0
ppm (t1)

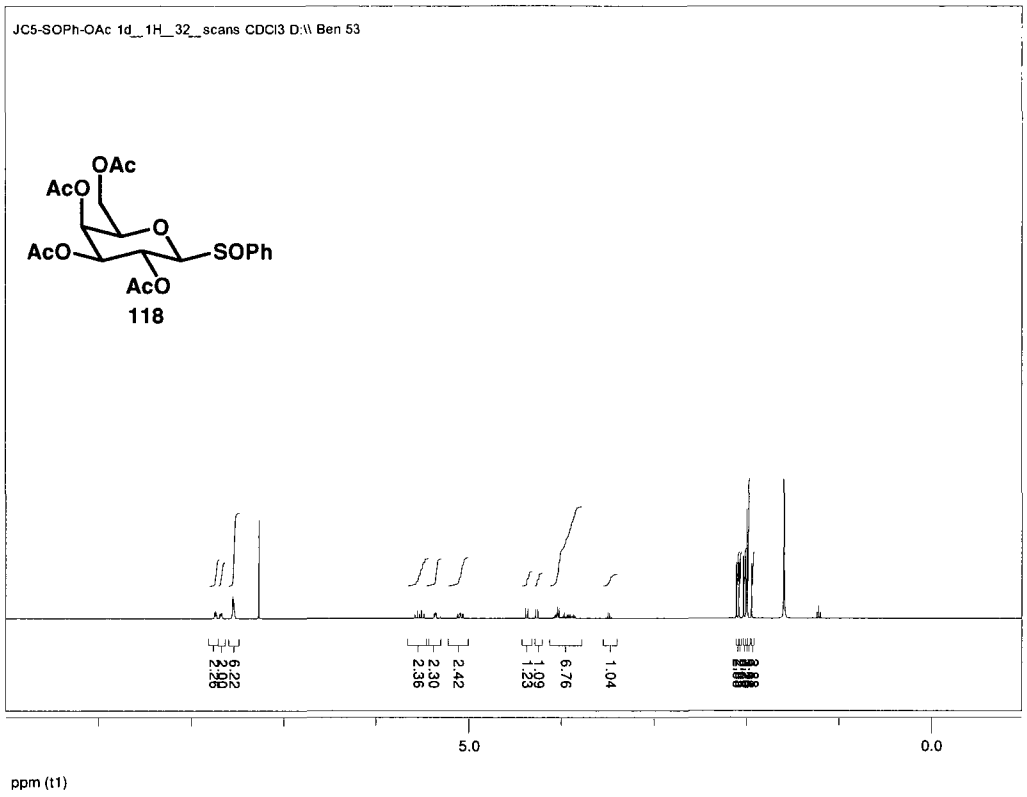
JC5-SOPh-OAc 1d__1H__32__scans CDCl3 D:\\ Ben 53
OAc
AcO
AcO
O
SOPh
AcO
118
2.26
2.99
9.22
2.36
2.30
2.42
1.23
1.99
6.76
1.04
5.0
0.0
ppm (t1)

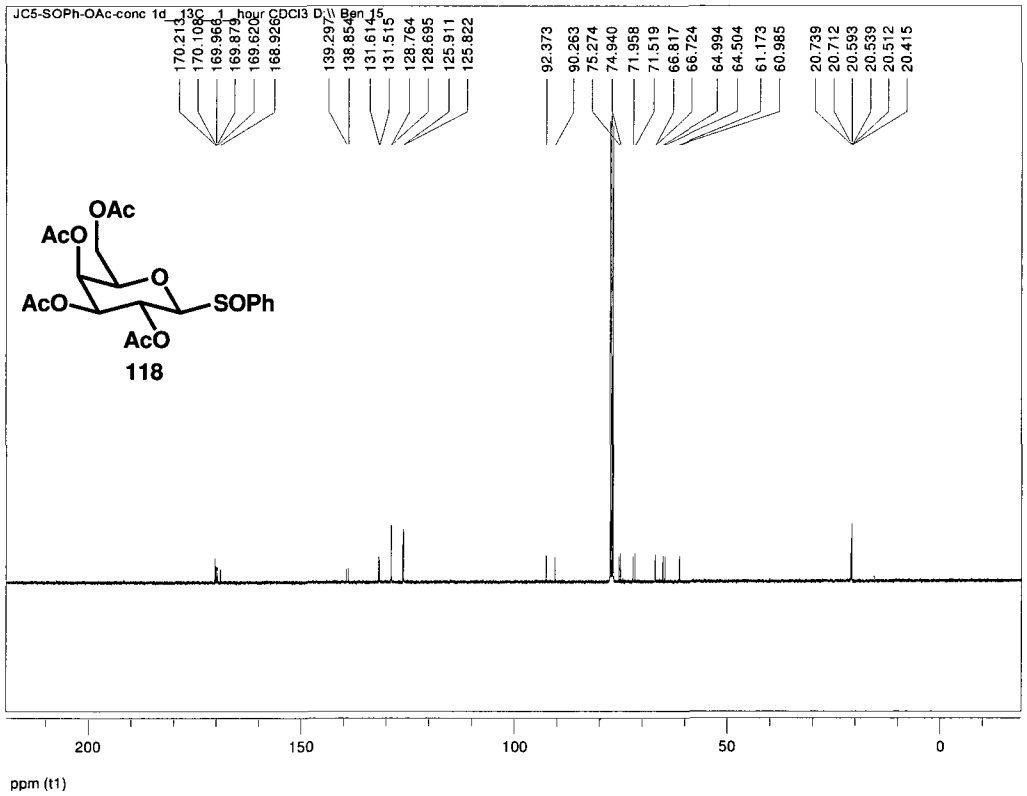
JC5-SOPh-OAc-conc 1d__13C__1__hour CDCl3 D:\\ Ben 15
170.213
170.108
169.964
169.879
169.620
168.926
139.297
138.854
131.614
131.515
128.764
128.695
125.911
125.822
92.373
90.263
75.274
74.940
71.958
71.519
66.817
66.724
64.994
64.504
61.173
60.985
20.739
20.712
20.593
20.539
20.512
20.415
OAc
AcO
AcO
O
SOPh
AcO
118
200
150
100
50
0
ppm (t1)

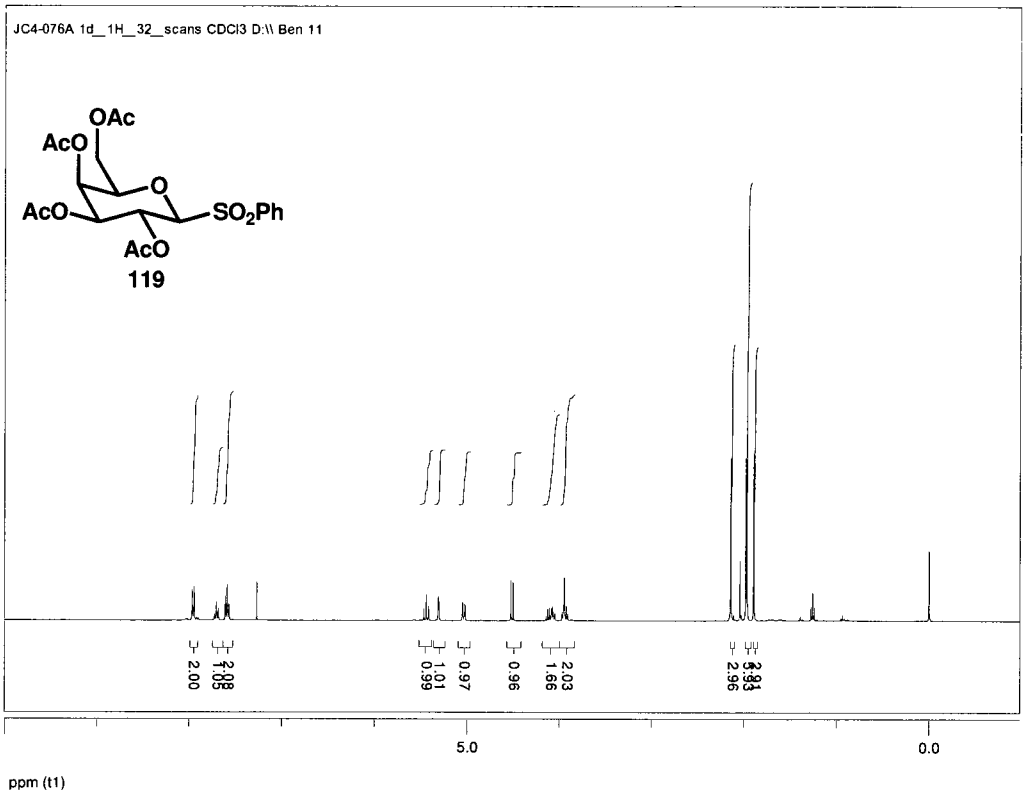
JC4-076A 1d__1H__32__scans CDCl3 D:\\ Ben 11
OAc
AcO
O
AcO
SO2Ph
AcO
119
2.00
2.08
2.05
1.01
0.99
0.97
0.96
1.66
2.03
2.96
5.0
0.0
ppm (t1)